POLITECHNIKA GDAŃSKA

Kontrola procesowa za pomocą technik czujnikowych nowych metod selektywnego oczyszczania biogazu ze związków uciążliwych zapachowo

ROZPRAWA DOKTORSKA

mgr inż. Edyta Słupek

Gdańsk, 2023

Imię i nazwisko autora rozprawy: Edyta Słupek
Dyscyplina naukowa: nauki chemiczne

ROZPRAWA DOKTORSKA

Tytuł rozprawy w języku polskim: Kontrola procesowa za pomocą technik czujnikowych nowych metod selektywnego oczyszczania biogazu ze związków uciążliwych zapachowo

Tytuł rozprawy w języku angielskim: Process control using sensor techniques of new methods for the selective purification of biogas from odor nuisance compounds

Promotor
podpis
dr hab. inż. Jacek Gębicki, prof. PG
Promotor pomocniczy
podpis
dr inż. Patrycja Makoś-Chełstowska

Gdańsk, rok 2023

OŚWIADCZENIE

Autor rozprawy doktorskiej: Edyta Słupek

Ja, niżej podpisana, oświadczam, iż jestem świadoma, że zgodnie z przepisem art. 27 ust. 1 i 2 ustawy z dnia 4 lutego 1994 r. o prawie autorskim i prawach pokrewnych (t.j. Dz.U. z 2021 poz. 1062), uczelnia może korzystać z mojej rozprawy doktorskiej zatytułowanej:

Kontrola procesowa za pomocą technik czujnikowych nowych metod selektywnego oczyszczania biogazu ze związków uciążliwych zapachowo

do prowadzenia badań naukowych lub w celach dydaktycznych.[1]

Świadoma odpowiedzialności karnej z tytułu naruszenia przepisów ustawy z dnia 4 lutego 1994 r. o prawie autorskim i prawach pokrewnych i konsekwencji dyscyplinarnych określonych w ustawie Prawo o szkolnictwie wyższym i nauce (Dz.U.2021.478 t.j.), a także odpowiedzialności cywilno-prawnej oświadczam, że przedkładana rozprawa doktorska została napisana przeze mnie samodzielnie.

Oświadczam, że treść rozprawy opracowana została na podstawie wyników badań prowadzonych pod kierunkiem i w ścisłej współpracy z promotorem dr hab. inż. Jackiem Gębickim i promotorem pomocniczym dr inż. Patrycją Makoś-Chełstowską.

Niniejsza rozprawa doktorska nie była wcześniej podstawą żadnej innej urzędowej procedury związanej z nadaniem stopnia doktora.

Wszystkie informacje umieszczone w ww. rozprawie uzyskane ze źródeł pisanych i elektronicznych, zostały udokumentowane w wykazie literatury odpowiednimi odnośnikami, zgodnie z przepisem art. 34 ustawy o prawie autorskim i prawach pokrewnych.

Potwierdzam zgodność niniejszej wersji pracy doktorskiej z załączoną wersją elektroniczną.

Gdańsk, dnia ....
                                                           podpis doktoranta

Ja, niżej podpisana, wyrażam zgodę/~~nie wyrażam zgody~~* na umieszczenie ww. rozprawy doktorskiej w wersji elektronicznej w otwartym, cyfrowym repozytorium instytucjonalnym Politechniki Gdańskiej.

Gdańsk, dnia ....
                                                           podpis doktoranta

*niepotrzebne usunąć

---

[1] Art. 27. 1. Instytucje oświatowe oraz podmioty, o których mowa w art. 7 ust. 1 pkt 1, 2 i 4–8 ustawy z dnia 20 lipca 2018 r. – Prawo o szkolnictwie wyższym i nauce, mogą na potrzeby zilustrowania treści przekazywanych w celach dydaktycznych lub w celu prowadzenia działalności naukowej korzystać z rozpowszechnionych utworów w oryginale i w tłumaczeniu oraz zwielokrotniać w tym celu rozpowszechnione drobne utwory lub fragmenty większych utworów.
2. W przypadku publicznego udostępniania utworów w taki sposób, aby każdy mógł mieć do nich dostęp w miejscu i czasie przez siebie wybranym korzystanie, o którym mowa w ust. 1, jest dozwolone wyłącznie dla ograniczonego kręgu osób uczących się, nauczających lub prowadzących badania naukowe, zidentyfikowanych przez podmioty wymienione w ust. 1.

OPIS ROZPRAWY DOKTORSKIEJ

Autor rozprawy doktorskiej: Edyta Słupek

Tytuł rozprawy doktorskiej w języku polskim: Kontrola procesowa za pomocą technik czujnikowych nowych metod selektywnego oczyszczania biogazu ze związków uciążliwych zapachowo

Tytuł rozprawy w języku angielskim: Process control using sensor techniques of new methods for the selective purification of biogas from odor nuisance compounds

Język rozprawy doktorskiej: polski

Promotor rozprawy doktorskiej: dr hab. inż. Jacek Gębicki, prof. uczelni

Promotor pomocniczy rozprawy doktorskiej*: dr inż. Patrycja Makoś-Chełstowska

Data obrony:

Słowa kluczowe rozprawy doktorskiej w języku polskim: biogaz, absorpcja, ciecze głęboko eutektyczne, kontrola procesowa

Słowa kluczowe rozprawy doktorskiej w języku angielskim: biogas, absorption, deep eutectic solvents, process control

Streszczenie rozprawy w języku polskim: W obecnym czasie dużą uwagę zwraca się na opracowanie efektywnej technologii oczyszczania biogazu do gazu wysokometanowego. Głównym celem rozprawy doktorskiej było opracowanie ekonomicznie opłacalnych absorbentów do efektywnego oczyszczania strumieni biogazu z substancji uciążliwych zapachowo. Procesy absorpcji fizycznej prowadzono z wykorzystaniem zaprojektowanych i otrzymanych dotąd jeszcze nie publikowanych sorbentów na bazie cieczy głęboko eutektycznych (*ang. Deep Eutectic Solvents, DES*). Przeprowadzone badania wykazały konkurencyjność DES do obecnie stosowanych konwencjonalnych sorbentów. W przeprowadzonych badaniach wykazano także przydatność matryc czujnikowych do monitorowania procesów absorpcyjnego uzdatniania biogazu. Uzyskane wyniki stanowią kompleksową charakterystykę uzdatniania biogazu z lotnych związków odorotwórczych. Przedstawione cele cząstkowe zrealizowano i przedstawiono w ośmiu publikacjach naukowych, które stanowią podstawę niniejszej rozprawy doktorskiej.

Streszczenie rozprawy w języku angielskim: Currently, considerable attention is being paid to the development of efficient technologies for the purification of biogas into high methane gas. The main objective of this dissertation was to develop economically viable absorbents for the efficient purification of biogas streams from odor-nuisance substances. Physical absorption processes were performed using designed and obtained as yet unpublished sorbents based on Deep Eutectic Solvents (DES). These studies showed the competitiveness of DES over the currently used conventional sorbents. This study also demonstrated the suitability of sensor arrays for monitoring the absorption of biogas treatment processes. The results provide a comprehensive characterization of biogas treatment of volatile odor-forming compounds. The presented partial objectives were realized and presented in eight scientific publications, which formed the basis of this dissertation.

Składam serdeczne podziękowania
Promotorowi dr hab. inż. Jackowi Gębickiemu,
za zaufanie, opiekę merytoryczną oraz wieloletnią współpracę.

Dziękuję również
Promotorce Pomocniczej dr inż. Patrycji Makoś-Chełstowskiej
za życzliwość, przyjaźń oraz wsparcie, na które zawsze mogłam liczyć.

Pracownikom oraz Doktorantom Katedry Inżynierii Procesowej i Technologii
Chemicznej dziękuję za okazaną wszechstronną pomoc.

Szczególne podziękowania składam moim Rodzicom
za wychowanie, troskę oraz wiarę w moje możliwości.

Kacper, Tobie dziękuję za Twoją wyrozumiałość, cierpliwość
oraz nieocenione wsparcie.

Spis treści

Wykaz skrótów i akronimów

Skrót/akronim	Nazwa w języku polski	Nazwa w języku angielskim
A	Aceton	Acetone
AP	Aldehyd propionowy	Propionaldehyde
B	Benzen	Benzene
BuOH	Butanol	Butanol
C	Kamfora	Camphor
C-one	Karwon	Carvone
ChCl	Chlorek choliny	Choline Chloride
CF	Chloroform	Chloroform
CO	Tlenek węgla	Carbon Monoxide
CH	Cykloheksan	Cyclohesane
CO_2	Dwutlenek węgla	Carbon Dioxide
CNG	Sprężony gaz ziemny	Compressed Natural Gas
COSMO-RS	Model ekranowania dla rzeczywistych rozpuszczalników	Conductor-Like Screening Model For Realistic Solvent
CH_4	Metan	Methane
ChCl	Chlorek choliny	Choline Chloride
DA	Kwas dekanowy	Decanoic Acid
DDA	Kwas dodekanowy	Dodecanoic Acid
DCM	Dichlorometan	Dichloromethane
DEG	Glikol dietylenowy	Diethylene glycol
DES	Ciecze głęboko eutektyczne	Deep Eutectic Solvents
DFT	Teoria funkcjonału gęstości	Density Functional Theory
DMDS	Disiarczek dimetylu	Dimethyl Disulfide
D3	Heksametylocyklotrisiloksan	Hexamethylcyclotrisiloxane
D4	Oktametylocyklotetrasiloksan	Octamethylcyclotetrasiloxane
D5	Dekametylocyklopentasiloksan	Decamethylcyclopentasiloxane
E	Etylobenzen	Ethylbenzene
Eu	Eukaliptol	Eucalyptol
EG	Glikol etylenowy	Ethylene Glycol
EPA	Analiza Potencjału Elektrostatycznego	Electrostatic Potential Analysis
ESP	Analiza potencjału elektrostatycznego	Electrostatic Potential Analysis
FA	Kwas mrówkowy	Formic Acid
FF	Furfural	Furfural
FTIR	Spektroskopia w podczerwieni z transformacją Fouriera	Fourier Transformed Infrared Spectroscopy
FPD	Detektor płomieniowo-fotometryczny	Flame Photometric Detector
FID	Detektor płomieniowo-jonizacyjny	Flame Ionization Detector
G	Gwajakol	Guaiacol
GC	Chromatografia gazowa	Gas Chromatography
GC-O	Chromatografia gazowa połączona z olfaktometrią dynamiczną	Gas Chromatography combined with Dynamic Olfactometry
GC-MS-O	Chromatografia gazowa połączona z spektrometrem mas oraz olfaktometrią dynamiczną	Gas Chromatography combined with a Mass Spectrometer and Dynamic Olfactometry
Gly	Glicerol	Glycerol
H	Stała Henry'ego	Henry's constant
H_2	Wodór	Hydrogen
HBA	Akceptor wiązania wodorowego	Hydrogen Bond Acceptor
HBD	Donor wiązania wodorowego	Hydrogen Bond Donor
H_2S	Siarkowodór	Hydrogen Sulphide
H_2SO_4	Kwas siarkowy (VI)	Sulphuric Acid (VI)
HS-GC-FID	Analiza fazy nadpowierzchniowej przy użyciu chromatografii gazowej sprzężonej z detektorem płomieniowo-jonizacyjnym	Headspace analysis using gas chromatography coupled with a flame ionization detector
IL	Ciecze jonowe	Ionic Liquid
IEA	Międzynarodową Agencje Energetyczna	International Energy Agency
K	Współczynników podziału para-ciecz	Vapor-Liquid Partition Coefficients

M	Mentol	*Menthol*
MLR	Wielokrotna regresja liniowa	*Multiple Linear Regression*
MP	Temperatura topnienia	*Melting Points*
N₂	Azot	*Nitrogen*
NH₃	Amoniak	*Ammonia*
NMR	Spektroskopia Magnetycznego Rezonansu Jądrowego	*Nuclear Magnetic Resonance Spectroscopy*
OA	Kwas oktanowy	*Octanoic Acid*
OECD	Organizacja Współpracy Gospodarczej i Rozwoju	*Organisation for Economic Cooperation and Development*
OZE	Odnawialne źródło energii	*Renewable Energy Source*
Ph	Fenol	*Phenol*
PLS	Regresja częściowa najmniejszych kwadratów	*Partial Least Squares Regression*
PSA	Adsorpcja zmiennociśnieniowa	*Pressure Swing Adsorption*
RDG	Analiza Gradientu Gęstości	*Reduced Density Gradient*
RE	Rada Europejska	*European Council*
RMSE	Błąd Średniokwadratowy	*Root Mean Square Error*
RT	Temperatura Pokojowa	*Room temperature*
SOₓ	Tlenki siarki	*Sulfur Oxides*
Syr	Syringol	*Syringole*
SiO₂	Krzemionka	*Silica*
SiₓOᵧ	Krzemiany	*Silicates*
Lev	Kwas lewulinowy	*Levulinic Acid*
LZO	Lotne związki organiczne	*Volatile Organic Compounds*
L2	Heksametylodisiloksan	*Hexamethyldisiloxane*
L3	Oktametylotrisiloksan	*Octamethyltrisiloxane*
L4	Dekametylotetrasiloksan	*Decamethyltetrasiloxane*
MOS	Czujnik półprzewodnościowy z tlenkiem metalu	*Metal Oxid Semiconductor*
NA	Kwas nonanowy	*Nonanoic Acid*
O₂	Tlen	*Oxygen*
OECD	Organizacja Współpracy Gospodarczej i Rozwoju	*Organisation for Economic Cooperation And Development*
T	Toluen	*Toluene*
TAC	Całkowity Roczny Koszt	*Total Annual Cost*
Th	Tymol	*Thymol*
TBABr	Bromek tetrabutyloamoniowy	*Tetrabutylammonium Bromide*
TBPCl	Chlorek tetrabutylofosfoniowy	*Tetrabutylphosphonium Chloride*
TCE	Tetrachloroetan	*Tetrachloroethane*
TCEtOH	2,2,2-trichloroetanol	*2,2,2-Trichloroethanol*
TCD	Detektor cieplno-przewodnościowy	*Thermal Condictivity Detector*
TCM	Czterochlorek węgla	*Carbon Tetrachloride*
TEABr	Bromek tetraetyloamoniowy	*Tetraethylammonium Bromide*
TEBAC	Chlorek trietylobenzyloamoniowy	*Trimethyl Benzylammonium Chloride*
TEG	Glikol trietylenowym	*Triethylene Glycol*
TMABr	Bromek tetrametyloamoniowy	*Tetramethylammonium Bromide*
TPABr	Bromek tetrapropyloammoniowy	*Tetrapropylammonium Bromide*
TriEG	Glikol trietylenowy	*Triethylene glycol*
Th	Tymol	*Thymol*
U	Mocznik	*Urea*
UDA	Kwas Undekanowy	*Undecanoic Acid*
UE	Unia Europejska	*European Union*
V	Wanilina	*Vanilin*
VA	Kwas wanilinowy	*Vanilin Acid*
VOCC	Lotne związki chloroorganiczne	*Volatile Organochlorine Compounds*
VOSiC	Lotne związki krzemoorganiczne	*Volatile Organosilicon Compounds*
VSC	Lotne związki siarkoorganiczne	*Volatile Organosulfur Compounds*
X	Ksylen	*Xylene*

1. Wprowadzenie

Rozwój cywilizacyjny jest nierozerwalnie związany z wykorzystaniem surowców energetycznych. Obecnie paliwa kopalne dostarczają około 90% całkowitego zapotrzebowania na energię, która pochodzi ze źródeł nieodnawialnych takich jak węgiel kamienny, gaz ziemny oraz ropa naftowa [1]. Wyczerpywanie się paliw konwencjonalnych oraz wojna rosyjsko-ukraińska doprowadziły do podwyżek cen gazu ziemnego, a tym samym zmusiły Radę Europejską (RE) do weryfikacji obowiązujących dyrektyw 2012/27/UE oraz (UE) 2018/2011 dotyczących efektywności energetycznej oraz promowania wykorzystania energii ze źródeł odnawialnych [2]. W nowelizacjach nałożono duży nacisk na rozwój technologii niskoemisyjnych biopaliw gazowych tj. borowodoru oraz biometanu [3]. Założono, że dostawcy paliw z każdego państwa członkowskiego Unii Europejskiej (UE) będą zobowiązani do dostarczania paliw i energii elektrycznej ze źródeł odnawialnych w ilości, która pozwoli na osiągnięcie redukcji emisji gazów cieplarnianych o co najmniej 13% do 2030 r względem paliw konwencjonalnych. Nowelizacja Dyrektywy RED II dotyczy również ilości dostarczanej energii ze źródeł odnawialnych (OZE) przez sektor transportu, który musi być na poziomie co najmniej 0,2% w 2022 r., 0,5% w 2025 r. i 2,2% w 2030 r w odniesieniu do paliw nieodnawialnych [4]. Dodatkowo w grudniu 2021 roku Komisja Europejska ogłosiła nowelizację dyrektywy gazowej UE (2009/73/WE) [5], która dotyczy rozbudowania dyrektywy o pakiet dekarbonizacyjny [6]. Wprowadzone nowelizacje powinny doprowadzić do szybkiego rozwoju technologii biopaliw niskoemisyjnych, które mogą zmniejszyć import lub całkowicie zastąpić gaz ziemny [7].

Obecnie energia pochodząca z biogazu oraz biometanu jest postrzegana jako rdzeń gospodarki w obiegu zamkniętym [8], która posiada duży potencjał w kwestii redukcji gazów cieplarniach [9,10]. Najbardziej rozpowszechnioną i praktyczną ścieżką do produkcji biogazu ze źródeł odnawialnych jest rozkład materii organicznej w wyniku sekwencyjnej czteroetapowej procedurze składającej się z hydrolizy, kwasogenezy, acetogenezy oraz metanogenezy [11]. Obecnie hydroliza stanowi najbardziej problematyczny i długotrwały etap, ponieważ obejmuje rozkład wielkocząsteczkowej, skomplikowanej oraz różnorodnej struktury biomaterii, która coraz częściej pozyskiwana jest z materiałów odpadowych z różnych gałęzi przemysłu, rolnictwa, a także z osadów ściekowych [12–14]. Wykorzystanie materiałów odpadowych tj.: obornik, gnojowica, pozostałości rolnicze, rośliny energetyczne, produkty uboczne przemysłu rolno-spożywczego lub oczyszczalni ścieków i innych odpadów organicznych jest zgodne z zasadami zrównoważonego rozwoju oraz gospodarką w obiegu zamkniętym (gospodarką cyrkularna). Jednak wsad na bazie materiałów odpadowych wpływa znacząco na wzrost ładunku zanieczyszczeń otrzymywanego surowego strumienia biogazu [7]. Surowy strumień biogazu oprócz podstawowych składników w postaci metanu (CH_4; 35–70% obj.) oraz dwutlenku węgla (CO_2; 15–50% obj.) zawiera również zmienne ilości zanieczyszczeń gazowych w tym: tlenek węgla (CO; 0–3% obj.), azot (N_2; 5-20% obj.), tlen (O_2; 0–5% obj.), wodór (H_2; 0–3% obj.), parę wodną (0–10% obj.), a także około 1-2% obj. pozostałych zanieczyszczeń w tym: siarkowodór (H_2S), amoniak (NH_3) oraz szerokie spektrum lotnych związków organicznych, np. węglowodory aromatyczne i alifatyczne, terpeny oraz związki tleno-, krzemo-, siarko-, azoto- i chloro-organiczne [15]. Obecność i ilość zanieczyszczeń ściśle zależy od rodzaju i składu wykorzystywanego wsadu, który poddawany jest fermentacji beztlenowej [16].

W literaturze opisywanych jest wiele metod oczyszczania biogazu, które różnią się między sobą specyfiką realizowania procesu technologicznego. Główne technologie uszlachetniania biogazu opierają się przede wszystkim na absorpcji fizycznej i chemicznej, adsorpcji, adsorpcji zmiennociśnieniowej, separacji membranowej, separacji kriogenicznej i biologicznej [17,18]. Pomimo postępującego ciągłego rozwoju metod oczyszczania większość z nich wymaga stosowania toksycznych rozpuszczalników, wysokich kosztów eksploatacji i znacznych nakładów inwestycyjnych. Dodatkowo wykorzystywane obecnie technologie są niewystarczające w celu wykorzystania biogazu jako paliwa do pojazdów w postaci sprężonej lub upłynnionej oraz do ciągłego zatłaczania biogazu do sieci przesyłowych. W ramach rozprawy doktorskiej opracowano kilka nowych „zielonych" absorbentów do usuwania licznych grup zanieczyszczeń odorotwórczych zidentyfikowanych w strumieniach biogazu pochodzenia rolniczego, wysypiskowego oraz ściekowego. Przeprowadzone badania miały na celu uzupełnienie obecnego stanu wiedzy dotyczącego wyjaśnienia zjawisk zachodzących w czasie procesu absorpcji oraz przedstawienie kompleksowego rozwiązania oczyszczania biogazu ze związków odorotwórczych. W ramach pracy przedstawiono również niskobudżetową metodę kontroli procesowej uzdatniania biogazu z wykorzystaniem matryc czujnikowych, która zmniejsza koszty operacyjne całego procesu i może być stosowana w rutynowych analizach.

1.1. Zanieczyszczenia biogazu

Obecność zanieczyszczeń w biogazie powoduje wiele problemów technologicznych i środowiskowych. Zanieczyszczenia nieorganiczne, których stężenia łącznie mogą wynosić do 65% objętości pozyskiwanego biogazu, stanowią balast znacząco obniżający wartość biogazu. Bardzo często surowy biogaz oprócz siarkowodoru (H_2S) zawiera inne formy związków siarki, np. tlenki siarki (SOx) lub kwas siarkowy (VI) (H_2SO_4), które powstają w wyniku spalania H_2S. Surowy strumień biogazu, a zwłaszcza gaz wysypiskowy może zawierać lotne związki siarkoorganiczne (*ang. Volatile Organosulfur Compounds*, VSC) tj.: siarczki, dwusiarczki czy tiole [12]. Emisja VSC jest głównie związana z beztlenową degradacją materiału organicznego zawierającego siarkę lub podgrzewaniem materiału wsadowego. VSC mogą być również wytwarzane podczas procesów tlenowych (np. kompostowania) ze względu na obecność ognisk bytowania beztlenowców [19]. Stężenia VSC ściśle uzależnione są od surowca użytego do produkcji biogazu, jednak zazwyczaj mieszczą się w zakresie od 0,16 do 19,51 mg/m^3 [12]. Związki odorotwórcze z grupy VSC posiadają niskie progi wyczuwalności zapachowej, jednak ich śladowe ilości powodują wydzielanie się nieprzyjemnego zapachu, który stanowi poważne problemy dla zdrowia publicznego pod względem problemów zdrowotnych tj.: dyskomfort, podrażnienie oczu, zawroty głowy, wymioty i bóle głowy [20–22]. VSC charakteryzują się również wysoką reaktywnością, toksycznością oraz właściwościami korozyjnymi. Wytwarzane przez VSC agresywne środowisko korozyjne powoduje wiele problemów eksploatacyjnych, tj.: zmniejszenie żywotności urządzeń technologicznych oraz zwiększenie kosztów operacyjnych w obszarze czynności konserwacyjnych tj.: wymiana oleju silnikowego czy świec zapłonowych [20].

Wśród pozostałych, niepożądanych, składników biogazu do szczególnie uciążliwych zanieczyszczeń zaliczane są węglowodory monoaromatyczne szczególnie benzen, toluen, etylobenzen oraz ksylen (BTEX). Ilość BTEX w biogazie jest zróżnicowana i zależy od surowca wykorzystywanego w procesie fermentacji. Związki z grupy BTEX posiadają potwierdzony potencjał rakotwórczy, a także mogą negatywnie wpływać na jakość środowiska [23–25]. Ze względu na toksyczny charakter BTEX, stężenie w powietrzu atmosferycznym jest regulowane prawnie. Obecnie nie ma żadnych regulacji prawnych dotyczących maksymalnych stężeń BTEX w strumieniach biogazu, których obecność może również negatywnie wpływać na zdrowie i środowisko [26,27]. W wielu pracach potwierdzono, że biogaz wysypiskowy posiada wyższe wartości BTEX niż biogaz pozyskany z odpadów rolniczych [12,28]. Wynika to z faktu składowania na wysypiskach śmieci materiałów przemysłowych (tj.: farby, gumy, kosmetyki czy kleje) do produkcji, których rozpuszczalniki z grupy BTEX są wykorzystywane [28–30]. BTEX w surowym strumieniu biogazu powstają podczas utleniania pośrednich produktów. Zakres stężeń zanieczyszczeń w postaci BTEX w biogazie mieści się w zakresie od 94 do 1906 mg/m^3 [31]. Biogaz zawierający wysokie stężenia BTEX powoduje korozję oraz przyczynia się do niedrożności układów silnikowych [32,33]. Dlatego bardzo ważne jest aby przed dalszym wykorzystaniem biogazu, węglowodory monoaromatyczne zostały usunięte.

Do kolejnej grupy problematycznych technologicznie zanieczyszczeń organicznych, mogących występować w biogazie należą lotne związki chloroorganiczne (*ang. Volatile Organochlorine Compounds*, VOCC). VOCC występują głównie w biogazie pozyskanym z odpadów z oczyszczalni ścieków i składowisk odpadów [12]. Całkowite stężenie VOCC w surowym strumieniu biogazu mieści się w zakresie od 259 do 1239 mg/m^3 [34–37]. Najczęściej w biogazie można zidentyfikować 1,1,1-trichloroetan, 1,1-dichloroetan, 1,1-dichloroetan, 1,2-dichloroetan, 1,2-dichloroetan, tetrachlorek węgla, chloroform, tetrachloroetylen, tetrachloroetan, dichlorometan i trichloroeten [34,35,38–40]. Zanieczyszczenia VOCC pochodzą z chemikaliów wykorzystywanych do oczyszczania ścieków i wody, utylizacji rozpuszczalników oraz czynników chłodniczych, a także odpadów stałych, np. polichlorku winylu [41]. Podczas procesu spalania biogazu, który zawiera VOCC dochodzi do reakcji chloru z tlenem oraz wodą, w wyniku czego tworzy się kwas solny, który posiadają właściwości silnie korozyjne [42]. Podczas spalania biogazu zawierającego VOCC może dochodzić do przekształcenia zanieczyszczeń w toksyczne polifluorowcowane dioksyny oraz związki furanowe [43]. Niekontrolowana emisja VOCC do atmosfery prowadzić może do:

- zubożenia warstwy ozonowej w stratosferze,
- powstawania smogu fotochemicznego,
- zwiększenia efektu cieplarnianego,
- obniżenia lokalnej jakości powietrza.

W celu ochrony środowiska, zwiększenia wartości opałowej, obniżenia awaryjności silników przetwarzających biogaz w energię, a także sprostania wymogom jakościowym stawianym biopaliwom - surowy biogaz musi być poddany procesom uzdatniania z VOCC [44,45].

Do kolejnych zanieczyszczeń należących do lotnych związków organicznych LZO (*ang. Volatile Organic Compounds*, VOC), które występują w biogazie pozyskanym z osadów z oczyszczalni ścieków [46,47] lub odpadów wysypiskowych [48,49] należą lotne związki krzemoorganiczne (*ang. Volatile Organosilicon Compounds*, VOSiC). Bardzo często w literaturze VOSiC, definiowane są jako siloksany i pod taką nazwą znajdują szerokie zastosowanie w produktach wykorzystywanych do higieny osobistej, w środkach czystości, tekstyliach oraz laminatach papierniczych, które stanowią odpady komunalne. Zawartość siloksanów w biogazie jest bardzo zmienna i głównie zależy od charakterystyki odpadów, wieku i stanu składowiska, oraz warunków atmosferycznych. Do głównych zanieczyszczeń VOSiC zaliczane są heksametylocyklotrisiloksan (D3), oktametylocyklotetrasiloksan (D4), dekametylocyklopentasiloksan (D5), heksametylodisiloksan (L2) i oktametylotrisiloksan (L3). D4 stanowi około 60% wszystkich siloksanów. W aktualnych raportach rocznych opublikowanych przez Międzynarodową Agencje Energetyczną (*ang. International Energy Agency, IEA*) oraz Organizację Współpracy Gospodarczej i Rozwoju (*ang. Organisation for Economic Cooperation and Development, OECD*) wykazano, że średnie stężenie siloksanów w strumieniach biogazu z oczyszczalni ścieków oraz składowisk odpadów na obszarze UE mieści się w zakresie od 0,2 mg/m^3 aż do 400 mg/m^3 [34,50]. Dla porównania w amerykańskich raportach wykazano znacznie niższe zawartości siloksanów w biogazie pozyskanym z osadów z oczyszczalni ścieków, wynoszące maksymalnie do 38 mg/m^3 biogazu [51]. Podczas spalania biogazu zawierającego siloksany wydziela się krzem, który następnie łączy się z tlenem tworząc osady z twardej krzemionki (SiO_2) lub krzemianów (Si_xO_y). Powstałe osady krzemionkowe doprowadzić mogą do ścierania się części silnika lub tworzenia się warstw obniżających przewodnictwo cieplne oraz zmniejszających właściwości smarne. Ponadto powstające osady zmieniają geometrię komory spalania turbin, kotłów oraz silników spalinowych w wyniku czego emitowane są większe ilości substancji szkodliwych, tj.: tlenku węgla czy formaldehydu, które negatywnie wpływają na środowisko [52]. Wymienione powyżej zanieczyszczenia nie tylko obniżają właściwości energetyczne biogazu ale również zmniejszają wydajność konwersji i żywotność komór spalania, a tym samym zwiększają koszty operacyjne i konserwacyjne biogazowni.

1.2. Produkcja biogazu w Europie

Obecnie większość biogazu wyprodukowanego zarówno w Polsce, jak i w pozostałych krajach Unii Europejskiej spalana jest w agregatach kogeneracyjnych produkując energię elektryczną i cieplną [53]. Wynika to z uwagi na umiejscowienie większości biogazowni, które zlokalizowane są w dużej odległości od zabudowań mieszkalnych i przemysłowych. Dodatkowo poziom wykorzystania wytworzonej energii jest niewielki i zazwyczaj pokrywa jedynie zapotrzebowanie energetyczne instalacji zlokalizowanych na terenie zakładów wytwarzających biogaz. Bez wątpienia wybitnym liderem pod względem produkcji biogazu i liczby biogazowni w Europie są Niemcy, którzy w 2020 roku wyprodukowali 11 TWh biometanu w 242 biometanowniach. Otrzymywana energia pozyskiwana jest głównie z odpadów rolniczych (kiszonki kukurydzy) oraz roślin energetycznych [54][55]. W Wielkiej Brytanii, Szwajcarii i Francji działa ponad 600 biogazowni rolniczych. W Wielkiej Brytanii najczęściej wykorzystywanym substratem są ścieki, osady ściekowe i bioodpady komunalne. Rozwój biogazu pozyskiwanego z osadów ściekowych wynika z obowiązujących przepisów, które ograniczają wykorzystywanie roślin energetycznych. W Wielkiej Brytanii istnieją również znaczne ograniczenia dotyczące rodzaju instalacji oraz miejsca wybudowania biogazowni. W ostatnich latach na terenie Francji zauważalny jest silny rozwój przydomowych i scentralizowanych biogazowni, których celem jest odzyskiwanie biogazu do produkcji energii elektrycznej na potrzeby działalności samoobsługowej. Surowce wykorzystywane do produkcji biogazu obejmują pozostałości z oczyszczalni ścieków, odpady z frakcji bio, odpady rolnicze, przemysłowe oraz składowiska. W Szwajcarii ilość biogazowni jest porównywalna do Francji, a wykorzystywane odpady są zbliżone do surowców wykorzystywanych w Wielkiej Brytanii, jednak zgłaszana ilość produkcji energii jest prawie trzy razy niższa w porównaniu z Francją [56–58]. Natomiast w Szwecji funkcjonują 71 biogazownie rolnicze w których wykorzystywany jest osad ściekowy oraz bioodpady, odpady rolne, przemysłowe oraz komunalne Warto zwrócić uwagę, że ilość energii produkowanej rocznie przez Szwedzkie biogazownie jest 3,4 razy wyższa niż w Austrii, która posiada 287 rolniczych biogazowni i wykorzystuje jako wsad przede wszystkim obornik [57,59]. W Polsce w 2021 roku funkcjonowało 128 biogazowni rolniczych w których wyprodukowano 342,9 m^3 biogazu rolniczego, co umożliwiło wytworzenie 732,6 GWh energii [60,61]. Surowce wykorzystywane w Polsce to głównie odpady rolnicze, obornik oraz rośliny energetyczne. Rozwój przemysłu biogazowego w Europie jest bezsprzeczny, choć dynamika zależy od poszczególnych krajów. Każdy z krajów UE przedstawia charakterystyczne modele, które opierają się na zastosowaniu różnych surowców odpadowych. Jednak aby móc zatłoczyć biogaz do sieci lub wykorzystać go jako paliwo transportowe musi on spełniać wymagania jakościowe gazu wysokometanowego.

Aktualnie kraje UE zmagają się z brakiem ujednoliconych rozporządzeń oraz dyrektyw odnoszących się jednoznacznie do parametrów jakościowych dla bioenergii pozyskiwanej z OZE. W zależności od kraju UE zakresy stężeń poszczególnych składników, a także dopuszczalne rodzaje zanieczyszczeń, różnią się w znacznym stopniu. Ogólne wytyczne dotyczące możliwości zatłaczania biogazu do sieci przesyłowych w państwach UE zawarte są w Dyrektywie Parlamentu Europejskiego i Rady 2009/73/WE z dnia 13 lipca 2009 r. W Polsce, zgodnie z Rozporządzeniem Ministra Gospodarki z dnia 24 sierpnia 2011r. w sprawie szczegółowego zakresu obowiązku potwierdzania danych dotyczących wytwarzanego biogazu rolniczego wprowadzanego do sieci dystrybucyjnej gazowej (Dz.U. 2011 nr 187 poz. 1117) wprowadzono możliwość zatłaczania biogazu do sieci gazu wysokometanowego o ile zatłaczany biogaz spełnia wymagania dla parametrów energetycznych i jakościowych stawianych dla danego typu gazu. Ze względu na brak specjalnych uregulowań dla biogazu wytwarzanego z osadów ściekowych oraz odpadów komunalnych w 2018 roku Rozporządzenie wygasło. Obecnie obowiązuje Rozporządzeniem Ministra Gospodarki z dnia 2 lipca 2010 r. w sprawie szczegółowych warunków funkcjonowania systemu gazowego (Dz.U. z 2010 r. Nr 133, poz. 891) [62] oraz normami PN-C-04753:2011 i PN-C-04752:2011. W przypadku zastosowania biogazu jako paliwa transportowego w Polsce przyjmuje się wymagania jakościowe tożsame dla sprężonego gazu ziemnego (ang. *Compressed Natural Gas*, CNG). Jakość gazu ziemnego wykorzystywanego jako paliwo do pojazdów jest zawarta w Rozporządzeniu Ministra Energii z dnia 30 czerwca 2016 r. w sprawie wymagań jakościowych dla sprężonego CNG oraz standaryzowana w normie PN-EN ISO 15403-1:2010 i PKN ISO/TR 15403-2:2010. W Tabeli 1 przedstawiono parametry jakościowe biometanu, które obowiązują w Polsce, Niemczech oraz Francji [62–64]. Konwersja odpadów w energię poprzez produkcję biogazu to nie tylko realna opcja z ogromnym potencjałem zmniejszenia, a nawet wyeliminowania zależności od paliw kopalnych, ale także zrównoważony i wydajny sposób wytwarzania zdecentralizowanej energii przy mniejszym śladzie węglowym. Proponowane podejście jest zgodne z założeniami i celami nowelizacji dyrektywy RED II. W kontekście zgromadzonej wiedzy można stwierdzić, że zarówno względy ekonomiczne, środowiskowe, jak i polityczne przemawiają za oczyszczaniem biogazu do postaci biometanu. Jednak obecnie brakuje odpowiedniej technologii uzdatniania biogazu, która wyeliminuje problemy w obecnie stosowanych metodach oraz umożliwi skuteczne i tanie oczyszczanie biogazu do biometanu, który można wykorzystać nie tylko do produkcji energii w jednostkach kogeneracyjnych, ale również jako paliwo do silników i turbin gazowych, gaz sieci przesyłowych, uzdatniacz do przechowywania i konserwacji owoców i warzyw, paliwo do ogniw paliwowych [65,66].

Tabela 1. Parametry jakościowe biometanu [62–64].

Parametry	Jednostka	Kraj		
		Polska	Niemcy	Francja
CH_4	[%]	94,0– 97,0	> 96,0	≥ 86
CO_2	[%]	≤ 3	< 6,0	≥ 2,5
H_2S	[mg/Nm³]	≤ 7,0	≤ 5,0	≤ 5,0
H_2	[%]	≤ 0,5	≤ 5,0	≤ 6,0
O_2	[%]	≤ 0,2	≤ 3,0	< 0,1
NH_3	[mg/m³]		≤ 3,0	≤ 3,0
H_2O	[%]	≤ 1	-	-
VOSiC	[mg/Nm³]	≤ 30,0	<0,5	<0,5
VOC	[mg/Nm³]	≤ 25,0	-	≤ 1,0 (Cl) ≤ 10,0 (F)
Merkaptany	[mg/Nm³]	≤ 16,0	≤ 15,0	≤ 6,0
Zawartość siarki całkowitej	[mg/Nm³]	≤ 40,0	< 30,0	< 75, 0-100,0
Zawartość par rtęci	[µg/m³]	30,0	≤ 5,0	≤ 1,0
Temperatura punktu rosy wody (ciśnienie 5,5 MPa)	[˚C]	≤ +3,7 (1,04– 30,10) ≤ -5,0 (1,11– 31,03)	Temperatura otoczenia	≤ -5 at P_{max}
Wartość opałowa	[MJ/m³]	≥ 31,0	30,2-47,2	34,2-46,08
Wartość liczby Wobbego	[MJ/m³]	45,0–54,0	46,1-56,5	48,2-56,5
Zawartość pyłu	[mg/m³]	≤ 1,0	Technicznie wolny	< 5,0

1.3. Metody oczyszczania biogazu

Obecnie do tradycyjnych metod uzdatniania strumieni gazowych, najczęściej zaliczane są takie techniki jak: absorpcja, adsorpcja, adsorpcja zmiennociśnieniowa, separacja membranowa oraz separacja

kriogeniczna i biologiczna [67]. Procesy absorpcji można klasyfikować jako procesy fizyczne oraz chemiczne. W absorpcji fizycznej wykorzystywane są rozpuszczalniki niereaktywne np. woda, natomiast w absorpcji chemicznej rozpuszczalniki reaktywne, takie jak monoetanoloamina (MEA) [68]. Oczyszczanie z wykorzystaniem procesów absorpcyjnych należy do prostych i wydajnych procesów, lecz główną wadą związaną z zastosowaniem konwencjonalnych rozpuszczalników organicznych jest ich niebezpieczny charakter chemiczny oraz energochłonny proces regeneracji i niewystarczająca rozpuszczalność wszystkich zanieczyszczeń [69]. Techniki adsorpcyjne należą do technik suchych, wolnych od chemikaliów oraz wykorzystujących adsorbenty, np. zeolity. Jednak są to procesy złożone i stosunkowo drogie [70]. Procesy membranowe klasyfikowane są do procesów suchych bez użycia związków chemicznych lecz wymagają dużego nakładu energii. Dodatkowo wprowadzany gaz, wymaga wstępnej obróbki, która zwiększa koszt całego procesy [71]. Dzięki zastosowaniu procesów kriogenicznych możliwe jest otrzymanie biometanu o wysokiej czystości, jednak jest to proces również energochłonny [72]. Wykorzystanie metod biologicznych posiada zalety w tym niskie zapotrzebowanie na energię, łagodne warunki procesowe. Jednak jest to metoda wymagająca pod względem doboru, adaptacji oraz ciągłego dostarczania składników odżywczych dla mikroorganizmów [73]. Ze względu na wszystkie wady i zalety obecnie stosowanych metod coraz częściej tworzone są techniki zintegrowane, które łączą wiele metod (Tabela 2).

Obecnie metody oparte na wykorzystaniu absorpcji fizycznej wykazują wysoką skuteczność usuwania lotnych związków organicznych (LZO) z fazy gazowej przy użyciu odpowiednio dobranych absorbentów [74,75]. Fizyczna absorpcja obejmuje różne rodzaje rozpuszczalników takich jak woda, związki organiczne i oleje. Wybór odpowiedniego absorbentu jest kluczem do skutecznego zastosowania absorpcji. Absorbent powinien charakteryzować się wysoką zdolnością absorpcji LZO, wysoką temperaturą wrzenia, niską prężnością pary, niską lepkością, niskim współczynnikiem podziału ciecz-para, bezpieczeństwem i brakiem toksyczności oraz niskim kosztem. Z ekonomicznego i środowiskowego punktu widzenia, woda wydaje się być najlepszym absorbentem do usuwania LZO z biogazu. Jednak większość LZO jest hydrofobowa i tylko niektóre z nich można absorbować za pomocą wody. Najpopularniejszym fizycznym absorbentem do usuwania o wysokiej wydajności H_2S, CO_2, merkaptanów i siloksanów jest SelexolTM (eter dimetylowy glikolu polietylenowego) licencjonowany przez UOP LLC [76–78]. W porównaniu z innymi rozpuszczalnikami SelexolTM ma wyższą lepkość, co zmniejsza szybkość przenoszenia masy. Ponadto potrzeba schłodzenia absorbentu jest główną wadą tego procesu, powodującą wysokie koszty inwestycyjne i operacyjne [79,80]. Oleje mineralne są również popularnymi rozpuszczalnikami do absorpcji LZO z biogazu. Wydajność absorpcji zależy głównie od rodzaju oleju mineralnego, a także temperatury procesu i czasu kontaktu rozpuszczalnika z zanieczyszczonym biogazem. Spośród testowanych olejów mineralnych, najwyższą skutecznością w usuwaniu związków organicznych z fazy gazowej wykazują olej silnikowy, olej silikonowy 47V20, Seriola 1510 i polialfaolefina [81]. Jednak podczas procesu absorpcji powstaje mgła olejowa, która łączy się z biogazem, co zmniejsza wartość energetyczną spalanego biogazu. Zastosowanie olejów mineralnych jako absorbentów wymaga także ich schłodzenia przed procesem absorpcji [82–84]. Wiele prac opisuje zastosowanie etanoloamin (monoetanoloaminy, dietanoloaminy, trietanoloaminy itp.) do absorpcji LZO z faz gazowych. Jednak ograniczeniami takich rozpuszczalników chemicznych są wysokie zapotrzebowanie na energię do regeneracji rozpuszczalnika, znaczna degradacja aminy i straty spowodowane parowaniem, a także problemy z korozją elementów konstrukcyjnych [67,84–87]. Inne rozpuszczalniki organiczne, tj. poli(dimetylosiloksan) [88], adypiniandi(2-etyloheksylo) [89] i roztwór środka powierzchniowo czynnego [90], mogą być również stosowane do absorpcji LZO. Większość z wykorzystywanych absorbentów zaliczana jest do grupy szkodliwych rozpuszczalników organicznych, które podczas użytkowania same ulegają procesowi degradacji w wyniku czego doprowadzają do korozji urządzeń procesowych. Ponadto proces ich regeneracji jest skomplikowany i wiąże się z dużym nakładem energetycznym [91]. Ze względu na ciągle istniejące wady obecnie stosowanych absorbentów do usuwania LZO, nadal poszukuje się alternatywnych „zielonych absorbentów", które zastąpią obecnie stosowane rozpuszczalniki organiczne oraz umożliwią otrzymanie wysokometanowego gazu, który można zatłaczać do sieci przesyłowych lub wykorzystywać jako paliwo transportowe w postaci sprężonej lub upłynnionej.

Do niedawna alternatywnymi absorbentami dla rozpuszczalników organicznych były ciecze jonowe (*ang. Ionic Liquids*, ILs), które początkowo uważano za idealne absorbenty ze względu na ich nielotność, niepalność, niewybuchowość oraz możliwość dostrojenia pozostałych właściwości fizykochemicznych w oparciu o dobór odpowiedniego kationu i anionu [92]. ILs wykazywały odpowiednie właściwości absorpcyjne w zakresie wychwytywania zanieczyszczeń nieorganicznych tj.: CO_2 [93,94], H_2S [95–97], NH_3 [98,99] oraz H_2O [100]. W kwestii uzdatniania biogazu z zanieczyszczeń organicznych opublikowano nieliczne prace naukowe dotyczące usuwania siloksanów [101], toluenu [102,103], dichlorometanu [102], siarczku dimetylu oraz disiarczku dimetylu [103]. We wszystkich pracach efektywność usuwania LZO była

określana na podstawie współczynnika podziału para-ciecz oraz współczynnika dyfuzji. Dynamiczne procesy absorpcyjne były pomijane ze względu na wysoki koszt, skomplikowaną syntezę, udowodnioną znikomą biodegradowalność [104,105].

Tabela 2. Zalety i wady głównych technik wykorzystywanych do oczyszczania biogazu.

Technika	Zalety	Wady
Absorpcja fizyczna z użyciem wody jako absorbentu	- wysoka wydajność (> 97% CH_4), - łatwość użycia, - niski koszt użytkowania - niskie zużycie energii elektrycznej, - najczęściej stosowana metoda,	- straty CH_4 (ok. 2%), - wysokie zapotrzebowanie na wodę (nawet przy regeneracji), - możliwość spieniania, - zatykanie z powodu wzrostu bakterii, - nieefektywny dla wielu grup związków chemicznych ze względu na ich ograniczoną rozpuszczalność,
Absorpcja fizyczna z użyciem rozpuszczalników organicznych jako absorbentów	- wysoka wydajność (97 – 99% CH_4), - wzrost wydajności usuwania względem użytego absorbentu, - energiczny bardziej korzystny niż woda, - możliwa regeneracja z niskotemperaturowym ciepłem odpadowym,	- wymagane związki organiczne, - trudna obsługa, - drogie inwestycje i obsługa, - wymagane ogrzewanie do pełnej regeneracji,
Absorpcja chemiczna	- wysoka jakość CH_4, - nie wymaga sprężania gazu ,	- metoda droga, - do regeneracji wymagane ciepło, - proces korozyjny, - wymagane mocne kwasy, - stosowanie zasad powoduje reakcję z CO_2, tworząc węglany, - możliwość pienienia podczas procesu,
Adsorpcja	- nie wymaga użycia rozpuszczalników organicznych, - łatwy w obsłudze i szeroko stosowany, - wysoka zdolność adsorpcji, - niskie koszty,	- utrata zdolności adsorpcyjnej po regeneracji, - wstępna obróbka jest konieczna do usuwania wody, związków chlorowcowanych i siarczków - stosuje się węgiel aktywny, - konieczność regeneracji adsorbentu za pomocą dużej ilości gazów,
Adsorpcja zmiennociśnieniowa	- wysoka wydajność (95–98% CH_4), - nie wymaga użycia rozpuszczalników organicznych - zwartość, - bardzo powszechne w branżach na małą skalę - łatwo skalowalny,	- droga inwestycja i obsługa, - straty CH_4 w przypadku nieprawidłowego działania zaworów, - wymagane wstępne uzdatnianie H_2S i wody, - skomplikowana kontrola procesu, - wysokie zużycie energii elektrycznej (0.25 kWh/Nm^3),
Separacja membranowa	- prostota i łatwość obsługi, - konfiguracja modułowa, - nie wymaga chemikaliów, - wysoka niezawodność, - duża powierzchnia i mała objętość,	- wysoki straty CH_4 (<10%), - zatykanie i obrastanie membran, - kosztowny, - brak wykorzystania do gazu, wysypiskowego lub biogazu ściekowego,
Separacja kriogeniczna	- dobra wydajność (90–98% CH_4), - nie wymaga chemikaliów - wysoka czystość CH_4 (99 %), - najmniejsze straty CH_4 (<1%), - czysty CO_2 jest otrzymywany jako produkt uboczny, - łatwy w obsłudze,	- wysokie koszty inwestycji i eksploatacji, - wymagana wysoka energia, - konieczna jest obróbka wstępna w celu wyeliminowania zanieczyszczeń, - wydajność i technologia nie są bardzo wykazane, - technicznie złożona procedura,
Separacja biologiczna	- Przyjazna środowisku, - nie wymaga chemikaliów, - niskie koszty eksploatacji, - prostota, - możliwość ponownego użycia,	- długi czas działania procesu, - niska wydajność usuwania,

W celu zwalczania powyższych ograniczeń w 2003 roku Abbot i inni [106] zaproponowali nową klasę ekologicznych absorbentów na bazie cieczy głęboko eutektycznych (*ang. Deep Eutectic Solvents*, DES). DES to mieszanina eutektyczna składająca się z dwóch lub więcej związków chemicznych w określonym stosunku molowym. W strukturze DES jeden ze składników pełni rolę donora wiązań wodorowych (*ang. Hydrogen Bond Donor,* HBD), a drugi akceptora wiązań wodorowych (*ang. Hydrogen Bond Acceptor,* HBA).

Ze względu na powstanie pomiędzy HBA i HBD specyficznych oddziaływań niekowalencyjnych obserwuje się znaczny spadek temperatury topnienia DES w porównaniu z czystymi HBA i HBD [107]. Dodatkowo DES charakteryzują się zbliżonymi właściwościami fizykochemicznymi do ILs, jednak są uważane za mniej toksyczne, bardziej biodegradowalne oraz opłacalne, a przede wszystkim ich otrzymywanie jest prostsze i wolne od produktów ubocznych. Porównanie właściwości DES z konwencjonalnymi absorbentami oraz ILs przedstawiono w Tabeli 3.

Tabela 3. Porównanie właściwości fizykochemicznych sorbentów [108–117].

Właściwości	Woda	Aminy	IL	DES
Synteza	Nie	Nie	Wielostopniowa	Łatwe mieszanie
Zastosowanie	Jednofunkcyjny	Jednofunkcyjny	Wielofunkcyjny	Wielofunkcyjny
Regulowanie	Nie	Nie	Wysokie	Wysokie
Stabilność termiczna	Niska	Niska	Regulowana, ogólnie wysoka	Regulowana, ogólnie wysoka
Temperatura wrzenia	100°C	111-350°C	>250°C	Wyższe niż inne rozpuszczalniki (214-1 774°C)
Przyjazny dla środowiska	Tak	Nie	Nie wszystkie	Tak
Toksyczność	Nie	Tak	Często zwiększa toksyczność w kontakcie z systemami wodnymi	Dopuszczalne profile toksyczności
Korozyjność	Wysoka	Wysoka	Niska	Niska
Biodegradowalność	Łatwo	Łatwo	Trudno	Łatwo
Biodegradowalny	Tak	Nie	Słabo	Tak
Gęstość oraz lepkość	Niska	Średnia	Regulowana, zazwyczaj wyższa niż w pozostałych rozpuszczalnikach	Regulowana, zazwyczaj niższa niż w ILs
Napięcie powierzchniowe	Wysokie	Niskie	Niższe niż wody i wyższe niż amin	Niskie
Prężność par	Wysokie	Wysokie	Niska	Niska
Palność	Nie	Tak	Nie	Nie
Charakter	Neutralny	Zasadowy	Zasadowy/neutralny/kwasowy	Zasadowy/neutralny/kwasowy
Rodzaj absorpcji	Fizyczna	Chemiczna/ Fizyczna	Fizyczna	Fizyczna
Zdolność absorpcji	Średnia	Średnia	Wysoka	Wysoka
Koszt	Niski	Umiarkowany	Wysoki	Niski

Korzystne właściwości DES takie jak różnorodna i efektywna interakcja z nieorganicznymi oraz organicznymi zanieczyszczeniami za pośrednictwem wiązań wodorowych lub słabszych oddziaływań elektrostatycznych, wielokrotna zdolność do regeneracji, przyczyniła się do rosnącej liczby publikacji naukowych dotyczących zastosowania DES jako medium do separacji. Największą popularność zyskały DES w zastosowaniu jako rozpuszczalniki ekstrakcyjne, absorpcyjne oraz modyfikatory adsorbentów oraz membran [118–123]. Do tej pory stosunkowo dobrze opisano zastosowanie DES do wychwytywania nieorganicznych szkodliwych cząsteczek gazowych, tj. dwutlenku węgla, wody, amoniaku, siarkowodoru czy dwutlenku siarki z powietrza, paliw gazowych, biogazu i gazów przemysłowych [124–132]. Od 2017 roku w literaturze obserwuje się wzrost zainteresowania nad zastosowaniem DES do absorpcji LZO (takich jak toluen, aldehyd octowy oraz dichlorometan) z modelowych strumieni gazowych. W prezentowanych pracach ocena skuteczności zastosowania DES do wychwytywania LZO ogranicza się jedynie do wyznaczenia współczynników podziału para-ciecz (K) przy użyciu techniki statycznej fazy nadpowierzchniowej. W praktyce procedura HeadSpace polega na umieszczeniu określonej objętości DES w fiolce o pojemności 20 mL i dodaniu niewielkiej ilości dokładnie odmierzonych ilości LZO. Następnie fiolki są zamykane za pomocą

nakrętki z membraną i termostatowane przez 24 h w określonej temperaturze. Po upływie 24 h faza nadpowierzchniowa analizowana jest za pomocą chromatografii gazowej sprzężonej z selektywnymi detektorami. Otrzymane mniejsze stężenia LZO w fazie nadpowierzchniowej (gazowej) wskazują na lepszą interakcję, powinowactwo oraz absorpcję z wykorzystaniem DES. Opisaną procedurę jako pierwsza przedstawiła Moura i in. W pracy wyznaczano współczynnik podziału K pomiędzy toluenem, a DES na bazie czwartorzędowych soli amoniowych oraz fosfoniowych połączonych w odpowiednich stosunkach molowych z glikolami oraz kwasami organicznymi. W badaniach potwierdzono, że największą zdolność pochłaniania lotnych węglowodorów monoaromatycznych ma DES, składający się z bromku tetrabutyloamoniowego (TBABr) i kwasu dekanowego (DA) w stosunku molowym 1:2. Otrzymane wartości K były znacznie niższe w porównaniu z wodą oraz zbliżone do wcześniej publikowanych wyników dla absorbentów na bazie cieczy jonowych oraz oleju silikonowego (K=0,001) [133–135]. Podobne wyniki Moufawad i in. uzyskali podczas testowania współczynników podziału para-ciecz dla toluenu, n-heptanu i 1-decenu w tym samym jonowym DES. Praca ta potwierdziła, że największe powinowactwo zarówno do węglowodorów monoaromatycznych, jak i alifatycznych ma TBABr:DA (1:2) [136]. Aby w pełni ocenić przydatność DES jako absorbentów do usuwania LZO ze strumieni gazowych, konieczne jest uwzględnienie zarówno powinowactwa DES do zanieczyszczeń, jak i innych parametrów procesowych takich jak: skład matrycy gazowej, przepływ modelowego strumienia biogazu, dodatek wody do DES, stężenie początkowe zanieczyszczeń, temperaturę oraz ciśnienie, które mają kluczowy wpływ na efektywność procesu absorpcji. W tym celu niezbędne jest prowadzenie badań w układzie dynamicznym, będącym zminiaturyzowaną wersją instalacji przemysłowych. Obecnie tylko w kilku pracach wykazano usuwanie LZO w układzie dynamicznym. Większość badań koncentrowała się wyłącznie na usuwaniu pojedynczych zanieczyszczeń takich jak aceton (A), dichlorometan (DCM), T, L2, D4 z modelowego strumienia biogazu, którym był gaz obojętny - azot (N$_2$) [136,137]. W badaniach wykazano, że zdolność oraz efektywność absorpcji zależy od siły powstających oddziaływań niekowalencyjnych pomiędzy zanieczyszczeniem, a absorbentem. Dla acetonu, dichlorometanu, toluenu otrzymano najwyższe wartości absorpcji na poziomie 2,66 mg/g, 988 mg/g, 304 mg/g z wykorzystaniem DES na bazie tymolu:kwasu dekanowego (Th:DA (1:1)), chlorku tetrabutylofosfoniowego: kwasu lewulinowego (TBPCl:Lev (1:1)), chlorku trietylobenzyloamoniowego: fenolu (TEBAC:Ph (1:3)) [91,138,139]. W badaniach wykazano, że wartości efektywność absorpcji TEBAC:Ph (1:3) były znacząco wyższe w porównaniu z cieczami jonowymi [EMIM][Tf2N] (223 mg/g) oraz konwencjonalnego absorbentu na bazie glikolu tetraetylowego - TEG (163 mg/g) w tych samych warunkach procesu [91]. Jednak rzetelne porównanie obecnie wykorzystywanych DES jest trudne ze względu na odmienne warunki procesu absorpcji dynamicznej oraz różne metody oceny efektywności DES. Obecnie wszystkie publikowane badania z wykorzystaniem procesów dynamicznych były przeprowadzone w skali laboratoryjnej. Dlatego należy zwrócić szczególną uwagę, że w literaturze obecnie brakuje badań uzdatniania strumieni gazowych z wykorzystaniem DES, w których wykonana zostanie rzetelna charakterystyka i optymalizacja warunków procesowych absorpcji, której efektem końcowym będzie przeprowadzenie badań w powiększonej skali z wykorzystaniem rzeczywistych strumieni gazowych.

1.4. Kontrola procesowa

Zapewnienie jakości i efektywności procesów przemysłowych ma ogromne znaczenie w poszukiwaniu alternatywnych i ekonomicznie opłacalnych metodach uzdatniania biogazu. Idealny system monitoringu technologicznego powinien składać się z szeregu częstych, cyklicznych badań i czynności, które umożliwią dokładną analizę składu substratu, masy pofermentacyjnej i biogazu. Prawidłowo zaprojektowany i wdrożony monitoring umożliwia rzetelny przepływ informacji w procedurach eksploatacyjnych w całym zakresie pracy biogazowni. Monitoring procesów technologicznych powinien rozpocząć się na etapie rozruchu procesu i być kontynuowany przez cały okres eksploatacji. Dokładny system monitoringu technicznego pozwala na zmniejszenie ryzyka wystąpienia problemów technologicznych oraz w razie ich wystąpienia na natychmiastowe odtworzenie i ustabilizowanie produkcji biogazu [140]. Głównym celem monitoringu i sterowania technologicznego jest optymalizacja, utrzymanie i stabilizacja produkcji bioenergii. Skuteczny monitoring umożliwia racjonalne gospodarowanie zasobami biogazowni, przy jednoczesnym wzroście produktywności bioenergii oraz deprecjacji produkcji i emisji zanieczyszczeń do atmosfery [141]. Warto zwrócić uwagę, że Dla porównania koszty monitoringu stanowią ułamek strat, jakie biogazownia może ponieść w przypadku długotrwałych przestojów, awarii czy wahań produkcji biogazu.

Obecnie do kontroli procesów technologicznych podczas produkcji i oczyszczania strumieni biogazu stosuje się najczęściej techniki analityczne oparte głównie na chromatografii gazowej (*ang. Gas Chromatography, GC*) [142,143]. Konwencjonalne pomiary z wykorzystaniem metody referencyjnej opartej na jednowymiarowej chromatografii gazowej dostarczają dogłębnych informacji nie tylko w zakresie

dotyczącym składu biogazu lecz również odnoszą się do środowiska atmosferycznego wokół biogazowni. Jednak pomiary chromatograficzne są tymczasowe i tylko w niewielkim stopniu pozwalają na identyfikację zakłóceń procesowych w czasie rzeczywistym. Dlatego też, coraz częściej poszukuje się nowych technik pomiarowych, które będą komplementarne z chromatografią gazową. Obecnie zastosowanie komplementarnych technik doprowadziło do połączenia jedno- i wielowymiarowych analiz GC z olfaktometrią dynamiczną (GC-O) [144,145] oraz systemem detekcji opartym na spektrometrii mas (GC-MS-O) [146–148]. Badania olfaktometryczne charakteryzują się wysokim kosztem (szkolenie panelistów) oraz wysokimi wymaganiami związanymi z prowadzeniem akredytowanego laboratorium olfaktometrycznego [145]. W związki z tym, większość uczelni i zakładów przemysłowych stosuje proste systemy chromatograficzne sprzężone z selektywnymi detektorami, tj.: detektor płomieniowo-jonizacyjnym (*ang. Flame Ionization Detector*, FID), detektor cieplno-przewodnościowy (*ang. Thermal Conductivity Detector*, TCD), detektor płomieniowo-fotometryczny (*ang. Flame Photometric Detector, FPD*) lub detektor spektrometrii mas (*ang. Mass Spectrometry Detector, MS*).

Stosowane analityczne systemy kontroli umożliwiają analizę ilościową oraz jakościową kontrolowanego produktu, jednak monitoring jest prowadzony w trybie pracy „off-line" lub „in-line", który uniemożliwia natychmiastową korektę prowadzonych procesów. Dlatego też, należy obiektywnie stwierdzić, że obecnie poszukuje się nowych metod do oczyszczania strumieni biogazu oraz nowych metod kontroli procesów, które obniżyłyby koszty inwestycyjne oraz umożliwiłyby kontrolę w trybie „on-line". W przypadku próbek gazowych systemy multisensoryczne stanowią obiecującą alternatywą dla technik analitycznych. Obecnie matryce czujników gazowych są coraz częściej stosowane jako metody alternatywne zarówno dla technik chromatograficznych, jak i olfaktometrycznych w takich dziedzinach, jak monitoring jakości powietrza [149], ocena skuteczności procesów dezodoryzacji [150,151] czy optymalizacja i automatyzacja bioprocesów [152]. Matryce czujnikowe przeznaczone są zazwyczaj do szybkiej i ogólnej analizy składu mieszaniny gazów bez jej podziału na poszczególne składniki. Stosowane podejście umożliwia przypisanie danej mieszaniny gazów do wzorców w bazie danych i na tej podstawie dostarcza jakościowych informacji np. o procesach kompostowania [153,154]. Składowiska odpadów są kolejną grupą obiektów komunalnych, w których zaimplementowano matryce sensorowe. Gębicki i wsp. [155] kontrolowali jakość powietrza w pobliżu miejskiego składowiska odpadów, wykorzystując dwa rodzaje matryc czujników gazu. Jednym z nich było komercyjnie dostępne urządzenie (HERACLES II), a drugim samodzielnie zbudowany prototyp matrycy czujnikowej z czterema czujnikami, które na podłożu metalowym zawierają cienką warstwę tlenków np. miedzi, cynku lub cyny (*ang. Metal Oxid Semiconductor, MOS*) oraz jednym czujniku fotojonizacyjnym i dwoma czujnikami elektrochemicznymi. Jako technikę referencyjną wykorzystano olfaktometrię terenową, a matryce czujnikowe zostały wytrenowane do klasyfikacji analizowanych próbek powietrza.

Obecnie widoczna jest ciągła intensyfikacja badań zmierzających w kierunku przystosowania matryc czujnikowych do ilościowego oznaczania związków chemicznych. Moufid i wsp. [156] opracowali wydajny i czuły system monitorowania zapachów w celu zminimalizowania uciążliwości zapachowych i zanieczyszczenia środowiska. Wykorzystując regresję częściową najmniejszych kwadratów (*ang. Partial Least Squares Regression, PLS*) wyniki chromatograficzne skorelowano z wynikami otrzymanymi z matrycy czujnikowej. O podobnym zastosowaniu matryc czujnikowych donosili Delgado-Rodrigues i wsp. [157]. Autorzy porównali dwie metody monitorowania związków zapachowych emitowanych podczas kompostowania w miejskiej oczyszczalni ścieków. Do ilościowego oznaczania związków z gazów kompostowych wykorzystali GC-MS oraz matrycę złożoną z 10 czujników typu MOS. Regresja PLS została wykorzystana do kalibracji i treningu matrycy czujnikowej względem stężeń określonych substancji wyznaczonych metodą GC-MS. Opracowane modele matematyczne zostały sprawdzone przy użyciu narzędzi statystycznych, tj. t-testu i F-testu. W literaturze porównywane są najczęściej mocne i słabe strony wykorzystywania matryc czujnikowych do kontroli procesowej w celu wykazania ich innowacyjności i pionierskiego zastosowania (Tabel 4). Jednak w chwili obecnej brakuje rzetelnego porównania kontroli procesowej uzdatniania strumieni gazowych w odniesieniu do oceny jakości działania matryc czujnikowych, która skupiałaby się na określeniu poziomu równoważności wyników uzyskanych z matryc czujnikowych w porównaniu z wynikami uzyskanymi z metody referencyjnej (GC).

Tabela 4. Zalety i wady wykorzystania matryc czujnikowych oraz chromatografii gazowej do kontroli procesowej.

Matryce czujnikowe	
Zalety	**Wady**
Kontrola procesu w systemie "on-line"	Zmienność odpowiedzi czujników związana z czynnikami środowiskowymi (temperatura i wilgotność względna)
Układ czujników w postaci łatwo wymienialnych podzespołów	Starzenie lub zatrucie czujników

Łatwość kalibracji	Brak możliwości analiz jakościowej
Stosunkowo wysoka dokładność (błędy < 10%)	Wielowymiarowość generowanego sygnału
Szybki czas odpowiedzi (10-120 s)	Skomplikowana identyfikacja sygnałów
Niska granica wykrywalności (do poziomu ppb)	
Niski koszt	

Metoda referencyjna – chromatografia gazowa	
Zalety	**Wady**
Analiza ilościowa oraz jakościowa	Konieczność transportu próbek
Wysoka rozdzielczość, powtarzalność, odtwarzalność oraz dokładność	Ograniczone zakresy pomiarowe wynikające z granicy oznaczalności danych związków oraz z trudnością z przygotowaniem wieloskładnikowych wzorców gazowych
Identyfikacja wszystkich związków obecnych w mieszaninie kalibracyjnej	Reprezentatywność próbki zależy od wielu czynników
Mała objętość próbki do analizy	Potencjalny rozkład termiczny niestabilnych lotnych związków organicznych
	Zakłócenia wynikające z interakcji pomiędzy komponentami
	Wpływ parametrów metrologicznych na granicę oznaczalności oraz wykrywalności
	Wysokie koszty

Reasumując obecnie istnieje realne zapotrzebowanie na opracowanie efektywnej i korzystnej ekonomicznie technologii uzdatniania biogazu do parametrów gazu wysokometanowego (gazu ziemnego i sprężonego gazu ziemnego). Najkorzystniejszym rozwiązaniem wydaje się być wykorzystanie stosowanych powszechnie płuczek absorpcyjnych, które będą kompatybilne z nowym typem efektywnych i skutecznych absorbentów. Dodatkowo należy obiektywnie stwierdzić, że oprócz poszukiwania nowych metod do oczyszczania strumieni biogazu poszukuje się również nowych metod kontroli procesowej, która umożliwi ciągłą oraz bezobsługową kontrolę w systemie in-line lub on-line.

2. Cele badawcze

Głównym celem niniejszej rozprawy doktorskiej było opracowanie nowych i ekonomicznie opłacalnych sorbentów do efektywnego oczyszczania strumieni biogazu z substancji uciążliwych zapachowo oraz wykazanie możliwości zastosowania matryc czujnikowych do monitorowania procesu uzdatniania biogazu do gazu wysokometanowego.

Realizacja celu rozprawy doktorskiej obejmuje następujące zadania badawcze:

1) Opracowanie nowych sorbentów na bazie cieczy głęboko eutektycznych (ang. Deep Eutectic Solvent, DES) do efektywnego oczyszczania strumienia biogazu w oparciu o możliwość projektowania właściwości fizykochemicznych DES poprzez dobór odpowiedniego akceptora i donora wiązań wodorowych.
2) Otrzymanie zaprojektowanych DES.
3) Zbadanie podstawowych właściwości fizykochemicznych zaprojektowanych i otrzymanych DES.
4) Zbadanie struktury chemicznej DES oraz interakcji pomiędzy HBA i HBD w celu wytworzenia DES.
5) Wykorzystanie materiałów sorpcyjnych na bazie DES do efektywnego i selektywnego usuwania zanieczyszczeń z modelowego strumienia biogazu w procesie absorpcji fizycznej.
6) Określenie interakcji pomiędzy DES i zanieczyszczeniami podczas procesu absorpcji.
7) Zastosowanie alternatywnej techniki monitorowania procesu oczyszczania strumienia biogazu z wykorzystaniem matryc czujnikowych oraz porównanie otrzymanych wyników z metodą referencyjną chromatografią gazową sprzężoną z selektywnymi detektorami.
8) Wykazanie konkurencyjności absorbentów na bazie DES do obecnie stosowanych konwencjonalnych sorbentów.

3. Opis badań

Przedstawione cele cząstkowe zrealizowano i przedstawiono w ośmiu publikacjach naukowych, które stanowią podstawę niniejszej rozprawy doktorskiej. Otrzymane wyniki eksperymentalne wykazały duży potencjał nowych materiałów sorpcyjnych na bazie cieczy głęboko eutektycznych do absorpcyjnego oczyszczania strumienia biogazu. W badaniach wykazano przydatność matryc czujnikowych do monitorowania procesu absorpcji. Kontrola procesowa umożliwiła wyznaczenie efektywności procesu usuwania licznych zanieczyszczeń występujących w biogazie zarówno na wysokich, jak i niskich poziomach stężeń. Uzyskane wyniki stanowią kompleksową charakterystykę procesu oczyszczania strumieni biogazu.

Wymienione poniżej publikacje naukowe zostały załączone w Rozdziale 8.

1. **E. Słupek**, P. Makoś, J.Gębicki, Deodorization of model biogas by means of novel non- ionic deep eutectic solvent, Arch. Environ. Prot. 46 (2020) 41–46. (https://doi.org/10.24425/aep.2020.132524)
2. **E. Słupek,** P. Makoś, Absorptive Desulfurization of Model Biogas Stream Using Choline Chloride- Based Deep Eutectic Solvents, Sustainability. 12 (2020) 1619. (https://doi.org/10.3390/su12041619)
3. **E. Słupek**, P. Makoś-Chełstowska, & J. Gębicki, Removal of Siloxanes from Model Biogas by Means of Deep Eutectic Solvents in Absorption Process. Materials, 14 (2021) 241. (https://doi.org/10.3390/ma14020241)
4. P. Makoś-Chełstowska, **E. Słupek**, A. Kramarz, & J. Gębicki, New Carvone-Based Deep Eutectic Solvents for Siloxanes Capture from Biogas. Int. J. Mol. Sci., 22 (2021) 9551. (https://doi.org/10.3390/ijms22179551)
5. P. Makoś-Chełstowska, **E. Słupek**, & J. Gębicki, Deep eutectic solvents – based green absorbents for effective volatile organochlorine compounds removal from biogas. GREEN CHEMISTRY, 23 (2021) 4814-4827. (https://doi.org/10.1039/d1gc01735g) (Reproduced from Ref. Green Chemistry with permission from the Royal Society of Chemistry)
6. P. Makoś-Chełstowska, **E. Słupek,** , A. Kramarz, D. Dobrzyniewski, B. Szulczyński, & J. Gębicki, Green monoterpenes based deep eutectic solvents for effective BTEX absorption from biogas. CHEMICAL ENGINEERING RESEARCH & DESIGN,. 188 (2022), s.179-196. (https://doi.org/10.1016/j.cherd.2022.09.047) (CC-BY-NC-ND) (4.0))
7. **E. Słupek,** P. Makoś-Chełstowska, D. Dobrzyniewski, B. Szulczyński, & J. Gębicki, Process Control of Biogas Purification Using Electronic Nose. CHEMICAL ENGINEERING TRANSACTIONS, 82 (2020) 427- 432. (https://doi.org/10.3303/cet2082072)
8. **E. Słupek**, P. Makoś, & J. Gębicki, Theoretical and Economic Evaluation of Low-Cost Deep Eutectic Solvents for Effective Biogas Upgrading to Bio-Methane. ENERGIES, 13 (2020) 3379. (https://doi.org/10.3390/en13133379)

3.1. Absorpcja lotnych związków organicznych

W początkowej fazie badań otrzymano niejonowy DES złożony z naturalnych i nietoksycznych składników, tj. gwajakol (G), kamfora (C) i kwas lewulinowy (Lev) w stosunku molowym 1:1:3 (**Publikacja 1**). W badaniach zwrócono szczególną uwagę, aby składniki tworzące absorbenty otrzymywane były z łatwo dostępnych materiałów odpadowych, pochodzących z innych procesów produkcji biogazu, np. hydrolizy lub fermentacji beztlenowej. W celu charakterystyki dla G:C:Lev (1:1:3) wykonano podstawowe badania fizykochemiczne (gęstość, lepkość dynamiczna) w warunkach ciśnienia atmosferycznego oraz w zakresie temperatur od 25 do 50°C, co jest zwykłym zakresem temperatur pracy kolumny absorpcyjnej. DES wykorzystano jako absorbent do usuwania dichlorometanu (DCM), toluenu (T), heksametylodisiloksanu (L2) oraz aldehydu propionowego (AP). Powinowactwo absorbentu do DCM, T oraz L2 oceniono za pomocą współczynników podziału ciecz-para (K). Testy powinowactwa przeprowadzono w szklanych fiolkach, które termostatowano w temperaturze 25 i 50°C przez 48 godzin. Badania przeprowadzono dla wody, n-heksadekanu oraz nowego dotąd jeszcze nie publikowanego G:C:Lev (1:1:1) i znanych DES powstałych poprzez zmieszanie czwartorzędowej soli amoniowej (chlorku choliny - ChCl) z mocznikiem (U), kwasem lewulinowym (Lev) oraz glikolem dietylenowym (DEG) w odpowiednim stosunku molowym. Stężenia LZO w

fazie gazowej oznaczono za pomocą analizy fazy nadpowierzchniowej przy użyciu chromatografii gazowej sprzężonej z detektorem płomieniowo-jonizacyjnym (HS-GC-FID). Na podstawie bilansu masowego oznaczono stężenia LZO w fazie ciekłej. Otrzymane wyniki współczynnika K dla G:C:Lev (1:1:3) i n-heksadekanu były zbliżone niezależnie od temperatury, co potwierdza skuteczność zaproponowanego DES w usuwaniu LZO. Zaobserwowany brak widocznych zmian podczas zmiany temperatury jest bardzo ważny w przypadku przemysłowego zastosowania DES, ponieważ temperatura strumienia biogazu wytwarzanego w przemyśle nie zawsze jest stabilna. Najniższe wartości K, na poziomie <0,001 uzyskano dla toluenu. W kolejnej części badań dla toluenu przeprowadzono badania absorpcji z wykorzystaniem układu dynamicznego. Jako modelowy strumień biogazu zastosowano gaz inertny (azot) zanieczyszczony parami toluenu na poziomie 50 ppm v/v. W warunkach dynamicznych określono wpływ prędkości przepływu modelowego strumienia biogazu oraz objętość absorbentu w zakresie 20-70 mL/min oraz 15-50 mL. Efektywność absorpcji monitorowano na wlocie i wylocie z kolumny barbotażowej za pomocą GC-FID. W wyniku szeregu przeprowadzonych badań otrzymano najkorzystniejsze warunki absorpcji:

- natężenie przepływu modelowego strumienia biogazu - 50 mL/min
- objętość absorbentu - 50 mL.

Uzyskane najkorzystniejsze warunki przetestowano do procesu absorpcji mieszaniny wszystkich badanych zanieczyszczeń (T, PA, DCM i L2) w stężeniu 50 ppm v/v oraz temperaturze 25°C. Uzyskane krzywe absorpcji zilustrowały znaczącą zależność czasu efektywnego usuwania DCM, T, L2, AP od ich struktury. Mniejsza zdolność absorpcyjna DCM oraz AP mogła wynikać z większej konkurencyjności oddziaływań tworzonych przez T and L2 z G:C:Lev (1:1:3). Ponadto w cyklu badań wykonano proces regeneracji i możliwość ponownego wykorzystania DES, które są bardzo ważne z ekonomicznego punktu widzenia. W badaniach wykorzystano proces adsorpcji na węglu aktywnym do usuwania LZO z DES. Wyniki wskazują, że LZO można całkowicie usunąć z DES, a zregenerowany DES może być ponownie użyty co najmniej pięć razy bez znaczącej utraty zdolności absorpcyjnej. Otrzymane wyniki eksperymentalne wykazały duży potencjał G:C:Lev (1:1:3) do absorpcyjnego oczyszczania rzeczywistych strumieni biogazu.

3.2. Absorpcja lotnych związków siarkoorganicznych

W ramach **Publikacji 2** zwrócono szczególną uwagę na proces odsiarczania strumieni biogazu z disiarczku dimetylu (DMDS), który jest uznawany za przedstawiciela lotnych związków siarkoorganicznego (*ang. Volatile Organosulfur Compounds*, VSC). W tym celu otrzymano trzy jonowe DES przez połączenie chlorku choliny (ChCl) z fenolem (Ph), glikolem etylenowym (EG) oraz kwasem lewulinowym (Lev) w stosunku molowym 1:2. W celu wytypowania najlepszego DES przeprowadzono proces absorpcji w układzie dynamicznym, w którym zastosowano najkorzystniejsze warunki, które otrzymano w ramach **Publikacji 1** (objętość DES - 50 mL oraz natężenie przepływu modelowego strumienia biogazu - 50 mL/min). Proces absorpcji prowadzono w temperaturze 25°C z początkowym stężeniem DMDS na poziomie 1 mg/Nm^3. Efektywność absorpcji monitorowano na wlocie i wylocie z kolumny barbotażowej za pomocą GC-FID. Najwyższą efektywność absorpcji otrzymano dla ChCl:Ph (1:2), dla którego krzywa przebicia do 800 minut była jedynie w 30% nasycona zanieczyszczeniami, dopiero po kolejnych 300 minutach gwałtownie wzrosła. Pozostałe DES: ChCl:EG (1:2) i ChCl:Lev (1:2) wykazały nieco niższe wartości krzywych przebicia do 600 i 800 minut. W otrzymanych krzywych przebicia zaobserwowano, że zdolność i szybkość wchłaniania DMDS maleje wraz ze wzrostem lepkości DES. Wyższe wartość lepkości absorbentów utrudniają proces przenoszenia masy, przez co efektywny czas absorpcji drastycznie maleje co widoczne jest na uzyskanych krzywych przebicia. Najwyższą efektywność absorpcji uzyskano dla ChCl:Ph (1:2), który charakteryzował się najniższą wartością lepkości dynamicznej. Dla najlepszego DES przeprowadzono szereg badań, pod kątem doboru najkorzystniejszych parametrów procesowych, które mają decydujący wpływ na praktyczne zastosowanie DES. W badaniach uwzględniono wpływ:

- objętości DES - 15-50 mL,
- natężenia przepływu modelowego strumienia biogazu - 20-70 mL/min,
- stężenia początkowego DMDS - 0,1-100,0 mg/Nm^3,
- temperatury procesu - 25-60°C.

W toku badań potwierdzono, że objętość DES, natężenie przepływu oraz temperatura procesu na poziomie 50 mL, 50 mL/min i 25°C to nadal najkorzystniejsze parametry. Dodatkowo wykazano, że początkowa ilość DMDS w modelowym strumieniu biogazu ma jedynie niewielki wpływ na zdolność i szybkość absorpcji. Jest to korzystne ze względu na zmienne ilości DMDS w rzeczywistych strumieniach biogazu. W optymalnych warunkach DMDS był usuwany z wysoką wydajnością przez 800 min. Po upływie 800 minut zaobserwowano stopniowe przesycenie ChCl:Ph (1:2). W celu lepszego zrozumienia otrzymanych różnic w krzywych przebicia

oraz wyjaśnienia mechanizmów usuwania DMDS z fazy gazowej za pomocą DES zastosowano badania strukturalne z zastosowaniem spektroskopii w podczerwieni z transformacją Fouriera (*ang. Fourier Transformed Infrared Spectroscopy*, FTIR). Na widmach FTIR nie zaobserwowano przesunięć wynikających z powstania oddziaływań S–H···π, O–H···S i C–H···S. W celu lepszego zrozumienia oraz wykazania interakcji wykonano obliczenia z zastosowaniem teorii funkcjonału gęstości (*ang. Density Functional Theory, DFT*), analizy potencjału elektrostatycznego (*ang. Electrostatic Potential Analysis, ESP*) oraz analizy zmniejszonego gradientu gęstości (*ang. Reduced Density Gradient, RDG*). Podczas analizy teoretyczne zoptymalizowano najbardziej prawdopodobne i stabilne konfiguracje w fazie gazowej ChCl:Ph-DMDS, ChCl:Lev-DMDS i ChCl:EG-DMDS na poziomie teorii B3LYP/6-311++G**. Powstałe kompleksy DES-DMDS nie wykazały oddziaływań o silnym charakterze wiązań wodorowych, jednak potwierdziły występowanie słabych wiązań elektrostatycznych - interakcje van der Waalsa, które były główną siłą napędową usuwania DMDS z modelowego strumienia biogazu. W celu dokładnego przetestowania DES dla przesyconego ChCl:Ph (1:2) przeprowadzono badania regeneracji z wykorzystaniem procesu barbotaż azotem oraz proces adsorpcji z wykorzystaniem trzech adsorbentów węgiel aktywny, żel krzemionkowy oraz tlenek glinu. Najwyższą skuteczność cyklu absorpcji-desorpcji DMDS otrzymano z zastosowaniem barbotażu azotem. Zregenerowany ChCl:Ph (1:2) może zostać ponownie wykorzystany co najmniej pięciokrotnie bez znaczącej utraty zdolności absorpcyjnej oraz bez zmian w swojej strukturze co zostało potwierdzone za pomocą analizy FTIR.

3.3. Absorpcja lotnych związków krzemoorganicznych

W kolejnej części badań zwrócono szczególną uwagę na absorpcyjne usuwanie siloksanów z modelowego strumienia biogazu z wykorzystaniem DES. W **Publikacji 3** przedstawiono badania przesiewowe dwudziestu jonowych DES składających się z bromku tetrapropyloamoniowego (TPABr) jako akceptora wiązań wodorowych (HBA) oraz glikoli (tj. glikol etylenowy (EG), glicerol (Gly), glikol trietylenowy (TriEG), glikol tetraetylenowy (TEG), glikol dietylenowy (DEG)) jako donorów wiązań wodorowych (HBD) w różnym stosunku molowym (1:3; 1:4; 1:5; 1:6, HBA:HBD) oraz rozpuszczalników konwencjonalnych (tj. woda oraz glikol etylenowy). Badania przesiewowe przeprowadzono przy użyciu modelu ekranowania dla rzeczywistych rozpuszczalników (*ang. Conductor-Like Screening Model for Realistic Solvent, COSMO-RS*) opartego na porównaniu rozpuszczalności siloksanów w DES. Największą rozpuszczalność zarówno liniowych (heksametylodisiloksan (L2), oktametylotrisiloksan (L3)), jak i cyklicznych (oktametylocyklotetrasiloksan (D4)) siloksanów otrzymano dla DES złożonego z TPABr i TEG w stosunku molowym 1:3. Zachodzące interakcję pomiędzy TPABr i TEG oraz pomiędzy TPABr:TEG (1:3) i siloksanami określono za pomocą metody FTIR oraz badań teoretycznych opartych na analizie σ-profili (opisującej rozkład prawdopodobieństwa pola powierzchni z gęstością ładunku) oraz analizie σ-potencjałów (opisującej powinowactwo między składnikami mieszaniny). Otrzymane badania teoretyczne wskazały, że tworzenie wiązań wodorowych pomiędzy grupą -OH z cząsteczki DES, a grupą -O- z siloksanów jest najbardziej prawdopodobną siłą napędową procesu absorpcji siloksanów.

W kolejnej części badań otrzymano DES przez zmieszanie TPABr z TEG w stosunku molowym 1:3. Dla TPABr:TEG (1:3) określono podstawowe właściwości fizykochemicznych, tj. lepkość dynamiczna, gęstość i temperatura topnienia (*ang. Melting Points, MP*). Brak zmian lepkości podczas zmian częstotliwości obrotów na minutę wskazuje, że TPABr:TEG (1:3) jest cieczą newtonowską. Wydajność absorpcyjną usuwania siloksanów z fazy gazowej z wykorzystaniem TPABr:TEG (1:3) wyznaczono w układzie dynamicznym. Dla dynamicznego procesu absorpcji wyznaczono główne parametry procesowe, tj. temperatura procesu (25-50°C), objętość DES (15-50 mL), rodzaj gazu matrycowego (czysty N_2 oraz N_2:CH_4 2:1 obj.) oraz natężenie przepływu biogazu (10-50 mL/min). Stężenie gazowych siloksanów w modelowym strumieni biogazu utrzymywano na stałym poziomie wynoszącym 50 mg/dm^3. Efektywność absorpcji monitorowano na wlocie i wylocie z kolumny barbotażowej przy użyciu GC-FID, natomiast stężenie metanu przy użyciu GC-TCD. Przeprowadzone badania wykazały, że najkorzystniejsze parametry absorpcji siloksanów to:

- objętość DES - 50 mL,
- temperatura procesu - 25°C,
- natężenie przepływu modelowego strumienia biogazu - 50 mL/min.

Zastosowanie modelowego strumienia biogazu w postaci mieszaniny N_2:CH_4 (2:1 obj.) wykazały zmniejszoną o 20-80 minut chłonność DES w porównaniu z czystym azotem. W optymalnych warunkach siloksany usuwano z fazy gazowej z wysoką wydajnością do 375, 280 i 5300 minut odpowiednio dla L2, L3 oraz D4. Otrzymane krzywe przebicia oraz wydajności wchłaniania są znacznie wyższe w porównaniu do olejów mineralnych. W badaniach wykazano również, że nowy DES na bazie TPABr:TEG (1:3) można łatwo

regenerować z wykorzystaniem barbotażu azotem w podwyższonej temperaturze (90°C). Skuteczność desorpcji osiągnięto na poziomie 99,999%, która była utrzymywana do 5 cykli regeneracyjnych.

Ze względu na bardzo częste występowanie siloksanów w biogazie w **Publikacji 4** wykonano przesiewowe badania dla 90 niejonowych hydrofobowych DES. Jako absorbenty wytypowano DES złożone z dwóch składników chemicznych, które można łatwo wyekstrahować ze źródeł naturalnych, tj. rośliny lub biomasa. DES składały się z karwonu (C-one), kamfory (C), tymolu (Th), waniliny (V), gwajakolu (G), kwasu lewulinowego (Lev), kwasu wanilinowego (VA), kwasu dekanowego (DA), kwasu undekanowego (UA) i kwasu dodekanowego (DDA), które połączono ze sobą w stosunku molowym 1:1. Przy wykorzystaniu modelu COSMO-RS wyznaczono i porównano współczynniki aktywności DES względem siloksanów liniowych: L2, L3, dekametylotetrasiloksan (L4) oraz cyklicznych: heksametylocyklotrisiloksan (D3) i dekametylocyklopentasiloksan (D5). Największe powinowactwo w badaniach teoretycznych do siloksanów otrzymano dla DES na bazie karwonu (C) w połączeniu z kwasami organicznymi tj. DA, UDA oraz DDA. Ze względu na to w kolejnej części badań otrzymano DES przez zmieszanie C z DA, UDA oraz DDA w odpowiednim stosunku molowym. Dla nowych DES na bazie C:DA (1:1), C:DDA (3:1) oraz C:UDA (1:1) wyznaczono podstawowe właściwości fizykochemicznych DES, które charakteryzowały się niskimi wartościami lepkości oraz gęstości. W celu dokładniej charakterystyki nowych DES wykonano badania teoretyczne oparte na analizie σ-profili oraz σ-potencjałów oraz badania eksperymentalne z wykorzystaniem spektroskopii FTIR oraz spektroskopii magnetycznego rezonansu jądrowego *(ang. Nuclear Magnetic Resonance Spectroscopy, NMR).* Zestawienie wszystkich badań umożliwiło określenie mechanizmów tworzenia DES oraz absorpcji siloksanów z wykorzystaniem DES. Wykazano, że wiązania wodorowe odgrywają dominującą rolę w tworzeniu DES, natomiast słabsze oddziaływania niezwiązane są odpowiedzialne za skuteczność usuwania siloksanów z biogazu. W celu określenia wydajności absorpcyjnego usuwania siloksanów z fazy gazowej z wykorzystaniem DES przeprowadzono procesy dynamiczne. Efektywność absorpcji monitorowano na wlocie i wylocie z kolumny barbotażowej przy użyciu GC-FID, natomiast stężenie metanu oraz dwutlenku węgla przy użyciu GC-TCD. Proces absorpcji prowadzono przy zastosowaniu objętości DES na poziomie 50 mL, szybkości przepływu 50 mL/min oraz temperaturze procesu 25°C. W tej części badań wykazano, że najskuteczniejszym absorbentem o zdolności absorpcyjnej do 5600 minut okazał się DES złożone z C:DA (1:1). Nasycenie C:DA (1:1) było najdłuższe dla cyklicznych siloksanów D3 i D4, natomiast najszybciej przesycał się liniowy L2. Otrzymane różnice w efektywności absorpcji mogły wynikać z wartości prężności par i polarności, które dla L2 były znacznie większe w porównaniu z innymi siloksanami. Ponadto, cykliczne siloksany posiadają większą liczbę wiązań Si···O w stosunku do liniowych siloksanów, co również może wpływać na zwiększenie powinowactwa do DES. W dalszych badaniach dla najlepszego DES (C:DA (1:1)) określono wpływ głównych parametrów procesowych: prędkości przepływu w zakresie przepływu laminarnego 25-70 mL/min oraz rodzaju matrycy modelowego strumienia biogazu (N_2 oraz $CH_4:CO_2$ 2:1 obj.). Stężenie siloksanów utrzymywano na tym samym poziomie 30 g/m^3. C:DA (1:1) wysyciło się związkami L2, L3 i L4 po około 5500 min (50 mL/min) i 6000 min (25 mL/min), D3 5000 min (50 mL/min) i 6000 min (25 mL/min) oraz D5 6000 min dla 50 i 25 mL/min. Największe różnice w czasie absorpcji pomiędzy przepływami 75, 50 i 25 mL/min zaobserwowano dla związków liniowych. Przeprowadzone badania potwierdziły, że cykliczne siloksany wykazywały większe powinowactwo do DES niż liniowe. Zmiana matrycy z czystego azotu na mieszaninę $CH_4:CO_2$ 2:1% v/v w początkowej fazie procesu absorpcji doprowadziła do sorpcji siloksanów oraz metanu i dwutlenku węgla. Całkowity ubytek metanu wynosił około 1%. Otrzymana wartość mieści się w dopuszczalnych normach stosowanych podczas procesów przemysłowych. W przypadku dwutlenku węgla zaobserwowano znacznie dłuższy czas efektywnego wychwytywania CO_2. Wydłużona absorpcja CO_2 jest korzystna pod względem dalszego zastosowania C:DA (1:1). Ze względu na wysoką selektywność wychwytywania siloksanów z jednoczesnym usuwaniem dwutlenku węgla proponowana procedura absorpcji ma duży potencjał do oczyszczania rzeczywistych strumieni biogazu. W końcowym etapie badań wykonano regenerację C:DA (1:1). Najwyższą skuteczność desorpcji zaobserwowano dla barbotażu azotem w temperaturze 150°C. Pełną desorpcję siloksanów uzyskano po 90 minutach. Wykazano, że cykl absorpcji-desorpcji można prowadzić pięciokrotnie bez zmiany wydajności procesu oraz bez zmian w strukturze DES, co potwierdzono za pomocą widm FTIR oraz NMR.

3.4. Absorpcja lotnych związków chloroorganicznych

Lotne związki chloroorganiczne (*ang. Volatile Organochloride Compound, COCC*) stanowią problematyczną grupę zanieczyszczeń biogazu z grupy LZO. Dlatego, też w **Publikacji 5** przetestowano nowe dotąd jeszcze nie publikowane niejonowe DES jako rozpuszczalniki do absorpcyjnego usuwania

dichlorometanu (DCM), chloroformu (CF), czterochlorku węgla (TCM), 2,2,2-trichloroetanolu (TCEtOH), 1,1,2,2-tetrachloroetanu (TCE) z modelowego strumienia biogazu. Niejonowe DES otrzymano przez połączenie: kamfory (C), gwajakolu (G), syringolu (Syr) i kwasu lewulinowego (Lev) w odpowiednim stosunku molowym. W wyniku badań eksperymentalnych otrzymano DES na bazie C:G (1:1), C:Lev (1:2), G:Lev (1:1) oraz Syr:Lev (1:1), dla których określono podstawowe właściwości fizykochemiczne, tj. lepkość, gęstość i temperatura topnienia. Nowe DES przebadano pod względem strukturalnym, z zastosowaniem techniki NMR oraz FTIR. Zastosowanie techniki NMR potwierdziło, że otrzymane DES przebiegło bez dodatkowych reakcji ubocznych, ponieważ zidentyfikowane sygnały przypisano wyłącznie do sygnałów HBA oraz HBD, które tworzyły konkretny DES. Uzyskane informacje z widm FTIR wskazują jedynie na powstawanie silnych wiązań wodorowych pomiędzy HBA i HBD. Nie wskazują jednak liczby wiązań wodorowych, ich dokładnej lokalizacji oraz informacji o słabszych oddziaływaniach, czyli oddziaływaniach elektrostatycznych w strukturach DES. Dlatego też, w kolejnej części badań wykorzystano obliczenia z zastosowaniem teorii funkcjonału gęstości DFT, aby uzyskać wgląd w zachodzące integracje w DES na poziomie atomowym. Najbardziej prawdopodobne i stabilne kompleksy DES zostały zoptymalizowane geometrycznie na poziomie teorii B3LYP/6-311++G**. W kolejnym etapie badań teoretycznych przeprowadzono analizę gradientu gęstości (*ang. Reduced Density Gradient*, RDG), która miała na celu klasyfikację i identyfikację wszystkich oddziaływań niekowalencyjnych występujących pomiędzy składnikami DES. Analiza RDG umożliwia identyfikację trzech rodzajów oddziaływań, tj. wiązań wodorowych, sił van der Waalsa i odpychania sterycznego. Badania teoretyczne poszerzono o analizę potencjału elektrostatycznego (*ang. Electrostatic Potential Analysis*, EPA) w celu wykazania najbardziej prawdopodobnych i najbardziej stabilnych obszarów ataku elektrofilowego oraz przewidywania, w jaki sposób różne geometrie elementów DES mogą ze sobą oddziaływać.

W badaniach eksperymentalnych przeprowadzono procesy absorpcyjnego usuwania COCC. W celu określenia wydajności procesów absorpcyjnych z wykorzystaniem DES wyznaczono główne parametry procesowe, tj.:

- rodzaj DES - C:Gu (1:1); C:Lev (1:2); Gu:Lev (1:1); Syr:Lev (1:1),
- temperatura absorpcji - 20-60°C,
- natężenie przepływ gazu - 25-75 mL/min,
- skład gazu - CH_4:CO_2:N_2:H_2O w stosunku; 81:15:2:2; 66:30:2:2; 51:45:2:2 % obj.,
- początkowe stężenie COCC - 0,5-10,0 mg/m^3,
- temperatura procesu regeneracji (barbotaż azotem) - 20-100°C.

Stężenie gazowych zanieczyszczeń monitorowano na wlocie i wylocie z kolumny barbotażowej przy użyciu techniki GC-FID, natomiast skład modelowego strumienia biogazu z wykorzystaniem GC-TCD.

W wyniku przeprowadzonych badań otrzymano najkorzystniejsze parametry usuwania COCC z modelowego strumienia biogazu: rodzaj DES - Syr:Lev (1:1), temperatura procesu - 25˚C, natężenie przepływu modelowego strumienia biogazu - 50 mL/min. Zastosowanie metanu w modelowej mieszaninie w postaci CH_4:CO_2:N_2:H_2O w stosunku objętościowym 81:15:2:2, 66:30:2:2 i 51:45:2:2 obj. zmniejszyło pojemność absorpcyjną DES średnio o 0,7% w porównaniu z czystym azotem. W wyniku zwiększeni stężenia dwutlenku węgla z 0 do 30% zaobserwowano zmniejszenie pojemności i szybkości absorpcji COCC, a co za tym idzie skrócenie efektywnego czasu absorpcji COCC z 138 do 89 min. Kolejne zwiększenie stężenia CO_2 z 30 i 45% nie doprowadziło do istotnych zmian w efektywnym czasie absorpcji COCC. Nieoczekiwane wyniki uzyskano dla TCEtOH, gdzie zaobserwowano, że wraz ze wzrostem stężenia CO_2 w biogazie następuję efektywny wzrost czasu wchłaniania TCEtOH z 640 do 1200 min. Najprawdopodobniej wynika to z faktu, że grupa -OH z TCEtOH może tworzyć silne wiązania wodorowe zarówno z DES, jak i CO_2. Zwiększenie stężenia COCC w strumieniu biogazu z 0,5 do 1 mg/cm^{-3} nie spowodowało istotnych różnic w czasie absorpcji. Dalszy wzrost do 10 mg/m^{-3} doprowadził do zauważalnego skrócenia czasu przesycenia DES z 612,1 do 211,8 min dla DCM. W badaniach regeneracyjnych wykazano, że barbotaż azotem w 100°C przez 60 minut jest najefektywniejszy sposobem umożliwiającym przeprowadzenie do 10 cykli absorpcji-desorpcji bez zmian w strukturze DES co potwierdzono za pomocą analizy FTIR.

W najkorzystniejszych warunkach procesu pojemność absorpcyjna dla DCM, CF, TCM, TCE i TCEtOH wynosiła odpowiednio 304, 420, 360, 292 oraz 661 mg COCC/g DES. Otrzymane wartości dla Syr:Lev (1:1) podczas usuwania DCM są wyższe o około 98 mg/g w porównaniu z absorbentami na bazie ILs. W celu dokładniejszej analizy i lepszego poznania i wyjaśnienia mechanizmów zachodzących podczas procesu usuwania COCC w procesie absorpcji, kompleksy DES- COCC scharakteryzowano metodą FTIR oraz metodami obliczeniowymi mechaniki kwantowej. W widmach FTIR po absorpcji COCC, nastąpiło przesunięcie grupy –OH i grupy C=O w kierunku wyższych wartości liczby falowej. Zaobserwowane zmiany potwierdziły, że proces absorpcji może odbywać się poprzez tworzenie słabych wiązań wodorowych

pomiędzy grupą -COOH (pochodzącą z Syr:Lev), a atomem chloru (pochodzącą z COCC). Dodatkowo otrzymane wyniki RDG wykazały, że oddziaływania van der Waalsa występują we wszystkich kompleksach DES-COCC, z wyjątkiem kompleksów DES-TCEtOH, w których współistniały zarówno wiązania wodorowe, jak i oddziaływania van der Waalsa.

3.5. Absorpcja lotnych związków organicznych z grupy BTEX

W ramach **Publikacji 6** otrzymano DES poprzez połączenie: kamfory (C), karwonu (C-one), eukaliptolu (Eu), furfuralu (FF), chlorku choliny (ChCl), bromku tetrametyloamoniowowego (TMABr), bromku tetraetyloamoniowego (TEABr), bromku tetrapropyloamoniowego (TPABr), bromku tetrabutyloamoniowego (TBABr), gwajakolu (G), syringolu (Syr), mentolu (M), tymolu (Th), waniliny (V), kwasu mrówkowego (FA), kwasu oktanowego (OA), kwasu nonanowego (NA), kwasu dekanowego (DA), kwasu dodekanowego (DDA) oraz kwasu lewulinowego (Lev), które zmieszano w stosunku molowym 1:1. Otrzymane DES zastosowano jako rozpuszczalniki do absorpcyjnego usuwania benzenu (B), toluenu (T), etylobenzenu (E) oraz ksylenu (X) z modelowego strumienia biogazu. Z 99 przetestowanych DES tylko 39 kompleksów eutektycznych okazało się cieczami w temperaturze pokojowej. Ze względu na stosunkowo dużą liczbę nowych DES przeprowadzono preselekcję DES poprzez porównanie teoretycznych stałych Henry'ego (H), które zostały wyznaczone za pomocą modelu COSMO-RS. Najniższe wartości stałych K, a tym samym największą rozpuszczalność BTEX otrzymano dla DES na bazie C:OA (1:1), C:DA (1:1), C-one:OA (1:1), C-one:NA (1:1), C-one:DA (1:1), C-one:Lev (1:1) oraz Eu:OA (1:1). Dla wybranych DES określono podstawowe właściwości fizykochemiczne (tj. temperatura topnienia, gęstość, lepkość oraz napięcie powierzchniowe) oraz wykonano badania strukturalne z zastosowaniem metod NMR oraz FTIR. W celu wytypowania najefektywniejszego DES przeprowadzono absorpcję BTEX w układzie dynamicznym, w którym zastosowano najkorzystniejsze warunki uzyskane w ramach wcześniejszych badań, tj. temperatura procesu 25°C, ciśnienie biogazu 10 kPa, objętość DES 50 mL, natężenie przepływu modelowego biogazu 50 mL/min, stężenie początkowe BTEX 2000 mg/m^3. Stężenie gazowych zanieczyszczeń monitorowano na wlocie i wylocie z kolumny barbotażowej przy użyciu techniki GC-FID. W celu dokładniejszej preselekcji DES wykonano również szybkie porównanie eksperymentalnych stałych Henry'ego (K). Badania wykonano techniką HS-GC-FID zgodnie z procedurą opisaną w **Publikacji 1.** Preselekcje eksperymentalnych K wykonano w dwóch wariantach. Pierwszy dotyczył rozpuszczalności pojedynczych zanieczyszczeń w DES, drugi natomiast rozpuszczalności mieszaniny BTEX. Uzyskane wartości stałych K w obu wariantach różnią się od siebie tylko nieznacznie. Wyniki z procesów dynamicznych oraz uzyskanych wartości stałych K wykazały, że chłonność BTEX zależy zarówno od rodzaju HBD, HBA, jak i struktury BTEX. DES złożony z Eu i OA w stosunku molowym 1:1 charakteryzowały się najwyższą chłonnością BTEX. W badanach wykazano, że na efektywność absorpcji BTEX ma wpływ nie tylko struktura składników i silnie hydrofobowy charakter DES, ale także właściwości fizykochemiczne tj. niska lepkość, wysokie napięcie powierzchniowe i stosunkowo niska temperatura topnienia. W celu wyjaśnienia zachodzących interakcji pomiędzy DES a BTEX, wykorzystano badania molekularne oparte na obliczeniach teoretycznych DFT, RGD oraz EPA. Za pomocą badań teoretycznych wykazano, że główna siłą napędową wychwytywania BTEX były oddziaływania elektrostatyczne tj. oddziaływania van der Waalsa oraz oddziaływania π-π pomiędzy BTEX oraz DES.

W kolejnej części badań określono wpływ matrycy na efektywność absorpcji Eu:OA (1:1). Porównano efektywność absorpcji BTEX z obojętnego strumienia azotu oraz z modelowej mieszaniny biogazu składającego się z CH$_4$:CO$_2$:N$_2$ w stosunku objętościowym 5:3:2. Skład zanieczyszczeń kontrolowana za pomocą GC-FID, natomiast modelowego strumienia biogazu z wykorzystaniem GC-TCD. Otrzymane wyniki wykazały, że zastosowanie modelowego strumienia biogazu skraca czas absorpcji, a tym samym zmniejsza zdolność absorpcji DES. Wynika to z tworzenia się konkurencyjnych interakcje, najprawdopodobniej pomiędzy CH$_4$···HBA oraz CO$_2$···HBD powstają wiązania wodorowe w wyniku których następuje częściowa absorpcja CH$_4$ i CO$_2$. W związku z dodatkową absorpcją głównych składników biogazu zmniejsza się wydajność wchłaniania BTEX. Największe zmiany w efektywności absorpcji widoczne są dla benzenu, którego czas skrócił się o ok 1000 minut. W celu wykazania konkurencyjności nowych absorbentów na bazie DES, dynamiczne procesy absorpcyjnego usuwania BTEX przeprowadzono na komercyjnie dostępnym absorbencie (Genosorbie). Procesy absorpcji prowadzono w takich samych warunkach jak dla Eu:OA (1:1) z wykorzystaniem modelowej mieszaniny biogazu złożonej z CH$_4$:CO$_2$:N$_2$ (5:3:2 obj.). Podczas badań dla Eu:OA (1:1) uzyskano najkrótszy czas absorpcji zanieczyszczeń dla benzenu, który wynosił 4048 minut. Z kolei najdłuższy czas uzyskano dla toluenu, etylobenzenu i ksylenu, które wynosiły odpowiednio 5334, 5790 i 5800 minut. Bardzo podobny trend usuwania BTEX można zaobserwować w przypadku Genosorbu dla którego najkrótszy czas absorpcji uzyskano również dla benzenu wynoszący 3118 min. Dla pozostałych

zanieczyszczeń otrzymano zbliżone lecz niższe wartości wynoszące dla toluenu, etylobenzenu i ksylenu, odpowiednio 4319, 5731 i 5859 min. Otrzymane wyniki wskazują, że nowy DES może być dobrą alternatywą dla dostępnych i stosowanych obecnie absorbentów w przemyśle. W celu wyjaśnienia mechanizmów wychwytywania BTEX wykorzystano analizy teoretyczne oparte na modelu COSMO-RS oraz analizy eksperymentalne przy wykorzystaniu technik FTIR oraz NMR. W badaniach wykazano, że główna siłą napędową usuwania BTEX przy zastosowaniu Eu:OA (1:1) oraz Genosorbu są słabsze oddziaływania niekowalencyjne, tj. oddziaływania van der Waalsa.

Dla Eu:OA (1:1) przeprowadzono również proces absorpcji w powiększonej skali w celu potwierdzenia przydatności DES. Zwiększenie skali obejmowało 10-krotne zwiększenie objętości DES do 500 mL oraz natężenia przepływu modelowego strumienia biogazu $CH_4:CO_2:N_2$ (5:3:2 obj.) do 500 mL/min. Proces absorpcji przeprowadzono w dwóch wariantach temperaturowych. Pierwszą kolumnę absorpcyjną utrzymywano w temperaturze pokojowej (RT), a drugą ochłodzono do 10°C. W obu wariantach proces efektywnego wychwytu benzenu jest prawie dwukrotnie krótszy w porównaniu z ETX. Czas przebicia DES dla benzenu wynosił odpowiednio 5000 min i 6500 min, toluenu od 10500 min do 13700 min, dla etylobenzenu i ksylenu odpowiednio od około 11500 min do 15000 min (25 i 10°C). Uzyskany czas absorpcji w temperaturze 10°C jest proporcjonalnie dłuższy w porównaniu z RT. Zależność między wzrostem wydajności procesu absorpcji, a spadkiem temperatury jest dobrze znana i wynika z egzotermicznego charakteru procesu absorpcji. Otrzymany stopień absorpcji BTEX wraz ze spadkiem temperatury z 25 do 10°C wzrasta z 51,9 do 55,4%. Tę samą tendencję otrzymano w przypadku absorpcji metanu, gdzie stopień wchłaniania wzrasta z 0,73 do 0,81%. Z punktu widzenia przemysłowych procesów absorpcyjnych wzrost rozpuszczalności CH_4 w absorbentach jest niekorzystny Otrzymana wartość rozpuszczalności metanu osiąga maksymalnie 2% [158]. Jest to wartość, która nie przekracza dopuszczalnej wartości. W przypadku CO_2 zaobserwowano znikomą rozpuszczalność w DES. Z otrzymanych wyników można zatem stwierdzić, że proces absorpcji jest selektywny dla związków z grupy węglowodorów monoaromatycznych. W przeprowadzonych procesach absorpcyjnych w powiększonej skali otrzymano całkowitą zdolność absorpcji BTEX na poziomie 0,05 g/g (25 °C) oraz 0,056 g/g (10°C). Otrzymane wartości są porównywalne z dostępnymi na rynku absorbentami. Niski koszt produkcji DES, możliwość wielokrotnej regeneracji bez wpływu na strukturę DES i bez znaczącego obniżenia wydajności absorpcji, sprawiają, że DES jest doskonałą „zieloną" alternatywą dla pozostałych mediów absorpcyjnych.

3.6. Kontrola procesowa

W kolejnej części badań szczególną uwagę zwrócono na wykazanie przydatności alternatywnej metody kontroli procesowej z wykorzystaniem matrycy czujników gazu do monitorowania procesów absorpcyjnych. W **Publikacji 7** wykorzystano i sprawdzono prototyp matrycy czujnikowej zbudowanej z dwóch czujników typu MOS: TGS2600 i TGS2611. Wybór prezentowanych modeli czujników wynikał z ich wysokiej czułości na LZO, niski koszt, długą żywotność oraz łatwość przetwarzania sygnału. Prototyp matrycy czujnikowej oraz technikę referencyjną (GC-FID) wykorzystano jako metody kontroli procesowej absorpcyjnego uzdatniania modelowego strumienia biogazu z LZO. Modelowy strumień biogazu składał się z mieszaniny $CH_4:CO_2$ w stosunku objętościowym 75:25 oraz zanieczyszczeń tj.: cykloheksan (CH), 1-butanol (BuOH), toluen (T), disiarczek dimetylu (DMDS) i aldehyd propionowy (AP) na poziomie 16 ppm v/v. Badania absorpcji w układzie dynamicznym prowadzono w temperaturze pokojowej z zastosowaniem absorbentów na bazie DES (C:G (1:1) i ChCl:U (1:2)) oraz rozpuszczalników organicznych (n-heksadekan). Próbki biogazu monitorowano na wlocie i wylocie z kolumny barbotażowej.

Kontrola procesowa z wykorzystaniem matrycy czujnikowej polegała na poborze próbek gazowych na wlocie i wylocie kolumny barbotażowej, które były kierowane do worków typu TEDLAR przez określony czas. Z worków Tedlarowych badana próbka była kierowana do komory czujnikowej. Prędkość przez komorę pomiarową była stała i wynosiła 300 mL/min. Ze względu na wysokie stężenie metanu próbki przed wlotem do komory pomiarowej były rozcieńczane powietrzem. Matryca czujnikowa pracowała w trybie stop - czas przepływu próbki przez komorę wynosił 60 sekund oraz flow - czas zatrzymania próbki w komorze pomiarowej wynosił 30 sekund. Uzyskane sygnały z czujników automatycznie były zapisywane w pamięci komputera za pomocą przetwornika analogowo-cyfrowego. Zarejestrowane sygnały konwertowano do przestrzeni dwuwymiarowej. Konwersja sygnału umożliwiła określenie procentowej efektywności uzdatniania biogazu, którą porównano efektywnością absorpcji otrzymaną za pomocą metody referencyjnej. Porównane efektywności uzdatniania nie różnią od siebie znacząco. Największe różnice na poziomie 24-31% dla wszystkich absorbentów otrzymano względem DMDS. Różnice te wynikały z bardzo niskich wartości czułości na DMDS obu zastosowanych czujników w matrycy czujnikowej. Ze względu na to sygnały DMDS były znacznie niższe, a błąd oszacowania efektywności uzdatniania większy.

Wyniki uzyskane w ramach **Publikacji 7** wykazały, że matryce czujnikowe mogą być z powodzeniem wykorzystywane do monitorowania procesu oczyszczania biogazu metodą absorpcyjną. Zastosowanie alternatywnej, znacznie tańszej, metody względem chromatografii gazowej, umożliwia znacznie krótszy czas pojedynczej analizy oraz łatwą możliwość automatyzacji procesu. W ramach **Publikacji 7** wykazano również, że nowo otrzymany DES na bazie C:G (1:1) wykazuje najwyższe wartości skuteczności oczyszczania modelowego biogazu zarówno z pojedynczych LZO, jak i z ich mieszaniny. Ze względu na duży potencjał wykorzystania matryc czujnikowych do monitorowania procesów absorpcyjnego uzdatniania biogazu w **Publikacji 6** (którą dokładnie opisano w podrozdziale 3.4) wykonano kontrolę procesową za pomocą metody referencyjnej (GC-FID) oraz z wykorzystaniem metody alternatywnej. Matryca czujnikowa wykorzystana w **Publikacji 6** została zbudowana z 5 czujników typu MOS (TGS2600, TGS2602, TGS2603, TGS823, TGS8100) oraz PID-A12, które są czułe na LZO; czujnika SHT25 czułego na zmiany temperatury, wilgotności i ciśnienia atmosferycznego; czujnika NDIR, który jest czuły na CH_4 oraz CO_2. Skonstruowana matryca czujnikowa umożliwiła kontrolę stężeń BTEX w zakresie od 0 do 6600 mg/m^3 oraz dwutlenku węgla i metanu w zakresie 0-100% v/v. Kontrola procesowa z wykorzystaniem matrycy czujnikowej polegała na poborze próbek gazowych do worków typu TEDLAR na wlocie i wylocie kolumny barbotażowej, następnie pomiary czujnikowe wykonywano automatycznie w trybie stop-flow (30s-30s). Otrzymane sygnały czujników rejestrowano za pomocą przetwornika analogowo-cyfrowego i konwertowano go za pomocą dedykowanego oprogramowania. Do analizy sygnałów uzyskanych z matrycy czujnikowej wykorzystano analizę statystyczną opartą na wielokrotnej regresji liniowej (ang. *Multiple Linear Regression,* MLR). Opracowany modele predykcyjny umożliwił określenie liniowej zależności pomiędzy zmiennymi niezależnymi (sygnał czujnika), a zmienną zależną (stężenie zanieczyszczenia). Sygnały z każdego czujnika zostały skalibrowane i zweryfikowany zarówno względem temperatury 25°C, jak i 10°C. Podczas prowadzonych testów kalibracyjnych wykazano, że eukaliptol składnik Eu:OA (1:1) wykazał emisję, która miała wpływ na sygnał czujników gazu. Dlatego też, opracowano sześć modeli MLR: dla strumienia wlotowego (całkowite stężenie BTEX w 10°C i 25°C) oraz strumienia wylotowego (całkowite stężenie BTEX w 10°C i 25°C), jeden wspólny model MLR dla wlotu i wylotu dwutlenku węgla oraz jeden dla metanu w tej samej konfiguracji. Modele MLR dla BTEX opracowano w celu uzyskania przewidywanej całkowitej powierzchni pików chromatograficznych badanych związków. Dla pięciu z sześciu przygotowanych modeli wartości R^2 były większe niż 0,9850. Najniższe wartości R^2 osiągnięto dla strumienia wlotowego BTEX w temperaturze 25°C, które wyniosły 0,9629, co nadal jest więcej niż zadowalające. Emisja eukaliptolu w strumieniach wylotowych wyraźnie wpływa na sygnały z czujnika PID. Dlatego też, dopiero po zmniejszeniu odpowiedzi matrycy na sygnał pochodzący od eukaliptolu stężenia BTEX obliczone za pomocą przygotowanych modeli MLR były zbliżone do wyników chromatograficznych. Opracowane modele MLR posłużyły do obliczenia efektywności procesu absorpcji. Wyniki stężeń określone za pomocą matrycy czujnikowej porównano z chromatografią gazową. Do oceny zgodności i dokładności przygotowanych modeli względem referencyjnych pomiarów chromatograficznych wykorzystano błąd średniokwadratowy (*ang. Root Mean Square Error – RMSE*), który jest najczęściej stosowaną metodą do określania błędu modelu w przewidywaniu zmiennych wyjściowych. Najniższe wartości RMSE na poziomie 0,017 otrzymano dla BTEX w procesie w temperaturze 10°C, natomiast najwyższe na poziomie 0,039 dla dwutlenku węgla w procesie w temperaturze 25°C. Uzyskane wyniki wskazują, że wartości stężeń sumarycznych BTEX, CH_4 i CO_2 w biogazie na wlocie i wylocie nie różnią się istotnie od uzyskanych technikami referencyjnymi. Uzyskane wyniki potwierdzają, że matryce czujników gazowych wraz z odpowiednio dobranym modelem matematycznym mogą charakteryzować się podobnie wysokim poziomem jakości jak wyniki uzyskane techniką chromatografii gazowej. Prezentowany model matrycy czujnikowej oprócz wielu zalet posiada również dwa główne ograniczenia przede wszystkim skala prowadzonych badań oraz możliwość wyznaczenia jedynie sumy BTEX. Z tego względu zaproponowana matryca czujnikowa nie nadawałaby się do bezpośredniego wykorzystania w przemyśle. Jednak zaproponowana alternatywna metoda kontroli procesowej docelowo może świetnie zapełnić lukę pomiędzy czujnikami gazów selektywnymi dla określonych związków chemicznych, a technikami chromatograficznymi.

3.7. Ocena DES

Z ekonomicznego punktu widzenia całkowity koszt technologii absorpcyjnego uzdatniania biogazu w dużym stopniu zależy od ceny absorbentu. Ze względu na to w **Publikacji 8** zbadano wpływ 23 DES złożonych z czwartorzędowych soli amoniowych i tanich składników organicznych jako potencjalne absorbenty do usuwania siloksanów, CO_2 i H_2S z modelowego strumienia biogazu. Do wstępnej preselekcji DES wykorzystano teoretyczny model COSMO-RS. Badania przeprowadzono w analogiczny sposób jak w badaniach opisywanych powyżej. W wyniku teoretycznego obliczenia współczynnika aktywności, entalpii

nadmiarowej oraz stałych Henry'ego badane DES podzielono na trzy grupy. Pierwsza posiadająca największy potencjał do rozpuszczania wszystkich zanieczyszczeń, druga wykazująca efektywną absorpcję tylko do siloksanów oraz trzecią, która nie wykazywała potencjału absorpcji do badanych zanieczyszczeń. Do dalszych badań wytypowano tylko dwa DES na bazie ChCl:U (1:2) i ChCl:OA (1:2), dla których wykonano analizy σ-profilów i σ-potencjału dzięki którym potwierdzono, że główną siłą napędową procesu absorpcji są interakcje elektrostatyczne pomiędzy zanieczyszczeniami biogazu, a DES. W dalszej części badań wykonano analizy ekonomiczne procesów absorpcyjnych wykonywanych za pomocą płuczki (wodnej, aminowej oraz DES), adsorpcji zmiennociśnieniowej oraz separacji membranowej. Jednoznaczne oszacowanie kosztów dla poszczególnych technologii jest trudne ze względu na różnice w kosztach komponentów, materiałów i mediów oraz lokalnych uwarunkowań. Obliczenie całkowitego rocznego kosztu (*ang. Total Annual Cost, TAC*) procesu uszlachetniania biogazu, umożliwiło porównanie kosztów różnych technologii pomiędzy sobą. Wartość TAC dla ChCl:U (1:2) wynosiła 982 510 ± 78 601 EUR i była bardzo zbliżony do TAC dla adsorpcji zmiennociśnieniowej (970 000 EUR). Natomiast dla ChCl:OA (1:2) otrzymano TAC w wysokości 1 095 685 ± 87 654 EUR, której wartość była bardzo zbliżone do TAC dla płuczki aminowej (1 104 000 EUR) i separacji membranowej (1 061 000 EUR). Najniższą wartość TAC otrzymano dla płuczki wodnej (880 000 EUR). Na podstawie TAC obliczono koszt jednostkowy za 1 m^3 czystego biometanu który można uporządkować w następującej kolejność: płuczka aminowa > separacja membranowa > ChCl:OA (1:2) > ChCl:U (1:2) > PSA > płuczka wodna. Dla absorpcji fizycznej z wykorzystaniem DES koszt jednostkowy wynosił 0,35 ± 0,03 EUR/m^3 dla ChCl:U (1:2) oraz 0,37 ± 0,03 EUR/m^3 dla ChCl:OA (1:2). Uzyskane wyniki wskazują na duży potencjał DES w uzdatnianiu biogazu do wysokiej jakości bio-metanu o właściwościach porównywalnych z gazem ziemnym.

Tabela 5 przedstawia kompleksową charakterystykę wszystkich przebadanych w ramach pracy doktorskiej absorbentów na bazie DES, które wykorzystano do uzdatniania biogazu z zanieczyszczeń odorotwórczych. W charakterystyce procesów szczególną uwagę zwrócono na rodzaj użytego DES, rodzaj usuwanych zanieczyszczeń, pojemność/szybkość absorpcyjną DES, koszt DES oraz rodzaj kontroli procesowej.

Tabela 5. Podsumowanie badań absorpcji zanieczyszczeń odorotwórczych z grupy LZO ze strumieni gazowych z wykorzystaniem DES.

DES	LZO	Statyczna analiza przestrzeni nad roztworem	Współczynniki podziału para-ciecz (K) / stała prawa Henry'ego	Dynamiczny proces absorpcji	Modelowy strumień biogazu	Czas nasycenia [min]	Zdolność absorpcji (rozpuszczalność) [mg/g]	Kontrola procesowa	Rodzaj regeneracji cykle absorpcji/ desorpcji	Koszt DES
G:C:Lev (1:1:3)	T AP DCM L2	Warunki: - stężenie: 50 ppm v/v - temperatura: 25 °C - objętość DES: 1,0 mL - czas: 48h	<0,001 0,008 0,057 <0,001	Warunki: - prędkość przepływu: 50 mL/min - objętość DES: 50 mL - stężenie: 50 ppm v/v - ciśnienie: 10 kPa	N_2	1800 1200 1000 2500	n.d.	GC-FID	Adsorpcja na: - węglu aktywnym - cykle: 5	33,0 €
ChCl:U (1:2)	T AP DCM L2		0,026 0,010 0,057 0,012	n.d	n.d	n.d	n.d	GC-FID	n.d	44,6 €
ChCl:Lev (1:2)	T AP DCM L2		0,035 0,008 0,075 0,0085	n.d	n.d	n.d	n.d	GC-FID	n.d	42,5 €
ChCl:DEG (1:2)	T AP DCM L2		0,076 0,010 0,038 0,0096	n.d	n.d	n.d	n.d	GC-FID	n.d	56,9 €
ChCl:Ph (1:2)	DMDS	n.d.	n.d.	Warunki: - prędkość przepływu: 50 mL/min - objętość DES: 50 mL - stężenie: 1 mg/m³	N_2	1050 800 600	n.d.	GC-FID	Adsorpcja na: - węglu aktywny, - żelu krzemionkowy, - tlenku glinu. - cykle: 5	50,6 €
ChCl:EG (1:2)										37,5 €
ChCl:Lev (1:2)										42,5 €
TPABr:TEG (1:3)	L2 L3 D4	n.d.	n.d.	Warunki: - prędkość przepływu: 50 mL/min - objętość DES: 50 mL - stężenie: 1 mg/m³	$CH_4:CO_2$ (2:1 obj.)	375 280 5300	380 g/L 230 g/L 5000 g/L	GC-FID-TCD	Barbotaż azotem: -przepływ: 50 mL/min - temperatura: 90°C - czas: 3h - cykle: 10	66,1 €
C:DA (1:1)	L2 L3 L4 D3 D5	n.d.	n.d.	Warunki: - prędkość przepływu: 50 mL/min - objętość DES: 50 mL - stężenie: 30 g/m³ - ciśnienie: 10 kPa - temperatura: 25°C	$CH_4: CO_2$ (2:1 obj.)	5000 5500 6000 5200 5500	n.d.	GC-FID-TCD	Barbotaż azotem: -przepływ: 70 mL/min - temperatura: 150°C - czas: 90 min - cykle: 5	35,5 €
C:UDA (1:1)	L2 L3 L4 D3 D5					500 1000 1400 1100 1100				95,1 €
C:DDA (1:1)	L2 L3 L4 D3 D5					400 2000 1000 1000 1000				44,0 €

c.d. Tabela 5. Podsumowanie badań absorpcji zanieczyszczeń odorotwórczych z grupy LZO ze strumieni gazowych z wykorzystaniem DES.

DES	LZO	Statyczna analiza przestrzeni nad roztworem	Współczynniki podziału para-ciecz (K) / stała prawa Henry'ego	Dynamiczny proces absorpcji	Modelowy strumień biogazu	Czas nasycenia [min]	Zdolność absorpcji (rozpuszczalność) [mg/g]	Kontrola procesowa	Rodzaj regeneracji cykle absorpcji/ desorpcji	Koszt DES
C:Gu (1:1)	DCM CF TCM TCE TCEtOH	n.d.	n.d.	Warunki: - prędkość przepływu: 50 mL/min - objętość DES: 50 mL - stężenie: 0,5 mg/m³ - ciśnienie: 10 kPa -temperatura: 25°C	$CH_4:CO_2:H_2O:N_2$ (58:38:2:2 obj.)	500 620 400 600 1200	215,0 561,5 320,0 262,4 275,3	GC-FID-TCD	Barbotaż azotem: -przepływ: 70 mL/min - temperatura: 100°C - czas: 1h - cykle: 10	32,78 €
C:Lev (1:2)	DCM CF TCM TCE TCEtOH					275 220 225 280 650	181,0 401,5 143,5 248,0 198,15			24,02 €
Gu:Lev (1:1)	DCM CF TCM TCE TCEtOH					200 550 250 350 800	130,7 399,5 115,8 154,0 161,2			36,02 €
Syr:Lev (1:1)	DCM CF TCM TCE TCEtOH					800 700 450 580 1200	304,0 420,0 360,0 292,0 661,0			263,5 €
C:Gu (1:1)	CH BuOH T DMDS AP	n.d.	n.d.	Warunki: - prędkość przepływu: 500 mL/min - objętość DES: 1000 mL - stężenie: 2000 mg/m³ - temperatura: 25°C	$CH_4:CO_2$ (75:25 obj.)	n.d.	n.d.	GC- FID matryca czujników: - TGS2600 - TGS2611	n.d.	32,78 €
ChCl:U (1:2)	CH BuOH T DMDS AP									44,6 €
E:OA (1:1)	B T E X	Warunki: - stężenie: 1,5 µL/mL - temperatura: RT - objętość DES: 0,5 mL - czas: 24h	n.d.	Warunki: - prędkość przepływu: 500 mL/min - objętość DES: 500 mL - stężenie: 2000 mg/m³ - temperatura: 10°C - ciśnienie: 1 atm	$CH_4:CO_2:N_2$ (5:3:2 obj.)	6500 13700 11500 11500	Suma BTEX: 56	GC-FID-TCD Matryca czujników: - TGS2600 - TGS2602 - TGS2603 - TGS823 - TGS8100 - PID-A12 - NDIR	Barbotaż azotem: - temperatura: 120°C - czas: 3h - cykle: 10	43 €
	B T E X		0,027 0,018 0,013 0,013	Warunki: - prędkość przepływu: 500 mL/min - objętość DES: 500 mL - stężenie: 2000 mg/m³ - ciśnienie: 1 atm - temperatura: 25°C		5000 10500 15000 15000	Suma BTEX: 50			

c.d. Tabela 5. Podsumowanie badań absorpcji zanieczyszczeń odorotwórczych z grupy LZO ze strumieni gazowych z wykorzystaniem DES.

DES	LZO	Statyczna analiza przestrzeni nad roztworem	Współczynniki podziału para-ciecz (K) / stała prawa Henry'ego	Dynamiczny proces absorpcji	Modelowy strumień biogazu	Czas nasycenia [min]	Zdolność absorpcji (rozpuszczalność) [mg/g]	Kontrola procesowa	Rodzaj regeneracji cykle absorpcji/ desorpcji	Koszt DES
C:DA (1:1)	B T E X	Warunki: - stężenie: 1,5 µL/mL - temperatura: RT - objętość DES: 0,5 mL - czas: 24h	0,035 0,024 0,020 0,019	Warunki: - prędkość przepływu: 50 mL/min - objętość DES: 50 mL - stężenie: 2000 mg/m³ - ciśnienie: 10 kPa - temperatura: 25°C	N₂	1536 3221 4452 4562	n.d.	GC-FID	Barbotaż azotem: - temperatura: 120°C - czas: 3h - cykle: 10	35,5 €
C:OA (1:1)	B T E X		0,034 0,027 0,021 0,020			2365 3251 4571 4579				29,9 €
C-one:Lev (1:1)	B T E X		0,038 0,028 0,026 0,025			2103 3065 4498 4507				62,4 €
C-one:OA (1:1)	B T E X		0,031 0,029 0,021 0,019			3108 3215 4165 4007				58,4 €
C-one:NA (1:1)	B T E X		0,033 0,023 0,022 0,020			2789 4256 4259 4264				31,1 €
C-one:DA (1:1)	B T E X		0,035 0,026 0,016 0,015			1997 4984 5845 5856				63,8 €
ChCl:U (1:2)	L2 L3 D4	n.d.	n.d.	Warunki: - prędkość przepływu: 913 m³/h - objętość DES: 2,35 m³ - stężenie: 200 ppm v/v - ciśnienie: 100 kPa - temperatura: 20°C	CH₄:CO₂:H₂S (68:31:1 obj.)	1313,4 1245,6 1470,6	1,42 mol/L 0,99 mol/L 1,09 mol/L	-	Kolumna odpędowa: - temperatura 115–125 ◦C - ciśnienie powietrza ok 140-170 kPa. - strumień powietrza wlotowego 403 m3/h - cykle: 73 i 60	44,6 €
ChCl:OA (1:2)	L2 L3 D4					223,8 120,6 187,2	0,24 mol/L 0,10 mol/L 0,14 mol/L	-		50,3 €

4. Wnioski końcowe

Niniejsza praca, przedstawia nowe i ekonomicznie opłacalne sorbenty do efektywnego oczyszczania strumieni biogazu z substancji uciążliwych zapachowo oraz wykazuje możliwość zastosowania matryc czujnikowych do monitorowania procesu uzdatniania biogazu do gazu wysokometanowego. W ramach pracy otrzymano następujące potencjalne korzyści, które stanowią nowość naukową:

1) Otrzymano nowe sorbenty na bazie cieczy głęboko eutektycznych DES (nigdy wcześniej niepublikowanych) z nietoksycznych, tanich i łatwo dostępnych związków.
2) Przygotowane DES stanowią nową klasę absorbentów, a koncepcja ich otrzymywania nawiązuje do aktualnych trendów zielonej chemii.
3) Szczegółowe badania mechanizmów powstawania DES, oparte na technikach spektroskopowych i obliczeniowym modelowaniu molekularnym, znacznie zwiększyły obecny stan wiedzy na temat wpływu poszczególnych oddziaływań pomiędzy HBA i HBD podczas tworzenie nowych DES.
4) Badania szeregu właściwości fizykochemicznych nowych DES dostarczyły ważnych informacji przy doborze warunków procesów absorpcyjnych. Otrzymane informacje stanowią przydatny zbiór danych, który może być wykorzystywany przez szerokie grona odbiorców przy doborze warunków innych technik separacyjnych.
5) Badania eksperymentalne połączone z badaniami teoretycznymi nad usuwaniem zanieczyszczeń odorotwórczych z wykorzystaniem nowych DES dostarczyły wielu informacji, które umożliwiły lepsze zrozumienie zachodzących mechanizmów podczas procesu absorpcji fizycznej. Uzyskane wyniki z pewnością przyczynią się w przyszłości do racjonalnego projektowania zadaniowych DES-ów.
6) Przeprowadzone badania wpływu wielu parametrów (rodzaj zanieczyszczeń, stężenie, temperatura, czas, objętość absorbentów, szybkość przepływu modelowego strumienia biogazu) na proces absorpcji uzupełniły stan wiedzy dotyczący przydatności DES do procesów absorpcji.
7) Przeprowadzone badania z zastosowaniem alternatywnej techniki kontroli procesowej potwierdziły, że nowa metodyka z wykorzystaniem matrycy czujników gazowych jest w pełni uzasadniona i porównywalna na akceptowalnym poziomie z chromatografia gazową.
8) W przeprowadzonych badaniach wykazano konkurencyjność absorbentów na bazie DES do obecnie stosowanych konwencjonalnych sorbentów, zarówno w zakresie możliwości regeneracyjnych jak i budżetowych.
9) Wszystkie przedstawione procesy absorpcyjne z wykorzystaniem DES i kontrolą procesową z zastosowaniem matryc czujnikowych charakteryzują się wysokim potencjałem aplikacyjnym.

Przedstawione wyniki badań opisują kompleksową charakterystykę procesu absorpcyjnego oczyszczania biogazu ze związków odorotwórczych z wykorzystaniem nowych absorbentów oraz nowego zastosowania matrycy czujników gazu do kontroli procesów absorpcyjnych.

5. Literatura

[1]   OECD, IEA, OECD Green Growth Studies: Preliminary version, 2011.

[2]   C.A.L.S. Institute, DYREKTYWA PARLAMENTU EUROPEJSKIEGO I RADY, Bruksela, 2022. https://doi.org/10.2833/239077.

[3]   E. Commission, Commission Proposes New EU Framework to Decarbonise Gas Markets, Promote Hydrogen and Reduce Methane Emissions, Energy Transitions Futur. Gas EU. (2020) 37–89. https://doi.org/10.1007/978-3-030-32614-2_3.

[4]   BP, Statistical Review of World Energy 2021, London, UK, 2021.

[5]   E. Commission., Proposal for a Directive of the European Parliament and of the Council on Common Rules for the Internal Markets in Renewable and Natural Gases and in Hydrogen, Brussels, Belgium, 2010. https://doi.org/10.1017/cbo9780511664885.046.

[6]   T. Nevzorova, V. Kutcherov, Barriers to the wider implementation of biogas as a source of energy: A state-of-the-art review, Energy Strateg. Rev. 26 (2019) 100414. https://doi.org/10.1016/j.esr.2019.100414.

[7]   International Energy Agency, Outlook for biogas and biomethane. Prospects for organic growth, IEA Publ. (2020) 1–93. https://www.iea.org/reports/outlook-for-biogas-and-biomethane-prospects-for-organic-growth, License: CC BY 4.0.

[8]   M.-A. Eyl-Mazzega, C. Mathieu, K. Boesgaard, S. Cornot-Gandolphe, J. Daniel-Gromke, V. Denysenko, J. Liebetrau, Renewable gas and regulation in Germany , Denmark , Italy , and Netherlands, 2019. https://www.ifri.org/en/publications/etudes-de-lifri/biogas-and-biomethane-europe-lessons-denmark-germany-and-italy.

[9]   S. Alberici, M. Moultak, J. Peters, The future role of biomethane, (2021).

[10]   National Centre for Emission Management (KOBiZE), Poland ' s National Inventory Report 2022_lata 1988-2020, Poland, Warsaw, 2022. https://unfccc.int/documents/461818.

[11]   L. Appels, J. Baeyens, J. Degrève, R. Dewil, Principles and potential of the anaerobic digestion of waste-activated sludge, Prog. Energy Combust. Sci. 34 (2008) 755–781. https://doi.org/10.1016/j.pecs.2008.06.002.

[12]   J.I. Salazar Gómez, H. Lohmann, J. Krassowski, Determination of volatile organic compounds from biowaste and co-fermentation biogas plants by single-sorbent adsorption, Chemosphere. 153 (2016) 48–57. https://doi.org/10.1016/j.chemosphere.2016.02.128.

[13]   M.Y. Mustafa, R.K. Calay, E. Román, Biogas from Organic Waste - A Case Study, Procedia Eng. 146 (2016) 310–317. https://doi.org/10.1016/J.PROENG.2016.06.397.

[14]   M.A. Perea-Moreno, E. Samerón-Manzano, A.J. Perea-Moreno, Biomass as renewable energy: Worldwide research trends, Sustainability. 11 (2019). https://doi.org/10.3390/su11030863.

[15]   S. Rasi, Biogas Composition and Upgrading to Biomethane Saija Rasi Biogas Composition and Upgrading to Biomethane, 2009.

[16]   S.Ã. Rasi, A. Veijanen, J. Rintala, Trace compounds of biogas from different biogas production plants, 32 (2007) 1375–1380. https://doi.org/10.1016/j.energy.2006.10.018.

[17]   S. Rasi, J. Läntelä, A. Veijanen, J. Rintala, Landfill gas upgrading with countercurrent water wash, Waste Manag. 28 (2008) 1528–1534. https://doi.org/10.1016/j.wasman.2007.03.032.

[18]   J. Lemus, M. Martin-Martinez, J. Palomar, L. Gomez-Sainero, M.A. Gilarranz, J.J. Rodriguez, Removal of chlorinated organic volatile compounds by gas phase adsorption with activated carbon, Chem. Eng. J. 211–212 (2012) 246–254. https://doi.org/10.1016/j.cej.2012.09.021.

[19]   E. Smet, H. Van Langenhove, Abatement of volatile organic sulfur compounds in odorous emissions from the bio-industry, Biodegradation. 9 (1998) 273–284. https://doi.org/10.1023/a:1008281609966.

[20]   F.A.T. Andersson, A. Karlsson, B.H. Svensson, J. Ejlertsson, Occurrence and abatement of volatile sulfur compounds during biogas production, J. Air Waste Manag. Assoc. 54 (2004) 855–861. https://doi.org/10.1080/10473289.2004.10470953.

[21]   B.P. Lomans, C. Van Der Drift, a Pol, H.J.M.O. Den Camp, Cellular and Molecular Life Sciences Microbial cycling of volatile organic sulfur compounds, Cell. Mol. Life Sci. 59 (2002) 575–588.

[22]   E. Smet, P. Lens, H. Van Langenhove, Treatment of waste gases contaminated with odorous sulfur compounds, Crit. Rev. Environ. Sci. Technol. 28 (1998) 89–117. https://doi.org/10.1080/10643389891254179.

[23]   A.N. Baghani, A. Sorooshian, M. Heydari, R. Sheikhi, S. Golbaz, Q. Ashournejad, M. Kermani, F. Golkhorshidi, A. Barkhordari, A.J. Jafari, M. Delikhoon, A. Shahsavani, A case study of BTEX characteristics and health effects by major point sources of pollution during winter in Iran, Environ. Pollut. 247 (2019) 607–617. https://doi.org/10.1016/J.ENVPOL.2019.01.070.

[24]   M.J. Milazzo, J.M. Gohlke, D.L. Gallagher, A.A. Scott, B.F. Zaitchik, L.C. Marr, Potential for city parks to reduce exposure to BTEX in air, Environ. Sci. Process. Impacts. 21 (2019) 40–50. https://doi.org/10.1039/c8em00252e.

[25]   C. Peng, J.W. Lee, H.T. Sichani, J.C. Ng, Toxic effects of individual and combined effects of BTEX on Euglena gracilis, J. Hazard. Mater. 284 (2015) 10–18. https://doi.org/10.1016/J.JHAZMAT.2014.10.024.

[26]   F. Abbasi, H. Pasalari, J.M. Delgado-Saborit, A. Rafiee, A. Abbasi, M. Hoseini, Characterization and risk assessment of BTEX in ambient air of a Middle Eastern City, Process Saf. Environ. Prot. 139 (2020) 98–105. https://doi.org/10.1016/J.PSEP.2020.03.019.

[27]   Y. Li, C.P. Alaimo, M. Kim, N.Y. Kado, J. Peppers, J. Xue, C. Wan, P.G. Green, R. Zhang, B.M. Jenkins, C.F.A. Vogel, S. Wuertz, T.M. Young, M.J. Kleeman, Composition and Toxicity of Biogas Produced from Different Feedstocks in California, Environ. Sci. Technol. (2019). https://doi.org/10.1021/acs.est.9b03003.

[28]   E. Durmusoglu, F. Taspinar, A. Karademir, Health risk assessment of BTEX emissions in the landfill environment, J. Hazard. Mater. 176 (2010) 870–877. https://doi.org/10.1016/j.jhazmat.2009.11.117.

[29]   J.G.C. Bretón, R.M.C. Bretón, S.M. Morales, J.D.W. Kahl, C. Guarnaccia, R. del Carmen Lara Severino, M.R. Marrón, E.R. Lara, M. de la Luz Espinosa Fuentes, M.P.U. Chi, G.L. Sánchez, Health risk assessment of the levels of BTEX in ambient air of one urban site located in leon, guanajuato, mexico during two climatic seasons, Atmosphere (Basel). 11 (2020). https://doi.org/10.3390/atmos11020165.

[30]   J. Zheng, M. Shao, W. Che, L. Zhang, L. Zhong, Y. Zhang, D. Streets, Speciated VOC emission inventory and spatial patterns of ozone formation potential in the Pearl River Delta, China, Environ. Sci. Technol. 43 (2009) 8580–8586. https://doi.org/10.1021/es901688e.

[31]   K.A.U. Johansson, Characterisation of contaminants in biogas before and after upgrading to vehicle gas, Rapp. SGC 246. (2012).

[32]   E. Ryckebosch, M. Drouillon, H. Vervaeren, Techniques for transformation of biogas to biomethane, Biomass and Bioenergy. 35 (2011) 1633–1645. https://doi.org/10.1016/j.biombioe.2011.02.033.

[33] E. Santos-Clotas, A. Cabrera-Codony, E. Boada, F. Gich, R. Muñoz, M.J. Martín, Efficient removal of siloxanes and volatile organic compounds from sewage biogas by an anoxic biotrickling filter supplemented with activated carbon, Bioresour. Technol. 294 (2019) 122136. https://doi.org/10.1016/J.BIORTECH.2019.122136.

[34] S. Rasi, J. Läntelä, J. Rintala, Trace compounds affecting biogas energy utilisation – A review, Energy Convers. Manag. 52 (2020) 3369–3375. https://doi.org/10.1016/j.enconman.2011.07.005.

[35] J. Rasi S., Veijanen, A., Rintala, Trace compounds of biogas from different biogas production plants, Energy. 32 (2007) 1375–1380. https://doi.org/10.1016/J.ENERGY.2006.10.018.

[36] I.A. Arkharov, E.N. Simakova, E.S. Navasardyan, Landfill Gas as Feedstock for Energy and Industrial Processes, Chem. Pet. Eng. 52 (2016) 547–551. https://doi.org/10.1007/s10556-016-0229-y.

[37] A. Jaffrin, N. Bentounes, A.M. Joan, S. Makhlouf, Landfill biogas for heating greenhouses and providing carbon dioxide supplement for plant growth, Biosyst. Eng. 86 (2003) 113–123. https://doi.org/10.1016/S1537-5110(03)00110-7.

[38] R.J. Spiegel, J.L. Preston, Technical assessment of fuel cell operation on landfill gas at the Groton, CT, landfill, Energy. 28 (2003) 397–409. https://doi.org/10.1016/S0360-5442(02)00118-4.

[39] H.C. Shin, J.W. Park, K. Park, H.C. Song, Removal characteristics of trace compounds of landfill gas by activated carbon adsorption, Environ. Pollut. 119 (2002) 227–236. https://doi.org/10.1016/S0269-7491(01)00331-1.

[40] F. Dincer, M. Odabasi, A. Muezzinoglu, Chemical characterization of odorous gases at a landfill site by gas chromatography-mass spectrometry, J. Chromatogr. A. 1122 (2006) 222–229. https://doi.org/10.1016/j.chroma.2006.04.075.

[41] B. V. Nielsen, S. Maneein, M.D. Mahmud Al Farid, J.J. Milledge, The effects of halogenated compounds on the anaerobic digestion of macroalgae, Fermentation. 6 (2020). https://doi.org/10.3390/FERMENTATION6030085.

[42] M.D. Rey, R. Font, I. Aracil, Biogas from MSW landfill: Composition and determination of chlorine content with the AOX (adsorbable organically bound halogens) technique, Energy. 63 (2013) 161–167. https://doi.org/10.1016/j.energy.2013.09.017.

[43] A. Buekens, H. Huang, Comparative evaluation of techniques for controlling the formation and emission of chlorinated dioxins/furans in municipal waste incineration, J. Hazard. Mater. 62 (1998) 1–33. https://doi.org/https://doi.org/10.1016/S0304-3894(98)00153-8.

[44] M. Miltner, A. Makaruk, M. Harasek, Review on available biogas upgrading technologies and innovations towards advanced solutions, J. Clean. Prod. 161 (2017) 1329–1337. https://doi.org/10.1016/J.JCLEPRO.2017.06.045.

[45] I. Angelidaki, L. Xie, G. Luo, Y. Zhang, H. Oechsner, A. Lemmer, R. Munoz, P.G. Kougias, Biogas Upgrading: Current and Emerging Technologies, Biofuels Altern. Feed. Convers. Process. Prod. Liq. Gaseous Biofuels. (2019) 817–843. https://doi.org/10.1016/B978-0-12-816856-1.00033-6.

[46] A.A. Bletsou, A.G. Asimakopoulos, A.S. Stasinakis, N.S. Thomaidis, K. Kannan, Mass loading and fate of linear and cyclic siloxanes in a wastewater treatment plant in Greece, Environ. Sci. Technol. 47 (2013) 1824–1832. https://doi.org/10.1021/es304369b.

[47] T. Matsui, S. Imamura, Removal of siloxane from digestion gas of sewage sludge, Bioresour. Technol. 101 (2010) S29–S32. https://doi.org/10.1016/j.biortech.2009.05.037.

[48] E.Y. Companioni-Damas, F.J. Santos, M.T. Galceran, Linear and cyclic methylsiloxanes in air by concurrent solvent recondensation-large volume injection-gas chromatography-mass spectrometry, Talanta. 118 (2014) 245–252. https://doi.org/10.1016/j.talanta.2013.10.020.

[49] M. Arnold, VTT RESEARCH NOTES 2496 Reduction and monitoring of biogas trace compounds, 2006. http://www.vtt.fi/publications/index.jsp.

[50] R. Dewil, L. Appels, J. Baeyens, Energy use of biogas hampered by the presence of siloxanes, Energy Convers. Manag. 47 (2006) 1711–1722. https://doi.org/10.1016/j.enconman.2005.10.016.

[51] P. Tower, New Techn0Logy for Removal of Siloxanes in Digester Gas Results in Lower Maintenance Costs and Air Quality Benefits in Power Generation Equipment, Proc. Water Environ. Fed. 2003 (2012) 440–447. https://doi.org/10.2175/193864703784639859.

[52] O. Sevimoğlu, B. Tansel, Effect of persistent trace compounds in landfill gas on engine performance during energy recovery: A case study, Waste Manag. 33 (2013) 74–80. https://doi.org/10.1016/J.WASMAN.2012.08.016.

[53] A.M. Klepacka, J. Skudlarski, E. Golisz, Aktualny stan sektora biogazu rolniczego w Polsce na tle krajów Unii Europejskiej, (n.d.) 203–212.

[54] J. Liebetrau, V. Denysenko, J.D. Gromke, IEA Bioenergy Task 37: Country Report Germany 2020, 2020. http://task37.ieabioenergy.com/country-reports.html?file=files/daten-redaktion/download/publications/country-reports/Germany 2020.pdf.

[55] M.A. Jaro, J.; Gräf, D.; Schimmel, Gas for Climate Report Market State and Trends in Renewable and Low-Carbon Gases in Europe, (2021). https://www.europeanbiogas.eu/wp-content/uploads/2021/12/Gas-for-Climate-Market-State-and-Trends-report-2021.pdf.

[56] J. Thual, French Report IEA TF 37, 2020. https://task37.ieabioenergy.com/wp-content/uploads/sites/32/2022/12/France_Country_report_05_2022.pdf.

[57] W.K. Biswas, M. John, Biogas solutions – sustainability, climate and conditions for implementation, 2022. https://doi.org/10.1002/9781119721079.ch1.

[58] C. Lukehurst, UK Country Report Task 37 (UK), 2017. https://task37.ieabioenergy.com/country-reports.

[59] N. Naffine, Country Report Australia, 2000. https://doi.org/10.1007/978-3-642-57256-2_2.

[60] M.. et al. Banasik, P.; Białowiec, A.; Czekała, W.; Chomiuk, D.; Dach, J.; Filipiak, I.; Fugol, M.; Kacała, M.; Kowalczyk-Juśko, A.; Kolasiński, Raport Biogaz w Polsce, 2021. https://magazynbiomasa.pl/raport-biogaz-w-polsce-2022-pobierz-i-czytaj-za-darmo/.

[61] O. and G.I.– N.R.I. Poland, REPORT THE AGRICULTURAL BIOGAS PLANTS, 2014. https://www.globalmethane.org/documents/Poland-Ag-Biogas-Plants-April-2014.pdf.

[62] ROZPORZĄDZENIE MINISTRA GOSPODARKI 1) z dnia 24 sierpnia 2011 r. w sprawie szczegółowego zakresu obowiązku potwierdzania danych dotyczących wytwarzanego biogazu rolniczego wprowadzonego do sieci dystrybucyjnej gazowej, (2011).

[63] O. Wesley, A. Yaqian, Z. Ange, N. Doan, P. Minh, A Review of Biogas Utilisation , Purification and Upgrading Technologies, Waste and Biomass Valorization. 8 (2017) 267–283. https://doi.org/10.1007/s12649-016-9826-4.

[64]   B. Workshop, European biomethane standards for grid injection and vehicle fuel use, (2017).

[65]   I.S. Chang, J. Zhao, X. Yin, J. Wu, Z. Jia, L. Wang, Comprehensive utilizations of biogas in Inner Mongolia, China, Renew. Sustain. Energy Rev. 15 (2011) 1442–1453. https://doi.org/10.1016/j.rser.2010.11.013.

[66]   Q. Sun, H. Li, J. Yan, L. Liu, Z. Yu, X. Yu, Selection of appropriate biogas upgrading technology-a review of biogas cleaning, upgrading and utilisation, Renew. Sustain. Energy Rev. 51 (2015) 521–532. https://doi.org/10.1016/j.rser.2015.06.029.

[67]   M. Persson, O. Jonsson, A. Wellinger, Biogas Upgrading To Vehicle Fuel Standards and Grid, 2007. http://task37.ieabioenergy.com/files/daten-redaktion/download/publi-task37/upgrading_report_final.pdf.

[68]   A. Carranza-Abaid, R.R. Wanderley, H.K. Knuutila, J.P. Jakobsen, Analysis and selection of optimal solvent-based technologies for biogas upgrading, Fuel. 303 (2021). https://doi.org/10.1016/j.fuel.2021.121327.

[69]   B. Kazmi, J. Haider, M.A. Qyyum, S. Saeed, M.R. Kazmi, M. Lee, Heating load depreciation in the solvent-regeneration step of absorption-based acid gas removal using an ionic liquid with an imidazolium-based cation, Int. J. Greenh. Gas Control. 87 (2019) 89–99. https://doi.org/10.1016/j.ijggc.2019.05.007.

[70]   B. Wu, X. Zhang, D. Bao, Y. Xu, S. Zhang, L. Deng, Biomethane production system: Energetic analysis of various scenarios, Bioresour. Technol. 206 (2016) 155–163. https://doi.org/10.1016/j.biortech.2016.01.086.

[71]   F.M. Baena-Moreno, E. le Saché, L. Pastor-Pérez, T.R. Reina, Membrane-based technologies for biogas upgrading: a review, Environ. Chem. Lett. 18 (2020) 1649–1658. https://doi.org/10.1007/s10311-020-01036-3.

[72]   M.A. Qyyum, J. Haider, K. Qadeer, V. Valentina, A. Khan, M. Yasin, M. Aslam, G. De Guido, L.A. Pellegrini, M. Lee, Biogas to liquefied biomethane: Assessment of 3P's–Production, processing, and prospects, Renew. Sustain. Energy Rev. 119 (2020) 109561. https://doi.org/10.1016/j.rser.2019.109561.

[73]   R. Kadam, N.L. Panwar, Recent advancement in biogas enrichment and its applications, Renew. Sustain. Energy Rev. 73 (2017) 892–903. https://doi.org/10.1016/j.rser.2017.01.167.

[74]   S. Zhang, H. He, Q. Zhou, X. Zhang, X. Lu, Y. Tian, Principles and strategies for green process engineering, Green Chem. Eng. 3 (2022) 1–4. https://doi.org/10.1016/j.gce.2021.11.008.

[75]   D.J.C. Constable, Green and sustainable chemistry – The case for a systems-based, interdisciplinary approach, IScience. 24 (2021) 103489. https://doi.org/10.1016/j.isci.2021.103489.

[76]   A. Ghayur, T.V. Verheyen, E. Meuleman, Biological and chemical treatment technologies for waste amines from CO_2 capture plants, J. Environ. Manage. 241 (2019) 514–524. https://doi.org/10.1016/j.jenvman.2018.07.033.

[77]   M. Scholz, B. Frank, F. Stockmeier, S. Falß, M. Wessling, Techno-economic analysis of hybrid processes for biogas upgrading, Ind. Eng. Chem. Res. 52 (2013) 16929–16938. https://doi.org/10.1021/ie402660s.

[78]   S.J. Hoff, D.S. Bundy, M.A. Nelson, B.C. Zelle, L.D. Jacobson, A.J. Heber, J. Ni, Y. Zhang, J.A. Koziel, D.B. Beasley, Emissions of ammonia, hydrogen sulfide, and odor before, during, and after slurry removal from a deep-pit swine finisher, J. Air Waste Manag. Assoc. 56 (2006) 581–590. https://doi.org/10.1080/10473289.2006.10464472.

[79]   P.J. E. Wheless, Siloxanes in landfill and digester gas update, 2004.

[80]   and D.J.W. N. Korens, D. R. Simbeck, Process Screening Analysis of Alternative Gas Treating and Sulfur Removal for Gasification, 2002.

[81]   G. Darracq, A. Couvert, C. Couriol, A. Amrane, D. Thomas, E. Dumont, Y. Andres, P. Le Cloirec, Erratum: Silicone oil: An effective absorbent for the removal of hydrophobic volatile organic compounds, J. Chem. Technol. Biotechnol. 86 (2011) 324. https://doi.org/10.1002/jctb.2545.

[82]   C. Rojas Devia, A. Subrenat, Absorption of a linear (l2) and a cyclic (d4) siloxane using different oils: Application to biogas treatment, Environ. Technol. (United Kingdom). 34 (2013) 3117–3127. https://doi.org/10.1080/09593330.2013.804588.

[83]   M. Feroskhan, S. Ismail, A review on the purification and use of biogas in compression ignition engines, Int. J. Automot. Mech. Eng. 14 (2017) 4383–4400. https://doi.org/10.15282/ijame.14.3.2017.1.0348.

[84]   L. Ghorbel, R. Tatin, A. Couvert, Relevance of an organic solvent for absorption of siloxanes, Environ. Technol. (United Kingdom). 35 (2014) 372–382. https://doi.org/10.1080/09593330.2013.828778.

[85]   A. Bello, R.O. Idem, Comprehensive Study of the Kinetics of the Oxidative Degradation of CO_2 Loaded and Concentrated Aqueous Monoethanolamine (MEA) with and without Sodium Metavanadate during CO_2 Absorption from Flue Gases, (2006) 2569–2579. https://doi.org/10.1021/ie050562x.

[86]   T. Supap, R. Idem, P. Tontiwachwuthikul, C. Saiwan, Analysis of monoethanolamine and its oxidative degradation products during CO_2 absorption from flue gases: A comparative study of GC-MS, HPLC-RID, and CE-DAD analytical techniques and possible optimum combinations, Ind. Eng. Chem. Res. 45 (2006) 2437–2451. https://doi.org/10.1021/ie050559d.

[87]   O.I. Maile, H. Tesfagiorgis, E. Muzenda, The potency of monoethanolamine in biogas purification and upgrading, South African J. Chem. Eng. 24 (2017) 122–127. https://doi.org/10.1016/j.sajce.2017.06.004.

[88]   Z. Xiang, Y. Lu, X. Gong, G. Luo, Absorption and desorption of gaseous toluene by an absorbent microcapsules column, J. Hazard. Mater. 173 (2010) 243–248. https://doi.org/10.1016/j.jhazmat.2009.08.075.

[89]   R. Hadjoudj, H. Monnier, C. Roizard, F. Lapicque, Measurements of diffusivity of chlorinated VOCs in heavy absorption solvents using a laminar falling film contactor, Chem. Eng. Process. Process Intensif. 47 (2008) 1478–1483. https://doi.org/10.1016/j.cep.2007.04.014.

[90]   B. Park, G. Hwang, S. Haam, C. Lee, I.S. Ahn, K. Lee, Absorption of a volatile organic compound by a jet loop reactor with circulation of a surfactant solution: Performance evaluation, J. Hazard. Mater. 153 (2008) 735–741. https://doi.org/10.1016/j.jhazmat.2007.09.016.

[91]   C. Dai, M. Chen, W. Mu, B. Peng, G. Yu, N. Liu, R. Xu, N. Wang, B. Chen, Highly efficient toluene absorption with π -electron donor-based deep eutectic solvents, Sep. Purif. Technol. 298 (2022) 121618. https://doi.org/10.1016/j.seppur.2022.121618.

[92]   C. Zhang, J. Wu, R. Wang, E. Ma, L. Wu, J. Bai, J. Wang, Study of the toluene absorption capacity and mechanism of ionic liquids using COSMO-RS prediction and experimental verification, Green Energy Environ. 6 (2021) 339–349. https://doi.org/10.1016/J.GEE.2020.08.001.

[93]   N.Y. Yusuf, M.S. Masdar, W.N.R.W. Isahak, D. Nordin, T. Husaini, E.H. Majlan, S.A.M. Rejab, C.L. Chew, Ionic liquid-impregnated activated carbon for biohydrogen purification in an adsorption unit, IOP Conf. Ser. Mater. Sci. Eng. 206 (2017). https://doi.org/10.1088/1757-899X/206/1/012071.

[94]   S. Sarmad, J.-P. Mikkola, X. Ji, CO_2 capture with Ionic liquids (ILs) and Deep Eutectic Solvents (DESs): a new generation of sorbents, Wiley-VCH. 10(2) (2016) 324–352. https://doi.org/10.1002/cssc.201600987.

[95]   R. Santiago, J. Lemus, A.X. Outomuro, J. Bedia, J. Palomar, Assessment of ionic liquids as H_2S physical absorbents by

thermodynamic and kinetic analysis based on process simulation, Sep. Purif. Technol. 233 (2020) 116050. https://doi.org/10.1016/j.seppur.2019.116050.

[96]   Y. Zhao, H. Gao, X. Zhang, Y. Huang, D. Bao, S. Zhang, Hydrogen Sulfi de Solubility in Ionic Liquids (ILs): An Extensive Database and a New ELM Model Mainly Established by Imidazolium- Based ILs, (2016). https://doi.org/10.1021/acs.jced.6b00449.

[97]   D. Hospital-benito, T. Welton, J.P. Hallett, Process Analysis of Ionic Liquid-Based Blends as H 2 S Absorbents: Search for Thermodynamic/Kinetic Synergies′, (2021). https://doi.org/10.1021/acssuschemeng.0c07229.

[98]   J. Palomar, M. Gonzalez-miquel, J. Bedia, F. Rodriguez, J.J. Rodriguez, Task-specific ionic liquids for efficient ammonia absorption, Sep. Purif. Technol. 82 (2011) 43–52. https://doi.org/10.1016/j.seppur.2011.08.014.

[99]   J. Lemus, J. Bedia, C. Moya, N. Alonso-Morales, M.A. Gilarranz, J. Palomar, J.J. Rodriguez, Ammonia capture from the gas phase by encapsulated ionic liquids (ENILs), RSC Adv. 6 (2016) 61650–61660. https://doi.org/10.1039/c6ra11685j.

[100]   J. De Riva, V. Ferro, C. Moya, M.A. Stadtherr, J.F. Brennecke, J. Palomar, International Journal of Greenhouse Gas Control Aspen Plus supported analysis of the post-combustion CO 2 capture by chemical absorption using the [P 2228][CNPyr] and [P 66614][CNPyr] AHA Ionic Liquids, Int. J. Greenh. Gas Control. 78 (2018) 94–102. https://doi.org/10.1016/j.ijggc.2018.07.016.

[101]   R. Santiago, C. Moya, J. Palomar, Siloxanes capture by ionic liquids: Solvent selection and process evaluation, Chem. Eng. J. 401 (2020) 126078. https://doi.org/10.1016/j.cej.2020.126078.

[102]   A.-S. Rodriguez Castillo, P.-F. Biard, S. Guihéneuf, L. Paquin, A. Amrane, A. Couvert, Assessment of VOC absorption in hydrophobic ionic liquids: Measurement of partition and diffusion coefficients and simulation of a packed column, Chem. Eng. J. 360 (2019) 1416–1426. https://doi.org/https://doi.org/10.1016/j.cej.2018.10.146.

[103]   G. Quijano, A. Couvert, A. Amrane, G. Darracq, C. Couriol, P. Le, L. Paquin, D. Carrie, Potential of ionic liquids for VOC absorption and biodegradation in multiphase systems, 66 (2011) 2707–2712. https://doi.org/10.1016/j.ces.2011.01.047.

[104]   Y. Zhao, J. Zhao, Y. Huang, Q. Zhou, X. Zhang, S. Zhang, Toxicity of ionic liquids: Database and prediction via quantitative structure-activity relationship method, J. Hazard. Mater. 278 (2014) 320–329. https://doi.org/10.1016/j.jhazmat.2014.06.018.

[105]   A. Romero, A., Santos, A., Tojo, J. & Rodríguez, Toxicity and biodegradability of imidazolium ionic liquids, J. Hazard. Mater. 151 (2008) 268–273. https://doi.org/10.1016/J.JHAZMAT.2007.10.079.

[106]   A.P. Abbott, G. Capper, D.L. Davies, R.K. Rasheed, V. Tambyrajah, Novel solvent properties of choline chloride/urea mixtures, Chem. Commun. 9 (2003) 70–71. https://doi.org/10.1039/b210714g.

[107]   W. Tang, Y. An, K.H. Row, Emerging applications of (micro) extraction phase from hydrophilic to hydrophobic deep eutectic solvents: opportunities and trends, TrAC - Trends Anal. Chem. 136 (2021) 116187. https://doi.org/10.1016/j.trac.2021.116187.

[108]   A.R. Mainar, E. Iruin, L.C. Colmenares, A. Kvasha, I. de Meatza, M. Bengoechea, O. Leonet, I. Boyano, Z. Zhang, J.A. Blazquez, An overview of progress in electrolytes for secondary zinc-air batteries and other storage systems based on zinc, J. Energy Storage. 15 (2018) 304–328. https://doi.org/10.1016/j.est.2017.12.004.

[109]   S. Werner, M. Haumann, P. Wasserscheid, Ionic Liquids in Chemical Engineering, Annu. Rev. Chem. Biomol. Eng. 1 (2010) 203–230. https://doi.org/10.1146/annurev-chembioeng-073009-100915.

[110]   S. Sowmiah, V. Srinivasadesikan, M.C. Tseng, Y.H. Chu, On the chemical stabilities of ionic liquids, 2009. https://doi.org/10.3390/molecules14093780.

[111]   N. Azizi, S. Dezfooli, M. Khajeh, M.M. Hashemi, Efficient deep eutectic solvents catalyzed synthesis of pyran and benzopyran derivatives, J. Mol. Liq. (2013). https://doi.org/10.1016/j.molliq.2013.05.011.

[112]   A.P. Abbott, J.C. Barron, K.S. Ryder, D. Wilson, Eutectic-Based Ionic Liquids with Metal-Containing Anions and Cations, (2007) 6495–6501. https://doi.org/10.1002/chem.200601738.

[113]   Y. Dai, J. Van Spronsen, G.J. Witkamp, R. Verpoorte, Y.H. Choi, Ionic liquids and deep eutectic solvents in natural products research: Mixtures of solids as extraction solvents, J. Nat. Prod. 76 (2013) 2162–2173. https://doi.org/10.1021/np400051w.

[114]   S.N. Turosung, B. Ghosh, Application of Ionic Liquids in the Upstream oil Industry-A Review, Int. J. Petrochemistry Res. 1 (2017) 50–60. https://doi.org/10.18689/ijpr-1000110.

[115]   E.L. Smith, A.P. Abbott, K.S. Ryder, Deep Eutectic Solvents (DESs) and Their Applications, Chem. Rev. 114 (2014) 11060–11082. https://doi.org/10.1021/cr300162p.

[116]   H. Vanda, Y. Dai, E.G. Wilson, R. Verpoorte, Y.H. Choi, Green solvents from ionic liquids and deep eutectic solvents to natural deep eutectic solvents, Comptes Rendus Chim. 21 (2018) 628–638. https://doi.org/10.1016/j.crci.2018.04.002.

[117]   Y. Marcus, Estimation of the Critical Temperatures of Some More Deep Eutectic Solvents from Their Surface Tensions, Adv. Mater. Sci. Eng. 2018 (2018) 2–5. https://doi.org/10.1155/2018/5749479.

[118]   W. Jiang, H. Jia, H. Li, L. Zhu, R. Tao, W. Zhu, H. Li, S. Dai, Boric acid-based ternary deep eutectic solvent for extraction and oxidative desulfurization of diesel fuel, Green Chem. (2019) 3074–3080. https://doi.org/10.1039/c9gc01004a.

[119]   L. Xu, Y. Luo, H. Liu, J. Yin, H. Li, W. Jiang, W. Zhu, Extractive desulfurization of diesel fuel by amide-based type IV deep eutectic solvents, J. Mol. Liq. 338 (2021) 116620. https://doi.org/10.1016/j.molliq.2021.116620.

[120]   L. Xu, H. Jia, D. Zhu, F. Huan, R. Liu, W. Jiang, W. Zhu, Hydrogen bonding boosted oxidative desulfurization by ZnCl 2 / boric acid / polyethylene glycol-based ternary deep eutectic solvents, J. Mol. Liq. 368 (2022) 120725. https://doi.org/10.1016/j.molliq.2022.120725.

[121]   M.K. Hadj-kali, Z. Salleh, E. Ali, R. Khan, M.A. Hashim, Separation of Aromatic and Aliphatic Hydrocarbons using Deep Eutectic Solvents: a Critical Review, Fluid Phase Equilib. 448 (2017) 152–167. https://doi.org/10.1016/j.fluid.2017.05.011.

[122]   M. Pätzold, S. Siebenhaller, S. Kara, A. Liese, C. Syldatk, D. Holtmann, Deep Eutectic Solvents as Efficient Solvents in Biocatalysis, Trends Biotechnol. 37 (2019) 943–959. https://doi.org/10.1016/j.tibtech.2019.03.007.

[123]   B. Jiang, J. Zhou, M. Xu, H. Dou, H. Zhang, N. Yang, L. Zhang, Multifunctional ternary deep eutectic solvent-based membranes for the cost-effective ethylene / ethane separation, J. Memb. Sci. 610 (2020) 118243. https://doi.org/10.1016/j.memsci.2020.118243.

[124]   F.P. Pelaquim, A. Marinho, B. Neto, I. Angela, L. Dalmolin, M. Conceic, Gas Solubility Using Deep Eutectic Solvents : Review and Analysis, Am. Chem. Soc. 60 (2021) 8607–8620. https://doi.org/10.1021/acs.iecr.1c00947.

[125]   K. Chandran, C. Fai, C. Devi, H. Fatimah, M. Zaid, A review on deep eutectic solvents : Physiochemical properties and its application as an absorbent for sulfur dioxide, J. Mol. Liq. 338 (2021) 117021. https://doi.org/10.1016/j.molliq.2021.117021.

[126]   R.J. Isaifan, A. Amhamed, Review on Carbon Dioxide Absorption by Choline Chloride / Urea Deep Eutectic Solvents, Adv.

Chem. (2018).

[127] I. Wazeer, M.K. Hadj-kali, I.M. Al-nashef, Utilization of Deep Eutectic Solvents to Reduce the Release of Hazardous Gases to the Atmosphere : A Critical Review, Molecules. (2021) 1–34.

[128] M. Atilhan, T. Altamash, S. Aparicio, Quantum chemistry insight into the interactions between deep eutectic solvents and SO2, Molecules. 24 (2019) 1–18. https://doi.org/10.3390/molecules24162963.

[129] D. Yang, Y. Han, H. Qi, Y. Wang, S. Dai, Efficient Absorption of SO2 by EmimCl-EG Deep Eutectic Solvents, ACS Sustain. Chem. Eng. 5 (2017) 6382–6386. https://doi.org/10.1021/acssuschemeng.7b01554.

[130] Y. Marcus, Gas solubilities in deep eutectic solvents, Monatshefte Für Chemie - Chem. Mon. 149 (2018) 211–217. https://doi.org/10.1007/s00706-017-2031-8.

[131] P. Janicka, J. Płotka-wasylka, J. Gębicki, Deep Eutectic Solvents and Their Uses for Air Purification, J. Ecol. Eng. 23 (2022) 181–190.

[132] Y. Chen, X. Han, Z. Liu, D. Yu, W. Guo, T. Mu, Capture of Toxic Gases by Deep Eutectic Solvents, ACS Sustain. Chem. Eng. (2020). https://doi.org/10.1021/acssuschemeng.0c01493.

[133] L. Moura, T. Moufawad, M. Ferreira, H. Bricout, S. Tilloy, E. Monflier, M.F. Costa Gomes, D. Landy, S. Fourmentin, Deep eutectic solvents as green absorbents of volatile organic pollutants, Environ. Chem. Lett. 15 (2017) 747–753. https://doi.org/10.1007/s10311-017-0654-y.

[134] G. Quijano, A. Couvert, A. Amrane, G. Darracq, C. Couriol, P. Le Cloirec, L. Paquin, D. Carrié, Absorption and biodegradation of hydrophobic volatile organic compounds in ionic liquids, Water. Air. Soil Pollut. 224 (2013). https://doi.org/10.1007/s11270-013-1528-y.

[135] M.J. Salar-García, V.M. Ortiz-Martínez, F.J. Hernández-Fernández, A.P. de los Ríos, J. Quesada-Medina, Ionic liquid technology to recover volatile organic compounds (VOCs), J. Hazard. Mater. 321 (2017) 484–499. https://doi.org/10.1016/j.jhazmat.2016.09.040.

[136] T. Moufawad, M. Costa Gomes, S. Fourmentin, Deep eutectic solvents as absorbents for VOC and VOC mixtures in static and dynamic processes, Chem. Eng. J. 448 (2022) 137619. https://doi.org/10.1016/J.CEJ.2022.137619.

[137] P. Villarim, E. Genty, J. Zemmouri, S. Fourmentin, Deep eutectic solvents and conventional solvents as VOC absorbents for biogas upgrading: A comparative study, Chem. Eng. J. 446 (2022) 136875. https://doi.org/10.1016/j.cej.2022.136875.

[138] C.C. Chen, Y.H. Huang, J.Y. Fang, Hydrophobic deep eutectic solvents as green absorbents for hydrophilic VOC elimination, J. Hazard. Mater. 424 (2022) 127366. https://doi.org/10.1016/J.JHAZMAT.2021.127366.

[139] M. Mu, X. Zhang, G. Yu, R. Xu, N. Liu, N. Wang, B. Chen, C. Dai, Effective absorption of dichloromethane using deep eutectic solvents, J. Hazard. Mater. 439 (2022) 129666. https://doi.org/10.1016/j.jhazmat.2022.129666.

[140] K. Boe, Online monitoring and control of the biogas process, 2006. http://citeseerx.ist.psu.edu/viewdoc/download?doi=10.1.1.125.2757&rep=rep1&type=pdf.

[141] J.B. Holm-Nielsen, P. Oleskowicz-Popiel, Process control in biogas plants, 1st ed., Elsevier Ltd., 2013. https://doi.org/10.1533/9780857097415.2.228.

[142] R. Nakakubo, H.B. Møller, A.M. Nielsen, J. Matsuda, Ammonia inhibition of methanogenesis and identification of process indicators during anaerobic digestion, Environ. Eng. Sci. 25 (2008) 1487–1496. https://doi.org/10.1089/ees.2007.0282.

[143] A.J. Ward, E. Bruni, M.K. Lykkegaard, A. Feilberg, A.P.S. Adamsen, A.P. Jensen, A.K. Poulsen, Real time monitoring of a biogas digester with gas chromatography, near-infrared spectroscopy, and membrane-inlet mass spectrometry, Bioresour. Technol. 102 (2011) 4098–4103. https://doi.org/10.1016/j.biortech.2010.12.052.

[144] R. LATTES, Annals New York Academy of Sciences: Discussion, Ann. N. Y. Acad. Sci. 135 (1966) 504–505. https://doi.org/10.1111/j.1749-6632.1966.tb45498.x.

[145] C.M. Delahunty, G. Eyres, J.P. Dufour, Gas chromatography-olfactometry, J. Sep. Sci. 29 (2006) 2107–2125. https://doi.org/10.1002/jssc.200500509.

[146] L. Cai, J.A. Koziel, Y.C. Lo, S.J. Hoff, Characterization of volatile organic compounds and odorants associated with swine barn particulate matter using solid-phase microextraction and gas chromatography-mass spectrometry-olfactometry, J. Chromatogr. A. 1102 (2006) 60–72. https://doi.org/10.1016/j.chroma.2005.10.040.

[147] P.A. Clausen, H.N. Knudsen, K. Larsen, V. Kofoed-Sørensen, P. Wolkoff, C.K. Wilkins, Use of thermal desorption gas chromatography-olfactometry/mass spectrometry for the comparison of identified and unidentified odor active compounds emitted from building products containing linseed oil, J. Chromatogr. A. 1210 (2008) 203–211. https://doi.org/10.1016/j.chroma.2008.09.073.

[148] K.K. Kleeberg, Y. Liu, M. Jans, M. Schlegelmilch, J. Streese, R. Stegmann, Development of a simple and sensitive method for the characterization of odorous waste gas emissions by means of solid-phase microextraction (SPME) and GC-MS/olfactometry, Waste Manag. 25 (2005) 872–879. https://doi.org/10.1016/j.wasman.2005.07.003.

[149] P. Oikonomou, A. Botsialasa, A. Olziersky, I. Stratakos, S. Katsikasc, D. Dimas, G. Sotiropoulos, D. Goustouridis, I. Raptis, M. Sanopoulou, Wireless sensor network based on a chemocapacitive sensor array for the real-time monitoring of industrial pollutants, Procedia Eng. 87 (2014) 564–567. https://doi.org/10.1016/j.proeng.2014.11.551.

[150] Z. Liang, J. Wang, Y. Zhang, C. Han, S. Ma, J. Chen, G. Li, T. An, Removal of volatile organic compounds (VOCs) emitted from a textile dyeing wastewater treatment plant and the attenuation of respiratory health risks using a pilot-scale biofilter, J. Clean. Prod. 253 (2020) 120019. https://doi.org/10.1016/j.jclepro.2020.120019.

[151] I.O. Cabeza, R. López, I. Giraldez, R.M. Stuetz, M.J. Díaz, Biofiltration of α-pinene vapours using municipal solid waste (MSW) – Pruning residues (P) composts as packing materials, Chem. Eng. J. 233 (2013) 149–158. https://doi.org/10.1016/J.CEJ.2013.08.032.

[152] S.N. Hidayat, T.R. Nuringtyas, K. Triyana, Electronic Nose Coupled with Chemometrics for Monitoring of Tempeh Fermentation Process, Proc. - 2018 4th Int. Conf. Sci. Technol. ICST 2018. 1 (2018) 1–6. https://doi.org/10.1109/ICSTC.2018.8528580.

[153] A.C. Romain, D. Godefroid, M. Kuske, J. Nicolas, Monitoring the exhaust air of a compost pile as a process variable with an e-nose, Sensors Actuators, B Chem. 106 (2005) 29–35. https://doi.org/10.1016/j.snb.2004.05.033.

[154] R. López, I. Giráldez, A. Palma, M. Jesús Díaz, Assessment of compost maturity by using an electronic nose, Waste Manag. 48 (2016) 174–180. https://doi.org/10.1016/j.wasman.2015.09.039.

[155] J. Gębicki, T. Dymerski, J. Namieśnik, Investigation of air quality beside a municipal landfill: The fate of malodour compounds as a model VOC, Environ. - MDPI. 4 (2017) 1–14. https://doi.org/10.3390/environments4010007.

[156] M. Moufid, B. Bouchikhi, C. Tiebe, M. Bartholmai, N. El Bari, Assessment of outdoor odor emissions from polluted sites using simultaneous thermal desorption-gas chromatography-mass spectrometry (TD-GC-MS), electronic nose in conjunction with advanced multivariate statistical approaches, Atmos. Environ. 256 (2021) 118449. https://doi.org/10.1016/j.atmosenv.2021.118449.

[157] M. Delgado-Rodríguez, M. Ruiz-Montoya, I. Giraldez, R. López, E. Madejón, M.J. Díaz, Use of electronic nose and GC-MS in detection and monitoring some VOC, Atmos. Environ. 51 (2012) 278–285. https://doi.org/10.1016/j.atmosenv.2012.01.006.

[158] T. Kvist, N. Aryal, Methane loss from commercially operating biogas upgrading plants, Waste Manag. 87 (2019) 295–300.

6. Dorobek naukowy

Dane wg bazy danych Scopus (data dostępu 16.05.2023r.):

Uwzględniając cykl publikacyjny:

Sumaryczna wartość IF: 35,406
Sumaryczna wartość MNiSW: 950
Indeks Hirscha: 13

Uwzględniając cały dorobek publikacyjny:

Sumaryczna wartość IF: 101,353
Sumaryczna wartość MNiSW: 2 420
Indeks Hirscha: 13

6.1. Publikacje naukowe w czasopismach z listy Clarivate Journal Citation Report (JCR)

1) Makoś-Chełstowska, P., **Słupek, E.,** Kucharska, K., Kramarz, A., & Gębicki, J. (2022). Efficient Extraction of Fermentation Inhibitors by Means of Green Hydrophobic Deep Eutectic Solvents. MOLECULES, 27, 157. DOI: 10.3390/molecules27010157. **Liczba punktów MNiSW: 140, IF: 4,927**

2) P. Makoś-Chełstowska, **E. Słupek,** , A. Kramarz, D. Dobrzyniewski, B. Szulczyński, & J. Gębicki, Green monoterpenes based deep eutectic solvents for effective BTEX absorption from biogas. CHEMICAL ENGINEERING RESEARCH & DESIGN,. 188 (2022), s.179-196.
(https://doi.org/10.1016/j.cherd.2022.09.047) **Liczba punktów MNiSW: 140, IF: 4,119**

3) Makoś-Chełstowska, P., **Słupek, E.,** & Małachowska, A. (2021). Superhydrophobic sponges based on green deep eutectic solvents for spill oil removal from water. JOURNAL OF HAZARDOUS MATERIALS, 425, 127972. DOI:10.1016/j.jhazmat.2021.127972. **Liczba punktów MNiSW: 200, IF: 14,224**

4) Makoś-Chełstowska, P., **Słupek, E.,** Gębicki, J. (2021). Deep eutectic solvents – based green absorbents for effective volatile organochlorine compounds removal from biogas. GREEN CHEMISTRY, 23, 4814-4827. DOI:10.1039/d1gc01735g. **Liczba punktów MNiSW: 200, IF: 11,034**

5) **Słupek, E.,** Makoś-Chełstowska, P., & Gębicki, J. (2021). Removal of Siloxanes from Model Biogas by Means of Deep Eutectic Solvents in Absorption Process. Materials, 14, 241. DOI:10.3390/ma14020241. **Liczba punktów MNiSW: 140, IF=3,748**

6) Makoś-Chełstowska, P., **Słupek, E.,** Kramarz A., & Gębicki, J. (2021). New Carvone-Based Deep Eutectic Solvents for Siloxanes Capture from Biogas. International Journal of Molecular Sciences, 22, 9551. DOI: 10.3390/ijms22179551. **Liczba punktów MNiSW: 140, IF=6,208**

7) Kucharska K., Makoś-Chełstowska P., **Słupek E.,** Gębicki J. (2021) Management of Dark Fermentation Broth via Bio Refining and Photo Fermentation. ENERGIES, 14, 6268. DOI: 10.3390/en14196268. **Liczba punktów MNiSW: 140, IF=3,252**

8) Kucharska, K., **Słupek, E.,** Cieśliński, H., & Kamiński, M. (2020). Advantageous conditions of saccharification of lignocellulosic biomass for biofuels generation via fermentation processes.

CHEMICAL PAPERS, 74, 1199-1209. DOI: 10.1007/s11696-019-00960-1. **Liczba punktów MNiSW: 40, IF=2,146**

9) Kucharska, K., Rybarczyk, P., Hołowacz, I., Konopacka-Łyskawa, D., **Słupek, E.,** Makoś-Chełstowska, P., Cieśliński, H., & Kamiński, M. (2020). Influence of alkaline and oxidative pre-treatment of waste corn cobs on biohydrogen generation efficiency via dark fermentation. BIOMASS & BIOENERGY, 141, 105691. DOI:.1016/j.biombioe.2020.105691. **Liczba punktów MNiSW: 100, IF=5,774**

10) **Słupek, E.,** & Makoś, P. (2020). Absorptive Desulfurization of Model Biogas Stream Using Choline Chloride-Based Deep Eutectic Solvents. Sustainability, 12, 1-16. DOI:10.3390/su12041619. **Liczba punktów MNiSW: 70, IF=3,889**

11) Makoś, P., **Słupek,** E., & Gębicki, J. (2020). Hydrophobic deep eutectic solvents in microextraction techniques–A review. MICROCHEMICAL JOURNAL, 152, 104384. DOI: 10.1016/j.microc.2019.104384. **Liczba punktów MNiSW: 70, IF=5,304**

12) Makoś, P., **Słupek, E.,** & Małachowska, A. (2020). Silica Gel Impregnated by Deep Eutectic Solvents for Adsorptive Removal of BTEX from Gas Streams. Materials, 13, 1894-1911. DOI:10.3390/ma13081894. **Liczba punktów MNiSW: 140, IF=3,748**

13) **Słupek, E**., Makoś, P., & Gębicki, J. (2020). Deodorization of model biogas by means of novel non-ionic deep eutectic solvent. Archives of Environmental Protection, 46, 41-46. DOI:10.24425/aep.2020.132524. **Liczba punktów MNiSW: 100, IF=1,851**

14) Makoś, P., **Słupek, E.,** & Gębicki, J. (2020). Extractive detoxification of feedstocks for the production of biofuels using new hydrophobic deep eutectic solvents – Experimental and theoretical studies. JOURNAL OF MOLECULAR LIQUIDS, 303, 113101. DOI: 10.1016/j.molliq.2020.113101. **Liczba punktów MNiSW: 100, IF=6,633**

15) **Słupek, E.,** Makoś, P., & Gębicki, J. (2020). Theoretical and Economic Evaluation of Low-Cost Deep Eutectic Solvents for Effective Biogas Upgrading to Bio-Methane. ENERGIES, 13, 3379. DOI: 10.3390/en13133379. **Liczba punktów MNiSW: 140, IF=3,252**

16) **Słupek, E.,** Makoś, P., Kucharska, K., & Gębicki, J. (2020). Mesophilic and thermophilic dark fermentation course analysis using sensor matrices and chromatographic techniques. CHEMICAL PAPERS, 74, 1573-1582. DOI:10.1007/s11696-019-01010-6. **Liczba punktów MNiSW: 40, IF=2,146**

17) **Słupek, E.,** Makoś-Chełstowska, P., Dobrzyniewski, D., Szulczyński, B., & Gębicki, J. (2020). Process Control of Biogas Purification Using Electronic Nose. CHEMICAL ENGINEERING TRANSACTIONS, 82, 427-432. DOI: 10.3303/cet2082072. **Liczba punktów MNiSW: 20, IF=1,032**

18) Kucharska, K., Cieśliński, H., Rybarczyk, P., **Słupek, E.,** Łukajtis, R., Wychodnik, K., & Kamiński, M. (2019). Fermentative Conversion of Two-Step Pre-Treated Lignocellulosic Biomass to Hydrogen. Catalysts, 9, 1-27. DOI:10.3390/catal9100858. **Liczba punktów MNiSW: 100, IF=4,501**

19) **Słupek, E.,** Kucharska, K., & Gębicki, J. (2019). Alternative methods for dark fermentation course analysis. SN Applied Sciences, 469, 1-8. DOI:10.1007/s42452-019-0488-2. **Liczba punktów MNiSW: 20, IF=2,114**

20) Kucharska, K., Łukajtis, R., **Słupek, E.,** Cieśliński, H., Rybarczyk, P., & Kamiński, M. A. (2018). Hydrogen Production from Energy Poplar Preceded by MEA Pre-Treatment and Enzymatic Hydrolysis. MOLECULES, 23(3029), 1-21. DOI:3390/molecules23113029. **Liczba punktów MNiSW: 100, IF: 4,927**

21) Łukajtis, R., Rybarczyk, P., Kucharska, K., Konopacka-Łyskawa, D., **Słupek, E.,** Wychodnik, K., & Kamiński, M. A. (2018). Optimization of Saccharification Conditions of Lignocellulosic Biomass under Alkaline Pre-Treatment and Enzymatic Hydrolysis. ENERGIES, 11(4), 1-27. DOI: 10.3390/en11040886. **Liczba punktów MNiSW: 140, IF=3,252**

22) Łukajtis, R., Kucharska, K., Hołowacz, I., Rybarczyk, P., Wychodnik, K., **Słupek, E.,** Nowak, P., & Kamiński, M. A. (2018). Comparison and Optimization of Saccharification Conditions of Alkaline Pre-Treated Triticale Straw for Acid and Enzymatic Hydrolysis Followed by Ethanol Fermentation. ENERGIES, 11(3), 639-663. DOI: 10.3390/en11030639. **Liczba punktów MNiSW: 140, IF=3,252**

6.2. Publikacje popularnonaukowe

1) **Rozdział w monografii: Słupek, E.,** Makoś, P., Gębicki, J., & Rogala, A. (2019). Purification of model biogas from toluene using deep eutectic solvents. E3S Web of Conferences, 116, 00078. DOI:10.1051/e3sconf/201911600078. **Liczba punktów MNiSW: 5.**

2) **Rozdział w monografii:** Makoś, P., **Słupek, E.,** Sobczak, J., Zabrocki, D., Hupka, J., & Rogala, A. (2019). Dimethyl ether (DME) as potential environmental friendly fuel. E3S Web of Conferences, 116, 00048. DOI: 10.1051/e3sconf/201911600048. **Liczba punktów MNiSW: 5.**

3) **Słupek, E.,** Makoś P., & Kamiński M., (2018) Metodyka oznaczania sumarycznej zawartości inhibitorów fermentacji ciemnej oraz monocukrów w brzeczkach fermentacyjnych techniką HPLC-RID-UV-VIS/DAD, Cam. Sep. 10 , 52 – 63.

4) Makoś P., **Słupek, E.,** & Kamiński M., (2018) Metodyka rozdzielania i oznaczania lotnych inhibitorów fermentacji w brzeczkach fermentacyjnych ciemnej fermentacji, techniką GC-MS. Cam. Sep. 10, 64 – 80.

5) Kucharska K., **Słupek E,.** & Kamiński M., (2019) Otrzymywanie BIOwodoru z odpadów lignocelulozowych, Gospodarka Odpadami, 20-23

6) Kucharska K., **Słupek E,.** & Kamiński M., (2019) Bioconversion of waste materials to hydrogen via dark fermentation using Enterobacter aerogenes, Aparatura Badawcza i Dydaktyczna 24 (1), 4-13.

6.3. Komunikaty plakatowe

1) **Edyta Słupek**, Patrycja Makoś-Chełstowska, Jacek Gębicki, Deep eutectic solvents based on symmetric quaternary ammonium salts for volatile organosulfur compounds removal from biogas, 5th International Conference on Applied Surface Science (ICASS), 25-28.04.2022, Majorka, Hiszpania.

2) Patrycja Makoś-Chełstowska, **Edyta Słupek**, Aleksandra Kramarz, Jacek Gębicki, Novel green deep eutectic solvents as efficiency absorbents for monoaromatic hydrocarbons capture from gaseous fuel streams, 5th International Conference on Applied Surface Science (ICASS), 25-28.04.2022, Majorka, Hiszpania

3) **Edyta Słupek**, Patrycja Makoś, Jacek Gębicki, Andrzej Rogala, Purification of model biogas from toluene using deep eutectic solvents, International Conference on Advances in Energy Systems and Environmental Engineering (ASEE19), 9-12.06.2019, Wrocław, Polska.

4) Patrycja Makoś, **Edyta Słupek**, Joanna Sobczak, Dawid Zabrocki, Jan Hupka, Andrzej Rogala, Dimethyl ether (DME) as a potential environmental friendly fuel – a review – International Conference on Advances in Energy Systems and Environmental Engineering (ASEE19), 9-12.06.2019, Wrocław, Polska.

5) **Edyta Słupek**, Karolina Kucharska, Jacek Gębicki, Mesophilic and thermophilic fermentation course analysis using sensor matrices, 46thInternational Conference of the Slovak Society of Chemical, 19-23.05.2019, Tatranske Matliare, Słowacja.

6) Karolina Kucharska, **Edyta Słupek**, Hubert Cieśliński, Marian Kamiński, Lignocellulosic biomass processing for hydrogen generation via dark fermentation, 46th International Conference of the Slovak Society of Chemical, 19-23.05.2019, Tatranske Matliare, Słowacja.

7) **Edyta Słupek**, Karolina Kucharska, Jacek Gębicki, Determination of gas composition during dark fermentation with the use of matrices sensors, IV edycja Interdyscyplinarnej Akademickiej Konferencji Ochrony Środowiska (IAKOŚ), 05-07.04.2019, Gdańsk, Polska.

8) Karolina Kucharska, **Edyta Słupek,** Jacek Gębicki, Management of lignocellulosic residues by means of dark fermentation, IV edycja Interdyscyplinarnej Akademickiej Konferencji Ochrony Środowiska (IAKOŚ), 05-07.04.2019, Gdańsk, Polska..

9) **Edyta Słupek**, Karolina Kucharska, Jacek Gębicki, Application of matrices sensor for dark fermentation course analysis, 11th Conference on Interdisciplinary Problems in Environment Protection and Engineering, 08.-10.04.2019, Polanica Zdrój, Polska.

10) **Edyta Słupek**, Karolina Kucharska, Marian Kamiński, Otrzymywanie biowodoru z odpadów lignocelulozowych, XIV Konferencja dla Miasta I Środowiska, Unieszkodliwianie Odpadów, 26.11.2018r, Warszawa.

Karolina Kucharska, **Edyta Słupek,** Marian Kamiński, Zastosowanie materiałów odpadowych do produkcji biogazów, zwłaszcza biowodoru, XIV Konferencja dla Miasta I Środowiska, Unieszkodliwianie Odpadów, 26.11.2018r, Warszawa.

6.4. Komunikaty ustne

1) **Edyta Słupek,** Absorpcyjne usuwanie związnków chemoorganicznych z biogazu z zastosowaniem cieczy eutektycznych, XV Konferencja Naukowa POL-EMIS 2021 Aktualne trendy w ochronie powietrza i klimatu – kontrola, monitoring, prognozowanie i ograniczanie emisji, 29-31.03.2021, Wrocław.

2) **Edyta Słupek**, Determination of gas composition during dark fermentation with the use of matrices sensors, IV edycji Interdyscyplinarnej Akademickiej Konferencji Ochrony Środowiska (IAKOŚ), 05-07.04.2019, Gdańsk, Poland – Zajęcie trzeciego miejsca w kategorii wystąpienie ustne**.**

3) **Edyta Słupek,** Karolina Kucharska, Marian Kamiński, Odpady lignocelulozowe jako surowiec do produkcji biopaliw gazowych, XIV Konferencja dla Miasta I Środowiska, Unieszkodliwianie Odpadów, 26.11.2018r, Warszawa.

6.5. Udział w projektach finansowanych ze źródeł zewnętrznych

1) **Wykonawca w projekcie** „Zagospodarowanie odpadów frakcji bio do dwuetapowego wytwarzania biowodoru z jednoczesnym uzdatnianiem strumieni gazowych za pomocą zielonych rozpuszczalników" (nr DEC- 2021/41/B/ST8/02395). Program: OPUS – Narodowe Centrum Nauki (NCN), Kierownik: dr inż. inż. Jacek Gębicki.

2) **Kierownik projektu** „Badania selektywnego usuwania lotnych związków siarkoorganicznych z modelowego strumienia biogazu z zastosowaniem cieczy eutektycznych" (nr nr UMO-2020/37/N/ST4/0292). Praca finansowana ze środków NCN w ramach projektu PRELUDIUM.

3) **Wykonawca w projekcie** „Nowe biosorbenty z materiałów odpadowych modyfikowane zielonymi rozpuszczalnikami do oczyszczania strumieni paliw gazowych" (nr UMO-2021/43/D/ST8/01791). Program: SONATA – Narodowe Centrum Nauki (NCN), Kierownik: dr inż. Patrycja Makoś-Chełstowska

4) **Wykonawca w projekcie** "COASTAL BiogasCluster on anaerobic digestion, environmental services and nutrients removal" (STHB.02.02.00-DE-0129/17-00). Program: Europejska Współpraca Terytorialna i Europejski Instrument Sąsiedztwa, Kierownik dr inż. Robert Aranowski.

6.6. Udział w projektach finansowanych ze źródeł wewnętrznych

1) **Wykonawca w projekcie** „Otrzymywanie i charakterystyka nowych materiałów absorpcyjnych do selektywnego usuwania zanieczyszczeń z biogazu" (nr DEC-34/2020/IDUB/I.3.3). Program: Inicjatywa Doskonałości – Uczelnia Badawcza – Argentum Triggering Research Grants, Kierownik: dr inż. Patrycja Makoś- Chełstowska

7. Spis załączników

Załącznik 1 Publikacja: E. Słupek, P. Makoś, J.Gębicki, Deodorization of model biogas by means of novel non- ionic deep eutectic solvent, Arch. Environ. Prot. 46 (2020) 41–46. (https://doi.org/10.24425/aep.2020.132524)

Załącznik 2 Publikacja: E. Słupek, P. Makoś, Absorptive Desulfurization of Model Biogas Stream Using Choline Chloride-Based Deep Eutectic Solvents, Sustainability. 12 (2020) 1619. (https://doi.org/10.3390/su12041619)

Załącznik 3 Publikacja: E. Słupek, P. Makoś-Chełstowska, & J. Gębicki, Removal of Siloxanes from Model Biogas by Means of Deep Eutectic Solvents in Absorption Process. Materials, 14 (2021) 241. (https://doi.org/10.3390/ma14020241)

Załącznik 4 Publikacja: P. Makoś-Chełstowska, **E. Słupek**, A. Kramarz, & J. Gębicki, New Carvone-Based Deep Eutectic Solvents for Siloxanes Capture from Biogas. Int. J. Mol. Sci., 22 (2021) 9551. (https://doi.org/10.3390/ijms22179551)

Załącznik 5 Publikacja: P. Makoś-Chełstowska, **E. Słupek**, & J. Gębicki, Deep eutectic solvents – based green absorbents for effective volatile organochlorine compounds removal from biogas. GREEN CHEMISTRY, 23 (2021) 4814-4827. (https://doi.org/10.1039/d1gc01735g) (Reproduced from Ref. Green Chemistry with permission from the Royal Society of Chemistry)

Załącznik 6 Publikacja: P. Makoś-Chełstowska, **E. Słupek,** , A. Kramarz, D. Dobrzyniewski, B. Szulczyński, & J. Gębicki, Green monoterpenes based deep eutectic solvents for effective BTEX absorption from biogas. CHEMICAL ENGINEERING RESEARCH & DESIGN,. 188 (2022), s.179-196 (https://doi.org/10.1016/j.cherd.2022.09.047) (CC-BY-NC-ND) (4.0))

Załącznik 7 Publikacja: E. Słupek, P. Makoś-Chełstowska, D. Dobrzyniewski, B. Szulczyński, & J. Gębicki, Process Control of Biogas Purification Using Electronic Nose. CHEMICAL ENGINEERING TRANSACTIONS, 82 (2020) 427-432. (https://doi.org/10.3303/cet2082072)

Załącznik 8 Publikacja: E. Słupek, P. Makoś, & J. Gębicki, Theoretical and Economic Evaluation of Low-Cost Deep Eutectic Solvents for Effective Biogas Upgrading to Bio-Methane. ENERGIES, 13 (2020) 3379. (https://doi.org/10.3390/en13133379)

Autorzy:

E. Słupek, P. Makoś, J.Gębicki

Tytuł publikacji:

Deodorization of model biogas by means of novel non- ionic deep
eutectic solvent

Czasopismo:

Archives of Environmental Protection

DOI:

10.24425/aep.2020.132524

Deodorization of model biogas by means of novel non-ionic deep eutectic solvent

Edyta Słupek, Patrycja Makoś*, Jacek Gębicki

Gdansk University of Technology, Faculty of Chemistry,
Department of Process Engineering and Chemical Technology, Gdańsk, Poland

*Corresponding author's e-mail: patrycja.makos@pg.edu.pl

Abstract: The paper presents new non-ionic deep eutectic solvent (DES) composed of natural and non-toxic components i.e. guaiacol, camphor and levulinic acid in 1:1:3 molar ratio as a promising absorbent for removal of selected volatile organic compounds (VOCs) including dichloromethane, toluene, hexamethyldisiloxane and propionaldehyde from model biogas.

The affinity of DES for VOCs was determined as vapour-liquid coefficients and the results were compared with several well-known DESs based on quaternary ammonium salt as well as n-hexadecane and water. For new DES, the absorption process was carried out under dynamic conditions.

The results indicate that non-ionic DES has high affinity and capacity for VOCs being comparable to n-hexadecane. In addition, absorbed VOCs could be easily desorbed from DES using activated carbon and absorbent could be re-use minimum five times without significant loss of absorption capacity.

Introduction

Biogas from wastewater treatment plants and landfill sites consist of 30–60% v/v methane, 15–30% v/v carbon dioxide, 5–20% v/v nitrogen, 1–10% v/v oxygen and about 1–2% v/v of other contaminants including hydrogen sulfide, ammonia and numerous volatile organic compounds (VOCs), i.e. aliphatic and aromatic hydrocarbons, siloxanes, volatile organosulfur and organohalogen compounds, and oxygenated organic compounds (Rasi et al. 2007). Impurities from biogas can have environmental impacts such as stratospheric ozone depletion, the greenhouse effect, and reduction in local air quality as well as effect damage to power equipment. In addition, the presence of odour compounds resulting from biogas production is a serious problem, especially for residents of areas immediately adjacent to production plants (Kozłowski et al. 2019; Szulczyński et al. 2017).

Currently, various technologies have been developed for the deodorization of biogas stream, i.e. chemical and physical absorption, adsorption, condensation, membrane separation, thermal or catalytic oxidation, biological treatment, biofiltration (Miller et al. 2018, 2019; Wieczorek et al. 2012) and advanced oxidation process (Baena-Moreno et al. 2019). Among the technologies, physical absorption is one of the most attractive technologies due to its simplicity, economical, safety, and its potential high efficiency for the removal of medium or high VOCs concentration from the gas phase. The most important parameter during the absorption process is the use of a suitable absorption solvent. Absorbents should

be characterized by high absorption capacity of VOCs, low vapor pressure, high-boiling point, high diffusion coefficient, low price, safety, and no toxicity. Some common solvents that may be useful for the removal of odorous compounds include water, mineral oils, alcohols, ketones, and amines (Noorain et al. 2019).

In recent years, in accordance with the principles of green chemistry, conventional absorbents have been replaced by new generation green solvents. Until recently, the studies have been focused on the application of ionic liquids (ILs) as absorbents due to their unique properties. However, several reports have pointed out the problems with biodegradability, high toxicity, difficult and expensive synthesis of most ILs (Romero et al. 2008). To overcome the disadvantages of ILs, eco-friendly solvent system named as deep eutectic solvents (DESs) was introduced (Abbott et al. 2003). The DESs are mixture mainly composed of two or three non-toxic and biodegradable compounds with a melting point lower than its individual components. Until now, DESs have been widely used in catalysis, analytical chemistry, separation processes and electrochemistry, water and air purification (Tang et al. 2015, Makoś et al. 2018, Makoś et al. 2018).

There are currently several reports in which DESs have been successfully used to remove inorganic impurities from the gas phase, i.e. water, carbon dioxide, sulfur dioxide, ammonia and hydrogen sulfide (Chen et al. 2019, Duan et al. 2019). To the best of our knowledge, only one study focused on the application of deep eutectic solvents for VOCs absorption. In this study, authors tested several DESs composed of choline chloride with

urea and with ethylene glycol, glycerol and levulinic acid in 1:2 molar ratio, mixtures composed of tetrabutylphosphonium bromide with glycerol (1:1 molar ratio), and with levulinic acid (1:6 molar ratio) as well as tetrabutylammonium bromide with decanoic acid in 1:2 molar ratio for absorption of toluene, acetaldehyde and dichloromethane (Moura et al. 2017). In studies, the DESs present similar absorption capacities for acetaldehyde (corresponding to 99.9% absorption of the initial VOC amount). Due to the high absorption potential of DESs, they can be used as an alternative to conventional organic solvents used for VOC absorption from a gas stream.

The paper discusses the novel non-ionic DESs based on a combination of ±camphor [C], guaiacol [G] and levulinic acid [Lev] in 1:1:3 molar ratio. The affinity of new DESs for selected VOCs including toluene (T), dichloromethane (DCM), hexamethyldisiloxane (HMDS) and propionaldehyde (PA) was determined and the results were compared with several well--known DESs based on quaternary ammonium salts as well as n-hexadecane and water. For new DES, the absorption process was carried out under dynamic conditions. The reusability and regeneration of DESs were also investigated.

Experimental

Materials and reagents

Camphor, guaiacol, levulinic acid, propionaldehyde, toluene, dichloromethane, hexadecane, hexamethyldisiloxane, choline chloride, urea, and diethylene glycol (purity ≥ 95%) were purchased from Sigma-Aldrich (USA). Compressed gases were used for the preparation of model biogas and chromatographic analysis such as nitrogen (purity N 5,5), air (purity N 5.0) generated by a DK50 compressor with a membrane dryer (Ekkom, Poland) and hydrogen (purity N 5.5) generated by a 9400 Hydrogen Generator (Packard, USA).

Procedures
Preparation and physicochemical properties of DESs
New non-ionic DESs, as well as ionic DESs, were synthesized by mixing [C], [G] and [Lev] in a 1:1:3 molar ratio and choline chloride [ChCl] with urea [U], diethylene glycol [DEG], and levulinic acid in 1:2 molar ratio. The eutectic mixtures were stirred magnetically at 60°C until homogeneous liquids were obtained. The liquids were then left to cool spontaneously to room temperature. Dynamic viscosity and density were measured over a wide range of temperature from 25 to 50°C which is the usual absorption tower operating temperature range. The viscosity was determined using BROOKFIELD LVDV-II+ viscometer (Labo--Plus, Poland). The density was measured by means of DMA 4500 (Anton, Paar, Poland). The determination of dynamic viscosity, and density of DESs were performed at atmospheric pressure.

Affinity of absorbents for the selected VOCs
The affinity of absorbents for VOCs was evaluated by means of vapor – liquid partition coefficients (K) defined as (1):

$$K = \frac{c_G}{c_L} \qquad (1)$$

Where: C_G – concentration of VOCs in the gas phase in the equilibrium with a liquid solution of concentration C_L in the solute. Affinity tests were carried out in 20 ml glass vials containing 1 ml of absorbents enriched with 50 ppm v/v of each VOCs. The vials were closed with PTFE-coated silicone rubber septa and sealed with aluminum caps. The vials were maintained in laboratory shaker at 25 and 50°C for 48 h. The concentration of VOCs in gas phase was determined using static headspace coupled to gas chromatography (HS-GC). The concentration of VOCs in liquid phases was calculated from a mass balance on the VOC after determination of VOCs in the gas phases. The measurements were carried out using gas chromatograph Autosystem XL equipped with flame ionization detector (FID) (PerkinElmer, USA), an HP-5 (30 m × 0.25 mm × 0.25 μm) capillary column and TurboChrom 6.1 software. The following conditions were used for the GC-FID analysis: injection port temperature 200°C, injection mode: split (15:1), detector temperature 320°C, detector gases flow rates: air 450 mL/min, hydrogen 45 mL/min, carrier gas (nitrogen) flow rate 2 mL/min and oven temperature 60°C.

Absorption process
The model biogas, as well as the absorption process, was prepared by means of the bubbling phenomenon. Nitrogen was passed through a 20-mL vial containing 1 mL of each VOCs. The formed mixture was diluted with a nitrogen stream to achieve the desired concentration of VOCs (50 ppm v/v) in the model biogas mixture. The nitrogen containing VOCs was passed through a 60-mL absorption column containing 50 mL of DES. The total flow of nitrogen and gaseous VOCs was kept constant at 50 mL/min. The concentration of VOCs was monitored at the inlet and outlet of the bubble column using GC-FID. The processes were carried out for 3000 minutes. The absorptivity (A) of VOCs in the DES was calculated using equation (2):

$$A = \frac{c_{in} - c_{out}}{c_{in}} \qquad (2)$$

Where: C_{in} – VOCs concentration of the inlet gas (ppm v/v), and C_{out} – VOCs concentration of the outlet gas (ppm v/v).

Regeneration and reusability of DES
After the absorption process, the VOCs absorbed in the DES were removed by means of adsorption with activated carbon. The DES containing VOCs was mixed with activated carbon in a glass vial and subsequently filtered using a PTFE – syringe filter with a pore size of 0.22 μm to ensure the complete removal of the activated carbon from the absorbent phase. The concentration of VOCs in DES was controlled using HS-GC-FID procedure described above. The absorption/desorption cycles were repeated five times.

Results and discussion

Physicochemical properties of new DES
In the first stage of research, the volatility of DES was studied by passing nitrogen through the new absorbents at two temperatures – 25 and 50°C. The gas phase after bubbling DES was analyzed by GC. No peaks were observed in the chromatogram, indicating a lack of DES volatility at the studied temperatures.

It is well-known that the viscosity and density of absorbents play an important role in the mass transfer process. The viscosity and density were highly affected by the nature of DES components and temperature. The density of new DES at 25°C (1.1123 g/cm³) as well as DESs composed of ChCl and urea (1.2001 g/cm³), levulinic acid (1.1371 g/cm³), and diethylene glycol (1.1143 g/cm³) are higher than conventional absorbents, i.e. hexadecane (0.7701 g/cm³) and water (0.9970 g/cm³), and they are decreasing with increasing temperature (Figure 1A).

The viscosity of new DES is lower compared to the viscosity of the most popular DESs and slightly higher compared to viscosity values of organic solvents (e.g. n-hexadecane which represent mineral oil and water) already used for the removal of VOCs from the gas phase.

Deodorization of VOCs from model biogas

A key feature for deodorization of biogas is the VOCs affinity for DESs. Table 1 summarized the vapor-liquid partition coefficients of four VOCs in new non-ionic DES, and the most popular ionic DESs as well as water and n-hexadecane.

The significant decrease in vapor-liquid partition coefficients for the studied absorbents, compared to water, indicates that a greater amount of selected VOCs are solubilized in these absorbents. All VOCs showed similar K values in DES composed of [G][C][Lev] (1:1:3) than those obtained for n-hexadecane which is one of the most common

organic solvents used for the removal of VOCs from gas phases. The partition coefficient values obtained for PA as well as for DCM are in the same order of magnitude than those observed for the other choline chloride-based DESs. For the T and HMDS, non-ionic DES ([G][C][Lev]) is the most effective absorbent, due to the lowest K values. Higher K values for PA were obtained using all DESs compared to water and n-hexadecane, which indicates a lower efficiency of DES absorption for compounds from the aldehydes group. Similar K values (higher than [G][C][Lev] (1:1:3) and n-hexadecane) were obtained for most VOCs using DES containing [ChCl] in their structure. This is probably due to the limited solubility of VOCs in [ChCl]. However, these results are lower than those for water, which indicates better sorption properties of ionic DESs. The partition coefficient values for most VOCs in DESs are comparable in 25°C and 50°C. This trend is very important for the industrial use of environmentally friendly solvents as absorbents because the temperature of the biogas stream generated in the industry is not always stable. At 25°C, the higher absorption efficiency of VOCs was observed, while at 50°C, lower absorption efficiency was noted. At higher temperatures, lower viscosity of absorbents is observed, which theoretically should increase the absorption capacity. On the other hand, higher temperatures may adversely affect the affinity of VOC for DES, which strongly depends on hydrogen bonds, electrostatic interactions, as well as $\pi - \pi$ interactions, which are probably reduced. The interaction of both effects affects similar affinity values of VOCs to DES
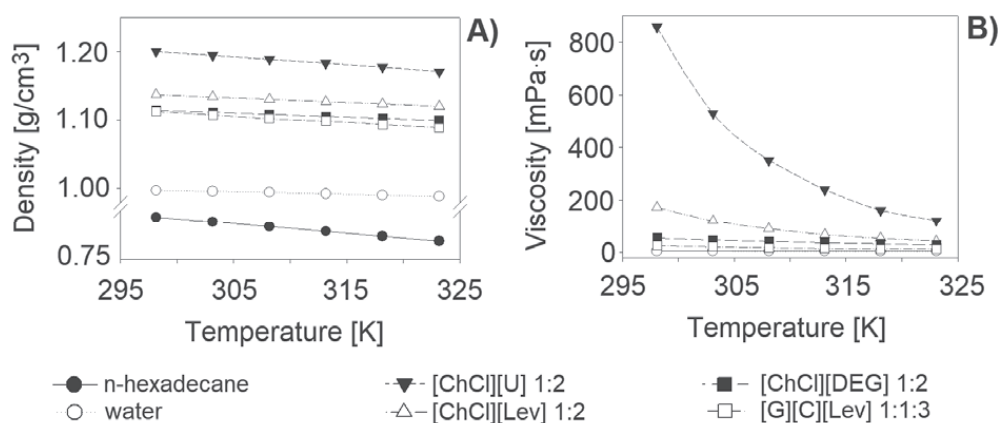
Fig. 1. A) Densities for absorbents as a function of temperature, B) Viscosities for absorbents as a function of temperature

Table 1. Vapour–liquid partition coefficients (K) of VOCs in absorbents at 25 and 50°C.

Absorbent	T		PA		DCM		HMDS	
	25°C	50°C	25°C	50°C	25°C	50°C	25°C	50°C
[G][C][Lev] (1:1:3)	<0.001	0.017	0.008	0.019	0.057	0.044	<0.001	<0.001
[ChCl][U] (1:2)	0.026	0.157	0.010	0,025	0.052	0.208	0.012	<0.001
[ChCl][Lev] (1:2)	0.035	0.091	0.011	0.026	0.075	0.081	0.0085	0.012
[ChCl][DEG] (1:2)	0.076	0.168	0.010	0.025	0.038	0.103	0.0096	0.018
n-hexadecane	<0.001	0.014	0.009	0.012	0.077	0.086	<0.001	<0.001
water	0.203	0.609	0.0045	0.015	0.112	0.251	0.61	0.86

in 25 and 50°C. The lower differences in the viscosity of absorbents in the temperature range, the greater the stability of the absorption process were observed.

In a dynamic system, two other parameters, i.e. flow rates and the volume of absorbent also have a significant influence on absorption efficiency. The studies were conducted under model conditions using nitrogen to verify only the interactions between VOCs and the new DES. In the studies, the effect of different flow rates between 20 and 70 mL/min were tested (Figure 2A). In the industrial point of view, the flow rate of contaminated biogas should be as high as possible. However, the results indicated that at a higher flow rate (above 50 mL/min), the absorption efficiency of VOCs was significantly decreased. Hence, 50 mL/min was chosen as the optimum flow rate by the proposed method. In the next step, the volume of absorbent between 15 and 50 mL was investigated (Figure 2B).

The results showed that with the increase in DES volume, the absorption capacity increased significantly and the time of complete saturation of DES increased from 950 min to 3000 minutes. The VOCs absorption capacity of DES was investigated for 50 ppm v/v concentration. Optimization studies for all compounds came out at a similar level. That is

why the paper presents only the most representative graphs obtained for T.

Figure 3 presents the absorption capacity of DES in optimum process conditions. The results indicate that the absorption capacity strongly influences the structure of VOCs. After 1200 minutes, DES was completely saturated with DCM and PA compounds. While at that time, the absorption capacity for toluene and HMDS was 0.26 and 0.52 respectively. The T and HMDS removal process could continue for 1800 minutes. The results are consistent with the vapor-liquid partition coefficient values. This indicates that the new DES can more effectively remove volatile siloxane compounds and aromatic hydrocarbons from the biogas stream.

Regeneration and reusability of DES

Regeneration and reusability of the DES for multiple uses as an absorbing solvent for VOCs removal are important in economics (Figure 4). In the studies, adsorption process based on activated carbon was applied to remove VOCs from DES. The results indicate that VOCs could be completely removed from DES and absorbent could be re-used minimum five times without significant loss of absorption capacity.
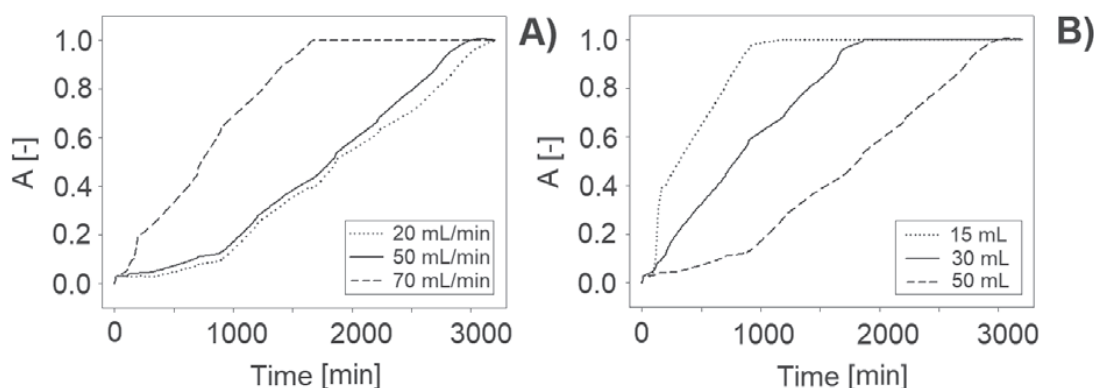
Fig. 2. Experimental breakthrough curves of T absorption with [G][C][Lev] (1:1:3 molar ratio) at different:
A) flow and B) volume of DES
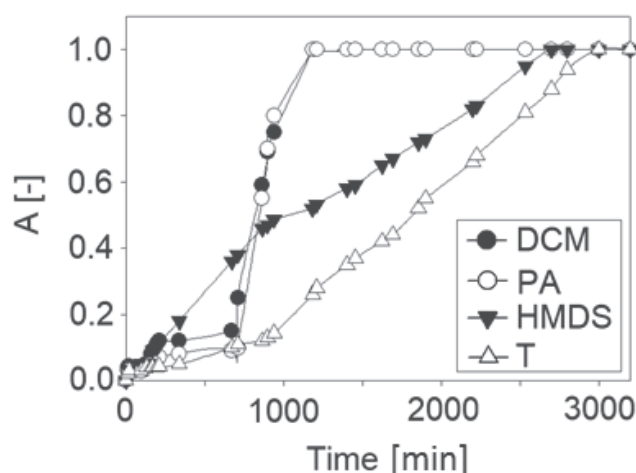
Fig. 3. VOCs absorption curves in [G][C][Lev] (1:1:3 molar ratio) at optimum conditions (25°C, 50 mL of DES, gas flow rate 50 mL/min, initial concentration of VOCs 50 ppm v/v)
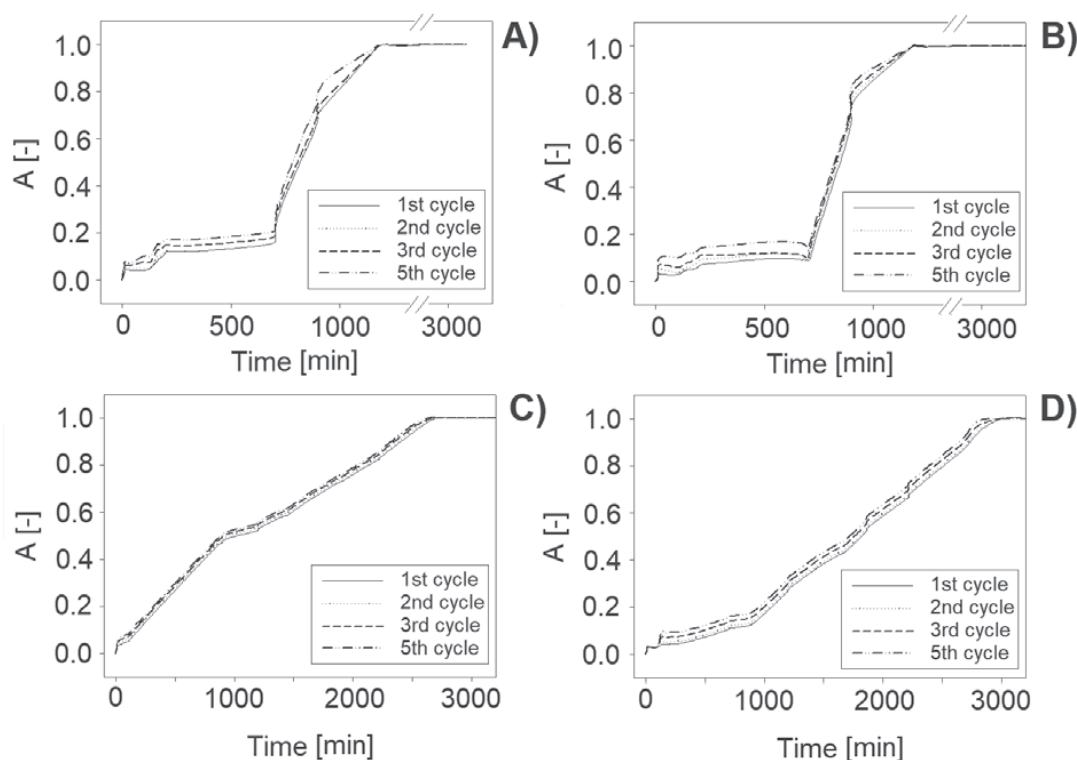
Fig. 34. Reusability of [G][C][Lev] (1:1:3 molar ratio): A) PA B) DCM C) HMDS D) T

Conclusions

The paper shows the new DES composed of natural non-toxic components including camphor, guaiacol and levulinic acid in 1:1:3 molar ratio as a promising candidate for implementation in the absorption process for the removal of VOCs from model biogas. The new DES confirms the high affinity and capacity for T, PA, DCM, and HMDS being comparable to n-hexadecane or higher than typical DESs composed of quaternary ammonium salts. In addition, the absorbed VOCs could be easily desorbed from DES using activated carbon and the absorption capacities are stable after five cycles. The obtained results indicate the great potential of the use of DES for the purification of real biogas streams.

References

Abbott, A.P., Capper, G., Davies, D.L., Rasheed, R.K. & Tambyrajah, V. (2003). Novel Solvent Properties of Choline Chloride/ Urea Mixtures. *Chemical Communication*, 0, 1, pp. 70–71, DOI: 10.1021/ja048266j.

Baena-Moreno, F. M., Rodríguez-Galán, M., Vega, F., Vilches, L. F. & Navarrete, B. (2019). Review: recent advances in biogas purifying technologies. *International Journal of Green Energy*, 16, 5, pp. 401–412, DOI: 10.1080/15435075.2019.1572610.

Chen, Y., Yu, D., Chen, W., Fu, L. & Mu, T. (2019). Water absorption by deep eutectic solvents. *Physical Chemistry Chemical Physics*, 21, 5, pp. 2601–2610, DOI: 10.1039/c8cp07383j.

Duan, X., Gao, B., Zhang, C. & Deng, D. (2019). Solubility and thermodynamic properties of NH3 in choline chloride-based deep eutectic solvents. *The Journal of Chemical Thermodynamics*, 133, 79–84, DOI: 10.1016/J.JCT.2019.01.031.

Kozłowski, K., Dach, J., Lewicki, A., Malińska, K., Do Carmo, I.E.P. & Czekała, W. (2019). Potential of biogas production from animal manure in Poland. *Archives of Environmental Protection*, 45, 3, pp. 99–108, DOI: 10.24425/aep.2019.128646.

Liu, F., Chen, W., Mi, J., Zhang, J.Y., Kan, X., Zhong, F.Y., Huang, K., Zheng, A. & Jiang, L. (2019). Thermodynamic and molecular insights into the absorption of H2S, CO$_2$, and CH$_4$ in choline chloride plus urea mixtures. *AIChE Journal*, 65, 5, pp. 1–10, DOI: 10.1002/aic.16574.

Makoś, P., Fernandes, A., Przyjazny, A. & Boczkaj, G. (2018). Sample preparation procedure using extraction and derivatization of carboxylic acids from aqueous samples by means of deep eutectic solvents for gas chromatographic-mass spectrometric analysis. *Journal of Chromatography A*, 1555, pp. 10–19, DOI: 10.1016/J. CHROMA.2018.04.054.

Makoś, P., Przyjazny, A. & Boczkaj, G. (2018). Hydrophobic deep eutectic solvents as "green" extraction media for polycyclic aromatic hydrocarbons in aqueous samples. *Journal of Chromatography A*, 1570, pp. 28–37, DOI: 10.1016/J.CHROMA.2018.07.070.

Miller, U., Sówka, I. & Adamiak, W. (2018). The application of Brij 35 in biofiltration of the air polluted with toluene vapours. *E3S Web of Conferences*, 44, pp. 1–8, DOI: 10.1051/e3sconf/20184400113.

Miller, U., Sówka, I. & Adamiak, W. (2019). The effect of betaine on the removal of toluene by biofiltration. *SN Applied Sciences*, 1, 9, pp. 1–8, DOI: 10.1007/s42452-019-0832-6.

Moura, L., Moufawad, T., Ferreira, M., Bricout, H., Tilloy, S., Monflier, E., Gomes, M.F.C., Landy, D. & Fourmentin, S. (2017). Deep eutectic solvents as green absorbents of volatile organic pollutants. *Environmental Chemistry Letters*, 15, 4, pp. 747–753, DOI: 10.1007/s10311-017-0654-y.

Noorain, R., Kindaichi, T., Ozaki, N., Aoi, Y. & Ohashi, A. (2019). Biogas purification performance of new water scrubber packed with sponge carriers. *Journal of Cleaner Production*, 214, pp. 103–111, DOI: 10.1016/J.JCLEPRO.2018.12.209.

Rasi, S., Veijanen, A. & Rintala, J. (2007). Trace compounds of biogas from different biogas production plants. *Energy*, 32, 8, pp. 1375–1380, DOI:10.1016/J.ENERGY.2006.10.018.

Romero, A., Santos, A., Tojo, J. & Rodríguez, A. (2008). Toxicity and biodegradability of imidazolium ionic liquids. *Journal of Hazardous Materials*, 151, 1, pp. 268–273, DOI: 10.1016/J. JHAZMAT.2007.10.079.

Szulczyński, B., Wasilewski, T., Wojnowski, W., Majchrzak, T., Dymerski, T., Namiésnik, J. & Gębicki, J. (2017). Different ways to apply a measurement instrument of E-nose type to evaluate ambient air quality with respect to odour nuisance in a vicinity of municipal processing plants. *Sensors (Switzerland)*, 17, 11, pp. 2671–2690, DOI: 10.3390/s17112671.

Tang, B., Zhang, H. & Row, K. H. (2015). Application of deep eutectic solvents in the extraction and separation of target compounds from various samples. *Journal of Separation Science*, 38, 6, pp. 1053–1064, DOI:10.1002/jssc.201401347.

Wieczorek, A. & Przybulewska, K. (2012). Examination of the biofiltration of air polluted with methyl isobutyl ketone. *Environment Protection Engineering*, 38, 1, pp. 51–58.

Dezodoryzacja modelowego strumienia biogazu z użyciem nowej niejonowej cieczy eutektycznej

Streszczenie: W pracy przedstawiono nową niejonową ciecz eutektyczną (DES) złożoną z naturalnych i nietoksycznych składników tj. gwajakol, kamfora i kwas lewulinowy w stosunku molowym 1:1:3, jako obiecujący absorbent do usuwania wybranych lotnych związków organicznych w tym dichlorometanu, toluenu, heksametylodisiloksanu oraz aldehydu propionowego.

W celu określenia powinowactwa DES do LZO, wyznaczono współczynniki podziału ciecz–para. Uzyskane wyniki porównano z popularnymi DES zawierającymi w strukturze czwartorzędową sól amoniową, a także z n-heksadekanem oraz wodą.

Dla nowej DES, proces absorpcji przeprowadzono również w warunkach dynamicznych. Wyniki wykazały, że nowa niejonowa DES charakteryzuje się dużym powinowactwem do wybranych LZO oraz dużą pojemnością sorpcyjną, a parametry te są porównywalne do n-heksadekanu.

Dodatkowo, zaabsorbowane LZO mogą być łatwo desorbowane przy użyciu węgla aktywnego. Dzięki temu, absorbent w postaci DES może być użyty minimum pięć razy bez znaczącego zmniejszenia pojemności sorpcyjnej.

Gdańsk, dnia 19.05.2023

dr inż. Patrycja Makoś-Chełstowska

(stopień/tytuł, imię i nazwisko)

Politechnika Gdańska

(Afiliacja)

OŚWIADCZENIE WSPÓŁAUTORA

Jako współautor pracy:. **"Deodorization of model biogas by means of novel non- ionic deep eutectic solvent"** oświadczam, że mój własny wkład polegał na konceptualizacji, metodologii, wizualizacji, prowadzeniu badań, zestawieniu i obróbce danych, przechowywaniu danych, przygotowaniu oryginalnego manuskryptu oraz przygotowaniu recenzji i redakcji ostatecznej wersji manuskryptu.

Jednocześnie wyrażam zgodę na przedłożenie ww. pracy przez mgr inż. Edytę Słupek jako część rozprawy doktorskiej w formie spójnego tematycznie zbioru artykułów opublikowanych w czasopismach naukowych.

Oświadczam, że samodzielna i możliwa do wyodrębnienia część ww. pracy wykazuje indywidualny wkład mgr inż. Edyty Słupek polegający na: konceptualizacji, metodologii, wizualizacji, prowadzeniu badań, zestawieniu i obróbce danych, przechowywaniu danych, przygotowaniu oryginalnego manuskryptu oraz przygotowaniu recenzji i redakcji ostatecznej wersji manuskryptu.

P. Makoś – Chełstowska

(podpis współautora)

Gdańsk, dnia 19.05.2023

dr inż. hab. Jacek Gębicki

(stopień/tytuł, imię i nazwisko)

Politechnika Gdańska

(Afiliacja)

OŚWIADCZENIE WSPÓŁAUTORA

Jako współautor pracy:. **"Deodorization of model biogas by means of novel non- ionic deep eutectic solvent"** oświadczam, że mój własny wkład polegał na nadzorowaniu wstępnego planu badań oraz realizacji badań, przygotowaniu recenzji oraz redakcji ostatecznej wersji manuskryptu, finansowaniu.

Jednocześnie wyrażam zgodę na przedłożenie ww. pracy przez mgr inż. Edytę Słupek jako część rozprawy doktorskiej w formie spójnego tematycznie zbioru artykułów opublikowanych w czasopismach naukowych.

Oświadczam, że samodzielna i możliwa do wyodrębnienia część ww. pracy wykazuje indywidualny wkład mgr inż. Edyty Słupek polegający na: konceptualizacji, metodologii, wizualizacji, prowadzeniu badań, zestawieniu i obróbce danych, przechowywaniu danych, przygotowaniu oryginalnego manuskryptu oraz przygotowaniu recenzji i redakcji ostatecznej wersji manuskryptu.

(podpis współautora)

Autorzy:

E. Słupek, P. Makoś

Tytuł publikacji:

Absorptive Desulfurization of Model Biogas Stream Using Choline
Chloride-Based Deep Eutectic Solvents

Czasopismo:

Sustainability

DOI:

10.3390/su12041619

Article

Absorptive Desulfurization of Model Biogas Stream Using Choline Chloride-Based Deep Eutectic Solvents

Edyta Słupek[ID] and Patrycja Makoś *[ID]

Department of Process Engineering and Chemical Technology, Faculty of Chemistry,
Gdansk University of Technology, G. Narutowicza St. 11/12, 80–233 Gdańsk, Poland; edyta.slupek@pg.edu.pl
* Correspondence: patrycja.makos@pg.edu.pl; Tel.: +48-508997100

check for updates

Abstract: The paper presents a synthesis of deep eutectic solvents (DESs) based on choline chloride (ChCl) as hydrogen bond acceptor and phenol (Ph), glycol ethylene (EG), and levulinic acid (Lev) as hydrogen bond donors in 1:2 molar ratio. DESs were successfully used as absorption solvents for removal of dimethyl disulfide (DMDS) from model biogas steam. Several parameters affecting the absorption capacity and absorption rate have been optimized including kinds of DES, temperature, the volume of absorbent, model biogas flow rate, and initial concentration of DMDS. Furthermore, reusability and regeneration of DESs by means of adsorption and nitrogen barbotage followed by the mechanism of absorptive desulfurization by means of density functional theory (DFT) as well as FT-IR analysis were investigated. Experimental results indicate that the most promising DES for biogas purification is ChCl:Ph, due to high absorption capacity, relatively long absorption rate, and easy regeneration. The research on the absorption mechanism revealed that van der Waal interaction is the main driving force for DMDS removal from model biogas.

Keywords: deep eutectic solvents; absorption; biogas; dimethyl disulfide; green solvents; desulfurization

1. Introduction

Currently, more and more attention is paid to the production of alternative high-quality fuels, including bio-methane, bio-hydrogen, bio-ethanol, bio-butanol, etc. Biogas is a modern form of bioenergy, which can be obtained in the process of dark fermentation using waste products from various industries and agriculture (agri-food and animal waste) [1–3]. Biogas usually contains 30%–60% *v/v* CH_4, 15%–30% *v/v* CO_2, 5%–20% *v/v* N_2, 1%–10% *v/v* O_2, and about 1%–2% *v/v* of other contaminants including H_2S, NH_3 and numerous of organic compounds [4–6]. Among the organic pollutants, volatile organosulfur compounds (VSCs) are one of the most important biogas impurities group. VSCs include sulfides, disulfides, thiophenes, and thiols, and the concentrations of them are strictly dependent on the raw material used for biogas production [7]. A typical range of VSCs concentration in biogas is shown in Table 1.

Table 1. Range concentrations volatile organosulfur compounds (VSCs) in the biogas stream [7].

VSCs	Concentration (mg/Nm^3 biogas)
dimethyl sulfide	1.25–2.76
carbon disulfide	1.62–5.91
2-propanethiol	0.50–1.19
1-propanethiol	2.87–19.51
2-butanethiol	0.79–4.65
thiophene	0.16–1.16
methyl propyl sulfide	0.35–1.76
dimethyl disulfide	0.39–1.14
dipropyl disulfide	0.76–3.16

Volatile organosulfur compounds are commonly found in many products and waste streams, causing technological and environmental problems [8,9]. VSCs are chemical compounds which are characterized by high toxicity, malodorousness, and high reactivity [10]. During biogas combustion, VSCs converted into toxic sulfur oxides (SOx) react with oxygen and water, forming sulfuric acid (H_2SO_4) which corrode the surface in the combustion chamber. Therefore, biogas pre-treatment is necessary to protect engines that convert biogas into energy and in order to protect an environment [11,12].

Currently, there are many technologies to remove impurities from biogas, which are classified into three main categories: physical (e.g., absorption, adsorption, condensation), chemical (e.g., catalytic oxidation, thermal oxidation, ozonation), and biological (e.g., bio-scrubbers, bio-filters, activated sludge) [13–16]. Most of these methods are expensive and complicated, therefore, more and more attention is paid to optimize them in terms of low energy consumption and high efficiency [17–20]. Among the technologies, physical absorption is one of the most attractive methods due to its simplicity, economical, safe, and its potential high impurities removal efficiency from gas steams [21]. The choice of a suitable absorbent is the key to successful impurities removal. "Perfect" absorbent should be characterized by non-toxic character, high absorption capacity, high-boiling point, low vapor pressure, high diffusion coefficient, low prices, and safety [22]. Several solvents that may be useful for the removal of impurities include water, mineral oils, alcohols, ketones, and amines [23–25]. However, in accordance with the trends of "green chemistry", conventional solvents should be replaced by new generation absorbents. Until recently, studies have focused on ionic liquids (ILs) as absorbents due to their unique properties [26]. However, the problems with their toxicity, stability, biodegradability, and expensive synthesis make them less than ideal solvents. Alternatives to ILs are deep eutectic solvents (DESs), which have similar physico-chemical properties. DESs are a mixture consisting mainly of two or three non-toxic and biodegradable compounds that are capable of forming eutectic liquids, based on the specific interaction between hydrogen bond donor (HBD) and hydrogen bond acceptor (HBA) [27,28]. Until now, DESs have been widely used for desulfurization of fuels [9], biomass pre-treatment [29], water and air purification [30,31], in catalysis [32], and analytical chemistry [27,33,34]. Till now, no studies have been in the literature published regarding the use of DESs as absorbents to remove volatile organosulfur compounds from the biogas stream. The studies presented in the literature are limited to the removal of inorganic compounds, i.e., H_2O, CO_2, H_2S, and NH_3 from gaseous phases [35–37]. Only a few works refer to their use to remove volatile organic compounds from the gas phase [38,39].

The paper describes the synthesis of DES composed of choline chloride (HBA) and phenol, ethylene glycol, levulinic acid (HBD) in a 1:2 molar ratio. The absorptive desulfurization was optimized on selection terms of DES type, temperature, absorbent volume, initial concentration of dimethyl disulfide (DMDS), and model biogas flow rate. Two most popular desorption methods including adsorption and nitrogen barbotage were investigated. For the better understand the mechanism of DMDS removal, FT-IR and density functional analysis were employed.

2. Materials and Methods

2.1. Reagends

The research was used reagents choline chloride (ChCl) (purity ≥99%), diethylene glycol (EG) (purity ≥95%), levulinic acid (Lev) (purity ≥98%), phenol (purity ≥99%), dimethyl disulfide (purity ≥98%), silica gel (SG) (grain diameter dp = 40 μm), active carbon (AC) (grain diameter dp = 0.3–0.5 mm), and aluminum oxide (III) (AO) (grain diameter dp = 40 μm) were purchased from Sigma-Aldrich (USA). Compressed gases such as nitrogen (purity N 5,5), air (purity N 5.0) generated by a DK50 compressor with a membrane dryer (Ekkom, Poland), and hydrogen (purity N 5.5) generated by a 9400 Hydrogen Generator (Packard, USA) were used for the preparation of model biogas, regeneration process, and chromatographic analysis.

2.2. Apparatures

Gas chromatograph Autosystem XL equipped with flame ionization detector (GC-FID) (PerkinElmer, USA), HP-5 (30 m × 0.25 mm × 0.25 μm) capillary column (Agilent Technologies, USA), TurboChrom 6.1 software (PerkinElmer, USA), and FT-IR Bruker Tensor 27 spectrometer (Bruker, USA) with an ATR accessory and OPUS software (Bruker, USA) were used.

2.3. Procedures

2.3.1. Preparation of DES

DESs were synthesized by mixing ChCl (HBA) with Ph, EG, and Lev (HBD) in a 1:2 molar ratio. The mixtures were stirred magnetically at 65 °C until homogeneous liquids were obtained. The liquids were then left to cool spontaneously to room temperature. The physico-chemical properties of the synthesized DES were presented in Table 2.

Table 2. Selected physico-chemical properties of deep eutectic solvents (DESs) reported in the literature.

HBA	HBD	HBA:HBD Molar Ratio	Melting Points (°C)	Density (g/cm^1) (25 °C)	Viscosity (cP) (25 °C)	Ref.
ChCl	Ph	1:2	−68.9	1.10	14	[40]
	Lev		Liquid at RT *	1.12	32	[41]
	EG		−66.0	1.12	37	[42]

* RT—room temperature.

2.3.2. Absorption Process

The absorption process was prepared by means of the barbotage phenomena. Nitrogen (model biogas stream) was passed through a 20-mL vial containing 5 mL of DMDS. The created mixture (nitrogen–DMDS) was diluted with a nitrogen stream to 1.0 mg/Nm^3 (DMDS) concentration. The model biogas stream containing DMDS was passed through an absorption column (total volume 60 mL) containing 50 mL of DES. The total flow of gaseous DMDS and nitrogen was kept constant at 50 mL/min. The concentration of DMDS was monitored at the inlet and outlet of the barbotage column using GC-FID. The processes were carried out for 1200 min. The absorptivity (A) of DMDS in the DES was calculated using Equation (1):

$$A = \frac{C_{in} - C_{out}}{C_{in}} \tag{1}$$

where C_{in}—initial DMDS concentration (ppm *v/v*),

C_{out}—DMDS concentration after absorption process (ppm *v/v*).

2.3.3. Regeneration of DESs

After the absorption process, DESs were regenerated using two popular methods, including nitrogen barbotage and adsorption. Nitrogen barbotage was carried on as follows: 4 mL of DES was barbotaged using nitrogen flow 50 mL/min for 2.5 or 5 h. Three types of adsorbents, i.e., AC, SG, and AO were used in the second type of regeneration process. All adsorbents were activated in a laboratory dryer at 120 °C for 2 h. The 4 mL of DES containing DMDS was mixed with 160 mg and 420 mg adsorbents in a vial. The vials were maintained in a laboratory shaker at 25 °C for 30 min, subsequently centrifuged for 5 min at 7000 rpm, and filtered through a 0.45 µm cellulose filter. The concentration of DMDS in DES (before and after regeneration) was controlled using static headspace coupled to gas chromatography (SHS-GC).

2.3.4. Chromatographic Analysis

GC temperature program was 120 °C; injection port temperature was 300 °C carrier gas–nitrogen (2 mL/min); injection mode: split 20:1; detector temperature was 300 °C; detector gases flow rates were hydrogen 40 mL/min and air 400 mL/min. DESs (2 mL) after regeneration were thermostated at 80 °C for 50 min. Then, 0.1 mL of gas phase was introduced into the GC injector. In order to monitor DMDS concentrations during the absorption process, 0.5 mL of model biogas was analyzed.

2.3.5. FT-IR Analysis

The following working parameters of FT-IR analysis were used: spectral range: 4000–550 cm^{-1}; number of background scans: 256; number of sample scans: 256; resolution: 4 cm^{-1}; slit width: 0.5 cm.

2.3.6. Theoretical Studies

The molecular structures and interactions between DES and DMDS were optimized using the B3LYP/6-311++G** level of theory with the dispersion corrected computational model using Orca 4.1.1 software package. All configurations were optimized for local minima using frequency calculations. The interaction energy for the gas phase between the DES and DMDS was calculated according to the following expression (Equation (2)):

$$\Delta E = E_{DES-HMDS} - (E_{DES} - E_{HMDS}) \tag{2}$$

where $E_{DES-HMDS}$—total energy of complex DES-DMDS (kcal/mol);

$\quad E_{DES}$—individual energy of DES (kcal/mol);

$\quad E_{HMDS}$—individual energy of HMDS (kcal/mol).

The counterpoise method has also been implemented to estimate the effects of the basis set superposition error (BSSE) on the interaction energy, based on previous studies [43]. Electrostatic potential analysis (ESP) and reduced density gradient analysis (RGD) were performed to the visual interpret the interaction nature in the DES-DMDS complex. Both RDG and ESP analysis were performed using Multiwfn software [44–46]. In order to the graphical presentation of the results, the Visual Molecular Dynamics 1.9.3, the software was used.

3. Results and Discussion

3.1. Optimization of Absorption Conditions

Optimization of absorption conditions using deep eutectic solvents was carried out for DMDS as the main representative of volatile organosulfur compounds commonly found in real biogas streams [7,47–50]. The process was optimized in terms of DES type, temperature, the volume of DES, model biogas flow, and initial concentration of DMDS.

3.1.1. Kind of DES

The selection of the absorption solvent is particularly important in the absorptive desulfurization process. Three types of DES were tested, including ChCl:Ph, ChCl:Lev, and ChCl:EG in a 1:2 molar ratio (Figure 1). In the experiment, the following pre-selected absorption conditions were used: 50 mL of DES; initial concentration of DMDS 1 mg/Nm^3, 25 °C temperature; model biogas flow rate 50 mL/min. Among the investigated DESs, ChCl:Ph shows the best absorption efficiency. After 800 min, the absorptivity value for ChCl:Ph was below 0.3 and then increased rapidly over the next 300 min, which indicates DES saturation. The saturation time of the other two DES was 600 and 800 min for ChCl:EG and ChCl:Lev, respectively. It can be noticed that the best result was obtained for DES which has the lowest viscosity value. As the viscosity increased, both the absorption capacity and absorption rate decreased. In DES with higher viscosity, the mass transfer is hindered, therefore it is preferable to use solvents with the lowest viscosity.
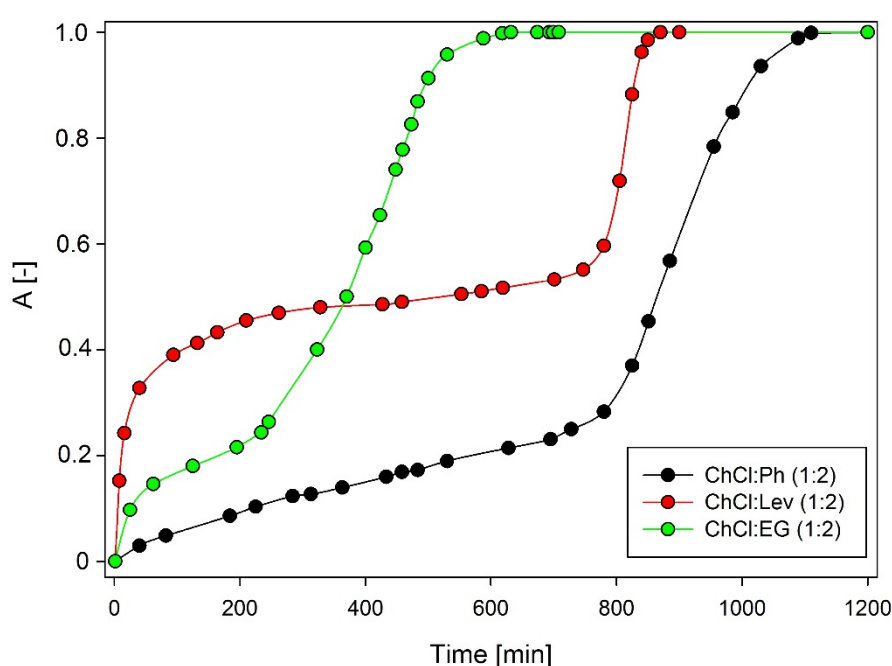
Figure 1. Dimethyl disulfide (DMDS) absorption curves using DES under optimum conditions.

It is worth noting that the viscosity of the DES increases when the amounts of hydroxyl groups in HBD increases. The existence of extra hydroxyl groups creates a more extensive hydrogen bond network which results in lower mobility of free species within the DES [28]. However, many other factors (except viscosity) also influence the DMDS removal efficiency, therefore in Section 3.2., the mechanism of absorptive desulfurization of model biogas was explained.

3.1.2. Volume of DES

In the studies, three-volume of DES in the range of 15–50 mL/min were investigated (Figure 2a). In the studies, other operating parameters, i.e., inlet concentration DMDS 1 mg/Nm^3, nitrogen flow rate 50 mL/min, and the temperature of process 25 °C, were constant. The results showed that with the increase in DES volume, the absorption efficiency increased significantly from 695 min to 1200 min. This is due to the fact that as the volume of the absorbent increases, the contact time between the gas phase and the liquid increases, due to which the saturation time is longer. Similar results were obtained in the work [51,52].
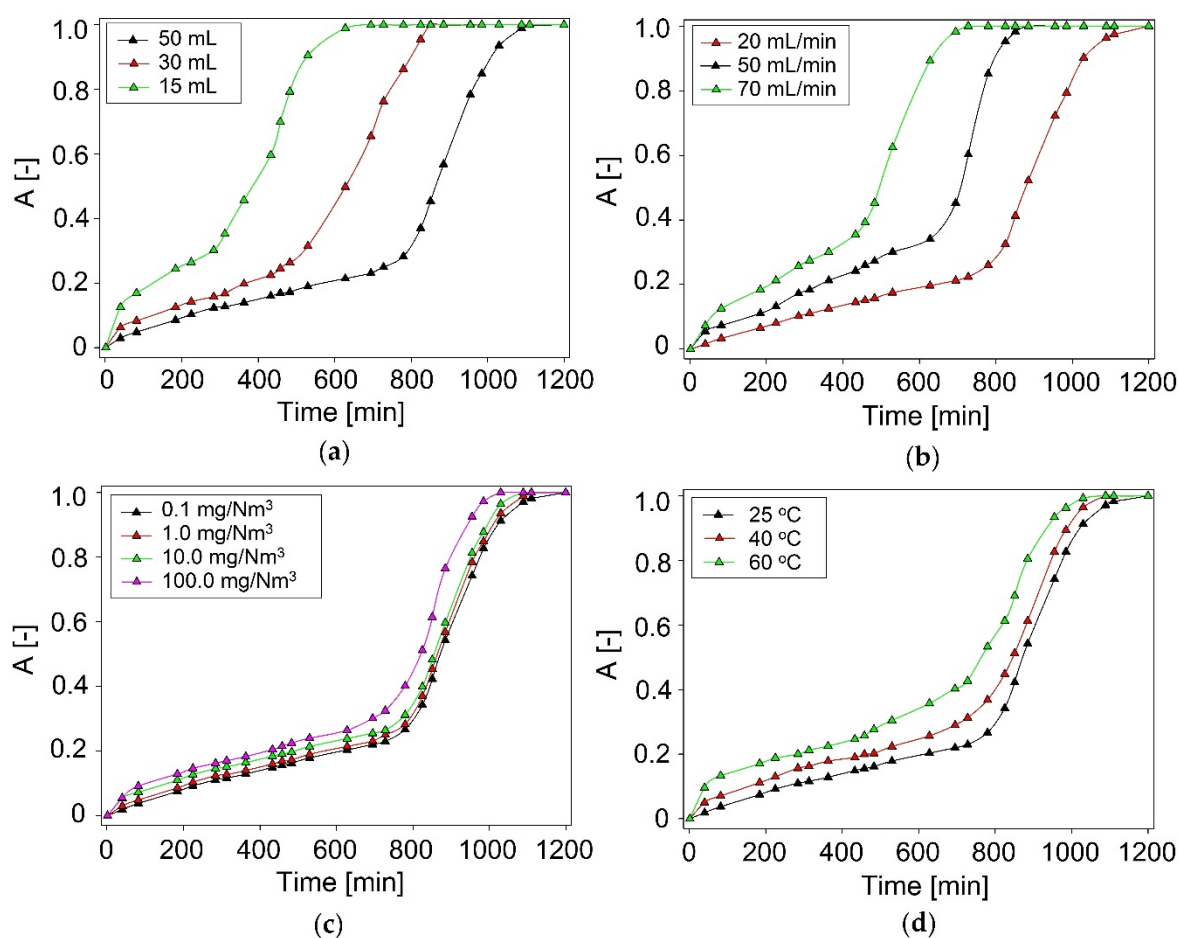
Figure 2. Experimental breakthrough curves of DMDS absorption with ChCl:Ph at different: (**a**) volume of DES; (**b**) biogas flow rate; (**c**) initial concentration of DMDS; (**d**) temperature.

3.1.3. Model Biogas Flow Rate

The next studied parameter was model biogas flow rate in the range of 20–70 mL/min (Figure 2b). From an industrial point of view, the flow rate of biogas should be as high as possible. The results indicate that the flow rate has a large impact on the overall DMDS capture process. As the flow rate increases from 20 to 70 mL/min, the DES saturation time is reduced from 1200 to 729 min. Similar results were obtained in the research [51–53]. This is due to the fact that as the flow velocity increases, the contact time of the polluted gas stream with the absorbent is reduced, which adversely affects the DMDS absorption process. However, only a slight change in saturation time is observed between the flow of 20 and 50 mL/min. Therefore, a 50 mL/min model biogas flow rate was considered as optimum value.

3.1.4. Initial Concentration of DMDS

In the studies, the initial concentration of DMDS in the range of 0.1–100 mg/Nm^3 was investigated (Figure 2c). The results indicate that the DMDS absorption efficiency remains fairly stable despite an increase in DMDS inlet concentration. This valuable result shows the ability of ChCl:Ph to the removal of DMDS in varying concentrations from real biogas steam which makes it desirable from an industrial point of view. Similar results were obtained in the work [54].

3.1.5. Temperature

Three temperature values, i.e., 25, 40, and 60 °C, were chosen to assess the influence of temperature on DMDS absorption behavior (Figure 2d). Theoretically, an increase in temperature affect the decreases

in DES viscosity and hence gas transfer rate are improved. The absorption curve reveals that by increasing DES temperature, the solubility of DMDS decreases. The decrease in solubility can be explained by the fact that the gas absorption process is normally exothermic. Therefore, the preferred temperature using DES is 25 °C, because in using this temperature the longest effective purification time for the biogas stream is achieved, lasting up to 1200 min. When the temperature is increased to 60 °C, the absorption time is reduced to 1010 min. Consequently, the absorption process can be performed at room temperature with minimal energy consumption. Similar results were obtained at work [55].

3.2. Mechanism of Absorption

3.2.1. FT-IR analysis

The experimental research on the mechanism of the absorption process was performed by FT-IR analysis. The spectra of pure DESs were compared with pure DMDS, and DES-DMDS complex spectra (Figure 3a–c). All characteristic bands that can be attributed to DMDS ($2909.32 \, cm^{-1}$—δs (CH) stretch, $1411.73 \, cm^{-1}$—δas (CH$_3$) def., $1302.68 \, cm^{-1}$—δs (CH$_3$) def., $692.82 \, cm^{-1}$—C-S stretch, $540.96 \, cm^{-1}$—S-S stretch) are visible in the ChCl:Ph-DMDS spectrum [56], which indicates the creation of the DES-DMDS complex (Figure 3a). Theoretically, in the absorptive DMDS removal process, both sulfur atoms can act as a donor in S–H···π and as an acceptor in O–H···S and C–H···S interactions [57–59]. However, on the FT-IR spectra, there are no shifts corresponding to this type of interaction. Therefore, other interactions must play a key role in the DMDS absorption process. Similar results were also obtained for ChCl:Lev (Figure 3b) and ChCl:EG (Figure 3c).

3.2.2. Molecular Modeling

In order to better understand the mechanisms of DMDS removal from the gas phase using DES, the density functional theory (DFT) was applied. For this purpose, the most probable and stable configurations in the gas phase of ChCl:Ph-DMDS, ChCl:Lev-DMDS, and ChCl:EG-DMDS was geometry optimized at the B3LYP/6-311++G** level of theory (Figure 4). The results indicate that in all complex, nonbonded interaction exists between choline and chloride atom (O-H···Cl), which can be identified as strong hydrogen bond because of short distance (below 2.5 Å) [60]. Hydrogen bonds also occur between the Cl atom and two phenol molecules such as Cl···H-O (2.32 Å) and Cl···H-O (2.44 Å) in the ChCl:Ph-DMDS complex, between Cl atom and carboxylic group of levulinic acid (Cl···H-OOC 2.07 Å), carboxylic groups of two levulinic acid molecules (OH···OH 1.88Å) in ChCl:Lev-DMDS, and between the Cl atom and hydroxyl group of one EG molecule (Cl···H-O 2.13 Å) as well as between both EG molecules (OH···HO 2.14 Å) in ChCl:EG-DMDS complex. However, between DMDS and all DES, there are no hydrogen bonds and only weak electrostatic bonds occur.

Electrostatic potential analysis (ESP) was used for visualization of total charge distribution and relative polarity of the studied DMDS structure and DESs-DMDS complexes. The ESP of DMDS, ChCl:Ph-DMDS, ChCl:Lev-DMDS, and ChCl:EG-DMDS are mapped onto their electron densities in Figure 5. The results indicate that the electropositive areas are around the hydrogen atoms whereas the electronegative area is around sulfur atoms, in the DMDS structure. In the ChCl:Ph-DMDS complex, a large electropositive area is around the nitrogen atom and electronegative areas are around Cl, O, and S atoms. During the absorption process, the electronegative region located around sulfur atoms in the DMDS molecule interacts with the electropositive area located around the nitrogen atom in the ChCl:Ph molecule. These interactions provide efficient DMDS removal from the model biogas. On the other hand, it can be concluded that HBA in the DES molecule has the greatest impact on the purification process. This phenomenon will be investigated in subsequent works. Similar results can be found in ChCl:Lev-DMDS and ChCl:EG-DMDS complex.
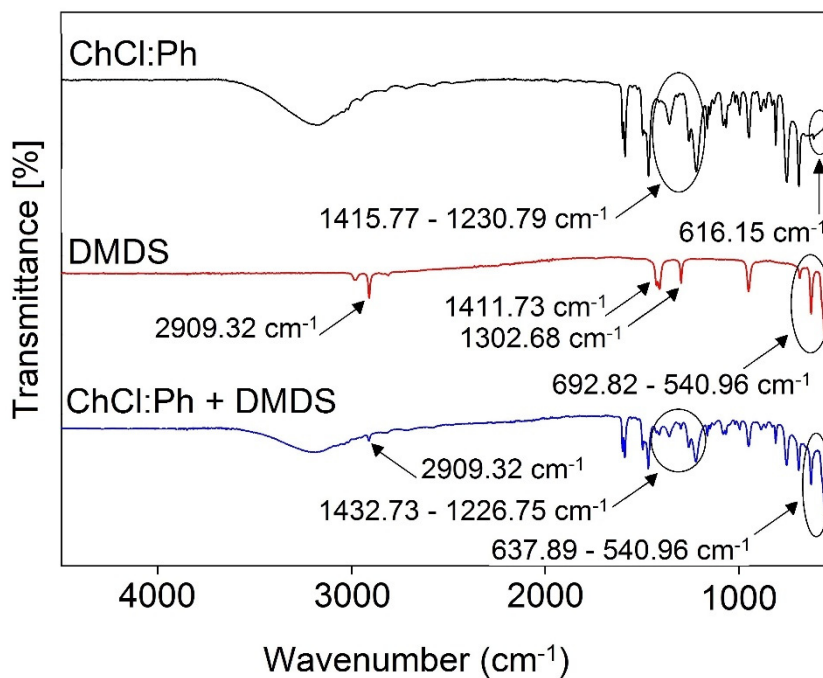
(**a**)
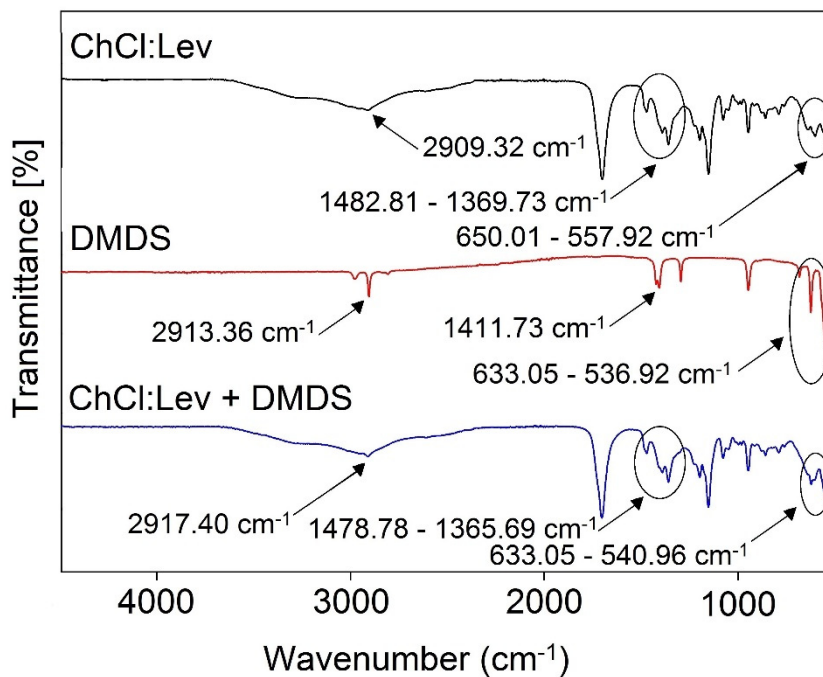
(**b**)

Figure 3. *Cont.*
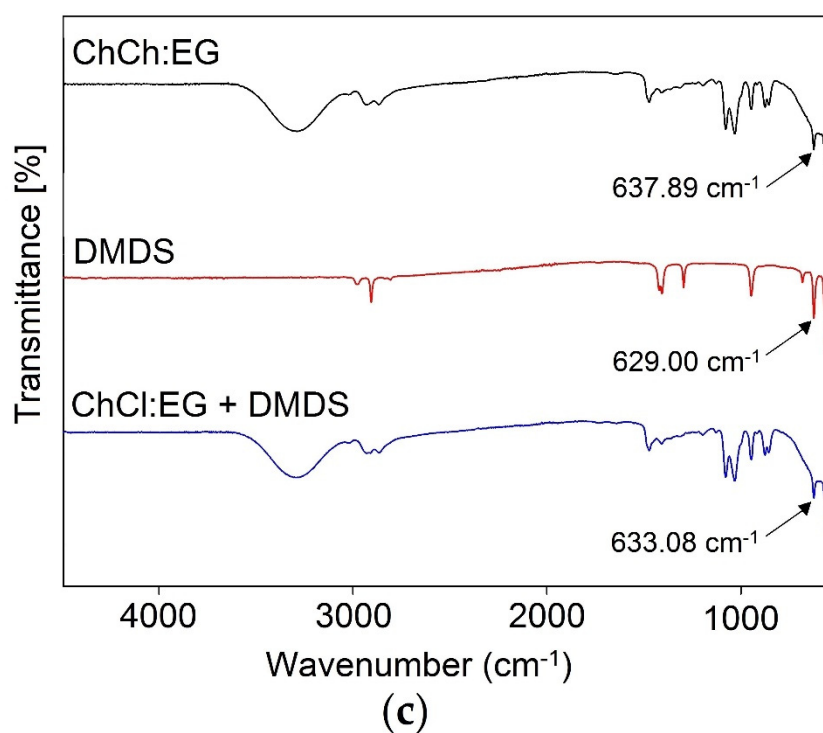
Figure 3. FT-IR spectra of: (**a**) pure ChCl:Ph, pure DMDS, and DES after the DMDS absorption process; (**b**) ChCl:Lev, pure DMDS, and DES after the DMDS absorption process; (**c**) pure ChCl:EG, pure DMDS, and DES after the DMDS absorption process.
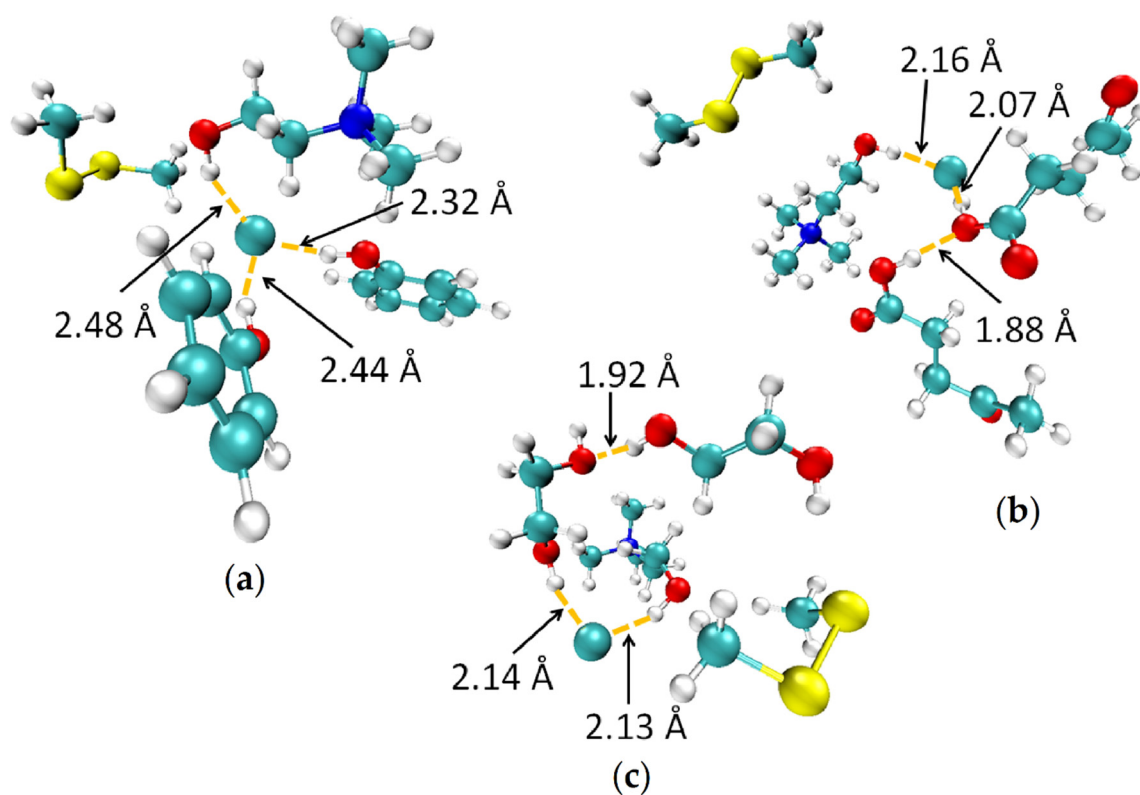
Figure 4. Optimized configurations of (**a**) ChCl:Ph-DMDS; (**b**) ChCl:Lev-DMDS; (**c**) ChCl:EG-DMDS. Carbon and chlorine atoms are displayed in light blue, nitrogen atoms are in dark blue, oxygen atoms are in red, sulfur atoms are in yellow, and hydrogen atoms are in white.
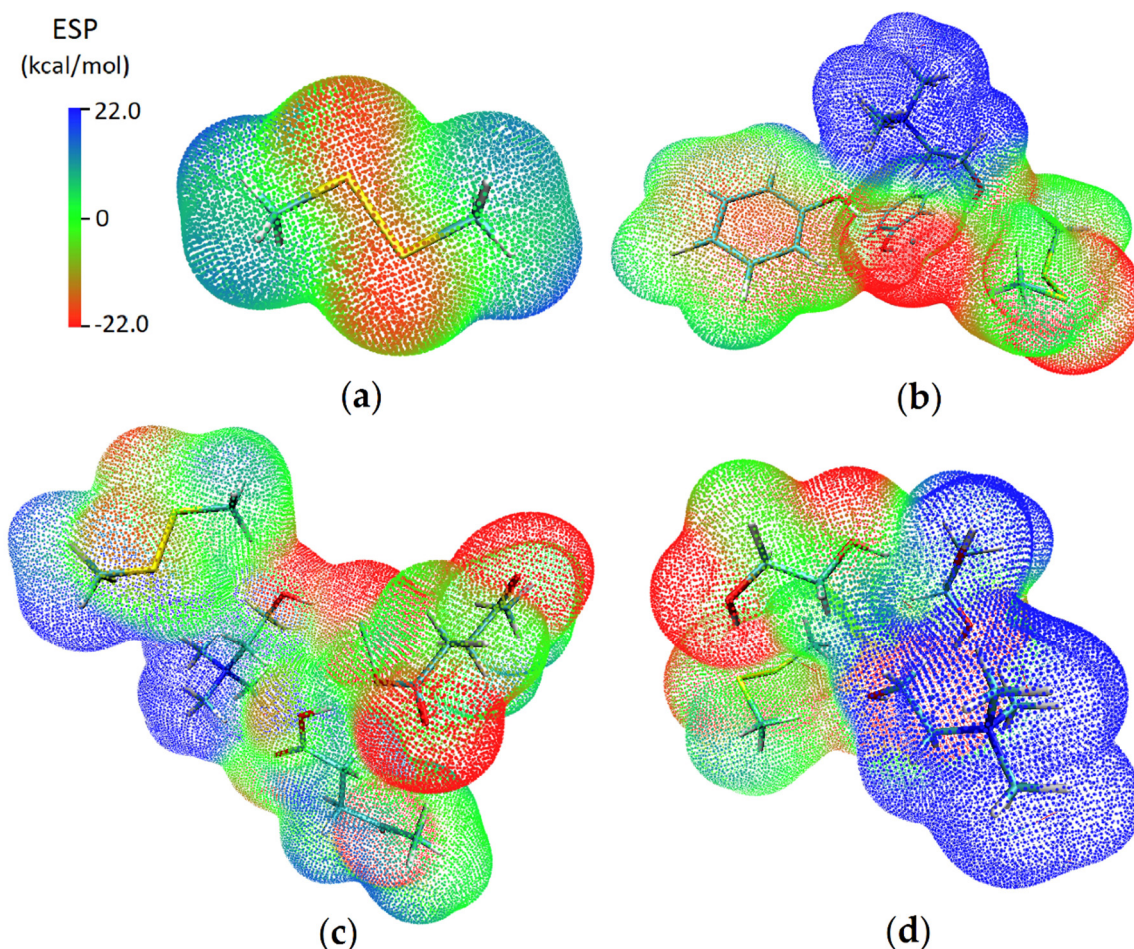
Figure 5. Electrostatic potential mapped on electron total density with an isovalue 0.001 for (**a**) DMDS; (**b**) ChCl:Ph-DMDS; (**c**) ChCl:Lev-DMDS; (**d**) ChCl:EG-DMDS. Blue color represents positive charges, red color represents negative charges.

The reduced density gradient (RDG) is a beneficial approach to distinguish and visualize various types of noncovalent interactions in real space. In the studies, the RDG analysis was used to visualized weak noncovalent interactions (i.e., hydrogen bond, van der Waals interaction, and repulsive effect), by plotting the RDG versus the electron density multiplied by the sign of the second Hessian eigenvalue, based on previous studies [44]. In Figure 6b,d,f, the green surfaces indicate van der Waals interaction, red surfaces indicate strong repulsion, and blue surfaces indicate an H-bond. The obtained data show that the three hydrogen bonds, as well as the van der Waals interaction, were formed between HBA and HBDs in all studied DES, which correspond to a large, negative sign($\lambda 2$)ρ value (from -0.04 to -0.02 au) and 0.01 au $<$ sign($\lambda 2$)ρ < 0.01 au, respectively, in 2D diagrams (Figure 6a,c,e). Furthermore, in ChCl:Ph-DMDS, strong repulsive bonds occur (sign($\lambda 2$)ρ $= 0.02$ au), due to the presence of an aromatic ring in the phenol molecule. In all the studied complexes, between DES and DMDS, only a van der Waals interaction occur. The surfaces of the van der Waals interaction increase following the order of ChCl:EG-DMDS $<$ ChCl:Lev-DMDS $<$ ChCl:Ph-DMDS. This indicates that the main driving force affecting DMDS removal from model biogas is the van der Waals interactions.
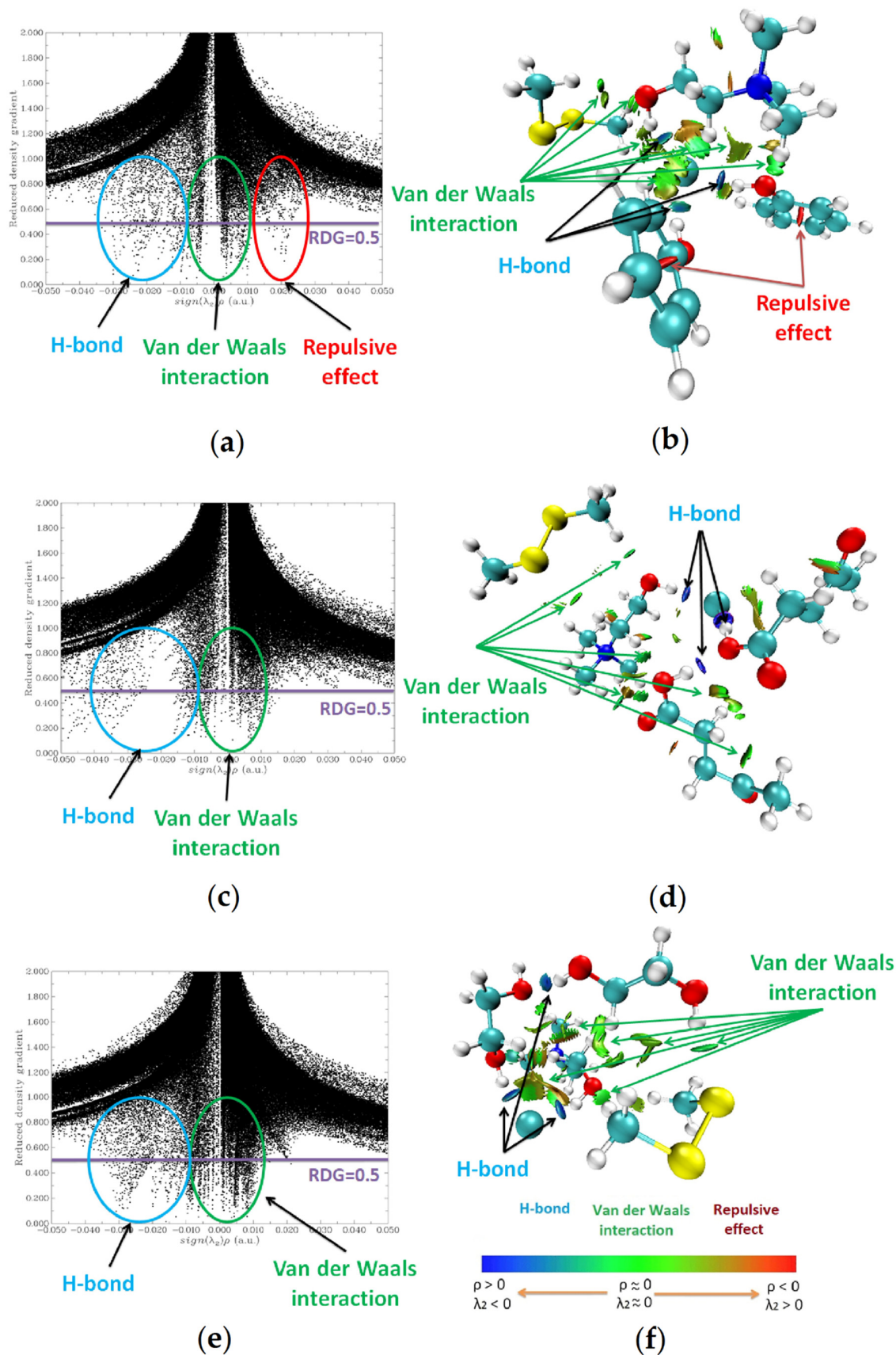
Figure 6. RDG isosurfaces (s = 0.5 a.u.) and 2D diagrams of electron density and its reduced density gradient for (**a**,**b**) ChCl:Ph-DMDS; (**c**,**d**) ChCl:Lev-DMDS; (**e**,**f**) ChCl:EG-DMDS.

The calculated interaction energy in the gas phase between DES and DMDS were −10.8, −3.7, and −9.6 kcal/mol for ChCl:Ph-DMDS, ChCl:Lev-DMDS, and ChCl:EG-DMDS, respectively. The lower interaction energy values stand for stronger interaction between DES and DMDS. The obtained data followed a similar trend to the experimental data: ChCl:Ph-DMDS < ChCl:EG-DMDS < ChCl:Lev-DMDS.

3.3. Regeneration and Reusability of DES

From an industrial point of view, the regeneration of DES is an essential and significant factor because it has a great impact on the operating cost. Therefore, regeneration of DES was carried on through one of the best-known regenerative methods, i.e., nitrogen barbotage (NG, which was carried for 2.5 and 5 h) and the adsorption process (with different types and amounts of adsorbents). In the adsorption process, three types of adsorbents were tested including SG, AC, and AO, in the amounts of 160 and 420 mg, which were added to 4 mL of each DES and shaken for 30 min. The results indicate that the nitrogen barboage is the most efficient desorption method. Desorption efficiency of DMDS from all DES after 5 h is higher than 99.999%. From ChCl:Ph, DMDS can be completely removed after 3 h (Figure 7).
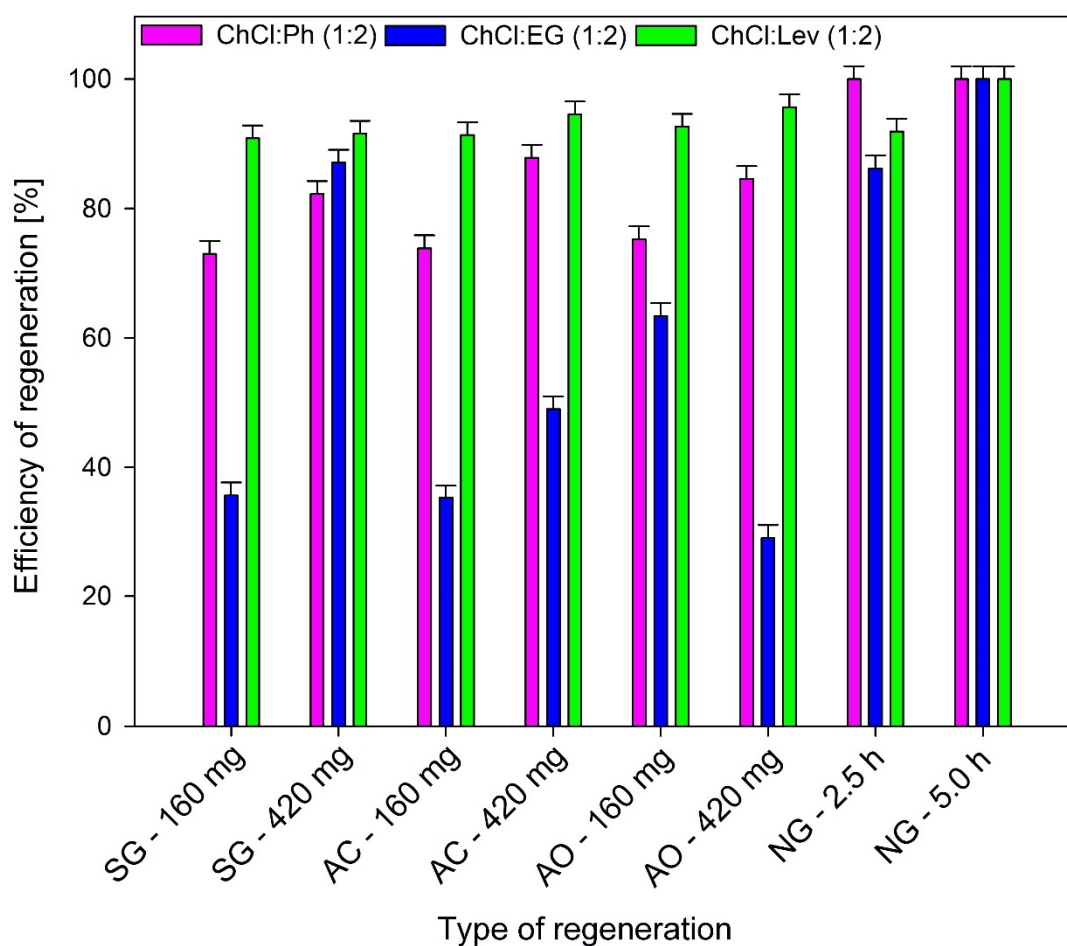
Figure 7. Regeneration efficiency of DESs after different regeneration methods.

For the remaining DES, this time should be extended, which would affect the cost of the process. In addition, the results show that slightly lower regeneration efficiencies for all DES were obtained using the adsorption process. The regeneration efficiency were in the range of 87.8%–84.5% for ChCl:Ph, 87.1%–63.4% for ChCl:EG, and 96.6%–91.3% ChCl:Lev. The highest absorption efficiency was obtained for 420 mg of SG. In most cases, the increase in adsorbent mass relative to the amount of DES containing

DMDS resulted in increased adsorption efficiency due to the increased adsorption surface. However, from an economical industrial point of view, the adsorbent amount should be as low as possible. Desorption is the most effective method to remove DMDS from ChCl:Lev. This is probably due to the low sorption capacity of ChCl:Lev and the absorption relatively small amount of DMDS.

The absorption−desorption results indicate that DMDS could be completely removed from DES and the absorbent could be reused for a minimum of five times without significant loss of absorption capacity DMDS (Figure 8a). In order to examine whether there were any structural changes in DES after the regeneration process (nitrogen barbotage), FT-IR analysis was used (Figure 8b–d). No additional peaks or shifts are observed in the DES spectra before and after regeneration, which indicates DES stability during the regeneration process.
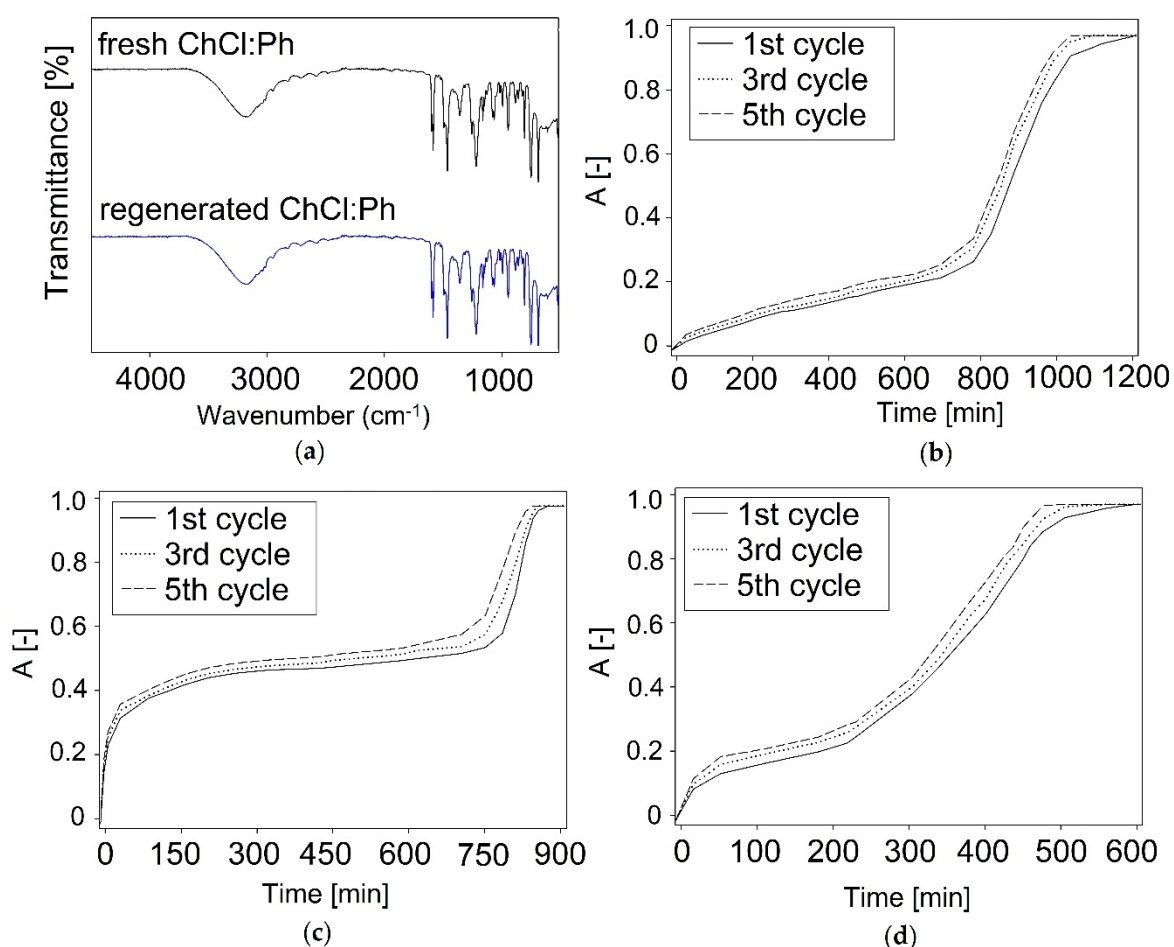
Figure 8. (**a**) FT-IR spectra recorded from on fresh ChCl:Ph, regenerated ChCl:Ph, and the reusability of DES: (**b**) ChCl:Ph; (**c**) ChCl:Lev; (**d**) ChCl:EG.

4. Conclusions

The choline chloride-based deep eutectic solvents have been synthesized and tested as alternative eco-friendly and green solvents for absorptive desulfurization of model biogas. Effect of selected absorption parameters including kind of DES, temperature, absorbent volume, model biogas flow rate, and initial concentration of DMDS were studied. It was found that the optimum absorption parameters for DMDS removal were absorption solvent ChCl:Ph in 1:2 molar ratio, 50 mL of DES, temperature 25 °C, and 50 mL/min flow rate. The influence of DMDS concentration indicates that the initial amount of DMDS in model biogas has only a minor effect on the absorption capacity and rate. In the optimum conditions, DMDS was removed with high efficiency for 800 min. After this time, the

gradual saturation of DES occurred. After the absorption process, ChCl:Ph in 1:2 molar ratio could be regenerated by means of nitrogen barbotage and reuse without loss absorption capacity.

The studies on the absorptive desulfurization mechanism indicate that the van der Waals interaction is the main driving force for the efficient removal of DMDS from model biogas.

The developed absorption process with the choline chloride-based deep eutectic solvents provides a promising alternative method for the removal of volatile organosulfur compounds from the real biogas stream.

The paper presents preliminary results of research on the removal of DMDS from a model biogas stream. However, due to the rich composition of real biogas samples, other volatile organic compound groups should also be included in future studies. In addition, in the future, to verify the suitability of the developed method, the studies using real samples of heavily contaminated biogas streams from sewage treatment plants and landfills will be carried out.

References

1. Guo, X.M.; Trably, E.; Latrille, E.; Carrre, H.; Steyer, J.P. Hydrogen production from agricultural waste by dark fermentation: A review. *Int. J. Hydrogen Energy* **2010**, *35*, 10660–10673. [CrossRef]

2. Słupek, E.; Makoś, P.; Kucharska, K.; Gębicki, J. Mesophilic and thermophilic dark fermentation course analysis using sensor matrices and chromatographic techniques. *Chem. Pap.* **2019**, in press.

3. Bastidas-Oyanedel, J.R.; Bonk, F.; Thomsen, M.H.; Schmidt, J.E. Dark fermentation biorefinery in the present and future (bio)chemical industry. *Rev. Environ. Sci. Biotechnol.* **2015**, *14*, 473–498. [CrossRef]

4. Persson, M.; Jonsson, O.; Wellinger, A. *Biogas Upgrading To Vehicle Fuel Standards and Grid*; ISBN IEA Bioenergy Task 37; IEA Bioenergy: London, UK, 2007.

5. Andrés, C.; Guardia, A.D.; Couvert, A.; Wolbert, D.; Le, S.; Soutrel, I.; Nunes, G. Odor concentration (OC) prediction based on odor activity values (OAVs) during composting of solid wastes and digestates. *Atmos. Environ.* **2019**, *201*, 1–12.

6. Papurello, D.; Soukoulis, C.; Schuhfried, E.; Cappellin, L.; Gasperi, F.; Silvestri, S.; Santarelli, M.; Biasioli, F. Monitoring of volatile compound emissions during dry anaerobic digestion of the Organic Fraction of Municipal Solid Waste by Proton Transfer Reaction Time-of-Flight Mass Spectrometry. *Bioresour. Technol.* **2012**, *126*, 254–265. [CrossRef] [PubMed]

7. Salazar Gómez, J.I.; Lohmann, H.; Krassowski, J. Determination of volatile organic compounds from biowaste and co-fermentation biogas plants by single-sorbent adsorption. *Chemosphere* **2016**, *153*, 48–57. [CrossRef]

8. Boczkaj, G.; Makoś, P.; Fernandes, A.; Przyjazny, A. New procedure for the control of the treatment of industrial effluents to remove volatile organosulfur compounds. *J. Sep. Sci.* **2016**, *39*. [CrossRef]

9. Makoś, P.; Boczkaj, G. Deep eutectic solvents based highly efficient extractive desulfurization of fuels—Eco-friendly approach. *J. Mol. Liq.* **2019**, 111916. [CrossRef]

10. Andersson, F.A.T.; Karlsson, A.; Svensson, B.H.; Ejlertsson, J. Occurrence and abatement of volatile sulfur compounds during biogas production. *J. Air Waste Manag. Assoc.* **2004**, *54*, 855–861. [CrossRef]

11. Sarmad, S.; Mikkola, J.-P.; Ji, X. CO_2 capture with Ionic liquids (ILs) and Deep Eutectic Solvents (DESs): A new generation of sorbents. *ChemSusChem* **2016**, *10*, 324–352. [CrossRef]

12. Sevimoğlu, O.; Tansel, B. Effect of persistent trace compounds in landfill gas on engine performance during energy recovery: A case study. *Waste Manag.* **2013**, *33*, 74–80. [CrossRef] [PubMed]

13. Sun, Q.; Li, H.; Yan, J.; Liu, L.; Yu, Z.; Yu, X. Selection of appropriate biogas upgrading technology-a review of biogas cleaning, upgrading and utilisation. *Renew. Sustain. Energy Rev.* **2015**, *51*, 521–532. [CrossRef]

14. Allegue, L.B.; Hinge, J. Biogas upgrading Evaluation of methods for H 2 S removal. *Dan. Technol. Inst.* **2014**, 31.

15. Mahmood, Q.; Zheng, P.; Cai, J.; Hayat, Y.; Hassan, M.J.; Wu, D.L.; Hu, B.L. Sources of sulfide in waste streams and current biotechnologies for its removal. *J. Zhejiang Univ. Sci. A* **2007**, *8*, 1126–1140. [CrossRef]

16. Burgess, J.E.; Parsons, S.A.; Stuetz, R.M. Developments in odour control and waste gas treatment biotechnology: A review. *Biotechnol. Adv.* **2001**, *19*, 35–63. [CrossRef]

17. Ryckebosch, E.; Drouillon, M.; Vervaeren, H. Techniques for transformation of biogas to biomethane. *Biomass Bioenergy* **2011**, *35*, 1633–1645. [CrossRef]

18. Nordlander, E.; Holgersson, J.; Thorin, E.; Thomassen, M.; Yan, J. Energy Efficiency Evaluation of two Biogas Plants. *Int. Conf. Appl. Energy* **2011**, 1661–1675.

19. Rossi, F.; Nicolini, A. A cylindrical Small Size Molten Carbonate Fuel Cell: Experimental Investigation on Materials and Improving Performance Solutions. *Fuel Cells* **2009**, *9*, 170–177. [CrossRef]

20. Rossi, F. A new geometry high performance small power MCFC. *J. Fuel Cell Sci. Technol.* **2004**, 1–6. [CrossRef]

21. Tippayawong, N.; Thanompongchart, P. Biogas quality upgrade by simultaneous removal of CO_2 and H_2S in a packed column reactor. *Energy* **2010**, *35*, 4531–4535. [CrossRef]

22. Noorain, R.; Kindaichi, T.; Ozaki, N.; Aoi, Y.; Ohashi, A. Biogas purification performance of new water scrubber packed with sponge carriers. *J. Clean. Prod.* **2019**, *214*, 103–111. [CrossRef]

23. Farooq, M.; Chaudhry, I.A.; Hussain, S.; Ramzan, N.; Ahmed, M. Biogas Up Gradation for Power Generation Applications in Pakistan. *J. Qual. Technol. Manag. Vol. Viiiissue Ii* **2012**, *VIII*, 107–118.

24. Wilk, A.; Więcław-Solny, L.; Tatarczuk, A.; Krótki, A.; Spietz, T.; Chwoła, T. Solvent selection for CO_2 capture from gases with high carbon dioxide concentration. *Korean J. Chem. Eng.* **2017**, *34*, 2275–2283. [CrossRef]

25. Xu, H.J.; Zhang, C.F.; Zheng, Z.S. Solubility of hydrogen sulfide and carbon dioxide in a solution of methyldiethanolamine mixed with ethylene glycol. *Ind. Eng. Chem. Res.* **2002**, *41*, 6175–6180. [CrossRef]

26. Romero, A.; Santos, A.; Tojo, J.; Rodríguez, A. Toxicity and biodegradability of imidazolium ionic liquids. *J. Hazard. Mater.* **2008**, *151*, 268–273. [CrossRef] [PubMed]

27. Makoś, P.; Słupek, E.; Gębicki, J. Hydrophobic deep eutectic solvents in microextraction techniques–A review. *Microchem. J.* **2020**, *152*, 104384. [CrossRef]

28. Zhang, Q.; De Oliveira Vigier, K.; Royer, S.; Jérôme, F. Deep eutectic solvents: Syntheses, properties and applications. *Chem. Soc. Rev.* **2012**, *41*, 7108–7146. [CrossRef]

29. Smink, D.; Kersten, S.R.A.; Schuur, B. Recovery of lignin from deep eutectic solvents by liquid-liquid extraction. *Sep. Purif. Technol.* **2019**, *235*, 116127. [CrossRef]

30. Florindo, C.; Branco, L.C.; Marrucho, I.M. Development of hydrophobic deep eutectic solvents for extraction of pesticides from aqueous environments. *Fluid Phase Equilibria* **2017**, *448*, 135–142. [CrossRef]

31. Zubeir, L.F.; Van Osch, D.J.G.P.; Rocha, M.A.A.; Banat, F.; Kroon, M.C. Carbon Dioxide Solubilities in Decanoic Acid-Based Hydrophobic Deep Eutectic Solvents. *J. Chem. Eng. Data* **2018**, *63*, 913–919. [CrossRef]

32. Pätzold, M.; Siebenhaller, S.; Kara, S.; Liese, A.; Syldatk, C.; Holtmann, D. Deep Eutectic Solvents as Efficient Solvents in Biocatalysis. *Trends Biotechnol.* **2019**, *37*, 943–959. [CrossRef] [PubMed]

33. Makoś, P.; Fernandes, A.; Przyjazny, A.; Boczkaj, G. Sample preparation procedure using extraction and derivatization of carboxylic acids from aqueous samples by means of deep eutectic solvents for gas chromatographic-mass spectrometric analysis. *J. Chromatogr. A* **2018**, *1555*, 10–19. [CrossRef] [PubMed]

34. Makoś, P.; Przyjazny, A.; Boczkaj, G. Hydrophobic deep eutectic solvents as "green" extraction media for polycyclic aromatic hydrocarbons in aqueous samples. *J. Chromatogr. A* **2018**, *1570*, 28–37. [CrossRef] [PubMed]

35. Sun, S.; Niu, Y.; Xu, Q.; Sun, Z.; Wei, X. Efficient SO_2 absorptions by four kinds of deep eutectic solvents based on choline chloride. *Ind. Eng. Chem. Res.* **2015**, *54*, 8019–8024. [CrossRef]

36. Yang, D.; Han, Y.; Qi, H.; Wang, Y.; Dai, S. Efficient Absorption of SO_2 by EmimCl-EG Deep Eutectic Solvents. *ACS Sustain. Chem. Eng.* **2017**, *5*, 6382–6386. [CrossRef]

37. Florindo, C.; Lima, F.; Branco, L.C.; Marrucho, I.M. Hydrophobic Deep Eutectic Solvents: A Circular Approach to Purify Water Contaminated with Ciprofloxacin. *ACS Sustain. Chem. Eng.* **2019**, *7*, 14739–14746. [CrossRef]

38. Moura, L.; Moufawad, T.; Ferreira, M.; Bricout, H.; Tilloy, S.; Monflier, E.; Costa Gomes, M.F.; Landy, D.; Fourmentin, S. Deep eutectic solvents as green absorbents of volatile organic pollutants. *Environ. Chem. Lett.* **2017**, *15*, 747–753. [CrossRef]

39. Słupek, E.; Makoś, P.; Gębicki, J.; Rogala, A. Purification of model biogas from toluene using deep eutectic solvents. *E3s Web Conf.* **2019**, *116*, 00078.

40. Ma, Y.; Wang, Q.; Zhu, T. Comparison of hydrophilic and hydrophobic deep eutectic solvents for pretreatment determination of sulfonamides from aqueous environments. *Anal. Methods* **2019**, *11*, 5901–5909. [CrossRef]

41. Florindo, C.; Oliveira, F.S.; Rebelo, L.P.N.; Fernandes, A.M.; Marrucho, I.M. Insights into the synthesis and properties of deep eutectic solvents based on cholinium chloride and carboxylic acids. *ACS Sustain. Chem. Eng.* **2014**, *2*, 2416–2425. [CrossRef]

42. Kalhor, P.; Ghandi, K. Deep eutectic solvents for pretreatment, extraction, and catalysis of biomass and food waste. *Molecules* **2019**, *24*, 4012. [CrossRef] [PubMed]

43. Simon, S.; Duran, M.; Dannenberg, J.J. How does basis set superposition error change the potential surfaces for hydrogen-bonded dimers? *J. Chem. Phys.* **1996**, *105*, 11024–11031. [CrossRef]

44. Johnson, E.R.; Keinan, S.; Mori-Sánchez, P.; Contreras-García, J.; Cohen, A.J.; Yang, W. Revealing noncovalent interactions. *J. Am. Chem. Soc.* **2010**, *132*, 6498–6506. [CrossRef] [PubMed]

45. Lu, T.; Chen, F. Quantitative analysis of molecular surface based on improved Marching Tetrahedra algorithm. *J. Mol. Graph. Model.* **2012**, *38*, 314–323. [CrossRef] [PubMed]

46. Lu, T.; Chen, F. Multiwfn: A multifunctional wavefunction analyzer. *J. Comput. Chem.* **2012**, *33*, 580–592. [CrossRef] [PubMed]

47. Noyola, A.; Morgan-sagastume, J.M.; Lo, J.E.; Ingenierı, I.D.; Escolar, C.; Universitaria, C.; Me, D.F. Treatment of biogas produced in anaerobic reactors for domestic wastewater: Odor control and energy/resource recovery. *Rev. Environ. Sci. Bio. Technol.* **2006**, *51*, 93–114. [CrossRef]

48. Ducom, G.; Radu-tirnoveanu, D.; Pascual, C.; Benadda, B.; Germain, P. Biogas—Municipal solid waste incinerator bottom ash interactions: Sulphur compounds removal. *J. Hazard. Mater.* **2009**, *166*, 1102–1108. [CrossRef]

49. Arespacochaga, N.D.; Valderrama, C.; Mesa, C.; Bouchy, L.; Cortina, J.L. Biogas deep clean-up based on adsorption technologies for Solid Oxide Fuel Cell applications. *Chem. Eng. J.* **2020**, *255*, 593–603. [CrossRef]

50. Privalova, E.; Rasi, S.; Mäki-Arvela, P.; Eränen, K.; Rintala, J.; Murzin, D.Y.; Mikkola, J.P. CO_2 capture from biogas: Absorbent selection. *RSC Adv.* **2013**, *3*, 2979–2994. [CrossRef]

51. Hsu, C.H.; Chu, H.; Cho, C.M. Absorption and reaction kinetics of amines and ammonia solutions with carbon dioxide in flue gas. *J. Air Waste Manag. Assoc.* **2003**, *53*, 246–252. [CrossRef]

52. Guo, Y.; Niu, Z.; Lin, W. Comparison of removal efficiencies of carbon dioxide between aqueous ammonia and NaOH solution in a fine spray column. *Energy Procedia* **2011**, *4*, 512–518.

53. Gonzalez-Garza, D.; Rivera-Tinoco, R.; Bouallou, C. Comparison of ammonia, monoethanolamine, diethanolamine and methyldiethanolamine solvents to reduce CO_2 greenhouse gas emissions. *Chem. Eng. Trans.* **2009**, *18*, 279–284.

54. Zhang, K.; Ren, S.; Yang, X.; Hou, Y.; Wu, W.; Bao, Y. Efficient absorption of low-concentration SO_2 in simulated flue gas by functional deep eutectic solvents based on imidazole and its derivatives. *Chem. Eng. J.* **2017**, *327*, 128–134. [CrossRef]

55. Lemus, J.; Bedia, J.; Moya, C.; Alonso-Morales, N.; Gilarranz, M.A.; Palomar, J.; Rodriguez, J.J. Ammonia capture from the gas phase by encapsulated ionic liquids (ENILs). *RSC Adv.* **2016**, *6*, 61650–61660. [CrossRef]

56. Meyer, M. Infrared, raman, microwave and ab initio study of dimethyl disulfide: Structure and force field. *J. Mol. Struct.* **1992**, *273*, 99–121. [CrossRef]

57. Biswal, H.S.; Chakraborty, S.; Wategaonkar, S. Experimental evidence of O-H-S hydrogen bonding in supersonic jet. *J. Chem. Phys.* **2008**, *129*. [CrossRef]

58. Biswal, H.S.; Wategaonkar, S. Sulfur, not too far behind O, N, and C: SH$\cdots\pi$ hydrogen bond. *J. Phys. Chem. A* **2009**, *113*, 12774–12782. [CrossRef]

59. Bhattacharyya, S.; Bhattacherjee, A.; Shirhatti, P.R.; Wategaonkar, S. O-H$\cdots$S hydrogen bonds conform to the acid-base formalism. *J. Phys. Chem. A* **2013**, *117*, 8238–8250. [CrossRef]

60. Minch, M.J. An Introduction to Hydrogen Bonding (Jeffrey, George A.). *J. Chem. Educ.* **1999**, *76*, 759. [CrossRef]

Gdańsk, dnia 19.05.2023

dr inż. Patrycja Makoś-Chełstowska
....
(stopień/tytuł, imię i nazwisko)

Politechnika Gdańska
....
(Afiliacja)

OŚWIADCZENIE WSPÓŁAUTORA

Jako współautor pracy:. **"Absorptive Desulfurization of Model Biogas Stream Using Choline Chloride-Based Deep Eutectic Solvents"** oświadczam, że mój własny wkład polegał na konceptualizacji, metodologii, konfiguracja układu eksperymentalnego oraz oprogramowania, prowadzeniu badań, zestawieniu i obróbce danych, przygotowaniu oryginalnego manuskryptu oraz przygotowaniu recenzji i redakcji ostatecznej wersji manuskryptu.

Jednocześnie wyrażam zgodę na przedłożenie ww. pracy przez mgr inż. Edytę Słupek jako część rozprawy doktorskiej w formie spójnego tematycznie zbioru artykułów opublikowanych w czasopismach naukowych.

Oświadczam, że samodzielna i możliwa do wyodrębnienia część ww. pracy wykazuje indywidualny wkład mgr inż. Edyty Słupek polegający na: konceptualizacji, metodologii, konfiguracja układu eksperymentalnego oraz oprogramowania, prowadzeniu badań, zestawieniu i obróbce danych, przygotowaniu oryginalnego manuskryptu oraz przygotowaniu recenzji i redakcji ostatecznej wersji manuskryptu.

....
(podpis współautora)

Autorzy:

E. Słupek, P. Makoś-Chełstowska, J.Gębicki

Tytuł publikacji:

Removal of Siloxanes from Model Biogas by Means of Deep Eutectic
Solvents in Absorption Process

Czasopismo:

Materials

DOI:

10.3390/ma14020241

Removal of Siloxanes from Model Biogas by Means of Deep Eutectic Solvents in Absorption Process

Edyta Słupek [ID], Patrycja Makoś-Chełstowska *[ID] and Jacek Gębicki

Department of Process Engineering and Chemical Technology, Faculty of Chemistry,
Gdansk University of Technology, G. Narutowicza St. 11/12, 80-233 Gdańsk, Poland;
edyta.slupek@pg.edu.pl (E.S.); jacek.gebicki@pg.edu.pl (J.G.)
* Correspondence: patrycja.makos@pg.edu.pl; Tel.: +48-508-997-100

Abstract: The paper presents the screening of 20 deep eutectic solvents (DESs) composed of tetrapropylammonium bromide (TPABr) and glycols in various molar ratios, and 6 conventional solvents as absorbents for removal of siloxanes from model biogas stream. The screening was achieved using the conductor-like screening model for real solvents (COSMO-RS) based on the comparison of siloxane solubility in DESs. For the DES which was characterized by the highest solubility of siloxanes, studies of physicochemical properties, i.e., viscosity, density, and melting point, were performed. DES composed of tetrapropylammonium bromide (TPABr) and tetraethylene glycol (TEG) in a 1:3 molar ratio was used as an absorbent in experimental studies in which several parameters were optimized, i.e., the temperature, absorbent volume, and model biogas flow rate. The mechanism of siloxanes removal was evaluated by means of an experimental FT-IR analysis as well as by theoretical studies based on σ-profile and σ-potential. On the basis of the obtained results, it can be concluded that TPABr:TEG (1:3) is a very effective absorption solvent for the removal of siloxanes from model biogas, and the main driving force of the absorption process is the formation of the hydrogen bonds between DES and siloxanes.

Keywords: absorption; biogas; deep eutectic solvents; siloxanes

1. Introduction

The production of energy from renewable sources is not only a choice resulting from the policy of environmental protection or care of the environment but is also an obligation imposed by the European Union in the form of numerous ordinances and international agreements [1]. Therefore, more and more EU countries are focusing their attention on managing waste materials from various industries for the production of biogas [2–5]. This approach is consistent with the theory of sustainable development. However, the obtained biogas is usually a multicomponent mixture containing both inorganic and organic substances, i.e., methane (30–60% *v/v*), carbon dioxide (15–30% *v/v*), water, ammonia, hydrogen sulfide, organosulfur compounds, siloxanes, and other linear and aromatic volatile organic compounds (VOCs) [6,7].

The chemical composition of the waste biogas changes depending on the type of raw materials used in the dark fermentation process. The presence of gaseous substances other than methane causes many technological and environmental problems. Particularly dangerous pollutants include siloxane compounds, which can appear in the biogas from municipal landfills or wastewater treatment plants [8,9]. During the combustion of such types of biogas, silicone may be released and combined with oxygen. This can lead to the formation of silica deposits. The silica deposits can cause abrasion of engine parts or the formation of layers that inhibit thermal conductivity or lubrication and clogged transmission lines [10]. Therefore, in order to eliminate the failure of engines converting biogas into energy and to meet the quality requirements for fuels, raw biogas must undergo several treatment processes. The oldest and most widely used process for the

treatment of gaseous streams is the application of water or amine scrubbers [11,12]. However, most siloxanes are hydrophobic, and only some of them, i.e., trimethylsilanol, can be absorbed with water because of their high solubility therein [13,14]. Amine scrubbers do not show satisfactory efficiency of siloxane removal either. Among the effective absorbents, there are mineral oils, mixtures of glycols, or inorganic acids [15–18]. Although the abovementioned absorption methods allow for the recovery of solvents, these methods have a significant disadvantage, which is their energy consumption resulting from the large amount of energy needed to regenerate the absorbent. Therefore, in recent years, more and more scientific research has been devoted to the search for new "green solvents" that will have higher purification efficiency of biogas streams with a simultaneous lower energy demand during regeneration [19].

In the last few years, ionic liquids (ILs) have attracted a lot of attention because they belong to the class of new solvents with a high affinity for CO_2 and a wide range of VOCs [20,21] In addition, ILs have a lower degradation rate, a lower energy requirement for solvent regeneration, and lower corrosive characteristics compared to conventional amine-based solvents [22]. The main disadvantages of ILs are their high viscosity, very high prices, and toxic character. Therefore, deep eutectic solvents (DESs) are a good alternative to ILs because they are much cheaper, less toxic, and more biodegradable [23]. These advantageous properties have made DESs widely used in various separation processes such as extraction [24–27], absorption [28–33], or adsorption [34]. So far, DES has not been used for the experimental removal of siloxanes from biogas. Only theoretical studies can be found in the literature [35].

The study presents screening of twenty-five deep eutectic solvents composed of tetrapropylammonium bromide (TPABr) as hydrogen bond acceptor (HBA) and glycols as hydrogen bond donors (HBDs) in various molar ratio as absorbents for removal of siloxanes from model biogas stream. For this proposal, the conductor-like screening model for real solvents (COSMO-RS) was used. The selection of DESs with the highest siloxane capacity potential was made on the basis of the calculated solubility. For DES (TPABr:TEG 1:3), which was characterized by the highest solubility of siloxanes, the study of its physicochemical properties, i.e., viscosity, density, and the melting point, was performed. Further on, optimization studies of the main parameters influencing the absorption processes were carried out. The mechanism of siloxane removal was evaluated by means of an experimental FT-IR analysis as well as theoretical studies based on σ-profile and σ-potential. To the best of our knowledge, this is the first study dedicated to the application of DES for experimental removal of siloxanes from the gas steams.

2. Materials and Methods

2.1. Materials

The following pure substances were used in this study: tetrapropylammonium bromide (TPABr) (purity ≥ 99.0%), tetraethylene glycol (TEG) (purity 99%), hexamethyldisiloxane (L2) (purity 98.5%), octamethyltrisiloxane (L3) (purity 98.5%), and octametylocyclotetrasiloxane (D4) (purity 98%) were purchased from Sigma Aldrich (St. Louis, MO, USA).

For the preparation of model biogas, compressed gases such as nitrogen (purity *N* 5.5) and methane (purity *N* 5.0) (Linde Gas, Łódź, Poland) were used. Additionally, for the GC analysis, compressed gases such as nitrogen (purity *N* 5.5), air (purity *N* 5.0) generated by a DK50 compressor with a membrane dryer (Ekkom, Cracow, Poland), and hydrogen (purity *N* 5.5) generated by a 9400 Hydrogen Generator (Packard, Detroit, MI, USA) were used.

2.2. Apparatus

The purification process was controlled by gas chromatography (Autosystem XL) (PerkinElmer, Waltham, MA, USA) coupled with a flame ionization detector (FID) (PerkinElmer, Waltham, MA, USA) and an HP-5 (30 m × 0.25 mm × 0.25 μm) capillary column (Agilent

Technologies, Santa Clara, CA, USA). In the investigations, the TurboChrom 6.1 software (PerkinElmer, Waltham, MA, USA), was used.

The following apparatus was used to evaluate the physicochemical properties: Bruker Tensor 27 spectrometer (Bruker, Billerica, MA, USA) with an ATR accessory and OPUS software (Bruker); BROOKFIELD LVDV-II + viscometer (Labo-Plus, Warsaw, Poland); DMA 4500 M (Anton Paar, Graz, Austria).

2.3. Procedures

2.3.1. COSMO-RS Studies

The geometry optimization of TPABr:TEG (1:3) was performed by means of the continuum solvation COSMO model at the BVP86/TZVP level of theory. The level of theory was used based on previous studies [35,36]. Multiple starting geometries of TPABr:TEG (1:3) were created and optimized in the gas phase to identify stable conformers. In the next step, the vibrational analysis was conducted to find the DES conformer correspond to the true energy minimum. Full geometry optimization was performed only for the most energetically favorable conformer.

In the studies, the COSMO-RS model was used for the screening of DESs using ADF COSMO-RS software (SCM, Netherlands). The relative solubility of siloxanes (x_j) in DESs were calculated using Equation (1):

$$log_{10}(x_j) = log_{10}\left[\frac{\exp\left(\mu_j^{pure} - \mu_j^{solvent} - \Delta G_{j,fusion}\right)}{RT}\right] \tag{1}$$

where: μ_j^{pure}—chemical potential of pure siloxanes (J/mol); $\mu_j^{solvent}$—chemical potential of siloxanes at infinite dilution (J/mol); $\Delta G_{j,fusion}$—fusion free energy of siloxanes (J/mol); R—universal gas constant = 8.314 (J/mol·K); T—temperature (K) [37–39].

2.3.2. Preparation of DES

The deep eutectic solvent was successfully synthesized by mixing TPABr and TEG in 1:3 molar ratio, on a magnetic stirrer under 800 rpm, at 80 °C. All components were dried in a vacuum oven before mixing. The mixing process was carried out for half an hour. The resulting liquid DES was left cooling to room temperature (RT).

2.3.3. Preparation of Model Impurities and Biogas

The model impurities were prepared by means of the barbotage process. Pure nitrogen was moved through a vial containing 1 mL of each siloxane. The obtained model impurities were diluted with a nitrogen stream to acquire a suitable concentration of siloxanes (50 mg/dm^3). This is the upper limit of the range of siloxane concentrations which can be identified in biogas [40].

The model biogas stream was prepared in two options. The first with the use of pure nitrogen, and the second with the use of a mixture of nitrogen and methane gases in the volume ratio of 2:1.

2.3.4. Absorption Process

The installation to separate the siloxanes consists of an absorption column, a stripper column, a heat exchanger, and a reboiler. Figure 1 shows the process of the absorption–desorption course of siloxanes using TPABr:TEG (1:3). The model polluted biogas stream containing a certain amount of methane and siloxanes is fed into the absorption column. The absorption process takes place under certain conditions maintained in the column (temperature of the process—Ta, the volume of DES—Va, flow rate of the biogas stream—wa). Pure methane from the top of the absorption column is collected. The next step in the entire process is desorbing the siloxanes from DES. For this purpose, the contaminated DES is directed into the stripper column which works in specific conditions (temperature

of the stripper process—Ts, time of the stripper process—ts). Owing to regeneration, it is possible to reuse DES, which has a major impact on the economics of the process.
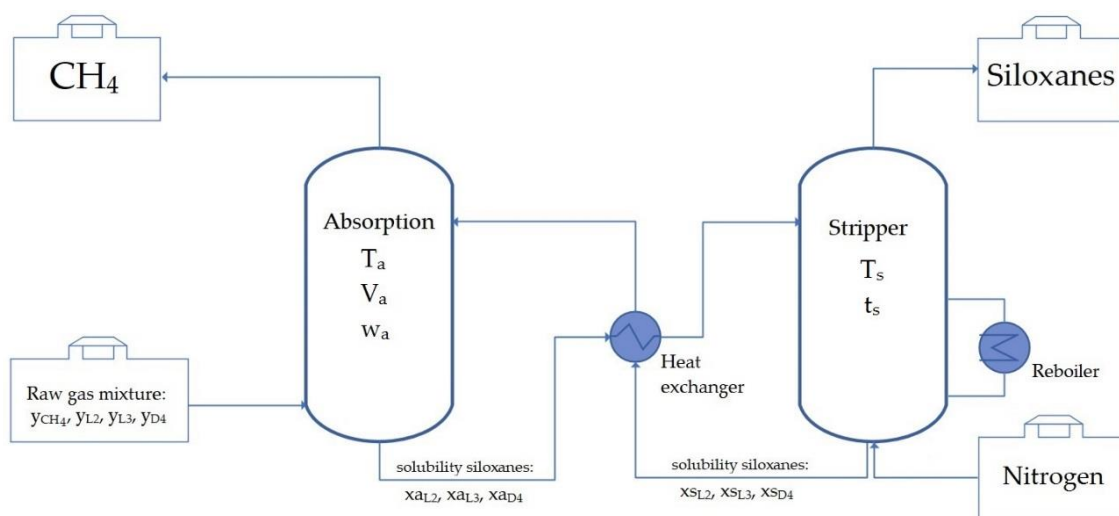
Figure 1. Simplified process flow diagram of siloxanes separation using deep eutectic solvent (DES).

The absorptivity (*A*) of siloxanes in the TPABr:TEG (1:3) was calculated using Equation (2):

$$A = \frac{C_{in} - C_{out}}{C_{in}} \ (\text{-}) \tag{2}$$

where c_{in}—initial siloxanes concentration (mg/dm³), c_{out}—siloxanes concentration after absorption process (mg/dm³).

2.3.5. Regeneration of DES

Following the selective absorption process of siloxanes, TPABr:TEG (1:3) was regenerated using nitrogen barbotage at an elevated temperature (80–100 °C). The regeneration process was carried out conducted in line with previous studies [24]. The regeneration experiments were conducted at 90 °C with an N_2 flow of 50 mL/min. The concentration of L2, L3, and D4 (before and after regeneration) in TPABr:TEG (1:3) was studied by means of gas chromatography.

2.3.6. Chromatographic Analysis

The degree and efficiency of the model biogas treatment were determined by gas chromatography coupled with a flame-ionization detector (GC-FID) (PerkinElmer, Waltham, MA, USA). The temperature of the GC oven was 120 °C, the detector temperature was 300 °C, the injection port temperature was 300 °C, the injection mode was split 5:1, and the carrier gas was nitrogen (2 mL/min).

2.3.7. Physicochemical Properties of DES
FT-IR Analysis

FT-IR spectra were taken using attenuated total reflectance (ATR) with the following operating parameters: number of background scans: 256, number of sample scans: 256; spectral range: 4000–550 cm^{-1}; resolution: 4 cm^{-1}; and slit width: 0.5 cm.

Viscosity and Density Measurements

The viscosity and density of the synthesized TPABr:TEG (1:3) were measured within a temperature range of 25–60 °C. The uncertainty measurement for the temperature was 0.5 °C. Additionally, the relationship between the viscosity and revolutions per minute abbreviated (RPM) in the temperature range 25–60 °C was determined.

Melting Point Measurements

The melting point (MP) was determined visually at atmospheric pressure by cooling DES samples to -50 °C, followed by a temperature increase at 0.1 °C/min. The temperature at which the initiation of the phase transformation was observed was adopted as the melting point.

3. Results and Discussion

3.1. COSMO-RS Molecular Simulation

3.1.1. Solubility of Siloxanes in DESs—Preselection of DES

The conductor-like screening model for real solvents (COSMO-RS) was used to calculate the solubility of siloxanes in pure glycols and water and in DESs composed with TPABr and glycols. Based on the previous studies, it can be deduced that COSMO-RS is a useful tool for solvent screening and predicting the impurities' solubility in conventional as well as non-conventional solvents [35,41,42]. In most of the published works, the selection of solvents is made on certain parameters, i.e., Henry's constant and activity coefficient. The results are often inconsistent. However, the most important parameter from the industrial point of view, solubility, is rarely reported [35,43]. Therefore, in this study, we calculated the solubility of individual siloxanes (L2, L3, and D4) in various DESs composed of TPABr as HBA and glycols, i.e., ethylene glycol (EG), glycerol (Gly), triethylene glycol (TriEG), tetraethylene glycol (TEG), and diethylene glycol (DEG), as HBD at various molar ratios (1:3; 1:4; 1:5; 1:6, HBA:HBD). These various molar ratios were selected on the basis of other studies which show that the melting point of most TPABr:glycols in 1:1, 1:2 complexes are higher than 20 °C [44,45]. This fact disqualifies the possibility of such DES as absorbents since one of the necessary conditions for absorbents is liquid at room temperature. The structures of HBA and HBDs are presented in Figure 2.
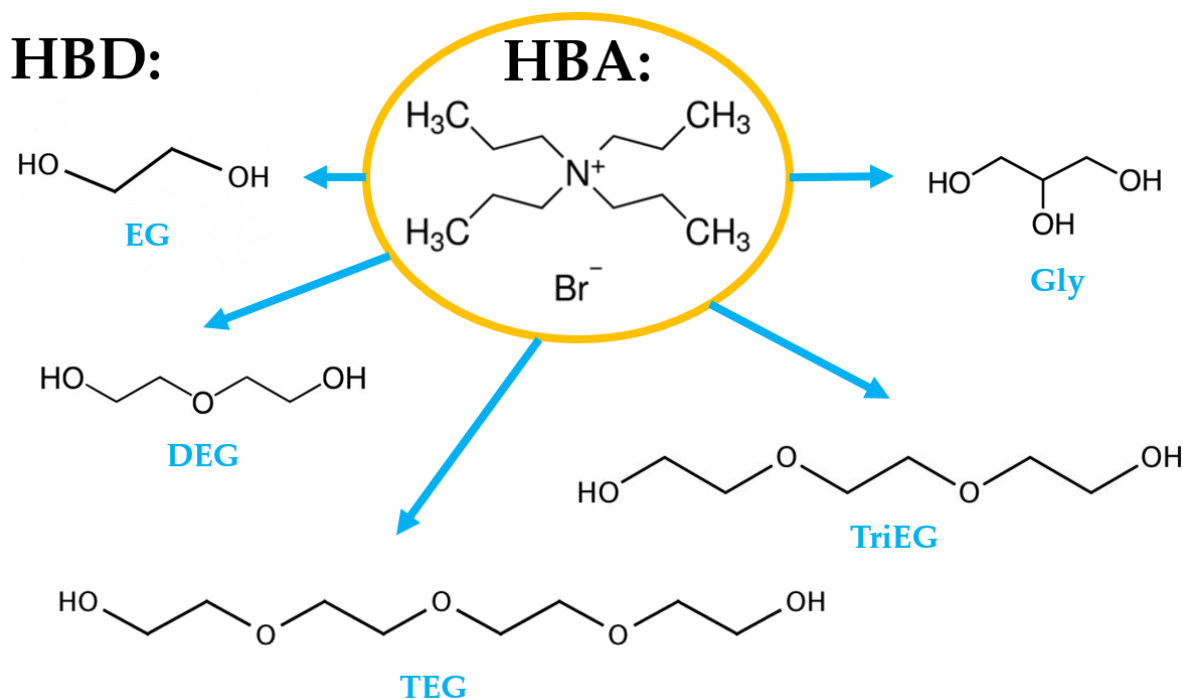
Figure 2. Structures of hydrogen bond acceptor (HBA) and hydrogen bond donors (HBDs).

Additionally, the solubility of siloxanes in pure glycols and water were taken into account. The obtained results are presented in Figures 3–5.
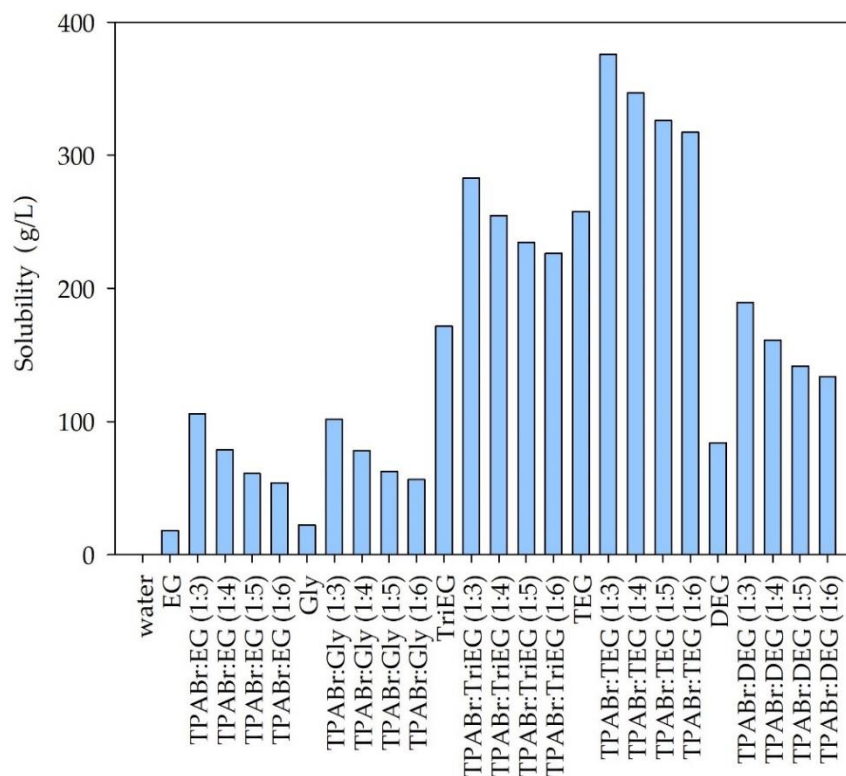
Figure 3. Solubility of hexamethyldisiloxane (L2) in DES and pure solvents.
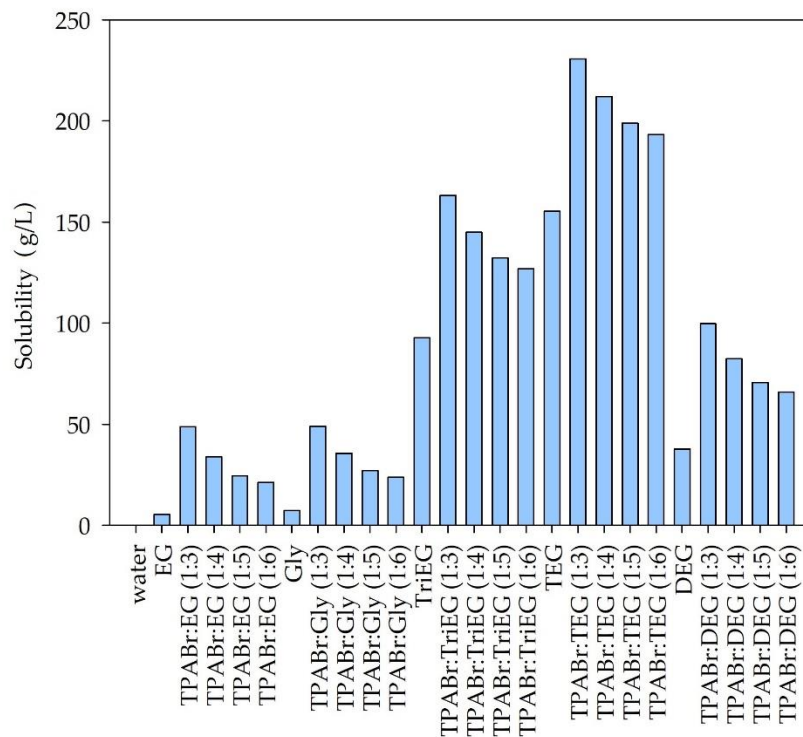
Figure 4. Solubility of octamethyltrisiloxane (L3) in DES and pure solvents.
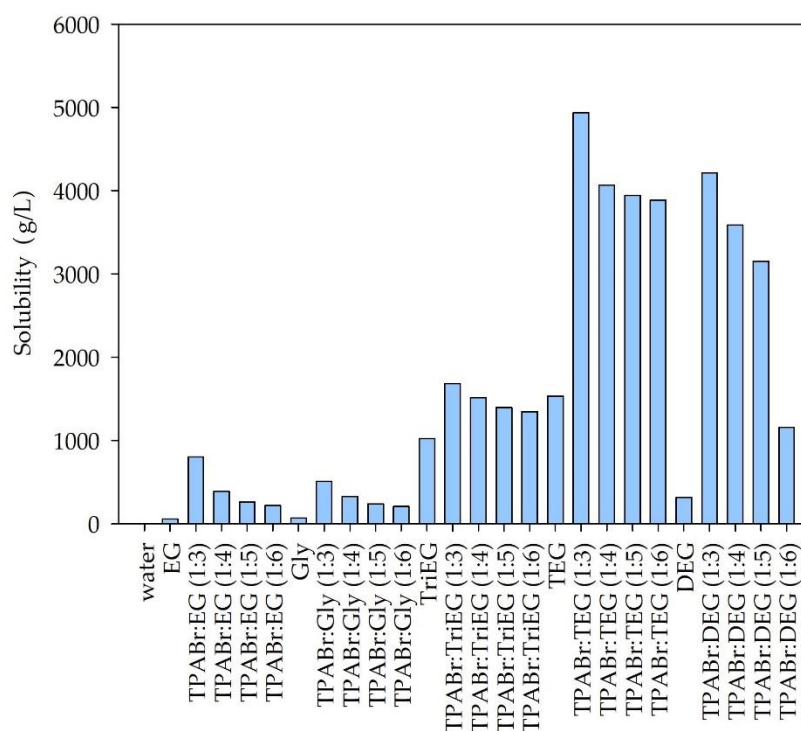
Figure 5. Solubility of octametylocyclotetrasiloxane (D4) in DES and pure solvents.

Among the tested solvents, water is the poorest solvent for siloxanes. The calculated solubility of individual siloxanes in water was 0.0054, 0.00011, and 0.027 g/L for L2, L3, and D4, respectively. This is due to the hydrophobic nature of most siloxanes [13,14]. From the industrial point of view, the ideal absorbents should be cheap and easily accessible. Due to the relatively high price of TPABr in comparison to the price of pure glycols, it would be advantageous to use pure EG, Gly, TriEG, TEG, or DEG to absorb siloxanes from biogas. However, the calculated solubility values are significantly lower for pure glycols compared to DES. The highest solubility can be observed for the DES composed of TPABr and glycols in 1:3 molar ratio. On the other hand, further increasing the amount of glycols in DES structures reduces the solubility of siloxanes. This indicates that both HBA and HBD take an active part in the absorption process by creating hydrogen or electrostatic bonds with siloxanes. COSMO-RS calculations indicate that D4, which represents cyclic siloxanes, shows higher solubility in DESs than linear siloxanes (L2 and L3). Similar results were obtained for ILs in the previous studies [46]. For linear siloxanes, as the length of the molecule decreases, their solubility in DESs increases. These are different results from those obtained for ionic liquids [46]. The highest solubility of both linear and cyclic siloxanes was obtained for DES composed of TPABr and TEG in 1:3 molar ratio. This is probably due to the formation of strong non-bonded interactions between TPABr:TEG (1:3) and siloxanes, i.e., hydrogen bonds between -OH group from TEG molecules, and O—a group from siloxanes. In order to obtain detailed information on the interactions between DES and siloxanes, analyses of σ-profiles and σ-potentials were performed. Due to the best siloxane dissolving ability of TPABr:TEG (1:3), only this DES was further investigated.

3.1.2. σ-Profile

A very important molecule-specific property in the COSMO-RS model is the σ-profile, which is the probability distribution of surface area with charge density (σ). Typically, σ-profile is presented as a histogram which can be divided into three regions i.e., HBA region σ > 0.0084 e/Å^2; non-polar region −0.0084 e/Å^2 < σ < 0.0084 e/Å^2; and HBD region σ < −0.0084 e/Å^2 [47]. The σ-profiles of TPA, Br, TEG, L2, L3, and L4 are shown in Figure 6.
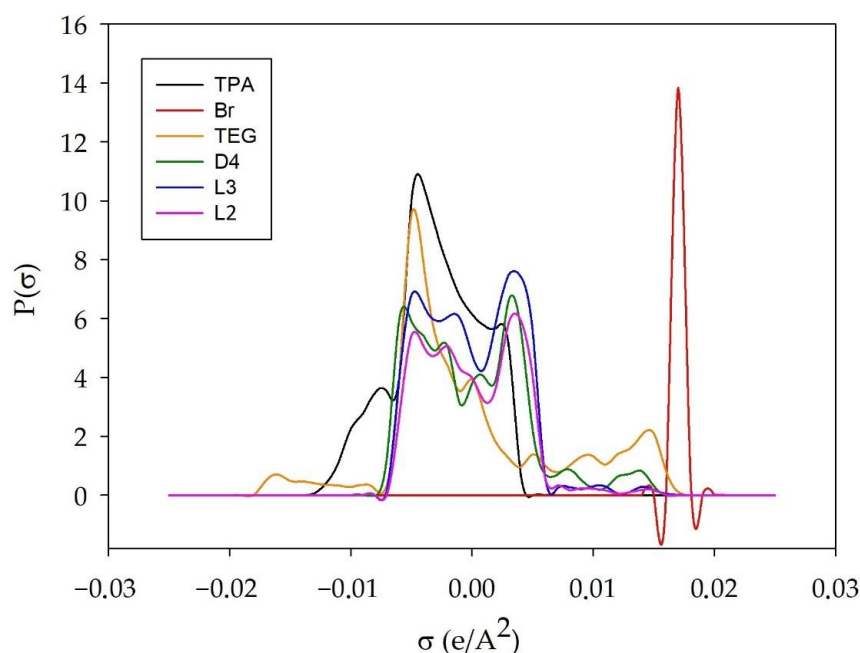
Figure 6. σ-Profile of TPABr:TEG (1:3), L2, L3, and L4.

The results indicate that the σ-profiles of all siloxanes are distributed within the non-polar and hydrogen bond acceptor region. There is no significant difference between σ-profiles of L2, L3, and D4. The only peak can be observed in the more positive region of the histogram for linear siloxanes. This indicates a slightly stronger hydrogen bond acceptor capacity of L2 and L3. Similar results were observed in other studies [35,46]. The distribution of TPA shows the concentration of the charge density mainly around 0, and a small concentration of the charge below -0.0084, which indicates the role of TPA as a hydrogen bond acceptor in hydrogen bond formation. The distribution of the bromide anion is located around 0.018 in the HBA area, which demonstrates a non-polar character and the possibility of H-bonding formation. On the other hand, the distribution of TEG is observed over the entire range of the σ-profile. This indicates that TEG can be both an acceptor and a hydrogen bond donor.

3.1.3. σ-Potential

The σ-potential is typically used to indicate the affinity between mixture components. The higher values of the positive μ (σ) suggest an increase in its repulsive behavior, and higher negative values of the μ (σ) indicate a stronger interaction between the molecules. Similarly to the σ-profile plot, the σ-potential plot is divided at the same three regions. The σ-potential for TPABr:TEG (1:3), L2, L3, and D4 are plotted in Figure 7. The obtained results indicate that all siloxanes almost overlap each other, which means that L2, L3, and D4 have similar molecular interaction properties with other molecules and with themselves. The shape of siloxanes σ-potential is negative in the HBA region and positive in the HBD region. This means that L2, L3, and D4 can be acceptors in H-bonding formation. However, the DES shape is negative in both these regions. This indicates that it is both an acceptor and a hydrogen bond donor. Therefore, the formation of hydrogen bonds is the most likely driving force in the process of removing siloxanes from biogas.

3.2. Structural and Physicochemical Properties of DES

3.2.1. FT-IR Analysis

Spectroscopic characterization is a very important aspect to determine the interaction between HBA (TPABr) and HBD (TEG). For this purpose, the FT-IR analysis was used in the study (Figure 8).
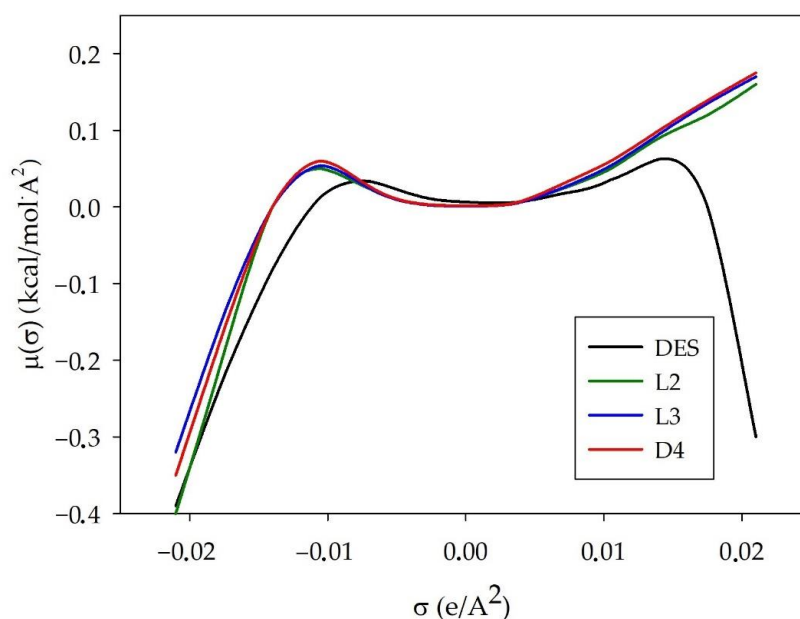
Figure 7. σ-Potential of TPAB:TEG (1:3) L2, L3, and L4.
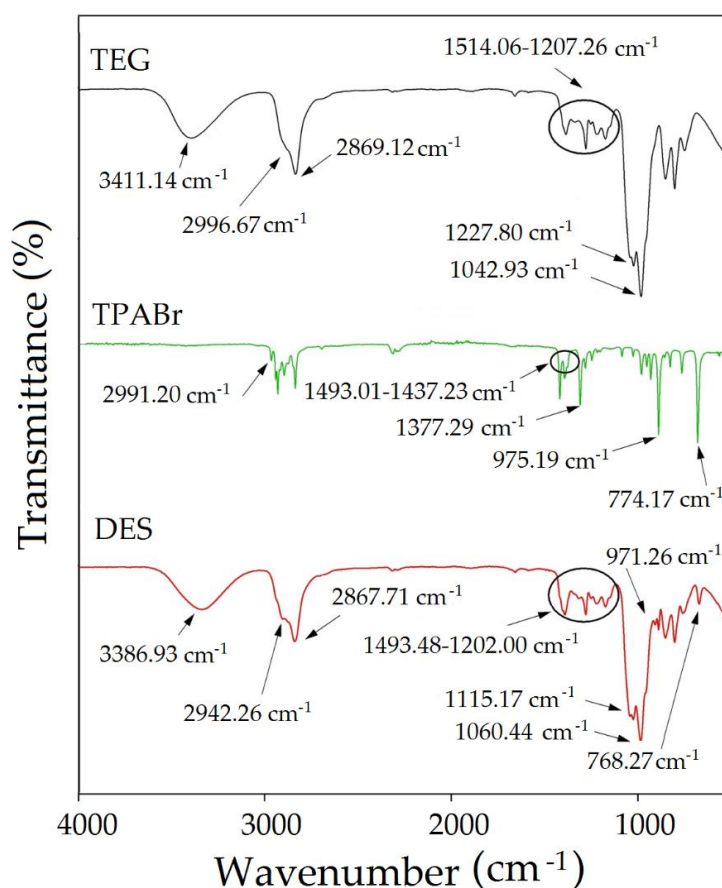
Figure 8. FT-IR spectrum for pure TPABr, TEG, and TPABr:TEG (1:3).

Figure 8 shows the mechanism of TBABr:TEG (1:3) formation. In the TPABr:TEG (1:3) spectrum, the shift of -OH group vibration towards lower values compared with pure TEG HBD (from 3411.14 to 3386.93 cm^{-1}) indicates the formation of O-H O or O-H Cl bonds. In addition, the broadening and shifts of the vibration towards lower values of the aliphatic C–H stretching bonds (from 2996.67 and 2869.12 cm^{-1} to 2942.26 and 2867.71 cm^{-1}) can be

observed. The shifts O-H O or O-H Cl, and C-H groups are most likely the consequence of hydrogen bond formation between TPABr and TEG [48,49]. Moreover, shifts of the OH group may result from the presence of C-O-C groups in the TEG. The C-O-C group are considered as the electronegative groups and tend to attract electrons on hydrogen in OH bands. The occurring interactions between TPABr and TEG can be confirmed by the shift of the C-O-C group towards lower values from 1227.80 to 1115.17 cm^{-1} and increasing the intensity of the OH group [50]. Similar vibration towards lower values can be seen in the peaks in the bands responding with H-bending, CH$_2$ deformation, and N-C-C bending bonds from 1514.06–1207.26 cm^{-1} to 1493.48–1202.00 cm^{-1}, and C-N bond symmetric stretching vibration from 774.17 to 768.27 cm^{-1} as well as redshift phenomena O-H and C-O-H stretching bonds from 1042.73 to 1060.44 cm^{-1}. The shifts confirm the interaction between the atoms in TPABr and TEG [51–53].

3.2.2. Viscosity and Density Measurements

It is well known that DES components and temperature have a dramatic effect on the absorbent density and viscosity. Basic physicochemical parameters of DES strongly influence the ability of the mass transfer capacity, which is of great importance for any changes in the absorption process [54,55]. In order to analyze the flow behavior of synthesized TPABr:TEG (1:3), the viscosity was studied in a function of shear rate ranging 10–50 rpm and temperature range 25–60 °C. The obtained results indicate that the viscosity of TBABr:TEG (1:3) decreases with increasing temperature. The increase in temperature causes the velocity of the particles in the liquid to increase, which reduces the intermolecular forces, resulting in a decrease in the TPABr:TEG (1:3) viscosity (Figure 9A). At room temperature, the viscosity of TPABr:TEG (1:3) is 84.6 mPas; it should be noted that it is much lower compared to the DESs which are presented in the literature. The dynamic viscosity of DES composed of tetrabutylammonium bromide (TBABr) and glycerol (Gly) or ethylene glycol (EG) in a molar ratio of 1:3 were 467.2 and 91.4 mPas, respectively [56]. A decrease in the viscosity value contributes to the increase in the capacity and rate of absorption because it makes the mass transfer easier. Therefore, DESs with lower value viscosities are more desirable for absorption processes.
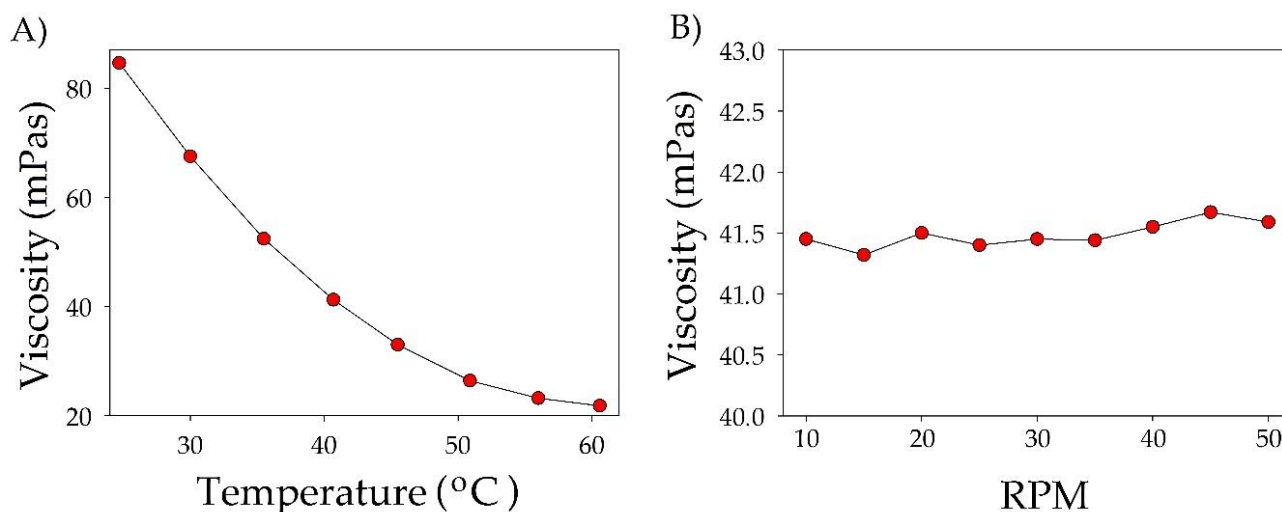
Figure 9. (**A**) Viscosity for TPABr:TEG (1:3) as a function of temperature in the range 25–60 °C. (**B**) Dependence of viscosity on turnover in the range 10–50 RPM in temperature 40 °C.

In Figure 9B, it can be observed that the viscosity of TPABr:TEG (1:3) remains almost constant throughout the range of the applied shear rate ranging. Therefore, it can be concluded that the obtained DES is a Newtonian liquid [57]. The possible shear thinning behavior can be attributed to different strengths of the H-bonding present in TPABr:TEG (1:3) which can start breaking with increasing RPM. However, deeper analysis is required

to confirm these assumptions. Similar behavior was also observed for another type of DES [58].

Another tested physicochemical parameter was density. The value of DES density decreases linearly with increasing temperature (Figure 10). At 20 °C, the density TPABr:TEG (1:3) is 1.5520 g/cm^3. However, it can be observed that with increased temperature (60 °C), the density value decreases to 1.5508 g/cm^3. The lower density values can be due to the fact that during heating, HBA and HBD in DES vibrate harder. These vibrates can cause molecular rearrangements between HBA and HBD, which can contribute to creating weaker interactions in the hydrogen bonding [59]. The obtained density of TPABr:TEG (1:3) is higher compared to the DESs which are composed of quaternary ammonium salts (ChCl or TBABr) [56,60].
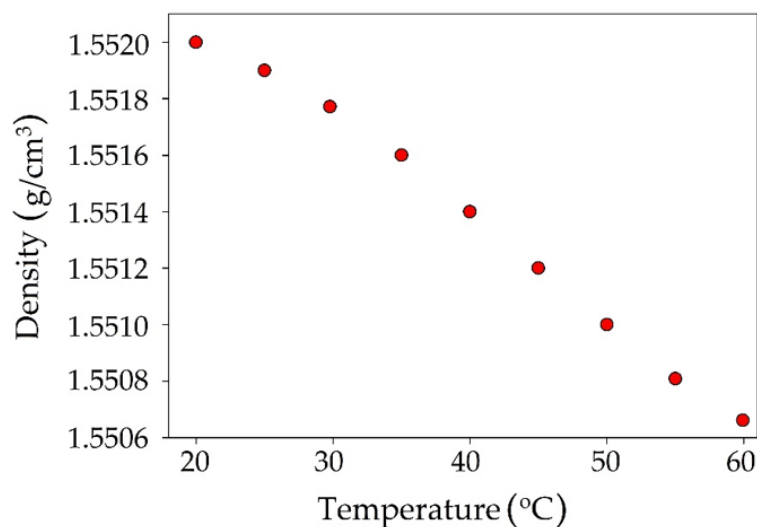
Figure 10. Density for TPABr:TEG (1:3) as a function of temperature in the range 25–60 °C.

3.2.3. Melting Point Measurements

The measured MP of TPABr:TEG (1:3) is −48 °C. As expected, the melting point of TPABr:TEG (1:3) is lower than the MP of pure TEG (−9.4 °C) [61]. The depression in the melting point of the mixture shows the formation of strong intermolecular interactions, i.e., hydrogen bonds between TPABr and TEG [62].

3.3. An Experimental Studies on Absorption of Siloxane Compounds

Optimization of the Absorption Process Conditions

In our research, the processes of absorption using a new DES based on TPABr:TEG (1:3) were carried out for purification of the model biogas stream from L2, L3, and D4 pollutants. The absorption processes were optimized in terms of the volume of TPABr:TEG (1:3), model biogas flow, and temperature.

The first optimized parameter was the volume of the TPABr:TEG (1:3) in the range of 15–50 mL/min (Figure 11). The results show that the volume of DES has a significant impact on the overall siloxane capture process. As the volume of DES increases from 15 to 50 mL/min, the DES saturation time increased from 150 to 320 min (L3—Figure 11B), from 140 to 400 min (L2—Figure 11A), and from 1551 to 5281 min (D4—Figure 11C). The increase in saturation time can be explained by increases in the contact time between the siloxane gas phase and the absorbent [63]. Increasing the volume of DES also contributes to an increase in the amount of active substance (TPABr:TEG (1:3)) and an increase in the number of active sites that are responsible for capturing of the siloxanes from DES.
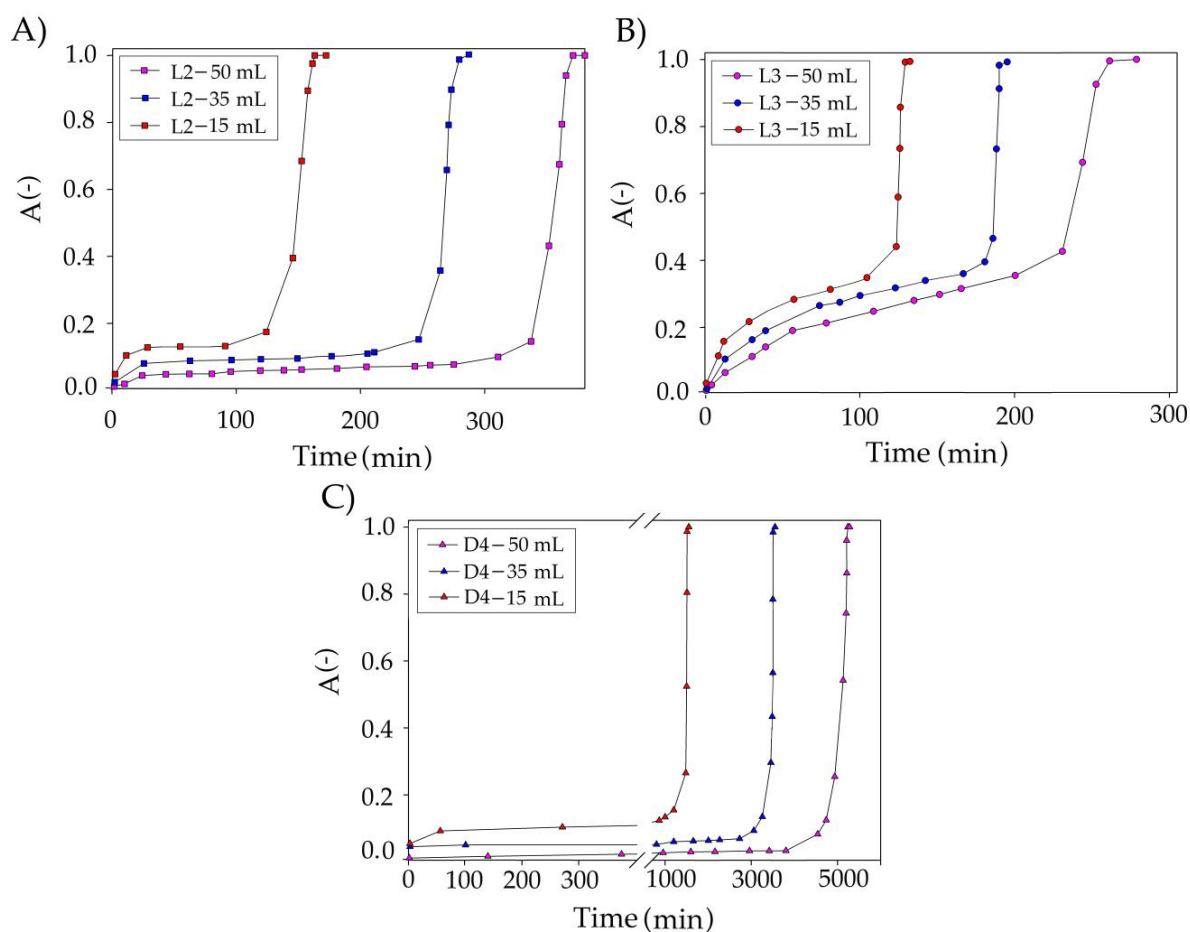
Figure 11. Experimental breakthrough curves of siloxane absorption with TPABr:TEG (1:3) at the different volumes of DES for (**A**) L2; (**B**) L3; and (**C**) D4.

The next studied parameter was model biogas flow rate in the range of 10–50 mL/min (Figure 12). The results indicate that the flow rate has only a minor effect on siloxane uptake compared to DES volume. The conducted research indicates that an increase in the flow rate from 10 to 50 mL/min slightly decreased the effectiveness of siloxane removal from the model biogas stream. Similar results were observed in the previous studies [29,64]. In the industrial technologies used with the use of a water scrubber, a flow of 88 mL/min is used to remove CO_2 or H_2S [65], whereas when using an amine scrubber, flows of 30 mL/min are used [66]. The reduction in the flow rate may result from the different viscosities of the use of the absorbent. Therefore, the assumed optimal value of 50 mL/min seems to be the rational and comparable value.

The temperature in the range of 25–50 °C was selected as the last parameter for optimizing the absorption conditions (Figure 13). An increase in temperature causes decreases in TPABr:TEG (1:3) viscosity. The lower viscosity improves the mass transfer efficiency and, hence, the siloxane removal efficiency should be higher. However, increasing the temperature does not extend the absorption process too much. This is likely due to the fact that the absorption process is normally exothermic [67]. Therefore, a temperature of 25 °C was adopted as optimal.
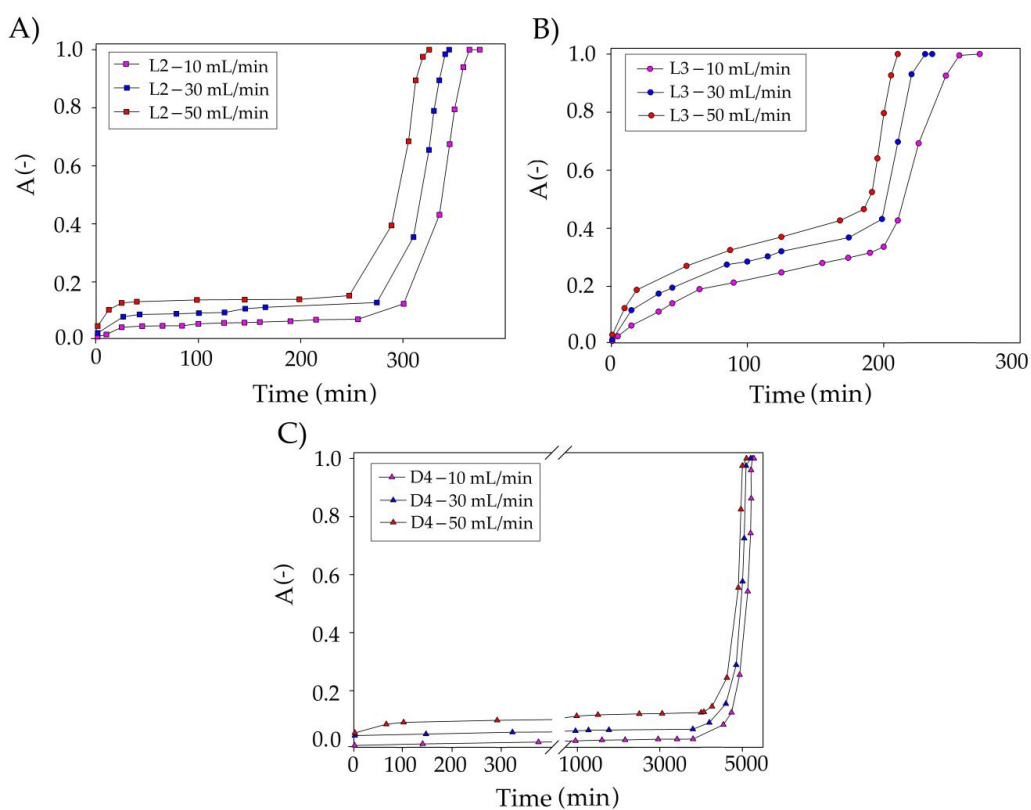
Figure 12. Experimental breakthrough curves of siloxane absorption with TPABr:TEG (1:3) at the different biogas flow rate for (**A**) L2; (**B**) L3; and (**C**) D4.
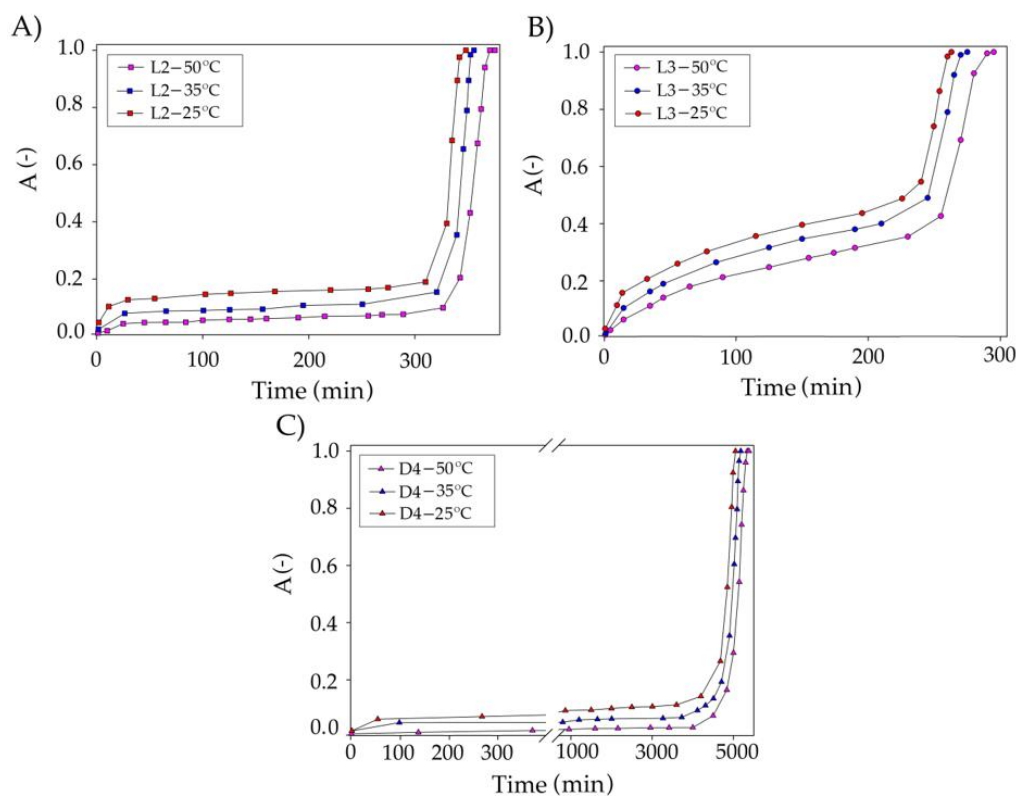
Figure 13. Experimental breakthrough curves of siloxane absorption with TPABr:TEG (1:3) at different temperatures for (**A**) L2; (**B**) L3; and (**C**) D4.

Owing to the conducted research, the optimum conditions for the removal of siloxanes from the model biogas stream were selected as a temperature of 25 °C, a DES volume of 50 mL, and a flow rate of 50 mL/min. The obtained dependence of the absorption efficiency on the duration of the absorption process of individual pollutants is shown in Figure 14A (with the use of pure nitrogen) and Figure 14B (with the use of a mixture of nitrogen and methane gases in the volume ratio 2:1).
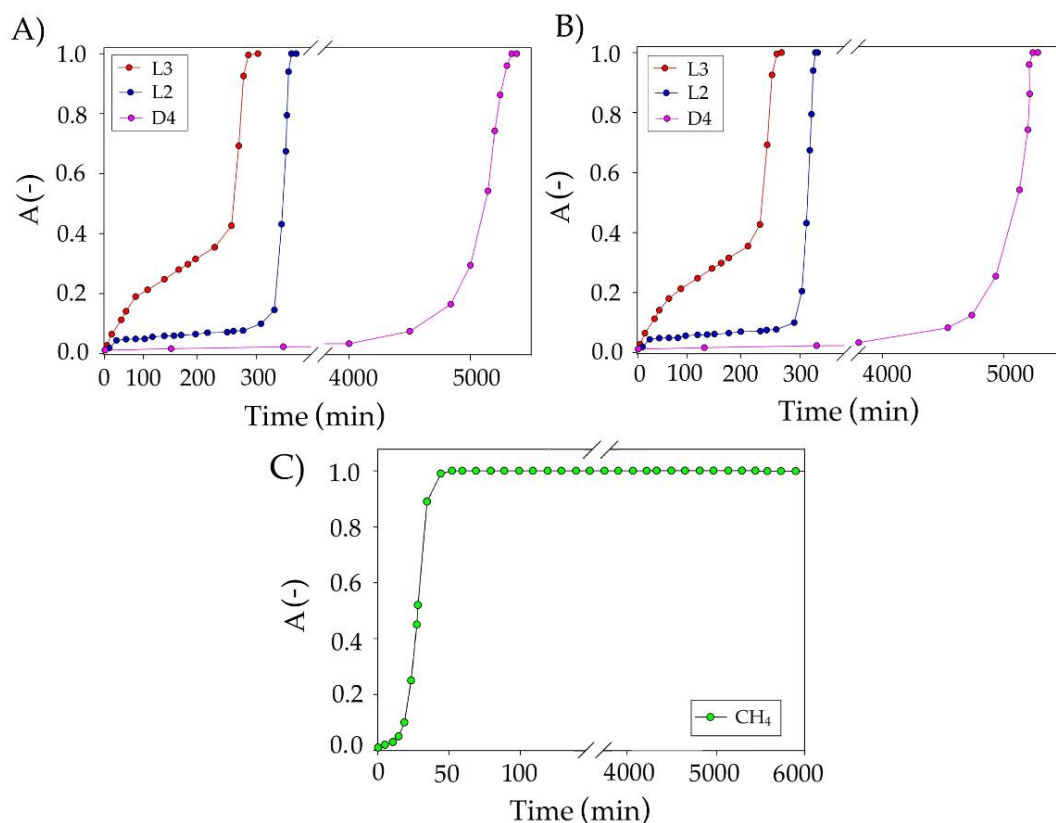
Figure 14. Experimental breakthrough curves of impurities absorption with TPABr:TEG (1:3) using (**A**) pure nitrogen and (**B**) mixture of nitrogen and methane at 2:1 volume ratio under optimum conditions, and (**C**) methane absorption curve using TPABr:TEG (1:3).

For D4 in pure N_2, after 5380 min of absorption process, a sharp increase in the supersaturation value was observed. While for D4 in the mixture of nitrogen:methane at 2:1 volume ratio, the saturation time was 5300 min. The oversaturation times of the other two siloxanes in N_2 were 400 and 300 min, while in N_2:CH_4 (2:1), they were 375 and 280 min, respectively, for L2 and L3. In the literature, there are very few works that focus on the capture of siloxanes from biogas. The results obtained in our studies can only be compared to the absorption in which the absorbent consists of amines, acids, or bases. However, it is well known that the strong bases and acids contribute to the cleavage of Si-O bonds and convert siloxanes to other volatile compounds with lower boiling points [68].

Devia and Subrenat [15] proposed L2 and D4 absorption into motor oil, cutting oil, and water-cutting oil. The studies showed the best results were obtained for motor oil for which the breakthrough curves obtained to allow for efficient removal of siloxanes were for 191.4 min (L2) and for 47.1 min (D4). The obtained results show that the proposed new DES-based absorbents show a much higher absorption capacity towards siloxanes than conventional solvents. In the studies, apart from monitoring the siloxane absorption process, the concentration of methane was also monitored (Figure 14C). The results show that complete saturation of TPABr:TEG (1:3) with methane occurs after 50 min of the process. The loss of methane in the entire process of siloxane absorption was within 5%.

3.4. FT-IR Studies on Absorption of Siloxane Compounds

The experimental study on the mechanism of the absorption process of siloxanes was conducted by FT-IR analysis. The obtained spectra of pure TPABr:TEG (1:3) and pure siloxanes were compared with the spectra of TPABr:TEG (1:3) after the absorption process (Figures 15–17). All of them identified the bands which can be observed in the FT-IR spectrum for pure siloxanes: Si-O-Si antisymmetric stretch bonds in the range 1000–1100 cm^{-1} and Si-C symmetric stretch bonds at 800 cm^{-1} are visible in the spectrum of the TPABr:TEG (1:3) after the absorption process [69]. In the spectrum after the absorption process, new peaks or significant band shifts cannot be observed. Only shifts of the -OH stretching vibration and aliphatic C-H stretching bonds are visible, which confirms the phenomena of physical absorptions. In addition, the shifts of -OH stretching vibration indicate that the hydroxyl group from TPABr:TEG (1:3) may interact with the oxygen atoms from siloxanes by forming hydrogen bonds, which is in accordance with the siloxane absorption [70]. Additionally, a shift of the bands originating from group C-O-C towards higher values from 1112.40 to 1123.83 cm^{-1} (Figure 15), 1123.54 cm^{-1} (Figure 16), and 1118.59 cm^{-1} (Figure 17) are observed. These shifts indicate that siloxane absorption can also occur through the interaction of silicon atom (Si-OH—827.67 cm^{-1} and SiO—752.14 cm^{-1} (Figure 15), Si-O—801.56 cm^{-1} (Figure 16), Si-OH and Si-O in the range 847.96–792.11 cm^{-1} (Figure 17)) with the oxygen atoms with C-O-C in the DES (1:3) [50].
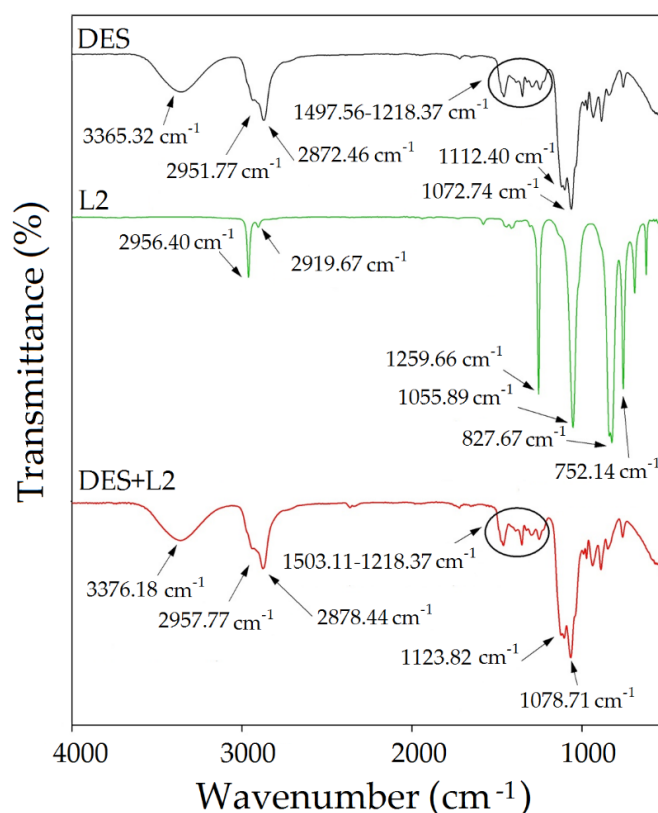
Figure 15. FT-IR spectrum for pure TPABr:TEG (1:3), pure L2 and complex TPABr:TEG + L2 (DES + L2).
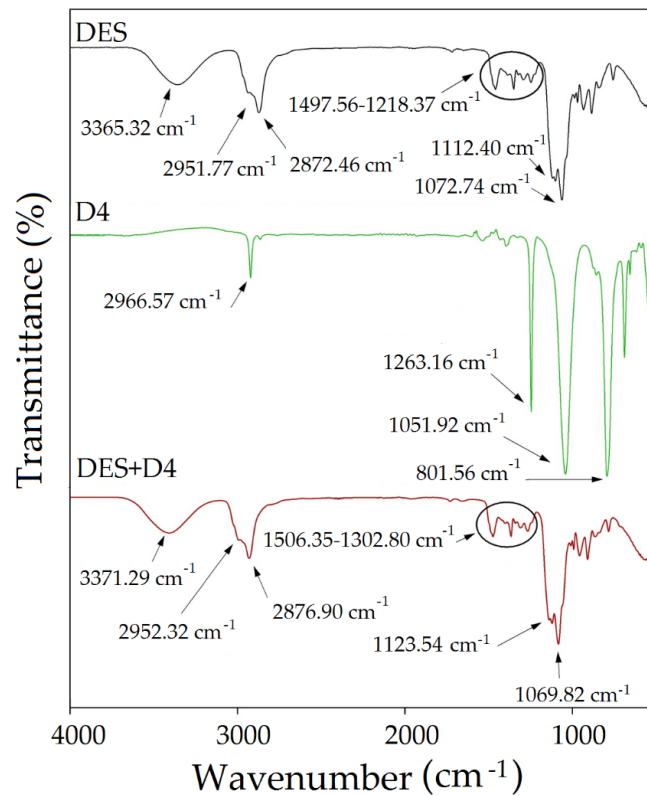
Figure 16. FT-IR spectrum for pure TPABr:TEG (1:3), pure D4 and complex TPABr:TEG + D4 (DES + D4).
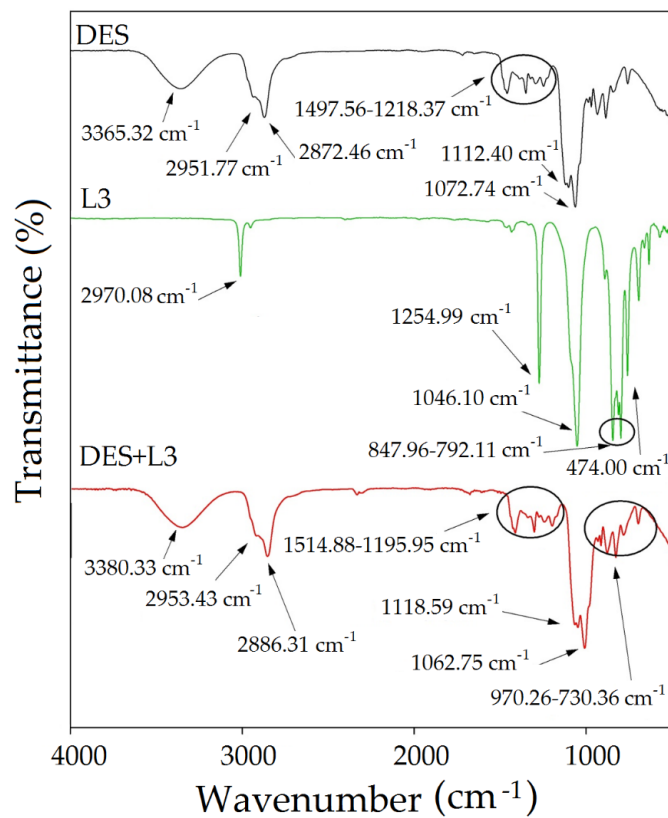
Figure 17. FT-IR spectrum for pure TPABr:TEG (1:3), pure L3 and complex TPABr:TEG + L3 (DES + L3).

3.5. Regeneration of DES

From the industrial point of view, the regeneration processes of absorbents are extremely important because they determine the final costs. The obtained results indicate that siloxanes can be completely removed from TPABr:TEG (1:3) using nitrogen barbotage conducted at a temperature of 90 °C for 3 h. TPABr:TEG (1:3) shows tall and almost unchanging L2, L3, and D4 removal efficiency for up to 10 regeneration cycles (Figure 18A). In addition, the thermal stability of TPABr:TEG (1:3) by means of FT-IR analysis was confirmed. The comparison of fresh and regenerated TPABr:TEG (1:3) spectrum indicates a lack of additional shifts and peaks in the regenerated TPABr:TEG (1:3) (Figure 18B). This confirms stability and effective regeneration of TPABr:TEG (1:3).
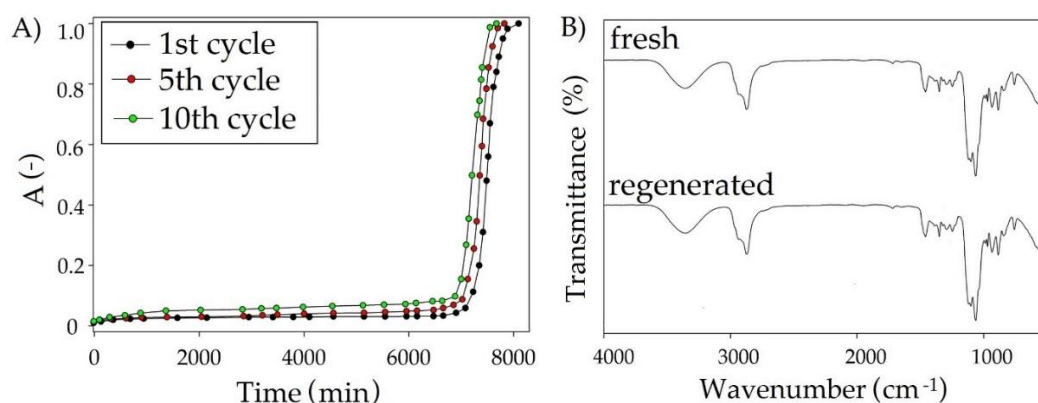
Figure 18. (**A**) Reusability of TPABr:TEG (1:3) on the example of removing L2, (**B**) FT-IR spectra from on fresh and regenerated TPABr:TEG (1:3).

4. Conclusions

In the paper, the solubility of siloxanes (L2, L3, and D4) in deep eutectic solvents (DESs) composed of tetrabutylammonium bromide and glycols as well as conventional solvents was investigated. The siloxane solubility was predicted by means of the COSMO-RS model where the highest solubility of both linear and cyclic siloxanes was present in the DES composed of TPABr and TEG in a 1:3 molar ratio. The chemical structures of TPABr:TEG (1:3) and the interaction structures between TPABr and TEG as well as between DES and siloxanes were reported using FT-IR spectroscopy. Furthermore, in order to confirm the interactions, the analyses of σ-profiles and σ-potentials were used.

The results of physicochemical properties indicate that TPABr:TEG (1:3) is a Newtonian liquid due to the lack of viscosity changes during shear changes, which contribute to only minor changes in siloxane removal efficiency with increasing temperature. In turn, carrying out the absorption process at a temperature of 25 °C is beneficial from an economic point of view. Under optimum conditions (50 mL of TPABr:TEG (1:3), 50 mL/min flow rate, and temperature 25 °C), the L2, L3, and D4 can be removed with high efficiency for 375, 280, and 5300 min, respectively. These are much better absorption efficiencies compared to mineral oils. In addition, TPABr:TEG (1:3) also can be easily regenerated up to 5 cycles without significantly changing the siloxane absorption efficiency. The studies on the absorptive mechanism to remove siloxanes indicate that the reason for the high solubility siloxanes in TPABr:TEG (1:3) is the formation of the strong hydrogen interactions between -OH group from DES molecule, and -O- a group from siloxanes.

The cost of the absorption process mainly depends on the type of absorbents. The estimated capital cost of the absorption process based on TPABr:TEG (1:3) is 126.05 €/L [71,72]. The DES price is higher than conventional absorbents prices which are 9.17 €/L for motor oil 5W40 from Elf) [73]; 33.42 €/L for cutting oil Hochleistungs-Schneidöl Alpha 93 from Jokish® GmbH [74]. However, it should be remembered that DES can be used for up to 5 cycles without changing the high efficiency of removing siloxanes from biogas. The initial price of 126.05 €/L can drop to 25.21 €/L. Therefore, DESs can be used as alternative absorbents.

Conflicts of Interest: The authors declare no conflict of interest.

References

1. Perea-Moreno, M.-A.; Salmeron-Manzano, E.; Perea-Moreno, A.-J. Biomass as Renewable Energy: Worldwide Research Trends. *Sustainability* **2019**, *11*, 863. [CrossRef]
2. Meyer, A.K.; Ehimen, E.A.; Holm-Nielsen, J.B. Future European biogas: Animal manure, straw and grass potentials for a sustainable European biogas production. *Biomass Bioenergy* **2018**, *111*, 154–164. [CrossRef]
3. Zhu, T.; Curtis, J.; Clancy, M. Promoting agricultural biogas and biomethane production: Lessons from cross-country studies. *Renew. Sustain. Energy Rev.* **2019**, *114*, 109332. [CrossRef]
4. Scarlat, N.; Dallemand, J.-F.; Fahl, F. Biogas: Developments and perspectives in Europe. *Renew. Energy* **2018**, *129*, 457–472. [CrossRef]
5. Barragán, E.A.; Ruiz, J.M.O.; Tigre, J.D.C.; Zalamea-León, E. Assessment of Power Generation Using Biogas from Landfills in an Equatorial Tropical Context. *Sustainability* **2020**, *12*, 2669. [CrossRef]
6. Persson, M.; Jonsson, O.; Wellinger, A. *Biogas Upgrading to Vehicle Fuel Standards and Grid*; IEA Bioenergy Task 37; Susanne AUER: Vienna, Austria, 2007.
7. Rincón, C.A.; De Guardia, A.; Couvert, A.; Wolbert, D.; Le Roux, S.; Soutrel, I.; Nunes, G. Odor concentration (OC) prediction based on odor activity values (OAVs) during composting of solid wastes and digestates. *Atmos. Environ.* **2019**, *201*, 1–12. [CrossRef]
8. Rasi, S. *Biogas Composition and Upgrading to Biomethane*; University of Jyväskylä: Jyväskylä, Finland, 2009; ISBN 978-951-39-3618-1.
9. Carrera-Chapela, F.; Donoso-Bravo, A.; Souto, J.A.; Ruiz-Filippi, G. Modeling the Odor Generation in WWTP: An Integrated Approach Review. *Water Air Soil Pollut.* **2014**, *225*, 1–15. [CrossRef]
10. Sevimoğlu, O.; Tansel, B. Effect of persistent trace compounds in landfill gas on engine performance during energy recovery: A case study. *Waste Manag.* **2013**, *33*, 74–80. [CrossRef]
11. Noorain, R.; Kindaichi, T.; Ozaki, N.; Aoi, Y.; Ohashi, A. Biogas purification performance of new water scrubber packed with sponge carriers. *J. Clean. Prod.* **2019**, *214*, 103–111. [CrossRef]
12. Vo, T.T.; Wall, D.M.; Ring, D.; Rajendran, K.; Murphy, J.D. Techno-economic analysis of biogas upgrading via amine scrubber, carbon capture and ex-situ methanation. *Appl. Energy* **2018**, *212*, 1191–1202. [CrossRef]
13. Rasi, S.; Läntelä, J.; Veijanen, A.; Rintala, J. Landfill gas upgrading with countercurrent water wash. *Waste Manag.* **2008**, *28*, 1528–1534. [CrossRef] [PubMed]
14. Rasi, S.; Läntelä, J.; Rintala, J. Upgrading landfill gas using a high pressure water absorption process. *Fuel* **2014**, *115*, 539–543. [CrossRef]
15. Devia, C.R.; Subrenat, A. Absorption of a linear (L2) and a cyclic (D4) siloxane using different oils: Application to biogas treatment. *Environ. Technol.* **2013**, *34*, 3117–3127. [CrossRef] [PubMed]
16. Ghorbel, L.; Tatin, R.; Couvert, A. Relevance of an organic solvent for absorption of siloxanes. *Environ. Technol.* **2013**, *35*, 372–382. [CrossRef]
17. Ajhar, M.; Travesset, M.; Yüce, S.; Melin, T. Siloxane removal from landfill and digester gas—A technology overview. *Bioresour. Technol.* **2010**, *101*, 2913–2923. [CrossRef]
18. Shen, M.; Zhang, Y.; Hu, D.; Fan, J.; Zeng, G. A review on removal of siloxanes from biogas: With a special focus on volatile methylsiloxanes. *Environ. Sci. Pollut. Res.* **2018**, *25*, 30847–30862. [CrossRef]
19. Schuur, B.; Brouwer, T.; Smink, D.; Sprakel, L.M. Green solvents for sustainable separation processes. *Curr. Opin. Green Sustain. Chem.* **2019**, *18*, 57–65. [CrossRef]
20. Zhang, S.; Zhang, X.; Dong, H.; Zhao, Z.; Zhang, S.; Huang, Y. Carbon capture with ionic liquids: Overview and progress. *Energy Environ. Sci.* **2012**, *5*, 6668–6681. [CrossRef]

21. Blanchard, L.A.; Hancu, D.; Beckman, E.J.; Brennecke, J.F. Green processing using ionic liquids and CO₂. *Nat. Cell Biol.* **1999**, *399*, 28–29. [CrossRef]

22. Reddy, R.G. Novel applications of ionic liquids in materials processing. *J. Phys. Conf. Ser.* **2009**, *165*, 1–6. [CrossRef]

23. Sarmad, S.; Mikkola, J.-P.; Ji, X. Carbon Dioxide Capture with Ionic Liquids and Deep Eutectic Solvents: A New Generation of Sorbents. *ChemSusChem* **2017**, *10*, 324–352. [CrossRef] [PubMed]

24. Makoś, P.; Fernandes, A.; Przyjazny, A.; Boczkaj, G. Sample preparation procedure using extraction and derivatization of carboxylic acids from aqueous samples by means of deep eutectic solvents for gas chromatographic-mass spectrometric analysis. *J. Chromatogr. A* **2018**, *1555*, 10–19. [CrossRef] [PubMed]

25. Makoś, P.; Przyjazny, A.; Boczkaj, G. Hydrophobic deep eutectic solvents as "green" extraction media for polycyclic aromatic hydrocarbons in aqueous samples. *J. Chromatogr. A* **2018**, *1570*, 28–37. [CrossRef] [PubMed]

26. Makoś, P.; Słupek, E.; Gębicki, J. Extractive detoxification of feedstocks for the production of biofuels using new hydrophobic deep eutectic solvents—Experimental and theoretical studies. *J. Mol. Liq.* **2020**, *308*, 113101. [CrossRef]

27. Makoś, P.; Słupek, E.; Gębicki, J. Hydrophobic deep eutectic solvents in microextraction techniques—A review. *Microchem. J.* **2020**, *152*, 104384. [CrossRef]

28. Słupek, E.; Makoś, P.; Gębicki, J. Deodorization of model biogas by means of novel non- ionic deep eutectic solvent. *Arch. Environ. Prot.* **2020**, *46*, 41–46. [CrossRef]

29. Słupek, E.; Makoś, P. Absorptive Desulfurization of Model Biogas Stream Using Choline Chloride-Based Deep Eutectic Solvents. *Sustainability* **2020**, *12*, 1619. [CrossRef]

30. Słupek, E.; Makos, P.; Dobrzyniewski, D.; Szulczynski, B.; Gebicki, J. Process control of biogas purification using electronic nose. *Chem. Eng. Trans.* **2020**, *82*. [CrossRef]

31. Shukla, S.K.; Mikkola, J.-P. Unusual temperature-promoted carbon dioxide capture in deep-eutectic solvents: The synergistic interactions. *Chem. Commun.* **2019**, *55*, 3939–3942. [CrossRef]

32. Trivedi, T.J.; Lee, J.H.; Lee, H.J.; Jeong, Y.K.; Choi, J.W. Deep eutectic solvents as attractive media for CO₂ capture. *Green Chem.* **2016**, *18*, 2834–2842. [CrossRef]

33. Shukla, S.K.; Mikkola, J.-P. Intermolecular interactions upon carbon dioxide capture in deep-eutectic solvents. *Phys. Chem. Chem. Phys.* **2018**, *20*, 24591–24601. [CrossRef] [PubMed]

34. Makoś, P.; Słupek, E.; Małachowska, A. Silica Gel Impregnated by Deep Eutectic Solvents for Adsorptive Removal of BTEX from Gas Streams. *Materials* **2020**, *13*, 1894. [CrossRef]

35. Słupek, E.; Makoś, P.; Gębicki, J. Theoretical and Economic Evaluation of Low-Cost Deep Eutectic Solvents for Effective Biogas Upgrading to Bio-Methane. *Energies* **2020**, *13*, 3379. [CrossRef]

36. Mu, T.; Rarey, J.; Gmehling, J. Performance of COSMO-RS with Sigma Profiles from Different Model Chemistries. *Ind. Eng. Chem. Res.* **2007**, *46*, 6612–6629. [CrossRef]

37. Klamt, A. Conductor-like Screening Model for Real Solvents: A New Approach to the Quantitative Calculation of Solvation Phenomena. *J. Phys. Chem.* **1995**, *99*, 2224–2235. [CrossRef]

38. Klamt, A. Prediction of the mutual solubilities of hydrocarbons and water with COSMO-RS. *Fluid Phase Equilib.* **2003**, *206*, 223–235. [CrossRef]

39. Klamt, A.; Eckert, F. COSMO-RS: A novel and efficient method for the a priori prediction of thermophysical data of liquids. *Fluid Phase Equilib.* **2000**, *172*, 43–72. [CrossRef]

40. Tansel, B.; Surita, S.C. Managing siloxanes in biogas-to-energy facilities: Economic comparison of pre- vs post-combustion practices. *Waste Manag.* **2019**, *96*, 121–127. [CrossRef]

41. Klamt, A. The COSMO and COSMO-RS solvation models. *Wiley Interdiscip. Rev. Comput. Mol. Sci.* **2018**, *8*, 1–11. [CrossRef]

42. Chu, Y.; He, X. MoDoop: An Automated Computational Approach for COSMO-RS Prediction of Biopolymer Solubilities in Ionic Liquids. *ACS Omega* **2019**, *4*, 2337–2343. [CrossRef]

43. Mullins, E.; Oldland, R.; Liu, Y.A.; Wang, S.; Sandler, S.I.; Chen, C.-C.; Zwolak, A.M.; Seavey, K.C. Sigma-Profile Database for Using COSMO-Based Thermodynamic Methods. *Ind. Eng. Chem. Res.* **2006**, *45*, 4389–4415. [CrossRef]

44. Jibril, B.E.-Y.; Mjalli, F.S.; Naser, J.; Gano, Z.S. New tetrapropylammonium bromide-based deep eutectic solvents: Synthesis and characterizations. *J. Mol. Liq.* **2014**, *199*, 462–469. [CrossRef]

45. García, G.; Aparicio, S.; Ullah, R.; Atilhan, M. Deep Eutectic Solvents: Physicochemical Properties and Gas Separation Applications. *Energy Fuels* **2015**, *29*, 2616–2644. [CrossRef]

46. Santiago, R.; Moya, C.; Palomar, J. Siloxanes capture by ionic liquids: Solvent selection and process evaluation. *Chem. Eng. J.* **2020**, *401*, 126078. [CrossRef]

47. Han, J.; Dai, C.; Yu, G.; Lei, Z. Parameterization of COSMO-RS model for ionic liquids. *Green Energy Environ.* **2018**, *3*, 247–265. [CrossRef]

48. Aissaoui, T. Neoteric FT-IR Investigation on the Functional Groups of Phosphonium- Based Deep Eutectic Solvents. *Pharm. Anal. Acta* **2015**, *6*, 10–12. [CrossRef]

49. Zhu, S.; Li, H.; Zhu, W.; Jiang, W.; Wang, C.; Wu, P.; Zhang, Q.; Li, H. Vibrational analysis and formation mechanism of typical deep eutectic solvents: An experimental and theoretical study. *J. Mol. Graph. Model.* **2016**, *68*, 158–175. [CrossRef]

50. Ghaedi, H.; Ayoub, M.; Sufian, S.; Lal, B.; Uemura, Y. Thermal stability and FT-IR analysis of Phosphonium-based deep eutectic solvents with different hydrogen bond donors. *J. Mol. Liq.* **2017**, *242*, 395–403. [CrossRef]

51. Shameli, K.; Bin Ahmad, M.; Jazayeri, S.D.; Sedaghat, S.; Shabanzadeh, P.; Jahangirian, H.; Shahri, M.M.; Abdollahi, Y. Synthesis and Characterization of Polyethylene Glycol Mediated Silver Nanoparticles by the Green Method. *Int. J. Mol. Sci.* **2012**, *13*, 6639–6650. [CrossRef]

52. Banjare, M.K.; Behera, K.; Satnami, M.L.; Pandey, S.; Ghosh, K.K. Self-assembly of a short-chain ionic liquid within deep eutectic solvents. *RSC Adv.* **2018**, *8*, 7969–7979. [CrossRef]

53. Maheswari, A.U.; Palanivelu, K. Carbon Dioxide Capture and Utilization by Alkanolamines in Deep Eutectic Solvent Medium. *Ind. Eng. Chem. Res.* **2015**, *54*, 11383–11392. [CrossRef]

54. Ruß, C.; König, B. Low melting mixtures in organic synthesis—An alternative to ionic liquids? *Green Chem.* **2012**, *14*, 2969–2982. [CrossRef]

55. Xydis, G.; Nanaki, E.A.; Koroneos, C.J. Exergy analysis of biogas production from a municipal solid waste landfill. *Sustain. Energy Technol. Assess.* **2013**, *4*, 20–28. [CrossRef]

56. Yusof, R.; Abdulmalek, E.; Sirat, K.; Rahman, M.B.A. Tetrabutylammonium Bromide (TBABr)-Based Deep Eutectic Solvents (DESs) and Their Physical Properties. *Molecules* **2014**, *19*, 8011–8026. [CrossRef]

57. Burrell, G.L.; Dunlop, N.F.; Separovic, F. Non-Newtonian viscous shear thinning in ionic liquids. *Soft Matter* **2010**, *6*, 2080–2086. [CrossRef]

58. Basaiahgari, A.; Panda, S.; Gardas, R.L. Acoustic, volumetric, transport, optical and rheological properties of Benzyltripropylammonium based Deep Eutectic Solvents. *Fluid Phase Equilib.* **2017**, *448*, 41–49. [CrossRef]

59. Verduzco, L.F.R. Density and viscosity of biodiesel as a function of temperature: Empirical models. *Renew. Sustain. Energy Rev.* **2013**, *19*, 652–665. [CrossRef]

60. Altamash, T.; Atilhan, M.; Aliyan, A.; Ullah, R.; Nasser, M.S.; Aparicio, S. Rheological, Thermodynamic, and Gas Solubility Properties of Phenylacetic Acid-Based Deep Eutectic Solvents. *Chem. Eng. Technol.* **2017**, *40*, 778–790. [CrossRef]

61. Sigma Aldrich. Safety Data Sheet Tetraethylene Glycol. Available online: https://www.sigmaaldrich.com/MSDS/MSDS/DisplayMSDSPage.do?country=PL&language=pl&productNumber=110175&brand=ALDRICH&PageToGoToURL=https%3A%2F%2Fwww.sigmaaldrich.com%2Fcatalog%2Fproduct%2Faldrich%2F110175%3Flang%3Dpl (accessed on 18 November 2020).

62. Abbott, A.P.; Boothby, D.; Capper, G.; Davies, D.L.; Rasheed, R.K. Deep Eutectic Solvents Formed between Choline Chloride and Carboxylic Acids: Versatile Alternatives to Ionic Liquids. *J. Am. Chem. Soc.* **2004**, *126*, 9142–9147. [CrossRef]

63. Hsu, C.H.; Chu, H.; Cho, C.M. Absorption and reaction kinetics of amines and ammonia solutions with carbon dioxide in flue gas. *J. Air Waste Manag. Assoc.* **2003**, *53*, 246–252. [CrossRef]

64. Yincheng, G.; Zhenqi, N.; Wenyi, L. Comparison of removal efficiencies of carbon dioxide between aqueous ammonia and Na–solution in a fine spray column. *Energy Procedia* **2011**, *4*, 512–518. [CrossRef]

65. Horikawa, M.; Rossi, F.; Gimenes, M.; Costa, C.M.; Da Silva, M. Chemical absorption of H2S for biogas purification. *Braz. J. Chem. Eng.* **2004**, *21*, 415–422. [CrossRef]

66. Ma, C.; Liu, C.; Lu, X.; Ji, X. Techno-economic analysis and performance comparison of aqueous deep eutectic solvent and other physical absorbents for biogas upgrading. *Appl. Energy* **2018**, *225*, 437–447. [CrossRef]

67. Lemus, J.; Bedia, J.; Moya, C.; Alonso-Morales, N.; Gilarranz, M.A.; Palomar, J.; Rodriguez, J.J. Ammonia capture from the gas phase by encapsulated ionic liquids (ENILs). *RSC Adv.* **2016**, *6*, 61650–61660. [CrossRef]

68. Ryckebosch, E.; Drouillon, M.; Vervaeren, H. Techniques for transformation of biogas to biomethane. *Biomass Bioenergy* **2011**, *35*, 1633–1645. [CrossRef]

69. Urasaki, N.; Wong, C. Separation of low molecular siloxanes for electronic application by liquid-liquid extraction. *IEEE Trans. Electron. Packag. Manuf.* **1999**, *22*, 295–298. [CrossRef]

70. Sun, S.; Niu, Y.; Sun, Z.; Xu, Q.; Wei, X. Solubility properties and spectral characterization of sulfur dioxide in ethylene glycol derivatives. *RSC Adv.* **2014**, *5*, 8706–8712. [CrossRef]

71. Sigma Aldrich. Tetraethylene Glycol. Available online: https://www.sigmaaldrich.com/catalog/product/aldrich/110175?lang=pl&region=PL (accessed on 11 December 2020).

72. Sigma Aldrich. Tetrapropylammonium Bromide. Available online: https://www.sigmaaldrich.com/catalog/product/aldrich/225568?lang=pl&region=PL (accessed on 11 December 2020).

73. Kolegaberlin Motor Oil. Available online: https://www.kolegaberlin.pl/product-pol-4300-Elf-Evolution-900-NF-5W40-5L.html (accessed on 30 November 2020).

74. Hoffmann Group. Cutting Oil. Available online: https://www.hoffmann-group.com/GB/en/houk/Power-tools-and-workshop-supplies/Cooling-lubricants/High-performance-cutting-oil-chlorine-free-Alpha-93/p/084210 (accessed on 30 November 2020).

Gdańsk, dnia 19.05.2023

dr inż. Patrycja Makoś-Chełstowska
....
(stopień/tytuł, imię i nazwisko)

Politechnika Gdańska
....
(Afiliacja)

OŚWIADCZENIE WSPÓŁAUTORA

Jako współautor pracy:. **"Removal of Siloxanes from Model Biogas by Means of Deep Eutectic Solvents in Absorption Process"** oświadczam, że mój własny wkład polegał na konceptualizacji, metodologii, wizualizacji, prowadzeniu badań, przechowywaniu danych, przygotowaniu oryginalnego manuskryptu oraz finansowaniu.

Jednocześnie wyrażam zgodę na przedłożenie ww. pracy przez mgr inż. Edytę Słupek jako część rozprawy doktorskiej w formie spójnego tematycznie zbioru artykułów opublikowanych w czasopismach naukowych.

Oświadczam, że samodzielna i możliwa do wyodrębnienia część ww. pracy wykazuje indywidualny wkład mgr inż. Edyty Słupek polegający na: konceptualizacji, metodologii, wizualizacji, prowadzeniu badań, zestawieniu danych oraz przygotowaniu oryginalnego manuskryptu

P. Makoś- Chełstowska
....
(podpis współautora)

Gdańsk, dnia 19.05.2023

dr inż. hab. Jacek Gębicki
....
(stopień/tytuł, imię i nazwisko)

Politechnika Gdańska
....
(Afiliacja)

OŚWIADCZENIE WSPÓŁAUTORA

Jako współautor pracy:. **"Removal of Siloxanes from Model Biogas by Means of Deep Eutectic Solvents in Absorption Process"** oświadczam, że mój własny wkład polegał na nadzorowaniu wstępnego planu badań oraz realizacji badań, przygotowaniu recenzji oraz redakcji ostatecznej wersji manuskryptu.

Jednocześnie wyrażam zgodę na przedłożenie ww. pracy przez mgr inż. Edytę Słupek jako część rozprawy doktorskiej w formie spójnego tematycznie zbioru artykułów opublikowanych w czasopismach naukowych.

Oświadczam, że samodzielna i możliwa do wyodrębnienia część ww. pracy wykazuje indywidualny wkład mgr inż. Edyty Słupek polegający na: konceptualizacji, metodologii, wizualizacji, prowadzeniu badań, zestawieniu danych oraz przygotowaniu oryginalnego manuskryptu.

....
(podpis współautora)

Autorzy:

P. Makoś-Chełstowska, **E. Słupek**, A. Kramarz, J. Gębicki

Tytuł publikacji:

New Carvone-Based Deep Eutectic Solvents for Siloxanes Capture from Biogas

Czasopismo:

International Journal of Molecular Sciences

DOI:

10.3390/ijms22179551

Article

New Carvone-Based Deep Eutectic Solvents for Siloxanes Capture from Biogas

Patrycja Makoś-Chełstowska [1,2] , Edyta Słupek [1] , Aleksandra Kramarz [1] and Jacek Gębicki [1,*]

1   Department of Process Engineering and Chemical Technology, Faculty of Chemistry,
    Gdansk University of Technology, 80-233 Gdansk, Poland; patrycja.makos@pg.edu.pl (P.M.-C.);
    edyta.slupek@pg.edu.pl (E.S.); olakramarz96@gmail.com (A.K.)
2   EcoTech Center, Gdańsk University of Technology, 80-233 Gdańsk, Poland
*   Correspondence: jacek.gebicki@pg.edu.pl

Abstract: During biogas combustion, siloxanes form deposits of SiO_2 on engine components, thus shortening the lifespan of the installation. Therefore, the development of new methods for the purification of biogas is receiving increasing attention. One of the most effective methods is physical absorption with the use of appropriate solvents. According to the principles of green engineering, solvents should be biodegradable, non-toxic, and have a high absorption capacity. Deep eutectic solvents (DES) possess such characteristics. In the literature, due to the very large number of DES combinations, conductor-like screening models for real solvents (COSMO-RS), based on the comparison of siloxane activity coefficient of 90 DESs of various types, were studied. DESs, which have the highest affinity to siloxanes, were synthesized. The most important physicochemical properties of DESs were carefully studied. In order to explain of the mechanism of DES formation, and the interaction between DES and siloxanes, the theoretical studies based on σ-profiles, and experimental studies including the ^{1}H NMR, ^{13}C NMR, and FT-IR spectra, were applied. The obtained results indicated that the new DESs, which were composed of carvone and carboxylic acids, were characterized by the highest affinity to siloxanes. It was shown that the hydrogen bonds between the active ketone group (=O) and the carboxyl group (-COOH) determined the formation of stable DESs with a melting point much lower than those of the individual components. On the other hand, non-bonded interactions mainly determined the effective capture of siloxanes with DES.

Keywords: biogas; deep eutectic solvents; siloxanes; conductor-like screening model for real solvents

1. Introduction

Currently, increasing attention is being paid to obtaining so-called "green energy" from waste materials [1–4]. An alternative to natural gas is biogas, which is currently produced in over 17,783 biogas plants located in Europe. However, not all biogas plants have the technology needed for effective biogas purification that is in line with the parameters of high-methane gas. According to data from 2020 in Europe, only 729 biogas plants produced high-methane gas. In Europe, the leader in the production of biomethane is Germany, which currently has 232 biogas plants equipped with a system for producing high-quality methane. France and the United Kingdom have 131 and 80 such technologies, respectively [5]. In Poland, there are over 300 biogas plants, and only a few of them are capable of producing biomethane [6]. Biogas that is not fully purified cannot be injected into the transmission grid or used as an alternative transport fuel [7].

Biogas is a product of the methane fermentation process, in which the raw materials are mostly agricultural, landfill, and sewage waste. Raw biogas has a very rich chemical composition. The composition of biogas is strongly dependent on the raw material used for its production. Biogas mainly consists of methane (CH_4) and carbon dioxide (CO_2). In addition, biogas contains a lot of impurities including inorganic gaseous compounds,

i.e., nitrogen, oxygen, hydrogen, ammonia, carbon monoxide and water vapor, and numerous volatile organic compounds (VOC), including sulfur, nitrogen, oxygen-containing compounds, siloxanes, terpenes, linear and aromatic hydrocarbons [8–10]. The total concentration of organic and inorganic impurities may even amount to 65% of the volume of the obtained biogas, constituting a ballast that significantly reduces its calorific value. The calorific value of pure CH_4 is 35.7 MJ/m^3, while the calorific value of biogas ranges from 16 to 23 MJ/m^3 [6]. In addition, biogas impurities can be harmful in many biogas applications, and they can have environmental impacts such as stratospheric ozone depletion, increasing of the greenhouse effect, and reductions in local air quality [11–13]. One of the more troublesome groups of pollutants is organosilicon compounds (siloxanes). During biogas combustion, trace amounts of siloxanes are converted into SiO_2 deposits and damage the engine surfaces. Therefore, biogas needs to be upgraded before combustion [14].

Treatment biogas methods can be classified into adsorption, physical and chemical absorption, biological, cryogenic, and membrane separation methods [15–19]. These methods are mainly used for the removal of carbon dioxide, water, ammonia, and hydrogen sulfide, and they are not suitable for removing volatile organic compounds from biogas [20,21]. Absorption is one of the oldest and best-known technologies for gas purification. Until now, absorption has been mainly used for the removal of inorganic chemical compounds such as carbon dioxide, hydrogen sulfide, siloxanes, and other trace contaminants from gaseous fuel streams. Most absorption processes use organic solvents as absorbents. Physical scrubbing based on organic solvents has many advantages over the main technologies used for biogas treatment. These include:

- Very high treatment efficiency with a properly selected solvent;
- Low methane losses (below 1%);
- Simple and relatively inexpensive technology;
- The capacity to be regenerated many times.

However, most of the used absorbents are substances that negatively affect the natural environment and require large amounts of energy for regeneration [22,23]. Due to this, it is necessary to explore new green biogas purification methods which will be effective for the removal of hydrophobic VOCs including siloxanes.

Data from the literature suggest ionic liquids (ILs) as promising media for VOCs capture from biogas, due to their unique properties [24,25] However, in recent years, it was shown that ILs can be toxic and non-biodegradable, and that their synthesis can be very costly and complicated [26]. Despite the high efficiency of VOCs removal, the disadvantages of ILs preclude their use in real industrial processes. In the last few years, new absorption media called deep eutectic solvents (DESs) were studied in detail. DES is a mixture of two or more chemical components, one of which is a hydrogen bond acceptor (HBA), and the second is a donor (HBD). Due to the formation of strong hydrogen bonds between components, DESs are characterized by significant depressions in melting points (MP) compared to pure compounds. DESs have similar physicochemical properties to ILs, i.e., negligible vapor pressure, non-volatility, thermal stability, high conductivity, and tunable miscibility. Additionally, they are also non-toxic and biodegradable, and their synthesis is simple and cheap [27–29]. Due to the favorable properties of DESs, they are used in many processes, i.e., extraction [30–34], sample preparation [35], absorption [36–39], adsorption [40], metal electrodeposition [41], and biotransformations [42]. In addition, there are a lot of studies on the application of DESs for the removal of inorganic contaminants from gas streams, i.e., those of CO_2 [43–45], H_2S [46], SO_2 [47], H_2O [48], NH_3 [49]. However, there is very little work on the capture of siloxanes using DESs.

The paper presents a screening of 90 new non-ionic hydrophobic deep eutectic solvents composed of natural ingredients, i.e., terpenes, carboxylic acids, and polyphenols. For this purpose, the conductor-like screening model for real solvents (COSMO-RS) based on the comparison of siloxane activity coefficient to various DESs was used. Due to the fact that new never-before-published carvone mixtures with organic acids were selected as the most effective DES absorbents, the detailed results of structural characterization of new DESs,

and their basic physicochemical properties, i.e., melting point, density, and viscosity, were described. The mechanism of siloxane absorption by DESs was studied by means of ^{1}H NMR, ^{13}C NMR and FT-IR spectroscopy, based on σ-profiles. In addition, the optimization studies of the main parameters affecting the siloxane absorption process were considered. The possibility of the DESs' regeneration was also examined.

2. Results and Discussion

2.1. Screening of DES

In the studies, the COSMO-RS model was used for the screening of DESs, which were characterized by the highest affinity to siloxanes. The screening tests were prepared for the most common siloxanes in biogas, i.e., hexamethyldisiloxane (L2), octamethyl-trisiloxane (L3), decamethyltetrasiloxane (L4), hexamethylcyclotrisiloxane (D3), and de-camethylcyclopentasiloxane (D5), which represented linear and cyclic siloxanes [13,50,51] The structures of siloxanes are presented in Figure 1.
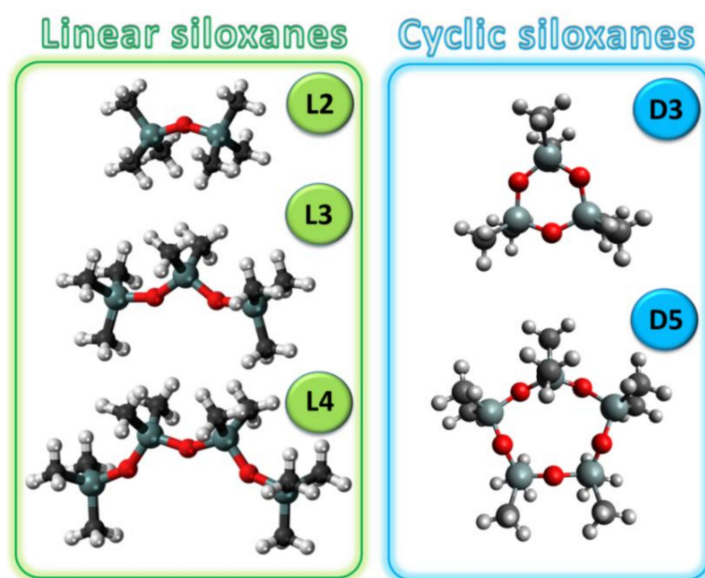
Figure 1. Structures of siloxanes used in the studies.

As solvents, DESs composed of two chemical components, which could be easily extracted from natural sources, i.e., plants or biomass, were tested. All components, i.e., carvone (C), camphor (Cam), thymol (Th), vanillin (V), guaiacol (Gu), levulinic acid (LA), vanillin acid (VA), decanoic acid (DA), undecanoic acid (UA), and dodecanoic acid (DDA), were mixed with each other at a 1:1 molar ratio. Based on the previous studies, the logarithmic activity coefficient (ln $(1/\gamma)$) was used to select the DES that exhibited the highest solubility of the siloxanes. This is a parameter that is directly related to the strength of interactions between molecules. The more negative the value, the greater the strength of the dominant interactions between siloxanes and DES, which indicates a greater affinity of solutes to solvents. In turn, the greater affinity of siloxanes to DES is responsible for their greater solubility. All calculations were performed at 20 °C and 101.325 kPa. The calculation results are presented in Figure 2. The paper presents only the most representative results for L2 and D3, which illustrated linear and cyclic siloxanes. The graphical results for the remaining siloxanes were omitted, as they fully corresponded to those obtained for L2 and D3. The obtained results indicated that L2 had a high affinity to most of the tested DES. However, completely different results were obtained for cyclic siloxane-D3. For this compound, lower logarithmic activity coefficients (ln $(1/\gamma)$ values) were obtained for DESs that were composed of carvone and carboxylic acids, i.e., decanoic, undecanoic acid, and dodecanoic acid, at a 1:1 molar ratio. The reason for the greater solubility of siloxanes in DESs that were composed of carvone and carboxylic acids was probably their specific

simple structures. The carvone had a carbonyl group that was capable of forming hydrogen bonds with the carboxyl group of DA, UA and DDA. The lack of additional groups in the HBA and HBD structures meant that oxygen from the Si−O−Si group in siloxanes had better access to the carboxyl group to which it could attach. The presence of other groups in the remaining DES, composed of, i.e., = O, -O-CH$_3$, -CH$_3$, caused the active sites to become covered, and thus, the interaction strength between the siloxanes and DES was reduced.
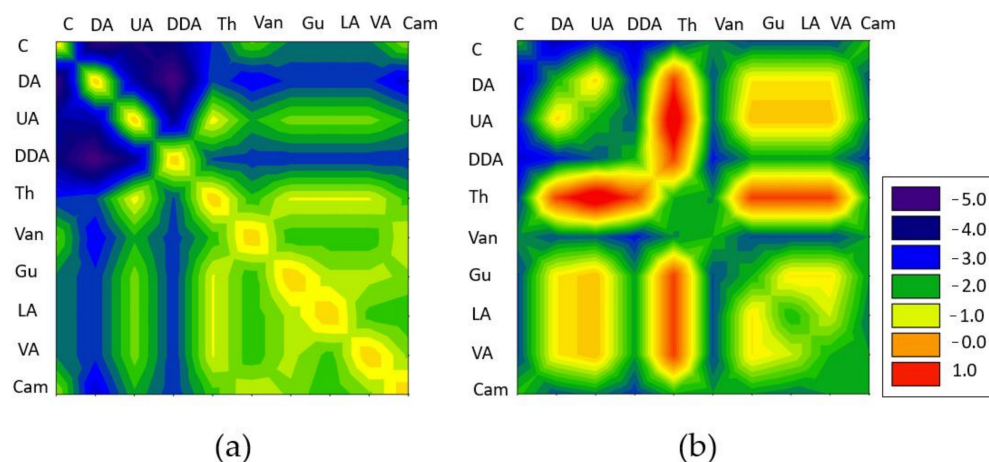
Figure 2. Screening of logarithmic activity coefficients of (**a**) L2 and (**b**) D3 in various DES mixtures at a 1:1 molar ratio.

In order to explain the obtained results, the σ-profiles of DESs' components and selected siloxanes were analyzed. The σ-profile is the molecule-specific property that determines the probability distribution of the surface area of molecules that have charge density [52,53]. Diagrams with σ-profiles of all studied molecules are presented in Figure 3. The σ-profile diagram could be divided into three segments, including an HBA region in the range of -0.025 eÅ^{-2} < σ < 0.01 eÅ^{-2}, an HBD region in the range of 0.01 eÅ^{-2} < σ < 0.025 eÅ^{-2}, and the segment between HBA and HBD that represents the non-polar region. Both the hydrogen bond donor and hydrogen bond acceptor segments indicated the potential of the studied components to form strong H bonds. The results for the σ-profiles indicated that DESs' components, depending on their structure, could be classified as hydrogen bond acceptor or donor groups. The first group was the HBA components, among which Cam and C could be distinguished, due to the active ketone group (=O) in the structures. The second group was that of the HBD components, to which Thy belonged due to the presence of a hydroxyl group (–OH) in the structure. Theoretically, all fatty acids (DA, UA, and DDA) could also be adapted to the HBD group. However, due to the specific structure of the carboxylic group (-COOH), fatty acids could be both donors and acceptors of hydrogen bonds. Therefore, they could be included in the third group, which also included Van (-CHO; -OH; -O-CH$_3$), Gu (-OH; -O-CH$_3$), LA (-COOH; = O) and VA (-COOH; -O-CH$_3$; -OH). These components could theoretically be mixed with each other and form hydrogen bonds, which could determine the formation of a stable eutectic mixture. For all the studied DES components, and siloxanes, a large peak in the non-polar region could be observed. This indicated that the siloxanes had a mostly non-polar character. Only small peaks around the HBA region could be observed in the σ-profile diagram of siloxanes, which indicated that siloxanes could also form H bonds with the –OH or –COOH group.
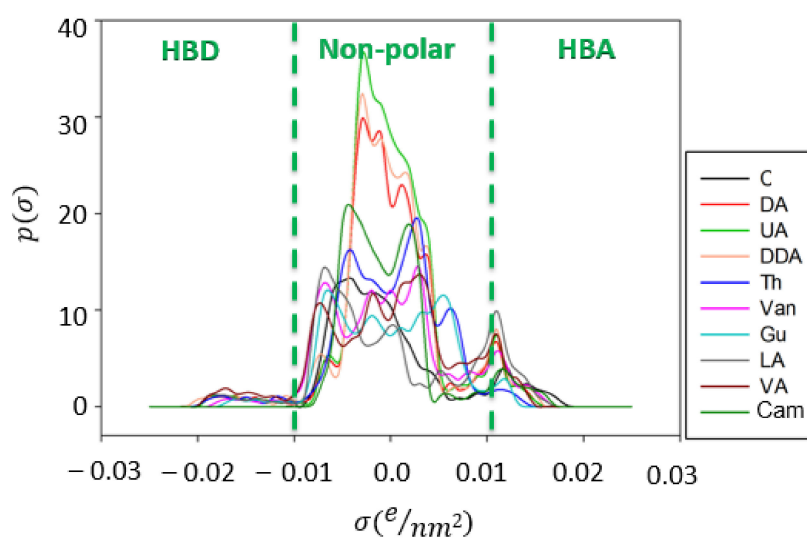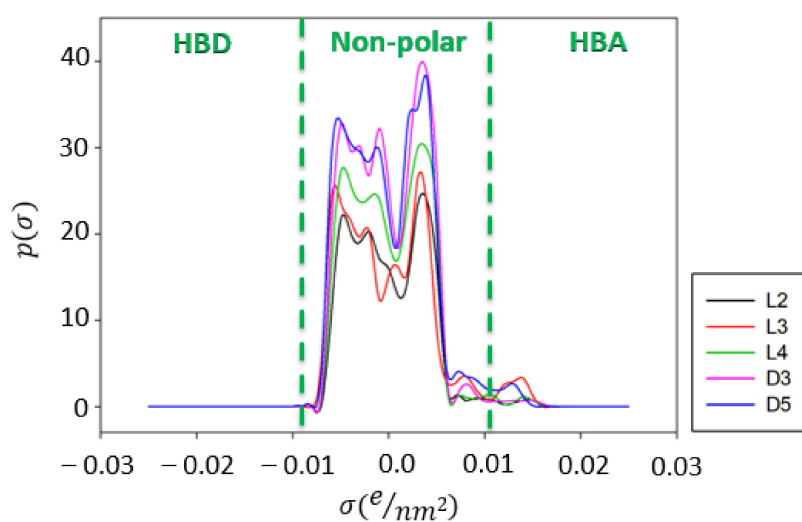
Figure 3. σ-profiles of (**a**) DES components and (**b**) siloxanes.

To confirm the results obtained using the σ-profiles, electrostatic potential (ESP) analysis was performed for DES components and selected siloxanes. The electrostatic potential of DESs and siloxanes are mapped onto electron densities in Figures 4 and 5. The positive potential regions are depicted as blue, red indicates negative potential, and white represents the potentials that are close to zero. The obtained results indicated that the electropositive area in DES component structures was located around the hydrogen atoms in the –C-H and –O-H groups. The electronegative area was located around the oxygen atom in the –O– and =O groups, and the neutral region was located around carbon atoms. During the formation of DESs, the electropositive area from one of the DES components (HBD) attracted the electronegative region of the second component (HBA). In this way, strong hydrogen bonds were formed between the DES compounds, resulting in the formation of stable DES. Figure 5 shows that, in all siloxane compounds, only a neutral region could be identified. This indicated that other weaker non-bonded interactions must play the dominant role in the capture of siloxane by DESs.
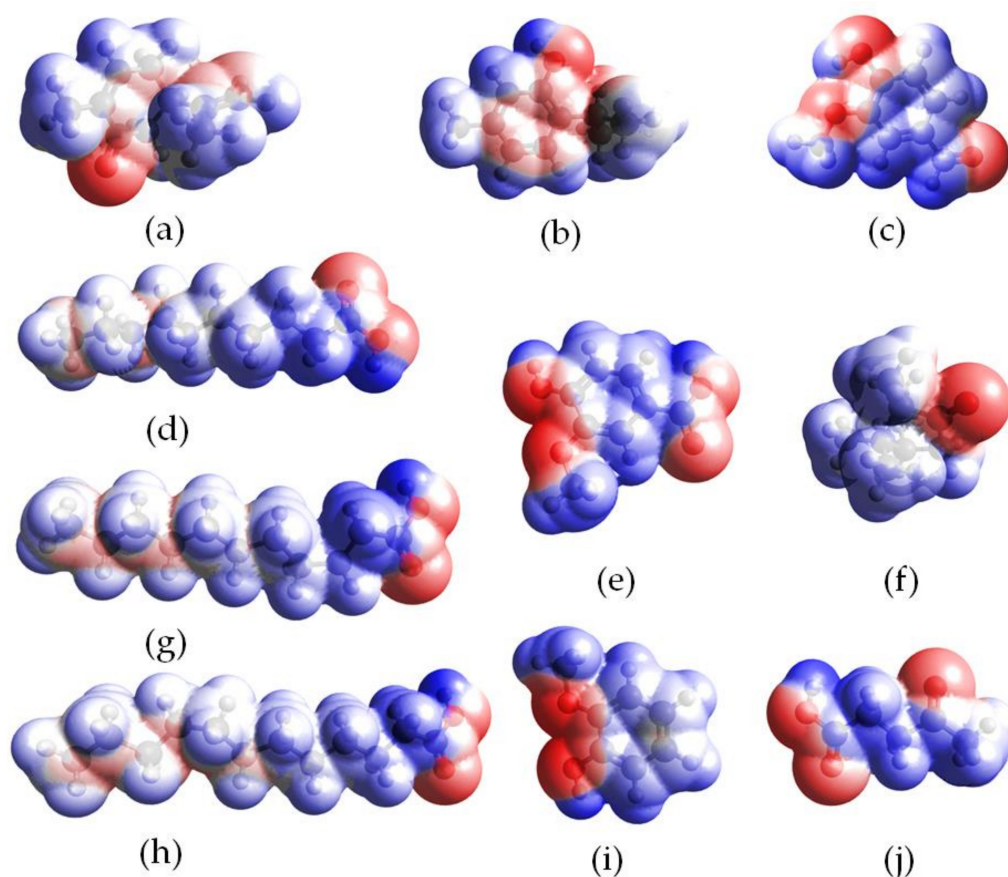
Figure 4. ESP mapped onto total electron density with an isovalue of 0.001 for DES components, i.e., (**a**) carvone, (**b**) thymol, (**c**) vanillin, (**d**) decanoic acid, (**e**) vanillic acid, (**f**) camphor, (**g**) undecanoic acid, (**h**) dodecanoic acid, (**i**) guaiacol and (**j**) levulinic acid. Blue color represents positive charges, red color represents negative charges, and white color represents neutral charges.
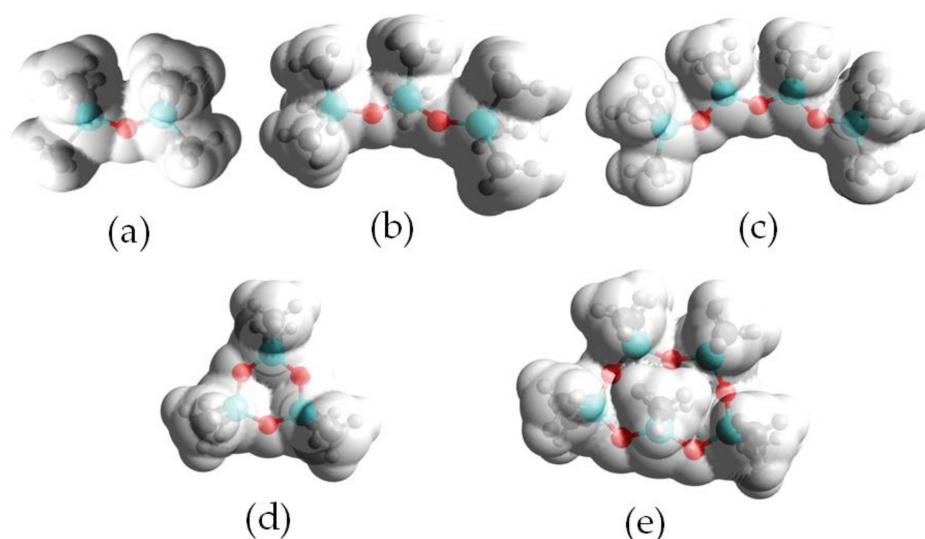
Figure 5. ESP mapped onto total electron density with an isovalue of 0.001 for siloxanes, i.e., (**a**) L2, (**b**) L3, (**c**) L4, (**d**) D3 and (**e**) D5. Blue color represents positive charges, red color represents negative charges, and white color represents neutral charges.

2.2. Synthesis of New DESs

From a technological point of view, only DESs, which ensure high solubility levels of linear and cyclic siloxanes, should be considered in further research. Therefore, in the next step, only DESs that were characterized by lower activity coefficient values were synthesized, including C:DA, C:UA, and C:DDA, at a 1:1 molar ratio. However, only C:DA and C:UA were in a liquid form at room temperature. Therefore, C:DDA was also synthesized at 2:1 and 3:1 molar ratios, and only C:DDA at a 3:1 ratio was liquid at room temperature.

2.3. An Experimental DESs Structural Characterization
2.3.1. Fourier Transform Infrared Spectroscopy (FT-IR)

FT-IR analysis provided a lot of important information about the structure of the synthesized DES. Based on the peak shifts, it was possible to determine which groups of individual substances were involved in the formation of DES, as well as to determine whether by-products were formed during the synthesis process. Figure 6 shows the spectra of pure substrates (HBA and HBD) and synthesized DESs. In the C:DA (1:1) spectrum, shifts of the stretching carbonyl band vibrations towards higher values, in comparison to both pure HBA (from 1693 cm^{-1} to 1708 cm^{-1}) and HBD (from 1668 cm^{-1} to 1676 cm^{-1}), were observed. This indicates that both groups, –COOH from DA and =O from C, were involved in the formation of a hydrogen bond. In addition, the γO-H deformation band (929 cm^{-1}), which could be observed in the DA spectrum, underwent distortion in the DES spectrum. In the DES spectrum, wide peaks within the wavelength number range from 965 to 891 cm^{-1} were observed. The deformation of the band of the -OH group confirmed the fact that it was involved in the formation of hydrogen bonds. Similar shifts were also observed in the spectra of the remaining DESs (C:UDA (1:1), and C:DDA (3:1)).
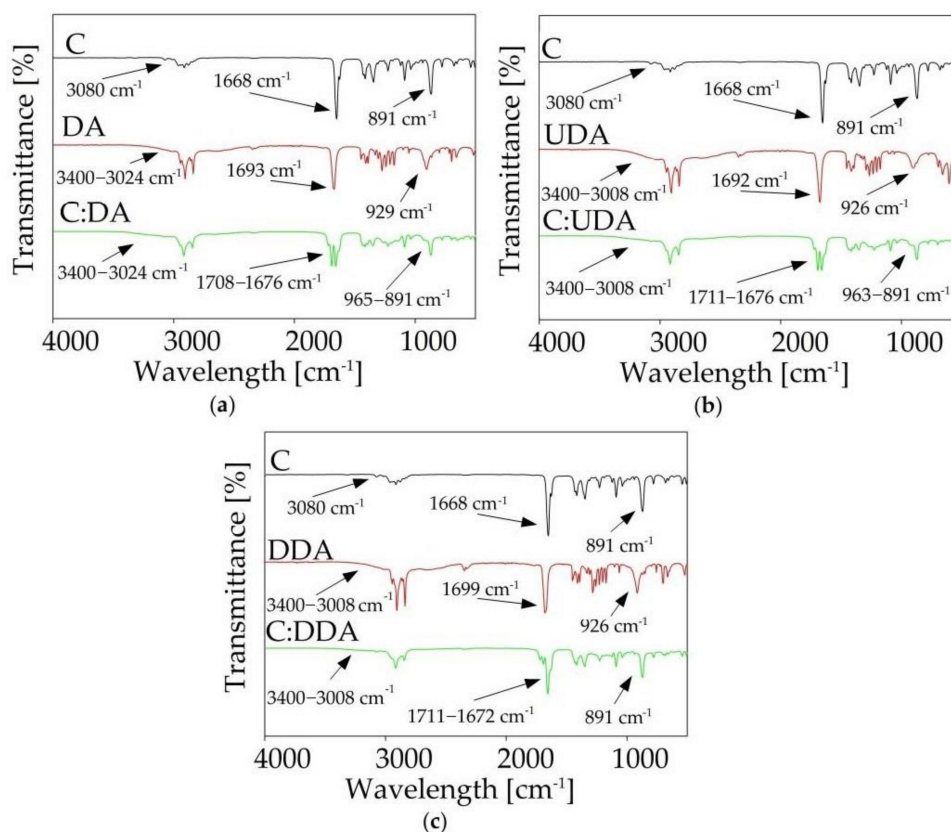
Figure 6. FT-IR spectra of pure components (HBA and HBD) and synthesized DES: (**a**) C:DA (1:1), (**b**) C:UDA (1:1), (**c**) C:DDA (3:1).

2.3.2. Nuclear Magnetic Resonance Spectroscopy (NMR)

The results of the ^{1}H NMR analysis confirmed the formation of hydrogen bonds between HBA (carvone) and various HBDs (i.e., DA, DDA and UDA). Spectra are presented in Figure 7 and Figures S1 and S2. The detailed values of chemical shifts are presented in Table 1, Tables S1 and S2. In the ^{1}H NMR spectra, shifts of hydrogen (H1) from the hydroxyl group that was present in the structure of carboxylic acids, towards lower values, were observed for DA (from 11.87 to 11.38 ppm) and DDA (from 11.87 to 10.69 ppm). For UDA, the shift towards higher values, from 10.4 to 11.43 ppm, was observed. The greatest differences in shifts could be observed for DES with DDA (about 0.2 ppm), and the lowest for DES with DA (about 0.1 ppm). This indicated that in DES composed of carvone and DDA, the strongest H-bonding occurred. All changes in the hydrogen signal from HBA were shifted towards lower values, except for H8. Hydrogen H8, which was shifted towards higher values in the DES spectrum, was located close to the oxygen atom from the carbonyl group. This may indicate that hydrogen bonds were formed in the vicinity of H8.
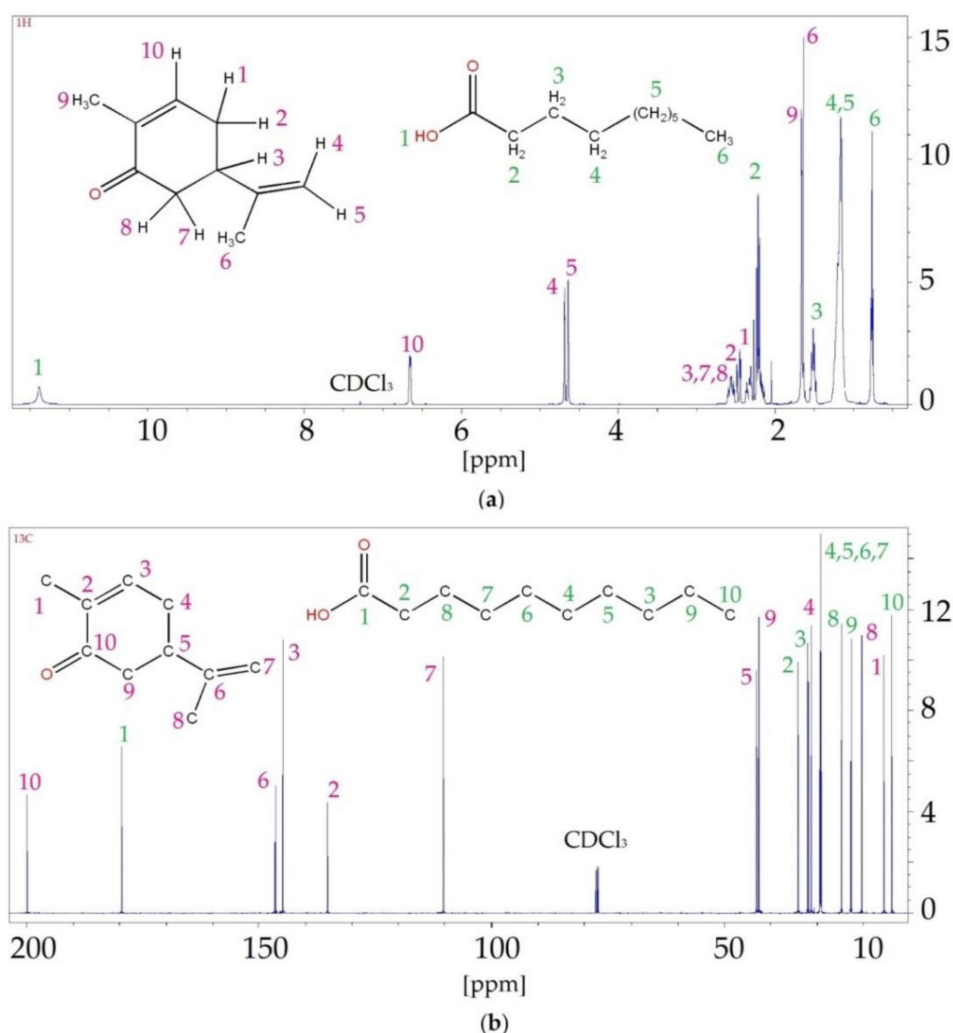
Figure 7. ^{1}H NMR (**a**) and ^{13}C NMR (**b**) spectrum of the C:DA (1:1).

Table 1. Chemical shift values from the ^{1}H NMR and ^{13}C NMR spectra for C:DA (1:1).

^{1}H NMR							
HBA		**DES**		**HBD**		**DES**	
atom	δ (ppm)	atom	δ (ppm)	atom	δ (ppm)	atom	δ (ppm)
H1	2.45	H1	2.31	H1	11.87	H1	11.38
H2	2.35	H2	2.30	H2	2.21	H2	2.21
H3	2.69	H3	2.56	H3	1.54	H3	1.51
H4	4.76	H4	4.68	H4	1.33	H4	1.19
H5	4.81	H5	4.64	H5	1.26	H5	1.15
H6	1.76	H6	1.63	H6	0.88	H6	0.76
H7	2.57	H7	2.48				
H8	2.35	H8	2.44				
H9	1.78	H9	1.66				
H10	6.77	H10	6.65				
^{13}C NMR							
C1	15.63	C1	15.48	C1	180.81	C1	179.50
C2	135.45	C2	135.27	C2	34.26	C2	33.96
C3	144.40	C3	144.74	C3	31.99	C3	31.77
C4	31.30	C4	31.12	C4	29.53	C4	29.32
C5	42.55	C5	42.89	C5	29.38	C5	29.17
C6	146.69	C6	146.40	C6	29.38	C6	29.16
C7	110.47	C7	110.33	C7	29.19	C7	28.98
C8	20.50	C8	20.26	C8	24.79	C8	24.62
C9	43.20	C9	42.35	C9	22.77	C9	22.55
C10	199.34	C10	199.7	C10	14.13	C10	13.92

In this study, ^{13}C NMR analysis was also performed. The observed shifts likewise indicated the formation of hydrogen bonds between the carvone and the fatty acids. This was confirmed by the C1 shifts in the carboxyl group in the acids and C10 in the carbonyl group in the carvone. In addition, shifts of carbons (C2 and C9) that were directly connected to the hydroxyl and carbonyl groups were also visible.

In both the ^{1}H NMR and ^{13}C NMR spectra of all DESs, only signals assigned to the substrates were observed. This indicated that no by-products were formed during the synthesis.

2.3.3. Physicochemical Properties of DESs

The melting point was one of the more important parameters that indicated the formation of DES. The chemical compounds that were used for the DESs synthesis were solid at room temperature. The MP of pure substrates was 25.2, 31.6, 28.6 and 43.2 °C for carvone, decanoic acid, undecanoic acid, and dodecanoic, respectively. For new DESs, a large depression in MP was observed. The melting points of new DESs were −19, −11.7 and −18.8 °C for C:DA (1:1), C:UDA (1:1) and C:DDA (3:1), respectively.

DES density and viscosity are physicochemical parameters that have a key influence on mass transfer processes [28]. Therefore, the dynamic viscosity of absorbents should be as low as possible, so that DES can be used for absorption processes. These are also parameters that largely depend on the HBD and HBA that are used for the DESs' synthesis.

The obtained results indicated that all of the studied DESs were characterized by relatively low viscosity. At 25 °C, the viscosity of the DESs ranged from 4 to 6 mPas. Compared to other DESs, i.e., tetraethylammonium chloride:oleic acid at a 1:3 molar ratio, and tetrabutylammonium bromide:decanoic acid (1:2), for which the viscosity was above 200 mPas, the obtained viscosity values were much lower [37,54]. This is a favorable feature since when DESs are used as absorption solvents, their viscosity should be as low as possible. The lower viscosity of the absorbents facilitates the mass transfer process. This is consistent with Walden's rule: the lower the viscosity, the greater the diffusion coefficient,

and vice versa. The viscosity of all DESs decreased with increasing temperature, which indicated normal liquid behavior (Figure 8a).
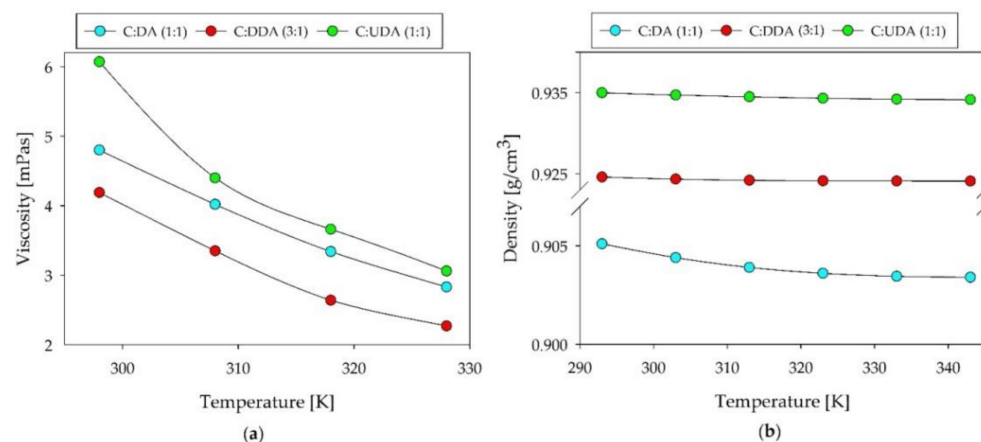
Figure 8. (**a**) Viscosity and (**b**) density of the new DESs.

The results of the DESs' density are presented in Figure 8b. The lowest density was obtained for C:DA (1:1), and the highest for C:UDA (1:1). With the increasing of the temperature from 20 to 70 °C, only slight changes in density could be observed. The largest visible differences were noticeable for C:DA (1:1) (about 0.002), and the lowest for C:DDA (3:1). The densities of the studies DES showed lower densities than water, ranging from 0.905 to 0.935 g/cm^3.

2.4. Absorption Process

Research on the siloxane absorption process from the model biogas stream was conducted for all synthesized DESs (C:DA (1:1), C:UDA (1:1) and C:DDA (3:1)). In the first part of the studies, as a model biogas, mixtures of nitrogen and siloxanes, such as L2, L3, L4, D3, and D5 at 30 g/m^3 concentration levels, were used. Pure nitrogen was used to exclude the effect of the matrix on the absorption capacity results. The flow rate was kept constant (50 mL/min) throughout the process. The research was carried out in accordance with the procedure described in previous works [36,39,55,56].

In this part of the study, the DESs that were characterized by the highest siloxane absorption capacity were selected. The obtained results are presented in Figure 9. All new DESs showed high siloxane absorption capacity. However, the most effective absorbent was DESs composed of C:DA (1:1). C:DA (1:1) displayed effective absorption capacity up to 5600 min. After this time, DES saturated and the process became ineffective. The saturation of DES (C:DA) was fastest for cyclic siloxanes D3 and D4. The time of the effective absorption process was 5217 min. The other DESs (C:UDA (1:1) and C:DDA (3:1)) showed a much shorter effective absorption capacity for siloxanes, as measured in terms of time (1500 and 1650 min). In addition, both DESs (C:UDA and C:DDA) were saturated most rapidly by the volatile linear siloxane (L2) (750 and 720 min), which indicates that the others siloxanes were more easily absorbed than L2. The vapor pressure and polarity of L2 were much greater compared to other linear siloxanes, which may have influenced the reduction in L2 removal from biogas. The cyclic siloxanes had a greater number of Si−O bonds relative to the linear siloxanes, which had great potential to form stronger bonds between siloxanes and DES. This may explain the greater affinity of cyclic siloxanes to-wards DESs.
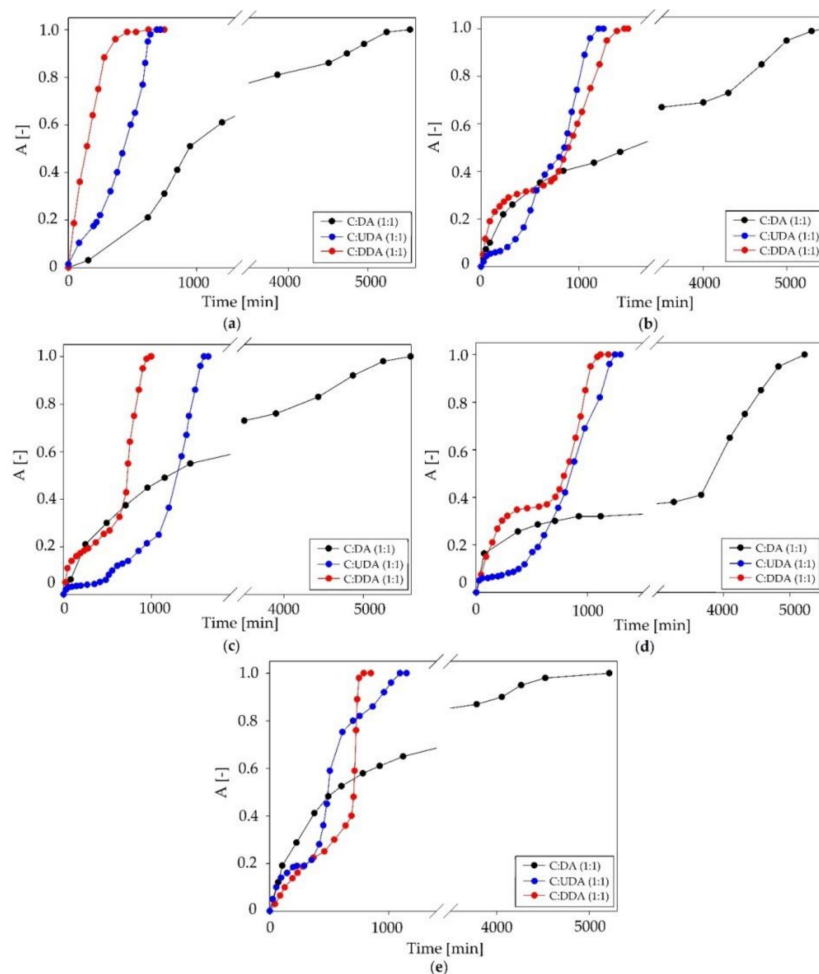
Figure 9. Absorption curves of the studied DESs for individual siloxanes: (**a**) L2, (**b**) L3, (**c**) L4, (**d**) D3 and (**e**) D5.

In the next part of the study, the most effective DES was subjected to further processes, in which the biogas stream consisted mainly of methane and carbon dioxide at a 2:1 v/v volume ratio. The concentration of siloxanes remained at the same level (30 g/m^3). The used concentrations of substances corresponded to the composition of the real biogas streams [13]. For C:DA (1:1), studies on the effect of the biogas flow rate, in the range from 25 to 75 mL/min, on the siloxanes removal efficiency were performed. This range corresponded to the laminar flow rate. The obtained results are presented in Figure 10. The shortest effective siloxane absorption time was obtained for the highest biogas flow of 75 mL/min. In turn, the longest absorption time was obtained at the flow rate of 25 mL/min. This was due to the fact that, with the increasing of the biogas flow rate, the contact time of siloxanes with DES was reduced, which adversely affected the absorption process [36,55]. DES was saturated with the L2, L3 and L4 compounds after about 5500 min (flow rate: 50 mL/min) and 6000 min (flow rate: 25 mL/min), with D3 after about 5000 min (flow rate: 50 mL/min) and 6000 min (flow rate: 25 mL/min), and D5 for both flow rates at about 6000 min. The greatest differences in the absorption time between the flows 75, 50, and 25 mL/min were observed for the linear compounds. This confirms that cyclic siloxanes presented more affinity to DES than linear ones.
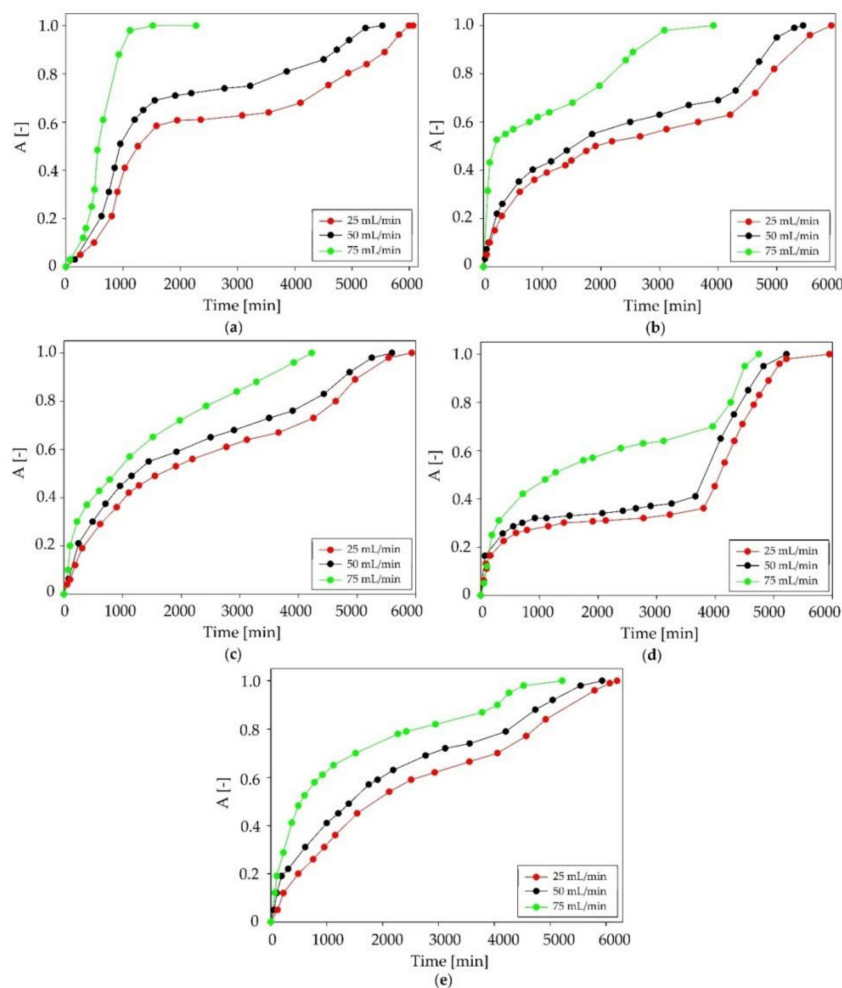
Figure 10. Absorption curves of C:DA (1:1) at various biogas flow rates in the range of 25–75 mL/min for individual siloxanes: (**a**) L2, (**b**) L3, (**c**) L4, (**d**) D3 and (**e**) D5.

During the absorption process, the content of the main components (CH_4 and CO_2) of the model biogas stream was also controlled. The absorption curves for CH_4 and CO_2 are presented in Figure 11. The obtained results indicated that, during the initial stage of the absorption process, both the CH_4 and CO_2 gases were also absorbed by DES. The C:DA (1:1) became saturated with methane in a very short time (after 50 min). Due to this, the methane loss was about 1%, which was within the acceptable range [55]. In contrast, the process of effectively capturing CO_2 took much longer, around 500 min. This was due to the presence of active oxygen in the CO_2 structure that could form competing strong hydrogen bonds with DES. The removal of CO_2 from biogas is advantageous because it is a gas that substantially reduces the calorific value of biogas [57]. Theoretically, CO_2 absorption should deteriorate the efficiency of siloxane capture due to the same active groups being present in the pollutant structures. However, due to the low efficiency of CO_2 removal with DES, only a minor effect of DES saturation with carbon dioxide on the efficiency of siloxane removal could be observed (Figure 12).
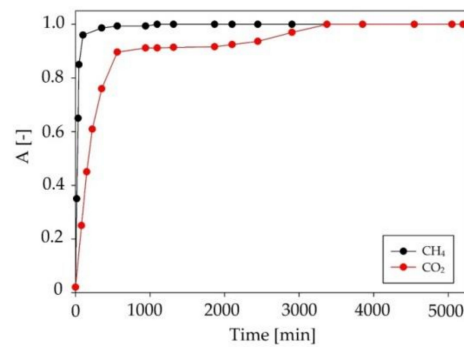
Figure 11. Absorption curves for methane and carbon dioxide in C:DA (1:1).
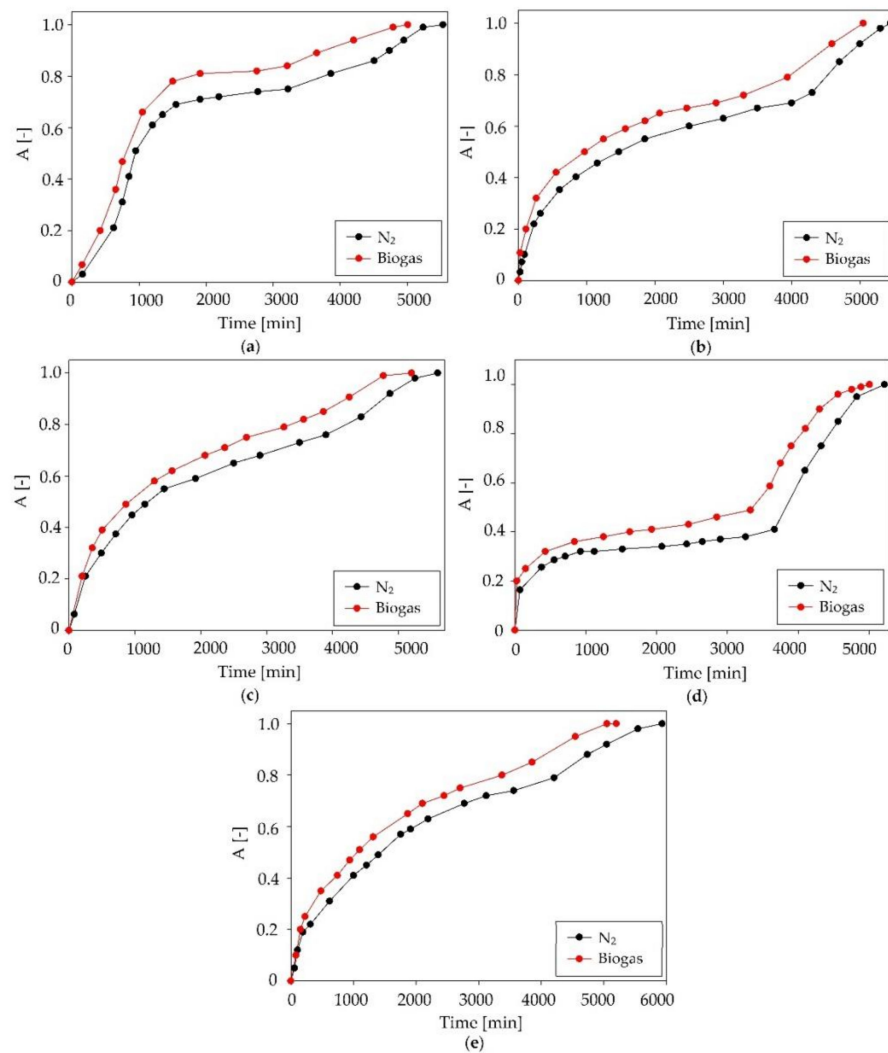
Figure 12. Absorption curves of C:DA (1:1) at various biogas matrix compositions for individual siloxanes: (**a**) L2, (**b**) L3, (**c**) L4, (**d**) D3 and (**e**) D5.

2.5. Mechanism of Siloxane Absorption

2.5.1. FT-IR Analysis

To confirm the effectiveness of the biogas purification process, FT-IR analyses of DESs before and after absorption were prepared. The obtained spectra are presented in Figure 13. In the spectra of DES after siloxane absorption, characteristic (Si-O-Si) bands were observed between 780 and 1260 cm^{-1}. This confirmed that siloxanes (S) were bound in DESs' active centers. The lack of band shifts in the vicinity of 3000–3500 cm^{-1} and 1670–1720 cm^{-1}

indicated that siloxanes did not combine with DES via hydrogen bonds, and that weaker non-bonded interactions played a major role in the absorption process.
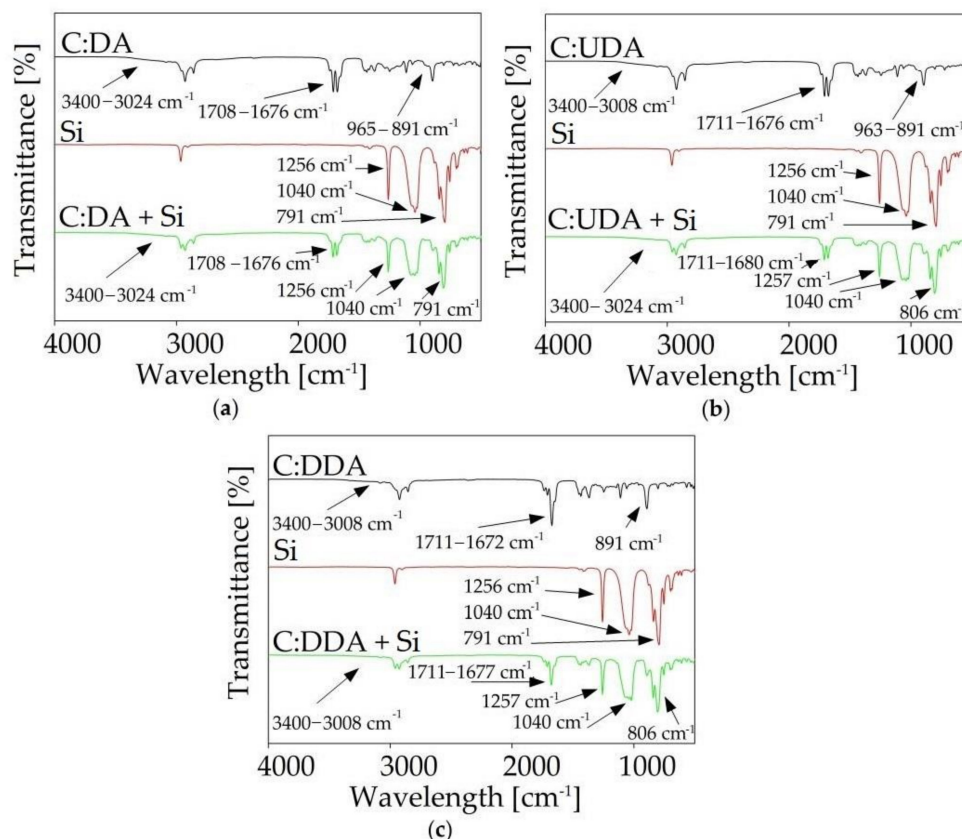
Figure 13. FT-IR spectra before and after siloxanes' (S) absorption for (**a**) C:DA (1:1), (**b**) C:UDA (1:1) and (**c**) C:DDA (3:1).

2.5.2. NMR Analysis

Additionally, DESs after the absorption process was subjected to ^{1}H NMR, and ^{13}C NMR analysis (Figure 14, and Figures S3 and S4). The detailed results of shifts values are summarized in Table 2, and Tables S3 and S4. In the ^{13}C NMR spectrum, all signals were shifted towards lower values. The greatest differences were visible at the C1 carbon shift (0.3–0.4 ppm) for each acid. Similar shifts were also observed for carvone-derived C10. In both cases, carbon atoms were directly bonded to oxygen atoms. This indicates that both C=O and -COOH groups were involved in the formation of weak non-bonded bonds with siloxanes. The ^{1}H NMR spectra showed similar results to those obtained for ^{13}C NMR. All signals were shifted towards lower values, and the greatest shift in values was observed for acid H1 (0.16–0.28 ppm). In addition, in both the ^{1}H NMR and ^{13}C NMR spectra, the signals from the siloxanes were visible. This confirms the effectiveness of the absorption process using DESs.

2.6. Desorption Process

From an industrial point of view, the absorbent regeneration process is extremely important. The possibility of multiple applications of sorption material significantly reduces the process costs [57]. On the other hand, the regeneration process is considered to be the main disadvantage of the absorption process due to its high energy consumption. Therefore, the desorption step should be optimized. In the studies, the desorption process was performed using the pure nitrogen bubbling process at elevated temperatures in range of 50–150 °C. The absorbent regeneration process was performed for the best absorbent, C:DA (1:1) (Figure 15). The obtained results indicated that the highest desorption efficiency was

observed for the process at a temperature of 150 °C. The complete siloxanes desorption was obtained after 90 min. Along with the decrease in process temperature, the desorption time was extended (up to 500 min at 70 °C). Below 70 °C, the desorption process was ineffective.
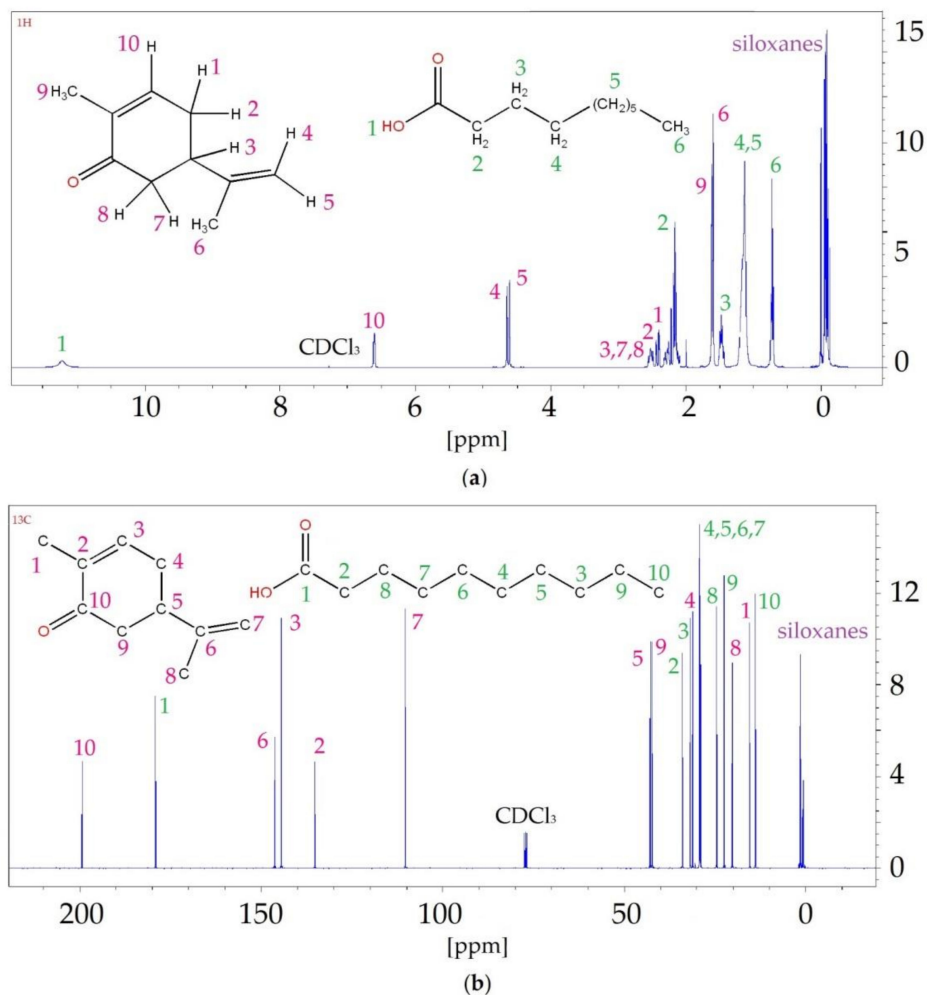
Figure 14. ^{1}H NMR (**a**) and ^{13}C NMR (**b**) spectra for C:DA (1:1) after the absorption process of siloxanes from the model biogas stream.
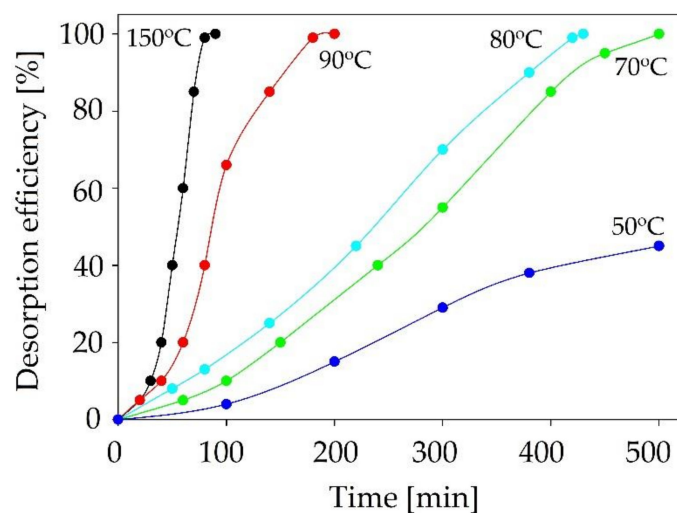
Figure 15. The effect of temperature on C:DA (1:1) in the desorption process.

Table 2. Chemical shift values from ^{1}H NMR and ^{13}C NMR spectra from individual DES components before and after the siloxane absorption process.

				^{1}**H NMR**				
	C		**C:DA (1:1)+Si**		**DA**		**C:DA (1:1)+Si**
atom	δ (ppm)	atom	δ (ppm)	atom	δ (ppm)	atom	δ (ppm)
H1	2.31	H1	2.26	H1	11.38	H1	11.22
H2	2.35	H2	2.31	H2	2.21	H2	2.17
H3	2.56	H3	2.52	H3	1.51	H3	1.48
H4	4.68	H4	4.64	H4	1.19	H4	1.16
H5	4.64	H5	4.61	H5	1.15	H5	1.13
H6	1.63	H6	1.59	H6	0.76	H6	0.74
H7	2.48	H7	2.44				
H8	2.44	H8	2.40				
H9	1.66	H9	1.62				
H10	6.65	H10	6.60				
				^{13}**C NMR**				
	C		**C:DA (1:1)+Si**		**DA**		**C:DA (1:1)+Si**
C1	15.48	C1	15.38	C1	179.50	C1	179.20
C2	135.27	C2	135.30	C2	33.96	C2	33.83
C3	144.74	C3	144.40	C3	31.77	C3	31.72
C4	31.12	C4	31.08	C4	29.32	C4	29.28
C5	42.89	C5	42.83	C5	29.17	C5	29.14
C6	146.40	C6	146.10	C6	29.16	C6	29.14
C7	110.33	C7	110.10	C7	28.98	C7	28.94
C8	20.26	C8	20.17	C8	24.62	C8	24.55
C9	42.35	C9	42.32	C9	22.55	C9	22.49
C10	199.7	C10	199.40	C10	13.92	C10	13.83

In the further part of the study, FT-IR spectra were obtained for the regenerated DES and compared with the fresh DES spectrum (Figure 16). In the FT-IR spectra, after the desorption process, no characteristic bands, derived from siloxanes, were observed. This indicates that the application of nitrogen bubbling at elevated temperatures is a suitable absorbent regeneration method.
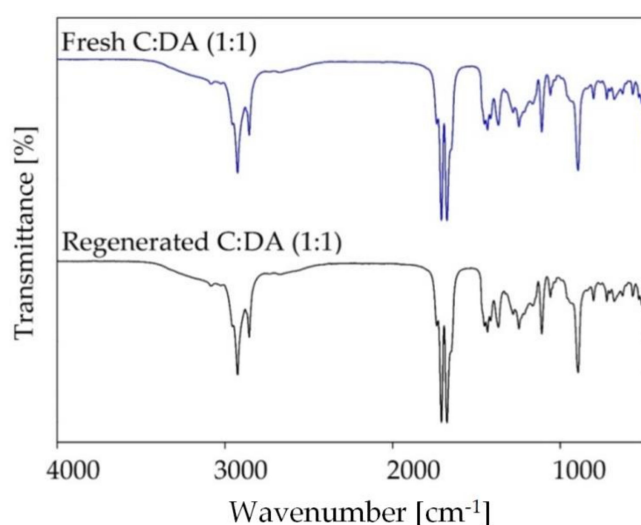
Figure 16. FT-IR spectra of the DES-based absorbent after the regeneration process.

In addition, C:DA (1:1) showed the ability to complete five regeneration cycles without changing the efficiency of the absorption process. The absorption curves for successive absorption cycles are presented in Figure 17. In comparison with the data in the literature,

the obtained results indicated a high efficiency of the regeneration process of DES, without a significant loss of absorption capacity. For example, the adsorption capacity of active carbon decreased by 65% after three siloxane adsorption/desorption cycles at 90 °C [58]. In other studies, a 30% reduction in adsorption capacity was observed after one cycle of the process carried out at a temperature of 160 °C for 4 h [59].
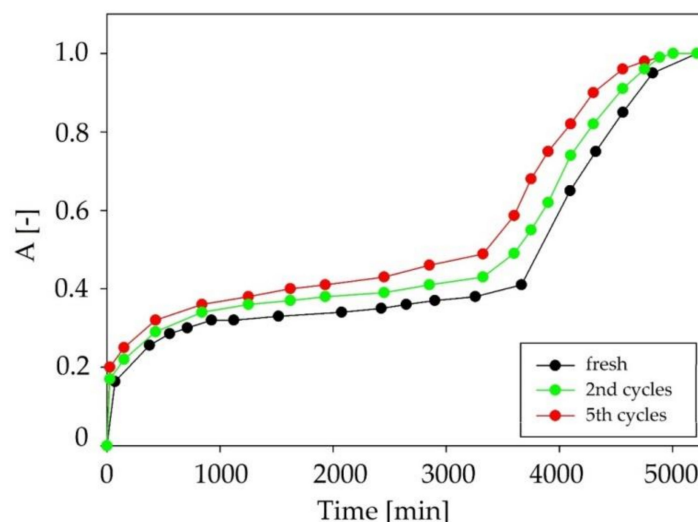
Figure 17. Absorption curves for fresh C:DA (1:1) and after 2 and 5 regeneration cycles.

3. Materials and Methods

3.1. Materials

The following chemicals were used in the studies: carvone (purity: ≥97%), decanoic acid (purity: ≥98%), undecanoic acid (purity: ≥97%), dodecanoic acid (purity: ≥98%), hexamethyldisiloxane (purity: ≥98.5%), octamethyltrisiloxane (purity: ≥98%), decamethyltetrasiloxane (purity: ≥97%), hexamethylcyclotrisiloxane (purity: ≥98%), decamethylcyclopentasiloxane (purity: ≥97%). All standards were purchased from Sigma Aldrich (St. Louis, MO, USA).

The following compressed gases were used to prepare the model biogas stream: nitrogen (purity: N 5.5), methane (purity: N 5.0) and carbon dioxide (purity: N 2.2). These were purchased from Linde Gas (Łódź, Poland).

For the GC analysis, compressed gases, such as helium (purity: N 5.0), nitrogen (purity: N 5.5), air (purity: N 5.0) and hydrogen (purity: N 5), were used. Air was generated by the DK50 compressor with a membrane dryer (Ekkom, Kraków, Poland), while hydrogen was generated by the Precision Hydrogen 1200 Generator (PEAK Scientific, Scotland, UK).

3.2. Apparatus

The efficiency of the siloxane absorption process was controlled by gas chromatography (Autosystem XL) (PerkinElmer, Waltham, MA, USA) with a flame ionization detector (FID) (PerkinElmer, Waltham, MA, USA), HP-5 (30 m × 0.25 mm × 0.25 μm) capillary column (Agilent Technologies, Santa Clara, CA, USA), and using TurboChrom 6.1 software (PerkinElmer, Waltham, MA, USA).

The methane and carbon dioxide contents in the biogas stream were monitored by means of gas chromatography (SRI Instruments, Earl St, Torrance, CA, USA) coupled with a thermal conductivity detector (TCD, SRI Instruments, Earl St, Torrance, CA, USA), and a packed column (Porapak Q 80/100, 2 m × 2 mm) (Restek, Bellefonte, PA, USA). In the investigations, the PeakSimple data system version 4.09 (exclusively licensed by SRI Inc., McLean, VA, USA) was used.

The following apparatuses were used to evaluate the structural and physicochemical properties: a Bruker Tensor 27 spectrometer (Bruker, Billerica, MA, USA) with an ATR

adapter and OPUS software (Bruker, Billerica, MA, USA), a Bruker Avance III HD 400 MHz (Bruker, Billerica, MA, USA), a BROOKFIELD LVDV-II + viscometer (Labo-Plus, Warsaw, Poland), a DMA 4500 M (Anton Paar, Graz, Austria), a Bruker Avance III HD 400 MHz (Bruker, Billerica, MA, USA) and a cryostat (HUBER, Edison, NJ, USA).

3.3. Procedures

3.3.1. COSMO-RS Studies

The fast screening of 90 DESs composed of natural ingredients, i.e., carvon (C), camphor (Cam), menthol (M), thymol (Th), vanillin (V), guaiacol (Gu), levulinic acid (LA), vanillin acid (VA), decanoic acid (DA), undecanoic acid (UA) and dodecanoic acid (DDA), was prepared using ADF COSMO-RS software (SCM, Netherlands). In the first part of the studies, the geometry optimization of all 90 deep eutectic solvents complexes composed of HBA and HBD in a 1:1 molar ratio was performed using the continuum solvation COSMO model at the BVP86/TZVP theoretical level. The geometry optimization studies were performed in the gas phase in order to find the most stable conformers, and then vibrational analysis was performed to identify the deep eutectic solvent conformer that corresponds to the true energy minimum. Only for the most energetically favorable conformer, full geometry optimization of deep eutectic solvents was prepared. Based on the activity coefficients, the DES with the highest affinity for siloxanes was selected. The activity coefficient was calculated using Equation (1):

$$\ln(\gamma_i) = \frac{\mu_i^{DES} - \mu_i^{p}}{RT} \tag{1}$$

where: μ_i^{sol}—chemical potential of siloxanes in DES;

μ_i^{p}—chemical potential of pure siloxanes;

R—universal gas constant (8.314 J/mol);

T—temperature (K).

3.3.2. DES Synthesis

Deep eutectic solvents were synthesized by mixing C with DA, UDA, and DDA at a 1:1 molar ratio. The stirring process was carried out on a magnetic stirrer at 800 RPM, at 60 °C. The obtained liquid DES was allowed to cool to room temperature. The chemical structures of HBA and HB, for the synthesis of DES, are presented in Figure 18.
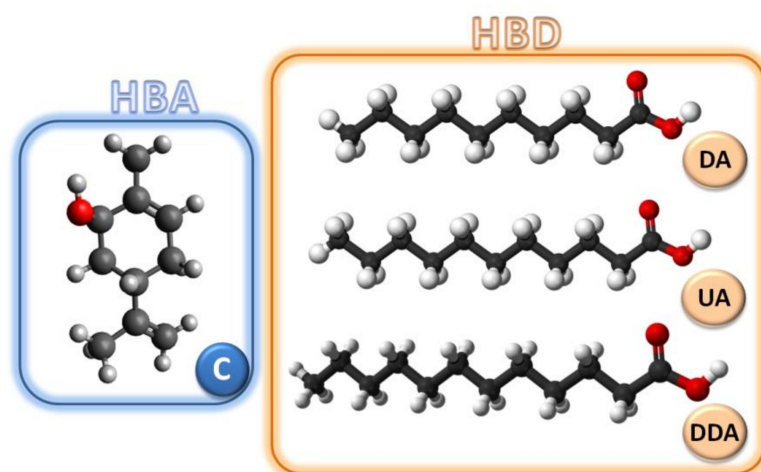
Figure 18. Structures of HBA and HBD used for DES synthesis.

3.3.3. DES Structural Characterization

FT-IR spectra were recorded using attenuated total reflection (ATR) with the following operating parameters: spectral range—4000–550 cm^{-1}; number of background scans—256; number of sample scans—256; resolution—4 cm^{-1}; slit width—0.5 cm. The NMR spectra of

the DESs were prepared by weighing 20 mg of a DESs and adding 0.7 mL of chloroform-d1. The measurements were carried out at 20 °C, with the use of the Bruker Avance III HD 400 MHz (Bruker, Billerica, MA, USA).

3.3.4. Physicochemical Properties of DES

The viscosity of the new DES was measured in the temperature range of 25–55 °C at 90 RPM. The density was measured in the temperature range of 20–70 °C. The measurement of uncertainty for the temperature was 0.5 °C. The melting points (MP) were measured using a cryostat. A quantity of 5 mL of the DESs was cooled to −50 °C and then a temperature increase of 1 °C/min was implemented. The MP of DES was determined visually. The point at which the first liquid drop appeared was taken as the melting point.

3.3.5. Preparation of Model Biogas

In the studies, two types of model biogas were used. Both model biogas streams were prepared using the bubbling method. In the first biogas stream, pure N_2 was passed through a 10-mL vial containing liquid siloxanes mixture (2 mL of L2 and D5, 3 mL of L3 and L4, and 1.6 g of solid D3 siloxane). Gas enriched with siloxanes was diluted with nitrogen in order to reach a 30 g/m^3 siloxanes concentration in the model biogas stream. In the second biogas stream, nitrogen was replaced with a mixture of CH_4 and CO_2 at a 2:1 *v/v* volume ratio.

3.3.6. Absorption Process

The scheme of the installation for absorption process is shown in Figure 19. In the process, the biogas stream was directed to the absorption column with 50 mL of DES, in which the siloxanes removal process took place based on the bubbling phenomenon. The pure biogas stream was discharged from the top of the absorption column. The absorption process was controlled at the inlet and outlet of the absorption column in terms of the effectiveness of the removal of siloxane impurities. Additionally, the concentration of CH_4 and CO_2 during the siloxane absorption process was also examined.
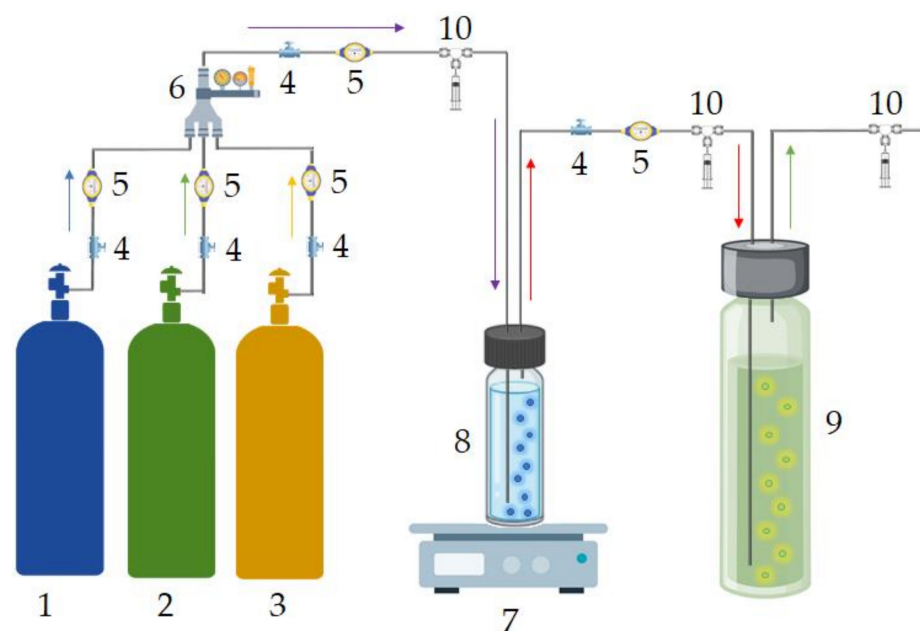
Figure 19. Siloxane absorption installation: 1-N_2 bottle; 2-CH_4 bottle; 3-CO_2 bottle; 4-valve; 5-flowmeter; 6-gas mixer; 7-hotplate; 8-vial with siloxanes; 9-vial with DES; 10-gas sample collection point.

The absorption efficiency (A) of siloxanes, methane, and carbon was calculated using Equation (2):

$$A = \frac{C_{in} - C_{out}}{C_{in}} \tag{2}$$

where: C_{in}—inlet siloxanes, CH_4, CO_2 concentration in biogas stream (g/m^3);

C_{out}—outlet siloxanes, CH_4, CO_2 concentration in biogas stream (g/m^3).

After the absorption process, DESs were regenerated by means of pure nitrogen bubbling. The regeneration experiments were carried out at the temperature of 90 °C with a nitrogen flow of 50 mL/min for 2 h. The efficiency of DESs after regeneration process was tested by means of GC analysis.

3.3.7. Gas Chromatographic Analysis

The siloxanes removal efficiency from the biogas stream was determined using the gas chromatography method coupled with a flame ionization detector (GC-FID). The following chromatographic condition was used: oven temperature program at 40 °C, ramped at 10 °C/min to 200 °C; FID detector temperature of 250 °C; injection port temperature of 200 °C; injection mode split of 5:1; nitrogen as carrier gas (180 mL/min).

The chromatographic methodology was validated based on the linearity, limits of detection (LOD), quantification (LOQ), precision, accuracy, and global uncertainty. Linearity was determined by the direct injection of siloxane standard mixtures at concentrations ranging from 0.005 to 50 g/m^3. The linearity of calibration was estimated using the correlation coefficient. The LOD was calculated from LOD=3·S/N, where S is analyte signal (mV), and N is noise level (mV). The LOQ was calculated from LOQ=3·LOD. The following results were obtained: LOD in range of 0.004–0.007 g/m^3, LOQ in range of 0.012–0.021 g/m^3, $R^2 > 0.997$; RSD < 5%.

The composition of the main components of the model biogas stream (methane and carbon dioxide) was monitored by means of gas chromatography coupled with a thermal conductivity detector (GC-TCD). The oven temperature was 40 °C, the detector temperature was 80 °C, the flow rate of the carrier gas (He) was 5 mL/min, and 200 μL of the gaseous sample was introduced into the column. Calibration was performed in the range of 5–50% v/v and 30–70% for CO_2 and CH_4, respectively. The method validation was performed as described above. The following results were obtained: LOD in range of 1–5% v/v; LOQ in the range of 3–15% v/v; $R^2 > 0.981$; RSD < 6%.

3.4. Conclusions

The paper presents new deep eutectic solvents composed of natural ingredients, including monoterpenes, fatty acids, and polyphenols, as suitable absorbent materials for the capture of siloxanes from biogas. The specific conclusions are as follows:

- Based on the COSMO-RS studies, among 90 eutectic mixtures, DESs composed of carveon and carboxylic acids, i.e., decanoic, undecanoic, and dodecanoic acid, have the highest affinity for siloxanes.
- Hydrogen bonds play a dominant role in the formation of DESs. On the other hand, weaker non-bonded interactions are responsible for the efficiency of the removal of siloxanes from biogas.
- From the industrial point of view, new DESs are characterized by favorable physico-chemical properties, i.e., low viscosity and density, and a low melting point, which enable efficient mass transfer even at low temperatures.
- DESs can be easily regenerated by bubbling at elevated temperatures, and their efficiency only slightly decreases after five cycles.
- The proposed absorption procedure based on DESs has great potential for the treatment of real biogas streams due to the high capture of siloxanes' selectivity.

References

1. Al-Hamamre, Z.; Saidan, M.; Hararah, M.; Rawajfeh, K.; Alkhasawneh, H.E.; Al-Shannag, M. Wastes and biomass materials as sustainable-renewable energy resources for Jordan. *Renew. Sustain. Energy Rev.* **2017**, *67*, 295–314. [CrossRef]
2. Hao, S.; Kuah, A.T.; Rudd, C.D.; Wong, K.H.; Lai, N.Y.G.; Mao, J.; Liu, X. A circular economy approach to green energy: Wind turbine, waste, and material recovery. *Sci. Total. Environ.* **2020**, *702*, 135054. [CrossRef]
3. Mahari, W.A.W.; Azwar, E.; Foong, S.Y.; Ahmed, A.; Peng, W.; Tabatabaei, M.; Aghbashlo, M.; Park, Y.-K.; Sonne, C.; Lam, S.S. Valorization of municipal wastes using co-pyrolysis for green energy production, energy security, and environmental sustainability: A review. *Chem. Eng. J.* **2021**, *421*, 129749. [CrossRef]
4. Kaur, A.; Bharti, R.; Sharma, R. Municipal solid waste as a source of energy. *Mater. Today Proc.* **2021**. [CrossRef]
5. Piechota, G.; Igliński, B. Biomethane in Poland—Current Status, Potential, Perspective and Development. *Energies* **2021**, *14*, 1517. [CrossRef]
6. Igliński, B.; Piechota, G.; Iwański, P.; Skarzatek, M.; Pilarski, G. 15 Years of the Polish agricultural biogas plants: Their history, current status, biogas potential and perspectives. *Clean Technol. Environ. Policy* **2020**, *22*, 281–307. [CrossRef]
7. Rasi, S. *Biogas Composition and Upgrading to Biomethane*; Lensu, A., Olsbo, P., Tynkkynen, M.-L., Eds.; Jyväskylä University Printing House: Jyväskylä, Finland, 2009.
8. Rasi, S.; Veijanen, A.; Rintala, J. Trace compounds of biogas from different biogas production plants. *Energy* **2007**, *32*, 1375–1380. [CrossRef]
9. Rasi, S.; Läntelä, J.; Rintala, J. Trace compounds affecting biogas energy utilisation–A review. *Energy Convers. Manag.* **2011**, *52*, 3369–3375. [CrossRef]
10. Macor, A.; Benato, A. A Human Health Toxicity Assessment of Biogas Engines Regulated and Unregulated Emissions. *Appl. Sci.* **2020**, *10*, 7048. [CrossRef]
11. Haak, L.; Roy, R.; Pagilla, K. Toxicity and biogas production potential of refinery waste sludge for anaerobic digestion. *Chemosphere* **2016**, *144*, 1170–1176. [CrossRef]
12. Li, Y.; Alaimo, C.P.; Kim, M.; Kado, N.Y.; Peppers, J.; Xue, J.; Wan, C.; Green, P.G.; Zhang, R.; Jenkins, B.M.; et al. Composition and Toxicity of Biogas Produced from Different Feedstocks in California. *Environ. Sci. Technol.* **2019**, *53*, 11569–11579. [CrossRef] [PubMed]
13. McBean, E.A. Siloxanes in biogases from landfills and wastewater digesters. *Can. J. Civ. Eng.* **2008**, *35*, 431–436. [CrossRef]
14. Santiago, R.; Moya, C.; Palomar, J. Siloxanes capture by ionic liquids: Solvent selection and process evaluation. *Chem. Eng. J.* **2020**, *401*, 126078. [CrossRef]
15. De Hullu, J.; Maassen, J.I.W.; van Meel, P.A.; Shazad, S.; Vaessen, J.M.P.; Bini, L.; Reijenga, J.C. *Comparing different biogas upgrading techniques*; Final Report for Eindhoven University of Technology; Eindhoven University of Technology: Eindhoven, The Netherlands, 20 July 2008.
16. Kvist, T.; Aryal, N. Methane loss from commercially operating biogas upgrading plants. *Waste Manag.* **2019**, *87*, 295–300. [CrossRef] [PubMed]

17. Adnan, A.I.; Ong, M.Y.; Nomanbhay, S.; Chew, K.W.; Show, P.L. Technologies for Biogas Upgrading to Biomethane: A Review. *Bioengineering* **2019**, *6*, 92. [CrossRef]

18. Sun, Q.; Li, H.; Yan, J.; Liu, L.; Yu, Z.; Yu, X. Selection of appropriate biogas upgrading technology-a review of biogas cleaning, upgrading and utilisation. *Renew. Sustain. Energy Rev.* **2015**, *51*, 521–532. [CrossRef]

19. Angelidaki, I.; Treu, L.; Tsapekos, P.; Luo, G.; Campanaro, S.; Wenzel, H.; Kougias, P.G. Biogas upgrading and utilization: Current status and perspectives. *Biotechnol. Adv.* **2018**, *36*, 452–466. [CrossRef]

20. Warren, W.K.E.H. A Techno-economic Comparison of Biogas Upgrading Technologies in Europe. Master's Thesis, Jyväskylän yliopisto—University of Jyväskylä, Jyväskylä, Finland, 2012; p. 44.

21. Hsu, C.H.; Chu, H.; Cho, C.M. Absorption and reaction kinetics of amines and ammonia solutions with carbon dioxide in flue gas. *J. Air Waste Manag. Assoc.* **2003**, *53*, 246–252. [CrossRef]

22. Zhang, Y.; Ji, X.; Xie, Y.; Lu, X. Thermodynamic analysis of CO2 separation from biogas with conventional ionic liquids. *Appl. Energy* **2018**, *217*, 75–87. [CrossRef]

23. Häckl, K.; Kunz, W. Some aspects of green solvents. *Comptes Rendus Chim.* **2018**, *21*, 572–580. [CrossRef]

24. Han, J.; Dai, C.; Yu, G.; Lei, Z. Parameterization of COSMO-RS model for ionic liquids. *Green Energy Environ.* **2018**, *3*, 247–265. [CrossRef]

25. Pham, T.P.T.; Cho, C.-W.; Yun, Y.-S. Environmental fate and toxicity of ionic liquids: A review. *Water Res.* **2010**, *44*, 352–372. [CrossRef] [PubMed]

26. Soltanmohammadi, F.; Jouyban, A.; Shayanfar, A. New aspects of deep eutectic solvents: Extraction, pharmaceutical applications, as catalyst and gas capture. *Chem. Pap.* **2021**, *75*, 439–453. [CrossRef]

27. Makoś, P.; Słupek, E.; Gębicki, J. Hydrophobic deep eutectic solvents in microextraction techniques–A review. *Microchem. J.* **2020**, *152*, 104384. [CrossRef]

28. Migliorati, V.; Sessa, F.; D'Angelo, P. Deep eutectic solvents: A structural point of view on the role of the cation. *Chem. Phys. Lett. X* **2019**, *2*, 100001. [CrossRef]

29. Makoś, P.; Przyjazny, A.; Boczkaj, G. Hydrophobic deep eutectic solvents as "green" extraction media for polycyclic aromatic hydrocarbons in aqueous samples. *J. Chromatogr. A* **2018**, *1570*, 28–37. [CrossRef]

30. Makoś, P.; Boczkaj, G. Deep eutectic solvents based highly efficient extractive desulfurization of fuels–Eco-friendly approach. *J. Mol. Liq.* **2019**, *296*, 111916. [CrossRef]

31. Ivanović, M.; Razboršek, M.I.; Kolar, M. Innovative Extraction Techniques Using Deep Eutectic Solvents and Analytical Methods for the Isolation and Characterization of Natural Bioactive Compounds from Plant Material. *Plants* **2020**, *9*, 1428. [CrossRef]

32. Cunha, S.C.; Fernandes, J.O. Extraction techniques with deep eutectic solvents. *TrAC Trends Anal. Chem.* **2018**, *105*, 225–239. [CrossRef]

33. Makoś, P.; Słupek, E.; Gębicki, J. Extractive detoxification of feedstocks for the production of biofuels using new hydrophobic deep eutectic solvents–Experimental and theoretical studies. *J. Mol. Liq.* **2020**, *308*, 113101. [CrossRef]

34. Makoś, P.; Fernandes, A.; Przyjazny, A.; Boczkaj, G. Sample preparation procedure using extraction and derivatization of carboxylic acids from aqueous samples by means of deep eutectic solvents for gas chromatographic-mass spectrometric analysis. *J. Chromatogr. A* **2018**, *1555*, 10–19. [CrossRef] [PubMed]

35. Słupek, E.; Makoś, P. Absorptive Desulfurization of Model Biogas Stream Using Choline Chloride-Based Deep Eutectic Solvents. *Sustainability* **2020**, *12*, 1619. [CrossRef]

36. Song, Y.; Chen, S.; Luo, F.; Sun, L. Absorption of Toluene Using Deep Eutectic Solvents: Quantum Chemical Calculations and Experimental Investigation. *Ind. Eng. Chem. Res.* **2020**, *59*, 22605–22618. [CrossRef]

37. Słupek, E.; Makos, P.; Dobrzyniewski, D.; Szulczynski, B.; Gebicki, J. Process control of biogas purification using electronic nose. *Chem. Eng. Trans.* **2020**, *82*. [CrossRef]

38. Słupek, E.; Makoś, P.; Gębicki, J. Deodorization of model biogas by means of novel non-ionic deep eutectic solvent. *Arch. Environ. Prot.* **2020**, *46*, 41–46. [CrossRef]

39. Makoś, P.; Słupek, E.; Małachowska, A. Silica Gel Impregnated by Deep Eutectic Solvents for Adsorptive Removal of BTEX from Gas Streams. *Materials* **2020**, *13*, 1894. [CrossRef]

40. Gomez, E.; Cojocaru, P.; Magagnin, L.; Vallés, E. Electrodeposition of Co, Sm and SmCo from a Deep Eutectic Solvent. *J. Electroanal. Chem.* **2011**, *658*, 18–24. [CrossRef]

41. Smith, E.L.; Abbott, A.; Ryder, K. Deep Eutectic Solvents (DESs) and Their Applications. *Chem. Rev.* **2014**, *114*, 11060–11082. [CrossRef]

42. García, G.; Aparicio, S.; Ullah, R.; Atilhan, M. Deep Eutectic Solvents: Physicochemical Properties and Gas Separation Applications. *Energy Fuels* **2015**, *29*, 2616–2644. [CrossRef]

43. Sarmad, S.; Mikkola, J.-P.; Ji, X. Carbon Dioxide Capture with Ionic Liquids and Deep Eutectic Solvents: A New Generation of Sorbents. *ChemSusChem* **2017**, *10*, 324–352. [CrossRef]

44. Zubeir, L.F.; van Osch, D.; Rocha, M.A.A.; Banat, F.; Kroon, M.C. Carbon Dioxide Solubilities in Decanoic Acid-Based Hydrophobic Deep Eutectic Solvents. *J. Chem. Eng. Data* **2018**, *63*, 913–919. [CrossRef]

45. Wu, H.; Shen, M.; Chen, X.; Yu, G.; Abdeltawab, A.A.; Yakout, S.M. New absorbents for hydrogen sulfide: Deep eutectic solvents of tetrabutylammonium bromide/carboxylic acids and choline chloride/carboxylic acids. *Sep. Purif. Technol.* **2019**, *224*, 281–289. [CrossRef]

46. Gholizadeh, F.; Kamgar, A.; Roostaei, M.; Rahimpour, M.R. Determination of SO2 solubility in ionic liquids: COSMO-RS and modified Sanchez-Lacombe EOS. *J. Mol. Liq.* **2018**, *272*, 878–884. [CrossRef]

47. Aissaoui, T.; AlNashef, I.; Benguerba, Y. Dehydration of natural gas using choline chloride based deep eutectic solvents: COSMO-RS prediction. *J. Nat. Gas Sci. Eng.* **2016**, *30*, 571–577. [CrossRef]

48. Zhong, F.; Huang, K.; Peng, H.-L. Solubilities of ammonia in choline chloride plus urea at (298.2–353.2) K and (0–300) kPa. *J. Chem. Thermodyn.* **2019**, *129*, 5–11. [CrossRef]

49. Gómez, J.S.; Lohmann, H.; Krassowski, J. Determination of volatile organic compounds from biowaste and co-fermentation biogas plants by single-sorbent adsorption. *Chemosphere* **2016**, *153*, 48–57. [CrossRef] [PubMed]

50. Santos-Clotas, E.; Cabrera-Codony, A.; Boada, E.; Gich, F.; Muñoz, R.; Martín, M.J. Efficient removal of siloxanes and volatile organic compounds from sewage biogas by an anoxic biotrickling filter supplemented with activated carbon. *Bioresour. Technol.* **2019**, *294*, 122136. [CrossRef]

51. Aissaoui, T.; Benguerba, Y.; AlOmar, M.K.; Alnashef, I.M. Computational investigation of the microstructural characteristics and physical properties of glycerol-based deep eutectic solvents. *J. Mol. Model.* **2017**, *23*, 23. [CrossRef] [PubMed]

52. García, G.; Atilhan, M.; Aparicio, S. A density functional theory insight towards the rational design of ionic liquids for SO2 capture. *Phys. Chem. Chem. Phys.* **2015**, *17*, 13559–13574. [CrossRef]

53. Moura, L.; Moufawad, T.; Ferreira, M.; Bricout, H.; Tilloy, S.; Monflier, E.; Gomes, M.C.; Landy, D.; Fourmentin, S. Deep eutectic solvents as green absorbents of volatile organic pollutants. *Environ. Chem. Lett.* **2017**, *15*, 747–753. [CrossRef]

54. Makoś-Chełstowska, P.; Słupek, E.; Gębicki, J. Deep eutectic solvent-based green absorbents for the effective removal of volatile organochlorine compounds from biogas. *Green Chem.* **2021**, *23*, 4814–4827. [CrossRef]

55. Słupek, E.; Makoś-Chełstowska, P.; Gębicki, J. Removal of Siloxanes from Model Biogas by Means of Deep Eutectic Solvents in Absorption Process. *Materials* **2021**, *14*, 241. [CrossRef] [PubMed]

56. Awe, O.W.; Zhao, Y.; Nzihou, A.; Minh, D.P.; Lyczko, N. A Review of Biogas Utilisation, Purification and Upgrading Technologies. *Waste Biomass Valorization* **2017**, *8*, 267–283. [CrossRef]

57. Słupek, E.; Makoś, P.; Gębicki, J. Theoretical and Economic Evaluation of Low-Cost Deep Eutectic Solvents for Effective Biogas Upgrading to Bio-Methane. *Energies* **2020**, *13*, 3379. [CrossRef]

58. Ortega, D.R.; Subrenat, A. Siloxane treatment by adsorption into porous materials. *Environ. Technol.* **2009**, *30*, 1073–1083. [CrossRef]

59. Gislon, P.; Galli, S.; Monteleone, G. Siloxanes removal from biogas by high surface area adsorbents. *Waste Manag.* **2013**, *33*, 2687–2693. [CrossRef]

dr inż. Patrycja Makoś-Chełstowska
....
(stopień/tytuł, imię i nazwisko)

Politechnika Gdańska
....
(Afiliacja)

OŚWIADCZENIE WSPÓŁAUTORA

Jako współautor pracy:. **"New Carvone-Based Deep Eutectic Solvents for Siloxanes Capture from Biogas"** oświadczam, że mój własny wkład polegał na konceptualizacji, metodologii, walidacji, analizie formalnej, prowadzeniu badań, wizualizacji, przygotowaniu oryginalnego manuskryptu oraz finansowaniu.

Jednocześnie wyrażam zgodę na przedłożenie ww. pracy przez mgr inż. Edytę Słupek jako część rozprawy doktorskiej w formie spójnego tematycznie zbioru artykułów opublikowanych w czasopismach naukowych.

Oświadczam, że samodzielna i możliwa do wyodrębnienia część ww. pracy wykazuje indywidualny wkład mgr inż. Edyty Słupek polegający na: konceptualizacji, metodologii, walidacji, analizie formalnej, prowadzeniu badań, wizualizacji oraz przygotowaniu oryginalnego manuskryptu.

....
(podpis współautora)

Gdańsk, dnia 19.05.2023

mgr inż. Aleksandra Kramarz
....
(stopień/tytuł, imię i nazwisko)

Politechnika Gdańska
....
(Afiliacja)

OŚWIADCZENIE WSPÓŁAUTORA

Jako współautor pracy:. **"New Carvone-Based Deep Eutectic Solvents for Siloxanes Capture from Biogas"** oświadczam, że mój własny wkład polegał na prowadzeniu badań, metodologii oraz przygotowaniu oryginalnego manuskryptu.

Jednocześnie wyrażam zgodę na przedłożenie ww. pracy przez mgr inż. Edytę Słupek jako część rozprawy doktorskiej w formie spójnego tematycznie zbioru artykułów opublikowanych w czasopismach naukowych.

Oświadczam, że samodzielna i możliwa do wyodrębnienia część ww. pracy wykazuje indywidualny wkład mgr inż. Edyty Słupek polegający na: konceptualizacji, metodologii, walidacji, analizie formalnej, prowadzeniu badań, wizualizacji oraz przygotowaniu oryginalnego manuskryptu.

....
(podpis współautora)

dr inż. hab. Jacek Gębicki
....
(stopień/tytuł, imię i nazwisko)

Politechnika Gdańska
....
(Afiliacja)

OŚWIADCZENIE WSPÓŁAUTORA

Jako współautor pracy:. **"New Carvone-Based Deep Eutectic Solvents for Siloxanes Capture from Biogas"** oświadczam, że mój własny wkład polegał na nadzorowaniu wstępnego planu badań oraz realizacji badań, przygotowaniu recenzji oraz redakcji ostatecznej wersji manuskryptu.

Jednocześnie wyrażam zgodę na przedłożenie ww. pracy przez mgr inż. Edytę Słupek jako część rozprawy doktorskiej w formie spójnego tematycznie zbioru artykułów opublikowanych w czasopismach naukowych.

Oświadczam, że samodzielna i możliwa do wyodrębnienia część ww. pracy wykazuje indywidualny wkład mgr inż. Edyty Słupek polegający na: konceptualizacji, metodologii, walidacji, analizie formalnej, prowadzeniu badań, wizualizacji oraz przygotowaniu oryginalnego manuskryptu.

....
(podpis współautora)

Autorzy:

P. Makoś-Chełstowska, **E. Słupek**, J. Gębicki

Tytuł publikacji:

Deep eutectic solvents – based green absorbents for effective volatile organochlorine compounds removal from biogas

Czasopismo:

Green Chemistry

DOI:

10.1039/d1gc01735g

PAPER

Check for updates

Deep eutectic solvent-based green absorbents for the effective removal of volatile organochlorine compounds from biogas†

Patrycja Makoś-Chełstowska, [ID] * Edyta Słupek [ID] and Jacek Gębicki [ID]

Volatile organochlorine compounds (VOXs) present in biogas can cause many technological and environmental problems. During the combustion of biogas containing VOXs, corrosion, as well as the formation of toxic by-products (polyhalogenated dioxins and furans) and further emission to the atmosphere, may occur. Therefore, in this study, a new procedure based on physical absorption was developed. In order to meet the requirements of green chemistry and green engineering, new deep eutectic solvents (DESs) composed of natural components were used in the absorption studies. Several physical properties of new DESs were determined, along with the absorbent formation mechanisms, by means of spectroscopic analysis and density functional theory. The most important absorption parameters, *i.e.*, the type of DES, gas flow rate, the type of matrix gas, temperature, and initial concentrations of VOXs were optimized. The obtained results indicate that DES composed of syringol and levulinic acid in a 1 : 1 molar ratio could efficiently absorb VOXs. The DES regeneration studies demonstrated that the absorption capacities of DES did not change after ten absorption-desorption cycles. Studies on the absorption mechanisms indicated that H-bonding and van der Waals interactions were the main driving forces for the removal of VOXs from biogas.

Introduction

Currently, biogas production is of growing importance because of its economic and environmental advantages.[1–3] Biogas is a biofuel formed from the decomposition of organic resources and waste in the anaerobic digestion process. The detailed chemical composition depends mostly on the kind of raw materials used in the fermentation process. Typically, biogas contains methane (30–70% v/v) and carbon dioxide (15–30% v/v), as well as small amounts of other gases, *i.e.*, nitrogen, oxygen, water vapour, hydrogen sulfide, ammonia, and numerous volatile organic compounds (VOCs).[4,5]

Nowadays, there is a need to develop an effective and economically advantageous technology of biogas treatment to optimize the parameters of high-methane gas (natural gas and compressed natural gas). The demand results from the introduction of a 2030 framework for climate and energy by the European Union (EU), in which there is 27% share of renewable energy consumption.[6] In addition, the UE parliament plans to increase the energy target to 35% by 2030. To achieve these targets, EU countries must significantly increase biogas production from waste materials and inject it into transmission networks or use it as a transport fuel. In order to introduce biogas into the natural gas network or use it as alternative transport fuels, biogas must be treated to meet certain quality parameters.

Volatile organochlorine compounds (VOXs) are one of the most technologically troublesome groups of chemical compounds in biogas. VOXs are mainly present in biogas from sewage treatment plants and landfills.[7] The total VOX concentration in the biogas stream is typically in the range of 259 to 1239 mg m^{-3}.[4,8–10] Typically, in the biogas stream, VOXs including 1,1,1-trichloroethane, 1,1-dichloroethane, 1,1-dichloroethene, 1,2-dichloroethane, 1,2-dichloroethene, carbon tetrachloride, chloroform, tetrachloroethylene, tetrachloroethane, dichloromethane, and trichloroethene can be identified.[4,8,11–13] They come from the chemicals used for wastewater and water treatment, disposal of solvents and refrigerants, as well as solid wastes, *i.e.*, polyvinyl chloride or other types of biomass.[14] During the biogas combustion process, chlorine compounds react with water vapour forming hydrochloric acid, which corrodes the surface in the combustion chamber. In addition, organic chlorinated compounds can also lead to the formation of toxic by-products, *i.e.*, polyhalogenated dioxins and furans in combustion processes.[15] Uncontrolled emission of VOXs into the atmosphere can lead

Department of Process Engineering and Chemical Technology, Faculty of Chemistry, Gdansk University of Technology, G. Narutowicza St. 11/12, 80-233 Gdańsk, Poland. E-mail: patrycja.makos@pg.edu.pl

†Electronic supplementary information (ESI) available. See DOI: 10.1039/d1gc01735g

to the destruction of the ozone layer and can contribute to the formation of photochemical smog as well as global warming.

Due to the aforementioned factors, the biogas purification step is a necessary process to protect engines and the environment.[16] There are several technologies dedicated to the removal of VOX from the gas stream: physical absorption, condensation, biofiltration, and adsorption based on activated carbon.[17–19] However, most of these methods require the application of toxic solvents, high running costs and capital investment costs, as well as long-time operation. The replacement or development of these techniques is one of the most important challenges of our day for the energy industry. Physical absorption is considered to be an appropriate method that meets the standards of green technology and engineering, which can have practical use in industry because it can be cheap, effective, and environmentally friendly.[20,21] However, the necessary condition is the selection of an appropriate solvent. The ideal absorbent should be characterized by low viscosity, relatively low toxicity, low vapor pressure, high boiling point, high absorption capacity, should be easy to regenerate, and low cost.[22] One of the solvents with all these characteristics is water. Water is commonly used in biogas purification processes, mainly for CO_2 capture.[23–25] However, since most of the volatile organochlorine compounds are hydrophobic, water is not an appropriate solvent in the absorption process. For hydrophobic components, silicone oil,[26] glycerol, squalene, dinonyl phthalate,[27] poly(N-methylpyrrole), and poly(N-methyl-pyrrole/polystyrenesulfonate),[28] are preferred. However, some of these solvents are toxic and do not have enough sorption capacity. Therefore, alternative "green solvents" are sought to substitute the currently used organic solvents. The first type of well-studied alternative solvents is ionic liquids (ILs), which are salts in the liquid state.[29,30] ILs have unique physicochemical properties that can be tunable through various suitable combinations of cations and ions. Despite the many advantages of ILs application as absorbents, including low vapor pressure, hydrophobicity or hydrophilicity, and high absorption capacity, they come with issues like toxicity, poor biodegradability, flammability, and expensive preparation and manufacturing.[30–33]

The second type of eco-friendly media utilized as absorbents are Deep Eutectic Solvents (DESs). DESs are eutectic mixtures consisting mainly of two or more compounds in a certain molar ratio. In a complex one of the components acts as a hydrogen bond donor (HBD) and the other as a hydrogen bond acceptor (HBA). Consequently, DESs have melting points (MP) lower than their separate components. The synthesis of DESs is simple, no by-products are formed and they do not require further treatment steps and expensive apparatus. DESs have similar physicochemical properties to ILs but in addition, DESs are characterized by non-toxicity, relatively good biodegradability, and the possibility for recyclability. Such features make DESs widely applied in the separation processes, i.e. extraction,[34–38] absorption,[39–44] and adsorption.[45] However, current studies on the application of DESs in gas separations are mainly limited to the removal of inorganic compounds

from gas streams, i.e., ammonia,[39] carbon dioxide,[46] hydrogen sulfide,[47] water,[48] or sulfur dioxide[49] from air, waste gases or hydrocarbon gases. Only a few reports describe volatile organic compounds, i.e. sulfides,[43] siloxanes,[22,50] toluene.[44,51] To the best of our knowledge, there are no works dedicated to the removal of volatile organochlorine compounds from model streams or real biogas streams using DESs. However, in the future, this approach can lead to creating a pioneering biogas purification technology in which the end product will be high-methane gas that can be directly introduced into transmission networks.

In practice, substances selected for DES synthesis should contain the following groups, –OH, –COOH, –O–CH₃, or =O, for the formation of stable DES structures.[52] Based on previous studies, the most stable DES complexes are formed by strong hydrogen bonds. Other weaker non-bonded interactions have a lower impact on the durability of DES structures in various processes.[53–55] The active groups of DES should interact with selected impurities but the interaction should not be too strong to allow the desorption of pollutants after the absorption process. However, DESs should not, or only slightly, absorb methane. It is acceptable to absorb a maximum of 2% methane.[56] To meet the requirements of the bio-refinery and sustainable development concept, components of DES should come from biomass, fermentation broth, or other readily available sources.[57]

This paper presents the synthesis of new, never-before-published deep eutectic solvents and their use as absorbents for the removal of VOXs from the model biogas stream. Several physical properties of DESs such as viscosity, density, and melting point have been investigated. Molecular characteristics of new DESs were studied by means of attenuated total reflectance Fourier transform infrared spectroscopy (ATR-FTIR), as well as proton and carbon-13 nuclear magnetic resonance spectroscopy (^1H NMR and ^{13}C NMR). Experimental results were compared with theoretical studies based on density functional theory (DFT). The absorption process was optimized in terms of DES selection, absorption temperature, gas flow, biogas compositions, and initial concentration of VOX. The possibility of the reusability and regeneration of DES was also examined. The mechanism of VOX removal from gas streams using DESs was explained by means of DFT and spectroscopic analysis.

Experimental

Materials

The following reagents were used in this study: ±camphor (C) with purity ≥95%, guaiacol (Gu) with purity ≥99%, syringole (Syr) with purity ≥98%, levulinic acid (Lev) with purity 97%, 1,1,2,2-tetrachloroethane (TCE) with purity ≥98%, 2,2,2-tri-chloroethanol (TCEtOH) with purity ≥99%, dichloromethane (DCM) with purity ≥99%, chloroform (CF) with purity ≥99%, carbon tetrachloride (TCM) with purity ≥99% were purchased from Sigma-Aldrich (USA).

High purity gases, *i.e.*, nitrogen (Linde Gas, Poland), air generated by a DK50 compressor with a membrane dryer (Ekkom, Poland), methane (Linde Gas, Poland), and hydrogen generated by Precision Hydrogen 1200 Generator (PEAK Scientific, Scotland, UK), were used for the preparation of biogas and chromatographic analysis.

Procedures

Preparation of DES. DESs were formed by combining ±camphor, guaiacol, syringole, and levulinic acid in a 1 : 1 molar ratio. DES composed of ±camphor and levulicic acid was mixed in a 1 : 2 mole ratio. The mixture of DES was stirred magnetically at 60 °C until a homogeneous liquid was obtained. The obtained DESs fluids were then left to cool to room temperature (RT).

Structural and physicochemical properties of DESs. For the structural analysis of new DESs, ATR-FTIR spectra were recorded by means of a Bruker Tensor 27 spectrometer (Bruker, USA) with an ATR accessory and OPUS software (Bruker, USA). The following parameters were used: spectral range: 4000–600 cm^{-1}; resolution: 4.5 cm^{-1}; number of sample scans 256; number of background scans 256; slit width 0.5 cm. In addition, NMR spectra of new DESs were prepared in 5 mm tubes by weighing 20 mg of a DES and inserting 0.7 mL of chloroform-d1. The measurements were carried out at 20 °C, using Bruker Avance III HD 400 MHz (Bruker, USA).

The melting points (MP) of DESs were determined visually by cooling DESs to −48 °C in a cryostat (HUBER, Germany), followed by a temperature increase at 1 °C min^{-1}. The MP was adopted as the temperature at which the first change in the DES aggregate state was observed. The density and viscosity of liquid DESs were measured using 5 mL of absorbents in a temperature range of 25 to 50 °C, with a BROOKFIELD LVDV-II+viscometer (Labo-Plus, Poland), and DMA 4500 M density meter (Anton Paar, Poland).

Absorption process. The biogas was prepared by means of bubbling. Nitrogen or a mixture of gases $CH_4 : CO_2 : N_2 : H_2O$ in various volume ratios was passed through a vial including 1 mL of all VOXs. The created stream was diluted with nitrogen (or gas mixture) to reach the desired concentration of VOXs in the biogas stream. In the next step, biogas was directed into the column containing the DES, in which the absorption process took place based on bubbling. The cleaned biogas stream was directed into the fume hood. The absorption setup used in this work is presented in Fig. 1.

During the absorption process, gas samples were collected before and after introduction into the absorption column and were analyzed by gas chromatography.

The absorption capacity (q) was calculated using eqn (1)–(3), in terms of the mass of the selected VOX absorbed (m_{VOX}) by the mass of DES (m_{DES}) used to attain complete saturation (t_{sat}):

$$\frac{d(m_{VOX})}{dt} = F \cdot C_{IN} - F \cdot C(t) \tag{1}$$
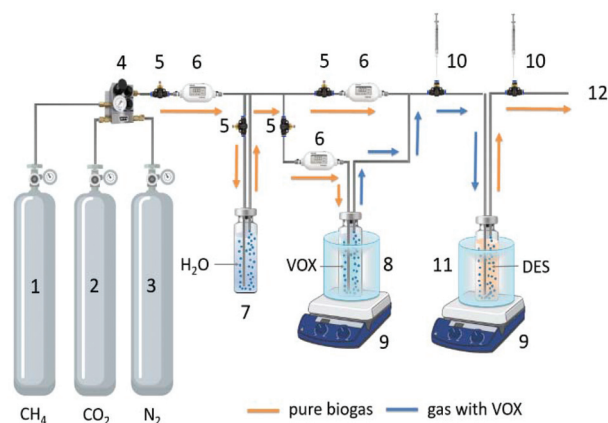
Fig. 1 Laboratory absorption setup: (1) bottle with methane; (2) bottle with carbon dioxide; (3) bottle with nitrogen; (4) gas mixer; (5) valve; (6) flowmeter; (7) vial with water; (8) thermostated vial with VOXs; (9) hotplate; (10) gas sample collection point; (11) thermostated vial with DES; (12) gas outlet.

$$m_{VOX} = F \cdot C_{IN} \cdot \left[t_{sat} - \int_0^{t_{sat}} \frac{C(t)}{C_{IN}} \cdot dt \right] \tag{2}$$

$$q = \frac{m_{VOX}}{m_{DES}} = \frac{F \cdot C_{IN}}{m_{DES}} \cdot \left[t_{sat} - \int_0^{t_{sat}} \frac{C(t)}{C_{IN}} \cdot dt \right] \tag{3}$$

where m_{VOX} is the VOX mass absorbed [g]; m_{DES} is the mass of DES (m_{DES}) used to attain complete saturation [g]; t_{sat} is the saturation time [min] (time when the VOX concentration in the outlet gas is the same as the initial VOX concentration); C_{IN} is the Initial concentration of VOX [g m^{-3}]; F is the Flow rate of the biogas passing through the absorption column [m^3 s^{-1}]; $C(t)$ is the concentration of the VOX in the outgoing biogas stream measured at intervals during the absorption process [g m^{-3}].

The absorption rate (N) was calculated using eqn (4):

$$N = \frac{G_{IN} \cdot Y_{IN} - G_{OUT} \cdot Y_{OUT}}{A} \tag{4}$$

where A is the gas–liquid interfacial area [m^2]; G_{IN}, G_{OUT} represent the flow rates [mol s^{-1}], which were calculated by determining the volumetric flow rates of mixed gas and the volume percentage of VOX in the biogas mixture; Y_{IN}, Y_{OUT} represent the mole percentage of VOX at the inlet and outlet gas stream.

The gas hold-up (ε_G) was measured using the volume expansion method[58] (eqn (5)):

$$\varepsilon_G = \frac{\Delta V}{\Delta V + V_{DES}} \tag{5}$$

ΔV – volume expansion after biogas dispersion [m^3]; V_{DES} – Volume of DES in absorption column [m^3]; The specific gas–liquid interfacial area (a) was calculated using eqn (6):

$$a = \frac{6 \cdot \varepsilon_G}{d_b \cdot (1 - \varepsilon_G)} \tag{6}$$

where d_b – bubble diameter [m].

The gas–liquid interfacial area (A) was calculated using eqn (7):

$$A = \mathrm{a} \cdot V_{\mathrm{DES}} \tag{7}$$

Absorption processes were carried out until the VOX concentration in the outlet gas was the same as the initial VOX concentration. Each absorption process was repeated three times.

Chromatographic analysis. Samples of biogas (0.2 mL) before, during, and after the absorption process were injected into the gas chromatograph Autosystem XL equipped with flame ionization detector (GC-FID) (PerkinElmer, USA), and HP-5 (30 m × 0.25 mm × 0.25 μm) capillary column (Agilent Technologies, USA) in order to determine VOX in the biogas stream. The following chromatographic parameters were used in the study: temperature of the oven 60 °C, injection port temperature 250 °C, the injection mode was split 5 : 1, detector temperature 300 °C, the carrier gas – nitrogen (flow rate: 1 mL min^{-1}). In addition, the second part of the sample (0.5 mL) before, during, and after the absorption process was injected into the gas chromatograph MG#5 (SRI Instruments, USA) equipped with a thermal conductivity detector (GC-TCD), and Porapack Q (80/100, 2 mm ID) (Restek, USA) packed column in order to study the concentration of CO_2, N_2, and CH_4 in the biogas stream. The following chromatographic parameters were used: temperature of the oven 40 °C, injection port temperature 60 °C, detector temperature 80 °C, the carrier gas – helium (flow rate: 5 mL min^{-1}). The water concentration in the biogas stream was analyzed by means of an HIH-4000-002 HONEYWELL sensor.

Theoretical studies theoretical studies. The structures of DESs, VOXs, and DES-VOX complexes were drawn using the Avogadro 1.2.0 program.[59] The Orca 4.2.1 software was applied to optimize the geometries of molecules as well as energy interactions between DES and VOX.[60] Gas-phase equilibrium geometries were fully optimized by means of DFT/B3LYP at the 6-311++G** basis set.[61] This level of theory is preferred to investigate the hydrogen bonding in ILs and DESs complexes.[34,49,62,63] The configurations of all ingredients and DESs complexes were inspected to be local minimum by frequency calculations. The interaction energies (ΔE_{int}) of the most stable complexes of all DES-VOX were determined at the B3LYP/6-311++G** level of theory using eqn (8):

$$\Delta E_{\mathrm{int}} = E_{\mathrm{DES-VOX}} - (E_{\mathrm{DES}} + E_{\mathrm{VOX}}) \tag{8}$$

where $E_{\mathrm{DES-VOX}}$ – total energy of DES–VOX complex [kcal mol^{-1}]; E_{DES} – total energy of selected DESs [kcal mol^{-1}]; E_{VOX} – total energy of selected VOX [kcal mol^{-1}].

The ΔE_{int} was calculated considering the basis set superposition error (BSSE) corrected by means of the counterpoise procedure.[64] Non-covalent interaction analysis (NCI) based on the Reduced Density Gradient (RDG) was applied in order to explain the nature and strength of the interactions for the studied complexes. Electrostatic Potential Analysis (ESP) was used for the visualization of the relative polarity as well as

determine the total charge distribution of the complexes. Both RDG and ESP procedures were made using the Multiwfn 3.7 program.[65–67] The graphical representation of the calculated results was made using Gnuplot and Visual Molecular Dynamics 1.9.3.[68] software.

Results and discussion

Synthesis and physical properties of DESs

In the studies, all DESs components, *i.e.*, camphor (C), levulinic acid (Lev), syringol (Syr), and guaiacol (Gu) were blended in a 1 : 1 molar ratio. However, only mixtures of Syr : Lev (1 : 1), C : Gu (1 : 1), Gu : Lev (1 : 1) were liquids at room temperature (RT). The remaining components were combined in molar ratios of 0.5 : 1 and 1 : 2. As a result of further synthesis, an additional liquid complex – C : Lev (1 : 2) was obtained. The other DESs, *i.e.*, C : Lev in 0.5 : 1 molar ratio, C : Syr in 0.5 : 1, 1 : 2 molar ratio, Syr : Gu 0.5 : 1, 1 : 2 were solid after cooling to RT.

The melting points (MP) of pure compounds that were used in the DESs synthesis, *i.e.*, C, Lev, Gu, and Syr, were 180 °C, 33 °C, 26 °C, and 50 °C, respectively. In the DESs mixtures, a meaningful depression of the MP with respect to the pure compounds was observed. The largest MP depression was observed for C : Gu (1 : 1) (lower than −48 °C). For the remaining DES, higher MPs were observed, which were −43 °C, −23 °C, and +8 °C for Gu : Lev (1 : 1); Syr : Lev (1 : 1), and C : Lev (1 : 2), respectively.

Density (ρ) is a typical property for DESs characterization, due to the significant impact on most of the technological processes. DESs densities are strongly dependent on temperature and exhibit higher values as compared to popular organic solvents. In our research, all DESs densities were measured in the temperature range from 293.15 to 323.15 K. The results of the tests are shown in Fig. 2A. All DESs were characterized by higher densities than most of the organic solvents, which were 1.0287 ± 0.041, 1.0597 ± 0.052, 1.1382 ± 0.049, and 1.1675 ± 0.047 g cm^{-3} for C : Gu (1 : 1), C : Lev (1 : 2), Gu : Lev (1 : 1), and Syr : Lev (1 : 1), respectively at 20 °C. The results presented in Fig. 2A indicate that the densities of DESs decreased with increasing temperature. This behavior can be explained by the increasing activity and molecular mobility, which caused the increase of the solution molar volume, thereby reducing the density.[69]

In the next step, the viscosities (η) of the liquid DESs were measured in the temperature range from 293.15 to 323.15 K. Viscosity is an important parameter of solvents in many industrial processes in which fluid flow systems are used. Most DESs have higher viscosities (>100 cP) as compared to water and conventional solvents, which can generate problems in the pumping, filtering, or stirring. Therefore, the dynamic viscosity of absorbents (DESs) should be as low as possible. The obtained results indicated that the highest viscosity measurement was attained at 20 °C for Syr : Lev (1 : 1) (31.1 ± 1.2 mPa s), followed by Gu : Lev (1 : 1) (30.0 ± 0.9 mPa s), and C : Lev
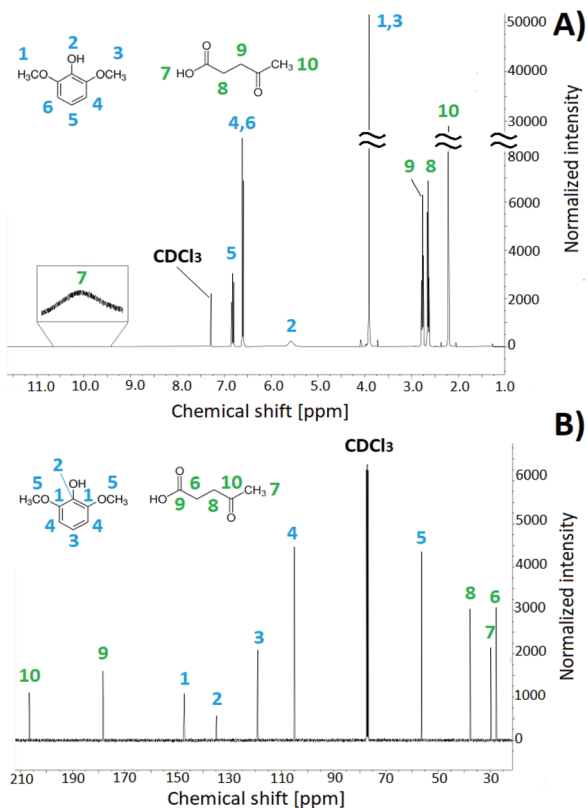
Fig. 2 (A) ^{1}H NMR spectra of Syr : Lev (1 : 1), (B) ^{13}C NMR spectra of Syr : Lev (1 : 1).
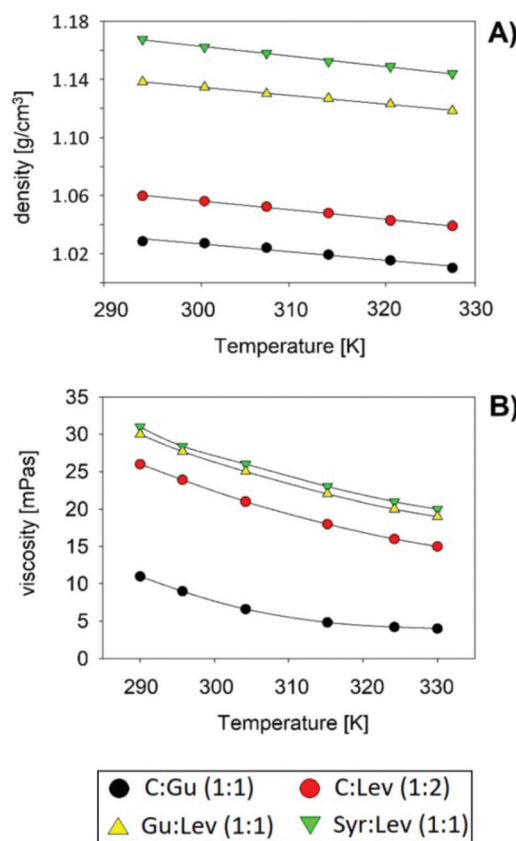

Fig. 3 (A) Density, and (B) viscosity of DESs in the range of 293.15 to 323.15 K.

(1 : 2) (26.2 ± 0.8 mPa s). In turn, the lowest viscosity was obtained for C : Gu (1 : 1) (10.9 ± 0.4 mPa s) (Fig. 2B). Similar to the observation of density behavior, the dynamic viscosity is strongly affected by temperature. As the temperature increased, the dynamic viscosities of all new absorbents drastically decreased. This is because the temperature increase in DES causes an increase in the average speed of the molecules in the liquid phase, which decreases the intermolecular forces. This can reduce the fluid resistance to flow (dynamic viscosity).[70]

Structural characterization of DESs formation

An experimental study on DES structural characterization. In order to experimentally explain the structures of the new DESs, ^{1}H NMR and ^{13}C NMR spectra were recorded (Fig. 3 and Fig. S1–S3†). NMR spectra allowed the identification of the atoms of HBA and HBD in DESs structures. The obtained results indicate that only signals from HBA and HBD are visible in the NMR spectra in all of the examined DESs. The absence of additional peaks in the NMR spectra confirmed that the synthesis reaction proceeded without additional side reactions.

In order to determine the interactions between ingredients in DESs, the proton and carbon chemical shifts ($\delta\delta$) were calculated. In the Syr : Lev (1 : 1) spectra, the differences in the chemical shifts of the proton in the hydroxyl group with con-

nection to pure syringol and with connection to DES were taken into account. The chemical shift of the proton in the hydroxyl group (–OH) in Syr : Lev (1 : 1) ($\delta\delta$ H-Syr : Lev = 5.51 ppm) decreased by 0.04 ppm (Fig. 3) in comparison to the chemical shift in pure syringol ($\delta\delta$ H-Syr = 5.55 ppm). The proton chemical shifts influence the carbon chemical shifts ($\delta\delta$). This effect was confirmed by the formation of a H-bond between the hydroxyl group (–OH) in syringol and the carbonyl group (C=O) in levulinic acid. Chemical shifts toward lower values were observed for the carbon atom connected to the OH group relative to pure syringol ($\delta\delta$ = 0.21 ppm), and for the carbon atom from the C=O group relative to pure levulinic acid ($\delta\delta$ = 0.80 ppm).

Similar chemical shift results were also obtained in the Gu : Lev (1 : 1) spectrum, in which the proton of the –COOH group with respect to pure levulinic acid ($\delta\delta$ = 0.12 ppm) shifted towards lower values. Additionally, in the ^{1}H NMR spectrum, the lower value of the proton shift of the –OH group with respect to pure guiacol was observed (Fig. S1†). In the Gu : Lev (1 : 1) spectrum, carbon chemical shifts ($\delta\delta$) towards lower values were observed for the C atom from the ketone group (Lev) ($\delta\delta$ = 0.14) and the carbon atom connected to the OH group (Gu) ($\delta\delta$ = 0.11 ppm) with respect to pure the pure components. This indicates that two hydrogen bonds between Gu and Lev were formed. In the DES-based on C : Lev (1 : 2)

(Fig. S2†) and C : Gu (1 : 1) (Fig. S3†), very similar proton and carbon chemical shifts (δδ) were also observed. In the C : Lev (1 : 2), proton chemical shifts towards lower values resulted from the connected O atom from the ketone group (C) to the H atom from of the COOH group (Lev), while in C : Gu (1 : 1) the proton chemical shifts come from the connected O atom from the ketone group (C) to the H atom from of the OH group (Gu). The resulting shifts were δδ = 0.10 ppm and δδ = 0.12 ppm, respectively. In addition, in C : Lev (1 : 2) the shifts towards lower values were observed, which resulted from the formation of hydrogen bonds between two COOH groups from two levulinic acid molecules. The calculated shift was 0.11 ppm. The described proton chemical shifts (δδ) affected the lower values of the carbon chemical shifts observed both in the C=O group (C) and in the COOH groups (Lev) in the C : Lev (1 : 2). The observed shifts were δδ = 0.79 ppm and δδ = 0.25 ppm, respectively. For the C : Gu (1 : 1), similar results were observed. The values of the carbon chemical shifts towards lower values both in the C=O group (C) and in the C–OH group (Gu) were δδ = 0.32 ppm and δδ = 0.05 ppm, respectively.

In the next part of the studies, Fourier transform infrared spectroscopy (FTIR) was used to identify structures of new DESs and study the interaction between HBA and HBD in DES complexes. The FT-IR spectra of pure HBA and HBD components and the newly created DESs are shown in Fig. 4. As is well known, DESs are created on the basis of specific intermolecular interactions (such as hydrogen bonds, dipole-dipole interactions, or van der Waals forces) between HBA and HBD. The location of the bonds depends on the structure of the HBA and HBD. In the FT-IR spectrum of Syr : Lev (1 : 1), the shift of the signal corresponding to the –OH stretching bonds relative to pure HBD (syringol) towards lower wavenumbers can be observed (Fig. 4). The shift is caused by hydrogen bond formation between syringol and levulinic acid.[71] In addition, the characteristic shifting of the bands corresponding to the

stretching vibrations of the C=O group towards higher wavenumbers (from 1703.64 cm^{-1} to 1707.17 cm^{-1}) relative to pure HBA (levulinic acid),[72] can be observed. Similar wavenumber shifts can be observed for the remaining DES (Fig. S4–S6†).

Theoretical studies on DESs formation. Information from spectroscopic analyses are not unambiguous, and they indicate the existence of strong hydrogen bonds between HBA and HBD. However, they do not indicate the number of hydrogen bonds, their exact location and information on weaker interactions, *i.e.*, electrostatic interactions in DESs structures. Therefore, additional quantum mechanical calculations based on DFT analysis were used to gain insight into the non-bonded interactions of all DESs at the atomic level.

The most likely and stable DESs complexes in the gas phase were geometrically optimized at the B3LYP/6-311++G** level of theory. DESs structures after geometric optimization are presented in Fig. 5A and S7.† The obtained results show that non-bonded interactions can be found between HBA and HBD, which can be identified as strong hydrogen bonds (H-bonds) because of the distances below 2.5 Å between atoms. In Syr : Lev (1 : 1), the distance between the ketone group in Lev and the hydroxyl group from Syr (=O⋯H–O) is 1.89 Å. In C : Gu (1 : 1), the distance is 1.83 Å between the ketone group in C and the hydroxyl group from Gu (=O⋯H–O). In G : Lev (1 : 1), two H-bonds existed between the hydroxyl group from Gu and the ketone group in Lev =O⋯H–O (1.85 Å), as well as between the hydroxyl group from Lev and the methoxy group from Gu O–H⋯O–CH$_3$ (1.83 Å). In C : Lev (1 : 2) two hydrogen bonds were also identified because of the short distances between the ketone group from C and hydroxyl group from one of the Lev molecules (=O⋯H–O) and hydroxyl groups from two Lev molecules O–H⋯H–O.

The classification and identification of all the non-covalent interactions (NCI) that exist between DESs components were
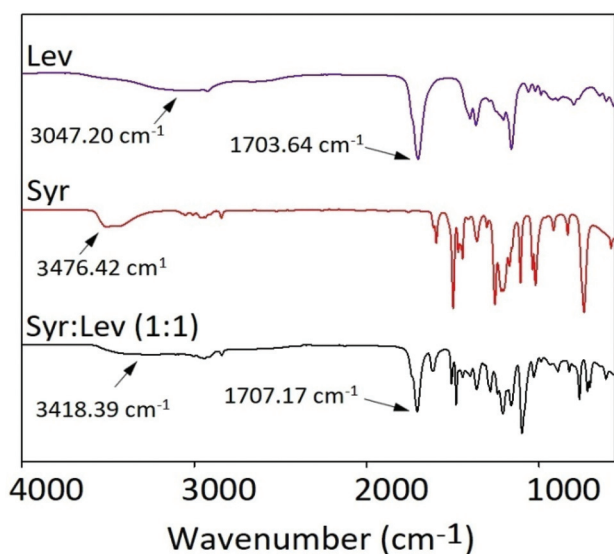
Fig. 4 FT-IR spectrum of pure Lev, Syr, and Syr : Lev (1 : 1).
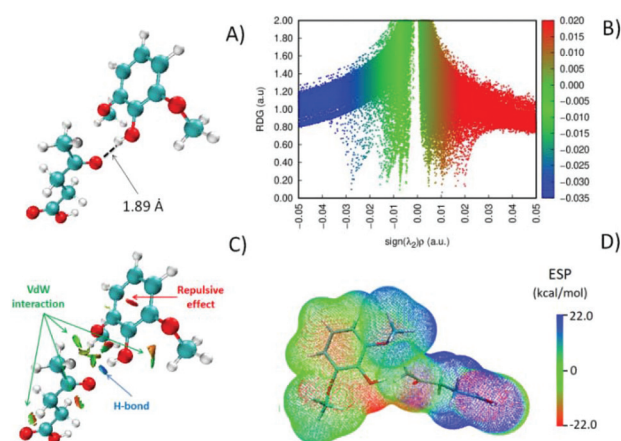
Fig. 5 (A) The structure of Syr : Lev (1 : 1) after geometric optimization; (B) 2D plots of RDG *versus* the electron density multiplied by the sign of the second Hessian eigenvalue for Syr : Lev (1 : 1). (C) Reduced density gradient (RDG) isosurfaces (s = 0.5 a.u.) of Syr : Lev (1 : 1). (D) Elecrostatic potential (ESP) mapped on electron total density with an isovalue of 0.001 for Syr : Lev (1 : 1).

conducted by means of reduced density gradient (RDG) analysis. The RDG analysis enables the identification of three types of interactions, *i.e.*, H-bonds, van der Waals forces, and steric repulsion.[49,73,74] Fig. 5B and Fig. S8† show the 2D plots of the reduced density gradient for Syr : Lev (1 : 1) and the rest of the DESs, respectively. The results show that in DESs complexes, three types of NCI co-exist: H-bonds, which correspond to the negative sign of $(\lambda_2)\rho$ (from −0.04 to −0.02 au); van der Waals interactions, −0.01 au < sign $(\lambda_2)\rho$ < 0.01 au; the repulsive effect, (sign $(\lambda_2)\rho$ < 0.02 au). The graphical interpretations of the obtained results are presented in Fig. 5C and Fig. S9,† where blue areas represent strong attractive effects (H-bonds); red areas indicate strong repulsive interactions; green areas denote weaker NCI, including van der Waals interactions. The results show that only one H-bond occurred between HBA and HBD in Syr : Lev (1 : 1), and C : Gu (1 : 1), while in C : Lev (1 : 2), and Gu : Lev (1 : 1), two hydrogen bonds were observed in DES complexes. In all DES, van der Waals interactions can be observed between HBA and HBD, and repulsive effects are due to the presence of aromatic rings in DESs structures. The coexistence of all identified NCI between DES components corresponds to the decrease in MP in DES complexes in comparison to the melting points of the individual compounds.[34,43]

In the next step of theoretical studies, the electrostatic potential analysis (EPA) was used to demonstrate the most likely and most stable regions for the electrophilic attack, and predict how the various geometries of DESs components could interact with each other. A comparison of the generated ESP maps for all studied DESs are presented in Fig. 5C and S10.† The negative electrostatic potentials are depicted as red, blue indicates positive potential, and green represents the potentials closer to zero. The results indicate that the electronegative areas are located around oxygen atoms in all DESs structures. The positive regions are over the hydrogen atoms in DESs molecules. Since the electronegative region is susceptible to electrophilic attack and electropositive is region prone to nucleophilic attack, it can be predicted that the electronegative area of HBA will be close to the electropositive area of HBD during the DESs formation. All complexes presented in Fig. 5C and Fig. S10† confirm this prediction. For example, when a Lev molecule interacts with a Syr molecule, the red region located around oxygen atom is attracted to the blue region around hydrogen in the hydroxyl group from Syr, forming hydrogen bond interactions. The same interaction behaviors were observed for the remaining DESs.

Absorption of VOX compounds

In order to systematically compare the absorption performance, the effects of several absorption factors including temperature, gas type, gas flow rate, inlet concentration, were studied.

Effects of DES type on the absorption process. The VOXs were absorbed in DES at 20 °C and 10 kPa pressure. The initial concentration of individual VOX compounds was 0,5 mg cm^{-3}. The VOX removal efficiency was analyzed by gas chromatography at 20 min intervals. Fig. 6 presents the VOX experi-

mental breakthrough curves of four types of DESs. All experimental breakthrough curves can be divided into two parts. In the first part of the curves, the outlet VOXs concentration increased significantly with time and gradually reached the breakthrough point. In the next part of the curves, the VOXs concentration reached saturation, and no further changes in concentration were observed. The obtained shape of the equilibrium curves is the result of the absorption law, which can be explained by the principle of the gas–liquid equilibrium of the system. In the absorption process, the mass transfer of VOX from biogas to DES and from DES to the biogas stream occur simultaneously. When the VOX concentration in DES reaches a certain ratio with the VOX concentration in the biogas stream, the rate of VOX mass transfer becomes equal to that of the desorption of VOX from DES (gas–liquid dynamic equilibrium).[75] The results indicate that the highest absorption capacity was observed for Syr : Lev (1 : 1) (Fig. 6). The absorption capacity for DCM, CF, TCM, TCE, and TCEtOH were 420 ± 22, 360 ± 16, 304 ± 11, 292 ± 8, and 661 ± 34 mg g^{-1}, respectively. Slightly lower absorption capacities were obtained for C : Gu (1 : 1). The absorption capacities were 365 ± 14, 320 ± 11, 275 ± 9, 266 ± 8, and 561 ± 18 mg g^{-1} for DCM, CF, TCM, TCE, and TCEtOH, respectively.

The obtained results indicate that the absorption capacities for the synthesized DES are higher as compared to other absorbents and solid adsorbents. The absorption capacity of the developed DES was up to 100 times greater than that of ionic deep eutectic solvents based on quaternary ammonium salts (*i.e.* choline chloride, tetrabutylammonium bromide or tetrapropylammonium bromide).[51] Ionic liquids have slightly lower absorption capacities as compared to the new DES.[76] However, their high price makes them almost impossible to use in industrial processes. Higher absorption capacities can be obtained for the metal-organic framework UiO-66, however, as in the case of ILs, the unit price for 1 kg of adsorbent is 79207.2 €.[77] This makes the process completely uneconomical despite its high efficiency. The prices of new DES vary depending on the components used to synthesize them. DESs prices can vary from 24.02 € to 263.5 € per 1 kg. The price is lower as compared to most of the absorbents and adsorbents described in the literature. The combination of price and high efficiency of VOX removal from biogas makes the new DESs have potential for industrial applications. The comparison of the available absorption and adsorption processes are presented in the Table S1.†

The absorption rate was determined for all processes. As expected, with time, a decrease in the absorption rate was observed. This is due to the decrease in the number of available DES active sites for VOX, which is associated with a reduction in the driving force of the absorption process (Fig. 6).[78] The absorption rate decrease is due to the decrease in the difference between the concentration of impurities in the gas and in DES phase. The combination of absorption rate and absorption capacity enables a complete evaluation of the absorption process, which is very important from an economic and industrial point of view. In Fig. 6, at the point of inter-
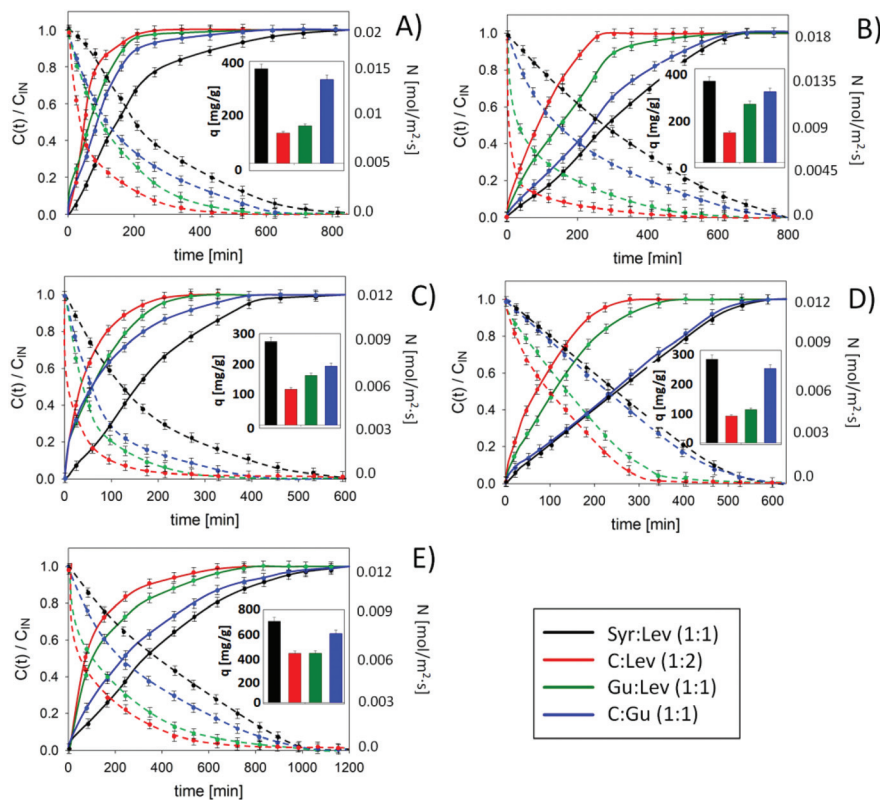
Fig. 6 Experimental breakthrough curves (solid line) and absorption rate (dashed line) of (a) DCM; (b) CF; (c) TCM; (d) TCE; (e) TCEtOH on different DESs (temperature 20 °C; inlet VOX concentration 0.5 mg cm^{-3}; gas flow 50 mL min^{-1}; matrix gas N$_2$).

section of the absorption curve and absorption rate curve, the time during which the absorption process is very fast and effective can be determined. After this time is exceeded, the absorbent must be regenerated because the absorption process becomes ineffective and uneconomical. For Syr : Lev (1 : 1), the times for quick and effective absorption were 193 ± 8, 290 ± 11, 170 ± 5, 252 ± 9, 385 ± 19 min for DCM, CF, TCM, TCE and TCEtOH, respectively. It is in some cases 11 times longer as compared to C : Lev (1 : 2).

Effects of temperature on the absorption process

Under real conditions, the produced biogas is immediately introduced into the treatment system. Depending on the fermentation method used, the temperature of the raw biogas varies from 35 to 40 °C, or from 50 to 55 °C for the mesophilic and thermophilic method, respectively.[79,80] When designing a new biogas plant, an economic analysis should be made.[22] At this stage, it is necessary to decide whether it is more profitable to apply additional biogas cooling before purification, or to regenerate or replace the absorbent more often. Therefore, it is very important to know how the increase in temperature affects the absorption capacity. Studies on the influence of temperature on the VOX absorption efficiency were carried out at intervals of 20 °C, 30 °C, 40 °C, 50 °C, and 60 °C. As expected, the capacity of VOX decreased by almost 50% with increasing temperature (Fig. 7A and S11†). This phenomenon

can be explained by the exothermic nature of the process for the absorption of VOX in DES. Higher temperature weakens the interactions between DES and VOX, allowing the VOX to leave the absorbent because of increased kinetic energy.[81]

Effects of gas flow and gas type on the absorption process. In the next part of the studies, the effect of gas flow rate in the range of 25–75 mL min^{-1} was determined (Fig. 7B and S12†). The obtained results indicated that in the range tested, the biogas flow rate had only a minor effect on the absorption capacity of VOX. As the flow rate increased from 25 to 75 mL min^{-1}, the Syr : Lev (1 : 1) absorption capacities of DCM, CF, TCM, TCE, and TCEtOH were slightly reduced from 426 ± 20 to 417 ± 19 mg g^{-1}, from 356 ± 17 to 349 ± 16 mg g^{-1}, from 305 ± 14 to 293 ± 11 mg g^{-1}, from 284 ± 14 to 278 ± 14 mg g^{-1}, and from 664 ± 22 to 661 ± 24 mg g^{-1}, respectively. Similar results were obtained for other DESs. This phenomenon can be explained by the fact that as the gas flow rate increased, the contact time of the biogas stream containing VOXs with the DES was reduced, which adversely affected the VOXs absorption process.[43] On the other hand, in industrial processes, the contaminated gas flow should be as high as possible in order to obtain a large volume of clean gas in the shortest time. Therefore, 75 mL min^{-1} was considered the optimal flow rate.

In the real biogas stream, the concentrations of methane and carbon dioxide ranged from 50 to 80% v/v, and from 15 to 45% v/v, respectively. Typically, the concentration of water
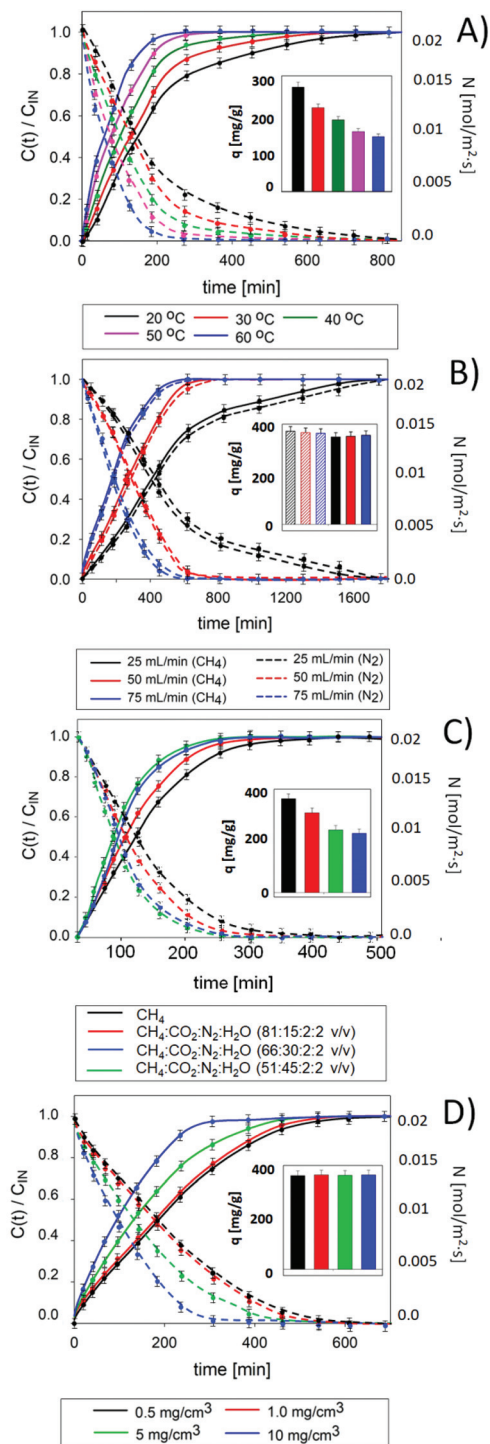
Fig. 7 Experimental breakthrough curves of DCM at (A) different temperatures for Syr : Lev (1 : 1) (inlet VOX concentration 0.5 mg cm³; gas flow 50 mL min⁻¹; matrix gas N2); (B) different gas flow rates for Syr : Lev (1 : 1) (inlet VOX concentration 0.5 mg cm³; temperature 20 °C); (C) different gas matrixes for Syr : Lev (1 : 1) (inlet VOX concentration 0.5 mg cm³; temperature 20 °C); (D) initial concentration for Syr : Lev (1 : 1) (gas flow 50 mL min⁻¹; temperature 20 °C).

vapor and nitrogen does not exceed 2% v/v. Therefore to recreate the real biogas stream under laboratory conditions, the type of matrix gas including pure nitrogen, pure methane or a mixture of gases, $CH_4 : CO_2 : N_2 : H_2O$ in $81 : 15 : 2 : 2$, $66 : 30 : 2 : 2$, and $51 : 45 : 2 : 2$ v/v were tested. As expected, nitrogen was not absorbed into the DES due to its neutral character. Therefore, the appearance of N_2 in the biogas stream did not affect the VOX absorption efficiency. The use of methane reduced the absorption capacity of DES by an average of 0.7% as compared to nitrogen (Fig. 7B and S12†). This is probably due to the absorption of CH_4 by Syr : Lev (1 : 1). Absorbed CH_4 can bind to Syr : Lev (1 : 1), thus blocking active sites. However, due to the only slight reduction in the DES absorption capacity, it can be concluded that the methane is only absorbed to a small extent, which is beneficial for the production of clean bio-methane from contaminated biogas. Based on the previous studies, methane is absorbed in most DES at a concentration of about 5%.[43,82,83] In commercial technologies (*i.e.* water scrubber, amine scrubber, membrane technologies), methane losses ranging from 0.04 to 1.97% v/v are observed.[56] Therefore, it can be concluded that the new method based on DES is within the acceptable range.

The substances that can negatively affect the removal of VOX from biogas are water and carbon dioxide. Both H_2O and CO_2 have active oxygen atoms in their structures, which can form strong hydrogen bonds with DES. The strong interaction of carbon dioxide and water with DES removes them from the gas phase. This is a positive development from the biogas purification point of view. However, it can also block the DES active sites to which VOX compounds are attached. As a rule, water is present in low concentrations in biogas, so its importance is lower than CO_2. In the real absorption process, the biogas is dried before introduction into the absorption column. The drying of the biogas takes place during its cooling. Part of the water vapor separates out as condensate. This process also removes other undesirable components, water-soluble gases and aerosols. The gas transmission setup includes condensate containers in which the water vapor condensate formed during cooling is collected.[84] As expected, the obtained results indicate that as the concentration of CO_2 in the biogas increased from 0 to 45% v/v, the absorption efficiency of most VOX decreased (Fig. 7C). A reduction in the absorptive capacity and rate of VOX was observed and consequently, there was a reduction in the effective VOX absorption time from 138 to 89 min. However, during VOX absorption from biogas containing 30 and 45% v/v CO_2, no significant difference in VOX absorption capacity and rate was observed. This is most likely due to the limited solubility of CO_2 in Syr : Lev (1 : 1). Very similar results were obtained for CF, TCE and TCM (Fig. S13†). Unexpected results were obtained for TCEtOH. With the increase in the concentration of carbon dioxide in the biogas at the inlet to the column, the absorption efficiency increased (absorption rate and capacity). The effective absorption time increased from 640 to 1200 min. This is probably because CO_2 molecules that attach to DES create additional active sites to which TCEtOH can attach. The –OH

group from TCEtOH can form strong hydrogen bonds with both DES and CO_2. However, the increase in CO_2 concentration from 30 to 45% v/v did not increase the absorption efficiency due to the limited solubility of CO_2 in DES.

Effects of VOXs type and their concentration on the absorption process. The average VOXs concentration in real biogas mostly depends on the kind of materials used for bio-methane production. Since VOXs concentrations are very variable, in the next part of the work, the influence of VOXs concentrations in the range of 0.5–10 mg cm^{-3} on the absorption process was studied. As expected, the obtained results indicate that the initial concentration of VOXs only had an impact on the saturation time; it did not affect the total DES absorption capacity (Fig. 7D and S14†). Increasing the VOXs concentration in the biogas stream from 0.5 to 1 mg cm^{-3} did not cause any significant differences in saturation time. However, a further increase in the concentration to 10 mg m^{-3} resulted in a noticeable reduction in the absorbent saturation time from 612.1 to 211.8 min for DCM (Fig. 7D). For the other DESs, the same behavior can be observed (Fig. S14†). This indicates that with an increase in the VOXs concentrations from 0.5 to 10.0 mg m^{-3}, the VOXs removal efficiency gradually decreased. This is due to the fact that increasing the VOXs concentration increases the molar ratio of VOXs/DES, resulting in the decreased absorption efficiency of VOXs.

The selectivity of individual VOX was determined by comparing the VOX absorption to the sum of all VOX absorptions in DES. The obtained results indicate that TCEtOH was characterized by the highest selectivity (TCEtOH/ΣVOX = 0.32). Slightly lower values were obtained for DCM (0.21) and CF (0.18), and the lowest values for TCM (0.15) and TCE (0.14). The high selectivity of TCEtOH is due to the presence of the –OH group in the structure, which can form strong hydrogen bonds with DES components. The remaining VOX do not have active groups in their structures; therefore, they will interact with DES only through weaker electrostatic bonds. On the basis of the obtained results, it can be concluded that with the increase in the content of chlorine atoms in the VOX structures, the electrostatic interactions weaken. For a detailed explanation, see the Mechanism of absorption section.

Regeneration of DES. From an industrial and economic point of view, absorbent regeneration is a very important factor because multiple uses of absorbent significantly reduce the cost of the process.[22] The obtained results as expected indicate that desorption efficiency increases with increasing temperature from 20 to 100 °C. The highest desorption efficiency of VOXs was obtained at 100 °C. At 100 °C, the complete desorption time was 60 minutes. However, at 80 °C, the time necessary for desorption increased to 180 minutes. Below 80 °C, even after 700 minutes of the process, 100% VOX removal from DES was not achieved. Similar results were obtained in previous studies.[85] The effect of temperature on VOXs desorption in Syr : Lev (1 : 1) is presented in Fig. 8. As shown in Fig. 8A and S15,† absorption capacity was only slightly lost after ten cycles (absorption–desorption). A comparison of the FT-IR spectra of fresh DES and DES after ten cycles of absorption-desorption showed no additional peaks or
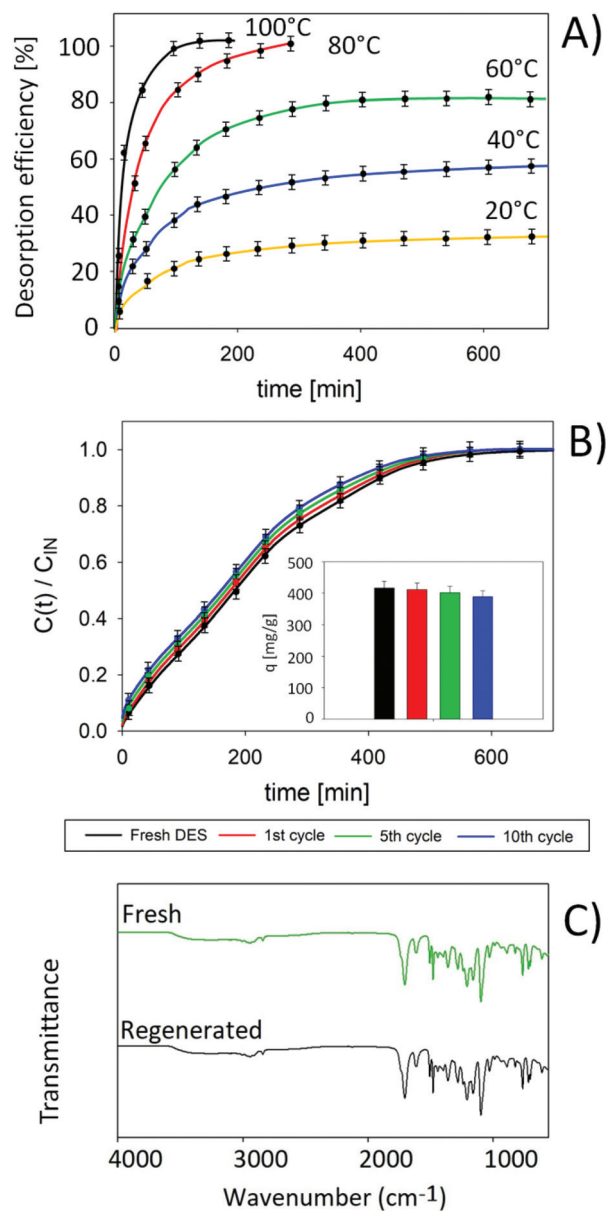
Fig. 8 VOXs absorption/desorption cycles of Syr : Lev (1 : 1): (A) The effect of temperature on Syr : Lev (1 : 1) desorption. (B) Experimental breakthrough curves of DCM after absorption/desorption cycles (gas flow 70 mL min^{-1}; matrix gas N_2; temperature 20 °C). (C) FT-IR spectra of fresh Syr : Lev (1 : 1) and regenerated DES.

band shifts (Fig. 8B). This indicates that Sy : Lev (1 : 1) is stable during multiple cycles and can be reused as a VOXs absorbent. In similar conditions, ILs based on 1-butyl-3-methylimidazolium thiocyanate [Bmim][SCN] showed only up to five effective DCM absorption-desorption cycles.[76]

Mechanism of absorption. In order to explain the absorption mechanism, DESs–VOX complexes were characterized by FT-IR, as well as quantum mechanical calculations. The FT-IR spectra of Syr : Lev (1 : 1) before and after the absorption of selected volatile organic halogens are presented in Fig. 9A and S16.† The comparison of the spectrum of pure Syr : Lev (1 : 1) with Syr : Lev
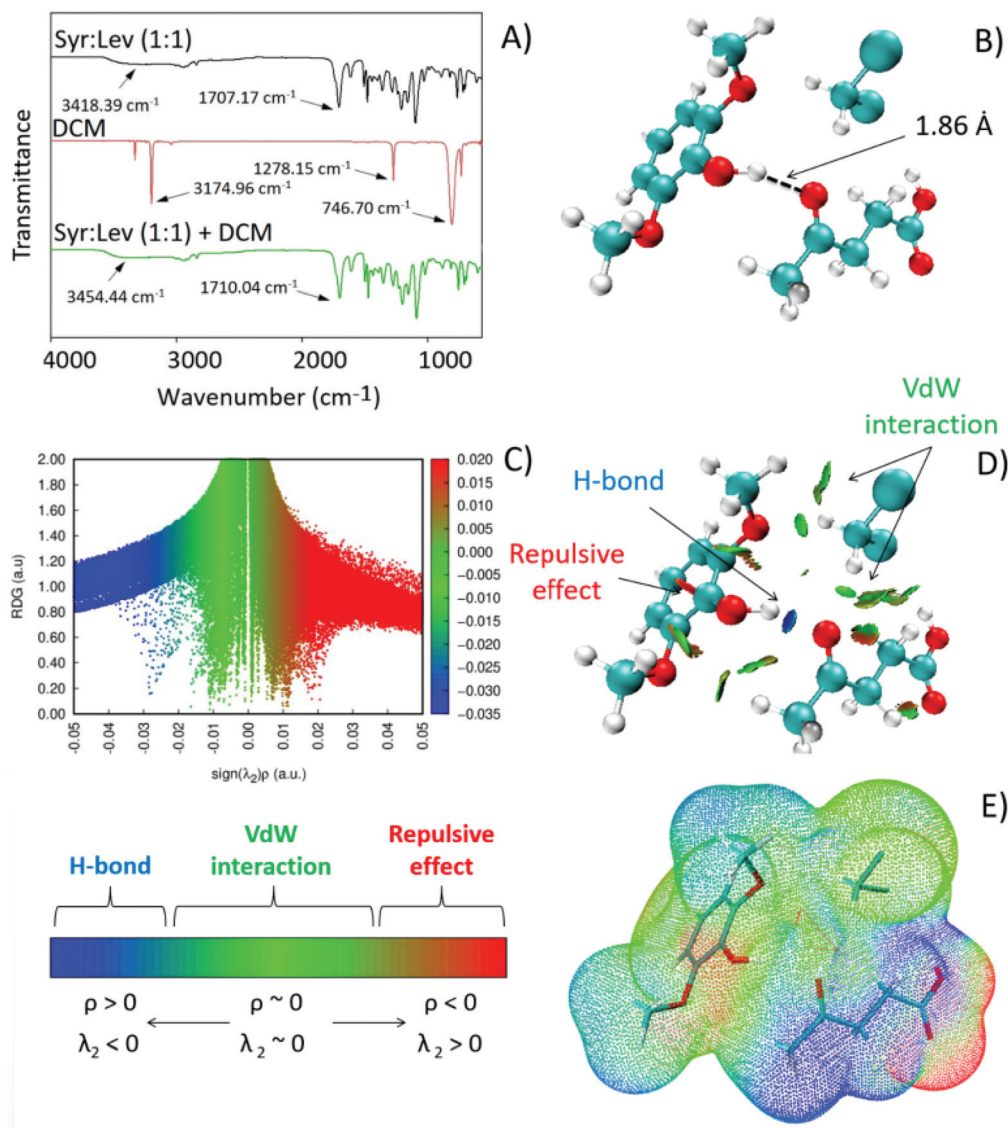
Fig. 9 (A) FT-IR spectra of pure Syr : Lev (1 : 1), pure DCM, and Syr : Lev (1 : 1) − DCM complex; (B) Syr : Lev (1 : 1) − DCM structure after geometric optimization; (C) 2D plots of RDG *versus* the electron density multiplied by the sign of the second Hessian eigenvalue for Syr : Lev (1 : 1) − DCM; (D) Reduced density gradient (RDG) isosurfaces (*s* = 0.5 a.u.) of Syr : Lev (1 : 1) − DCM; (E) Electrostatic potential (ESP) mapped on electron total density with an isovalue 0.001 for Syr : Lev (1 : 1) − DCM.

(1 : 1) after TCEtOH absorption showed the shift of the –OH bands towards higher values from 3418.39 cm^{-1} to 3446.81 cm^{-1}, as well as the carbonyl group towards higher values from 1707.17 cm^{-1} to 1712.82 cm^{-1} (Fig. S15†). The increase in the intensity of the –OH and C=O band confirmed the formation of a hydrogen bond between Syr : Lev (1 : 1), and the TCEtOH.[86] In addition, in the DES spectrum after the absorption of TCEtOH in the range 1097.76–714.13 cm^{-1} the vibrations assigned to the C–O stretching bond (1086.64 cm^{-1}), C–Cl bond (807.95 cm^{-1}), and C–H bending bond (709.96 cm^{-1}) present in pure TCEtOH are visible, which confirmed further interaction between Syr : Lev (1 : 1) and TCEtOH.[87] In the FT-IR spectra, after the absorption of DCM, CF, TCM, and TCE (Fig. 9A and S16†), there was a shift of the –OH group and the

C=O group towards higher wavenumber values. The observed changes confirmed that the absorption process may take place through the formation of weak hydrogen bonds between the COOH group (derived from Syr : Lev) and the chlorine atom (derived from VOX). Similar results were observed for C : Lev (1 : 2), C : Gu (1 : 1), and G : Lev (1 : 1) (Fig. S17–S19†).

The results of calculations indicated that non-bonded interactions exist between both components of DESs and all VOXs (Fig. 9B and S20–S23). Theoretically, chloride atoms of VOXs can interact with hydroxyl groups of DES (C–Cl···HO), or the C–H group can interact with carbonyl (C–H···O=) or hydroxyl groups of DESs (C–H···OH) forming weak hydrogen bonds.[88,89] However, C–H and Cl–C groups are weak donors and very weak acceptors, respectively. These groups can form only weak

hydrogen bonds. In the optimized complexes of Syr : Lev (1 : 1) – DCM, Syr : Lev (1 : 1) – CF, Syr : Lev (1 : 1) – TCM, and Syr : Lev (1 : 1) – TCE, the distances between the hydroxyl groups of DES components and chloride atoms of VOXs were greater than 2.5 Å, which indicates the absence of hydrogen bonds, and another interaction must play a major role in removing VOXs from the biogas stream. A similar phenomenon was observed for the remaining DES. Only in the Syr : Lev (1 : 1) – TCEtOH complex, two H-bonds exist between the hydroxyl group of TCEtOH and hydroxyl groups of Syr and Lev –OH···HO (1.79 and 1.8 Å), which may affect the higher absorption of TCEtOH as compared to other VOX. On the other hand, it was observed that when the TCEtOH molecule was attached to Syr : Lev (1 : 1), the H-bond between Syr and Lev in DES became weaker. Similar behavior was observed in the Gu : Lev (1 : 1) –TCEtOH complex, in which one of the existing hydrogen bonds between Gu and Lev was broken, and in its place an additional hydrogen bond between the carbonyl group of Lev and hydroxyl group of TCEtOH ═O···HO (1.94 Å) was formed. In C : Lev (1 : 2) – TCEtOH and C : Gu (1 : 1) – TCEtOH complexes, additional hydrogen bonds were formed between DESs and TCEtOH, and existing hydrogen bonds between DES components were not weakened or broken, which indicated the high stability of DESs during the absorption process.

The obtained results of the reduced density gradient analysis showed that van der Waals interactions occurred in all DES-VOX complexes, except for the DES-TCEtOH complexes in which both hydrogen bonding and van der Waals interactions coexisted (Fig. 9C and D and S24–S31†). The green surfaces of the van der Waals interaction increased following the order of C : Lev (1 : 2) < G : Lev (1 : 1) < C : Gu (1 : 1) < Syr : Lev (1 : 1), which is in line with the results obtained for the absorption processes. The obtained results showed that the non-covalent interactions (mainly van der Waals) are the main driving force for DCM, CF, TCM, and TCE removal from gas streams, while coexisting H-bonds and electrostatic interactions are responsible for the effective removal of TCEtOH.

The results of the electrostatic potential analysis of the VOXs compounds indicated that the electropositive areas were located around hydrogen atoms in DCM, CF, and TCEtOH. The electronegative areas were located around the oxygen and chloride atoms in VOX, and the neutral regions were located close to the carbon atoms (Fig. 9E and S32–S35). When VOXs (with exception of TCEtOH) interact with DESs, the electropositive regions located around hydrogen atoms in all DESs are attracted to the electronegative areas located close to chloride atoms in VOX. When TCEtOH interacts with DESs, the electropositive region located around the H atom in the hydroxyl group is attracted to the electronegative region located close to oxygen in the hydroxyl group, forming the H-bond interaction. The obtained interaction energies (ΔE_{int}) between all studied DESs and VOXs are presented in Table 1. The more negative values of interaction energies indicate stronger interactions between DES and VOX. It was observed that ΔE_{int} followed a similar trend to that of the experimental absorption capacity of VOX (C : Lev (1 : 2) > G : Lev (1 : 1) > C : Gu (1 : 1) > Syr : Lev (1 : 1)). Moreover, taking

Table 1 Interaction energies between DES and VOX

DES	Interaction energy [kcal mol^{-1}]				
	DCM	CF	TCM	TCEtOH	TCE
C : Lev (1 : 2)	−6.7	−6.1	−2.0	−10.5	−1.8
C : Gu (1 : 1)	−7.0	−5.3	−2.7	−11.5	−2.5
Gu : Lev (1 : 1)	−0.8	−0.4	−0.3	−1.9	−0.2
Syr : Lev (1 : 1)	−5.9	−5.3	−2.6	−8.2	−1.4

into account the individual VOX, the interaction energy can be ranked as follows TCE ~ TCM > DCM > TCEtOH, which is also in line with the results obtained experimentally.

Conclusions

New deep eutectic solvents composed of natural ingredients were successfully applied in the removal of volatile organochlorine compounds from the biogas stream in the absorption process. The influence of several absorption parameters, *i.e.*, the type of DES, gas flow rate, kind of matrix gas, temperature, and initial concentrations of VOXs, on the absorption process were studied. It was found that the Syr : Lev (1 : 1) had the highest absorption capacity for VOXs, at 20 °C. The other parameters, *i.e.* the initial concentration of VOXs and the gas flow, only affected the extension or reduction of the DES saturation time. However, they did not significantly affect the DES absorption capacity. In optimal conditions, the absorption capacities of DCM, CF, TCM, TCE, and TCEtOH were 304, 420, 360, 292, and 661 mg g^{-1}, respectively. The obtained result for the absorption capacity for DCM was higher by about 98 mg g^{-1} as compared to the results obtained with the use of ILs based on [Bmim][SCN].[76] After the absorption process, Syr : Lev (1 : 1) was successfully regenerated by means of nitrogen barbotage at 100 °C in one hour. The obtained results demonstrated that the absorption capacities of Syr : Lev (1 : 1) did not change after ten absorption-desorption cycles, which confirmed the stable reusable capacity. The theoretical and experimental studies on the mechanism of DESs formation and VOX absorption indicated that both H-bonding and van der Waals interactions between DES components contributed to the formation of stable eutectic mixtures. In addition, depending on the type of VOXs, only van der Waals or both hydrogen bonds and van der Waals interactions are the main driving forces for the removal of VOXs from model biogas. Therefore, the proposed procedure based on DESs has great potential for the purification of real biogas streams, and is in line with the green engineering strategy, as well as the European Union's strategy for obtaining renewable energy.

Author contributions

Patrycja Makoś-Chełstowska: Conceptualization, data curation, funding acquisition, formal analysis, investigation, method-

ology, supervision, writing – original draft, writing – review & editing. Edyta Słupek: Conceptualization, data curation, investigation, methodology, writing – original draft. Jacek Gębicki: Writing – review & editing.

Conflicts of interest

There are no conflicts to declare.

Acknowledgements

References

1 B. Stürmer, D. Leiers, V. Anspach, E. Brügging, D. Scharfy and T. Wissel, *Renewable Energy*, 2021, **164**, 171–182.

2 T. Tomić and D. R. Schneider, *Renewable Sustainable Energy Rev.*, 2018, **98**, 268–287.

3 L. Lijó, S. González-García, J. Bacenetti and M. T. Moreira, *Energy*, 2017, **137**, 1130–1143.

4 S. Rasi, J. Läntelä and J. Rintala, *Energy Convers. Manage.*, 2011, **52**, 3369–3375.

5 G. Piechota, B. Igliński and R. Buczkowski, *Energy Convers. Manage.*, 2013, **68**, 219–226.

6 N. Scarlat, J. F. Dallemand and F. Fahl, *Renewable Energy*, 2018, **129**, 457–472.

7 J. I. Salazar Gómez, H. Lohmann and J. Krassowski, *Chemosphere*, 2016, **153**, 48–57.

8 S. Rasi, A. Veijanen and J. Rintala, *Energy*, 2007, **32**, 1375–1380.

9 I. A. Arkharov, E. N. Simakova and E. S. Navasardyan, *Chem. Pet. Eng.*, 2016, **52**, 547–551.

10 A. Jaffrin, N. Bentounes, A. M. Joan and S. Makhlouf, *Biosyst. Eng.*, 2003, **86**, 113–123.

11 R. J. Spiegel and J. L. Preston, *Energy*, 2003, **28**, 397–409.

12 H. C. Shin, J. W. Park, K. Park and H. C. Song, *Environ. Pollut.*, 2002, **119**, 227–236.

13 F. Dincer, M. Odabasi and A. Muezzinoglu, *J. Chromatogr. A*, 2006, **1122**, 222–229.

14 B. V. Nielsen, S. Maneein, M. D. Mahmud Al Farid and J. J. Milledge, *Fermentation*, 2020, **6**(3), 85–107.

15 A. Buekens and H. Huang, *J. Hazard. Mater.*, 1998, **62**, 1–33.

16 O. W. Awe, Y. Zhao, A. Nzihou, D. P. Minh and N. Lyczko, *Waste and Biomass Valorization*, 2017, **8**, 267–283.

17 S. Rasi, J. Läntelä, A. Veijanen and J. Rintala, *Waste Manage*, 2008, **28**, 1528–1534.

18 J. Lemus, M. Martin-Martinez, J. Palomar, L. Gomez-Sainero, M. A. Gilarranz and J. J. Rodriguez, *Chem. Eng. J.*, 2012, **211–212**, 246–254.

19 M. Abtahi, K. Naddafi, A. Mesdaghinia, K. Yaghmaeian, R. Nabizadeh, N. Jaafarzadeh, N. Rastkari, S. Nazmara and R. Saeedi, *J. Environ. Health Sci. Eng.*, 2014, **12**, 1–7.

20 R. Guo, S. Lv, T. Liao, F. Xi, J. Zhang, X. Zuo, X. Cao, Z. Feng and Y. Zhang, *Resour., Conserv. Recycl.*, 2020, **153**, 104580.

21 G. Orsatti, F. Quatraro and M. Pezzoni, *Res. Policy*, 2020, **49**, 103919.

22 E. Słupek, P. Makoś and J. Gębicki, *Energies*, 2020, **13**, 3379.

23 I. Angelidaki, L. Xie, G. Luo, Y. Zhang, H. Oechsner, A. Lemmer, R. Munoz and P. G. Kougias, *Biomass, Biofuels, Biochem.*, 2019, 817–843.

24 E. Ryckebosch, M. Drouillon and H. Vervaeren, *Biomass Bioenergy*, 2011, **35**, 1633–1645.

25 Y. Xiao, H. Yuan, Y. Pang, S. Chen, B. Zhu, D. Zou, J. Ma, L. Yu and X. Li, *Chin. J. Chem. Eng.*, 2014, **22**, 950–953.

26 G. Darracq, A. Couvert, C. Couriol, A. Amrane, D. Thomas, E. Dumont, Y. Andres and P. Le Cloirec, *J. Chem. Technol. Biotechnol.*, 2010, **85**, 309–313.

27 G. F. Freeguard and R. Stock, *Trans. Faraday Soc.*, 1963, **59**, 1655–1662.

28 D. L. Feldheim, S. M. Hendrickson, M. Krejcik, C. M. Elliott and C. A. Foss, *J. Phys. Chem.*, 1995, **99**, 3288–3293.

29 A. S. Rodriguez Castillo, P.-F. Biard, S. Guihéneuf, L. Paquin, A. Amrane and A. Couvert, *Chem. Eng. J.*, 2019, **360**, 1416–1426.

30 S. N. Turosung and B. Ghosh, *Int. J. Petrochem. Res.*, 2017, **1**, 50–60.

31 A. Romero, A. Santos, A. Tojo and J. Rodríguez, *J. Hazard. Mater.*, 2008, **151**, 268–273.

32 K. Häckl and W. Kunz, *C. R. Chim.*, 2018, **21**, 572–580.

33 T. P. T. Pham, C. W. Cho and Y. S. Yun, *Water Res.*, 2010, **44**, 352–372.

34 P. Makoś, E. Słupek and J. Gębicki, *J. Mol. Liq.*, 2020, **308**, 113101–113112.

35 P. Makoś, A. Fernandes, A. Przyjazny and G. Boczkaj, *J. Chromatogr. A*, 2018, **1555**, 10–19.

36 P. Makoś and G. Boczkaj, *J. Mol. Liq.*, 2019, **296**, 111916–111927.

37 P. Makoś, A. Przyjazny and G. Boczkaj, *J. Chromatogr. A*, 2018, **1570**, 28–37.

38 P. Makoś, E. Słupek and J. Gębicki, *Microchem. J.*, 2020, **152**, 104384–104400.

39 F.-Y. Zhong, K. Huang and H.-L. Peng, *J. Chem. Thermodyn.*, 2019, **129**, 5–11.

40 T. Aissaoui, I. M. AlNashef and Y. Benguerba, *J. Nat. Gas Sci. Eng.*, 2016, **30**, 571–577.

41 H. Wu, M. Shen, X. Chen, G. Yu, A. A. Abdeltawab and S. M. Yakout, *Sep. Purif. Technol.*, 2019, **224**, 281–289.

42 Y. Zhang, X. Ji and X. Lu, *Renewable Sustainable Energy Rev.*, 2018, **97**, 436–455.

43 E. Słupek and P. Makoś, *Sustainability*, 2020, **12**, 1619–1635.

44 E. Słupek, P. Makoś and J. Gębicki, *Arch. Environ. Prot.*, 2020, **46**, 41–46.

45 P. Makoś, E. Słupek and A. Małachowska, *Materials*, 2020, **13**, 1894.

46 L. F. Zubeir, D. J. G. P. Van Osch, M. A. A. Rocha, F. Banat and M. C. Kroon, *J. Chem. Eng. Data*, 2018, **63**, 913–919.

47 H. Wu, M. Shen, X. Chen, G. Yu, A. A. Abdeltawab and S. M. Yakout, *Sep. Purif. Technol.*, 2019, **224**, 281–289.

48 Y. Chen, D. Yu, W. Chen, L. Fu and T. Mu, *Phys. Chem. Chem. Phys.*, 2019, **21**, 2601–2610.

49 M. Atilhan, T. Altamash and S. Aparicio, *Molecules*, 2019, **24**, 1–18.

50 E. Słupek, P. Makoś-Chełstowska and J. Gębicki, *Materials*, 2021, **14**, 1–20.

51 L. Moura, T. Moufawad, M. Ferreira, H. Bricout, S. Tilloy, E. Monflier, M. F. Costa Gomes, D. Landy and S. Fourmentin, *Environ. Chem. Lett.*, 2017, **15**, 747–753.

52 R. Chromá, M. Vilková, I. Shepa, P. Makoś-Chełstowska and V. Andruch, *J. Mol. Liq.*, 2021, **330**, 115617.

53 V. Migliorati, F. Sessa and P. D'Angelo, *Chem. Phys. Lett.: X*, 2019, **2**, 100001.

54 Z. Naseem, R. A. Shehzad, A. Ihsan, J. Iqbal, M. Zahid, A. Pervaiz and G. Sarwari, *Chem. Phys. Lett.*, 2021, **769**, 138427.

55 S. Khodaverdian, B. Dabirmanesh, A. Heydari, E. Dashtban-moghadam, K. Khajeh and F. Ghazi, *Int. J. Biol. Macromol.*, 2018, **107**, 2574–2579.

56 T. Kvist and N. Aryal, *Waste Manage.*, 2019, **87**, 295–300.

57 J. R. Bastidas-Oyanedel, F. Bonk, M. H. Thomsen and J. E. Schmidt, *Rev. Environ. Sci. Biotechnol.*, 2015, **14**, 473–498.

58 J. M. T. Vasconcelos, J. M. L. Rodrigues, S. C. P. Orvalho, S. S. Alves, R. L. Mendes and A. Reis, *Chem. Eng. Sci.*, 2003, **58**, 1431–1440.

59 S. Adams, P. De Castro, P. Echenique, J. Estrada, M. D. Hanwell, P. Murray-Rust, P. Sherwood, J. Thomas and J. Townsend, *J. Cheminf.*, 2011, **3**, 38.

60 F. Neese, *Wiley Interdiscip. Rev.: Comput. Mol. Sci.*, 2012, **2**, 73–78.

61 S. Grimme, J. Antony, S. Ehrlich and H. Krieg, *J. Chem. Phys.*, 2010, **132**, 154104–154115.

62 A. Gutiérrez, M. Atilhan and S. Aparicio, *Phys. Chem. Chem. Phys.*, 2018, **20**, 27464–27473.

63 T. Altamash, A. I. Amhamed, S. Aparicio and M. Atilhan, *Ind. Eng. Chem. Res.*, 2019, **58**, 8097–8111.

64 S. Simon, M. Duran and J. J. Dannenberg, *J. Chem. Phys.*, 1996, **105**, 11024–11031.

65 T. Lu and F. Chen, *J. Comput. Chem.*, 2012, **33**, 580–592.

66 T. Lu and F. Chen, *J. Mol. Graphics Modell.*, 2012, **38**, 314–323.

67 E. R. Johnson, S. Keinan, P. Mori-Sánchez, J. Contreras-García, A. J. Cohen and W. Yang, *J. Am. Chem. Soc.*, 2010, **132**, 6498–6506.

68 W. Humphrey, A. Dalke and K. Schulten, *J. Mol. Graphics*, 1996, **14**, 33–38.

69 A. Hayyan, F. S. Mjalli, I. M. Alnashef, T. Al-Wahaibi, Y. M. Al-Wahaibi and M. A. Hashim, *Thermochim. Acta*, 2012, **541**, 70–75.

70 R. Haghbakhsh, K. Parvaneh, S. Raeissi and A. Shariati, *Fluid Phase Equilib.*, 2018, **470**, 193–202.

71 N. F. Gajardo-Parra, M. J. Lubben, J. M. Winnert, Á. Leiva, J. F. Brennecke and R. I. Canales, *J. Chem. Thermodyn.*, 2019, **133**, 272–284.

72 B. D. Ribeiro, C. Florindo, L. C. Iff, M. A. Z. Coelho and I. M. Marrucho, *ACS Sustainable Chem. Eng.*, 2015, **3**, 2469–2477.

73 R. A. Boto, J. Contreras-García, J. Tierny and J. P. Piquemal, *Mol. Phys.*, 2016, **114**, 1406–1414.

74 G. Saleh, C. Gatti and L. Lo Presti, *Comput. Theor. Chem.*, 2012, **998**, 148–163.

75 X. Ma, M. Wu, S. Liu, J. Huang, B. Sun, Y. Zhou, Q. Zhu and H. Lu, *Chin. J. Chem. Eng.*, 2019, **27**, 2383–2389.

76 W. Wu, T. Li, H. Gao, D. Shang, W. Tu, B. Wang and X. Zhang, *Chin. J. Process Eng.*, 2019, **19**, 173–180.

77 Y. Zhou, L. Zhou, X. Zhang and Y. Chen, *Microporous Mesoporous Mater.*, 2016, **225**, 488–493.

78 H. Pashaei, A. Ghaemi and M. Nasiri, *RSC Adv.*, 2016, **6**, 108075–108092.

79 G. Tian, B. Yang, M. Dong, R. Zhu, F. Yin, X. Zhao, Y. Wang, W. Xiao, Q. Wang, W. Zhang and X. Cui, *Renewable Energy*, 2018, **123**, 15–25.

80 E. Słupek, P. Makoś, K. Kucharska and J. Gębicki, *Chem. Pap.*, 2020, **74**, 1573–1582.

81 J. Lemus, J. Bedia, C. Moya, N. Alonso-Morales, M. A. Gilarranz, J. Palomar and J. J. Rodriguez, *RSC Adv.*, 2016, **6**, 61650–61660.

82 C. H. Hsu, H. Chu and C. M. Cho, *J. Air Waste Manage. Assoc.*, 2003, **53**, 246–252.

83 Y. Guo, Z. Niu and W. Lin, *Energy Procedia*, 2011, **4**, 512–518.

84 M. Netušil, P. Ditl and S. Gupta, *Nat. Gas: Extr. End Use*, 2012, 3–22.

85 K. Zhang, Y. Hou, Y. Wang, K. Wang, S. Ren and W. Wu, *Energy Fuels*, 2018, **32**, 7727–7733.

86 S. Zhu, H. Li, W. Zhu, W. Jiang, C. Wang, P. Wu, Q. Zhang and H. Li, *J. Mol. Graphics Modell.*, 2016, **68**, 158–175.

87 R. Gautam, N. Kumar and J. G. Lynam, *J. Mol. Struct.*, 2020, **1222**, 128849.

88 W. Caminati, S. Melandri, A. Maris and P. Ottaviani, *Angew. Chem., Int. Ed.*, 2006, **45**, 2438–2442.

89 P. I. Nagy, *J. Phys. Chem. A*, 2013, **117**, 2812–2826.

Deep eutectic solvents – based green absorbents for effective volatile organochlorine compounds removal from biogas

Patrycja Makoś-Chełstowska [1]*, Edyta Słupek [1], Jacek Gębicki [1]

[1] Department of Process Engineering and Chemical Technology, Faculty of Chemistry, Gdansk University of Technology, G. Narutowicza St. 11/12, 80–233 Gdańsk, Poland; edyta.slupek@pg.edu.pl (E.S.); jacek.gebicki@pg.edu.pl (J.G.)

*Correspondence: patrycja.makos@pg.edu.pl; Tel.: +48-508-997-100
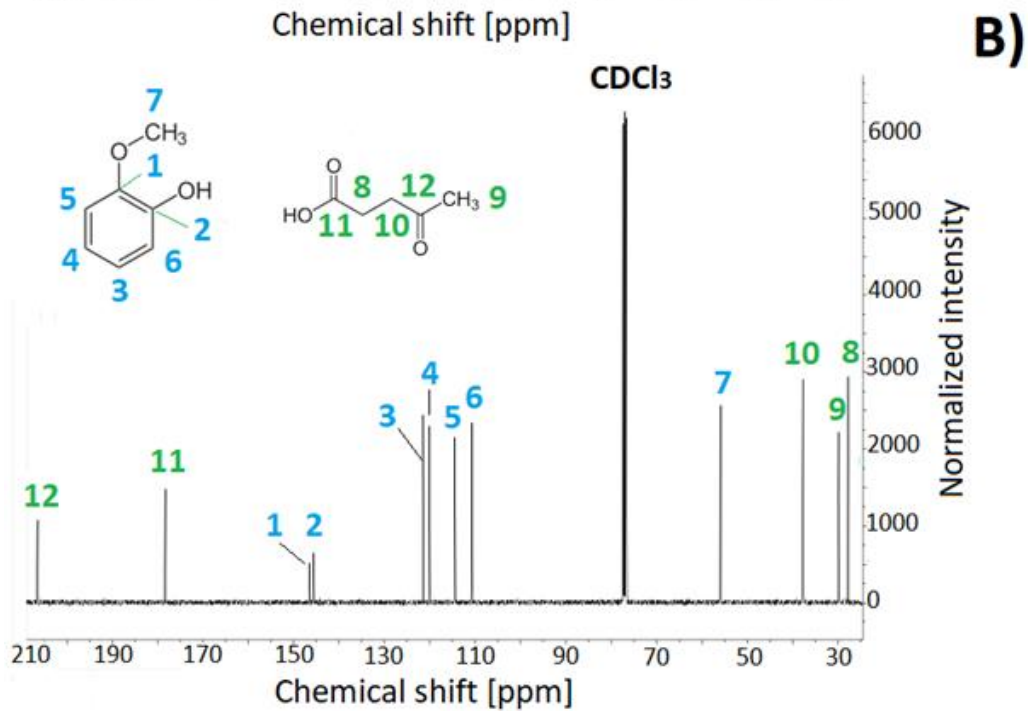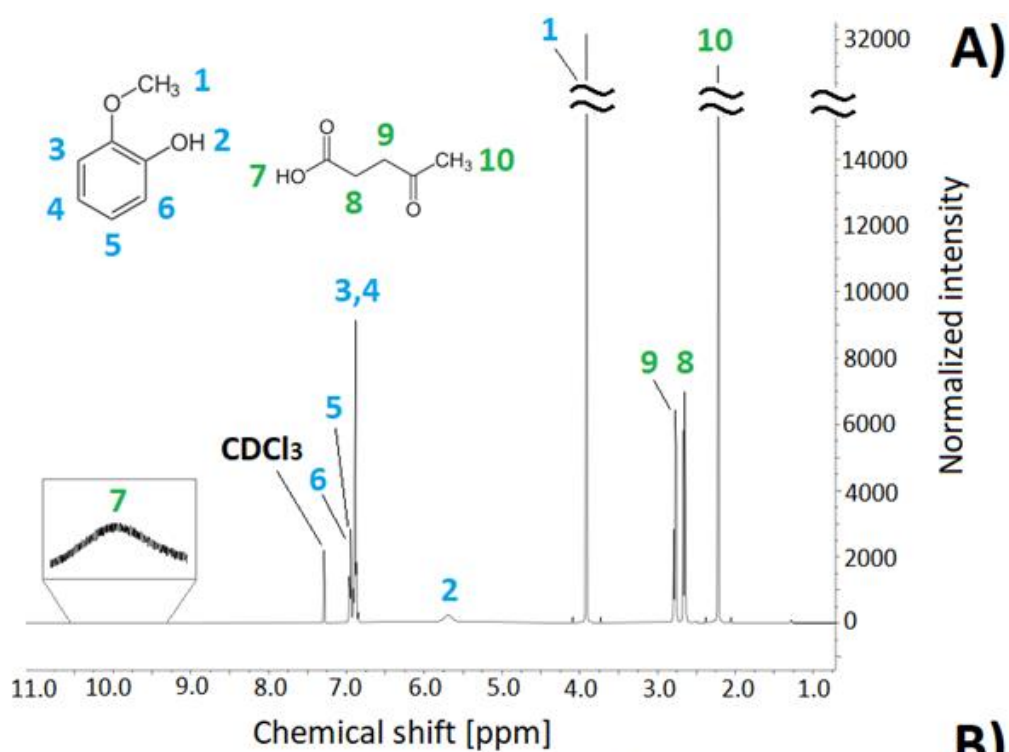
Figure S1 A) ¹H NMR spectra of Gu:Lev (1:1), B) ¹³C NMR spectra of Gu:Lev (1:1).
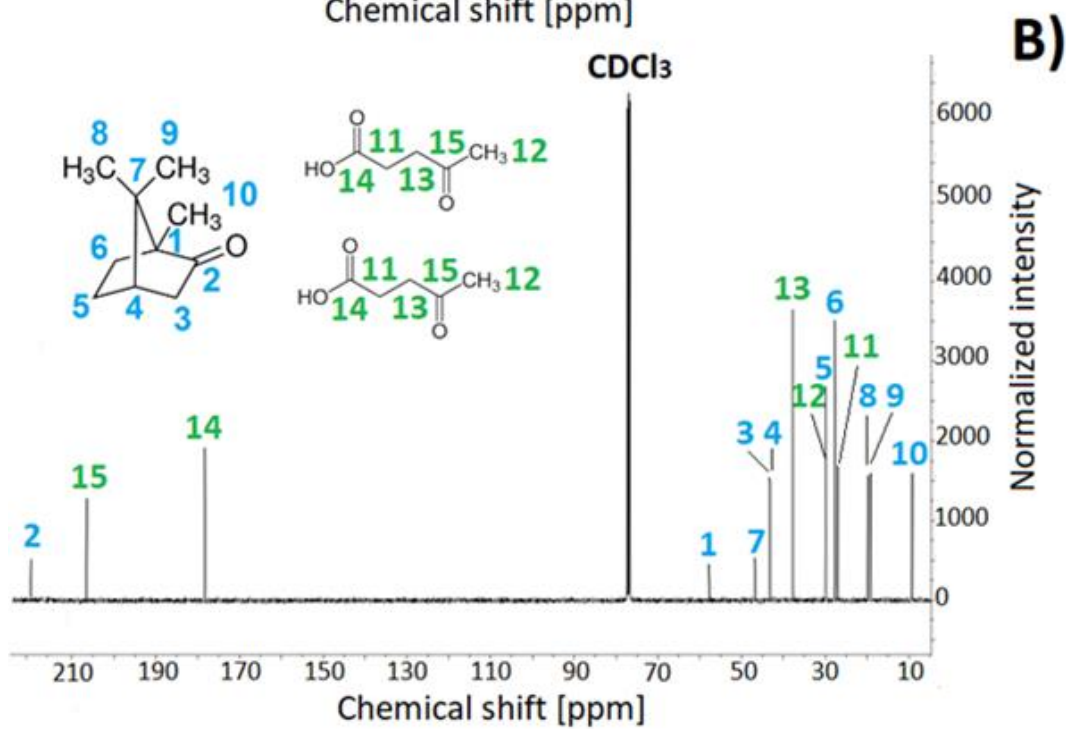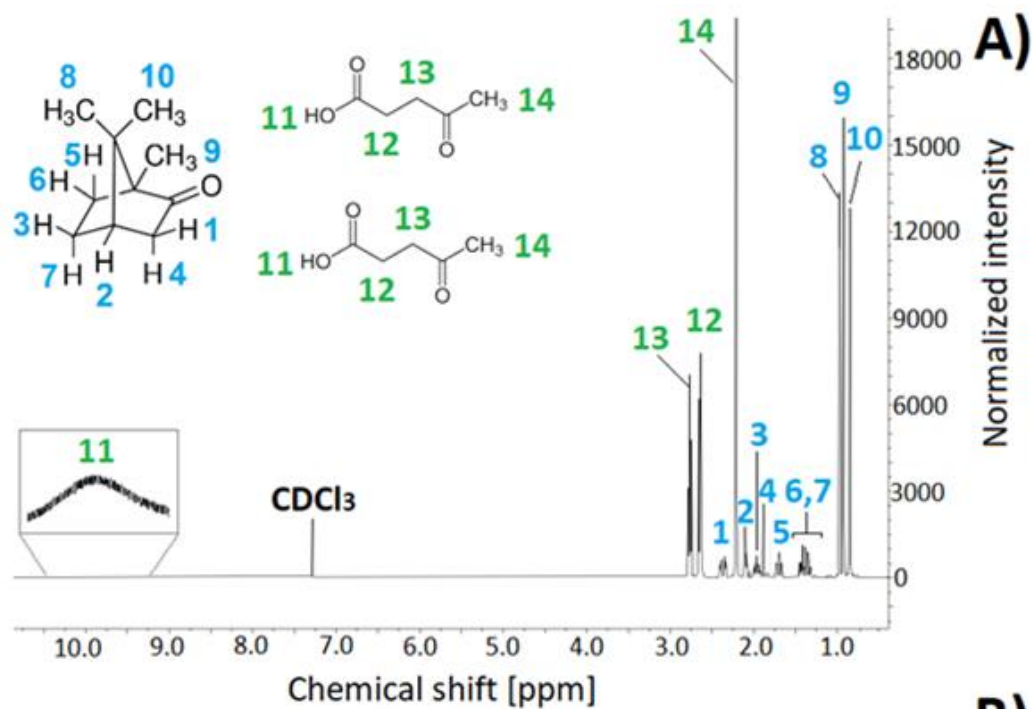
Figure S2 A) ^{1}H NMR spectra of C:Lev (1:2), B) ^{13}C NMR spectra of C:Lev (1:2).
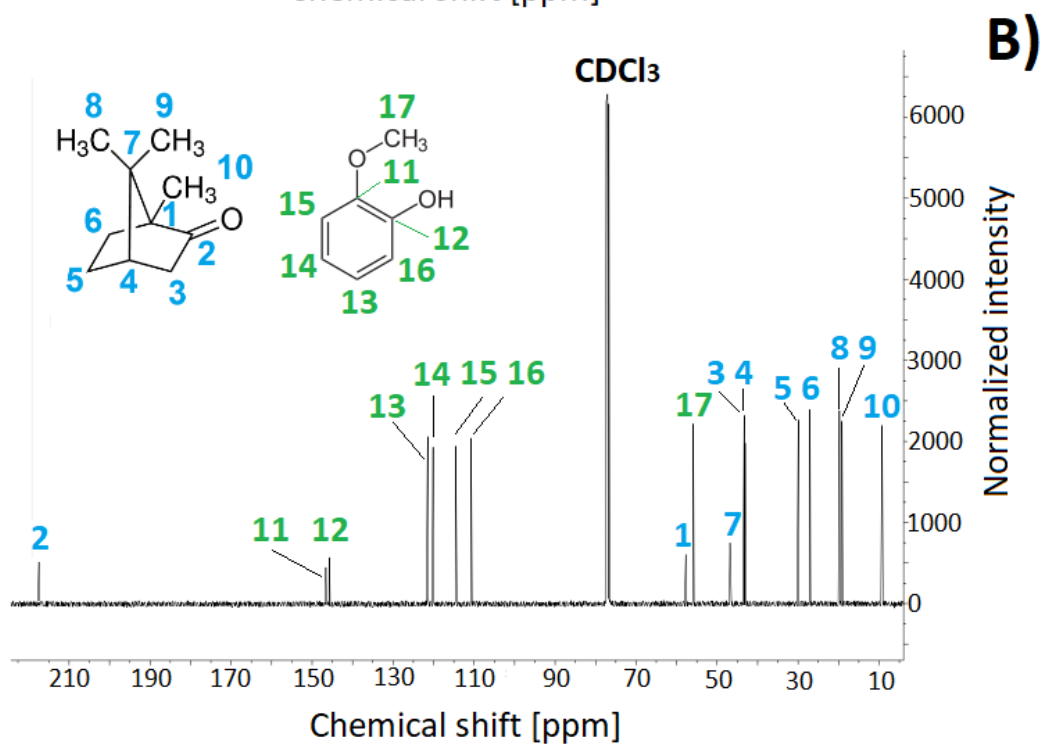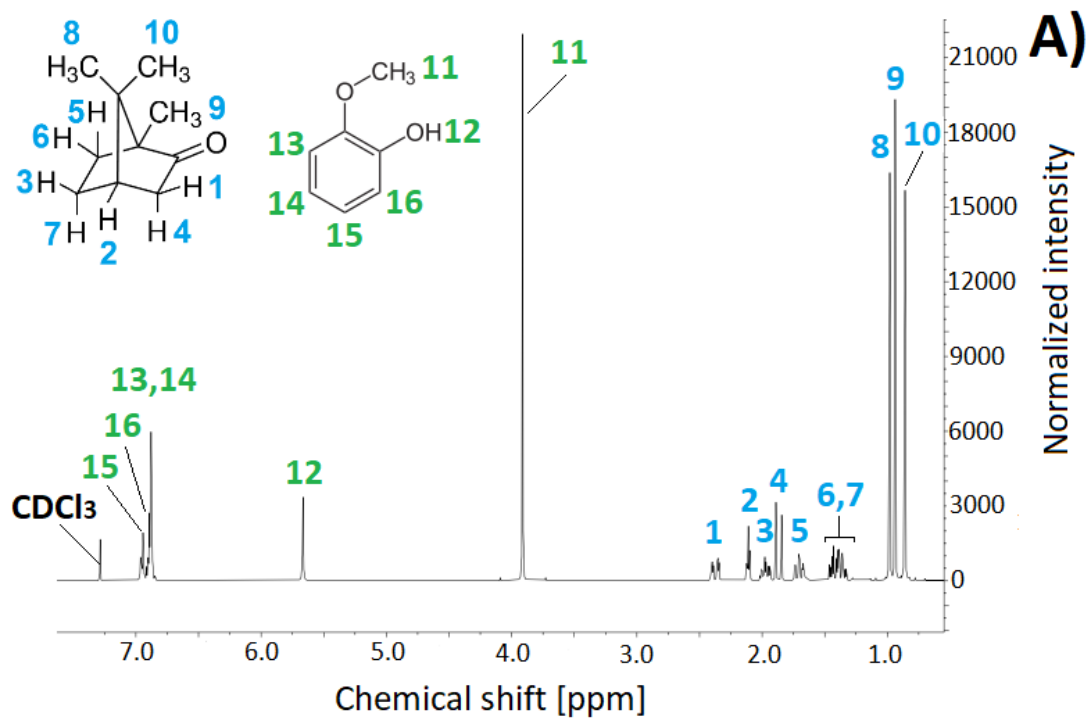
Figure S3 A) ^{1}H NMR spectra of C:Gu (1:1), B) ^{13}C NMR spectra of C:Gu (1:1).
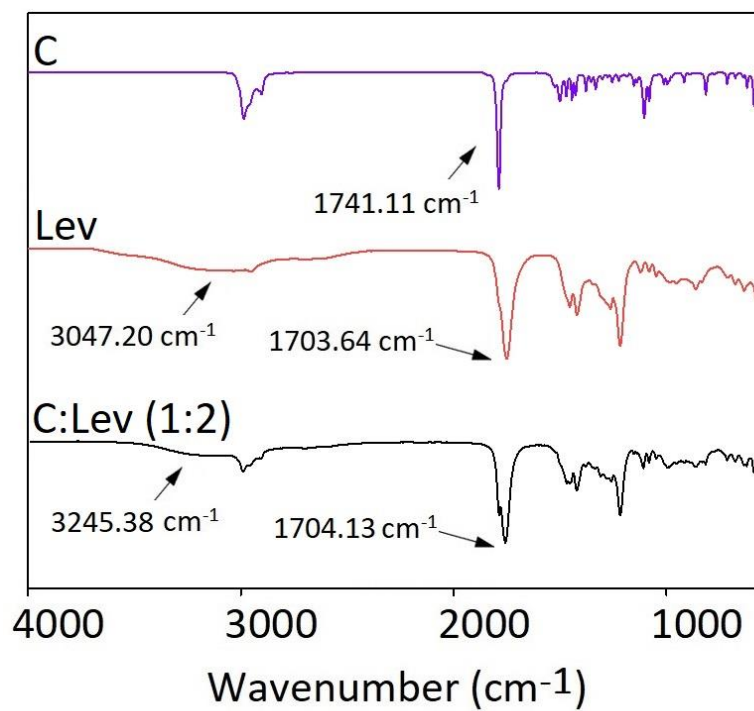
Figure S4 FT-IR spectrum for pure C, Lev, and C:Lev (1:2).
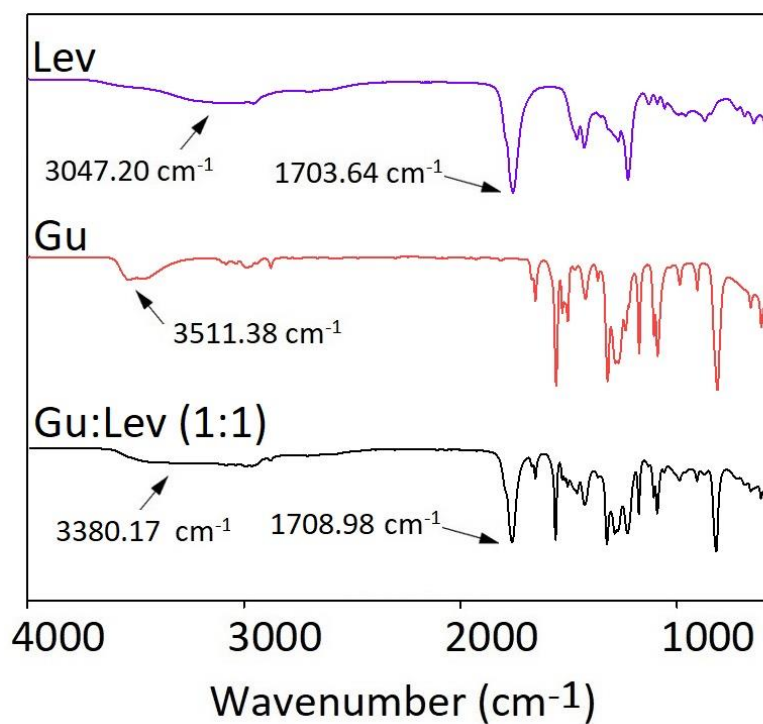
Figure S5 FT-IR spectrum for pure Lev, Gu, and Gu:Lev (1:1).
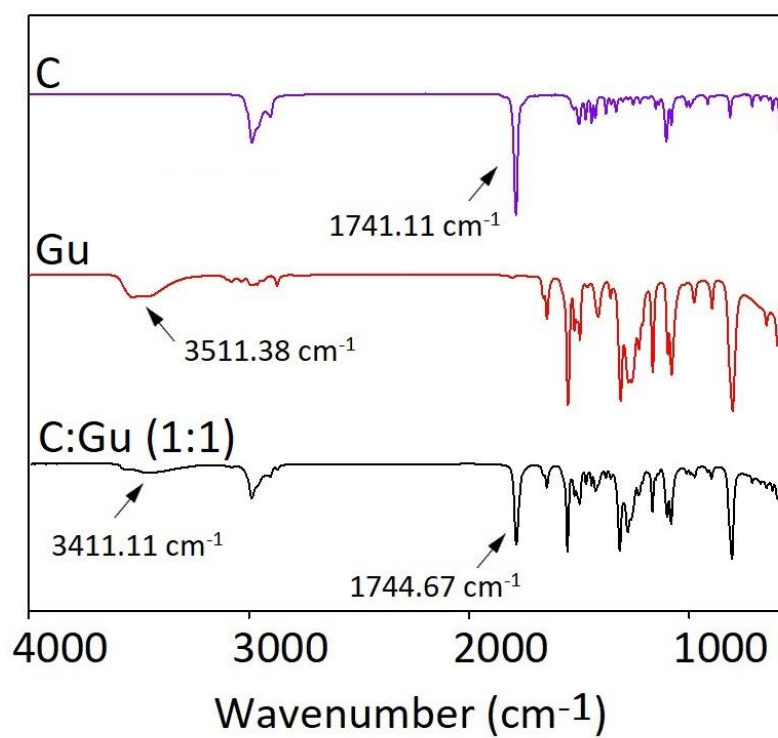
Figure S6 FT-IR spectrum for pure C, Gu, and C:Gu (1:1).
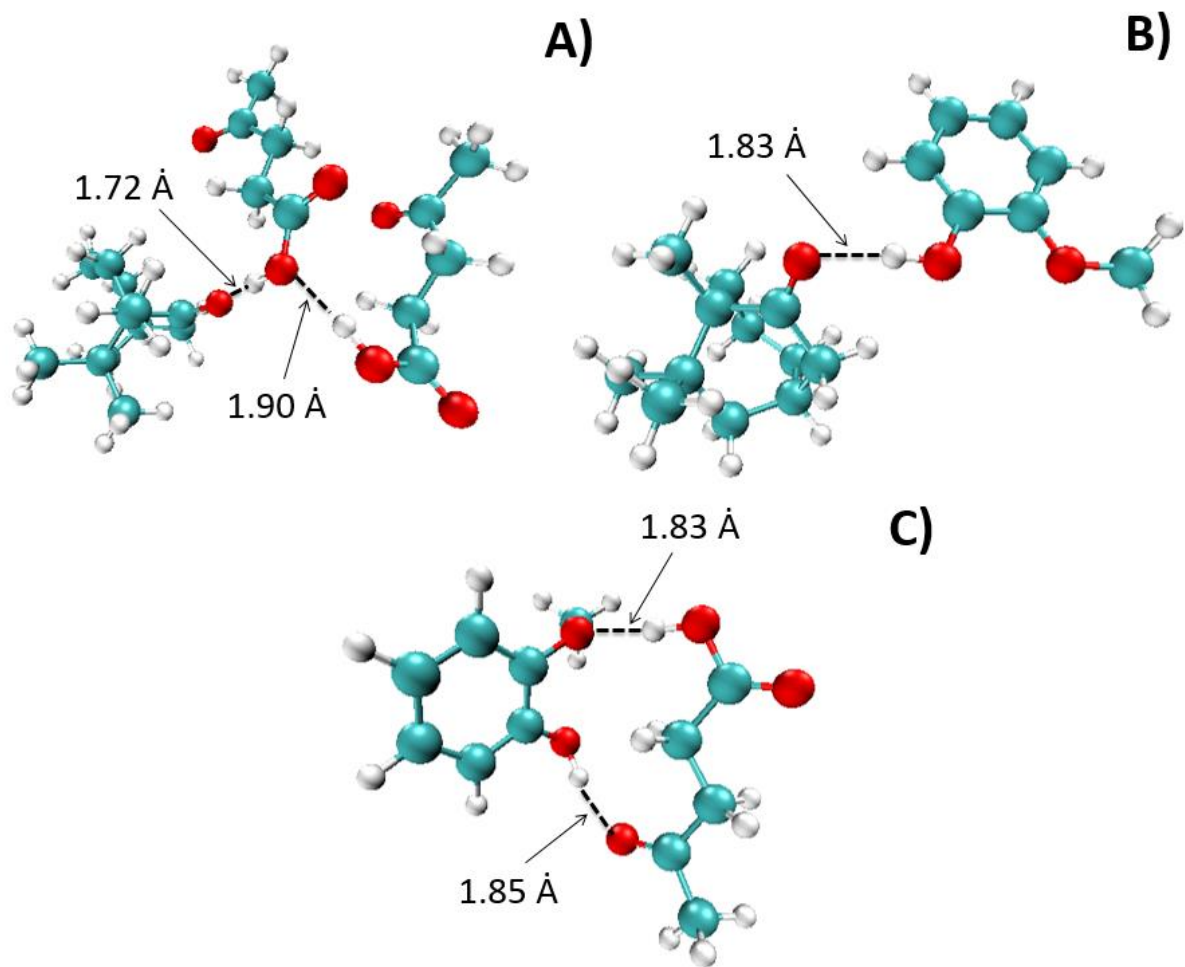
**Figure S7** The structures of DESs after geometric optimization: A) C:Lev (1:2); B) C:Gu (1:1); C) Gu:Lev (1:1).
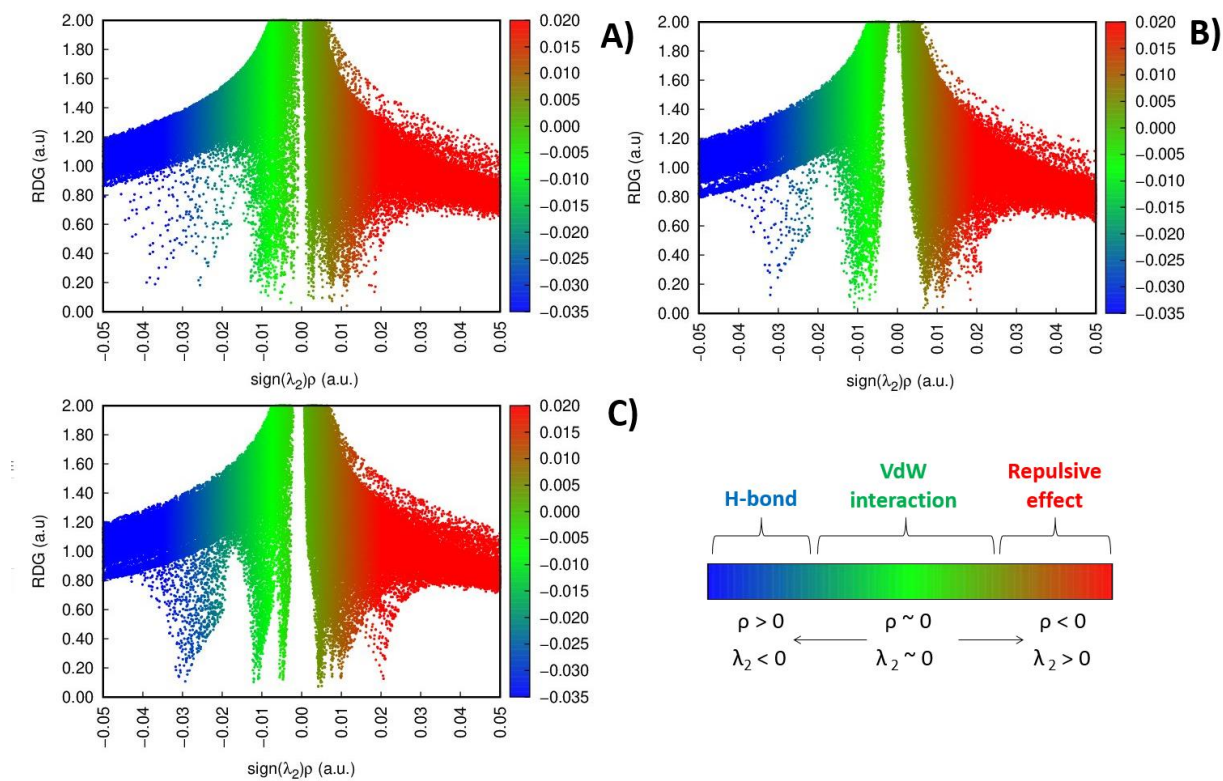
Figure S8 2D plots of RDG versus the electron density multiplied by the sign of the second Hessian eigenvalue for: A) C:Lev (1:2); B) C:Gu (1:1); C) Gu:Lev (1:1). The red area represents repulsive effects; blue area - H-bonding; green area - van der Waals interactions.
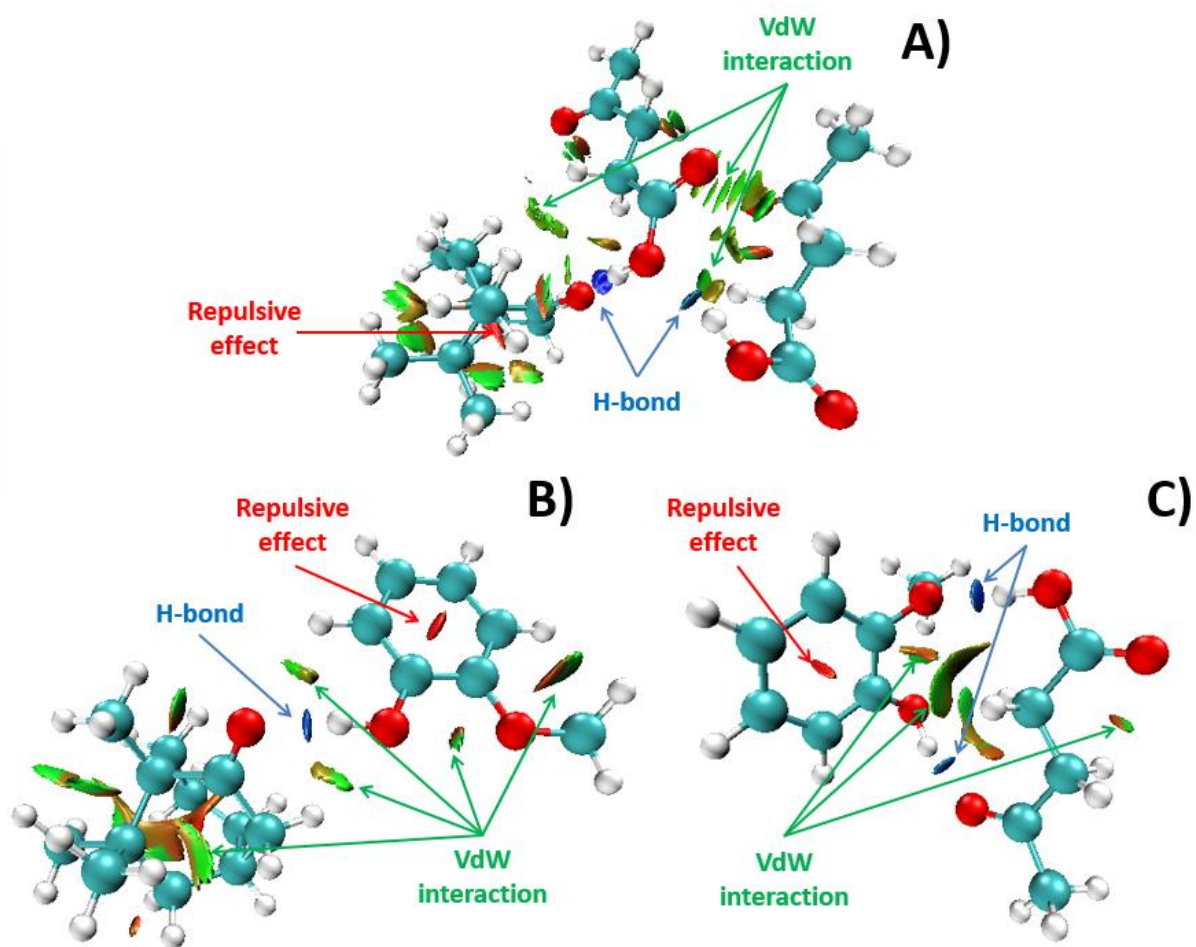
Figure S9 Reduced density gradient (RDG) isosurfaces (s=0.5 a.u.) of studied DESs: A) C:Lev (1:2); B) C:Gu (1:1); C) Gu:Lev (1:1). The red area represents repulsive effects; blue area - H-bonding; green area - van der Waals interactions.
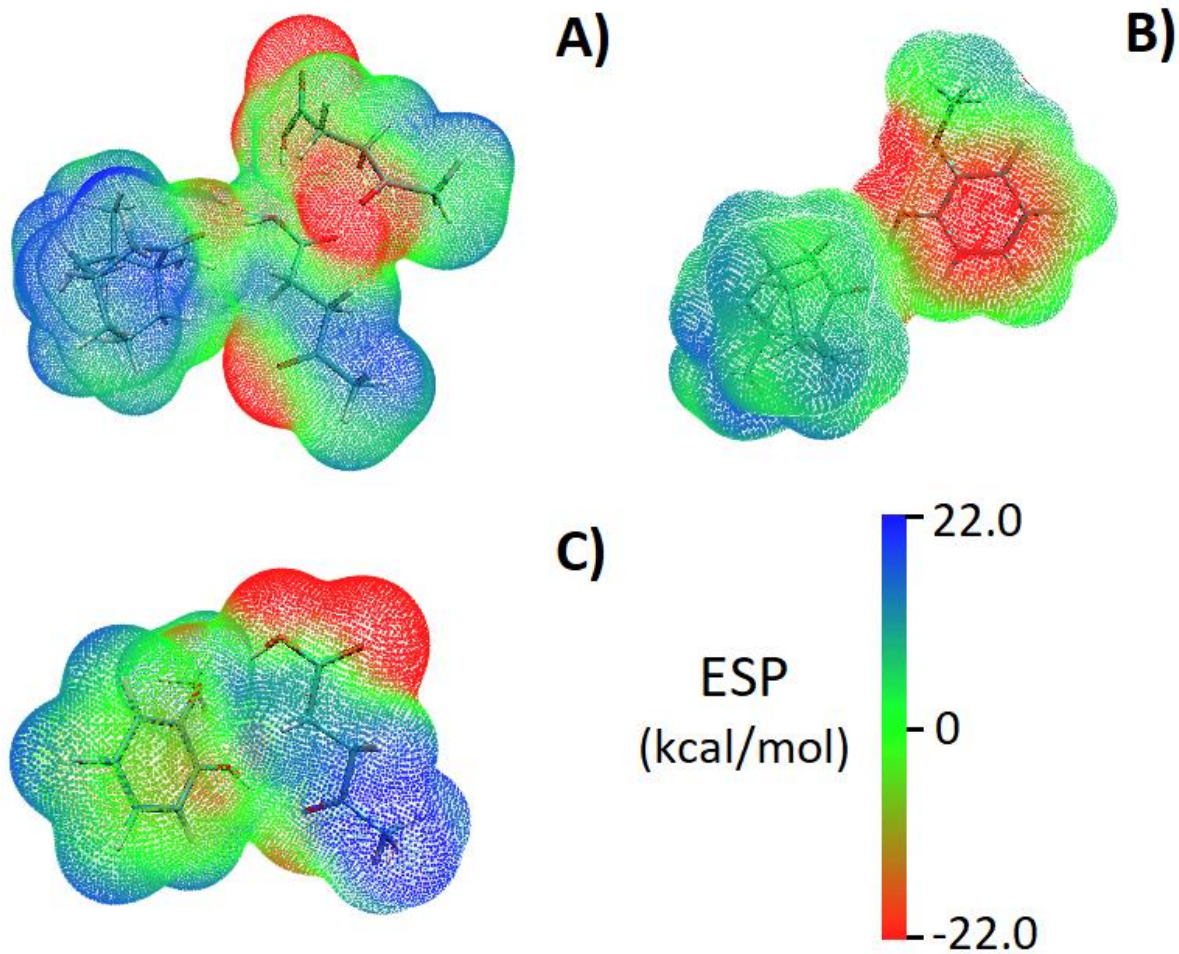
**Figure S10** Elecrostatic potential (ESP) mapped on electron total density with an isovalue 0.001 for: A) C:Lev (1:2); B) C:Gu (1:1); C) Gu:Lev (1:1). Blue area are positively charged; red regions are negatively charged; green are neutrally charged.
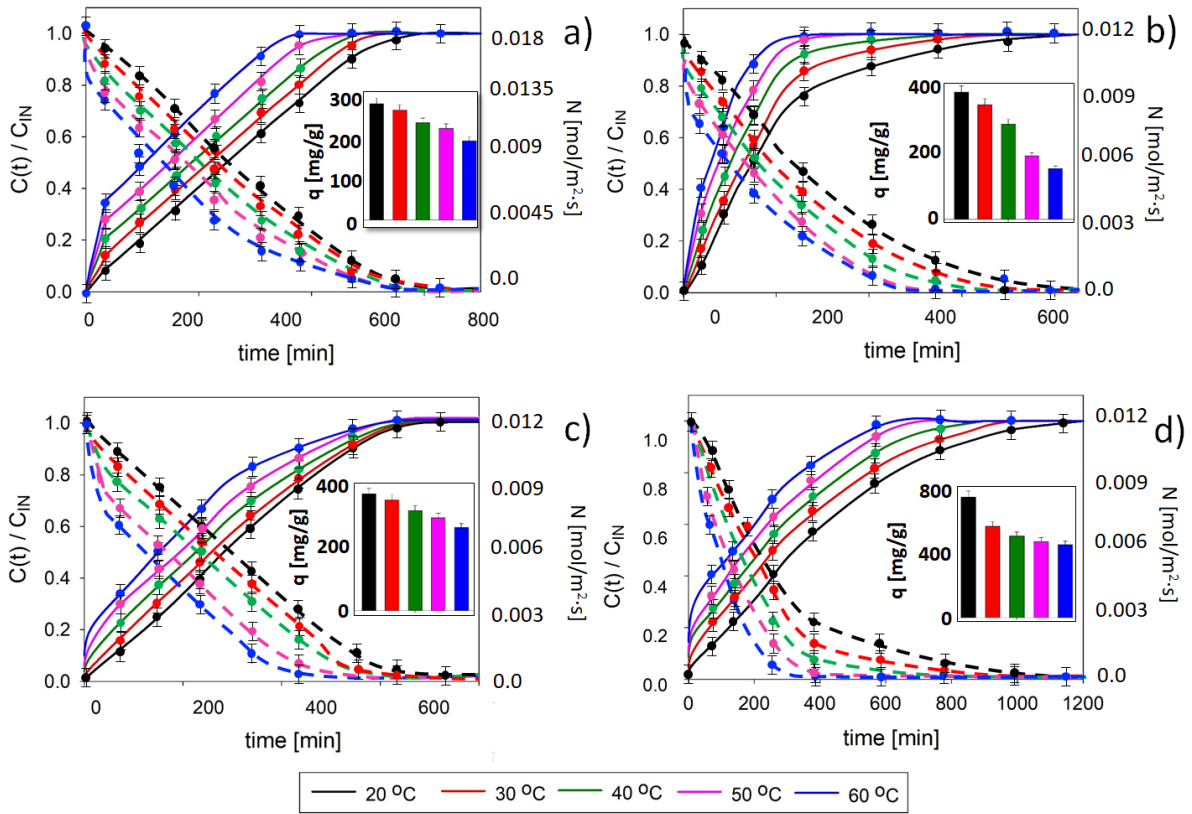
Figure S11 Experimental breakthrough curves of a) CF; b) TCM; c) TCE; d) TCEtOH at different temperatures for Syr:Lev (1:1) (inlet VOX concentration 0.5 mg/cm³; gas flow 50 mL/min; matrix gas N_2;).
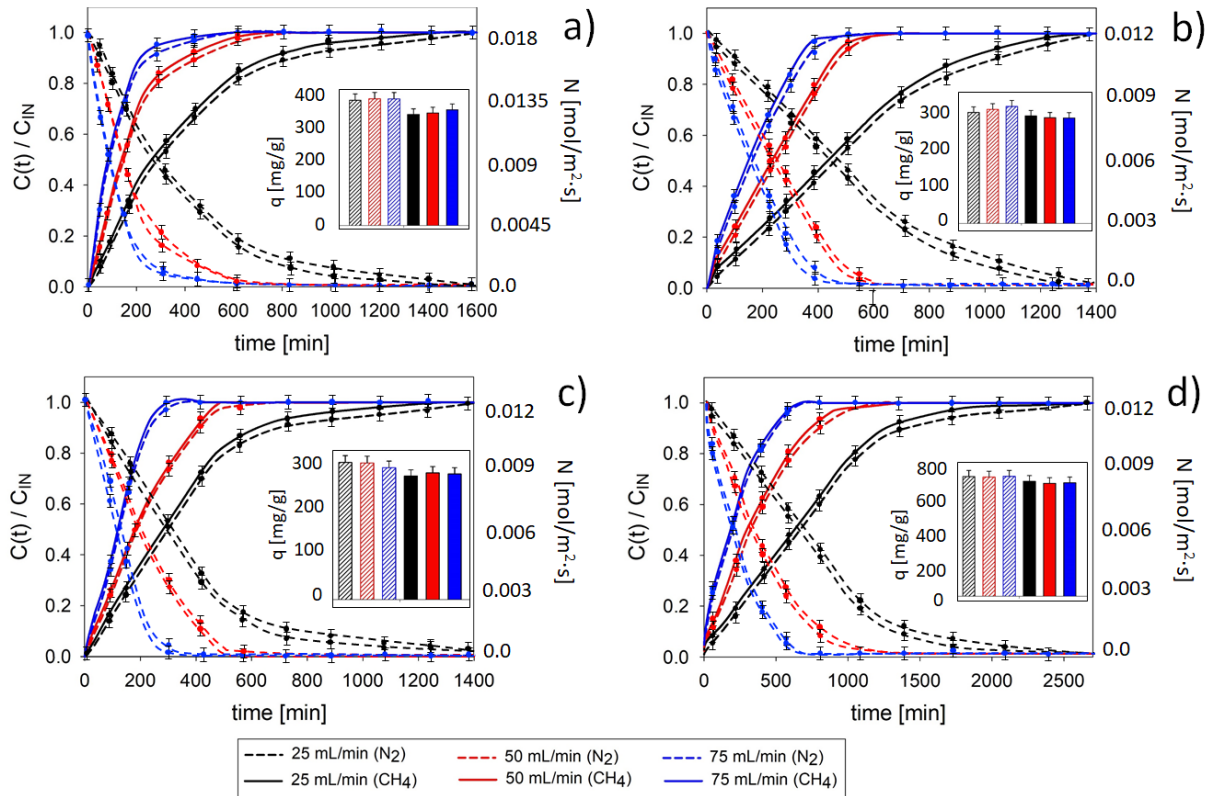
Figure S12 Experimental breakthrough curves of a) CF; b) TCM; c) TCE; d) TCEtOH at different gas flow rate for Syr:Lev (1:1) (inlet VOX concentration 0.5 mg/cm³; temperature 20°C).
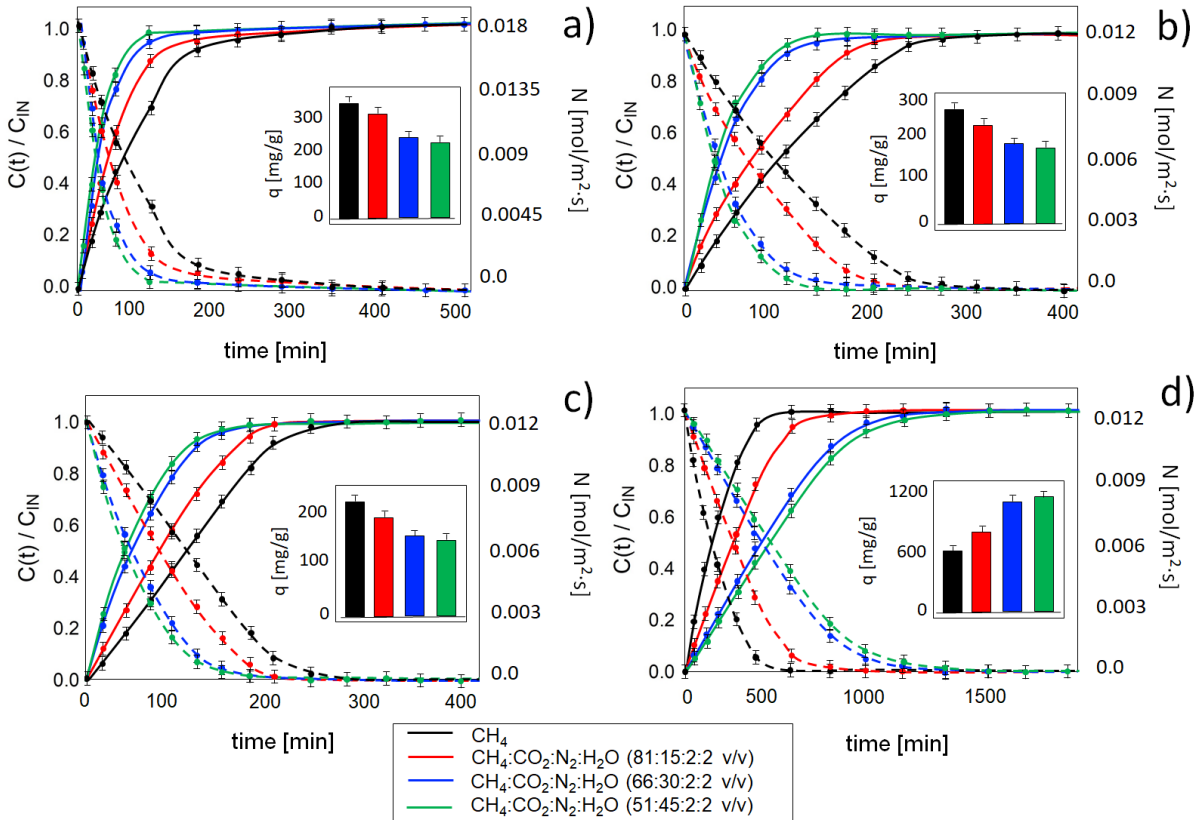
Figure S13 Experimental breakthrough curves of a) CF; b) TCM; c) TCE; d) TCEtOH at different gas matrix (inlet VOX concentration 0.5 mg/cm³; gas flow 50 mL/min; temperature 20°C).
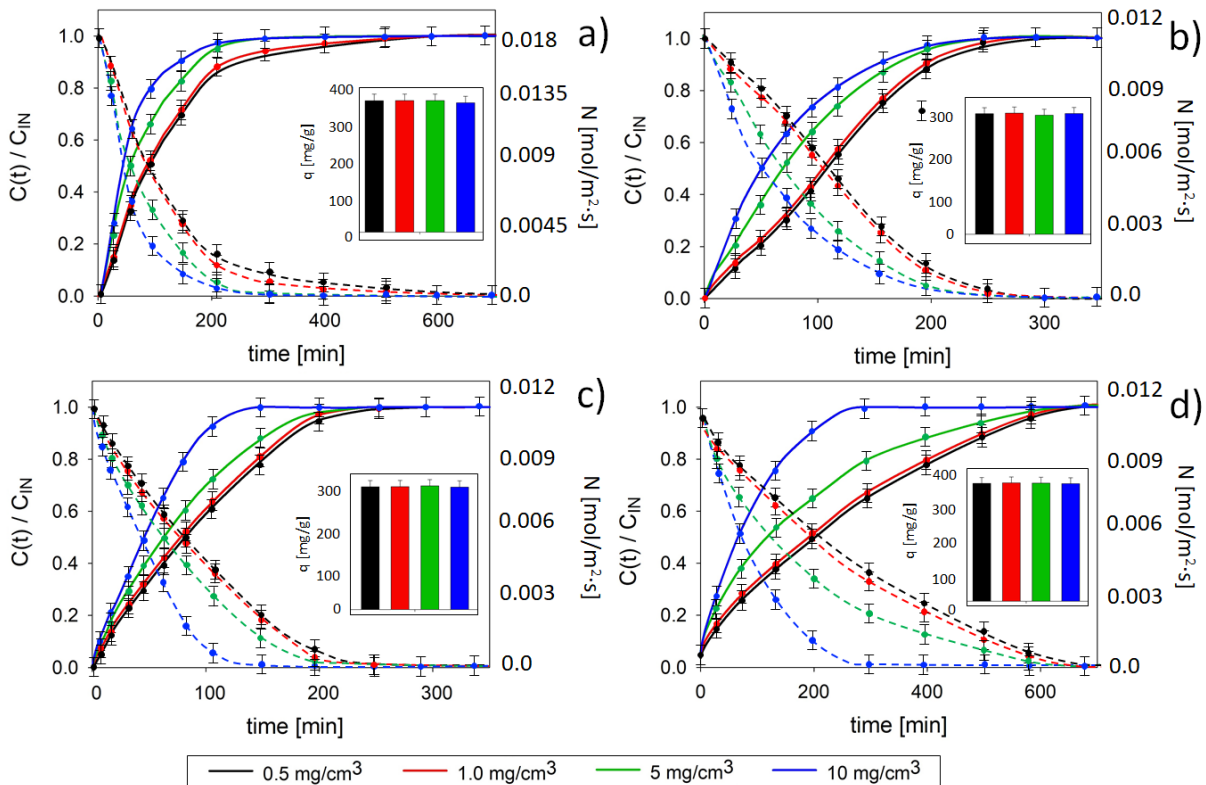
Figure S14 Experimental breakthrough curves of a) CF; b) TCM; c) TCE; d) TCEtOH at different initial concentration for Syr:Lev (1:1) (gas flow 70 mL/min; matrix gas N_2; temperature 20°C).
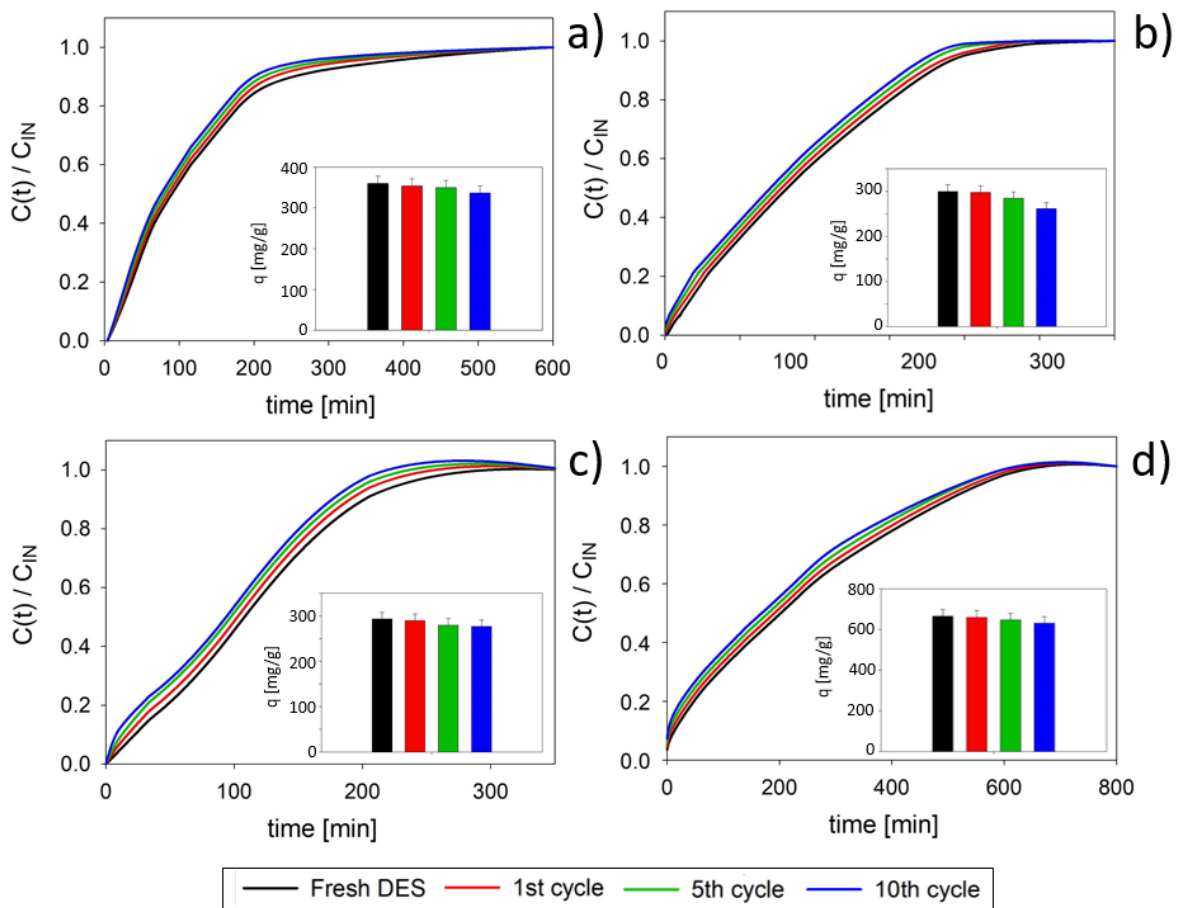
Figure S15 Experimental breakthrough curves of a) CF; b) TCM; c) TCE; d) TCEtOH after absorption/desorption cycles of Syr:Lev (1:1) (gas flow 70 mL/min; matrix gas N_2; temperature 20°C).
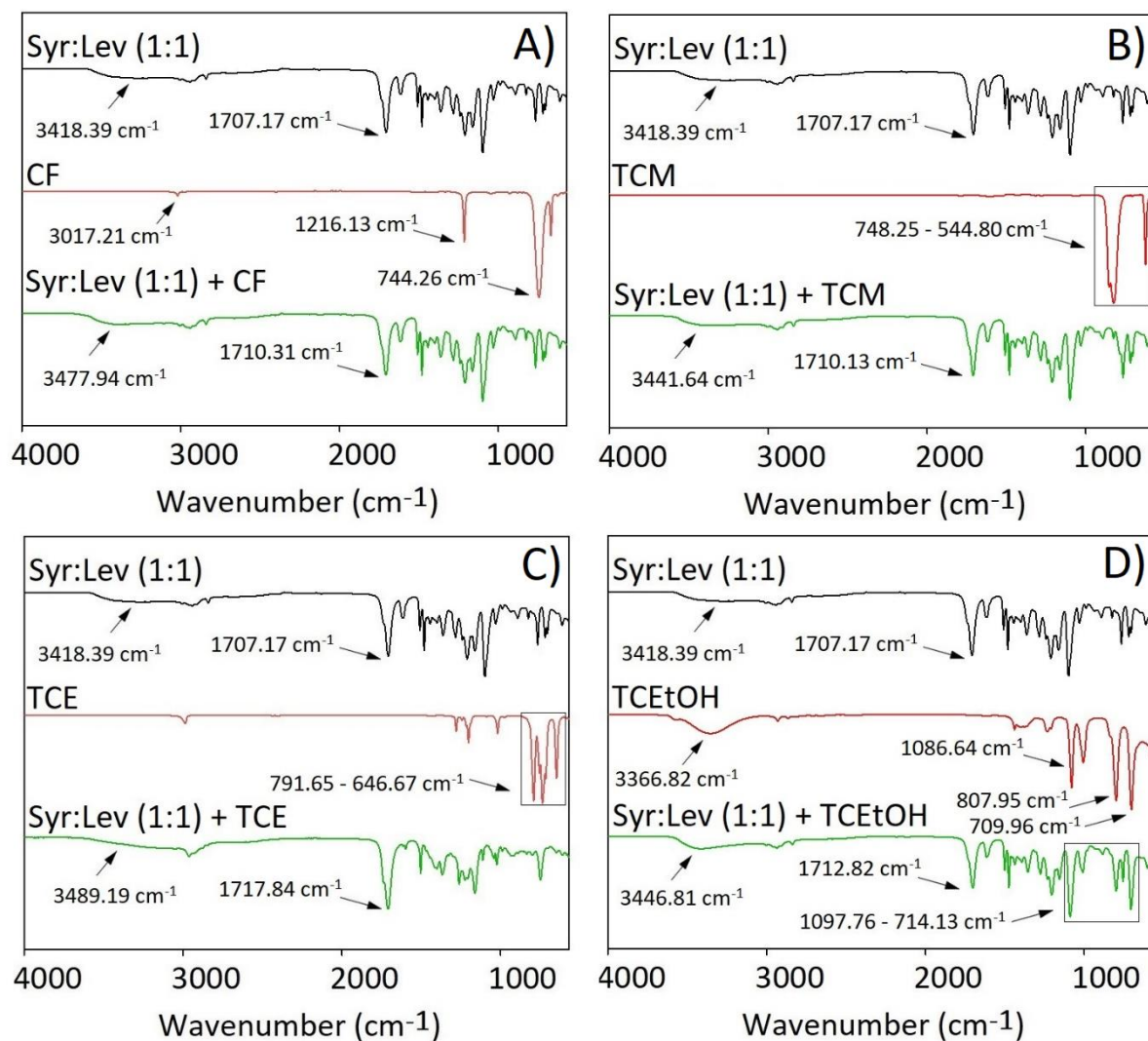
Figure S16 FT-IR spectra of pure Syr:Lev (1:1), pure VOXs, and Syr:Lev (1:1) − VOX complexes: A) Syr:Lev (1:1) − CF; B) Syr:Lev (1:1) - TCM; C) Syr:Lev (1:1) − TCE; D) Syr:Lev (1:1) - TCEtOH.
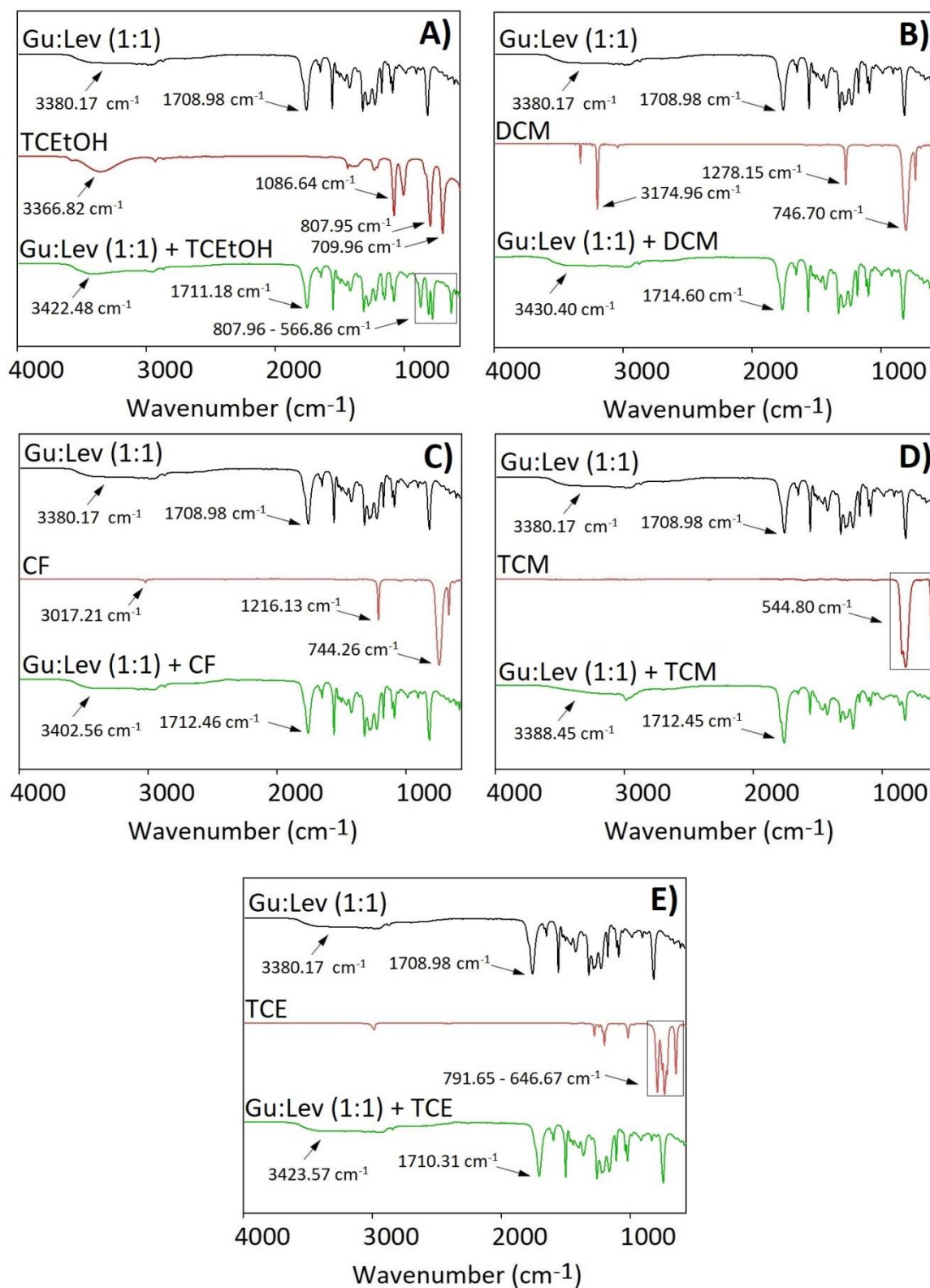
Figure S17 FT-IR spectra of pure Gu:Lev (1:1), pure VOXs, and Gu:Lev (1:1) – VOX complexes: A) Gu:Lev (1:1) - TCEtOH; B) Gu:Lev (1:1) - DCM; C) Gu:Lev (1:1) - CF; D) Gu:Lev (1:1) - TCM; E) Gu:Lev (1:1) – TCE.
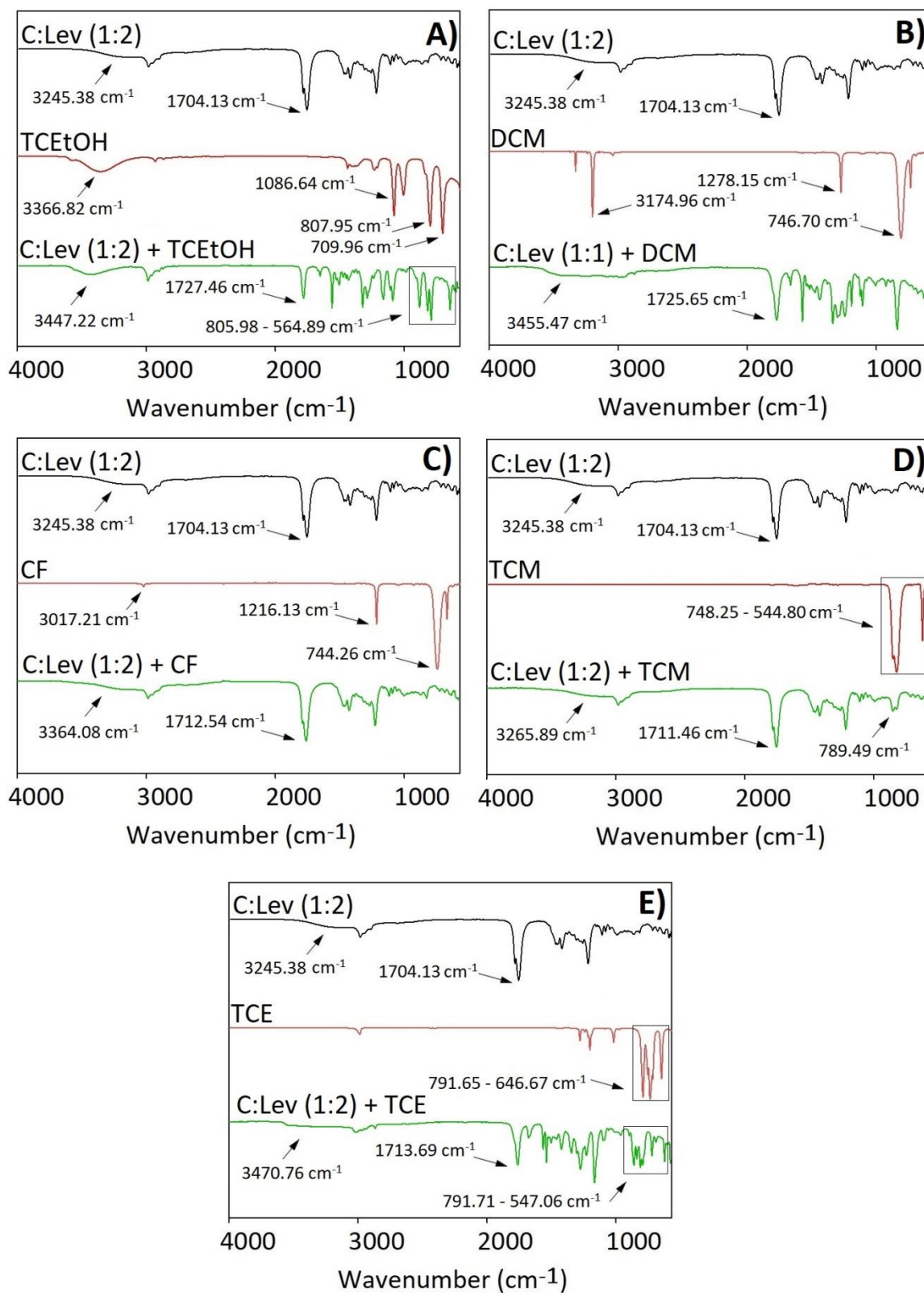
Figure S18 FT-IR spectra of pure C:Lev (1:2), pure VOXs, and C:Lev (1:2) – VOX complexes: A) C:Lev (1:2) - TCEtOH; B) C:Lev (1:2) - DCM; C) C:Lev (1:2) - CF; D) C:Lev (1:2) - TCM; E) C:Lev (1:2) – TCE.
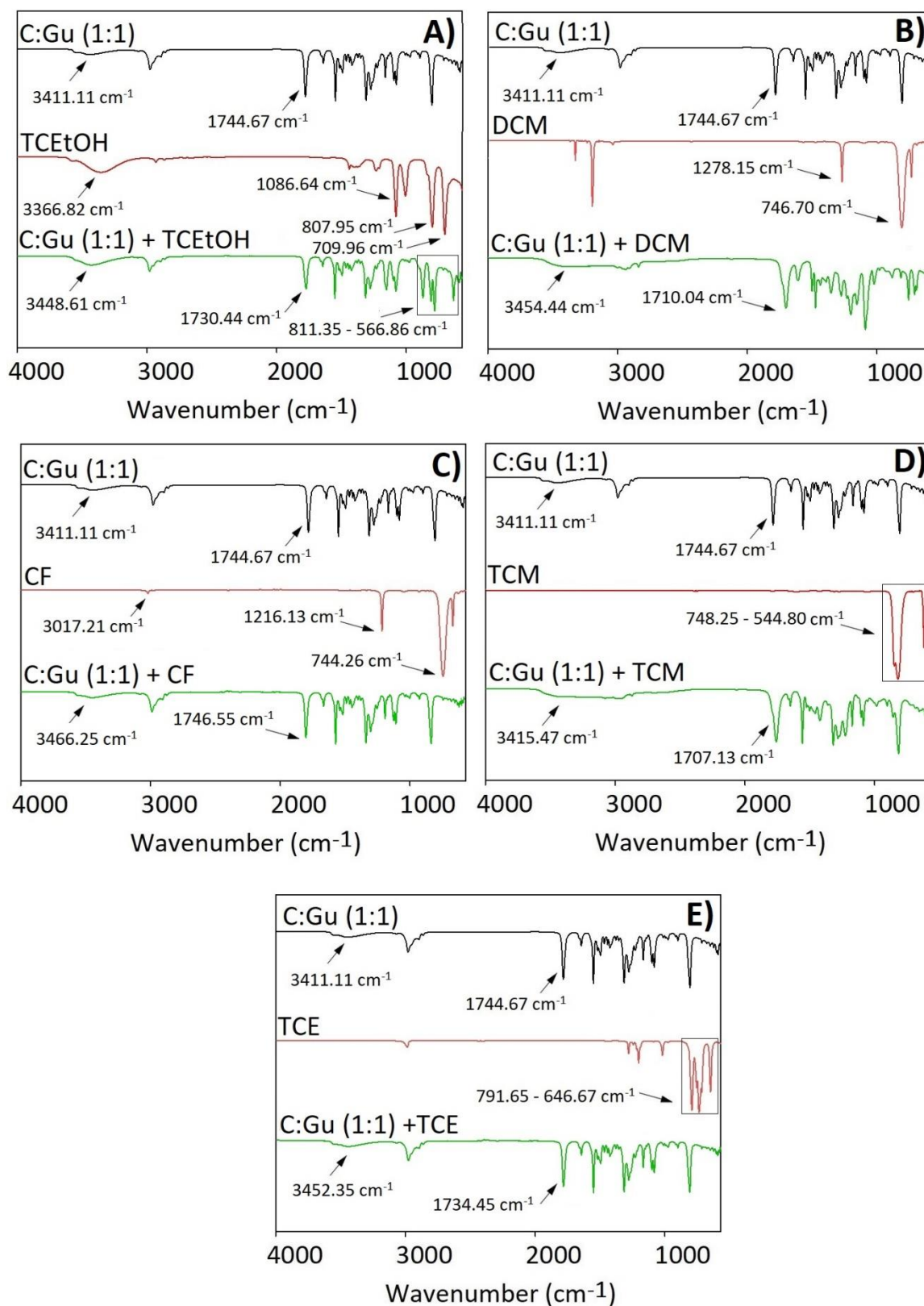
Figure S19 FT-IR spectra of pure C:Gu (1:1), pure VOXs, and C:Gu (1:1) – VOX complexes: A) C:Gu (1:1) - TCEtOH; B) C:Gu (1:1) - DCM; C) C:Gu (1:1) - CF; D) C:Gu (1:1) - TCM; E) C:Gu (1:1) – TCE.
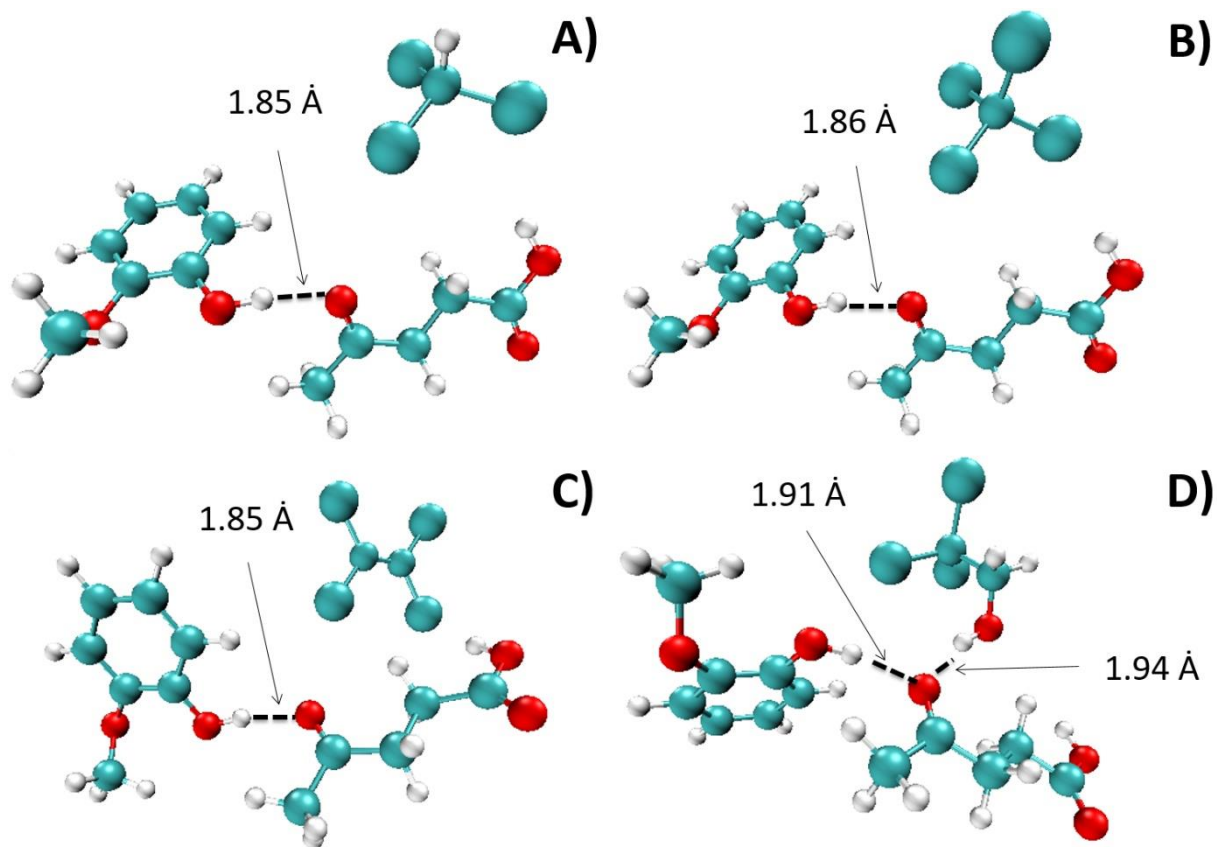
Figure S20 The structures of Syr:Lev (1:1) – VOX complexes after geometric optimization: a) A) Syr:Lev (1:1) – CF; B) Syr:Lev (1:1) – TCM; C) Syr:Lev (1:1) – TCE; D) Syr:Lev (1:1) – TCEtOH.
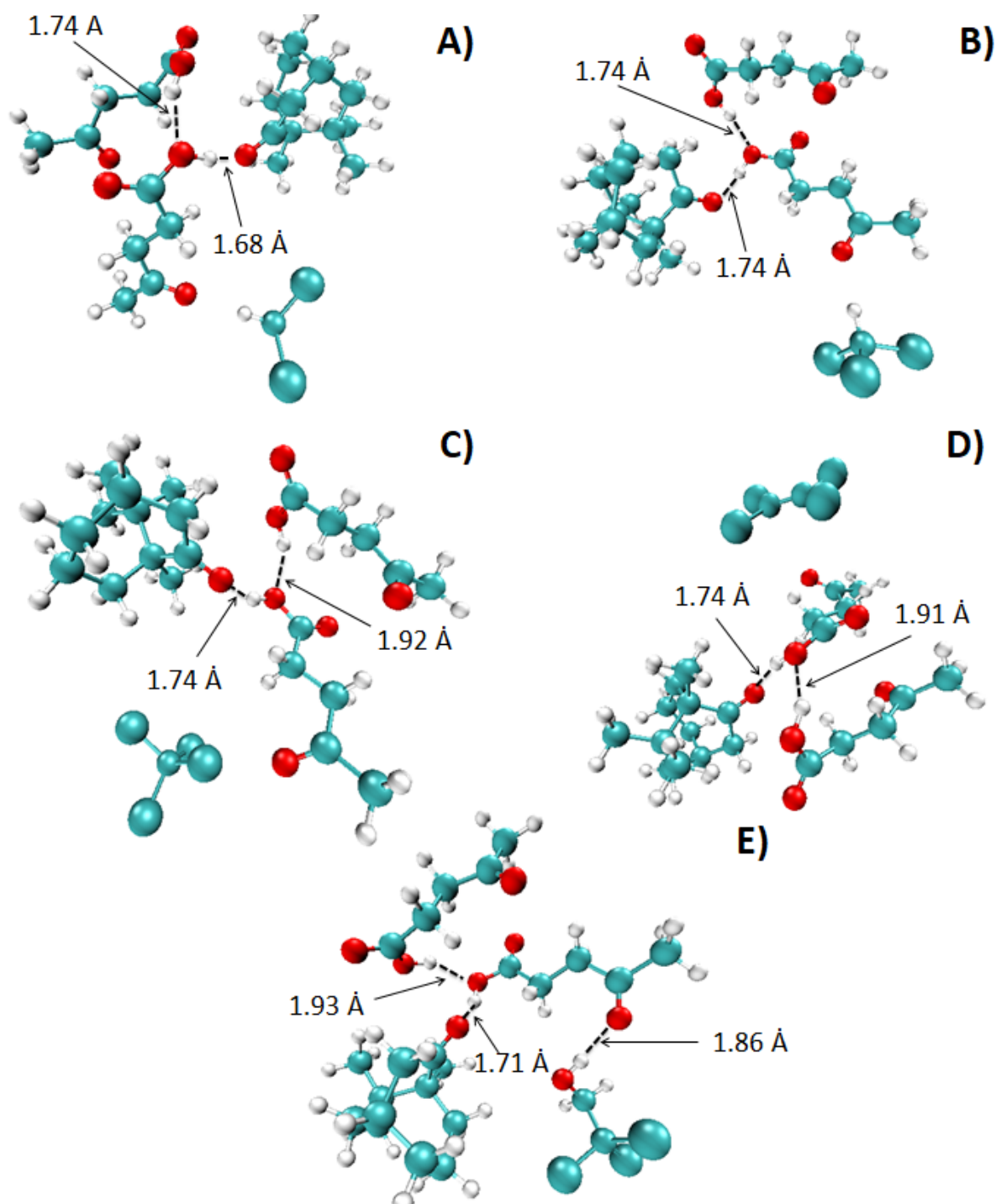
Figure S21 The structures of C:Lev (1:2) – VOX complexes after geometric optimization: A) C:Lev (1:2) – DCM; B) C:Lev (1:2)–CF; C) C:Lev (1:2) – TCM; D) C:Lev (1:2) – TCE; E) C:Lev (1:2) – TCEtOH.
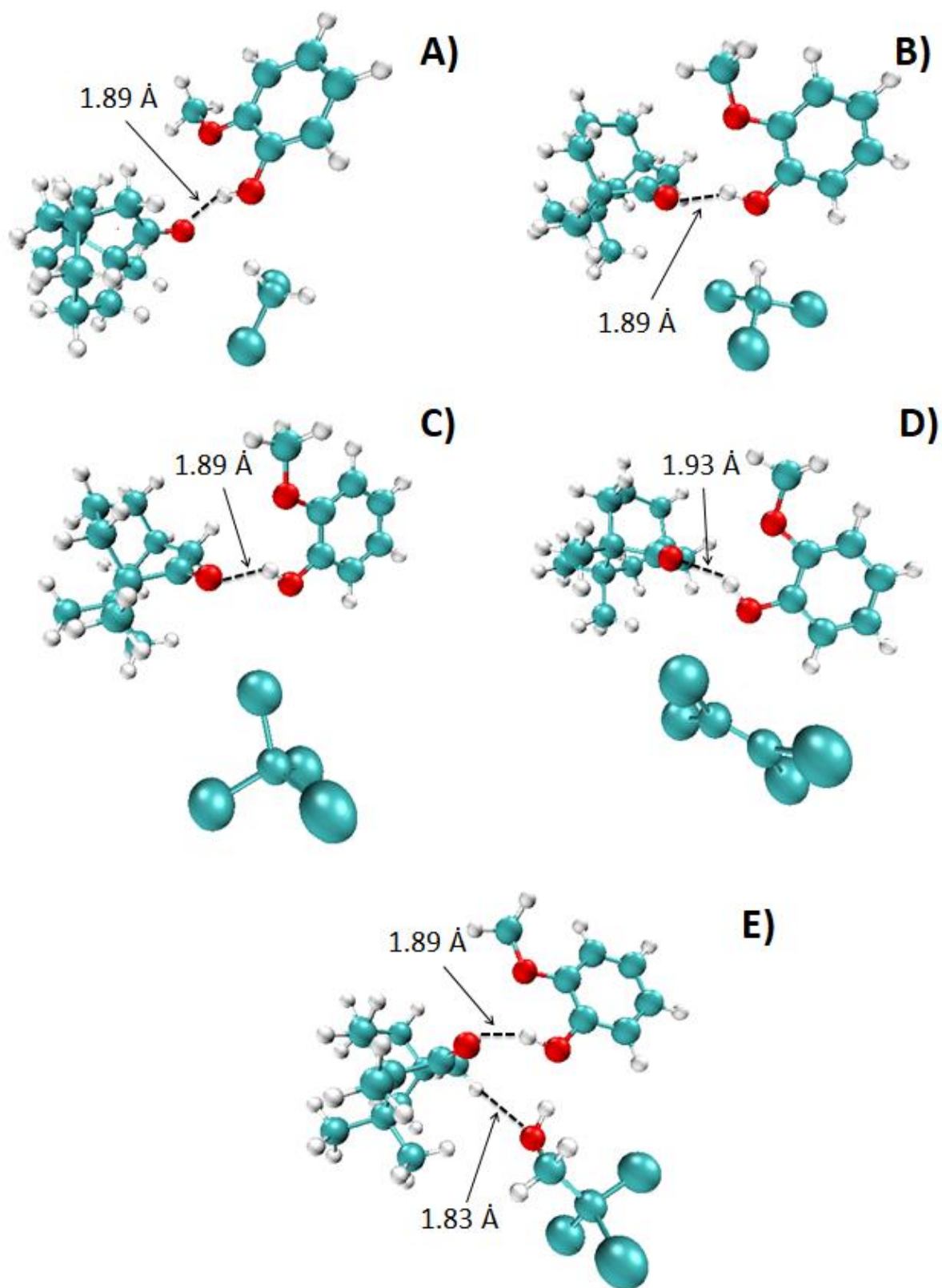
Figure S22 The structures of C:Gu (1:1) – VOX complexes after geometric optimization: A) C:Gu (1:1) – DCM; B C:Gu (1:1) - CF; C) C:Gu (1:1) – TCM; D) C:Gu (1:1) – TCE; E) C:Gu (1:1) – TCEtOH.
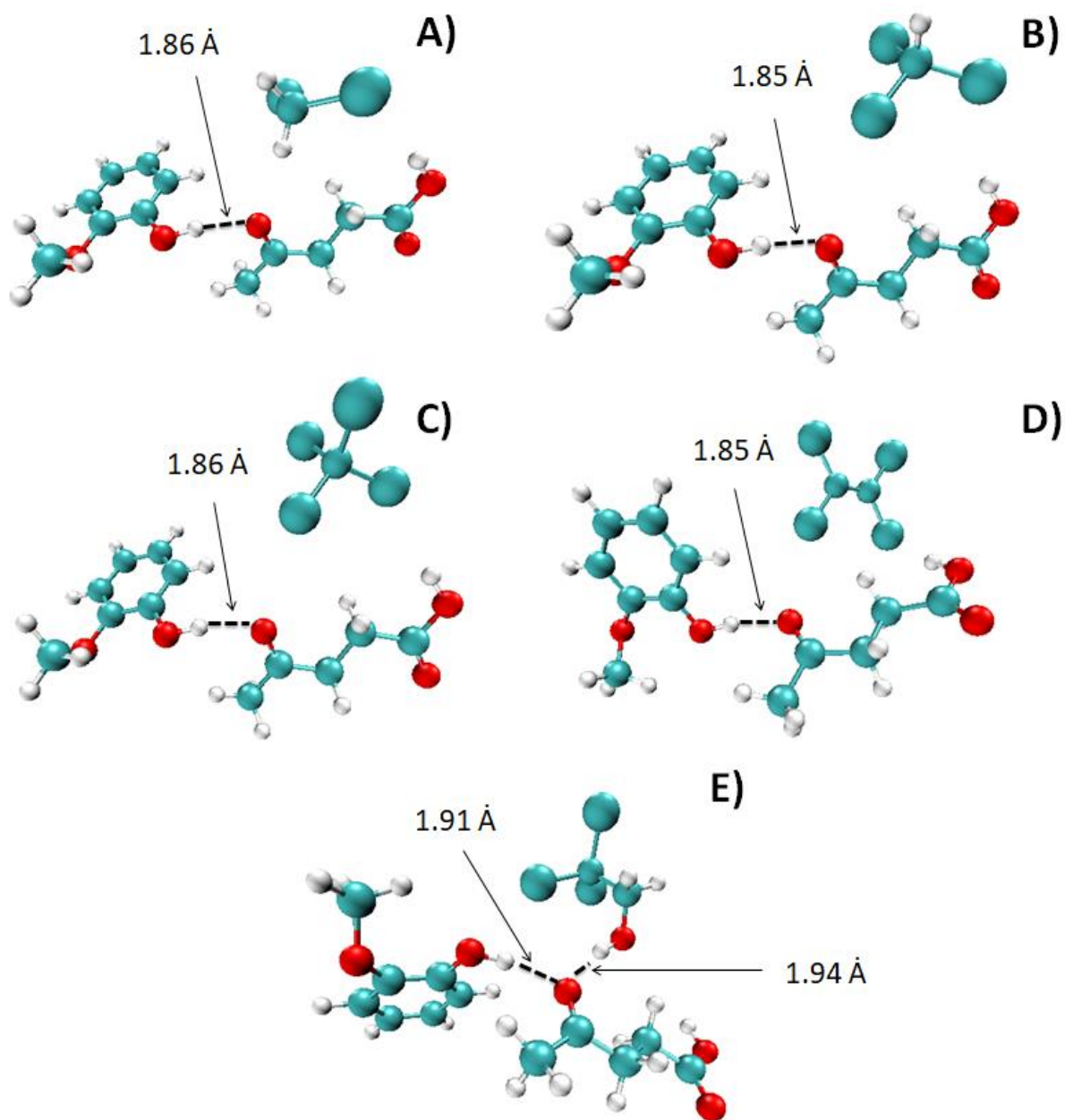
Figure S23 The structures of Gu:Lev (1:1) – VOX complexes after geometric optimization: A) Gu:Lev (1:1) – DCM; B Gu:Lev (1:1) - CF; C) Gu:Lev (1:1) – TCM; D) Gu:Lev (1:1) – TCE; E) Gu:Lev (1:1)– TCEtOH.
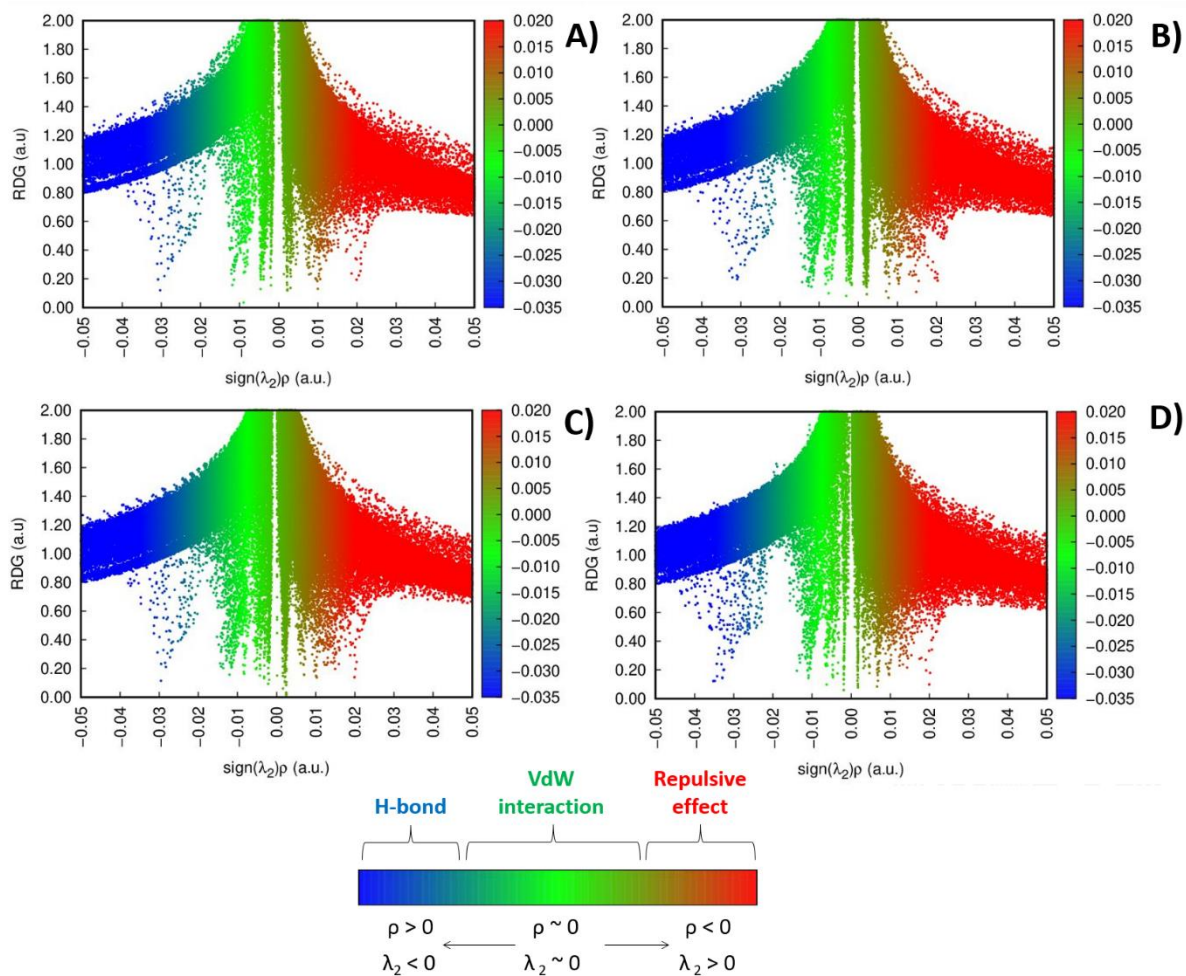
Figure S24 2D plots of RDG versus the electron density multiplied by the sign of the second Hessian eigenvalue for: ASyr:Lev (1:1) – CF; B) Syr:Lev (1:1) – TCM; C) Syr:Lev (1:1) – TCE; D) Syr:Lev (1:1) – TCEtOH. The red area represents repulsive effects; blue area - H-bonding; green area - van der Waals interactions.
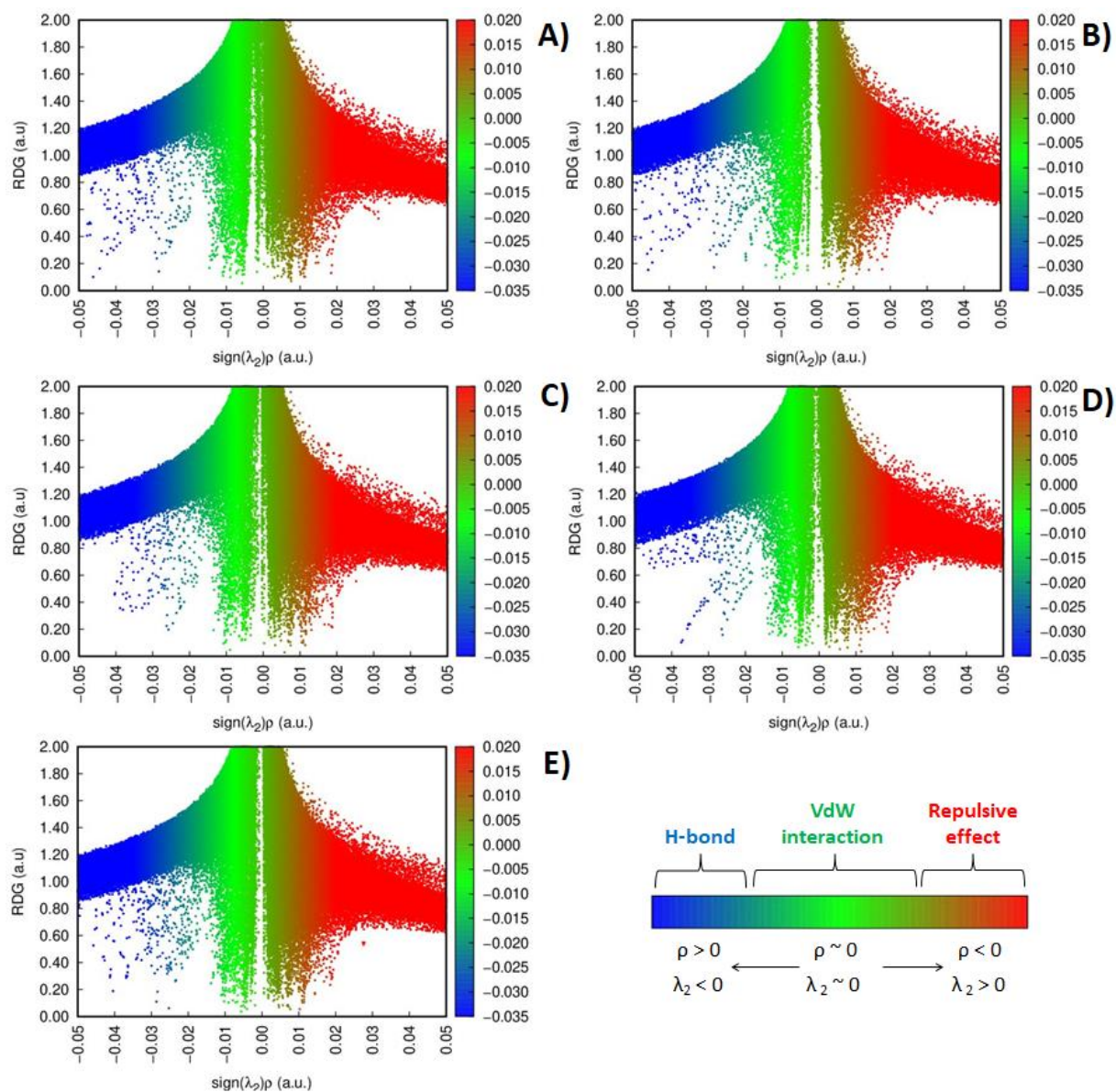
Figure S25 2D plots of RDG versus the electron density multiplied by the sign of the second Hessian eigenvalue for: A) C:Lev (1:2) − DCM; B) C:Lev (1:2)–CF; C) C:Lev (1:2)– TCM; D) C:Lev (1:2)– TCE; E) C:Lev (1:2)– TCEtOH. The red area represents repulsive effects; blue area - H-bonding; green area -van der Waals interactions.
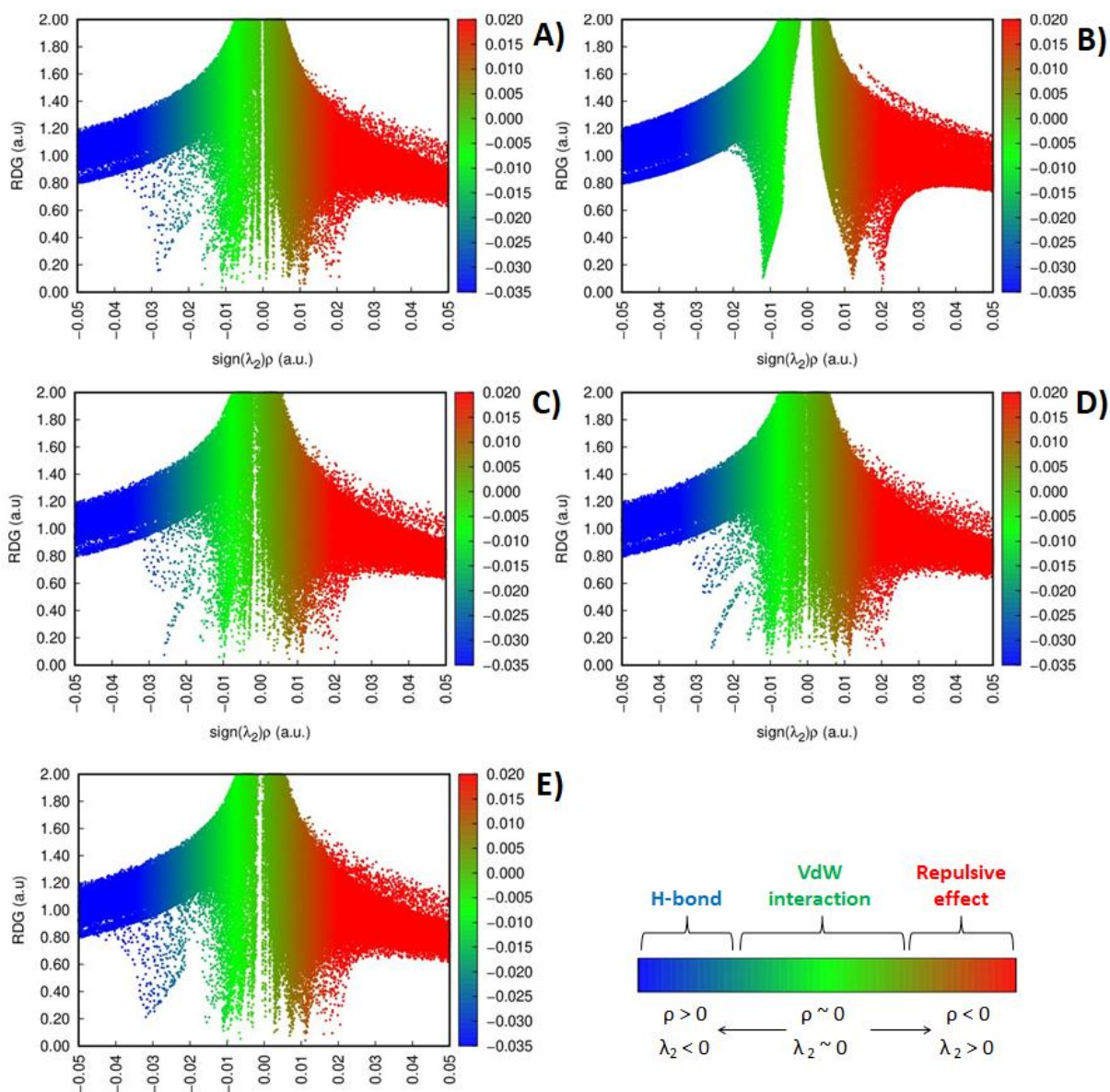
Figure S26 2D plots of RDG versus the electron density multiplied by the sign of the second Hessian eigenvalue for: A) C:Gu (1:1) – DCM; B) C:Gu (1:1) –CF; C) C:Gu (1:1) – TCM; D) C:Gu (1:1) – TCE; E) C:Gu (1:1) – TCEtOH. The red area represents repulsive effects; blue area - H-bonding; green area -van der Waals interactions.
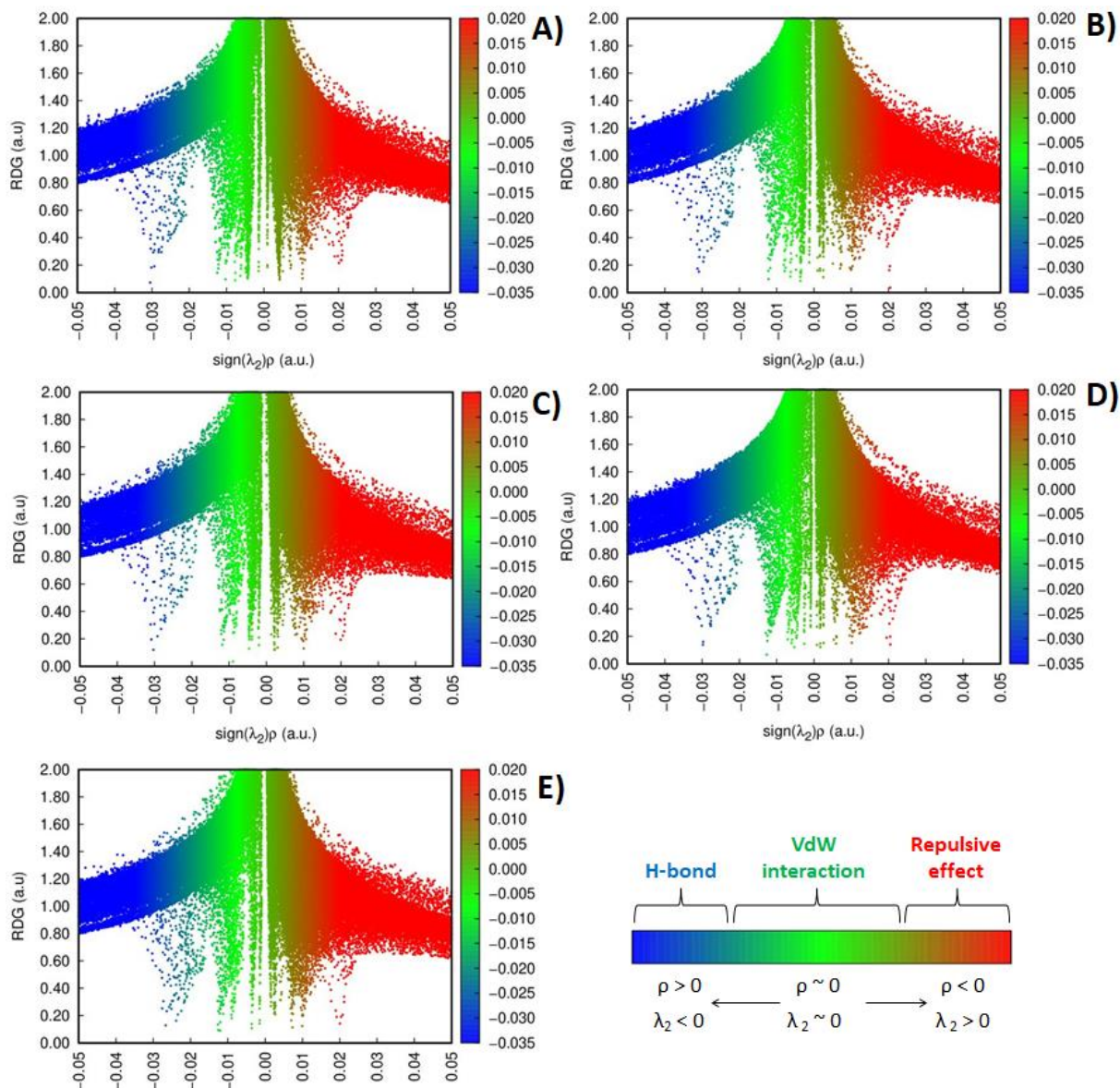
Figure S27 2D plots of RDG versus the electron density multiplied by the sign of the second Hessian eigenvalue for: A) G:Lev (1:1) – DCM; B) G:Lev (1:1) –CF; C) G:Lev (1:1) – TCM; D) G:Lev (1:1) – TCE; E) G:Lev (1:1) – TCEtOH. The red area represents repulsive effects; blue area - H-bonding; green area -van der Waals interactions.
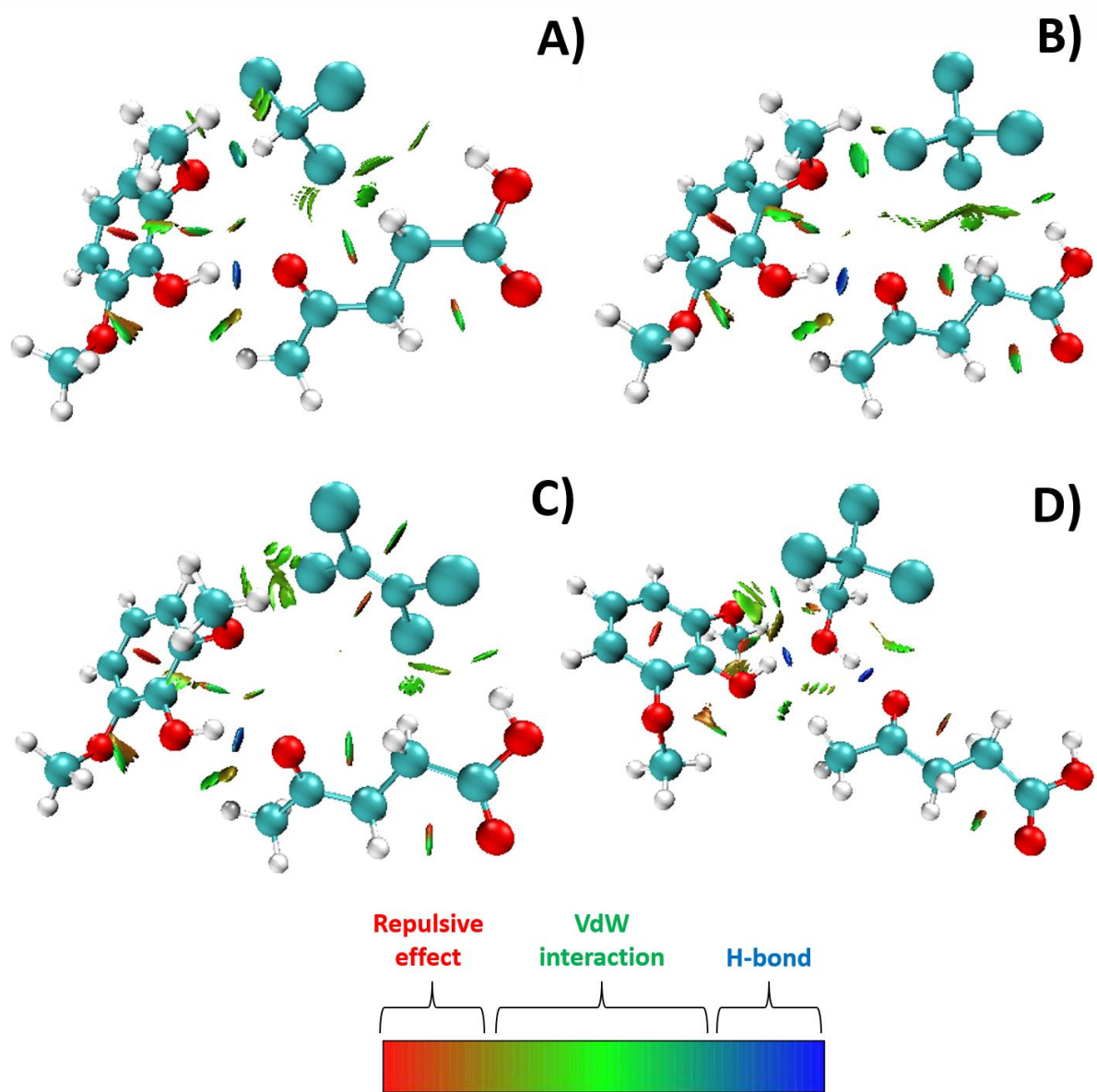
Figure S28 Reduced density gradient (RDG) isosurfaces (s=0.5 a.u.) of studied DES-VOX complexes: A) Syr:Lev (1:1) – CF; B) Syr:Lev (1:1) – TCM; C) Syr:Lev (1:1) – TCE; D) Syr:Lev (1:1) – TCEtOH. The red area represents repulsive effects; blue area - H-bonding; green area – van der Waals interactions.
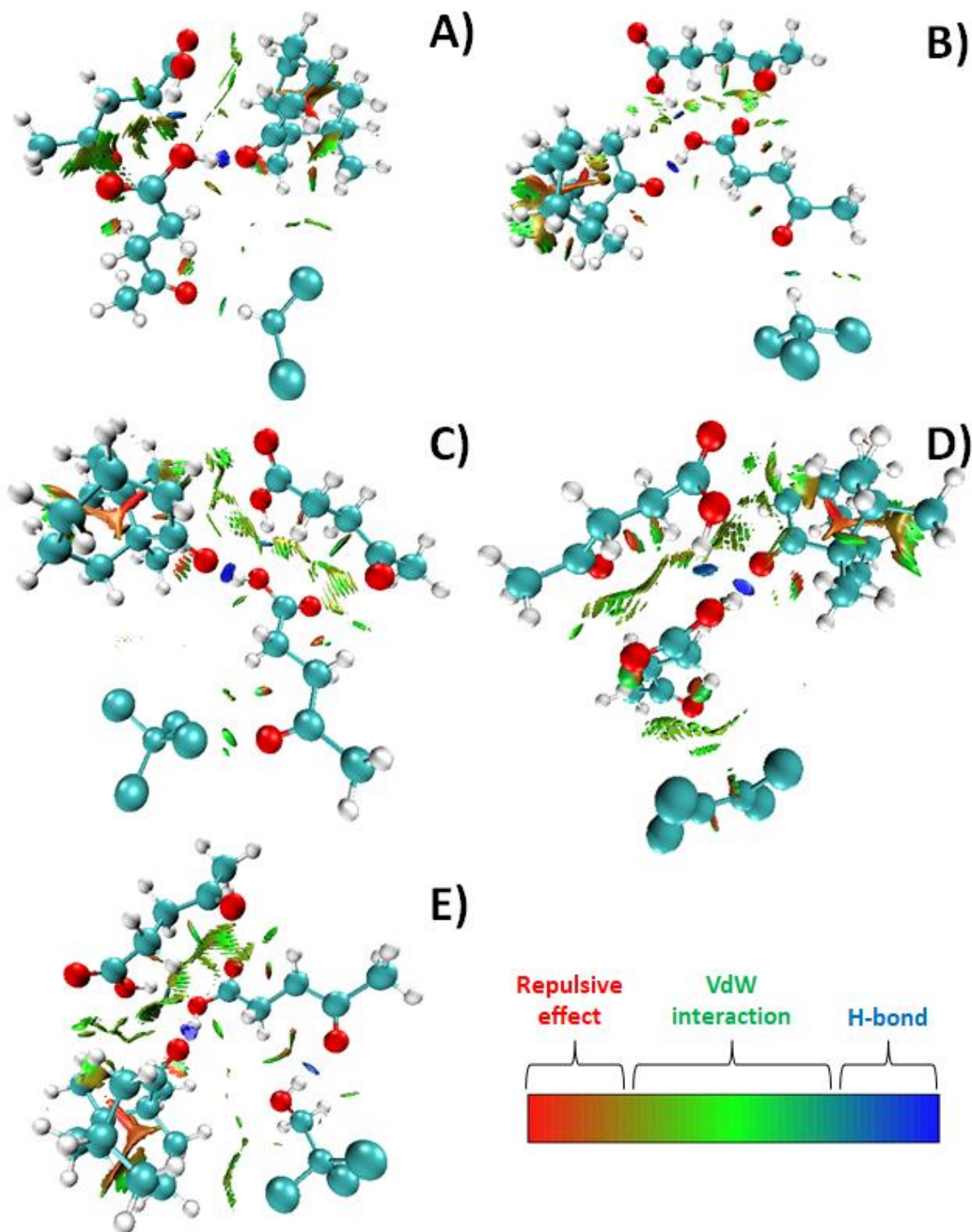
Figure S29 Reduced density gradient (RDG) isosurfaces (s=0.5 a.u.) of studied DES-VOX complexes: A) C:Lev (1:2) – DCM; B) C:Lev (1:2)–CF; C) C:Lev (1:2)– TCM; D) C:Lev (1:2)– TCE; E) C:Lev (1:2)– TCEtOH. The red area represents repulsive effects; blue area - H-bonding; green area -van der Waals interactions.
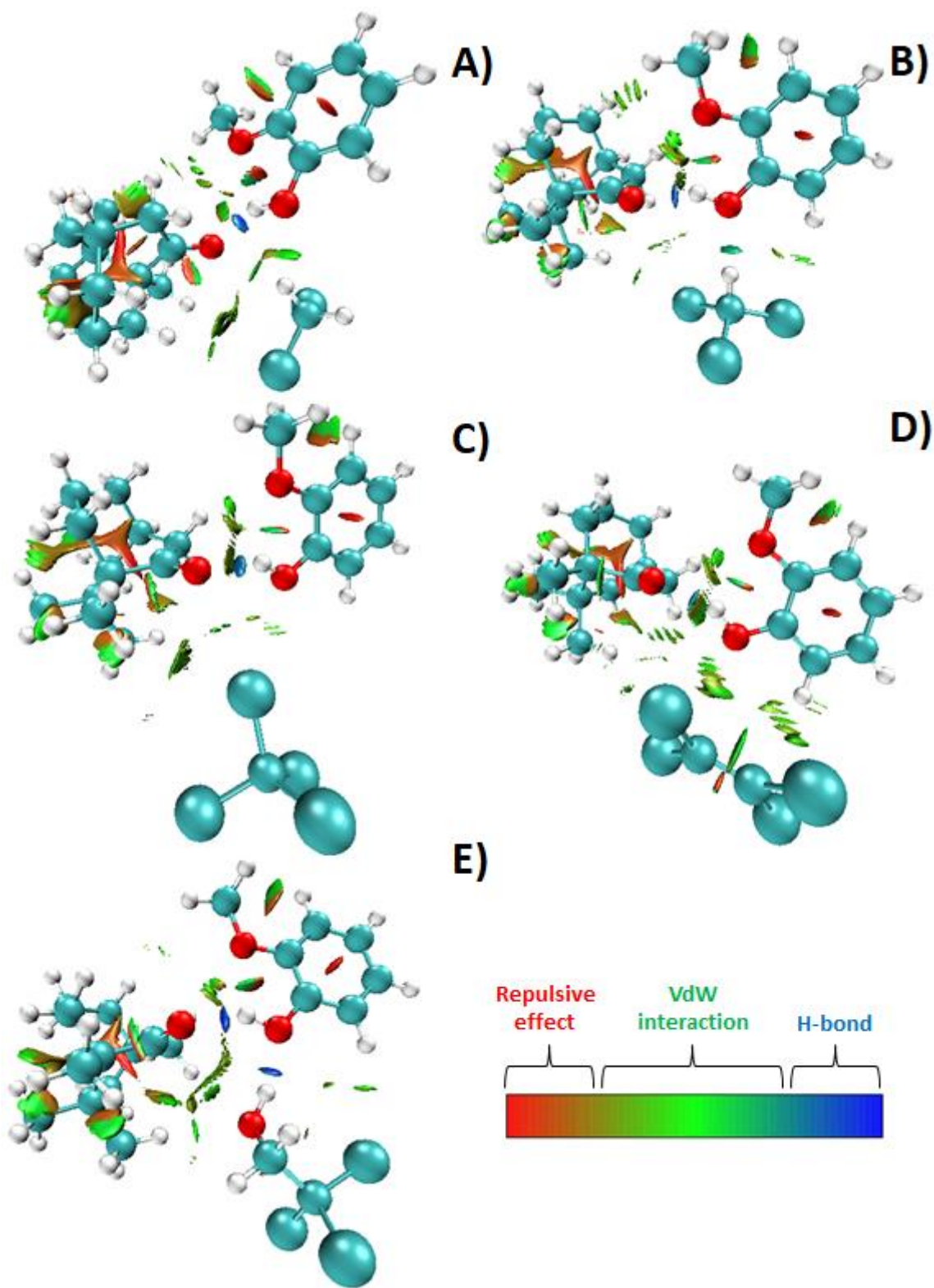
Figure S30 Reduced density gradient (RDG) isosurfaces (s=0.5 a.u.) of studied DES-VOX complexes: A) C:Gu (1:1) – DCM; B) C:Gu (1:1) –CF; C) C:Gu (1:1) – TCM; D) C:Gu (1:1) – TCE; E) C:Gu (1:1) – TCEtOH. The red area represents repulsive effects; blue area - H-bonding; green area -van der Waals interactions.
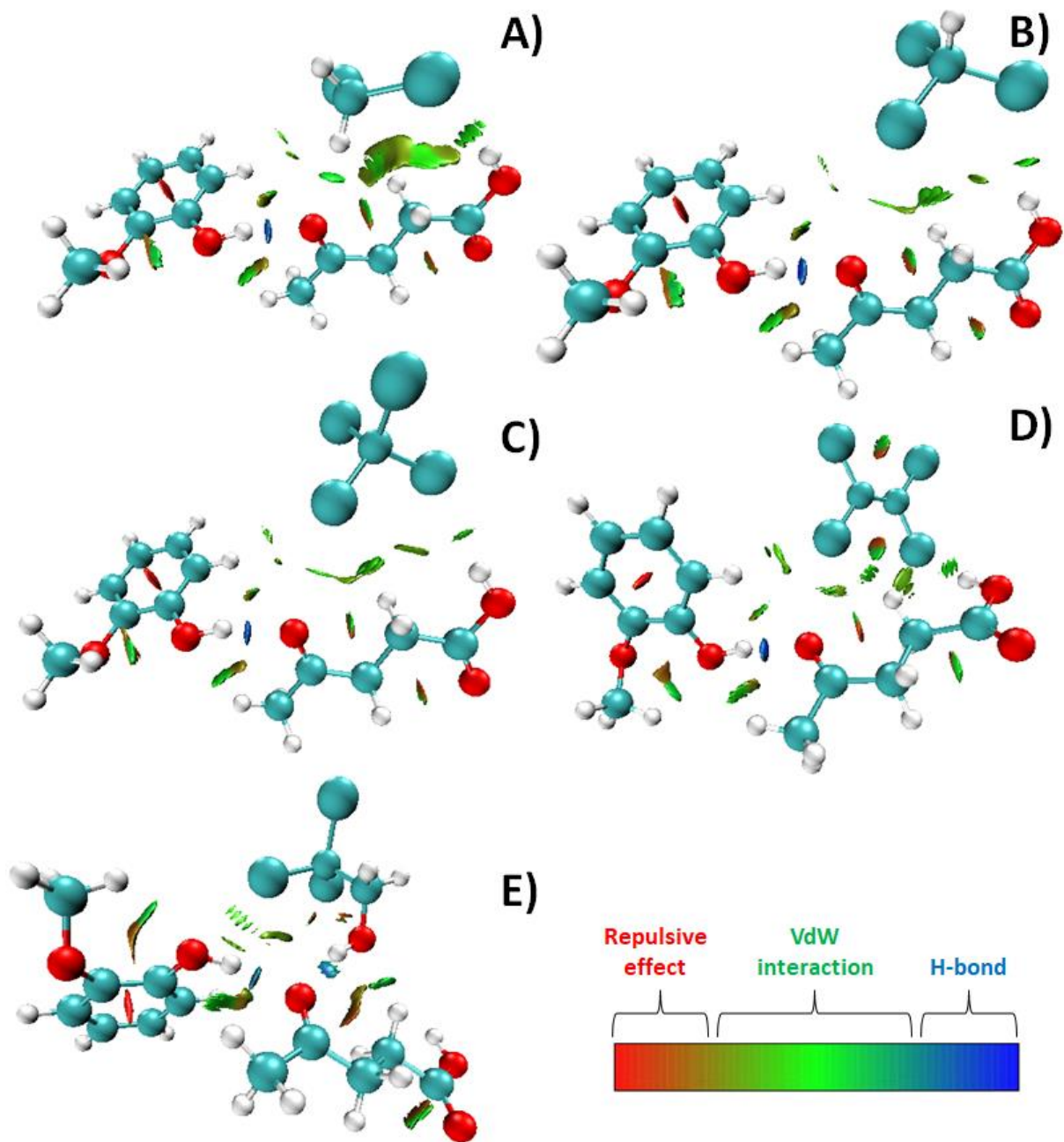
Figure S31 Reduced density gradient (RDG) isosurfaces (s=0.5 a.u.) of studied DES-VOX complexes: A) G:Lev (1:1) – DCM; B) G:Lev (1:1) –CF; C) G:Lev (1:1) – TCM; D) G:Lev (1:1) – TCE; E) G:Lev (1:1) – TCEtOH. The red area represents repulsive effects; blue area - H-bonding; green area -van der Waals interactions.
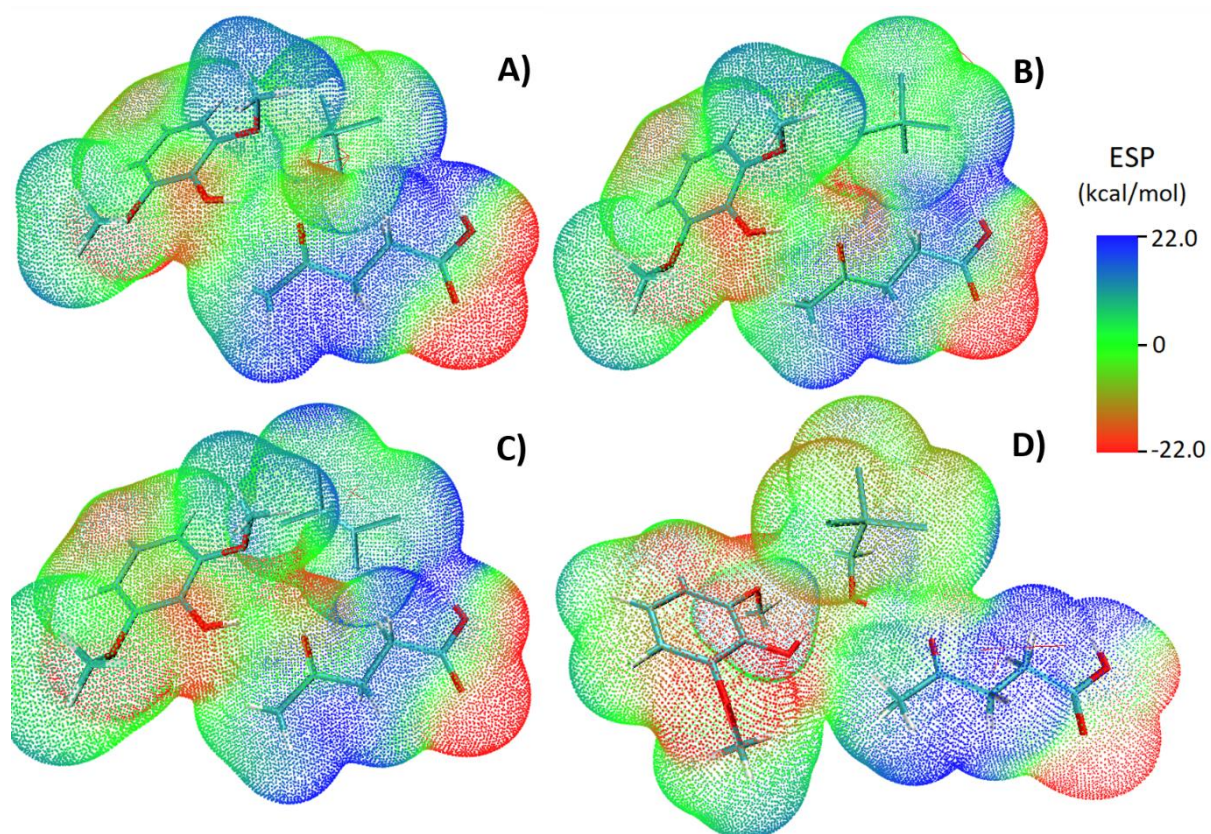
Figure S32 Electrostatic potential (ESP) mapped on electron total density with an isovalue 0.001 for: A) Syr:Lev (1:1) – CF; B) Syr:Lev (1:1) – TCM; C) Syr:Lev (1:1) – TCE; D) Syr:Lev (1:1) – TCEtOH. Blue area are positively charged; red regions are negatively charged; green are neutrally charged.
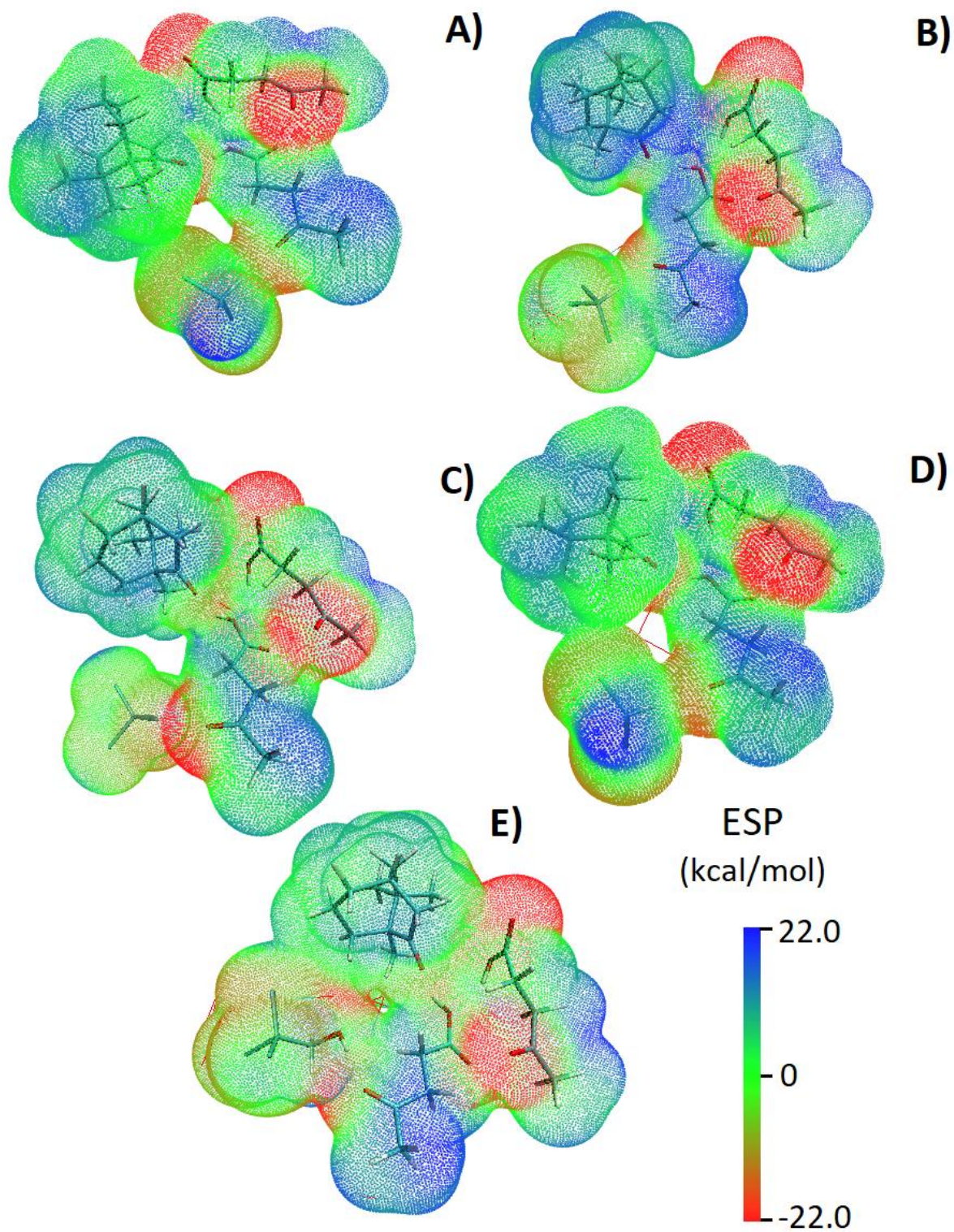
Figure S33 Electrostatic potential (ESP) mapped on electron total density with an isovalue 0.001 for: A) C:Lev (1:2) – DCM; B) C:Lev (1:2)–CF; C) C:Lev (1:2)– TCM; D) C:Lev (1:2)– TCE; E) C:Lev (1:2)– TCEtOH. Blue area are positively charged; red regions are negatively charged; green are neutrally charged.
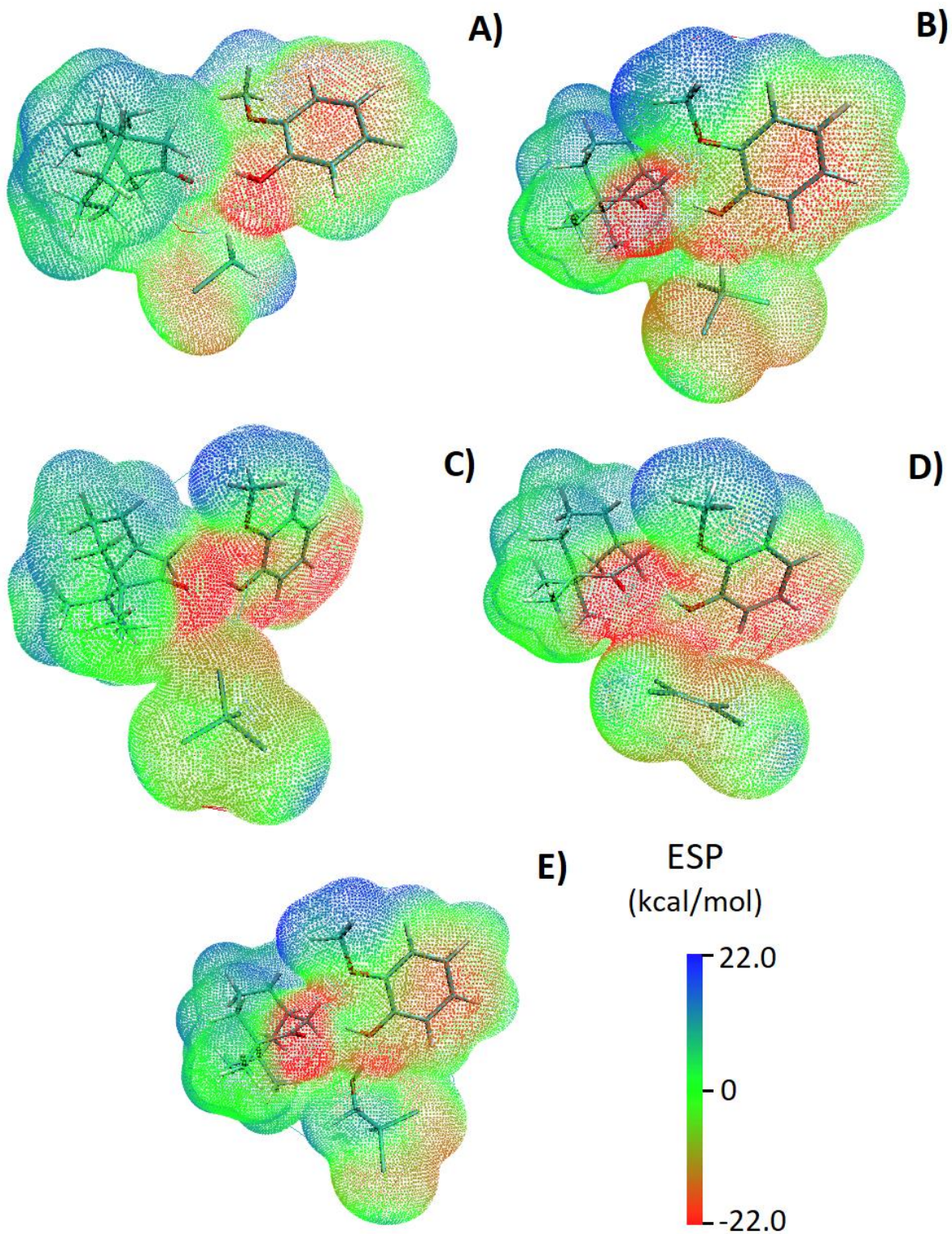
Figure S34 Electrostatic potential (ESP) mapped on electron total density with an isovalue 0.001 for: A) C:Gu (1:1) – DCM; B) C:Gu (1:1) - CF; C) C:Gu (1:1)– TCM; D) C:Gu (1:1)– TCE; E) C:Gu (1:1)– TCEtOH. Blue area are positively charged; red regions are negatively charged; green are neutrally charged.
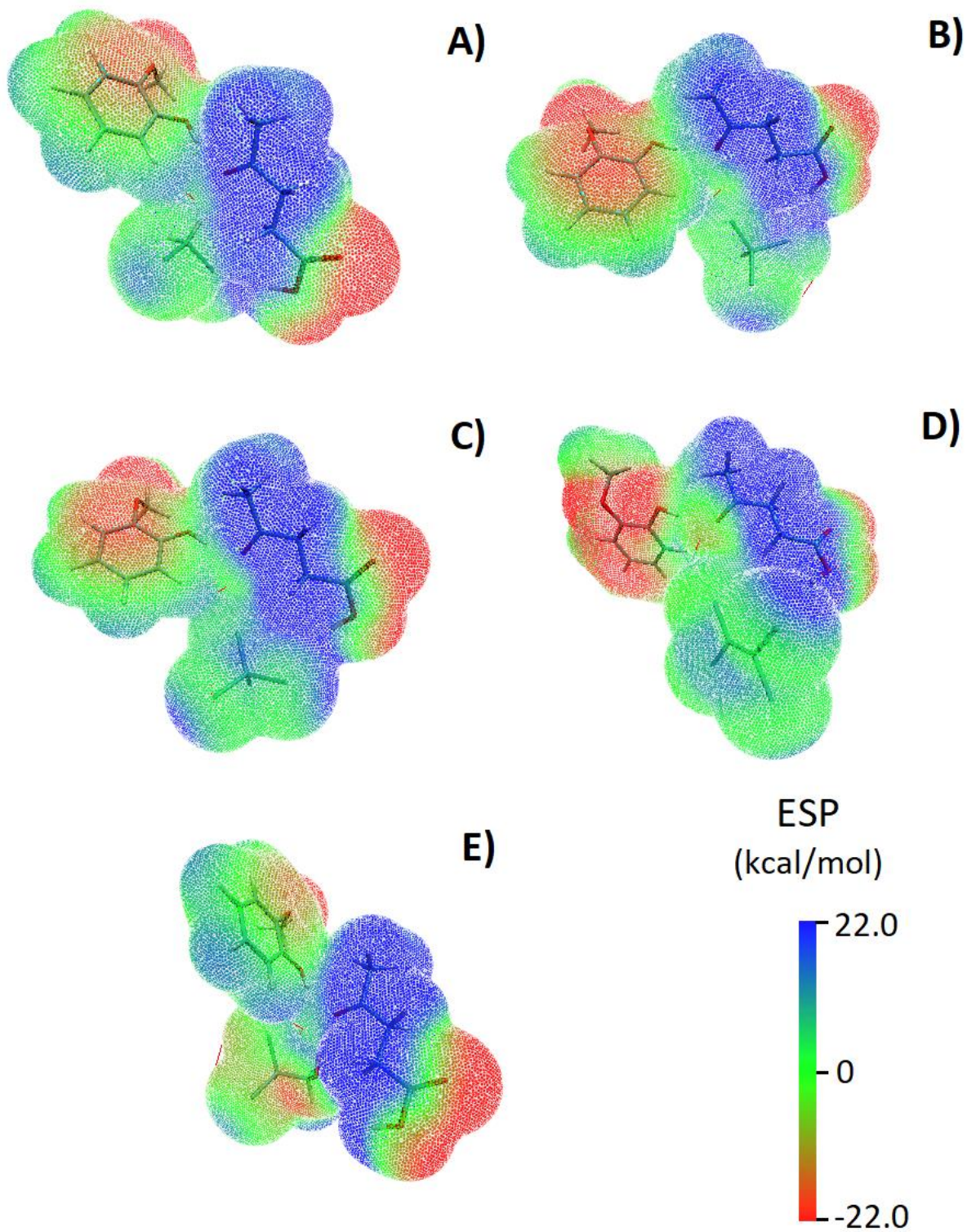
Figure S35 Electrostatic potential (ESP) mapped on electron total density with an isovalue 0.001 for: A) G:Lev (1:1) – DCM; B) G:Lev (1:1) –CF; C) G:Lev (1:1) – TCM; D) G:Lev (1:1) – TCE; E) G:Lev (1:1) – TCEtOH. Blue area are positively charged; red regions are negatively charged; green are neutrally charged.

Table S1 Comparison of the developed procedure of VOX absorption with other absorption or adsorption procedures.

Sorbent type	Type of VOX	Capacity [mg/g]	Gas type	Process conditions	Sorbent price per 1 kg	Ref.
ChCl:U (1:2)	DCM	0.2	air	Temperature: 30°C Flow rate: n.d. Pressure: n.d.	44.6 €	[1]
ChCl:EG (1:2)	DCM	0.26	air	Temperature: 30°C Flow rate: n.d. Pressure: n.d.	37.5 €	[1]
ChCl:Gly (1:2)	DCM	0.24	air	Temperature: 30°C Flow rate: n.d. Pressure: n.d.	40.1 €	[1]
ChCl:Lev (1:2)	DCM	0.27	air	Temperature: 30°C Flow rate: n.d. Pressure: n.d.	42.5 €	[1]
TBPB:Gly (1:1)	DCM	0.28	air	Temperature: 30°C Flow rate: n.d. Pressure: n.d.	199.9 €	[1]
TBPB:Lev (1:6)	DCM	0.29	air	Temperature: 30°C Flow rate: n.d. Pressure: n.d.	76.1 €	[1]
TBAB:DA (1:2)	DCM	0.3	air	Temperature: 30°C Flow rate: n.d. Pressure: n.d.	320.5 €	[1]
UiO-66	DCM	510.3	air	Temperature: 25°C Pressure: 44 kPa	79207.20 €	[2]
activated carbon	CF DCM CM	213.4 123.9 22.2	N_2	Temperature: 35°C Flow rate: 100 mL/min Pressure: 1.5 atm	12.16 €	[3]
ZIF-8/graphene oxide	DCM	240.0	air	Temperature: 25°C Flow rate: 20 ml/min.	7689.0 €	[4]
[Bmim][NTf2]	DCM	100	air	Temperature: 30°C Flow rate: n.d. Pressure: 10 kPa	950 €	[5]
[Bmim][PF6]	DCM	110	air	Temperature: 30°C Flow rate: n.d. Pressure: 10 kPa	2450.8 €	[5]
[Bmim][BF4]	DCM	130	air	Temperature: 30°C Flow rate: n.d. Pressure: 10 kPa	750 €	[5]
[Bmim][DCA]	DCM	140	air	Temperature: 30°C Flow rate: n.d. Pressure: 10 kPa	2494.5 €	[5]
[Bmim][SCN]	DCM	150	air	Temperature: 30°C Flow rate: n.d. Pressure: 10 kPa	892.8 €	[5]
[Emim][SCN]	DCM	120	air	Temperature: 30°C Flow rate: n.d. Pressure: 10 kPa	4934	[5]
Gu:C:Lev (1:1:3)	DCM	55	N_2	Temperature: 25°C Flow rate: 50 mL/min Pressure: 10 kPa	29.0 €	[6]
Syr:Lev (1:1)	DCM CF TCM TCE TCEtOH	304 420 360 292 661	Biogas (58% CH_4, 38 CO_2, 2% H_2O, 2% N_2)	Temperature: 25°C Flow rate: 50 mL/min Pressure: 10 kPa	263.5 €	This studies
C:Gu (1:1)	DCM CF TCM	215 561.5 320	Biogas (58% CH_4, 38 CO_2, 2% H_2O, 2% N_2)	Temperature: 25°C Flow rate: 50 mL/min Pressure: 10 kPa	32.78 €	This studies

	TCE	262.4				
	TCEtOH	275.3				
C:Lev (1:2)	DCM	181	Biogas (58% CH_4, 38 CO_2, 2% H_2O, 2% N_2)	Temperature: 25°C Flow rate: 50 mL/min Pressure: 10 kPa	24.02 €	This studies
	CF	401.5				
	TCM	143.5				
	TCE	248				
	TCEtOH	198.15				
Gu:Lev (1:1)	DCM	130.7	Biogas (58% CH_4, 38 CO_2, 2% H_2O, 2% N_2)	Temperature: 25°C Flow rate: 50 mL/min Pressure: 10 kPa	36.01 €	This studies
	CF	399.5				
	TCM	115.8				
	TCE	154				
	TCEtOH	161.2				

[Bmim][NTf2] - *1-Butyl-3-methylimidazolium bis(trifluoromethylsulfonyl)imide;* *[Bmim][PF6]* - *1-Butyl-3-methylimidazolium hexafluorophosphate;* *[Bmim][BF4]* - *1-Butyl-3-methylimidazolium tetrafluoroborate;* *[Bmim][DCA]* - *1-Butyl-3-methylimidazolium dicyanamide;* *[Bmim][SCN]* - *1-Butyl-3-methylimidazolium thiocyanate;* *[Emim][SCN]* - *1-Ethyl-3-methyl-imidazolium-thiocyanate;* *ChCl* – *choline chloride;* *CM*- *Chloromethane;* *DA* – *decanoic acid;* *EG* – *ethylene glycol;* *Gly* – *glycerol;* *U* – *urea;* *UiO-66* - *(Universitetet i Oslo) a metal organic framework;* *TBAB* – *tetrabutylammonium bromide;* *TBPB* - *tetrabutylphosphonium bromide*

References

[1]   L. Moura, T. Moufawad, M. Ferreira, H. Bricout, S. Tilloy, E. Monflier, M. F. Costa Gomes, D. Landy, S. Fourmentin, *Environ. Chem. Lett.* **2017**, *15*, 747–753.

[2]   L. Zhou, X. Zhang, Y. Chen, *Mater. Lett.* **2017**, *197*, 167–170.

[3]   J. Lemus, M. Martin-Martinez, J. Palomar, L. Gomez-Sainero, M. A. Gilarranz, J. J. Rodriguez, *Chem. Eng. J.* **2012**, *211–212*, 246–254.

[4]   Y. Zhou, L. Zhou, X. Zhang, Y. Chen, *Microporous Mesoporous Mater.* **2016**, *225*, 488–493.

[5]   W. Wu, T. Li, H. Gao, D. Shang, W. Tu, B. Wang, X. Zhang, *Guocheng Gongcheng Xuebao/The Chinese J. Process Eng.* **2019**, *19*, 173–180.

[6]   E. Słupek, P. Makoś, J.Gębicki, *Arch. Environ. Prot.* **2020**, *46*, 41–46.

Gdańsk, dnia 19.05.2023

dr inż. Patrycja Makoś-Chełstowska
....
(stopień/tytuł, imię i nazwisko)

Politechnika Gdańska
....
(Afiliacja)
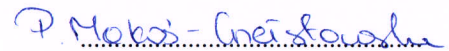
OŚWIADCZENIE WSPÓŁAUTORA

Jako współautor pracy:. **"Deep eutectic solvents – based green absorbents for effective volatile organochlorine compounds removal from biogas"** oświadczam, że mój własny wkład polegał na konceptualizacji, metodologii, analizie formalnej, nadzorowaniu, prowadzeniu badań, przygotowaniu oryginalnego manuskryptu, przygotowaniu recenzji i redakcji ostatecznej wersji manuskryptu oraz finansowaniu.

Jednocześnie wyrażam zgodę na przedłożenie ww. pracy przez mgr inż. Edytę Słupek jako część rozprawy doktorskiej w formie spójnego tematycznie zbioru artykułów opublikowanych w czasopismach naukowych.

Oświadczam, że samodzielna i możliwa do wyodrębnienia część ww. pracy wykazuje indywidualny wkład mgr inż. Edyty Słupek polegający na: konceptualizacji, gromadzeniu danych, prowadzeniu badań, metodologii oraz przygotowaniu oryginalnego manuskryptu.

(podpis współautora)

Gdańsk, dnia 19.05.2023

dr inż. hab. Jacek Gębicki
....
(stopień/tytuł, imię i nazwisko)

Politechnika Gdańska
....
(Afiliacja)

OŚWIADCZENIE WSPÓŁAUTORA

Jako współautor pracy:. **"Deep eutectic solvents – based green absorbents for effective volatile organochlorine compounds removal from biogas"** oświadczam, że mój własny wkład polegał na przygotowaniu recenzji oraz redakcji ostatecznej wersji manuskryptu.

Jednocześnie wyrażam zgodę na przedłożenie ww. pracy przez mgr inż. Edytę Słupek jako część rozprawy doktorskiej w formie spójnego tematycznie zbioru artykułów opublikowanych w czasopismach naukowych.

Oświadczam, że samodzielna i możliwa do wyodrębnienia część ww. pracy wykazuje indywidualny wkład mgr inż. Edyty Słupek polegający na: konceptualizacji, gromadzeniu danych, prowadzeniu badań, metodologii oraz przygotowaniu oryginalnego manuskryptu.

(podpis współautora)

Autorzy:

P. Makoś-Chełstowska, **E. Słupek,** A. Kramarz, D. Dobrzyniewski,

B. Szulczyński, J. Gębicki

Tytuł publikacji:

Green monoterpenes based deep eutectic solvents for effective BTEX
absorption from biogas

Czasopismo:

CHEMICAL ENGINEERING RESEARCH & DESIGN

DOI:

10.1016/j.cherd.2022.09.047

Green monoterpenes based deep eutectic solvents for effective BTEX absorption from biogas

Patrycja Makoś-Chełstowska[a,b,*], Edyta Słupek[a], Aleksandra Kramarz[a], Dominik Dobrzyniewski[a], Bartosz Szulczyński[a], Jacek Gębicki[a]

[a] Department of Process Engineering and Chemical Technology, Faculty of Chemistry, Gdansk University of Technology, 80–233 Gdansk, Poland
[b] EcoTech Center, Gdańsk University of Technology, 80–233 Gdańsk, Poland

A B S T R A C T

The combustion of biogas which contains significant amounts of monoaromatic hydrocarbons, i.e. benzene, ethylbenzene, toluene, and xylene (BTEX) can cause many technological, environmental, and health problems. Therefore, in these studies, a new physical absorption method based on deep eutectic solvents (DES) consisting of monoterpenes and carboxylic acids was developed for BTEX removal. A total of 39 DES were synthesized, of which seven were selected based on their affinity to BTEX, favorable physicochemical properties, and "green" character. Detailed structural (i.e. ^{1}H NMR, ^{13}C NMR, and FT-IR) and physicochemical experiments (i.e. melting point, density, viscosity, and surface tension) were performed for the DES. Then, DESs were used for the absorption process in both the laboratory and enlarged scale. BTEX absorption was monitored using two methods, including "in-situ" gas chromatography, and "online" sensors matrices. The crucial absorption parameters i.e. type of DES, temperature, and regeneration possibility were carefully studied. The mechanism of BTEX absorption was explained using experimental spectroscopic techniques and theoretical analysis based on the COSMO-RS model. The obtained results indicate that Eucalyptol:Octanoic acid can selectively capture BTEX from a biogas mixture due to the formation of electrostatic interaction. DES absorption capacity is 53.96 mg/g, which is comparable with commercially available absorbents.

© 2022 Published by Elsevier Ltd on behalf of Institution of Chemical Engineers.

1.   Introduction

Currently, an increase in demand for renewable energy production from natural sources can be observed. This is due to a number of factors, including the introduction of increasingly stringent climate policies limiting coal mining or assuming a phase-out of nuclear power plants, as well as the current war-induced fuel crisis. Therefore, more and more countries are considering the use of biogas from waste materials as renewable energy that could make countries less dependent on energy imports. The main problem in the widespread use of biogas is the presence of large amounts of organic and inorganic pollutants. Till now, many methods have been developed to purify biogas from inorganic substances, but there are still few technologies dedicated to the removal of volatile organic compounds from the biogas stream. One of the groups of problematic substances in biogas is monoarmomatic hydrocarbons including benzene, toluene, ethylbenzene, and xylenes (BTEX). These compounds are also one of the most common chemical pollutants of air, natural, and waste gasses (What is BTEX and why

is it important, 2022; Bretón et al., 2020). The presence of BTEX in biogas streams is mainly caused by the volatilization of intermediate products formed during fermentation processes. The concentration of BTEX in biogas streams can vary significantly depending on the raw material used in the fermentation process. Nevertheless, the concentration may vary from 94 to 1906 mg/m³ (Johansson, 2012). The presence of BTEX in biogas streams is unfavorable from ecological, public health, and industrial point of view (Abbasi et al., 2020; Li et al., 2019). Most of BTEX have a confirmed carcinogenic potential and adverse effects on the water and air environment (Baghani et al., 2019; Milazzo et al., 2019; Peng et al., 2015). In addition, combustion of biogas containing high concentrations of BTEX can cause corrosion, contamination, and clogging of engine systems (Rasi et al., 2011; Ryckebosch et al., 2011). Therefore, it is essential to remove monoaromatic hydrocarbons from biogas streams.

Currently, in the literature, we can find several methods dedicated to the removal of BTEX from biogas, including: absorption, catalytic oxidation, conventional adsorption, pressure swing adsorption, thermal swing adsorption, membrane, biological, and cryogenic methods (Santos-Clotas et al., 2019; Warren, 2012; Angelidaki et al., 2019; Awe et al., 2017; Rasi et al., 2014; Ma et al., 2018). Nevertheless, some of these methods show only low BTEX removal efficiency, longtime operation, require the use of toxic organic solvents, high capital investment, and running costs (Angelidaki et al., 2018). Therefore, the development of a cost-effective, efficient, "green" technology for BTEX removal from biogas streams is a major challenge for the energy industry. One of the most widely used industrial technology for volatile organic compounds (VOCs) captured from biogas is physical absorption. Physical scrubbing has some pros, including low operation and investment cost, good efficiency, and can be considered environmentally friendly if appropriate absorbents are used (Scholz et al., 2013). Among the available absorbents, the following can be distinguished triethylene glycol (Tazang et al., 2020), fluorocarbon surfactants (Xiao et al., 2015), polyethylene glycol, paraffin, water emulsion (Fang et al., 2016), and amines (Hatcher et al., 2013). However, most of these solvents are toxic and difficult to separate from the volatile organic compounds for the recycling process (Zhang et al., 2021). The green absorbent materials should be characterized by low vapor pressure, high boiling point, low viscosity, high absorption capacity, low cost and should be easy to regenerate (Słupek et al., 2020a).

Until recently, ionic liquids have been considered the ideal absorbents for the capture of BTEX from gaseous fuel streams (Zhang et al., 2021). However, their high price, non-biodegradable, and frequently toxic properties make them not widely used in the industrial purification of gaseous streams. In order to overcome the disadvantages of ionic liquids, a new type of green solvents named deep eutectic solvents (DESs) started to be considered as efficient media for biogas purification. According to the definition, DES is a complex which is consisting of a hydrogen bond donor (HBD) and hydrogen bond acceptor (HBA) with appropriate molar ratios. The specific non-covalent interactions created between HBA and HBD lead to the formation of DES with a much lower melting point compared to the individual components (Abbott et al., 2003; Smith et al., 2014). So far, many new DESs have been synthesized and successfully used in many separation processes, such as extraction, microextraction, absorption, and adsorption (Ghazali et al., 2019a; Hussin et al., 2021; Makoś and Boczkaj, 2019; Cunha and Fernandes, 2018; Makoś et al., 2020a, 2020b). Literature data show that DES is characterized by a high absorption capacity of carbon dioxide and other inorganic pollutants (including ammonia, hydrogen sulfide, water vapor, and sulfur dioxide) occurring in gaseous fuels, i.e. biogas. However, to ensure high efficiency of the removal of individual contaminants, it is necessary to choose the appropriate substances for DES formation. This is a crucial parameter because, as proven in previous works, the driving force of absorption processes using DES are non-covalent interactions between the absorbent and impurities, i.e., hydrogen bonds or electrostatic interactions. For example, to absorb CO_2 (hydrogen bond acceptor), it is necessary to use a DES that has at least one hydrogen bond donor group in the structure, i.e. -OH, -COOH, or -NH$_2$. The opposite is true for ammonia, which, due to its structure, is a good hydrogen bond donor, therefore a suitable DES for absorption should have acceptor groups, i.e. =O, or -O- (Shukla and Mikkola, 2018; García et al., 2015; Zubeir et al., 2018; Ghazali et al., 2019b; Luo et al., 2021; Wu et al., 2019). The mechanisms for removing inorganic contaminants from gas are currently fairly well known. Therefore, it is easy to speculate which DES might be suitable for capturing selected substances. However, knowledge of the VOC absorption capacity of gaseous streams with DES is very limited. Until now, the high absorption capacity of deep eutectic solvents has been proven for volatile organic silicon (Słupek et al., 2020a; Makoś et al., 2020a; Słupek et al., 2021; Makoś-Chełstowska et al., 2021a), sulfur (Słupek and Makoś, 2020), and chlorine compounds (Makoś-Chełstowska et al., 2021b). Among the compounds from the BTEX group, an attempt has been made to remove toluene from biogas (Moura et al., 2017; Słupek et al., 2020b). To the best of our knowledge, there are no works dedicated to the removal of all BTEX compounds from gas streams by means of deep eutectic solvents.

The paper describes the synthesis of new green monoterpenes based on deep eutectic solvents, their structural, and physicochemical properties (i.e. density, viscosity, surface tension, and melting point) as well as the application as efficient absorbents for BTEX capture from biogas. In this study, structural characterization of new absorbent materials and interaction between BTEX, and DES were analyzed using theoretical method based on the COSMO-RS model, and experimental techniques based on proton and carbon-13 nuclear magnetic resonance (^{1}H NMR and ^{13}C NMR), as well as Fourier transform infrared spectroscopy (FTIR). The absorption process was optimized in terms of the selection of the appropriate DES, and absorption temperature. Under optimal conditions, the absorption efficiency of DES was compared with a commercially available absorbent dedicated to biogas purification. The absorption processes were monitored using two methods, gas chromatography, and sensor matrices. The comparison of the two methods of process control was aimed at confirming the usefulness of the sensors' matrices in online research, due to shorter time of single analysis and its lower costs. The use of sensor arrays allow a real-time control of the absorption process, which in combination with an appropriately selected control algorithm can make the process fully autonomous (requiring little control by personnel). The validity of using gas sensor matrices as an alternative to chromatographic techniques has already been demonstrated, e.g.

to control biofiltration process (Szulczyński et al., 2018; Rybarczyk et al., 2020; López et al., 2011; Cabeza et al., 2013), odour monitoring (Romero-Flores et al., 2017), methane reforming process monitoring (Dobrzyniewski et al., 2021) and they also have high application potential in food industry (Pearce et al., 1993) or pharmaceutical industry (Spichiger and Spichiger-Keller, 2010).

2. Materials and methods

2.1. Materials

The following substances were used for the preparation of DES: ± camphor (Cam), carvone (C-one), eucalyptol (Eu), furfural (Fu), choline chloride (ChCl), tetramethylammonium bromide (TMABr), tetraethylammonium bromide (TEABr), tetrapropylammonium bromide (TPABr), tetra-butylammonium bromide (TBABr), guaiacol (G), syringol (S), menthol (M), thymol (Th), vanillin (V), formic acid (FA), octanoic acid (OA), nonanoic acid (NA), decanoic acid (DA), dodecanoic acid (DDA) and levulinic acid (Lev). For the preparation of contaminated biogas, monoaromatic hydrocarbons including benzene, toluene, ethylbenzene, and xylene were used. All reagents were obtained from Sigma Aldrich (St. Louis, MO, USA) with high purity ($\geq$ 98%). For the comparison of DES efficiency, a commercially available absorbent Genosorb ® 1843 (Clariant, USA) was used. High purity gases including nitrogen (purity N 5.0), methane (purity N 5.5), and carbon dioxide (purity N 4.5) were obtained from Linde Gas (Poland). The air was generated by a DK50 compressor with a membrane dryer (Ekkom, Poland), and hydrogen (purity N 5.5) generated by Precision Hydrogen 1200 Generator (PEAK Scientific, Scotland, UK). All gases were used for the preparation of a model biogas streams and chromatographic analysis.

2.2. Procedures

2.2.1. Preparation of DESs

DESs were prepared using the method described in previous studies (Makoś-Chełstowska et al., 2021a; Słupek and Makoś, 2020; Makoś-Chełstowska et al., 2021b). Two chemical compounds were mixed with each other in a proper molar ratio. In the next step, the mixture was stirred on a magnetic stirrer at 60 °C until a homogeneous liquid was formed. DES was cooled to the room temperature (RT).

2.2.2. Preselection of DESs based on Henry's law constant

The preselection of DES were prepared based on Henry's constants. Studies were performed using the headspace technique combined with gas chromatography-flame ionization detector (HS-GC-FID) in accordance with the procedure described in the previous works (Chai et al., 2005). Only DES that were liquids at room temperature were used for the test. Liquid DES (0.5 mL) was transferred to 20-mL headspace vials to which the 0.75 µL of each BTEX compound was added. The vials were then sealed and incubated at room temperature for 24 h. Then 100 µL of the headspace was introduced into the gas chromatograph. The concentration of BTEX in the gas phase (headspace) was determined on the basis of calibration curves prepared in accordance with the procedure presented in the previous works. The concentration of selected BTEX compounds in a liquid phase (DES) after headspace procedure was calculated according to Eq. 1:

$$V_1 \cdot C_0 = V_1 \cdot C_1 + V_g \cdot C_g \tag{1}$$

where: V_1 – DES volume [cm³];.

V_g – gas volume (headspace volume) [cm³];.

C_0 – initial concentration of BTEX in liquid sample (DES) [mol/m³];.

C_1 – concentration of selected BTEX in DES phase after headspace procedure [mol/m³];.

C_g – concentration of selected BTEX in gas phase after headspace procedure [mol/m³];.

The dimensionless Henry's law solubility constant was calculated according to Eq. 2:

$$H = \frac{C_g}{C_1} \tag{2}$$

2.2.3. Characterization of DESs

DESs viscosity and density measurements were made in the temperature range from 20° to 50°C. Measurements were made using the following apparatus BROOKFIELD LVDV-II+viscometer (Labo-Plus, Poland), and a DMA 4500 M density meter (Anton Paar, Poland). The surface tension (ST) of DES was measured using a tensiometer (A KRÜSS K9 model K9MK1) in the range of temperature of 20–50 °C. The tensiometer was stabilized for 30 min and calibrated using water at 20 °C. Then the 4 mL of DES was placed in a thermostated measuring cup. After reaching the appropriate temperature, the ST of DESs was measured automatically using A KRÜSS K9 within 3 s. The melting point (MP) of DESs was determined visually by cooling eutectic mixtures to – 25 °C in a cryostat (HUBER, Germany). Then the temperature was increased at 1 °C/min. The temperature at which the appearance of the first liquid drop was observed was taken as MP. Measurements of all physical properties of DES were repeated three times.

2.2.4. Mechanism of DESs formation, and BTEX absorption

The absorption mechanism and structural properties of new DESs were analyzed by ATR-FTIR spectroscopy by means of a Bruker Tensor 27 spectrometer (Bruker, USA) with an ATR accessory and OPUS software (Bruker, USA). The following parameters were adopted for the studies: 4000–600 cm⁻¹; the number of background and samples scans: 256; resolution: 4.5 cm⁻¹; slit width 0.5 cm. Additionally, nuclear magnetic resonance spectroscopy (NMR) measurements were performed in order to receive more deep insight into DES formation and the efficiency of BTEX absorption. Samples for NMR analysis were prepared in 5 mm tubes by weighing 20 mg of DES and inserting 0.4 mL of chloroform-d1. The NMR analysis was done out at 20 °C by means of Bruker Avance III HD 400 MHz (Bruker, USA).

For the theoretical examination of the mechanism of BTEX absorption, Conductor-like Screening Model for Real Solvents model (COSMO-RS) was used. For these propose, ADF COSMO-RS software (SCM, Netherlands) was used according to previous studies (Makoś-Chełstowska et al., 2021a, 2021b, 2022a). In the first stage, the geometry optimization of DES which were selected during HS-GC-FID analysis including Cam:OA, Cam:DA, C-one:OA, C-one:NA, C-one:DA, C-one:Lev, Eu:OA, main components of commercially available absorbent (i.e. tetraoxaoctadecane and pentaoxaheneicosane) and BTEX was prepared. The geometry optimization of all eight absorbent complexes in 1:1 molar ratio, and BTEX compounds was performed using the continuum solvation COSMO model at the BVP86/TZVP theoretical level. In order to find the most stable

conformers of studied compounds, optimization studies were performed in the gas phase. In the next step, the vibrational analysis was performed to find conformers that corresponds to the true energy minimum. The full geometry optimization of studies compounds was prepared only for the most energetically favorable conformers. For all absorbents, the affinity to BTEX was calculated by means of activity coefficient according to Eq. (3).

$$\ln(\gamma_i) = \frac{u_i^a - u_i^P}{RT} \tag{3}$$

where: u_i^a – chemical potential of selected BTEX in absorbent;.

u_i^P - chemical potential of pure BTEX compounds;.

R - universal gas constant (8.314 J/mol);.

T - temperature (K).

In order to visualize the charge distribution of absorbents and BTEX, the σ-profiles were calculated using the 3D surface charge densities.

2.2.5. Absorption and desorption process of BTEX

In this work, the absorption/desorption set-up was described in the previous work was used (Makoś-Chełstowska et al., 2021b). In the first stage, pure nitrogen was passed through a vial containing 1 mL of each BTEX compound. The obtained contaminated gas via bubbling phenomena was diluted with a model biogas stream (CH_4: CO_2: N_2 in 5:3:2 vol ratio) to 2000 mg/m³ concentration of BTEX. In the next step, the biogas stream was directed into the absorption column with an appropriate absorbent. The desorption process was carried out using the pure nitrogen barbotage method at elevated temperatures in the range of 100–120 °C consistent with previous research (Lawal et al., 2011).

During the absorption/desorption processes, the biogas samples were collected before and after introduction into the absorption/desorption column. The biogas samples were analyzed by gas chromatography and sensors matrix. Biogas purification processes were carried out until the concentration of BTEX in the inlet and outlet biogas were equal. In order to ensure the correctness of the results, the absorption processes were repeated three times. The absorption capacity (Q) was determined according to the previous studies (Makoś-Chełstowska et al., 2021b). To determine the absorption capacity of the absorbent, the volumetric flow rates of individual components of the gas mixture have been designated as the product of the volumetric flow rate of the gas mixture and the concentration of its components. For this purpose, by means of an Agilent ADM Flow Meter, the gas flow at the outlet of the absorption columns needs to be measured. Values of Q were calculated using Eqs. (4–6):

$$\frac{d(m_{BTEX})}{dt} = (F_{IN} \cdot C_{IN}(t) - F_{OUT}(t) \cdot C_{OUT}(t)) \cdot \bar{\rho}_{BTEX} \tag{4}$$

$$m_{BTEX} = \int_0^{t_{sat}} [F_{IN} \cdot C_{IN}(t) - F_{OUT}(t) \cdot C_{OUT}(t)] \, dt \cdot \bar{\rho}_{BTEX} \tag{5}$$

$$Q = \frac{m_{BTEX}}{m_A} \tag{6}$$

where: m_{BTEX} – BTEX mass absorbed [g];.

m_A - mass of absorbents used to obtain complete saturation [g];.

t_{sat} – saturation time of absorbents [s];.

C_{IN} – BTEX initial concentration in biogas [ppm v/v];.

C_{OUT} – BTEX outlet concentration in biogas [ppm v/v];.

$F_{IN,OUT}$ – Flow rate of the biogas at the inlet and outlet of the absorption column [m³/s];.

$\bar{\rho}_{BTEX}$ - average BTEX density at a given temperature [kg/m³].

The absorptivity of BTEX was calculated using the following Eq. 7:

$$A = \frac{A_{IN} - A_{OUT}}{A_{IN}} \tag{7}$$

where: A_{IN} – initial total peak area of BTEX compounds;.

A_{OUT} - total peak area of BTEX compounds after absorption process.

2.2.6. Process control

2.2.6.1. Chromatographic analysis. For the control of absorption/desorption process efficiency, biogas samples were analyzed by gas chromatography technique. In order to determine Henry's constants in static process and concentration BTEX in gas streams in a dynamic process, gas chromatograph Autosystem XL (PerkinElmer, USA) equipped with a capillary column an HP-5 (30 m × 0.25 mm × 0.25 μm) (Agilent Technologies, USA), and a flame ionization detector (GC-FID) (PerkinElmer, USA) was used. The chromatographic analysis was conducted under certain conditions: temperature of the oven 60 °C, injection port temperature 250 °C; the injection mode split 5:1, detector temperature 300 °C, the carrier gas – nitrogen (flow rate: 1 mL/min), amount of sample injected: 0.5 mL. For the determination of CH_4, CO_2, and N_2 in the biogas stream during the absorption process, the gas chromatograph GC MG#5 (SRI Instruments, USA) coupled to a thermal conductivity detector (GC-TCD), and equipped with a packed column Porapack Q (80/100, 2 mm ID) (Restek, USA) was used. The following conditions were used: temperature of the oven 40 °C, injection port temperature 60 °C, detector temperature 80 °C, the carrier gas – helium (flow rate: 5 mL/min), amount of sample injected: 2.0 mL.

2.2.6.2. Chemical gas sensor. In order to continuously monitor and control the absorption treatment of biogas, a matrix consisting of the commercially available gas sensor was constructed. Basic information about gas sensors used is shown in Table S1. The gas sensors were housed in separate PTFE chambers. This approach makes it possible to prevent the emissions of organic compounds into the measuring chamber and further reduces the absorption and chemical transformations of the gaseous substances. Due to the dependence of the output signal from PID-A12 gas sensors on variations in temperature, humidity, and atmospheric pressure, a sensor that controls these parameters was placed in an additional chamber. As a result, the lack of linearity of the PID output signal observed at higher concentrations can be corrected in the software during data analysis. Whereas, NDIR sensors capable of monitoring the presence of carbon dioxide and methane in process samples provide an analog voltage output proportional to the concentration of these gases, which is simultaneously linearized and temperature compensated. The constructed matrix allowed control of total BTEX concentrations in the range of 0–6600 mg/m³ while carbon dioxide and methane concentrations were monitored in the range of 0–100% by volume. The gas flow at the outlet of the absorption column was measured using an Agilent ADM Flow Meter, which provides continuous, real-time measurement of volumetric flow rate.

2.2.6.3. Gas sensor array measurement. The gas sensor array experimental setup is presented in Fig. S1. Process samples were collected at the inlet and outlet of the process and the bags made of TEDLAR film were used for this purpose. The three-way valve (V1) made it possible to alternate between the analyzed sample and the atmospheric air passing through the air filter to the measuring chamber. Purified air was directed to the measurement chamber after each analysis in order to regenerate the gas sensors and restore their input parameters. The flow rate of the sample and air was controlled using the rotation speed of the diaphragm pump. The pulse width modulation module (PWM) was responsible for regulating the supply voltage delivered to the pump motor, which fluctuations directly affect the pump speed and thus the flow rate. The sensor measurement was performed in the stop-flow mode: the sample flow time through the sensor chamber was 30 s, than by closing the valve (V2) the sample was retained in the chamber for another 30 s. Sensors signals were recorded using an analog-to-digital converter and processed by means of dedicated software. All manufacturer's requirements were taken into account when the electrical circuits for each sensor were prepared. The created system was controlled automatically by the Arduino control module. All analyzed samples were also subjected to gas chromatographic analysis, which was treated as a reference method.

2.2.6.4. Data analysis and processing. Data analysis and other calculations were performed using RStudio Desktop (v. 1.4.1717) software. Multiple linear regression (MLR) was selected as the calibration and validation model for the gas sensor array. Thus, linear relationships between independent (sensor's signals), and dependent (e.g. gas concentration, chromatographic peak area) variables were determined for carbon dioxide, methane, and total BTEX. Also, other methods of data analysis, e.g. Principal Component Analysis (PCA), Principal Component Regression (PCR), Partial Least Squares Regression (PLSR) can be used effectively for this purpose, especially when dealing with very complex sample matrices.

3. Results and discussion

3.1. DESs preparation and preselection

In the studies, all DESs were prepared by mixing HBA, i.e., Cam, C-one, Eu, Fu, ChCl, TMABr, TEABr, TPABr and TBABr, with different HBDs i.e. Lev, OA, NA, DA, DDA, G, S, V, M, Th and FA in 1:1 molar ratio. From 99 tested DES, only 39 eutectic complexes turned out to be liquids at room temperature. DES which met the first basic criterion of absorbents - were liquids at RT, were selected for further research. Due to the relatively large number of new DESs, a pre-selection of DES was performed. DES screening was performed based on the determination of Henry's constants. This parameter reflects the dissolving ability of BTEX in DES (Chen et al., 2022). The obtained results are shown in Fig. 1. The lower values of the Henry constants (H) correspond to the greater BTEX solubility in DES. The results indicate that the lowest values of H were obtained for xylene and ethylbenzene. Slightly higher values were obtained for ethylbenzene and the highest for benzene. This indicates that the alkyl groups form stronger non-covalent bonds with DES compared to the π interactions which is in line with previous work (Wang et al., 2017). It can be observed that BTEX compounds have the greatest affinity
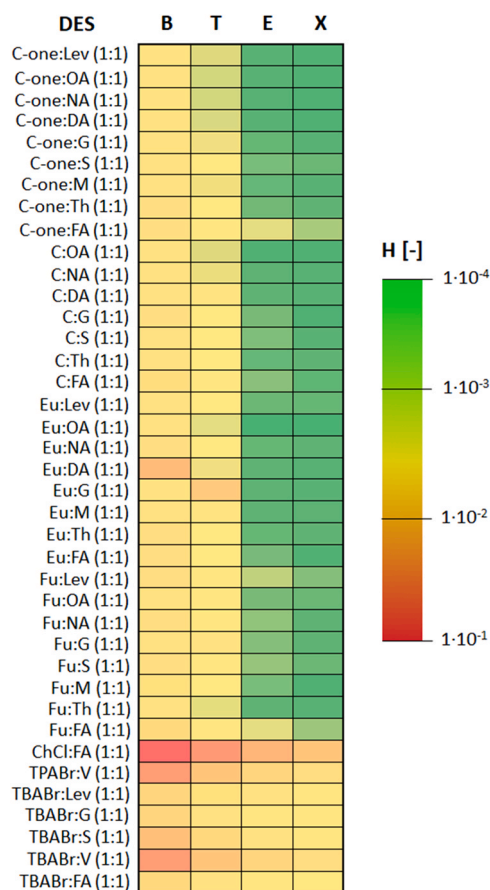

Fig. 1 – Henry's constants calculated for DES using the COSMO-RS model (according to the Eq. 2).

to non-ionic deep eutectic solvents. The affinity of mono-aromatic hydrocarbons to the ionic ones is significantly lower. These phenomena can be explained by the occurrence of very strong interaction between the cation and the anion in DES structures, that are stronger than the bonds formed between the DES and nonpolar impurities (Brouwer et al., 2021). The obtained results suggests that ionic interactions do not play a significant role in the BTEX absorption process. The most favorable results were obtained for DES consist of the monoterpenes acting as HBA in combination with carboxylic acids. The lowest Henry's constant values were obtained for DES consist of carvone, camphor, and eucalyptol as HBA, and carboxylic acids as HBD including: C:OA (1:1), C:DA (1:1), C-one:OA, C-one:NA, C-one:DA, C-one:Lev, and Eu:OA in 1:1 molar ratio. This suggests that the carboxyl group (-COOH) not only binds efficiently to the carbonyl group of the monoterpenes (= O) to form strong hydrogen bonds, but is also involved in the formation of strong inter-actions with BTEX compounds. Additionally, the specific structure of monoterpenes can lead to the formation of ad-ditional π-π interactions with monocarboxylic hydrocarbons. The coexistence of both types of interactions may affect the high absorption capacity of the new DES. Only DES with the highest absorption potential was used for further research.

3.2. Mechanism of DES formation

Due to the synthesis of new DES, which have not been pub-lished so far, their detailed structural studies were performed. In addition, understanding the interaction mechanisms be-tween HBA and HBD may play a key role in the selection of

optimal absorbents for biogas purification. Therefore, in this study, FT-IR analysis were performed for new DES and their individual components. Fig. S2 shows the FT-IR spectrum for the Eu:OA (1:1). On the DES spectrum, it can be observed the shift of wide bandwidth of stretching vibrations from O-H groups towards higher wavelengths (from 3002 cm^{-1} to 3014 cm^{-1}), and decreased peak intensity compared with the pure HBD. In the DES spectrum, intensity decrease, and shifts towards higher wavelengths are also observed for C=O stretching vibrations (from 1706 cm^{-1} to 1711 cm^{-1}) and C-O-C stretching vibrations (from 1080 cm^{-1} to 1081 cm^{-1}). The obtained results indicate that hydrogen bonding is formed between the carbonyl group from Eu and the carboxylic group from OA. Due to the presence of active oxygen atoms (-O-, or = O) in all tested HBA and carboxyl groups in HBD structures, similar band shifts can be observed in the spectra of the remaining DES (Fig. S3-S8). This suggests the formation of strong hydrogen bonds between HBA and HBD in all tested DES (Makoś-Chełstowska et al., 2021a; Ribeiro et al., 2015).

In addition, ^{1}H NMR and ^{13}C NMR spectra were performed to confirm the formation of hydrogen bonds between DES components and for the identification of potential synthesis by-products. NMR spectra of Eu:OA (1:1) are presented in Fig. S9, and the main shifts of peaks are summarized in Table S2. In the ^{1}H NMR spectrum, all identified peaks correspond to protons belonging to Eu and OA. This suggests that no by-products are formed during the DES synthesis.

Additionally, characteristic shifts in the ^{1}H NMR and ^{13}C NMR spectra of DES in comparison to pure substances can be observed. In ^{1}H NMR spectrum, mainly shifts toward lower values can be observed. The only exceptions are the (H1) and (H5) protons with Eu for which shifts towards higher values (from 2.02 to 2.19 ppm) can be observed. OA-derived protons are characterized by greater shift values than protons from Eu. The largest shift can be observed for the (H1) proton (from 11.60 ppm to 11.03 ppm). This is a proton from the O-H group of the carboxyl group. Such a large shift (by 57 ppm) proves the direct participation of this group in the formation of hydrogen bonds in DES. In the ^{13}C NMR spectrum, the shifts of values for most C atoms from both HBA and HBD towards lower values can be observed. Only for (C1) and (C2) from Eu, the shifts towards higher values can be observed. These shifts are affected by the direct bond with the oxygen atom in the Eu molecule, which actively participates in the formation of a hydrogen bond. The highest value of the shift can be observed for (C1) from the OA molecule (from 180.81 ppm to 178.70 ppm). This is because the C atom from the carboxyl group is involved in the formation of the hydrogen bond. NMR spectra were also performed for the remaining DES. For the rest of DES, similar behavior can be observed. Spectra and a list of shifts are presented in Figs. S10-S15.

3.3. Physicochemical properties of DESs

The practical application of DES requires knowledge of basic physicochemical properties including density, viscosity, surface tension, and melting point (MP). Therefore, all listed properties have been investigated in this work.

All studied DES are characterized by relatively significant depressions in melting point compared to pure HBA and HBD. MP of pure HBAs including Cam, C-one, and Eu are 175 °C, 25.2 °C, and 1.5 °C, respectively. While the MP of pure HBDs i.e. Lev, OA, NA, and DA, were 33 °C, 16.5 °C, 12.3 °C, and 31.6 °C, respectively. The greatest decrease in MP can be observed for

C-one:Lev (1:1) which equal – 25 °C. Slightly lower decrease in MP can be observed for the rest of DES including Eu:OA, C-one:OA, C-one:NA, C-one:DA, Cam:DA, Cam:OA, which are – 23, – 22, – 21, – 19, – 19, and – 8 °C, respectively.

The density of DES is a crucial parameter that significantly affects the mass transfer processes. The literature data indicate that most DESs are characterized by higher density than that of water, in the range of 1.00–1.35 g/cm^{3} at 20 °C (García et al., 2015). The densities of the tested DES are within the range of 0.9228–1.0397 g/cm^{3} at 20 °C. The density values of studied DES follows the order: C-one:Lev (1:1) > C-one:OA (1:1) > Cam:OA (1:1) > C-one:NA (1:1) > Cam:DA (1:1) > C-one:DA (1:1) > Eu:OA (1:1). It can be observed that the density of DES closely depends on the alkyl chain length of the carboxylic acids. An increase in the length of the carboxyl chain causes the increase in molar volume, which affects the decrease in the density value (Florindo et al., 2014). In addition, the density of DES strongly depends on temperature. The increase in temperature of eutectic mixtures affects the increase in the kinetic energy of the DES components, which causes a DES density decrease (Chemat et al., 2016; Hayyan et al., 2012). The densities of all tested DES at 20 – 50 °C are shown in Fig. 2a.

The next important property of absorbents is dynamic viscosity due to their strong influence on the mass transfer processes. Most DES are characterized by relatively high viscosity (> 100 cP) (Abbott et al., 2003; Smith et al., 2014; Makoś et al., 2020b), which significantly limits their usefulness in absorption processes. All tested DESs have lower viscosities than 10 mPas, and the value at 20 °C follows the order: Cam:DA (1:1) > C-one:Lev (1:1) > Cam:OA (1:1) > Eu:OA (1:1) > C-one:DA (1:1) > C-one:NA (1:1) > C-one:OA (1:1). This indicates that all DES can be successfully used for absorption. Obtained results indicate that the viscosity depends on the structure of both HBA and HBD. It can be observed that the viscosity of DES increases with the increasing length of the alkyl chain. This is in line with previous studies (Makoś-Chełstowska et al., 2022b). The higher viscosity value of C-one:Lev (1:1) compared to C-one:OA (1:1), C-one:NA (1:1), C-one:DA (1:1) can be explained by the additional carbonyl group in Lev structure. In addition, Fan et al. proved that the lifetime of the hydrogen bond also influences the viscosity value, which decreases in DES systems where HBA belongs to monocyclic unsaturated terpene ketones (Fan et al., 2021). The conducted research confirmed the theory of Fen et al. The lowest viscosity values were obtained for DES in which HBA was Carvone, which belongs to the group of terpene ketones. In addition, a close dependence of DES viscosity on temperature can be observed. As the temperature increase, the viscosity of DES decreases, which can be described by the Arrhenius or Vogel-Fulcher-Tammann model. This indicates the standard behavior of Newtonian liquids which can be explained by an increase in the average speed of DES molecules in the liquid phase at higher temperatures, which decreases the intermolecular forces. This causes a reduction of resistance of the fluid to flow and changes the viscosity (Haghbakhsh et al., 2018). Examined DES viscosity values at 20 – 50 °C are presented in Fig. 2b.

Another examined property of new DESs is surface tension (ST). This is another parameter that has a decisive effect on mass transfer process (Jiménez et al., 2001). The surface tension of DESs strongly depends on many factors, such as the temperature, type, and nature (hydrophobic or hydrophilic) of HBA and HBD. Knowledge of ST provides important information about the molecular influence on the
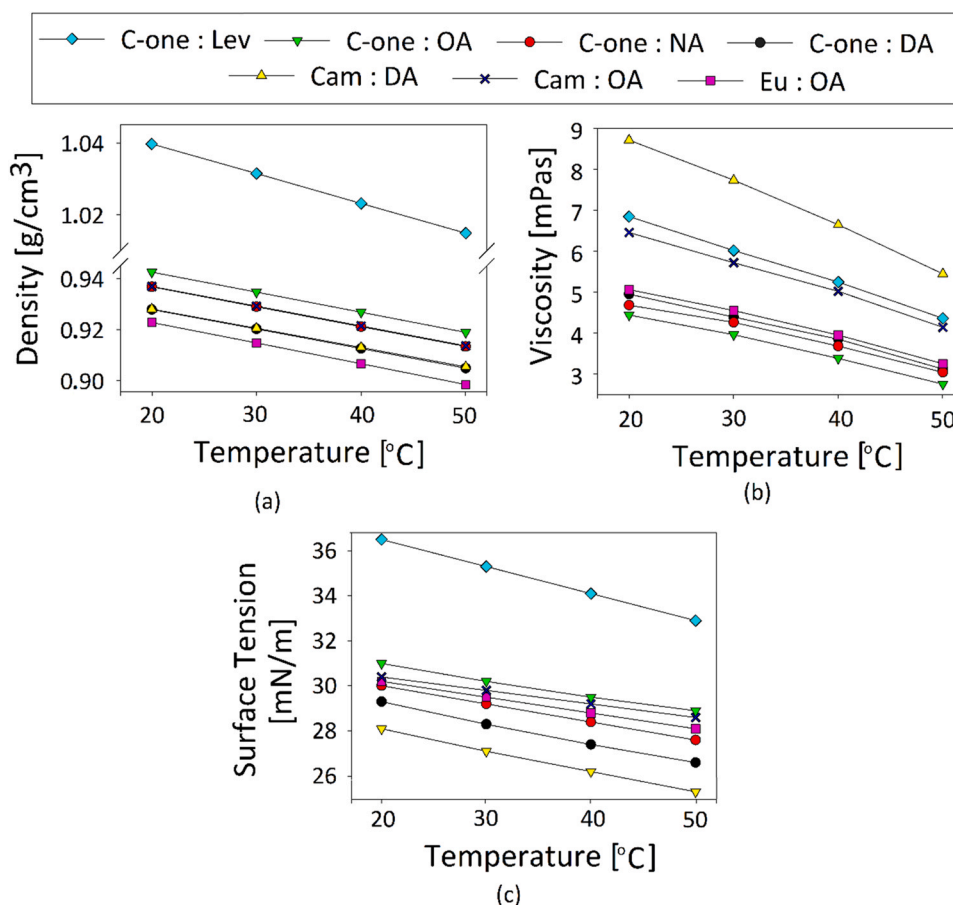
Fig. 2 – The (a) density, (b) viscosity, and (c) surface tension (ST) of DESs in the temperature range of 20–50 °C.

interactions in a mixture (Chen et al., 2019). In this study, the ST of DES was measured in the temperature range of 20–50 °C (Fig. 2c). Typically ST of DES is in the range of 40–65 mN·m^{-1} at 25 °C (Shahbaz et al., 2012; Kurnia et al., 2012). Experimental results indicate that the ST of studied DES composed of Carvone or Camphor as HBA and various carboxylic acids as HBD in a 1:1 molar ratio decreases with the increasing length of the HBD chain. This is probably due to the fact that with the increasing length of the acids chain the charge density decrease thus decrease the importance of electrostatic interactions between HBA and HBD. In addition, the obtained results show that the ST of all DES decreases with the increase in temperature. This is in line with the typical behavior of the liquids (Chen et al., 2019). As the temperature increases from 20 °C to 50 °C, a decrease in the ST value can be observed for C-one:Lev (1:1) from 36.5 mN/m to 32.9 mN/m, while for Cam:DA (1: 1) from 28.1 mN/m to 25.3 mN/m. This is due to the fact that increasing the DES temperature increases the molecular movement, the average kinetic energy, and reduces the forces of cohesion between molecules (weakening of the interaction between the HBA and HBD in DES) which causes the decrease in ST value (Abbott et al., 2011; Mjalli et al., 2014).

3.4. Absorption of BTEX

One of the key factors which have a decisive effect on the absorption efficiency of BTEX is a type of DES. Therefore a DES pre-selection was performed. For this purpose, the absorption processes were carried out under optimal conditions obtained in previous studies (Słupek et al., 2021, 2020b).

The procedures for collecting data from sensors and gas chromatography are included in the S.1. - Supplementary Materials (Fig. S16 - S17 and Table S3).

In the preselection studies, the only variable was the type of DES, and the other parameters were constant, i.e. temperature 25 °C, biogas pressure 10 kPa, the volume of DES 50 mL, biogas flow rate 50 mL/min, and initial concentration of BTEX 2000 mg/m^3. The initial concentrations used were higher than the BTEX content in the biogas stream. However, the concentration was adjusted to the content of all aromatics compounds in the biogas, which is between 35 and 1731 mg/m^3 (Salazar Gómez et al., 2016). An inert gas - nitrogen was used as the gas matrix to exclude other interactions resulting from affinity to other biogas components. The experimental breakthrough curves of seven different DESs are presented in Fig. 3. The obtained results indicate that the absorption capacity of BTEX depends both on the type of HBD, HBA, and the structure of BTEX. Based on a comparison of various DES composed of octanoic acid as HBD and different HBA, it can be observed that the absorption efficiency is ordered as follows, Eu > C-one > Cam. The time of effective absorption is 5852, 5556, and 4382 min for Eu:OA, C-one:OA, and Cam:OA, respectively. This order is due to the π-π interaction between aromatic groups of HBA and BTEX. In addition, the C-one and Cam contain in their structure the double bond of the carbonyl group that reduces structural availability and reduces the hydrophobic nature of DES, which negatively affects the effectiveness of the absorption process (López and Pascual-Villalobos, 2010). On the other hand, based on the comparison of the efficiency of the absorption with the use of DES composed of carvone as HBA and various carboxylic acids as HBD,
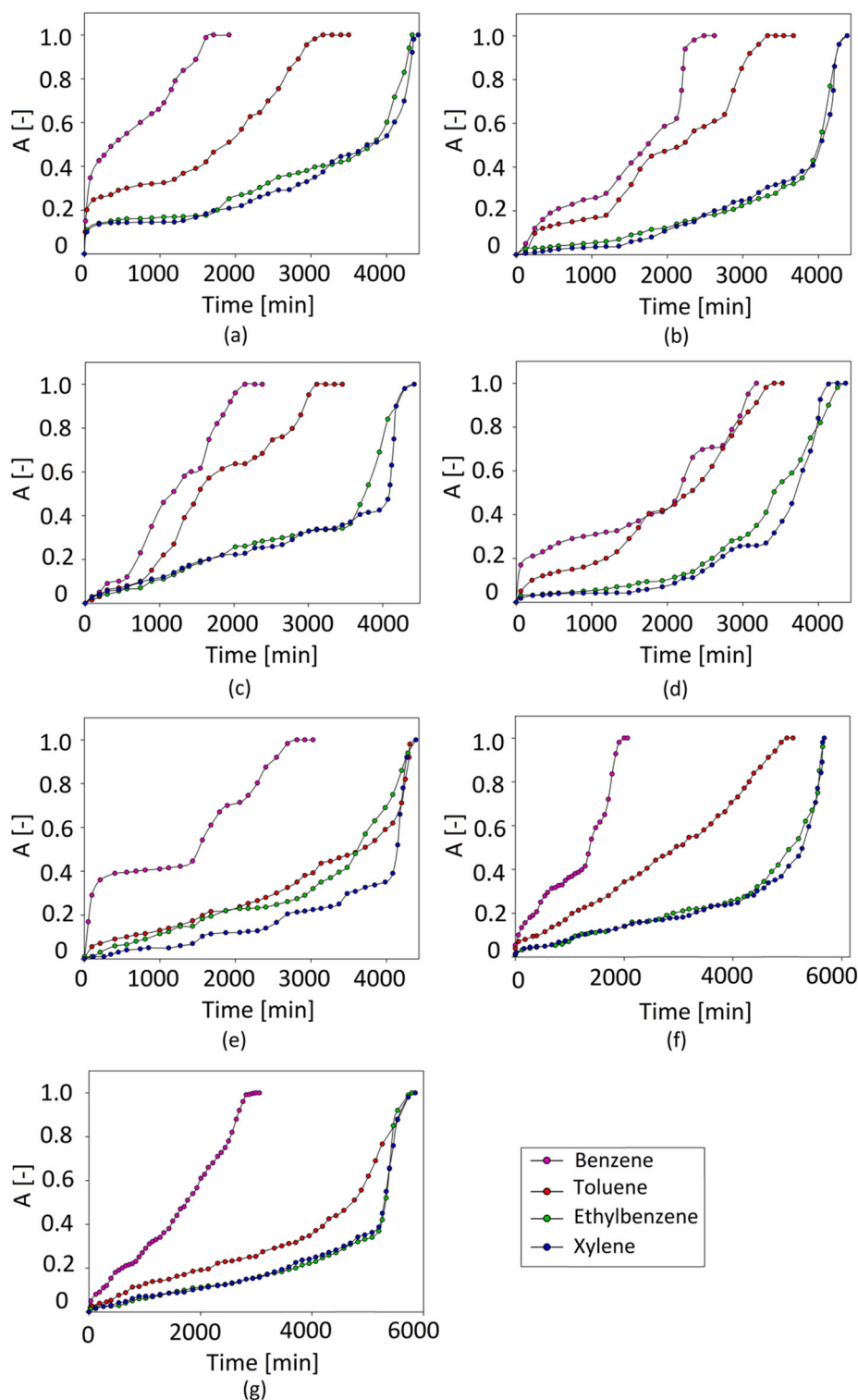
Fig. 3 – Experimental breakthrough curves of (a) Cam:DA (1:1); (b) Cam:OA (1:1); (c) C-one:Lev (1:1); (d) C-one:OA (1:1); (e) C-one:NA (1:1); (f) C-one:DA (1:1); (g) Eu:OA (1:1); on different DESs (temperature 25 °C; biogas (matrix gas N₂) flow 50 mL/min; inlet BTEX concentration 2000 mg/m³); the volume of the DES 50 mL; absorption column dimensions: height 10 cm and width 3 cm.

the following sequence can be observed C-one:DA > C-one:NA > C-one:OA > C-one:Lev. This is probably due to the fact that increasing the alkyl chain length of the HBD affects decreases the polarities of DESs. The highly nonpolar nature of DES has a positive effect on the rate and capacity absorption of BTEX (Chen et al., 2021). The absorption capacity is ordered according to the following sequence of BTEX: xylene > ethylbenzene > toluene > benzene, which is consistent with a growing number of methylene groups in the ring of

impurities. The differences between breakthrough patterns can be explained by the different interaction forces between BTEX and DES, as well as the physical properties of selected absorbents. Benzene is mainly able to the formation of π interaction with the DES functional group including –COOH, -CH₃, =CH₂, -O-, or =O. However, the strength of these interactions is similar in each case (Tsuzuki and Fujii, 2008). Therefore, it can be assumed that the changes in the breakthrough curves of benzene are caused by the physical

properties of DES. A comparison of benzene breakthrough curves shows a close dependence of DES supersaturation on their viscosity. As viscosity increases, DES is supersaturated faster, which is due to the hindrance of mass exchange. However, compounds that contain additional methyl or ethyl groups can form both π and other weak hydrogen bond interactions with carbonyl, ester, or carboxylic groups. As observed in previous studies, the strength of the weak hydrogen bonds (i.e. C-H⋯O) interaction increases with the length of the alkyl chain in hydrocarbons. This indicates that the methyl groups are actively involved in the formation of non-covalent bonds with DES, which is in line with the results obtained from Henry's constants and with previous works (Wang et al., 2017; Cabaleiro-Lago and Rodríguez-Otero, 2018). However, differences in the saturation points of DES indicate that the basic physical properties, i.e. the dynamic viscosity of the absorbents, also can affect the absorption efficiency of T, E, and X.

DES composed of Eu and OA in a 1:1 molar ratio is characterized by the highest absorption capacity. This proves that not only the structure of DES components and the strongly hydrophobic nature of DES affects the efficiency of BTEX absorption, but also the physicochemical properties i.e. low viscosity, high surface tension, and relatively low melting point. Both types of parameters play a significant role in the absorption process and it is difficult to clarify which one is more important. However, the combination of favorable physical properties with the specific structure of Eu:OA enhances the effect of DES absorption capacity. Therefore, further research was only done for the most favorable DES.

As observed in previous work, the presence of other substances in the gas can significantly affect the absorption capacity of DES. Therefore, a quick comparison of Henry's constants (according to the Eq. 2) was performed for the absorption of single impurities and the entire BTEX mixture from biogas under static conditions. The outcomes are shown in Fig. 4. The obtained results in the two variants are only slightly different from each other. This indicates that the coexistence of all BTEX in the biogas stream only slightly affects the absorption efficiency. This phenomenon can be explained by the lack of significant differences in the structures of all monoaromatic hydrocarbons, which could combine with functional DES groups and form competitive interactions.

In the next part of the studies, the influence of the matrix effect on the DES absorption efficiency has been investigated (Fig. 5). The BTEX absorption efficiency from pure nitrogen and from a model biogas mixture consisting of methane: carbon dioxide: nitrogen in a 5:3:2 vol ratio was compared. The composition of the model biogas mixture represents a typical matrix of real biogas streams (Janusz-Cygan et al., 2021). The obtained results indicate that the type of gas matrix affects the effective time of BTEX absorption. It can be noticed that the use of a model biogas stream reduces the absorption time and thus reduces the DES absorption capacity. This is due to the partial absorption of the main components of the biogas, i.e. CH_4 and CO_2. All tested DES are consist of HBA and HBD. Therefore, it is very likely that methane can easily bind to the hydrogen bond acceptor ($CH_4⋯HBA$), while carbon dioxide can easily bind to the hydrogen bond donor ($CO_2⋯HBD$), through non-covalent bonds (Altamash et al., 2019). Thus, competitive interactions can form that reduce the efficiency of BTEX uptake.
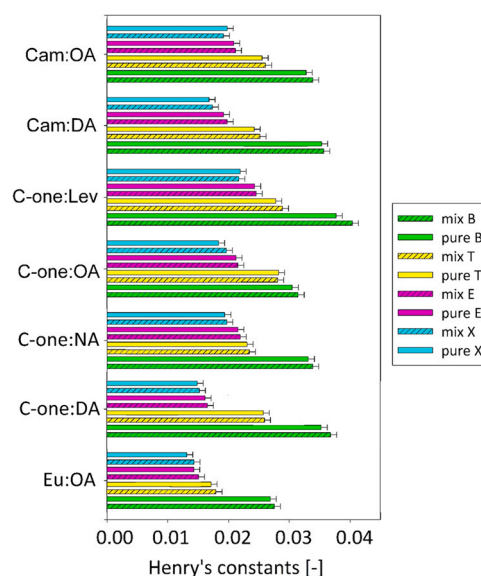

Fig. 4 – Henry's constants of the single impurities (solid column) and the BTEX mixture (hatch column) in DES. The total concentration of each of the impurities was 2000 mg/m³, at 25°C.

In addition, the most favorable DES was compared with commercially available absorbent which is mostly consist of tetraoxaoctadecane and pentaoxaheneicosane. The obtained results are presented in Fig. 6. The absorption processes were carried out using the model biogas mixture consisting of CH_4: CO_2: N_2 in a 5:3:2 vol ratio. The obtained results indicate that the new DES has an absorption capacity similar to that of a commercially available absorbent. The shortest impurities absorption time was obtained for the benzene, which was 4048 min. In turn, the longest time was obtained for the toluene, ethylbenzene, and xylene, which were 5334, 5790, 5800 min, respectively. The same BTEX removal trend can be observed for commercial absorbent. This indicates that the new DES may be a good alternative to commercially available sorbents. For which the shortest absorption time was achieved for benzene (3118 min). On the other hand, the absorption time was extended in the order of toluene, ethylbenzene and xylene, 4319, 5731 and 5859 min, respectively.

3.5. Mechanism of BTEX absorption

The absorption efficiency was also controlled at the structural level in order to explain the BTEX attachment mechanism for absorbents (DES and commercially available absorbent). For this purpose, the FT-IR and NMR analyses were carried out. Fig. S18 show FT-IR spectra of the Eu:OA (1:1) and Genosorb before and after the absorption process. The mechanisms of BTEX absorption were also explained for the rest of tested DES. The results are presented in Figs. S19-S49. On the Eu:OA (1:1) spectrum after absorption process, the characteristic peak from BTEX can be observed. The biggest changes are visible in the range of 3123–3000 cm⁻¹ (purple area), which can be assigned to the C_{Ar}-H stretching vibrations occurring in the aromatic ring. In addition, the structural changes in DES after the BTEX absorption process is also in the range 1631–1420 cm⁻¹ (blue area), and 907–633 cm⁻¹ (pink area). These changes are due to the emergence of the stretching vibrations C=C and the
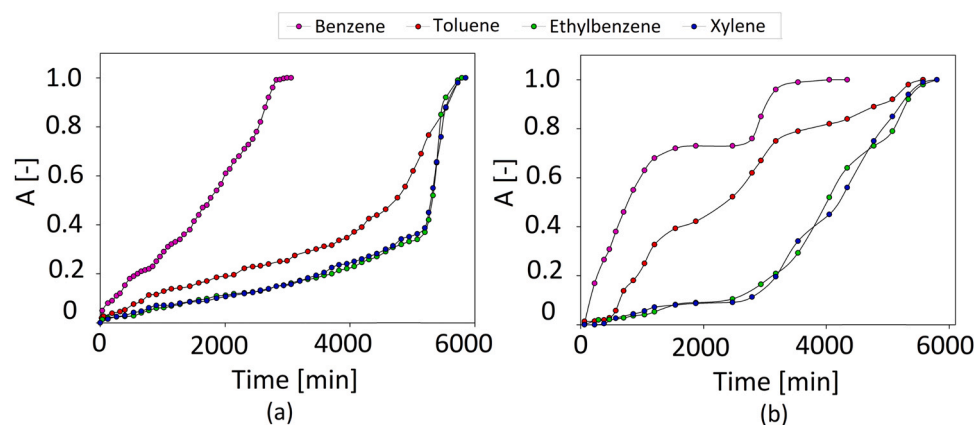
Fig. 5 – Experimental breakthrough curves of (a) Eu:OA (1:1) from pure nitrogen; (b) Eu:OA (1:1) from a model biogas mixture (CH$_4$:CO$_2$:N$_2$ 5:3:2 vol ratios) flow 50 mL/min; temperature 25 °C; inlet BTEX concentration 2000 mg/m^3, the volume of the DES 50 mL; absorption column dimensions: height 10 cm and width 3 cm.
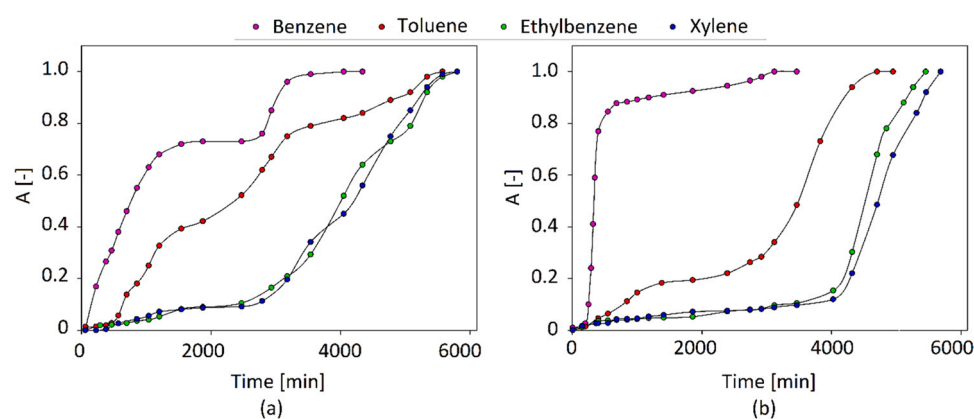

Fig. 6 – Experimental breakthrough curves of (a) Eu:OA (1:1) and (b) Genosorb (temperature 25 °C; biogas (matrix gas: CH$_4$:CO$_2$:N$_2$ 5:3:2 vol ratios) flow 50 mL/min; inlet BTEX concentration 2000 mg/m^3), the volume of the sorbent 50 mL; absorption column dimensions: height 10 cm and width 3 cm.

deformation vibrations outside the plane C$_{Ar}$-H, respectively. The above described mentioned chemical shifts suggest that the main driving force behind the BTEX absorption process is the formation of hydrogen bonds between DES and the aromatic ring with BTEX. This fact is also confirmed by the shifts signals with DES corresponding to the -OH groups from HBD and C═O from HBA, which are shifted towards the lower wavenumbers, from 3431 to 3014 cm^{-1} to 3415–3027 cm^{-1} and from 1711 cm^{-1} to 1708 cm^{-1}. For the remaining tested DES, very similar shifts can be observed.

The similar results can be observed for commercially available absorbent. The characteristic signals from BTEX are observed in very close ranges. In the spectrum after absorption process the following signals can be observed C$_{Ar}$-H stretching vibrations in the range of 3123–3000 cm^{-1} (purple area), stretching vibrations C═C 1631–1420 cm^{-1} (blue area), deformation vibrations outside the plane C$_{Ar}$-H 907–633 cm^{-1} (pink area). The peak from the C-O-C bond which are visible at the wavenumber of 1112 cm^{-1} on spectrum before absorption is shifted towards higher values (Fig. 7). This proves that ether group participates in the attachment of BTEX to the absorbent. It can be concluded that there are absorbent-BTEX bonds between the ether group (from Genosorb) and the aromatic group (from BTEX), which are the driving force behind the BTEX absorption process.

In the ^{1}H NMR and ^{13}C NMR spectra of both Eu:OA (1:1) and Genosorb after the absorption process all visible peaks

can be assigned to specific atoms derived from the Eu:OA (1:1) and BTEX (Fig. S50). This confirms that the absorption process is a physical one, without the formation of other substances by the reaction. In the ^{1}H NMR and ^{13}C NMR spectrum for Eu:OA (1:1) after the absorption process can be observed the shifts towards the higher values. For HBD the biggest differences in the NMR spectrum can be observed for protons (H1) and the carbon atom (C1), which are derived from the carboxyl group the octanoic acid. The described differences are at the levels 0.48 ppm and 0.9 ppm. In the case of HBA, the biggest differences can be observed for protons (H6), which come from the methyl group in close contact with the O atom, and the carbon atom (C6) which forms a -CH$_3$ group connected to an aromatic ring. The described differences signals are at the levels of 0.34 ppm and 0.46 ppm. This indicate that the interactions between BTEX and DES are mainly caused by the van der Waals forces between the aromatic ring and the carboxyl group of HBD. Similar behavior can be observed for Genosorb. All peaks in NMR spectra are shifted towards the higher values. Detailed values of chemical shifts for Eu:OA and Genosorb are presented in Table S4.

In order to understand the electrostatic interactions between absorbents and BTEX, σ-profiles were calculated. According to the definition, σ-profiles is a distribution function that relates the surface area of a molecule to the charge density of the surface (Han et al., 2018). Based on profiles
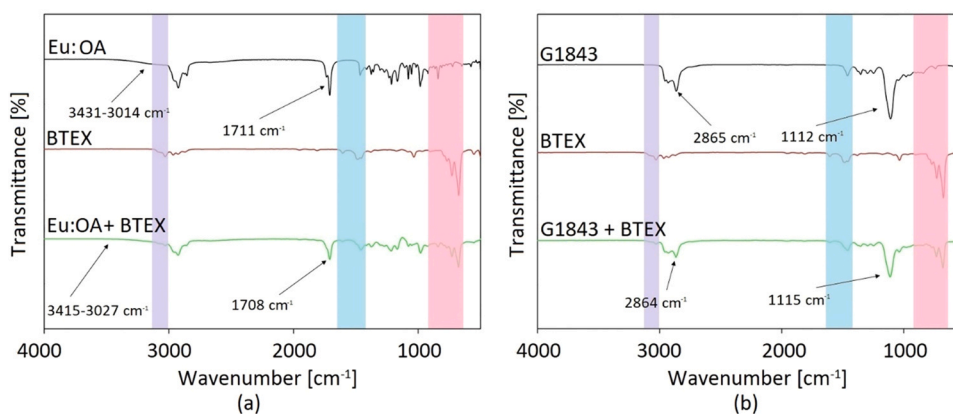
Fig. 7 – FT-IR spectrum before and after BTEX absorption for (a) Eu:OA (1:1) and (b) Genosorb.

results, it is possible to predict how the BTEX molecules will interact in an absorbent solute system, as well as the selectivity and solubility of BTEX in absorbents. In these studies, the generated σ-profile diagrams were divided into three regions. The segment between -0.0082 e/Å^2 and $+0.0082$ e/Å^2 charge density show that the studied compound readily undergoes van der Waals interactions. Segments below -0.0082 e/Å^2 and above $+0.0082$ e/Å^2 indicate that the molecule represents the possibility of the formation of hydrogen bonding. For all studied DES and commercially available absorbents, peaks in all segments can be identified (Fig. 8 and S51). However, the largest peaks are in the non-polar part and much smaller peaks are located in the HBA and HBD regions. The -O- and =O groups are responsible for the presence of peaks in the HBA region, and the -COOH group in the HBD region. This indicates that strong hydrogen bonds were formed in DESs between the HBA and HBD components. In order to confirm the obtained results, the electrostatic potential (ESP) analysis was also performed. The results are presented in Fig. 11 and S47 which show the ESP mapped electron total density with an isovalue 0.001 au for absorbents, and BTEX. The red area shows the negative potential region (–40 kcal/mol), the blue part of the surface represents the positive potential area (40 kcal/mol), and the white part - is the non-polar region (0 kcal/mol). In DES molecules, electropositive areas are located around the H atom in –CH$_3$, -CH$_2$, -CH, and –COOH groups. The electronegative regions are located in –O-, and =O group from HBA, and neutral regions are located in both HBA and HBD molecules around carbon atoms. When DES is created, the electronegative area from HBA attracted the electropositive area from HBD. Thus, strong hydrogen bonds are formed between the DES components. The presence of large non-polar surfaces also indicates that additionally, weaker non-covalent interactions, i.e. van der Waals interactions, are created between the DES components. Similar interaction can be observed between BTEX and DES or commercially available absorbent. Due to the presence of mainly non-polar regions in DES structures, weaker electrostatic interactions are the most likely driving force for the absorption process.

3.6. Increasing the scale of the absorption process

For the most favorable DES, the absorption process was also performed on an enlarged scale in order to confirm the usefulness of DES. The scale-up included a 10-fold increase in the volume of absorbent to 500 mL and increasing gas flow

rate up to 500 mL/min. The processes were carried out on a model biogas stream consist of CH$_4$:CO$_2$:N$_2$ in 5:3:2 vol ratios. The absorption process was made in two temperature variants. The first of the absorption column was maintained at room temperature (RT) and the second absorption column was cooled to 10 °C. The absorption curves are presented in Fig. 9. Based on the received data, similar absorption results can be observed compared to tests performed on a laboratory scale. In both processes, the order of saturation of the absorbent with aromatic compounds decreases with the decreasing volatility of the compounds. Benzene in both processes first breaks through the absorbent. The process of effective benzene capture is almost two times shorter compared to other substances. The DES breakthrough time for benzene is 5000 min and 6500 min in 25 and 10 °C, respectively. The dependence of DES absorption capacity on temperature is also visible for other monoaromatic hydrocarbons. The duration of absorption at a temperature reduced is proportionally higher compared to room temperature, for toluene from 10500 min to 13700 min, for ethylbenzene and xylene from about 11500–15000 min, respectively. The relationship between the increase in the efficiency of the absorption process and the decrease in temperature is well known and results from the exothermic nature of the absorption process (Muresan et al., 2015). Absorption curves for ethylbenzene and xylene have a similar shape and a similar breakthrough time, which is associated with a large chemical similarity of both compounds. In addition, it can be observed that the absorption rate for less volatile compounds increases when the more volatile compounds (for example benzene) have already saturated the absorbent. This is probably due to the attachment of the remaining monoaromatic hydrocarbons to the already absorbed molecules through π-π interactions.

By integrating the areas under the obtained curves over time, the total volume of methane, carbon dioxide, and BTEX used during the process was calculated (Figure 52). Then, assuming the density of substances, their masses were determined. The sorption capacity was calculated as the ratio of the difference between the determined masses of individual compounds in the inlet and outlet streams and the mass of the absorption liquid. Additionally, the degree of absorption of gas stream components during the process was determined. All the results obtained in this way are summarized in Table 1.

The obtained results indicate that degree of BTEX absorption increase from 51.9% to 55.4% with decreasing
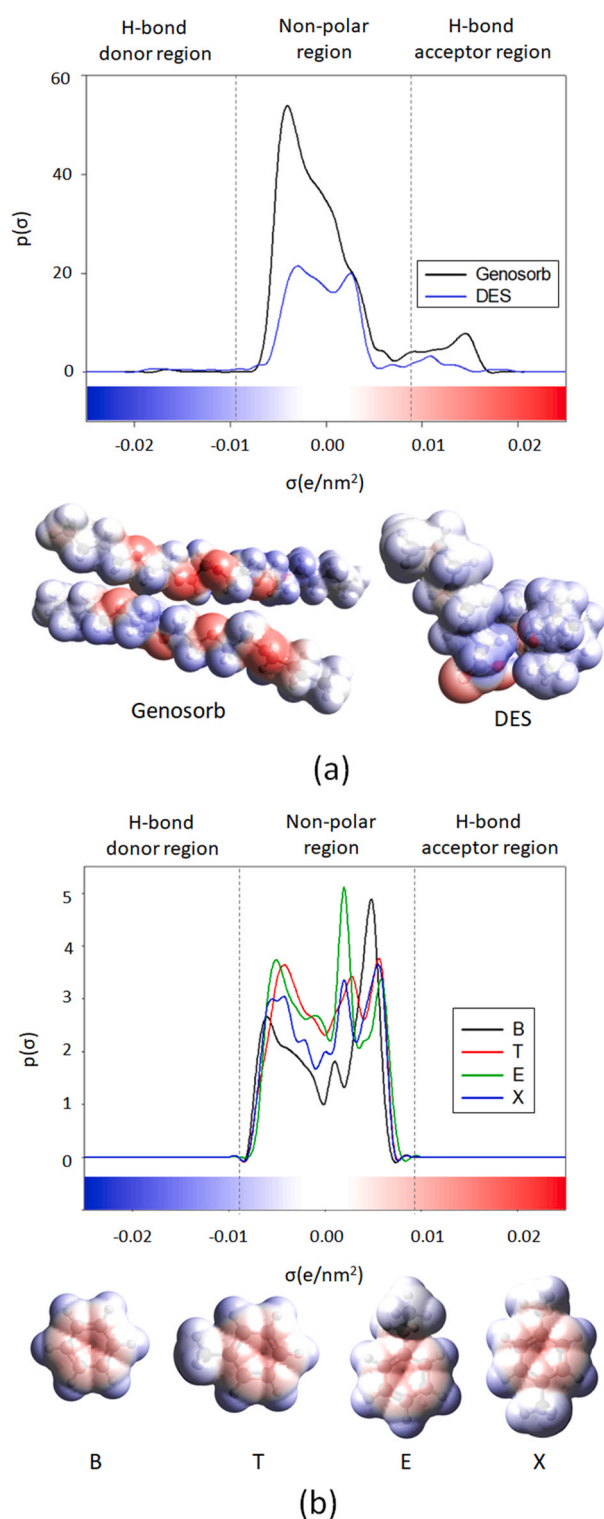
Fig. 8 – Sigma profile and electrostatic potential maps of a) Eu:OA (1:1) and commercially available absorbent; b) BTEX generated through COSMO-RS model.

temperature from 25° to 10°C. The same tendency can be observed for methane. For this molecule the degree of absorption increase from 0.73% to 0.81%. From the industrial absorption processes perspective, the increase in CH_4 solubility in absorbents is unfavorable, due to the fact that most industrial processes are carried out at 10°C. However, the increase in methane solubility is insignificant. The acceptable solubility of methane in the absorbent is 2% (Kvist and Aryal, 2019). The opposite behavior can be observed for carbon dioxide. However, the solubility of CO_2 in DES is also

negligible. Therefore, it can be concluded that the absorption process is selective for compounds from the group of monoaromatic hydrocarbons.

3.7. Comparison of process control methods

During the studies, two alternative methods for the control of absorption capacity were tested. Instrumental (analytical) techniques and a matrix of chemical gas sensors were used for process control and monitoring of tests performed. Gas chromatography with a flame ionization detector (GC-FID) and thermal conductivity detector (GC-TCD) were used as a reference method, which allowed qualitative and quantitative analysis of chemical compounds present in the tested samples.

The commercially available gas sensors were selected to construct the array and based on the signals received the mathematical models were developed. They show the correlation between the results obtained using the reference technique and sensor matrix. The use of widely available sensors makes it possible to easily reproduce the constructed array and to duplicate it many times, which would be difficult to achieve in the case of testing prototype sensors.

The prepared sensors array was calibrated and validated using Multiple Linear Regression (MLR). Since the process was conducted at two different temperatures, which are 10°C and 25°C, it was decided to develop separate models for each of these cases. This approach allowed to determine the impact of the absorption liquid components on the obtained gas sensor signals. It was expected that the eucalyptol emission, which was a component of the absorption liquid used, would affect the signals from the gas sensors, particularly the PID sensor. For this reason, based on the recorded matrix response signals six MLR models were developed: for the inlet stream (total BTEX in 10°C and total BTEX in 25°C) and outlet stream (total BTEX in 10°C and total BTEX in 25°C), one common MLR model for carbon dioxide inlet and outlet streams and one for methane in the same configuration. The MLR models for BTEX were developed to return the predicted total area of the chromatographic peaks of these compounds. Correlation charts for inlet and outlet streams, showing the accuracy of the prepared models, are presented in Fig. 10.

For methane and carbon dioxide, model gas mixtures were prepared to reflect the expected concentrations of these gases at the inlet and outlet streams of the process. The composition of the binary gas mixtures is shown in Table S5. The gas sensor array response was recorded for each mixture, with the analysis repeated three times. The number of gas calibration mixtures prepared was 42. Correlation charts of MLR models prepared for methane and carbon dioxide are shown in Figure 15.

The validity of using this method is confirmed by the values of the coefficients of determination (R^2) in the correlation plots. The value of coefficients of determination between chromatographic results and the values returned by prepared models are shown in Table S5. For five of the six prepared models the values of R^2 were more than 0.9850. The lowest values of R^2 was achieved for the BTEX inlet stream at 25°C and was equal to 0.9629, which is still more than satisfactory. It should be noted that eucalyptol emission in outlet streams clearly affects the signals from the PID sensor. Additionally, the emission depends on the process temperature. This is shown by the intercept values in the outlet
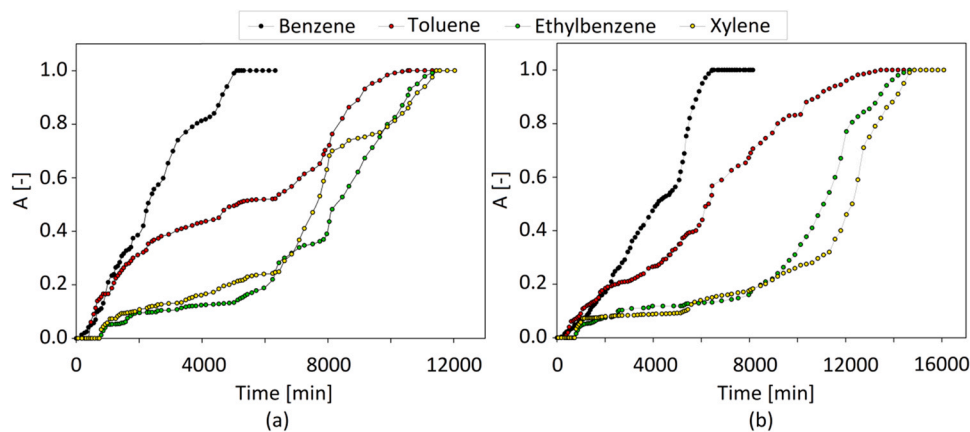
Fig. 9 – Absorption of BTEX (a) room temperature and (b) at 10 °C; absorption column dimensions: height 30 cm and width 5.5 cm.

stream models. Only after reduction of the matrix response to this eucalyptol the BTEX concentrations calculated using the prepared MLR models are similar to those obtained by chromatographic methods.

The developed MLR models were used to calculate the quantitative parameter of the description of the absorption process, which was absorptivity. The results of sensor matrices were compared with gas chromatography, which was a reference method. Fig. S53 presents the absorptivity parameter determination using a gas sensor array and gas chromatography throughout the process. The Root-Mean-Square Error (RMSE) for the entire range is presented in Table S6. RMSE is equal to 0.017 for the BTEX in the process carried out in the temperature of 10 °C, and 0.067 for the BTEX absorption process in 25 °C. In the case of methane and carbon dioxide the mean square errors reached slightly higher values. They were equal to 0.024 and 0.028 for methane in 10 °C and 25 °C. For carbon dioxide the calculated RMSE values are very similar as they are 0.031 at 10 °C and 0.039 in 25 °C respectively.

The obtained results indicate that the values of the total concentration of BTEX, CH_4 and CO_2 in biogas at the inlet and outlet do not differ significantly from this obtained using reference techniques. Additionally, such results demonstrate that sensor matrices could be satisfactorily used to control and monitor the absorption biogas purification processes. This study confirmed that the results obtained with the gas sensor array together with an appropriately selected mathematical model might be of similarly high level of quality as the results obtained using the gas chromatography technique (Fig. 11).

One of the limitations of sensor matrices is the possibility of measuring only the sum of BTEX concentration. There is no possibility to receive separate signals for individual compounds (inability to conduct qualitative analysis). However, from an industrial point of view, there is no need to measure separate compounds. Much more important is to measure the sum of impurities. A few additional challenges during sensor measurements are: the influence of temperature and humidity on the stability of the sensor's signals, multidimensionality of the generated signals (requires averaging by statistical methods) or complicated calibration on the basis of analytical procedures and regression models. Moreover, it should be noted that the research was conducted at laboratory scale. For this reason, the constructed array would not be able to be used directly in the process stream, but the next step will be to adapt the sensor array for operation under real conditions, e.g. using a dilution module to reduce gas concentration to required ranges.

Chromatographic techniques are characterized by high repeatability, reproducibility and accuracy and they give the possibility to identify all compounds present in a tested sample. In this regard, sensor arrays are no match for the instrumental techniques but if it is important to reduce the time of the analysis, investment costs or to automate the measurement process, they are an excellent alternative. Ultimately, gas sensor matrixes are intended to bridge the gap between gas sensors that are selective for specific chemical compounds and chromatographic techniques, which have a much broader field of application but are unsuitable for real-time measurements and require periodic maintenance and ensure the availability of high purity gases.

| Table 1 – Absorption capacity of DES.							
Compound	Inlet stream		Outlet stream		Calculated parameters		
	V [m³]	m [g]	V [m³]	M [g]	Δm [g]	Capacity [mg/g]	Degree of absorption [%]
Process in 10 °C							
CO_2	1.3	2375	1.25	2356	18.6	40	0.78
CH_4	3.1	2132	3.1	2115	17.4	37.3	0.81
BTEX	0.011	45.3	0.0049	20.2	25.1	53.9	55.4
Process in 25 °C							
CO_2	0.94	1765	0.93	1749.1	16	34.4	0.91
CH_4	2.44	1666	2.42	1654.2	12.2	26.2	0.73
BTEX	0.011	45	0.0052	21.5	23.2	49.7	51.9
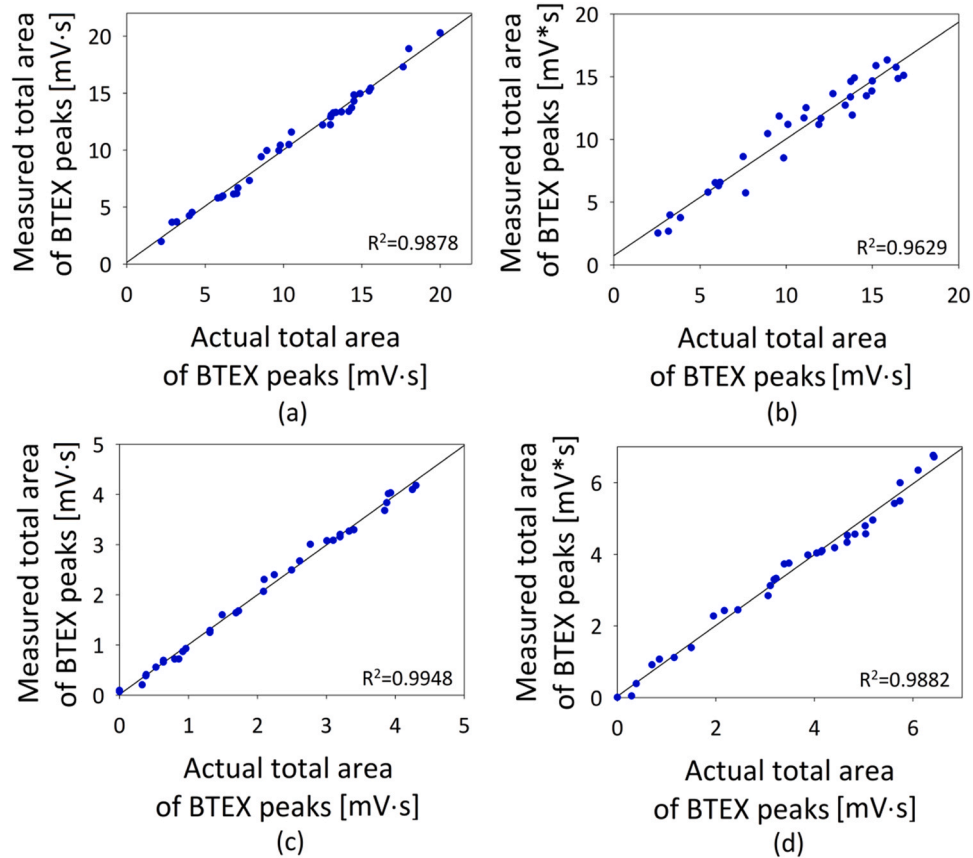
Fig. 10 – Actual and determined total area of chromatographic peaks correlation plot for inlet stream: (a) BTEX in 10 °C, (b) BTEX in 25 °C and outlet stream: (c) BTEX in 10 °C, (d) BTEX in 25 °C.

3.8.   *Regeneration process of DES*

From an economic and practical point of view, regeneration of the absorbents is a crucial feature. Therefore, the DES

regeneration processes after BTEX absorption were performed. The desorption process was carried out using conventional nitrogen barbotage in the temperature range 100–120 °C method. Based on the obtained results, it can be
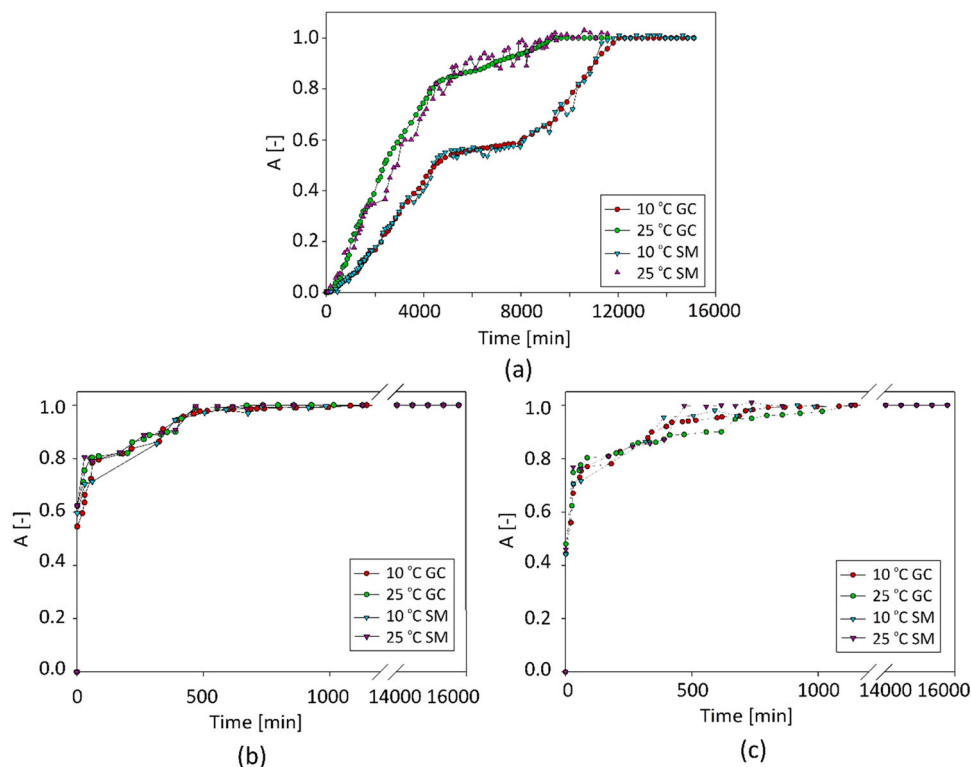
Fig. 11 – Absorption of (a) sum of BTEX; (b) CH_4; and (c) CO_2 controlled by gas chromatography (GC) and sensory matrix (SM).

Table 2 – Absorption capacity of toluene in various solvents.

Type of solvents	Abbreviation	Absorption capacity [g/g]	Gas matrix	Temperature [°C]	Price [€/kg]	Pressure [atm]	Literature
DES	Eu:OA (1:1)	0.056	model biogas (CH$_4$ 50%, CO$_2$ 30%, N$_2$ 20%)	10	43	1.0	This study
DES	Eu:OA (1:1)	0.050	model biogas (CH$_4$ 50%, CO$_2$ 30%, N$_2$ 20%)	25	43	1.0	This study
DES	LauA:DecA (1:2)	0.0035	nitrogen	30	27	n.d.	(Chen et al., 2021)
DES	Lid:DecA (1:2)	0.0023	nitrogen	30	533	n.d.	
DES	Thy:DecA (1:2)	0.0021	nitrogen	20	41	n.d.	
DES	TBPB:DecA (1:2)	0.00080	nitrogen	30	183	n.d.	
DES	DecA:OctN (1:2)	0.00068	nitrogen	30	18	n.d.	
DES	ChCl:Res (1:2)	0.00051	nitrogen	30	71	n.d.	
IL	[Bmim][NTf$_2$]	0.22	air	20	1600	1.17	(Universite, 2020)
IL	[Dmim][NTf$_2$]	0.34	air	20	6263	1.17	
IL	[Emim][Ac]	0.51	n.d.	25	1180	1	(Zhang et al., 2021)
IL	[Bmim][NTf$_2$]	0.15	n.d.	25	1600	1	
IL	[Bmim][Otf]	0.18	n.d.	25	1430	1	
IL	[Omim][PF$_6$]	0.31	n.d.	25	7920	1	
IL	[Hmpy][NTf$_2$]	0.21	n.d.	25	11860	1	
IL	[EMIM][BF$_4$]	0.12	synthetic air (21% O$_2$ and 79% N$_2$)	25	1330	1	(Ramos et al., 2020)
IL	[BMIM][BF$_4$]	0.24	synthetic air (21% O$_2$ and 79% N$_2$)	25	929	1	
IL	[HMIM][BF$_4$]	0.38	synthetic air (21% O$_2$ and 79% N$_2$)	25	16800	1	
IL	[BMIM][I]	0.17	synthetic air (21% O$_2$ and 79% N$_2$)	25	5600	1	
IL	[BMIM][PF$_6$]	0.29	synthetic air (21% O$_2$ and 79% N$_2$)	25	2276	1	
IL	[BMIM][HSO$_4$]	0.070	synthetic air (21% O$_2$ and 79% N$_2$)	25	1250	1	
IL	[BMIM][CH$_3$COO]	0.40	synthetic air (21% O$_2$ and 79% N$_2$)	25	1380	1	

observed that with the increase of the desorption temperature, the time of total BTEX removal was significantly shortened. At 120 °C, complete BTEX desorption was obtained after 1 h. In order to confirm the BTEX absorption-desorption capability, DES after regeneration was subjected into another absorption process. As shown in Fig. S54, hydrophobic Eu:OA (1:1) retains effective BTEX absorptivity at 95–97% during even ten consecutive regeneration cycles.

The absorption-desorption efficiency was also controlled at the structural level. Due to this the ^{1}H NMR, ^{13}C NMR and FT-IR absorption. The results are shown in Fig. S55. In all spectra, the signals from the BTEX that were identified in Figure 18 have disappeared. The spectra of fresh and regenerated DES are almost identical, which indicates that DES does not change its structure during the desorption process.

3.9.   Comparison of DES with other solvents

Currently, there are only a few studies in the literature relating to the absorption of BTEX from gas. Most of the work concerns the removal of toluene using ILs or DES. The comparison of DES efficiency with literature data is presented on Table 2. The obtained data indicate that Eu:OA (1:1) is characterized by higher absorption capacity of monoaromatic hydrocarbons in comparison to other DES, but the values are slightly lower than ILs. However, the cost of producing absorbents based on ILs is many times higher than for DES. In addition, the ILs have many others disadvantages such as the complicated synthesis, toxicity, and poor biodegradability. The disadvantages of ILs limit their large-scale use in absorption processes.

4.   Conclusions

Deep eutectic solvents based on monoterpenes were successfully synthesized and applied for BTEX absorption from

the biogas stream. The most important structural and physicochemical parameters that affected absorption efficiency were carefully studied. The obtained results indicate that DES consists of monoterpenes and carboxylic acids that are able to form strong hydrogen bonding and other weaker non-covalent interaction between active groups from HBA and HBA. The result of the interaction is the formation of stable eutectic mixtures, with a much lower melting point compared to pure ingredients, and favorable physicochemical properties, i.e. viscosity, density, and surface tension. From the tested DES, E:OA (1:1) is characterized by the highest absorption capacity of compounds from the BTEX group. This is due to the combination of its favorable physicochemical properties and the specific structure which selectively captures monoaromatic hydrocarbons by the formation van der Waals and π-π interactions between BTEX and DES. Absorption capacity depends on the absorption temperature and matrix composition. BTEX absorption capacity can vary from 0.05 to 0.056 g/g, which is comparable to commercially available absorbents. In addition, the low cost of DES production, the possibility of multiple regenerations without affecting the DES structure and without a significant reduction in the absorption efficiency, make DES an excellent green alternative to other absorption media.

Process control and monitoring was carried out using chromatographic techniques and self-constructed matrix of gas sensors. The controlled parameters of the absorption biogas treatment determined with the use of sensory techniques represents a similarly high level of quality as the results obtained with the gas chromatography. Thus, it was confirmed that real-time monitoring of absorption process is possible and there is no need to take any samples, conduct periodic maintenance of chromatographs and ensuring the availability of high purity gases. In other words, the analyzes showed that very similar or even identical results can be obtained faster and cheaper using gas sensors array, but they

do not allow quantitative analysis of tested samples. We conclude that the prepared sensor array, with the use of slight technical improvements, could be used on an industrial scale to supervise and control the ongoing process in real time in order to automate the process analysis.

CRediT authorship contribution statement

Patrycja Makoś-Chełstowska: Conceptualization, Methodology, Investigation, Writing – original draft, Writing – review & editing, Visualization, Supervision. **Edyta Słupek**: Investigation, Writing – original draft, Visualization, Conceptualization. **Aleksandra Kramarz**: Investigation, Writing – original draft. **Dominik Dobrzyniewski**: Investigation, Writing – original draft. **Bartosz Szulczyński**: Investigation, Writing – original draft. **Jacek Gębicki**: Writing – review & editing, Supervision.

Declaration of Competing Interest

The authors declare that they have no known competing financial interests or personal relationships that could have appeared to influence the work reported in this paper.

Acknowledgements

Appendix A. Supporting information

Supplementary data associated with this article can be found in the online version at doi:10.1016/j.cherd.2022.09.047.

References

What is BTEX and why is it important?, (n.d.). ⟨https://www.aeroqual.com/blog/what-is-btex⟩ (accessed March 29, 2022).

Bretón, J.G.C., Bretón, R.M.C., Morales, S.M., Kahl, J.D.W., Guarnaccia, C., del Carmen Lara Severino, R., Marrón, M.R., Lara, E.R., de la Luz Espinosa Fuentes, M., Chi, M.P.U., Sánchez, G.L., 2020. Health risk assessment of the levels of BTEX in ambient air of one urban site located in leon, guanajuato, mexico during two climatic seasons. Atmosphere (Basel) 11. https://doi.org/10.3390/atmos11020165

Johansson, K.A.U., 2012. Characterisation of contaminants in biogas before and after upgrading to vehicle gas, Rapp. SGC 246.

Abbasi, F., Pasalari, H., Delgado-Saborit, J.M., Rafiee, A., Abbasi, A., Hoseini, M., 2020. Characterization and risk assessment of BTEX in ambient air of a Middle Eastern City. Process Saf. Environ. Prot. 139, 98–105. https://doi.org/10.1016/J.PSEP.2020.03.019

Li, Y., Alaimo, C.P., Kim, M., Kado, N.Y., Peppers, J., Xue, J., Wan, C., Green, P.G., Zhang, R., Jenkins, B.M., Vogel, C.F.A., Wuertz, S., Young, T.M., Kleeman, M.J., 2019. Composition and toxicity of biogas produced from different feedstocks in California. Environ. Sci. Technol. https://doi.org/10.1021/acs.est.9b03003

Baghani, A.N., Sorooshian, A., Heydari, M., Sheikhi, R., Golbaz, S., Ashournejad, Q., Kermani, M., Golkhorshidi, F., Barkhordari, A., Jafari, A.J., Delikhoon, M., Shahsavani, A., 2019. A case study of BTEX characteristics and health effects by major point sources of pollution during winter in Iran. Environ. Pollut. 247, 607–617. https://doi.org/10.1016/J.ENVPOL.2019.01.070

Milazzo, M.J., Gohlke, J.M., Gallagher, D.L., Scott, A.A., Zaitchik, B.F., Marr, L.C., 2019. Potential for city parks to reduce

exposure to BTEX in air. Environ. Sci. Process. Impacts 21, 40–50. https://doi.org/10.1039/c8em00252e

Peng, C., Lee, J.W., Sichani, H.T., Ng, J.C., 2015. Toxic effects of individual and combined effects of BTEX on Euglena gracilis. J. Hazard. Mater. 284, 10–18. https://doi.org/10.1016/J.JHAZMAT.2014.10.024

Rasi, S., Läntelä, J., Rintala, J., 2011. Trace compounds affecting biogas energy utilisation - a review. Energy Convers. Manag. 52, 3369–3375. https://doi.org/10.1016/j.enconman.2011.07.005

Ryckebosch, E., Drouillon, M., Vervaeren, H., 2011. Techniques for transformation of biogas to biomethane. Biomass-.-. Bioenergy 35, 1633–1645. https://doi.org/10.1016/j.biombioe.2011.02.033

Santos-Clotas, E., Cabrera-Codony, A., Boada, E., Gich, F., Muñoz, R., Martín, M.J., 2019. Efficient removal of siloxanes and volatile organic compounds from sewage biogas by an anoxic biotrickling filter supplemented with activated carbon. Bioresour. Technol. 294, 122136. https://doi.org/10.1016/J.BIORTECH.2019.122136

Warren, W.K.E.H., 2012. A techno-economic comparison of biogas upgrading technologies in. Eur., MSc Thesis 44.

Angelidaki, I., Xie, L., Luo, G., Zhang, Y., Oechsner, H., Lemmer, A., Munoz, R., Kougias, P.G., 2019. Biogas upgrading: current and emerging technologies. Biofuels Altern. Feed. Convers. Process. Prod. Liq. Gaseous Biofuels 817–843. https://doi.org/10.1016/B978-0-12-816856-1.00033-6

Awe, O.W., Zhao, Y., Nzihou, A., Minh, D.P., Lyczko, N., 2017. A review of biogas utilisation, purification and upgrading technologies. Waste Biomass-.-. Valoriz. 8, 267–283. https://doi.org/10.1007/s12649-016-9826-4

Rasi, S., Läntelä, J., Rintala, J., 2014. Upgrading landfill gas using a high pressure water absorption process. Fuel 115, 539–543. https://doi.org/10.1016/j.fuel.2013.07.082

Ma, C., Liu, C., Lu, X., Ji, X., 2018. Techno-economic analysis and performance comparison of aqueous deep eutectic solvent and other physical absorbents for biogas upgrading. Appl. Energy 225, 437–447. https://doi.org/10.1016/j.apenergy.2018.04.112

Angelidaki, I., Treu, L., Tsapekos, P., Luo, G., Campanaro, S., Wenzel, H., Kougias, P.G., 2018. Biogas upgrading and utilization: Current status and perspectives. Biotechnol. Adv. 36, 452–466. https://doi.org/10.1016/J.BIOTECHADV.2018.01.011

Scholz, M., Frank, B., Stockmeier, F., Falß, S., Wessling, M., 2013. Techno-economic analysis of hybrid processes for biogas upgrading. Ind. Eng. Chem. Res. 52, 16929–16938. https://doi.org/10.1021/ie402660s

Tazang, N., Alavi, F., Javanmardi, J., 2020. Estimation of solubility of BTEX, light hydrocarbons and sour gases in triethylene glycol using the SAFT equation of state. Phys. Chem. Res 8, 251–266. https://doi.org/10.22036/pcr.2020.208933.1699

Xiao, X., Yan, B., Fu, J., Xiao, X., 2015. Absorption of gaseous toluene in aqueous solutions of some kinds of fluorocarbon surfactant. J. Air Waste Manag. Assoc. 65, 90–98. https://doi.org/10.1080/10962247.2014.968268

Fang, P., Tang, Z.J., Chen, X.B., Tang, Z.X., Chen, D.S., Huang, J.H., Zeng, W.H., Cen, C.P., 2016. Experimental study on the absorption of toluene from exhaust gas by paraffin/surfactant/water emulsion. J. Chem. 2016. https://doi.org/10.1155/2016/9385027

N. Hatcher, C. Jones, R. Weiland, Solubility of hydrocarbons and light ends in amines, Pet. Technol. Q. (2013).

Zhang, C., Wu, J., Wang, R., Ma, E., Wu, L., Bai, J., Wang, J., 2021. Study of the toluene absorption capacity and mechanism of ionic liquids using COSMO-RS prediction and experimental verification. Green. Energy Environ. 6, 339–349. https://doi.org/10.1016/J.GEE.2020.08.001

Słupek, E., Makoś, P., Gębicki, J., 2020a. Theoretical and economic evaluation of low-cost deep eutectic solvents for effective biogas upgrading to bio-methane. Energies 13, 3379. https://doi.org/10.3390/en13133379

Abbott, A.P., Capper, G., Davies, D.L., Rasheed, R.K., Tambyrajah, V., 2003. Novel solvent properties of choline chloride/urea

mixtures. Chem. Commun. 70–71. https://doi.org/10.1039/b210714g

Smith, E.L., Abbott, A.P., Ryder, K.S., 2014. Deep eutectic solvents (DESs) and their applications. Chem. Rev. 114, 11060–11082. https://doi.org/10.1021/cr300162p

Ghazali, Z., Hassan, N.H., Yarmo, M.A., Peng, T.L., Othaman, R., 2019a. Immobilization of choline chloride: urea onto mesoporous silica for carbon dioxide capture. Sains Malays. 48, 1025–1033. https://doi.org/10.17576/jsm-2019-4805-11

Hussin, F., Aroua, M.K., Yusoff, R., 2021. Adsorption of CO_2 on palm shell based activated carbon modified by deep eutectic solvent: breakthrough adsorption study. J. Environ. Chem. Eng. 9, 105333. https://doi.org/10.1016/J.JECE.2021.105333

Makoś, P., Boczkaj, G., 2019. Deep eutectic solvents based highly efficient extractive desulfurization of fuels – eco-friendly approach. J. Mol. Liq. 296, 111916–111927. https://doi.org/10.1016/j.molliq.2019.111916

Cunha, S.C., Fernandes, J.O., 2018. Extraction techniques with deep eutectic solvents. TrAC - Trends Anal. Chem. 105, 225–239. https://doi.org/10.1016/j.trac.2018.05.001

Makoś, P., Słupek, E., Małachowska, A., 2020a. Silica gel impregnated by deep eutectic solvents for adsorptive removal of BTEX from gas streams. Mater. (Basel) 13, 1894. https://doi.org/10.3390/ma13081894

Makoś, P., Słupek, E., Gębicki, J., 2020a. Extractive detoxification of feedstocks for the production of biofuels using new hydrophobic deep eutectic solvents – Experimental and theoretical studies. J. Mol. Liq. 308, 113101–113112. https://doi.org/10.1016/j.molliq.2020.113101

Shukla, S.K., Mikkola, J., 2018. Intermolecular interactions upon carbon dioxide capture in deep-eutectic solvents. Phys. Chem. Chem. Phys. 20, 24591–24601. https://doi.org/10.1039/c8cp03724h

García, G., Aparicio, S., Ullah, R., Atilhan, M., 2015. Deep eutectic solvents: physicochemical properties and gas separation applications. Energy Fuels 29, 2616–2644. https://doi.org/10.1021/ef5028873

Zubeir, L.F., Van Osch, D.J.G.P., Rocha, M.A.A., Banat, F., Kroon, M.C., 2018. Carbon dioxide solubilities in decanoic acid-based hydrophobic deep eutectic solvents. J. Chem. Eng. Data 63, 913–919. https://doi.org/10.1021/acs.jced.7b00534

Ghazali, Z., Yarmo, M.A., Othaman, R., 2019b. Confinement and characterization of deep eutectic solvent based on choline chloride:alcohol into nanoporous silica for CO_2 capture. AIP Conf. Proc. 2111. https://doi.org/10.1063/1.5111262

Luo, Q., Hao, J., Wei, L., Zhai, S., Xiao, Z., An, Q., 2021. Protic ethanolamine hydrochloride-based deep eutectic solvents for highly efficient and reversible absorption of NH3. Sep. Purif. Technol. 260, 118240. https://doi.org/10.1016/j.seppur.2020.118240

Wu, H., Shen, M., Chen, X., Yu, G., Abdeltawab, A.A., Yakout, S.M., 2019. New absorbents for hydrogen sulfide: deep eutectic solvents of tetrabutylammonium bromide/carboxylic acids and choline chloride/carboxylic acids. Sep. Purif. Technol. 224, 281–289. https://doi.org/10.1016/J.SEPPUR.2019.04.082

Słupek, E., Makoś-Chełstowska, P., Gębicki, J., 2021. Removal of siloxanes from model biogas by means of deep eutectic solvents in absorption process. Mater. (Basel) 14, 1–20. https://doi.org/10.3390/ma14020241

Makoś-Chełstowska, P., Słupek, E., Kramarz, A., Gębicki, J., 2021a. New carvone-based deep eutectic solvents for siloxanes capture from biogas. Int. J. Mol. Sci. 22, 9551–9574.

Słupek, E., Makoś, P., 2020. Absorptive desulfurization of model biogas stream using choline chloride-based deep eutectic solvents. Sustainability 12, 1619–1635. https://doi.org/10.3390/su12041619

Makoś-Chełstowska, P., Słupek, E., Gębicki, J., 2021b. Deep eutectic solvents – based green absorbents for effective volatile organochlorine compounds removal from biogas. Green. Chem. https://doi.org/10.1039/d1gc01735g

Moura, L., Moufawad, T., Ferreira, M., Bricout, H., Tilloy, S., Monflier, E., Costa Gomes, M.F., Landy, D., Fourmentin, S., 2017. Deep eutectic solvents as green absorbents of volatile

organic pollutants. Environ. Chem. Lett. 15, 747–753. https://doi.org/10.1007/s10311-017-0654-y

Słupek, E., Makoś, P., Gębicki, J., 2020b. Deodorization of model biogas by means of novel non- ionic deep eutectic solvent. Arch. Environ. Prot. 46, 41–46. https://doi.org/10.24425/aep.2020.132524

Szulczyński, B., Rybarczyk, P., Gębicki, J., 2018. Monitoring of n-butanol vapors biofiltration process using an electronic nose combined with calibration models. Mon. Fur Chem. 149, 1693–1699. https://doi.org/10.1007/s00706-018-2243-6

Rybarczyk, P., Szulczyński, B., Gebicki, J., 2020. Simultaneous removal of hexane and ethanol from air in a biotrickling filter-process performance and monitoring using electronic nose. Sustain 12. https://doi.org/10.3390/su12010387

López, R., Cabeza, I.O., Giráldez, I., Díaz, M.J., 2011. Biofiltration of composting gases using different municipal solid waste-pruning residue composts: Monitoring by using an electronic nose. Bioresour. Technol. 102, 7984–7993. https://doi.org/10.1016/J.BIORTECH.2011.05.085

Cabeza, I.O., López, R., Giraldez, I., Stuetz, R.M., Díaz, M.J., 2013. Biofiltration of α-pinene vapours using municipal solid waste (MSW) – Pruning residues (P) composts as packing materials. Chem. Eng. J. 233, 149–158. https://doi.org/10.1016/J.CEJ.2013.08.032

Romero-Flores, A., McConnell, L.L., Hapeman, C.J., Ramirez, M., Torrents, A., 2017. Evaluation of an electronic nose for odorant and process monitoring of alkaline-stabilized biosolids production. Chemosphere 186, 151–159. https://doi.org/10.1016/J.CHEMOSPHERE.2017.07.135

Dobrzyniewski, D., Szulczyński, B., Dymerski, T., Gębicki, J., 2021. Development of gas sensor array for methane reforming process monitoring. Sensors 21, 1–15. https://doi.org/10.3390/s21154983

Pearce, T.C., Gardner, J.W., Friel, S., Bartlett, P.N., Blair, N., 1993. Electronic nose for monitoring the flavour of beers. Analyst 4, 371–377. https://doi.org/10.1039/AN9931800371

Spichiger, S., Spichiger-Keller, U.E., 2010. Process monitoring with disposable chemical sensors fit in the framework of process analysis technology (PAT) for innovative pharmaceutical development and quality assurance. Chim. (Aarau) 64, 803–807. https://doi.org/10.2533/chimia.2010.803

Chai, X.S., Falabella, J.B., Teja, A.S., 2005. A relative headspace method for Henry's constants of volatile organic compounds. Fluid Phase Equilib. 231, 239–245. https://doi.org/10.1016/J.FLUID.2005.02.006

Makoś-Chełstowska, P., Słupek, E., Małachowska, A., 2022a. Superhydrophobic sponges based on green deep eutectic solvents for spill oil removal from water. J. Hazard. Mater. 425. https://doi.org/10.1016/j.jhazmat.2021.127972

Lawal, M.W.A., Stephenson, P., Sidders, J., Ramshaw, C., Yeung, H., 2011. Post-combustion CO_2 capture with chemical absorption: a state-of-the-art review. Chem. Eng. Res. Des. 89, 1609–1624.

Chen, C.C., Huang, Y.H., Fang, J.Y., 2022. Hydrophobic deep eutectic solvents as green absorbents for hydrophilic VOC elimination. J. Hazard. Mater. 424, 127366. https://doi.org/10.1016/J.JHAZMAT.2021.127366

Wang, W., Zhang, Y., Liu, W., 2017. Bioinspired fabrication of high strength hydrogels from non-covalent interactions. Prog. Polym. Sci. 71, 1–25. https://doi.org/10.1016/J.PROGPOLYMSCI.2017.04.001

Brouwer, T., Kersten, S.R.A., Bargeman, G., Schuur, B., 2021. trends in solvent impact on infinite dilution activity coefficients of solutes reviewed and visualized using an algorithm to support selection of solvents for greener fluid separations. Sep. Purif. Technol. 272, 118727. https://doi.org/10.1016/J.SEPPUR.2021.118727

Ribeiro, B.D., Florindo, C., Iff, L.C., Coelho, M.A.Z., Marrucho, I.M., 2015. Menthol-based eutectic mixtures: Hydrophobic low viscosity solvents. ACS Sustain. Chem. Eng. 3, 2469–2477. https://doi.org/10.1021/acssuschemeng.5b00532

Florindo, C., Oliveira, F.S., Rebelo, L.P.N., Fernandes, A.M., Marrucho, I.M., 2014. Insights into the synthesis and

properties of deep eutectic solvents based on cholinium chloride and carboxylic acids. ACS Sustain. Chem. Eng. 2, 2416–2425. https://doi.org/10.1021/sc500439w

Chemat, F., Anjum, H., Shariff, A.M., Kumar, P., Murugesan, T., 2016. Thermal and physical properties of (Choline chloride + urea + l-arginine) deep eutectic solvents. J. Mol. Liq. 218, 301–308. https://doi.org/10.1016/J.MOLLIQ.2016.02.062

Hayyan, A., Mjalli, F.S., Alnashef, I.M., Al-Wahaibi, T., Al-Wahaibi, Y.M., Hashim, M.A., 2012. Fruit sugar-based deep eutectic solvents and their physical properties. Thermochim. Acta 541, 70–75. https://doi.org/10.1016/j.tca.2012.04.030

Makoś, P., Słupek, E., Gębicki, J., 2020b. Hydrophobic deep eutectic solvents in microextraction techniques–a review. Microchem. J. 152. https://doi.org/10.1016/j.microc.2019.104384

Makoś-Chełstowska, P., Słupek, E., Małachowska, A., 2022b. Superhydrophobic sponges based on green deep eutectic solvents for spill oil removal from water. J. Hazard. Mater. 425, 127972. https://doi.org/10.1016/J.JHAZMAT.2021.127972

Fan, C., Sebbah, T., Liu, Y., Cao, X., 2021. Terpenoid-capric acid based natural deep eutectic solvent: Insight into the nature of low viscosity. Clean. Eng. Technol. 3, 100116. https://doi.org/10.1016/j.clet.2021.100116

Haghbakhsh, R., Parvaneh, K., Raeissi, S., Shariati, A., 2018. A general viscosity model for deep eutectic solvents: the free volume theory coupled with association equations of state. Fluid Phase Equilib. 470, 193–202. https://doi.org/10.1016/j.fluid.2017.08.024

Jiménez, E., Cabanas, M., Segade, L., García-Garabal, S., Casas, H., 2001. Excess volume, changes of refractive index and surface tension of binary 1,2-ethanediol + 1-propanol or 1-butanol mixtures at several temperatures. Fluid Phase Equilib. 180, 151–164. https://doi.org/10.1016/S0378-3812(00)00519-7

Chen, Y., Chen, W., Fu, L., Yang, Y., Wang, Y., Hu, X., Wang, F., Mu, T., 2019. Surface tension of 50 deep eutectic solvents: effect of hydrogen-bonding donors, hydrogen-bonding acceptors, other solvents, and temperature. Ind. Eng. Chem. Res. 58, 12741–12750. https://doi.org/10.1021/acs.iecr.9b00867

Shahbaz, K., Mjalli, F.S., Hashim, M.A., AlNashef, I.M., 2012. Prediction of the surface tension of deep eutectic solvents. Fluid Phase Equilib. 319, 48–54. https://doi.org/10.1016/j.fluid.2012.01.025

Kurnia, K.A., Mutalib, M.I.A., Man, Z., Bustam, M.A., 2012. Density and surface tension of ionic liquids [H2N–C2mim][PF6] and [H2N–C3mim][PF6]. J. Chem. Eng. Data 17025–17036.

Abbott, A.P., Harris, R.C., Ryder, K.S., D'Agostino, C., Gladden, L.F., Mantle, M.D., 2011. Glycerol eutectics as sustainable solvent systems. Green. Chem. 13, 82–90. https://doi.org/10.1039/c0gc00395f

Mjalli, F.S., Naser, J., Jibril, B., Alizadeh, V., Gano, Z., 2014. Tetrabutylammonium chloride based ionic liquid analogues and their physical properties. J. Chem. Eng. Data 59, 2242–2251. https://doi.org/10.1021/je5002126

Salazar Gómez, J.I., Lohmann, H., Krassowski, J., 2016. Determination of volatile organic compounds from biowaste and co-fermentation biogas plants by single-sorbent adsorption. Chemosphere 153, 48–57. https://doi.org/10.1016/j.chemosphere.2016.02.128

López, M.D., Pascual-Villalobos, M.J., 2010. Mode of inhibition of acetylcholinesterase by monoterpenoids and implications for pest control. Ind. Crops Prod. 31, 284–288. https://doi.org/10.1016/j.indcrop.2009.11.005

Chen, C.C., Huang, Y.H., Hung, S.M., Chen, C., Lin, C.W., Yang, H.H., 2021. Hydrophobic deep eutectic solvents as attractive media for low-concentration hydrophobic VOC capture. Chem. Eng. J. 424, 130420. https://doi.org/10.1016/j.cej.2021.130420

Tsuzuki, S., Fujii, A., 2008. Nature and physical origin of CH/p interaction: significant difference from conventional hydrogen bonds. Phys. Chem. Chem. Phys. 10, 2581–2583. https://doi.org/10.1039/b805489b

Cabaleiro-Lago, E.M., Rodríguez-Otero, J., 2018. On the nature of σ-σ, σ-π, and π-π stacking in extended systems. ACS Omega 3, 9348–9359. https://doi.org/10.1021/acsomega.8b01339

Janusz-Cygan, A., Jaschik, J., Tańczyk, M., 2021. Upgrading biogas from small agricultural sources into biomethane by membrane separation. Membr. (Basel). 11, 10–14. https://doi.org/10.3390/membranes11120938

Altamash, T., Amhamed, A.I., Aparicio, S., Atilhan, M., 2019. Combined experimental and theoretical study on high pressure methane solubility in natural deep eutectic solvents. Ind. Eng. Chem. Res. 58, 8097–8111. https://doi.org/10.1021/acs.iecr.9b00702

Han, J., Dai, C., Yu, G., Lei, Z., 2018. Parameterization of COSMO-RS model for ionic liquids. Green. Energy Environ. 3, 247–265. https://doi.org/10.1016/j.gee.2018.01.001

Muresan, V., Unguresan, M.L., Varodi, C., Szucs-Balazs, J.Z., 2015. Temperature influence over the absorption process of CO₂ in octane. Proc. - 2015 8th Rom. Tier. 2 Fed. Grid, Cloud High. Perform. Comput. Sci. ROLCG 2015, 1–5. https://doi.org/10.1109/ROLCG.2015.7367420

Kvist, T., Aryal, N., 2019. Methane loss from commercially operating biogas upgrading plants. Waste Manag 87, 295–300.

A. Universite, Development of a hybrid process, Membrane-Ionic Liquid (ILM), for gas treatment, (2020).

Ramos, V.C., Han, W., Yeung, K.L., 2020. A comparative study between ionic liquid coating and counterparts in bulk for toluene absorption. Green. Chem. Eng. 1, 147–154. https://doi.org/10.1016/j.gce.2020.10.008

Supplementary Materials

Green monoterpenes based deep eutectic solvents for effective BTEX absorption from biogas

Patrycja Makoś-Chełstowska[1,2,], Edyta Słupek[1], Aleksandra Kramarz[1], Dominik Dobrzyniewski[1], Bartosz Szulczyński[1] and Jacek Gębicki[1]

[1] Department of Process Engineering and Chemical Technology, Faculty of Chemistry, Gdansk University of Technology, 80-233 Gdansk, Poland
[2] EcoTech Center, Gdańsk University of Technology, 80-233 Gdańsk, Poland

S.1. The procedures for collecting data from sensors and gas chromatography

In the first step, of analyzing the data collected during the biogas absorption purification process, MLR models were created to find and mathematically describe the relationships between the gas sensor's signals and the concentration of individual gases (carbon dioxide, methane and total BTEX), which in this case was represented by the chromatographic peak areas. Since the process was conducted at two different temperatures, which are 10°C and 25°C, it was decided to develop separate models for each of these cases. This approach allowed to determine the impact of the absorption liquid components on the obtained gas sensor signals. It was expected that the eucalyptol emission, which was a component of the absorption liquid used, would affect the signals from the gas sensors, particularly the PID sensor. For this reason, based on the recorded matrix response signals six MLR models were developed: for the inlet stream (total BTEX in 10°C and total BTEX in 25°C) and outlet stream (total BTEX in 10°C and total BTEX in 25°C), one common MLR model for carbon dioxide inlet and outlet streams and one for methane in the same configuration.

The MLR models for BTEX were developed to return the predicted total area of the chromatographic peaks of these compounds. Correlation charts for inlet and outlet streams, showing the accuracy of the prepared models, are presented in Figure S13.

For methane and carbon dioxide, model gas mixtures were prepared to reflect the expected concentrations of these gases at the inlet and outlet streams of the process. The composition of the binary gas mixtures is shown in Table S2. The gas sensor array response was recorded for each mixture, with the analysis repeated three times. The number of gas calibration mixtures prepared was 42. Correlation charts of MLR models prepared for methane and carbon dioxide are shown in Figure S14.
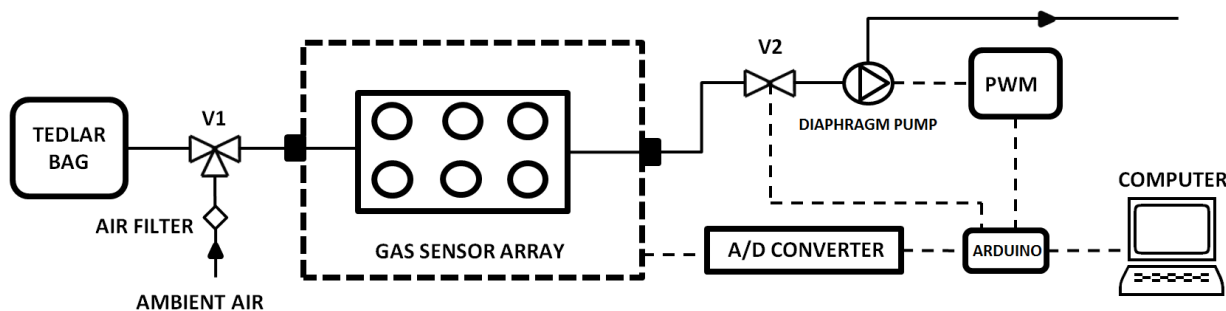
Figure S1 Gas sensor array experimental setup.
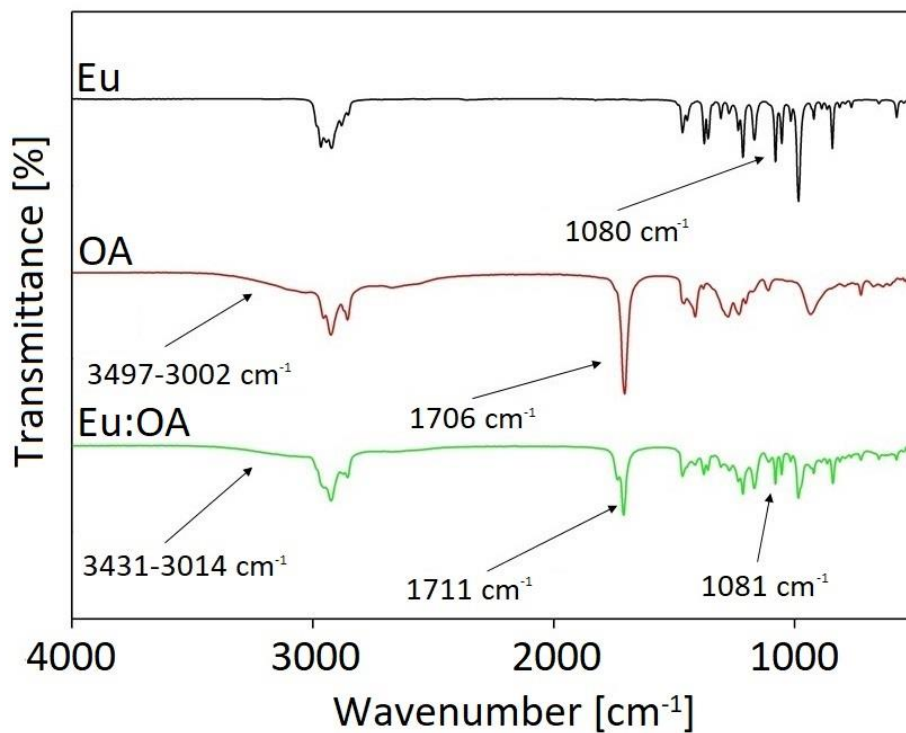
Figure S2 FT-IR spectrum of pure components Eu (HBA), OA (HBD), and Eu:OA (1:1).
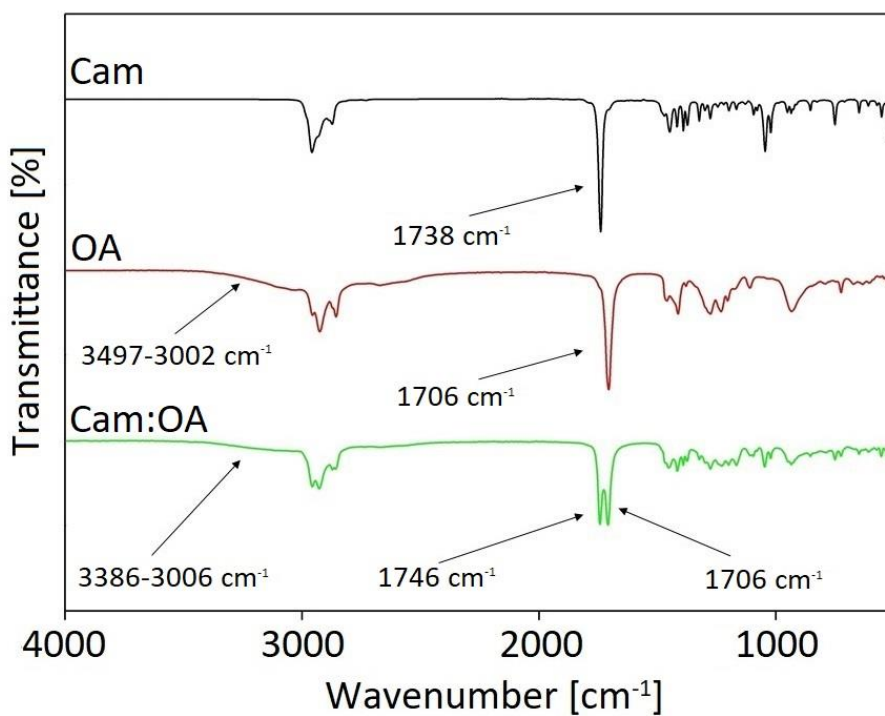
Figure S3 FT-IR spectrum of pure components Cam (HBA) and OA (HBD) and DES Cam:C8 (1:1).
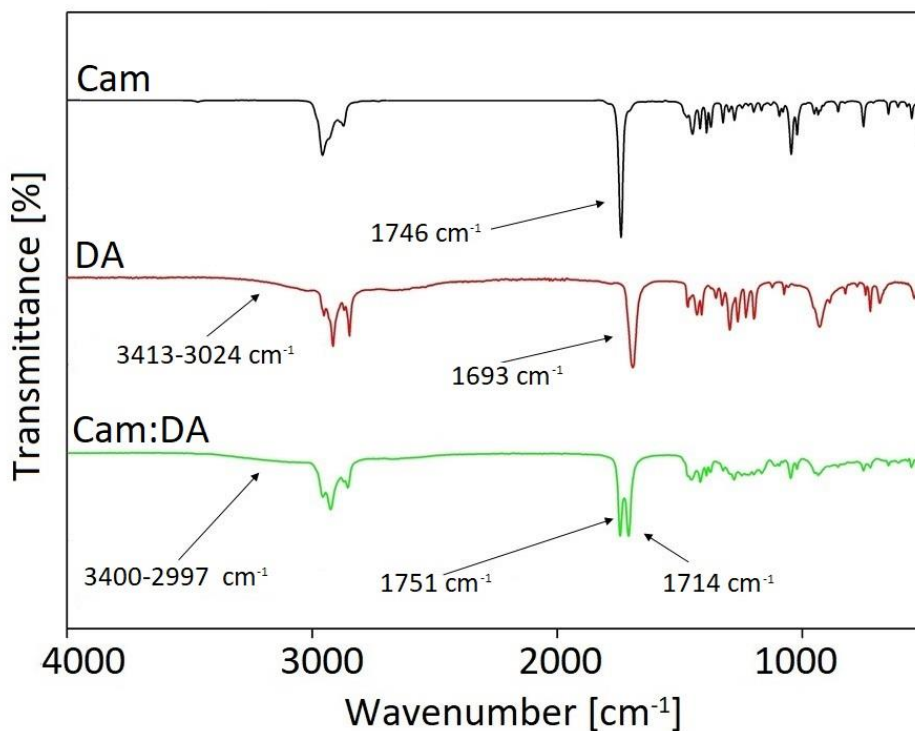
Figure S4 FT-IR spectrum of pure components Cam (HBA) and DA (HBD) and DES Cam:DA (1:1).
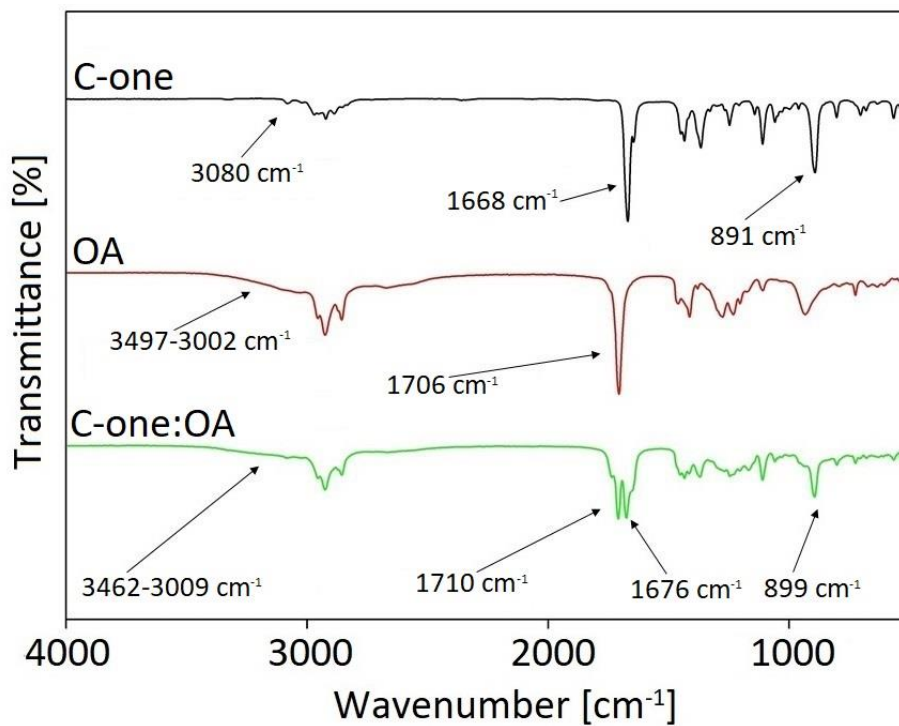
Figure S5 FT-IR spectrum of pure components C-one (HBA) and OA (HBD) and DES C-one:OA (1:1).
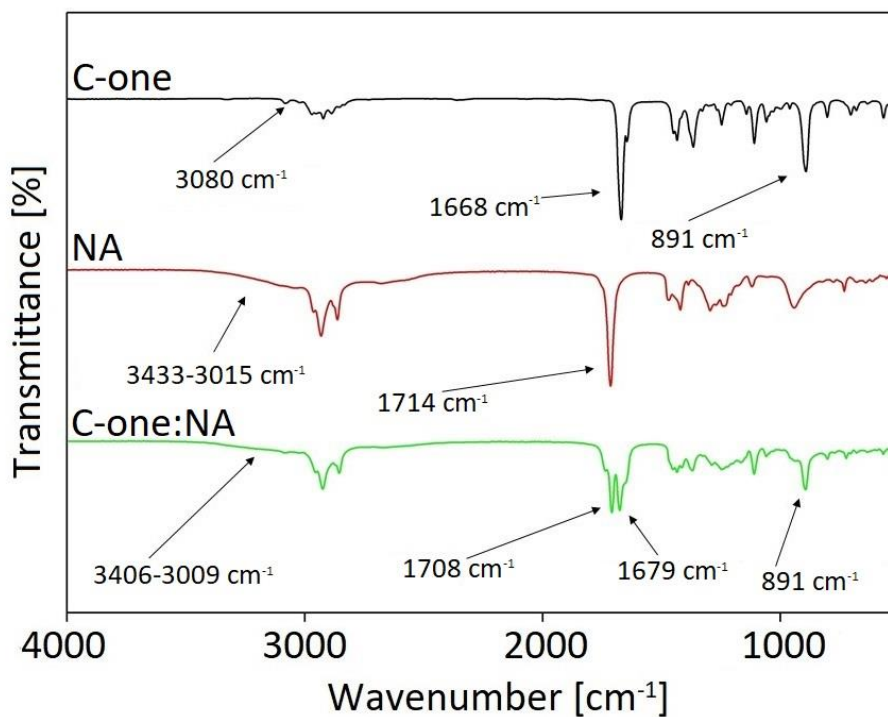
Figure S6 FT-IR spectrum of pure components C-one (HBA) and NA (HBD) and DES C-one:NA (1:1).
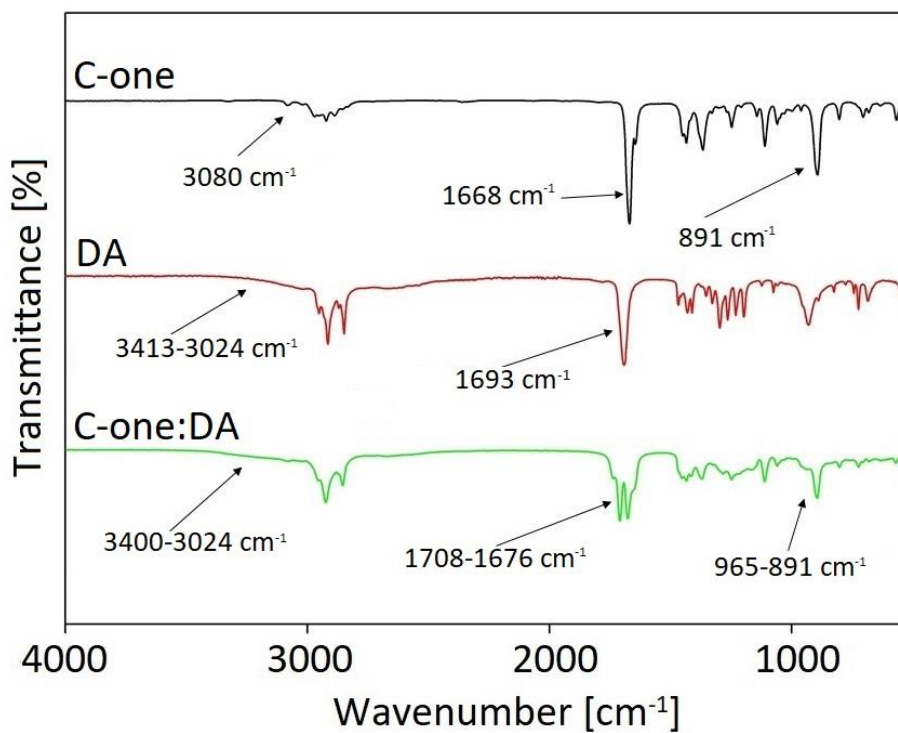
Figure S7 FT-IR spectrum of pure components C-one (HBA) and DA (HBD) and DES C-one:DA (1:1).
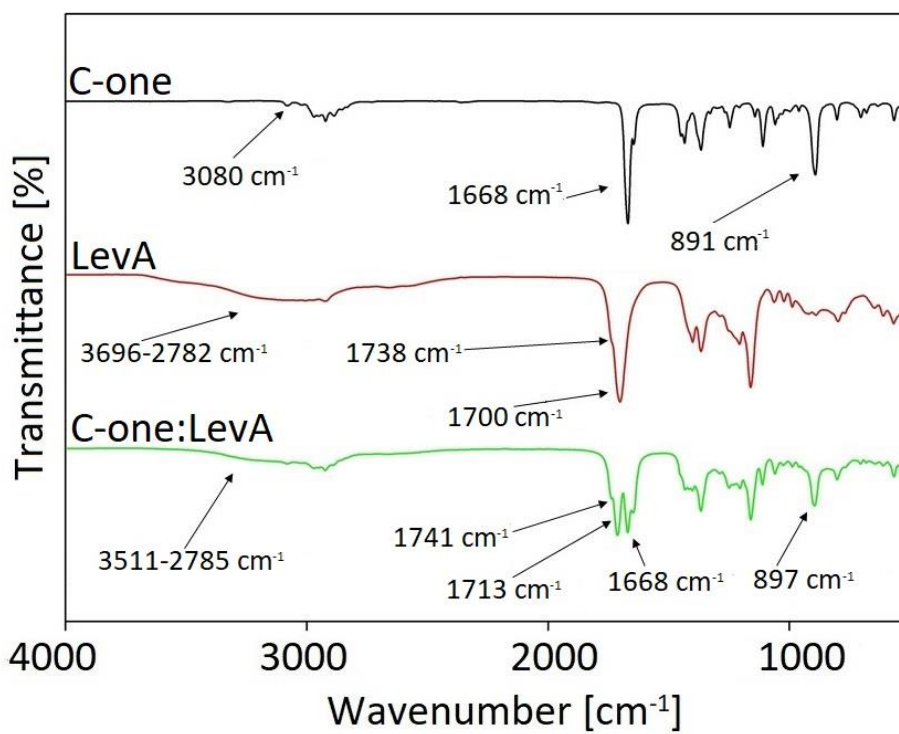
Figure S8 FT-IR spectrum of pure components C-one (HBA) and LevA (HBD) and DES C-one:LevA (1:1).
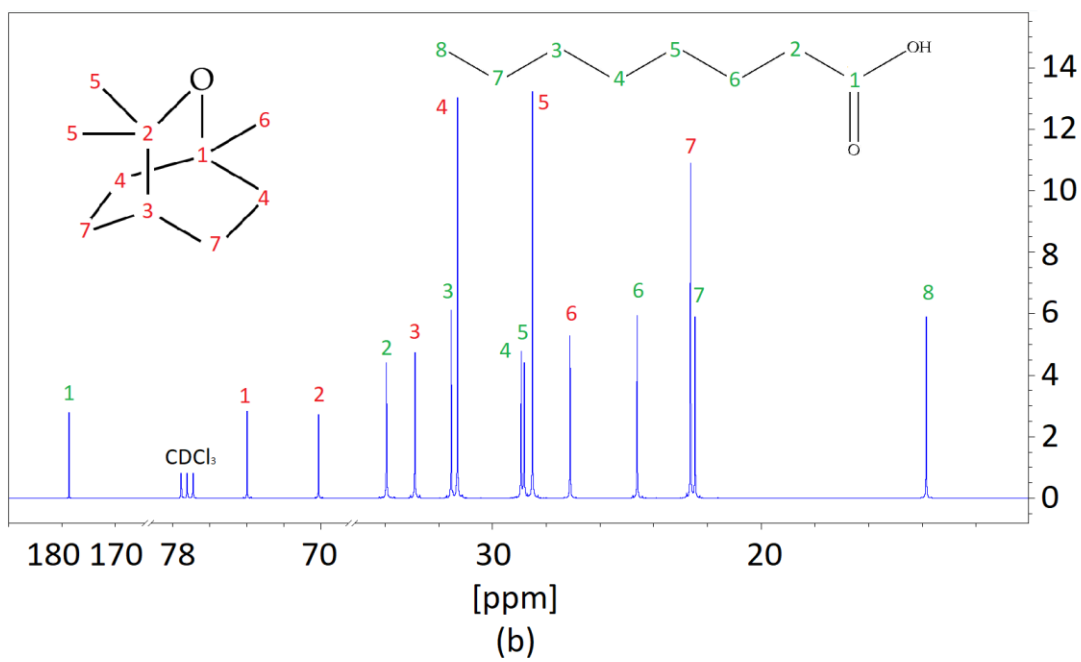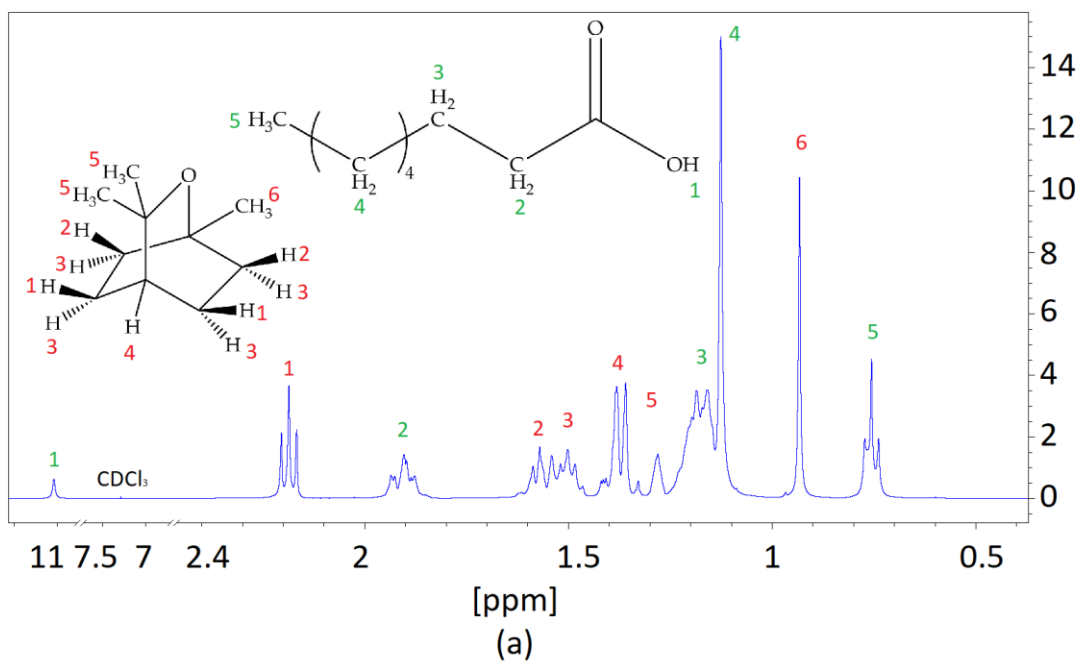
Figure S9 (a) ^{1}H NMR and (b) ^{13}C NMR spectra of Eu:OA (1:1).
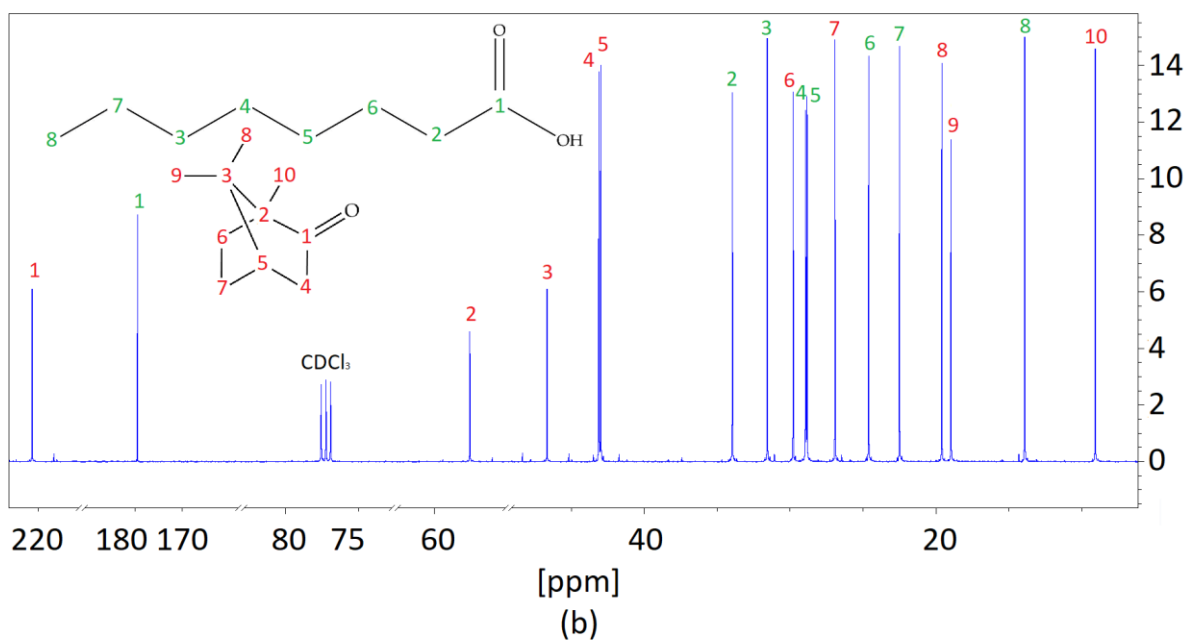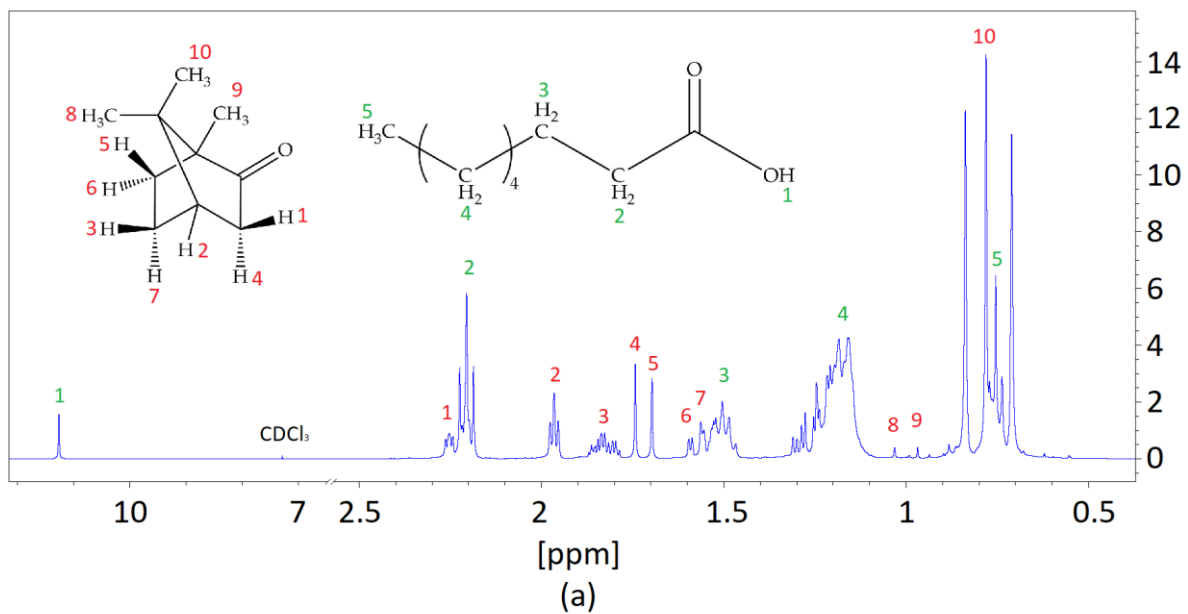
Figure S10 (a) ^{1}H NMR and (b) ^{13}C NMR of Cam:OA (1:1).
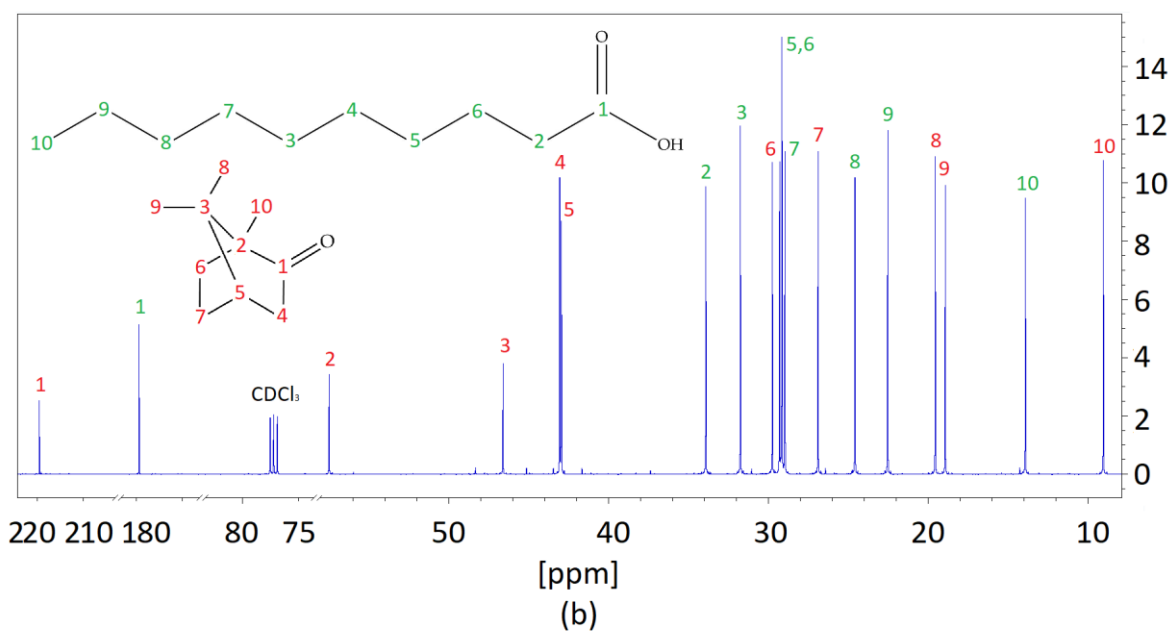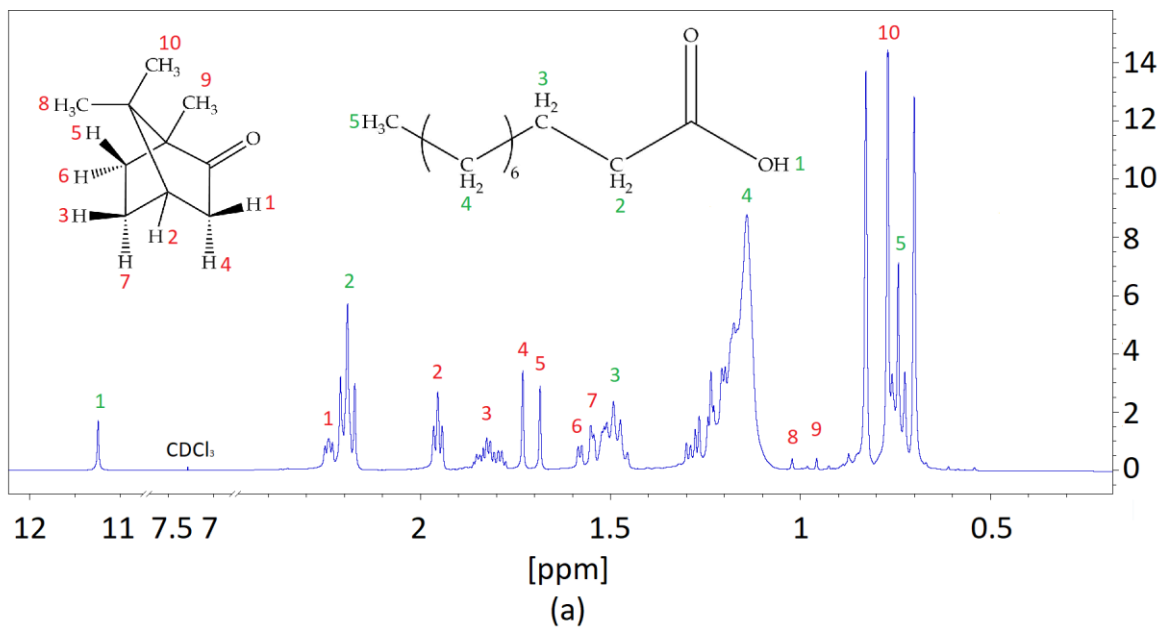
Figure S11 (a) ¹H NMR and (b) ¹³C NMR of Cam:DA (1:1).
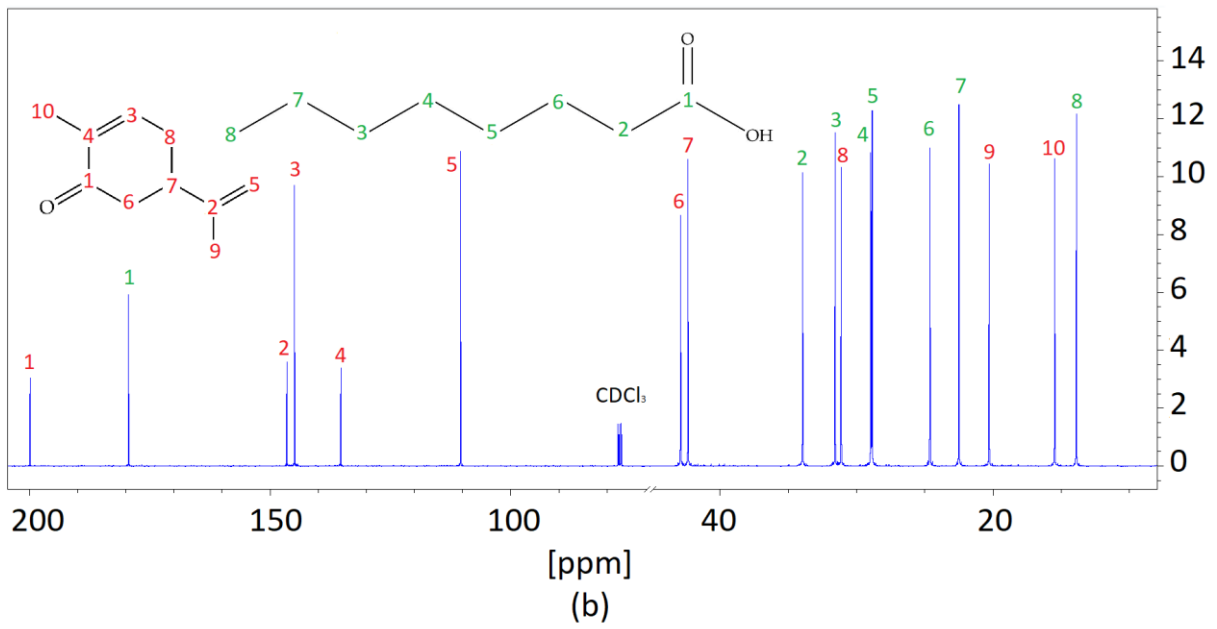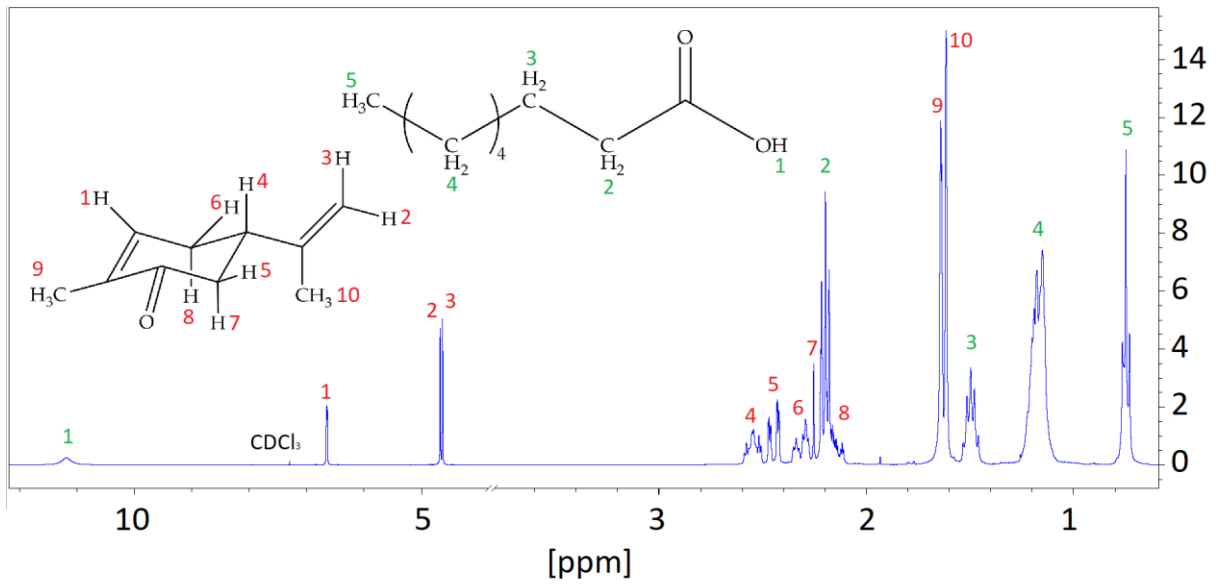
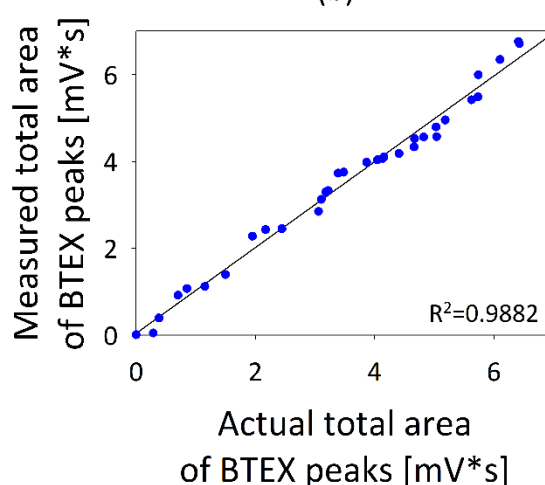**Figure S12** (a) ^{1}H NMR and (b) ^{13}C NMR of C-one:OA (1:1).
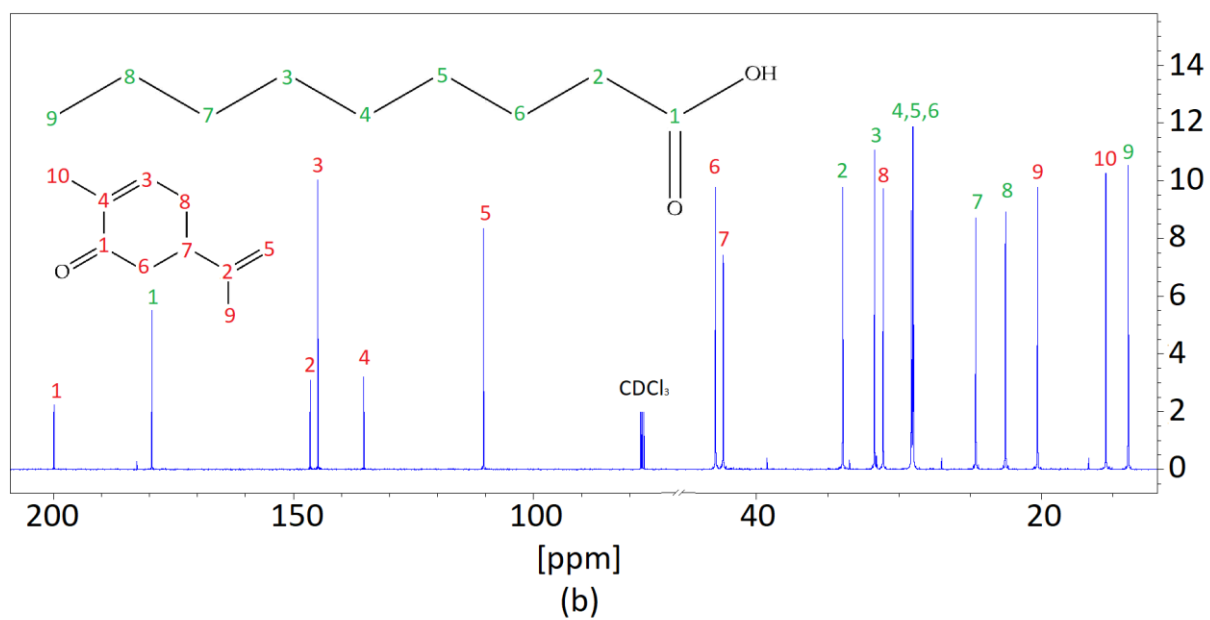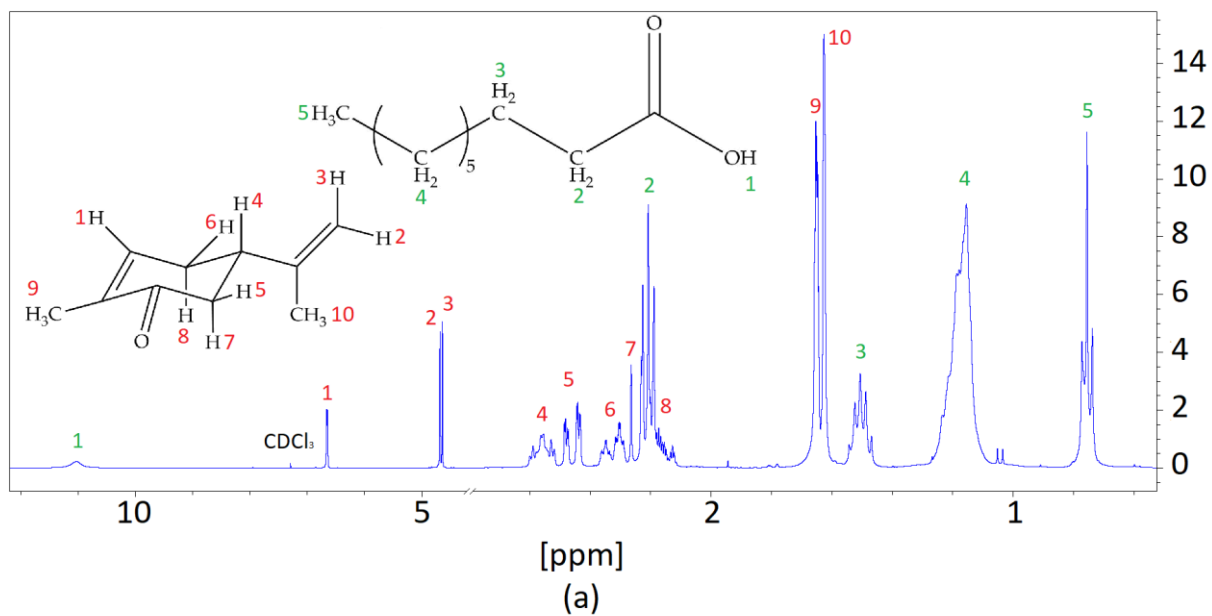
Figure S13 (a) ^{1}H NMR and (b) ^{13}C NMR of C-one:NA (1:1).
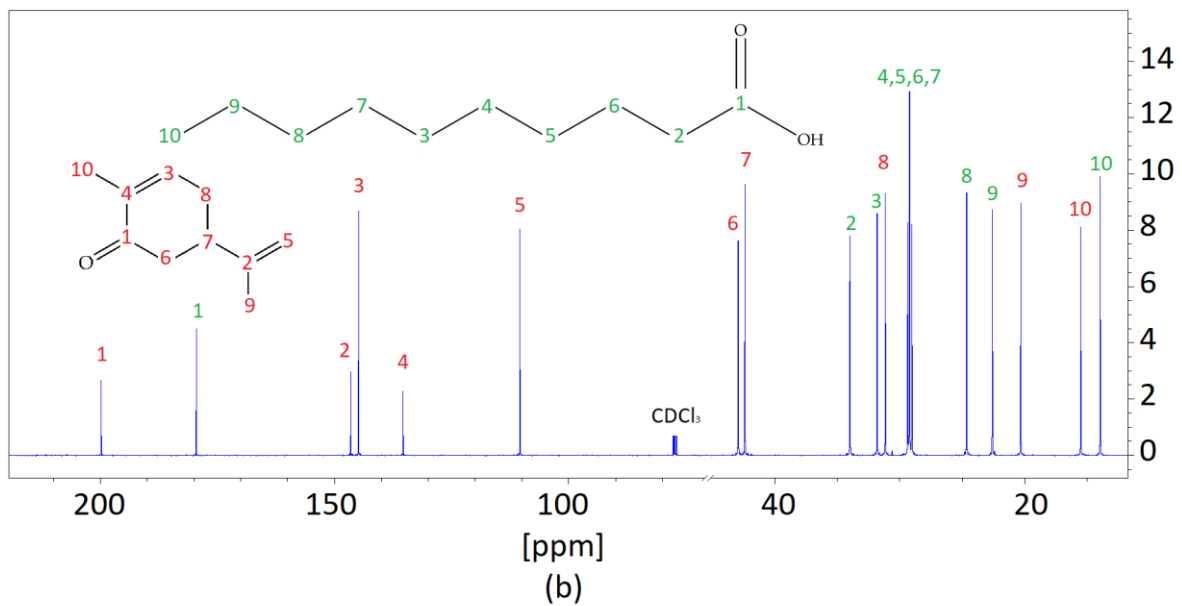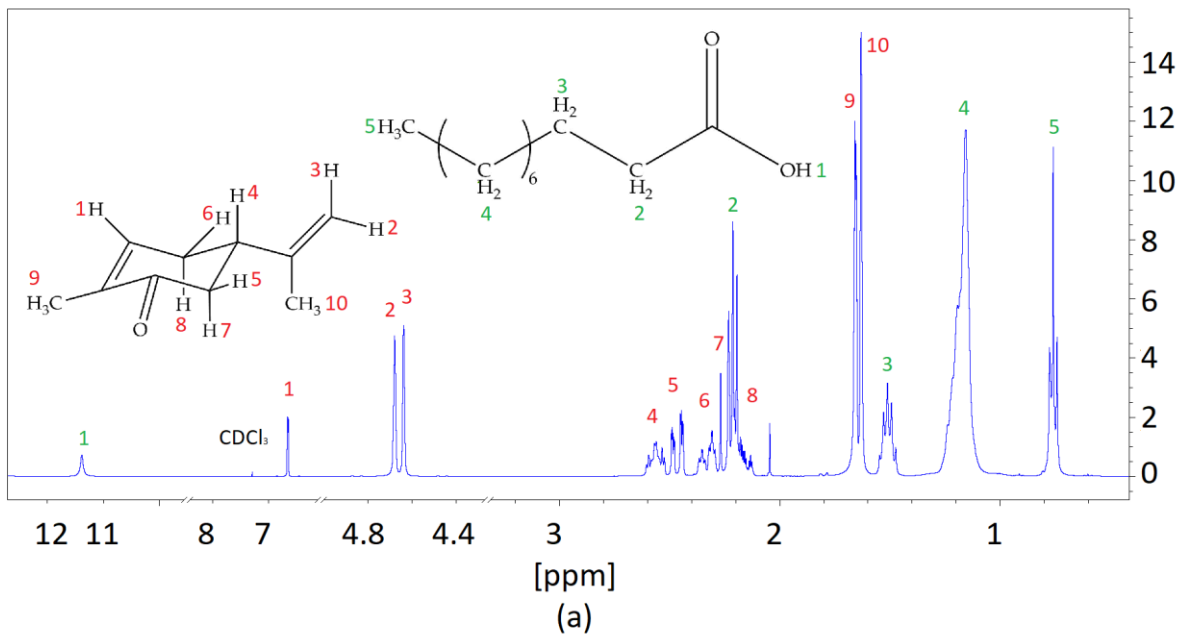
Figure S1 (a) ^{1}H NMR and (b) ^{13}C NMR of C-one:DA (1:1).
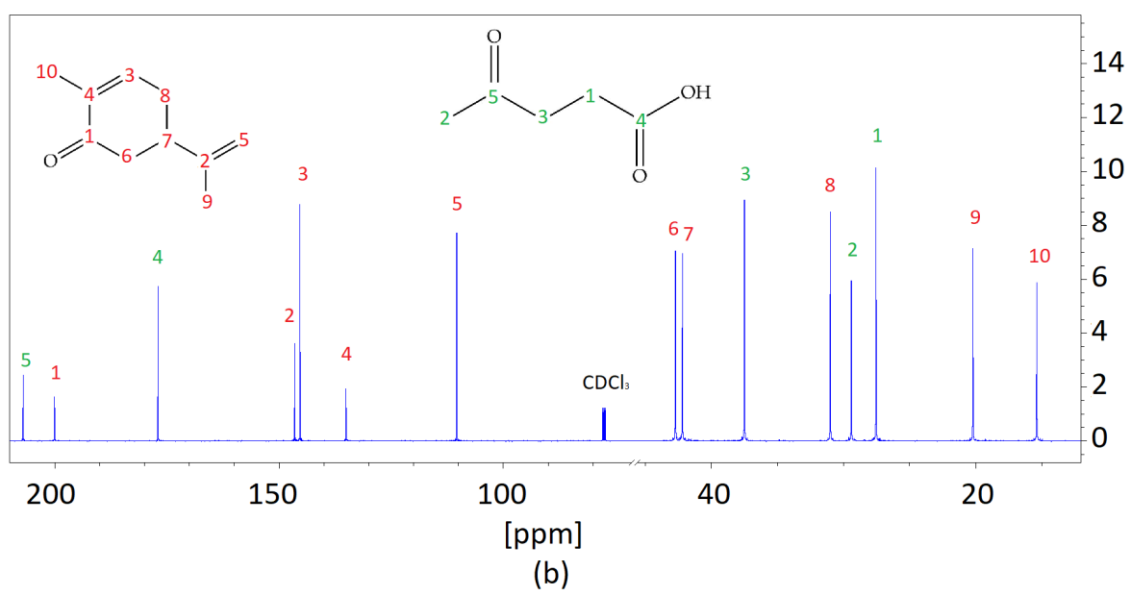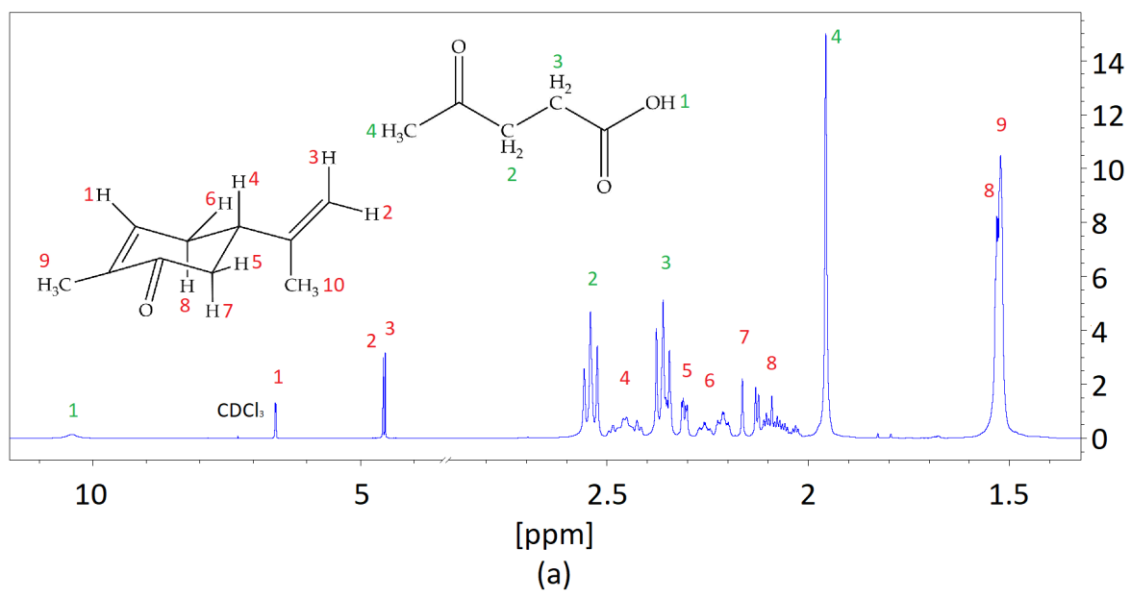
Figure S2 (a) ^{1}H NMR and (b) ^{13}C NMR of C-one:LevA (1:1).
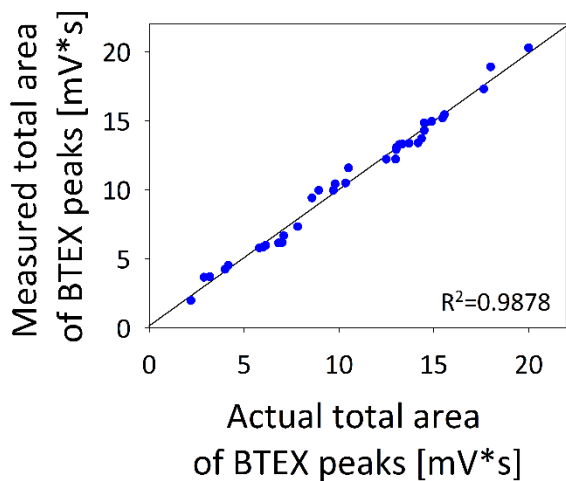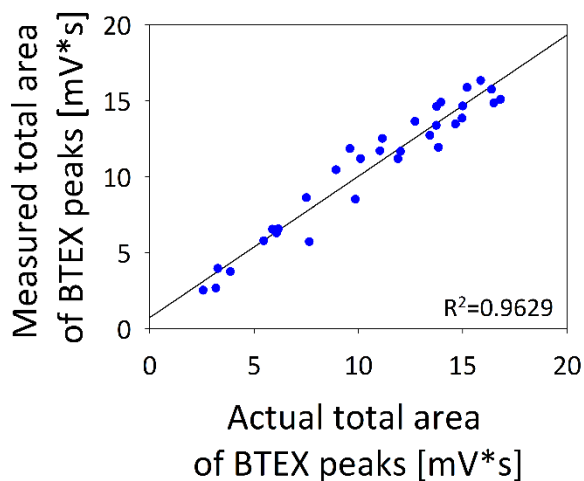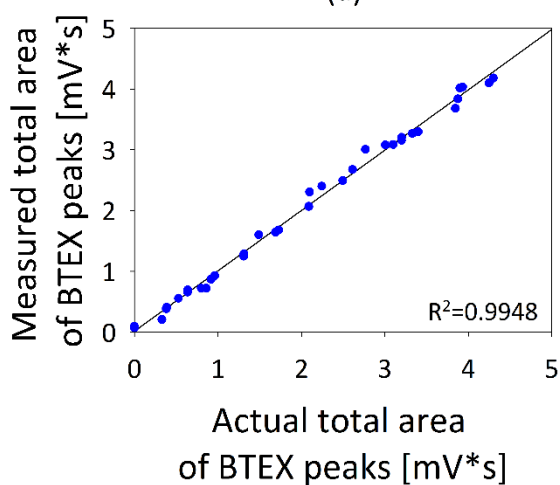
Figure S16 Actual and determined total area of chromatographic peaks correlation plot for inlet stream: (a) BTEX in 10°C, (b) BTEX in 25°C and outlet stream: (c) BTEX in 10°C, (d) BTEX in 25°C
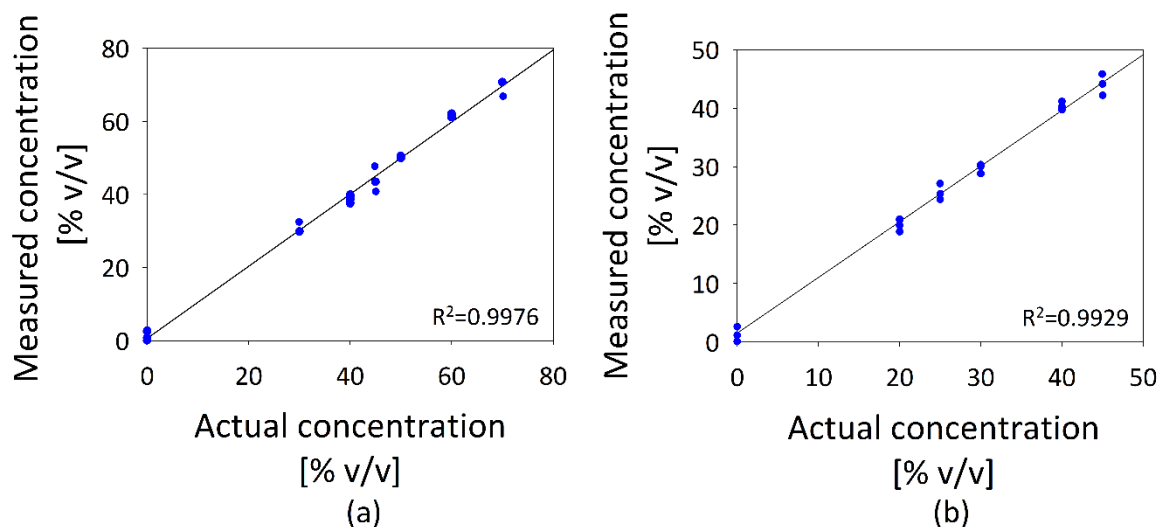
Figure S17 Actual and determined concentrations correlation plot for: (a) methane, (b) carbon dioxide.
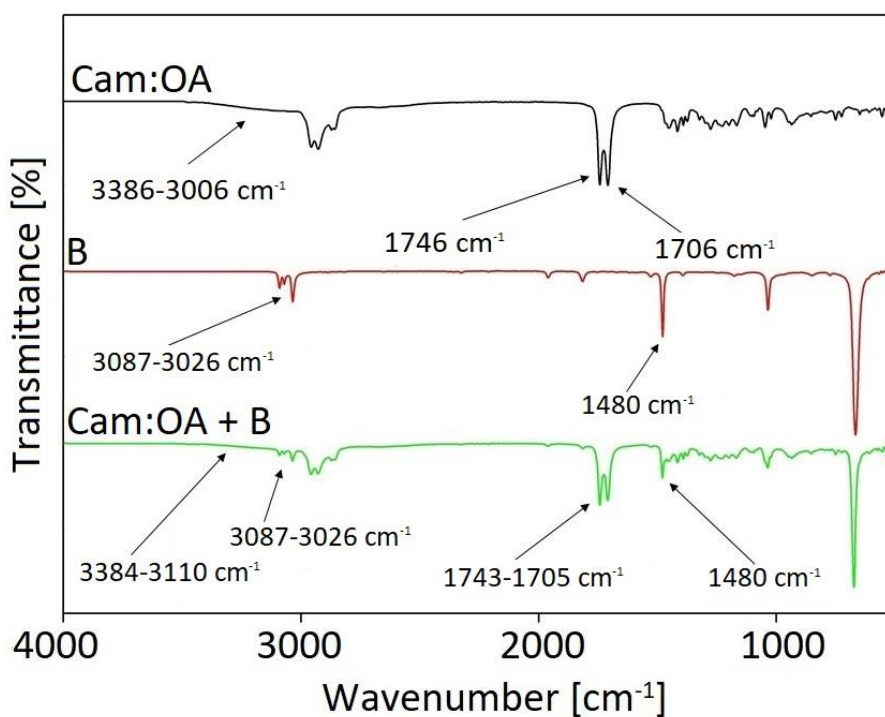

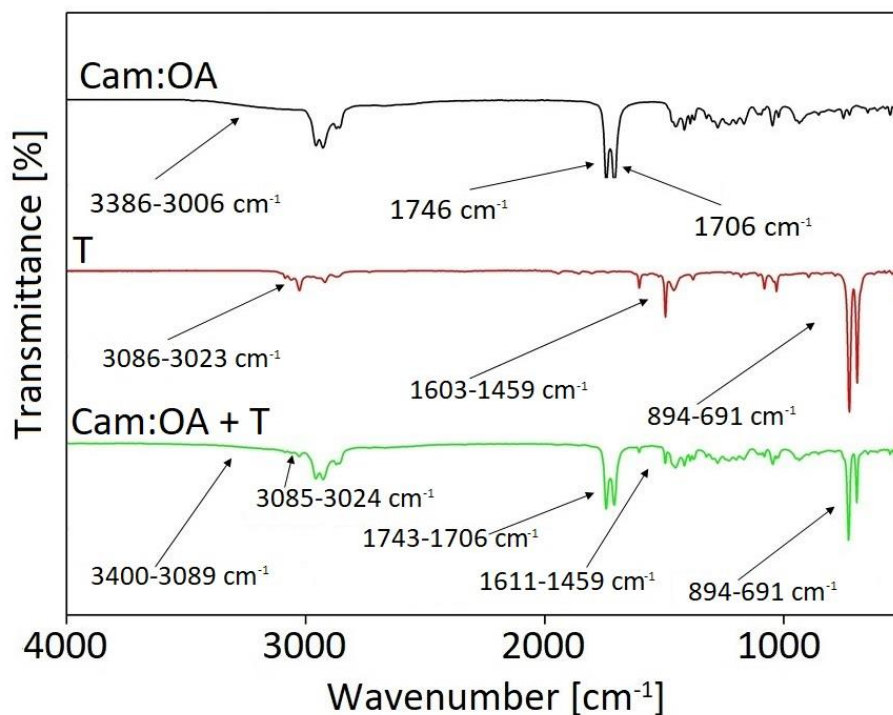**Figure S18** FT-IR spectra before and after benzene (B) absorption for Cam:OA (1:1).

Figure S19 FT-IR spectra before and after toluene (T) absorption for Cam:OA (1:1).
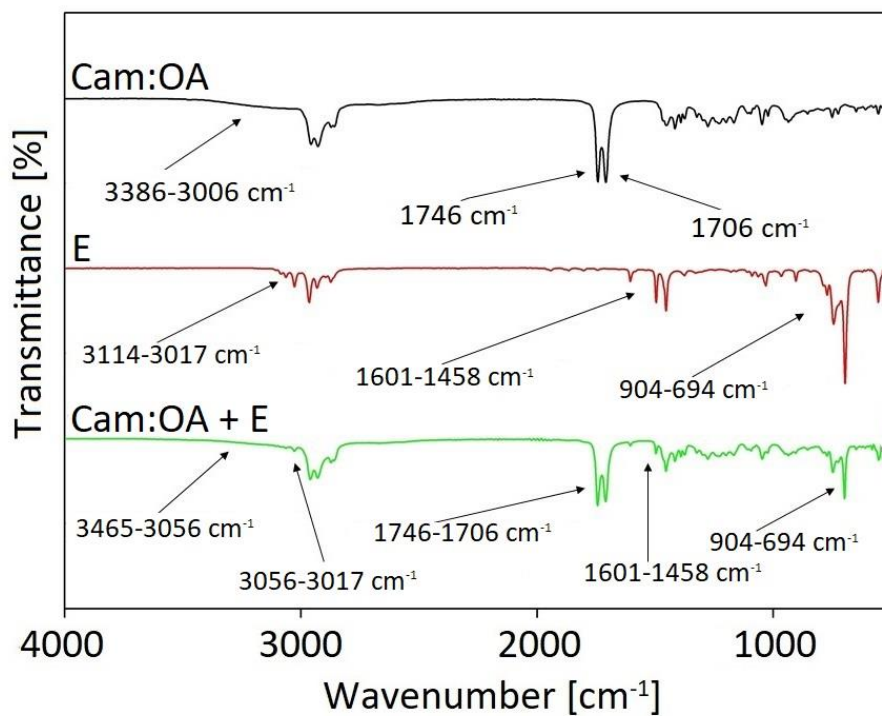

Figure S20 FT-IR spectra before and after ethylbenzene (E) absorption for Cam:OA (1:1).

Figure S21 FT-IR spectra before and after xylene (X) absorption for Cam:OA (1:1).

Figure S22 FT-IR spectra before and after benzene (B) absorption for Cam:DA (1:1).

Figure S23 FT-IR spectra before and after toluene (T) absorption for Cam:DA (1:1).

Figure S24 FT-IR spectra before and after ethylbenzene (E) absorption for Cam:DA (1:1).
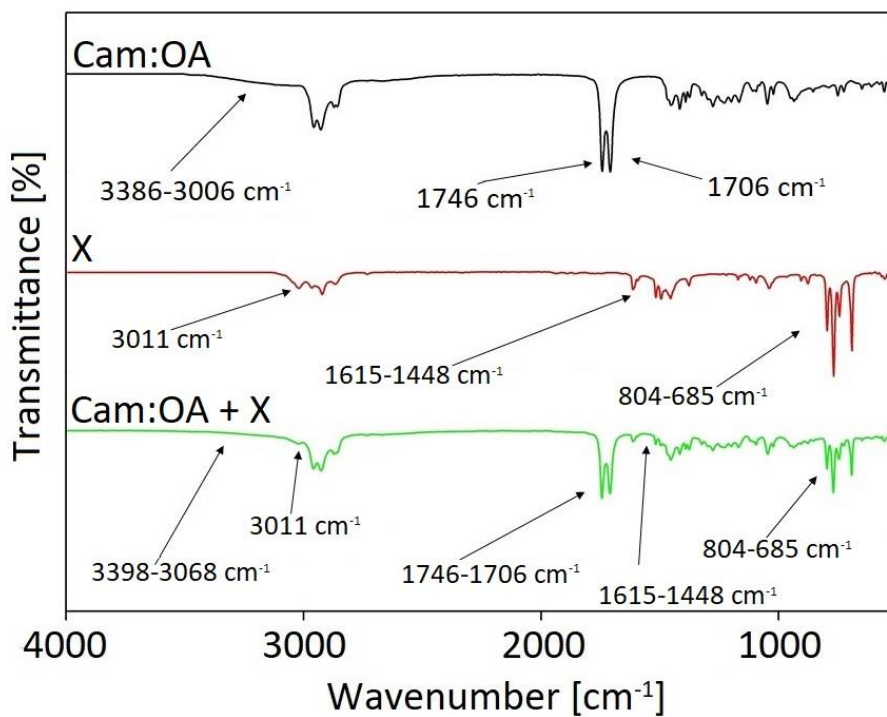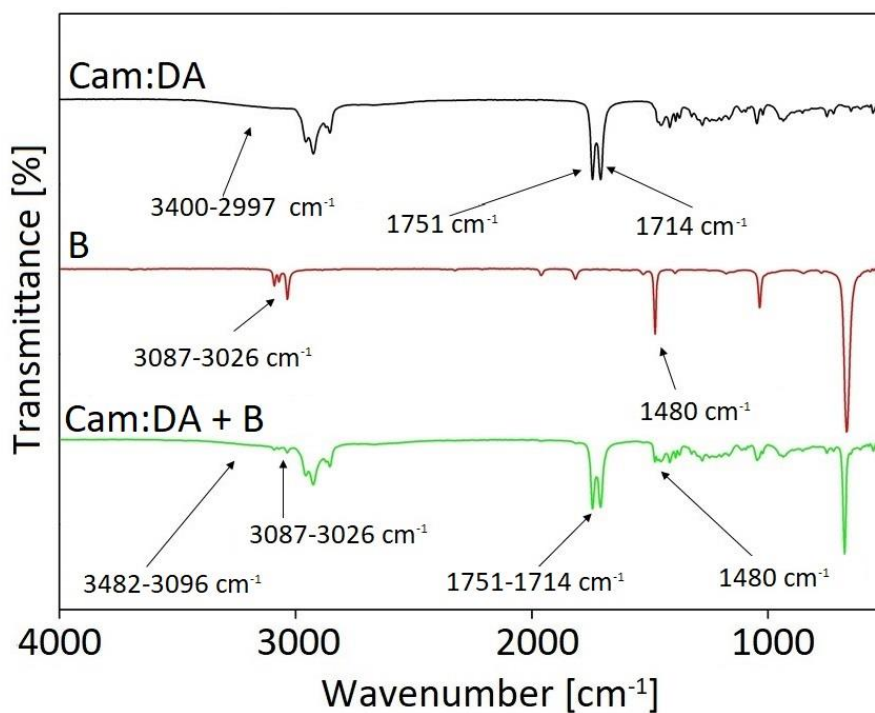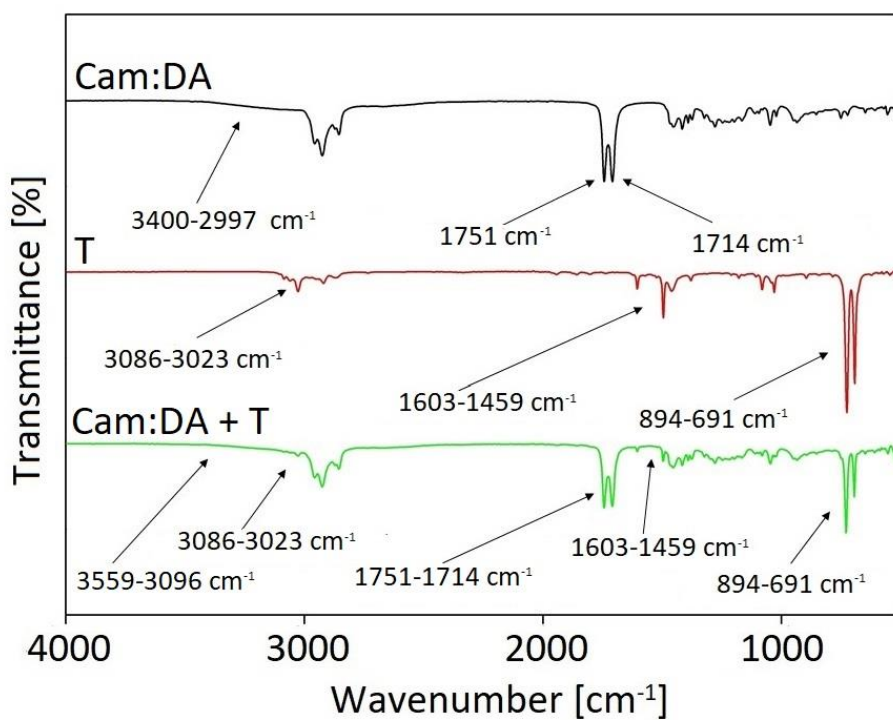
Figure S25 FT-IR spectra before and after xylene (X) absorption for Cam:DA (1:1).

Figure S26 FT-IR spectra before and after benzene (B) absorption for C-one:OA (1:1).

Figure S27 FT-IR spectra before and after toluene (T) absorption for C-one:OA (1:1).

Figure S28 FT-IR spectra before and after ethylbenzene (E) absorption for C-one:OA (1:1).

Figure S29 FT-IR spectra before and after xylene (X) absorption for C-one:OA (1:1).

Figure S30 FT-IR spectra before and after benzene (B) absorption for C-one:NA (1:1).

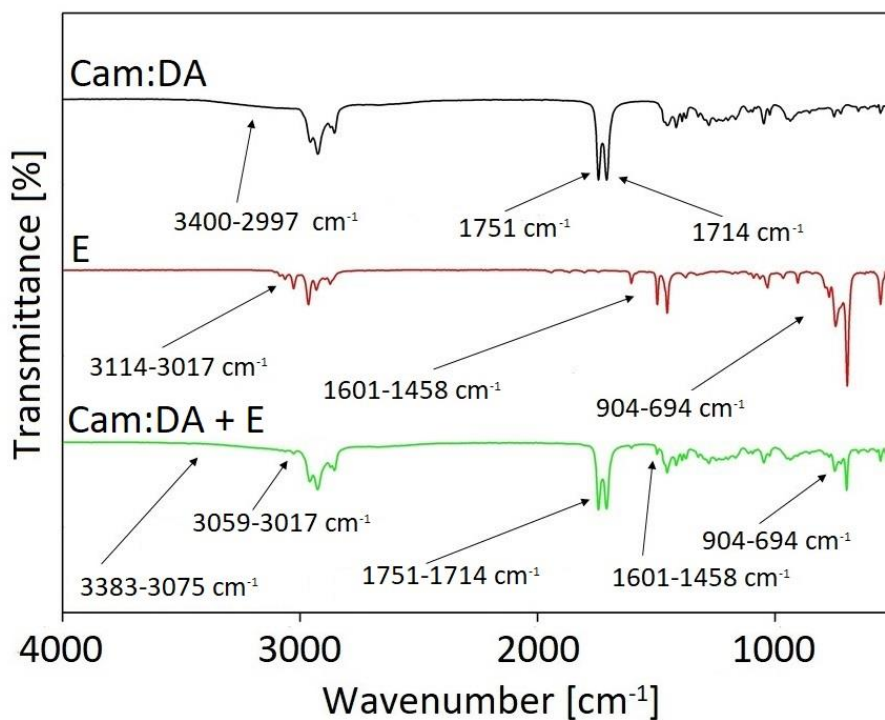**Figure S31** FT-IR spectra before and after toluene (T) absorption for C-one:NA (1:1).
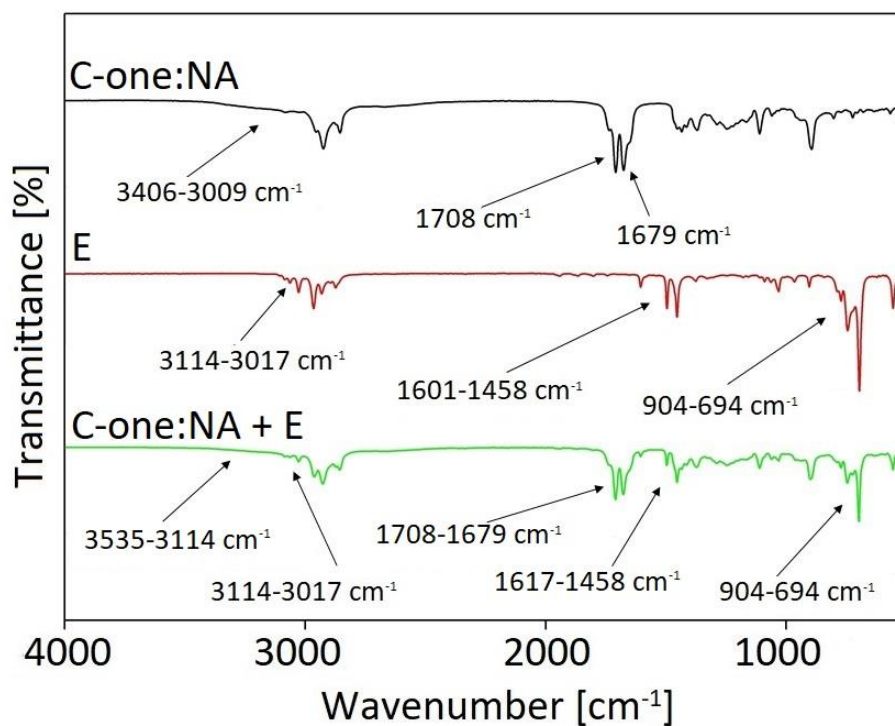
Figure S32 FT-IR spectra before and after ethylbenzene (E) absorption for C-one:NA (1:1).
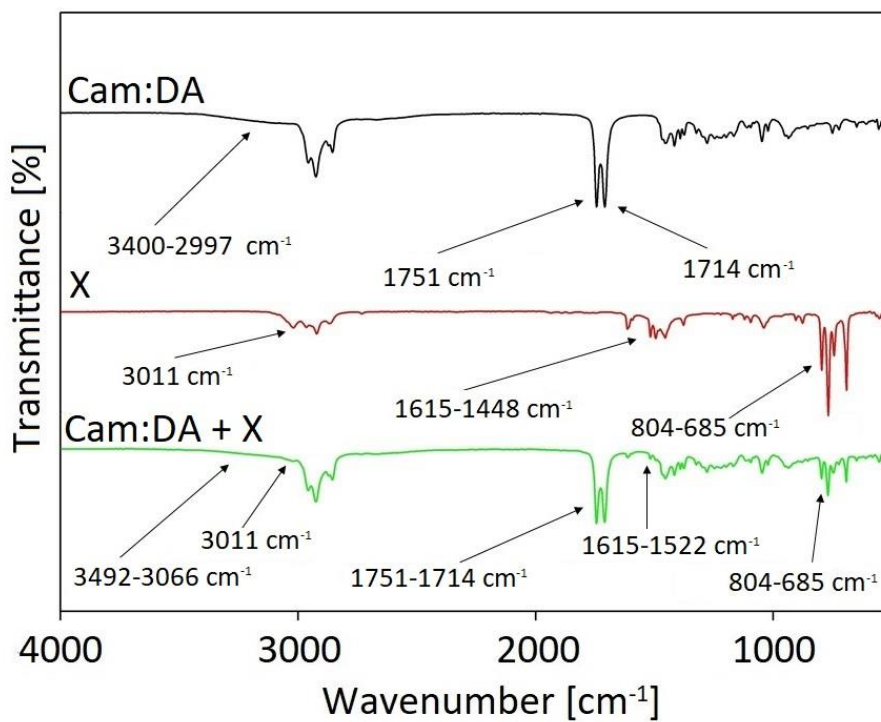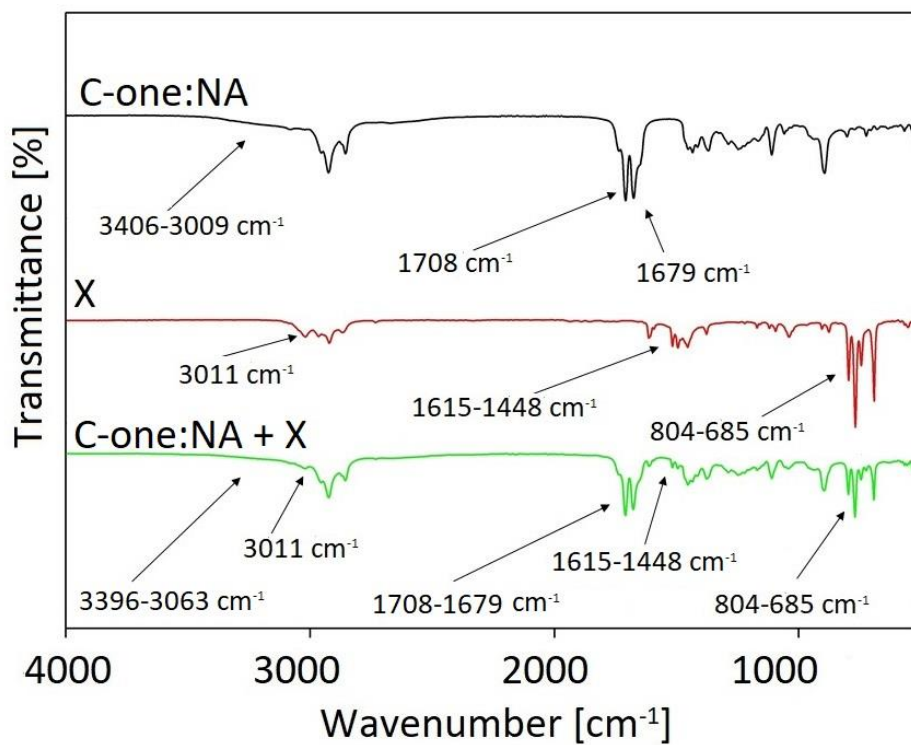
Figure S33 FT-IR spectra before and after xylene (X) absorption for C-one:NA (1:1).
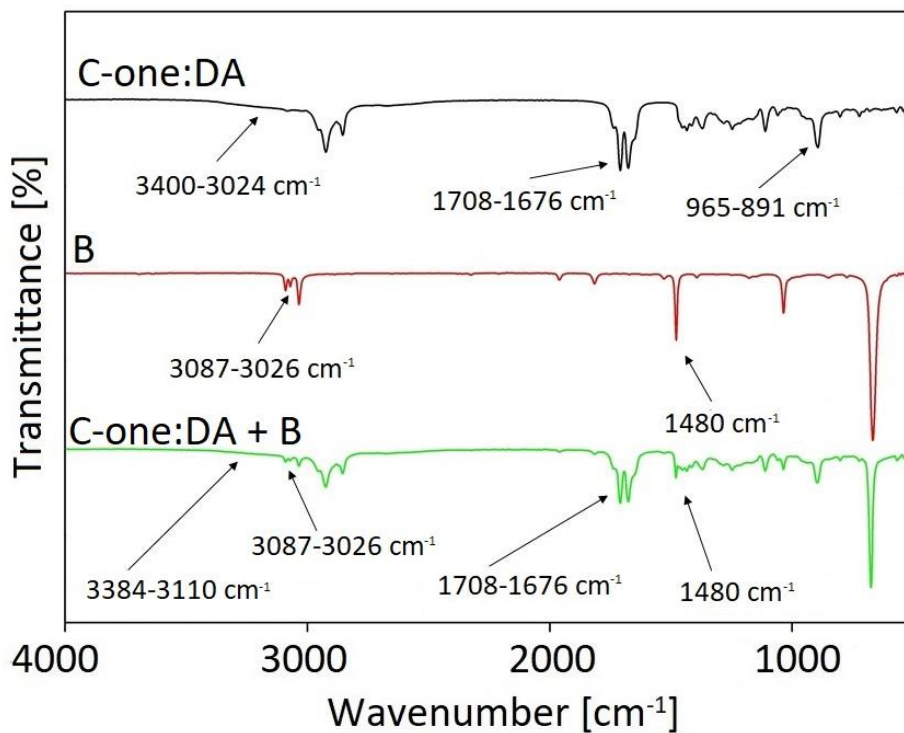
Figure S34 FT-IR spectra before and after benzene (B) absorption for C-one:DA (1:1).
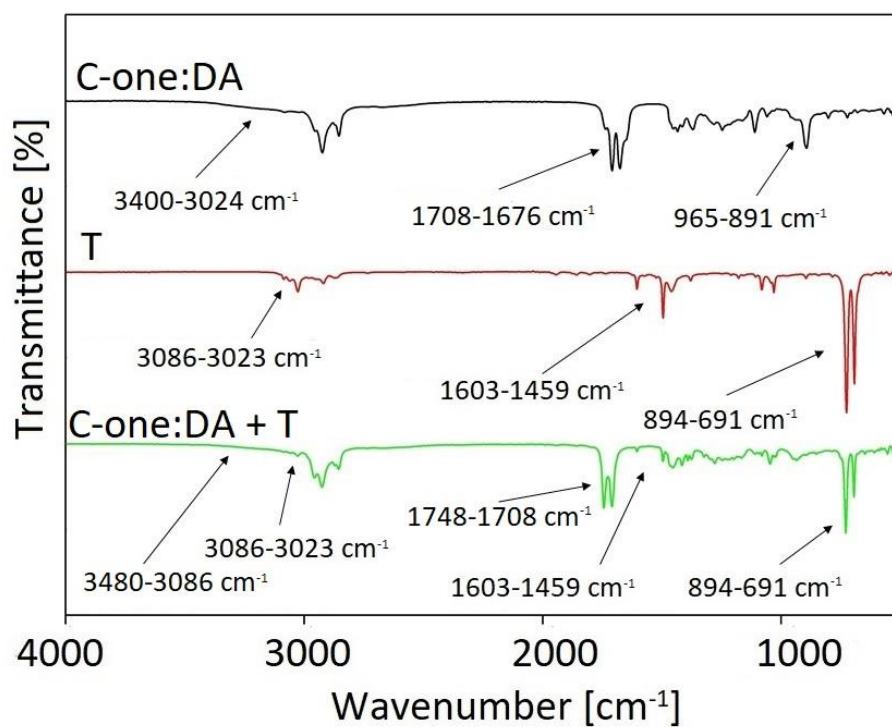
Figure S35 FT-IR spectra before and after toluene (T) absorption for C-one:DA (1:1).
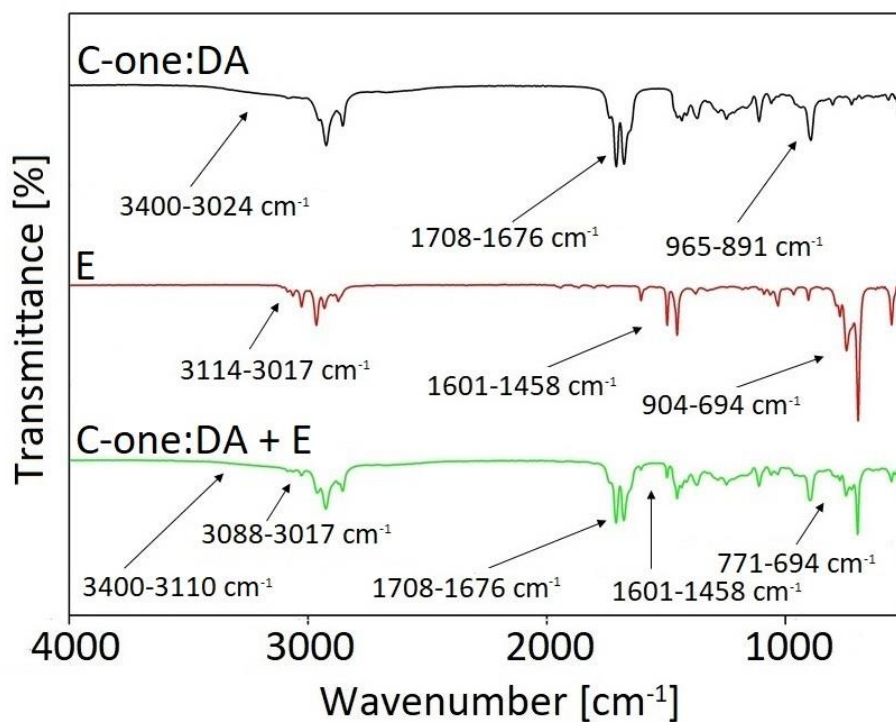
Figure S36 FT-IR spectra before and after ethylbenzene (E) absorption for C-one:DA (1:1).
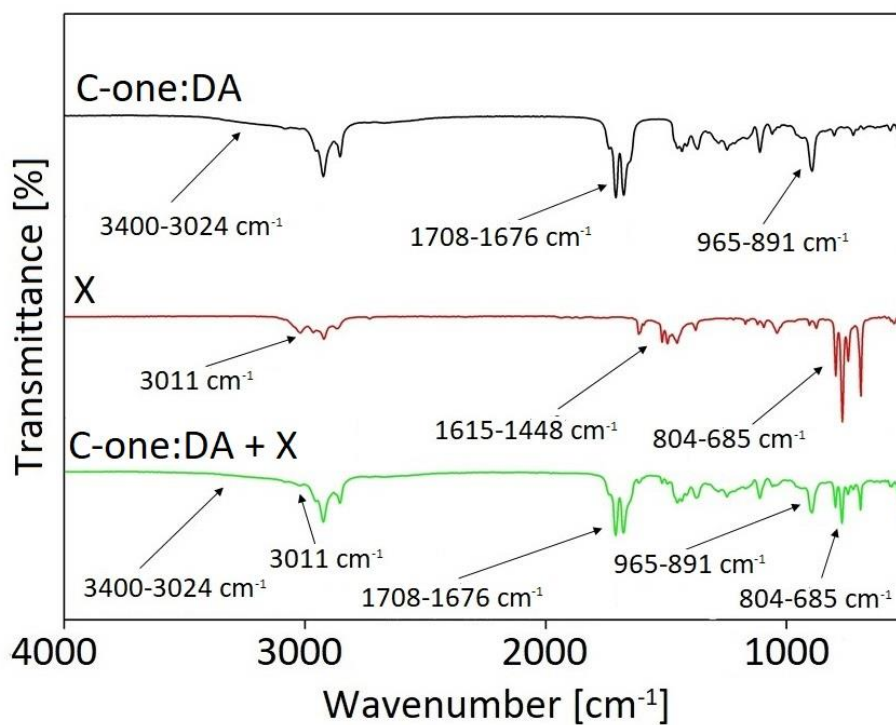
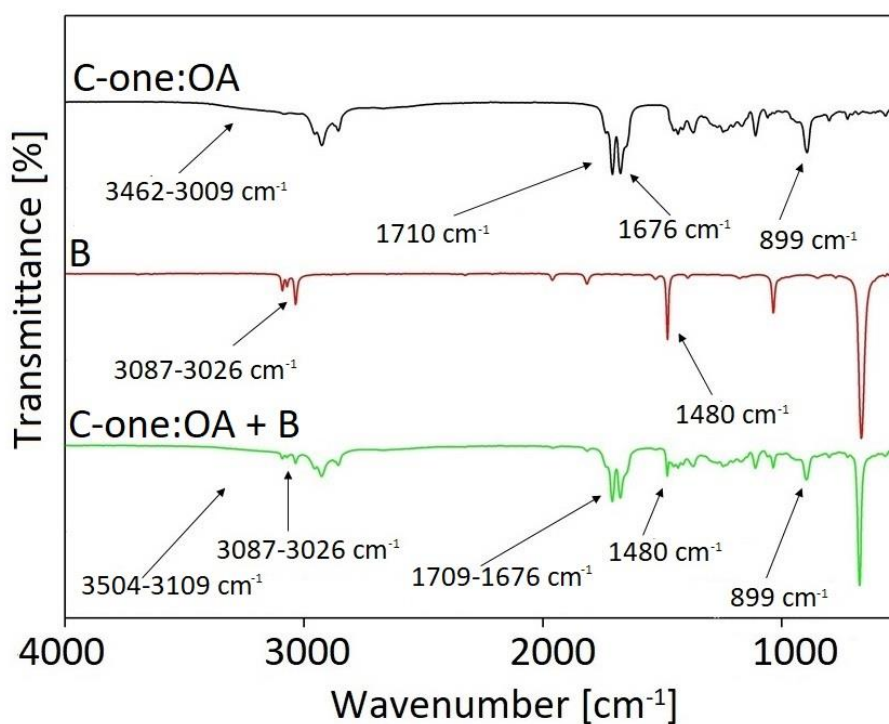**Figure S37** FT-IR spectra before and after xylene (X) absorption for C-one:DA (1:1).
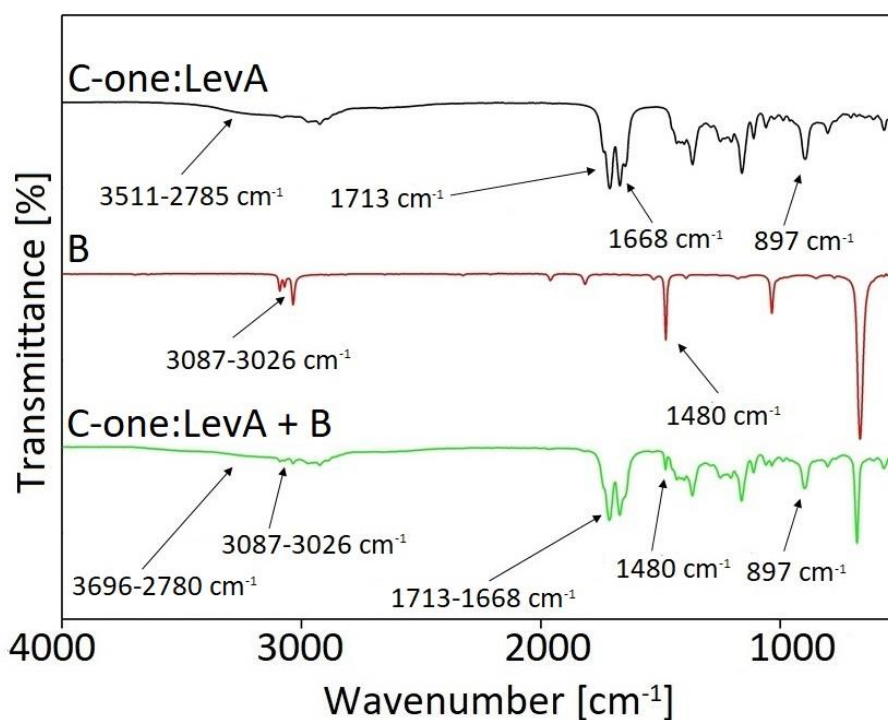
Figure S38 FT-IR spectra before and after benzene (B) absorption for C-one:LevA (1:1).
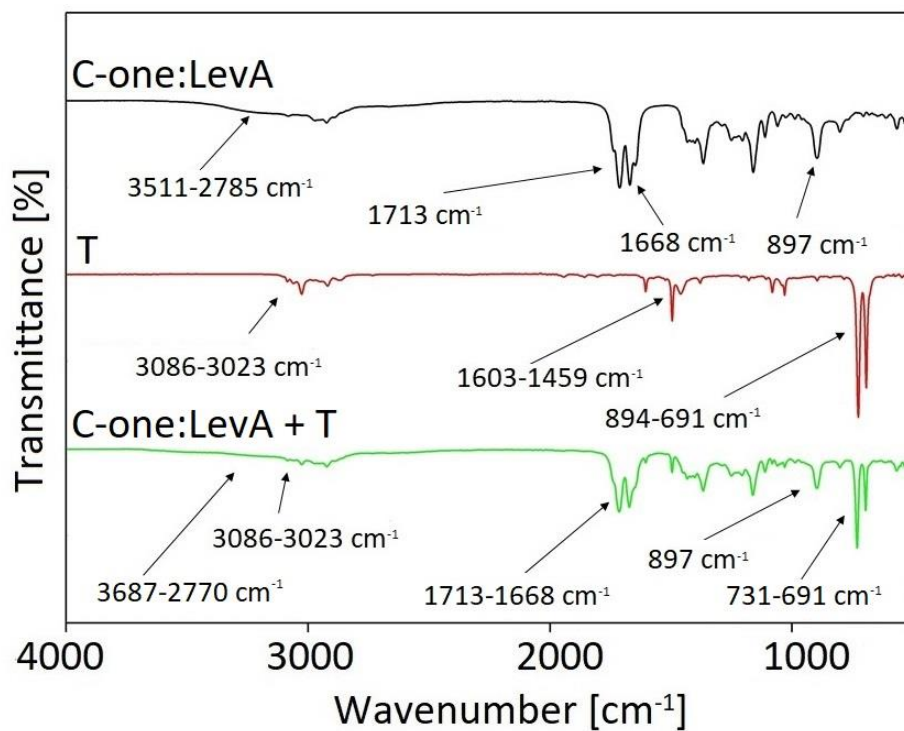
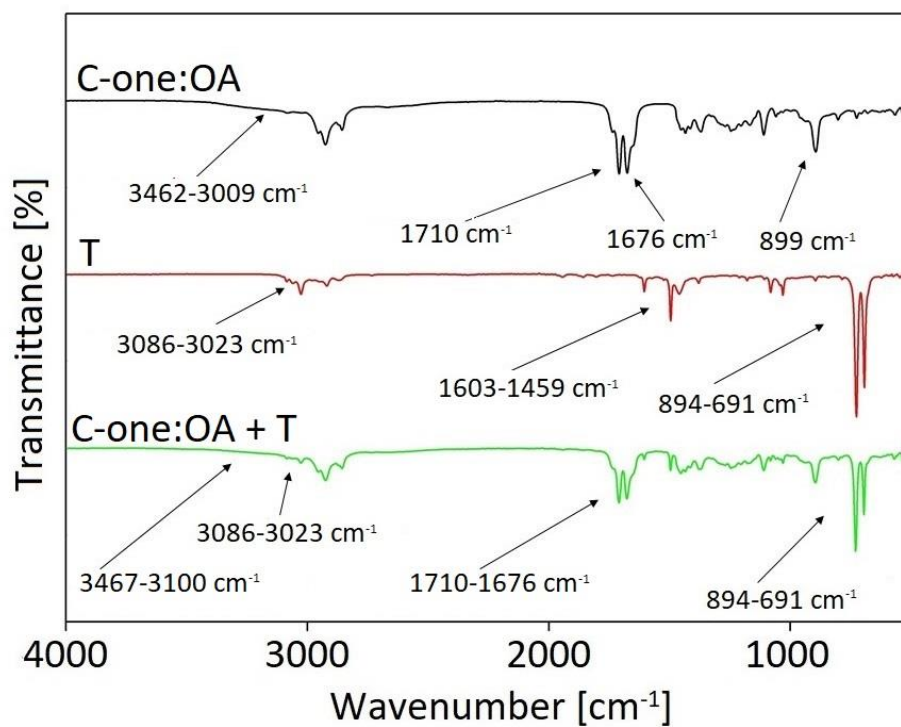**Figure S39** FT-IR spectra before and after toluene (T) absorption for C-one:LevA (1:1).
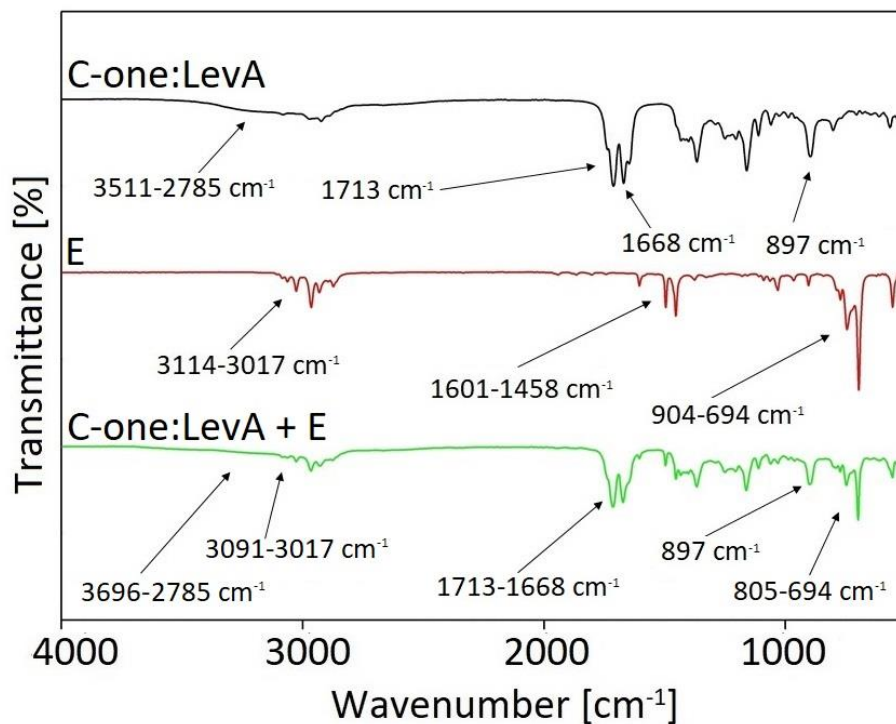
Figure S40 FT-IR spectra before and after ethylbenzene (E) absorption for C-one:LevA (1:1).
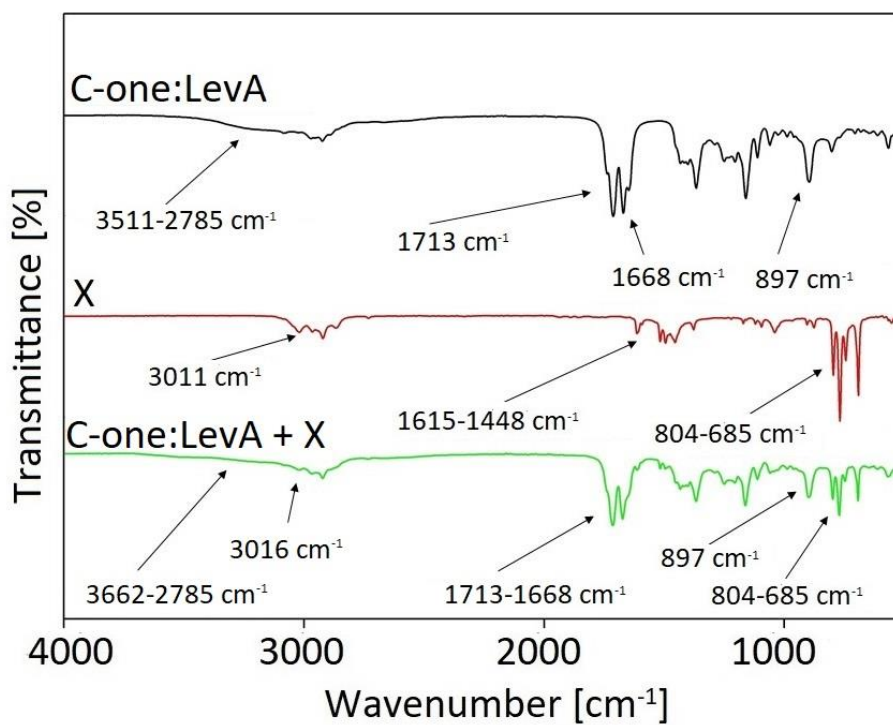
Figure S41 FT-IR spectra before and after xylene (X) absorption for C-one:LevA (1:1).
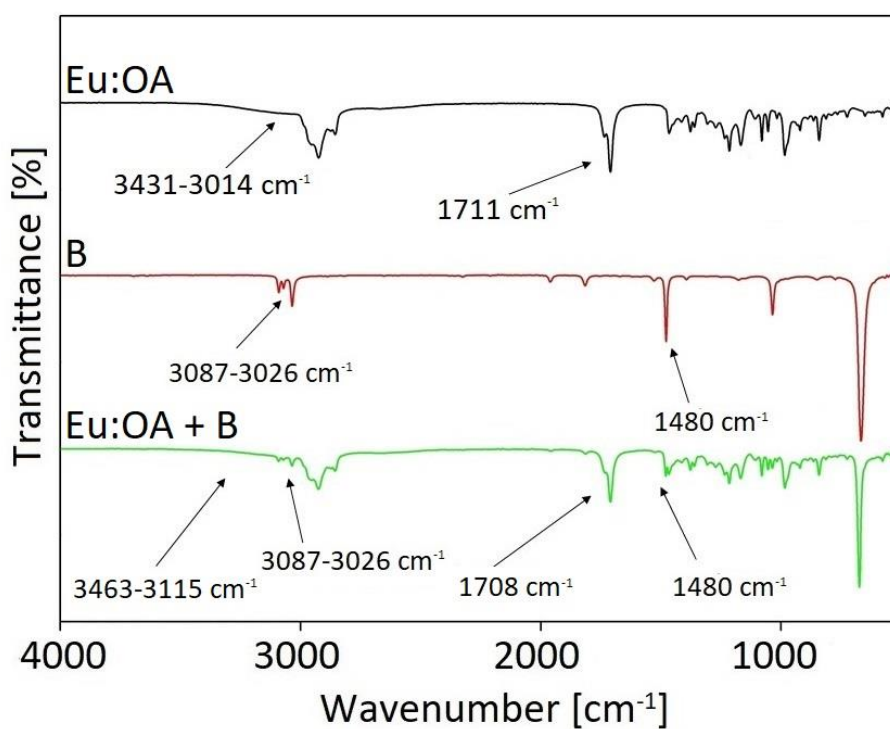
Figure S42 FT-IR spectra before and after benzene (B) absorption for Eu:OA (1:1).
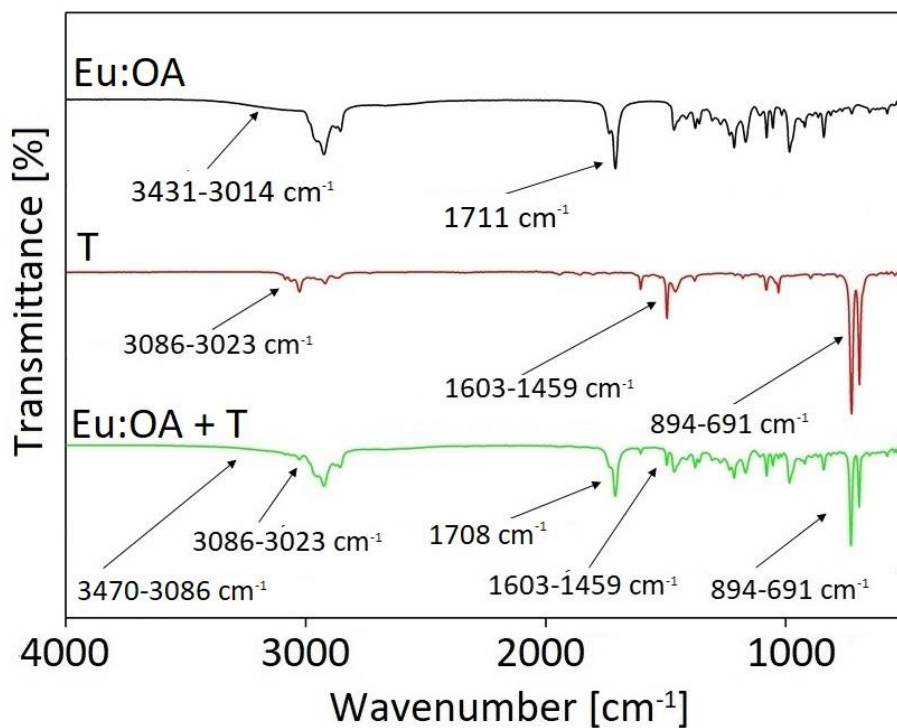
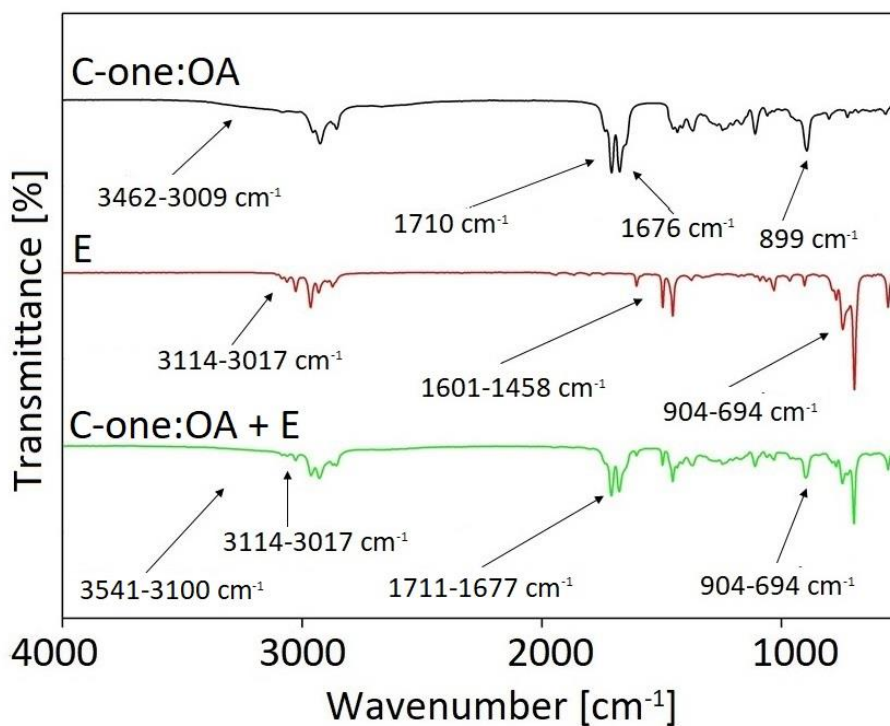**Figure S43** FT-IR spectra before and after toluene (T) absorption for Eu:OA (1:1).
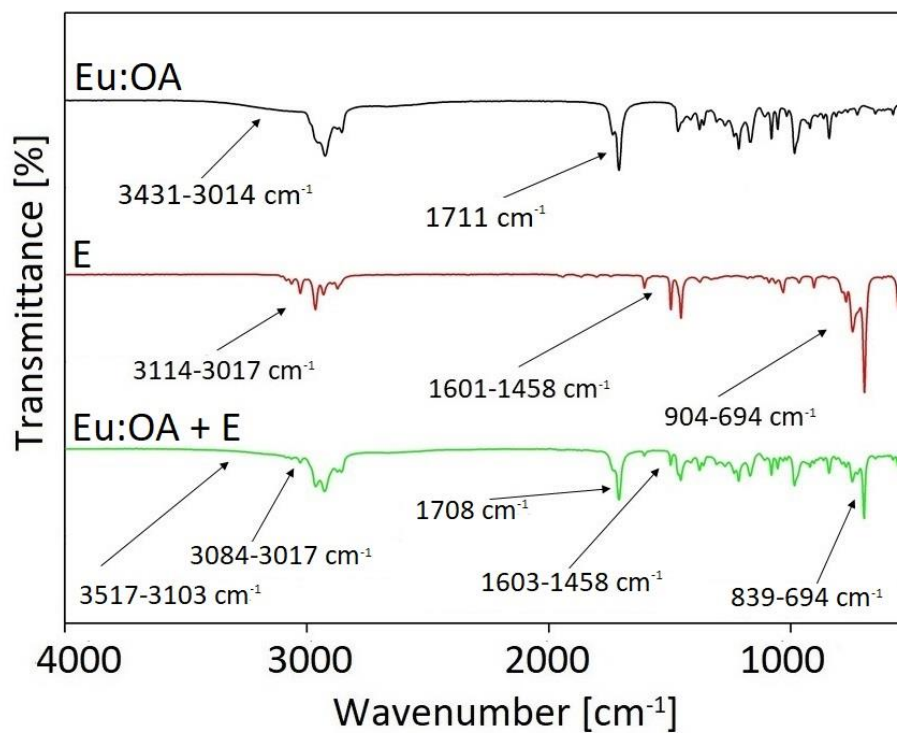
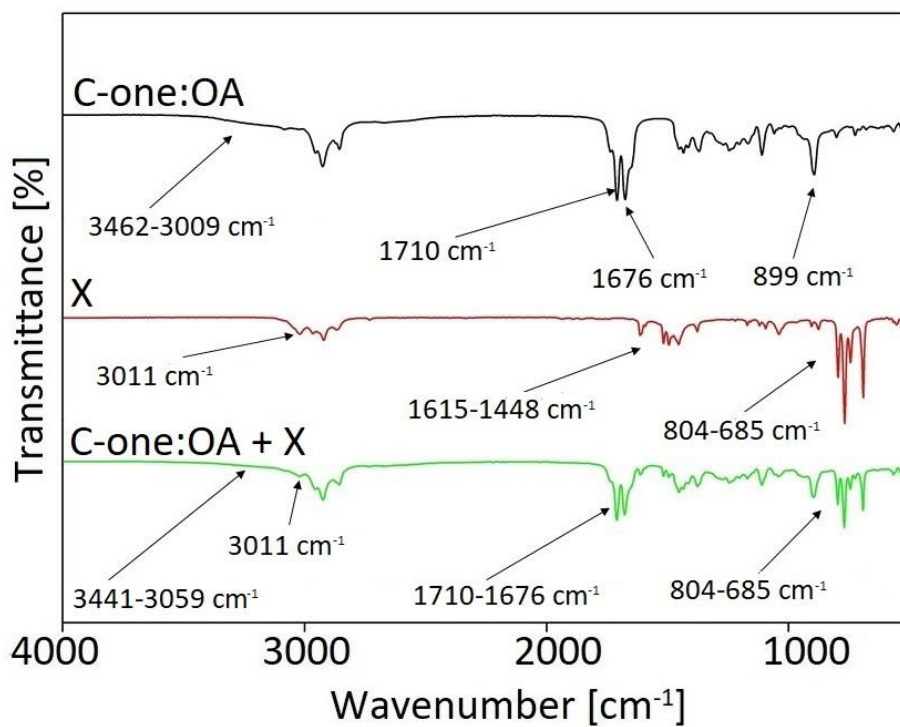**Figure S44** FT-IR spectra before and after ethylbenzene (E) absorption for Eu:OA (1:1).
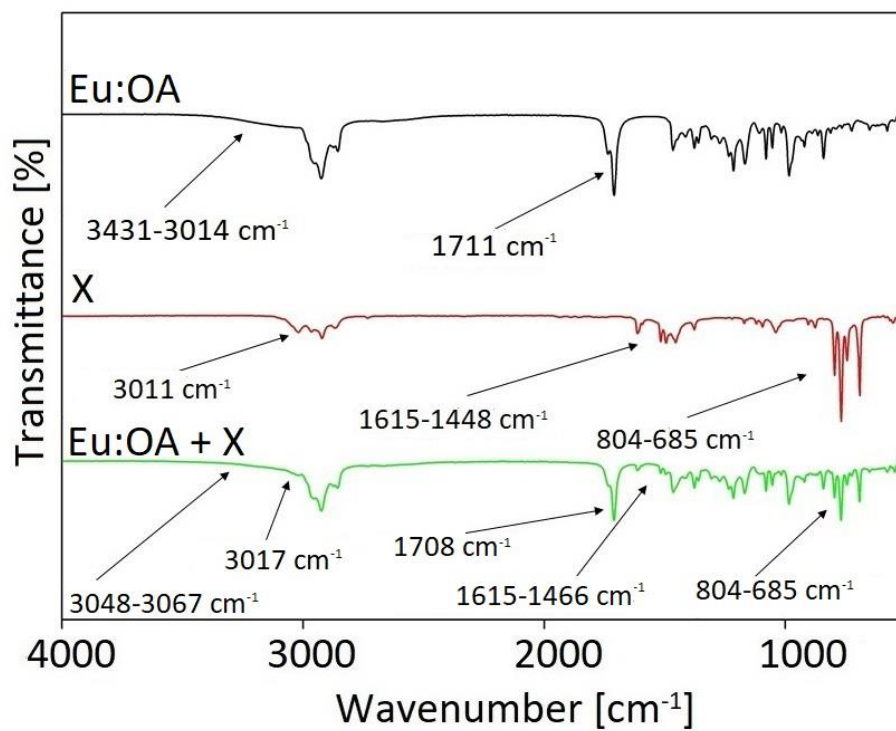
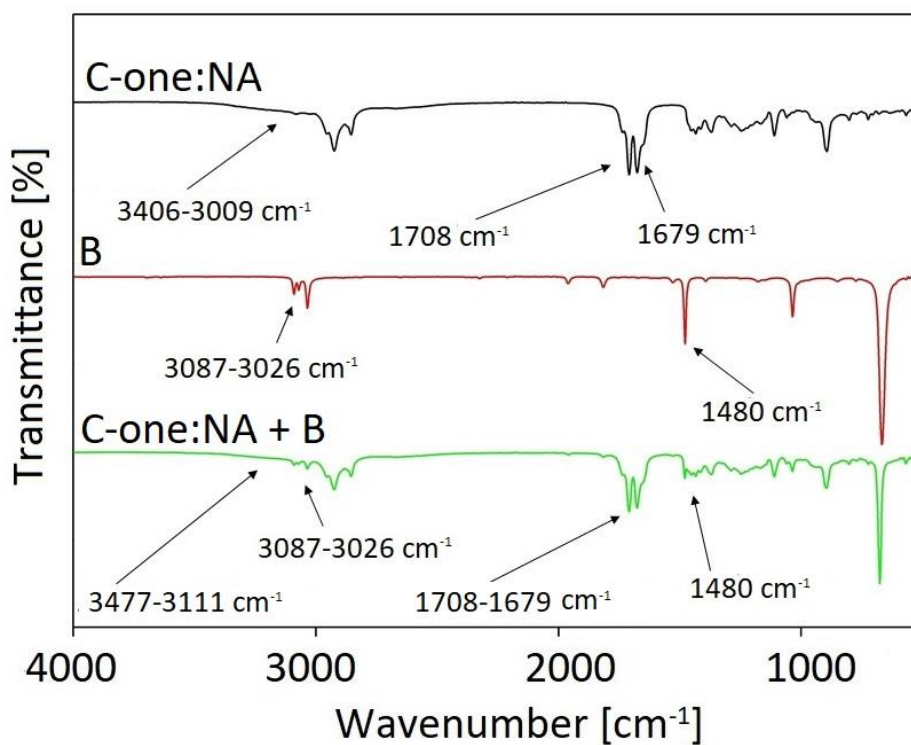**Figure S45** FT-IR spectra before and after xylene (X) absorption for Eu:OA (1:1).
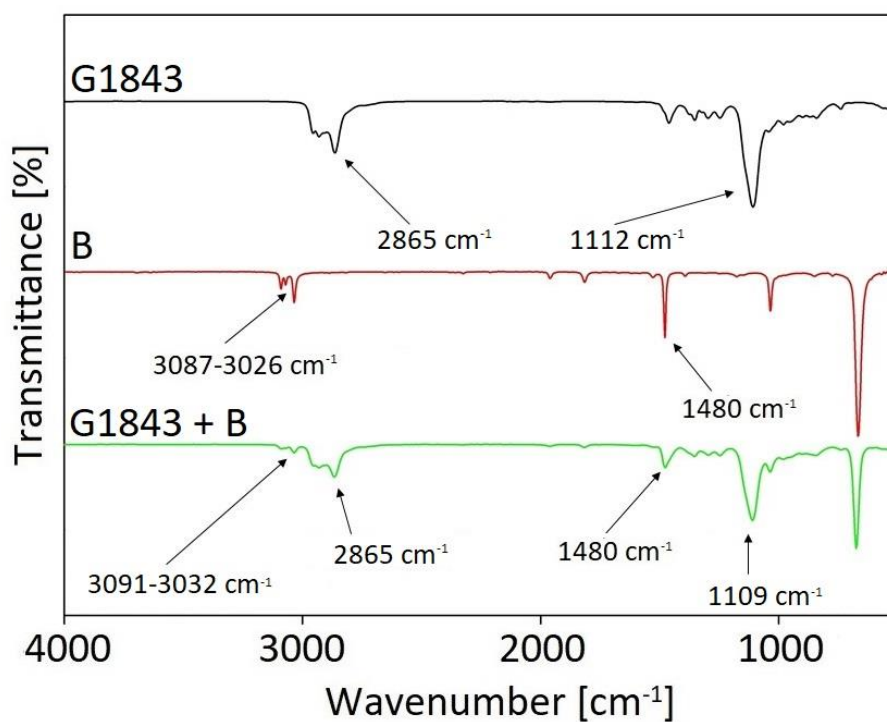
Figure S46 FT-IR spectra before and after benzene (B) absorption for G1843.

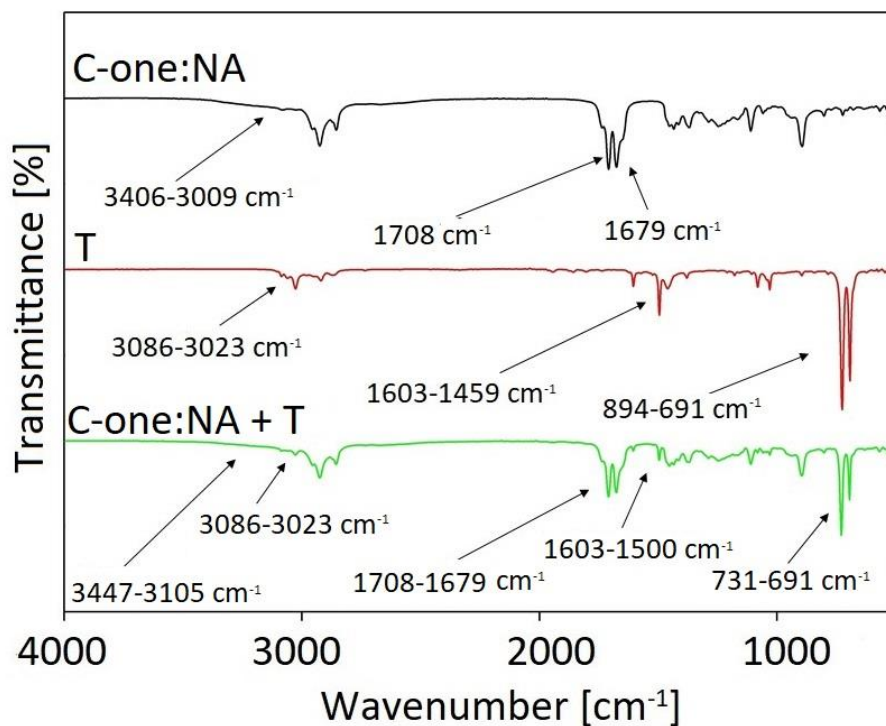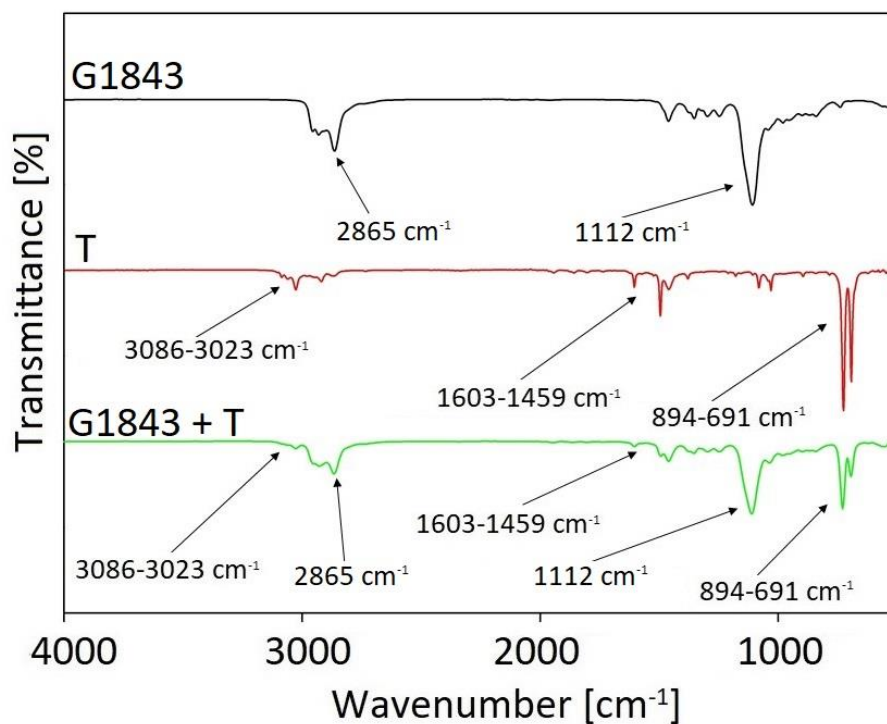**Figure S47** FT-IR spectra before and after toluene (T) absorption for G1843.
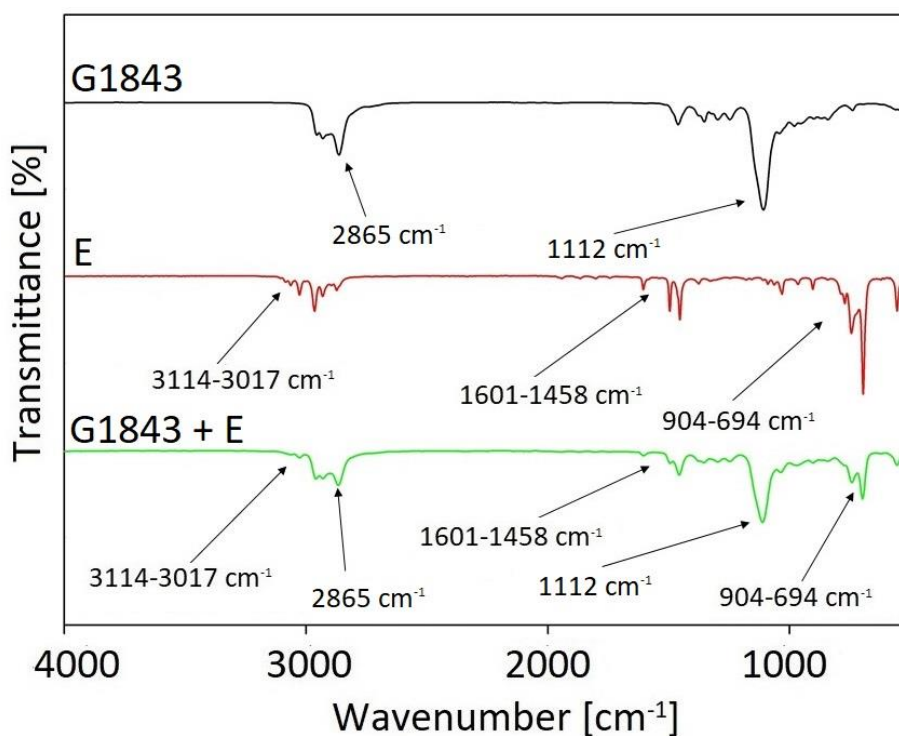
Figure S48 FT-IR spectra before and after ethylbenzene (E) absorption for G1843.
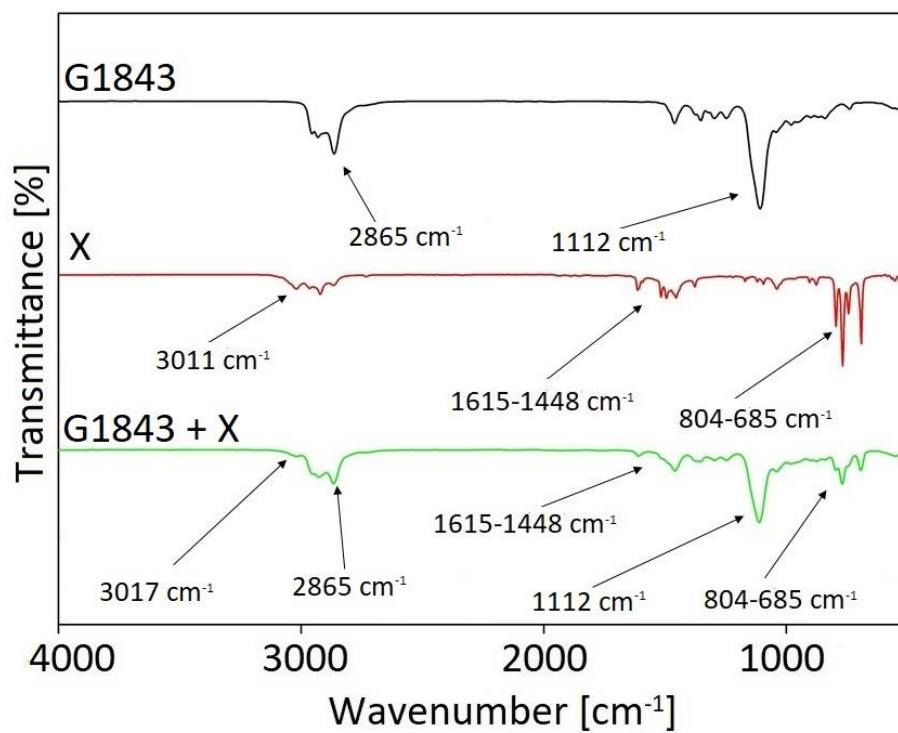
Figure S49 FT-IR spectra before and after xylene (X) absorption for G1843.
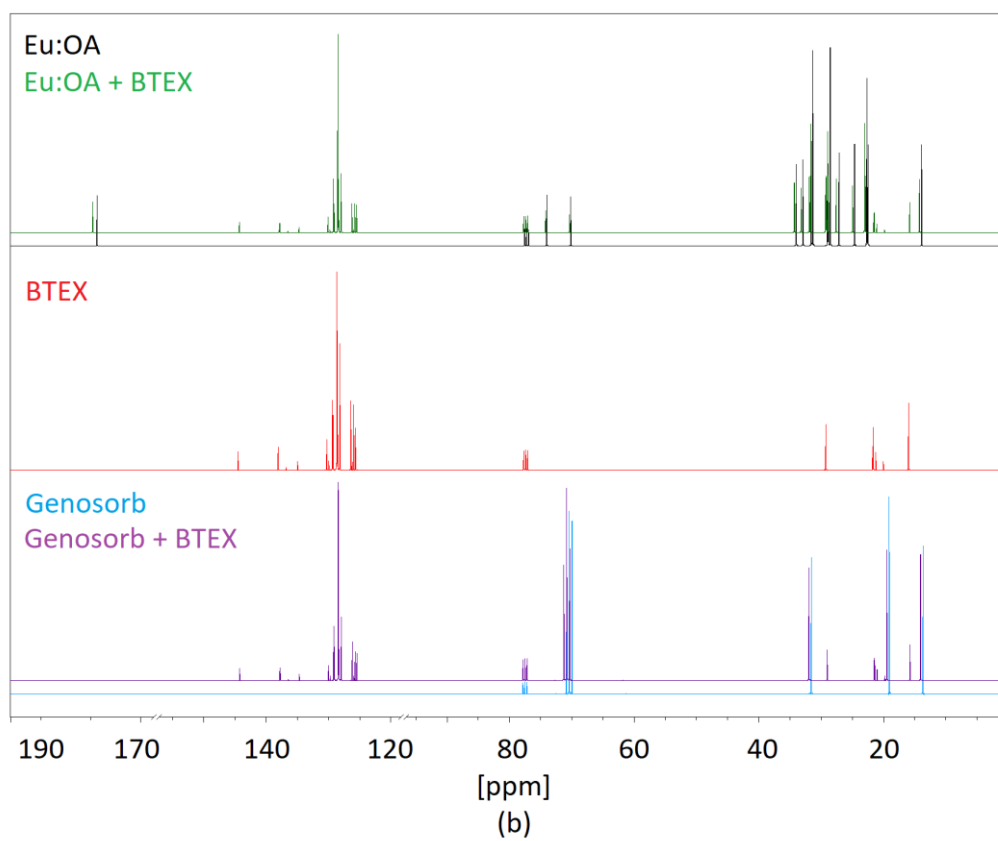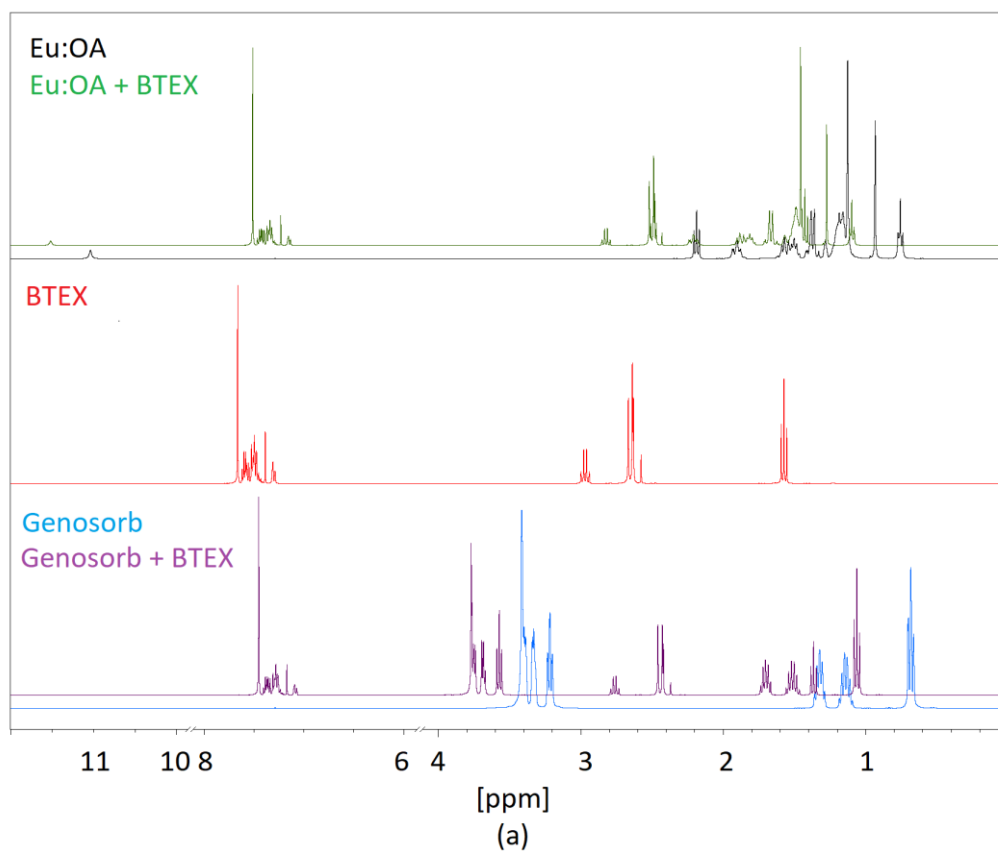
Figure S50 (a) ^{1}H NMR, (b) ^{13}C NMR spectra of Eu:OA (1:1) and Genosorb before and after BTEX absorption.
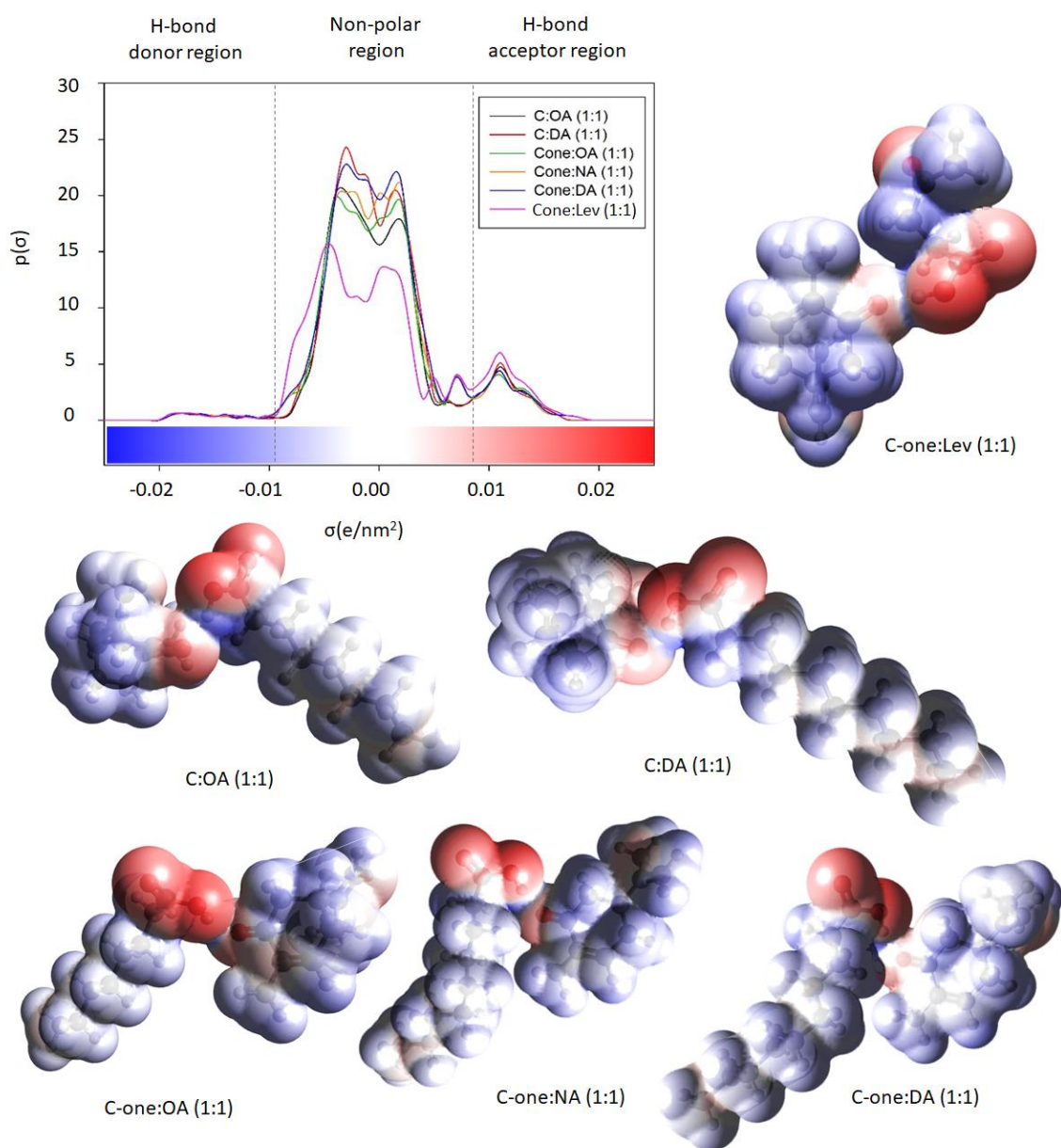
Figure S51 Sigma profile and electrostatic potential maps of a) Eu:OA (1:1) and commercially available absorbent; b) BTEX generated through COSMO-RS model.
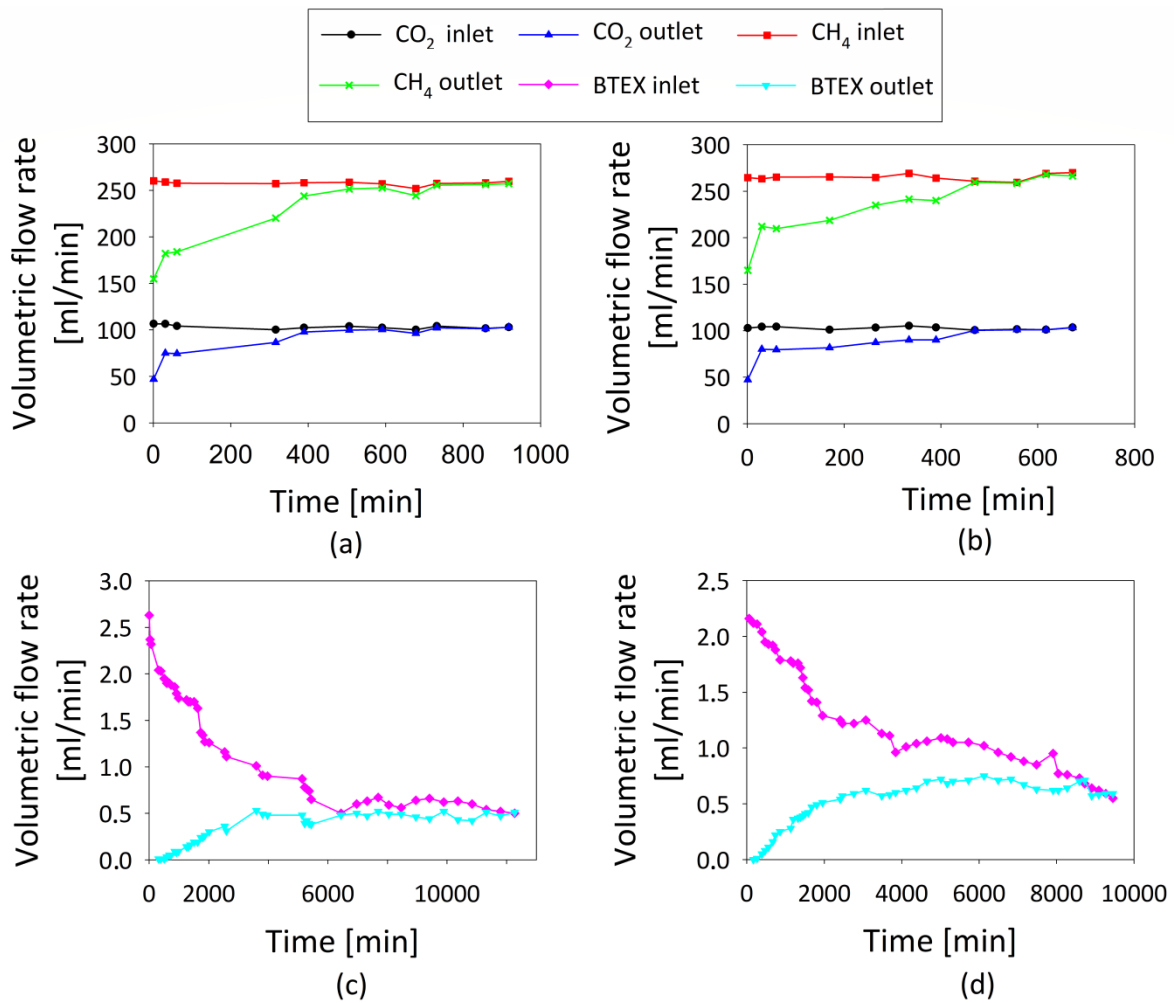
Figure S52 Volumetric flow rates of: (a) methane and carbon dioxide in 10°C; (b) methane and carbon dioxide in 25°C; (c) BTEX in 10°C; (d) BTEX in 25°C
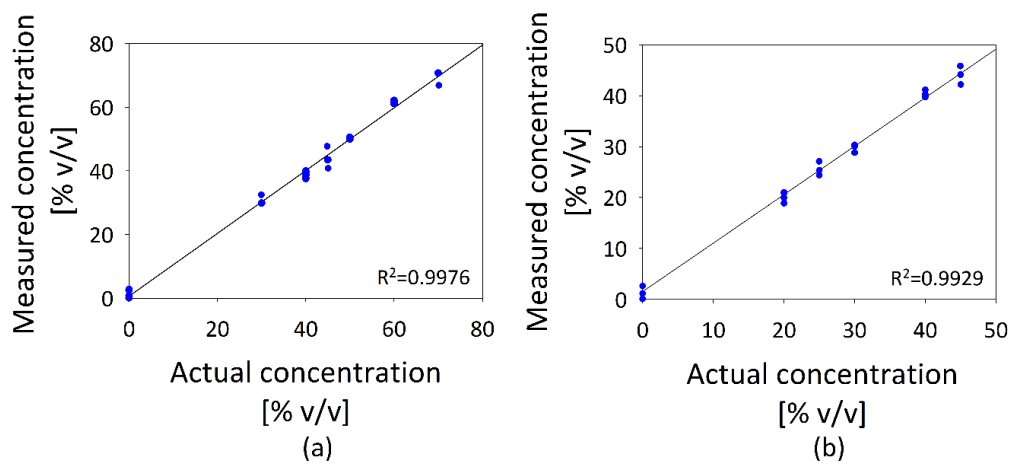
Figure 53. Actual and determined concentrations correlation plot for: (a) methane, (b) carbon dioxide
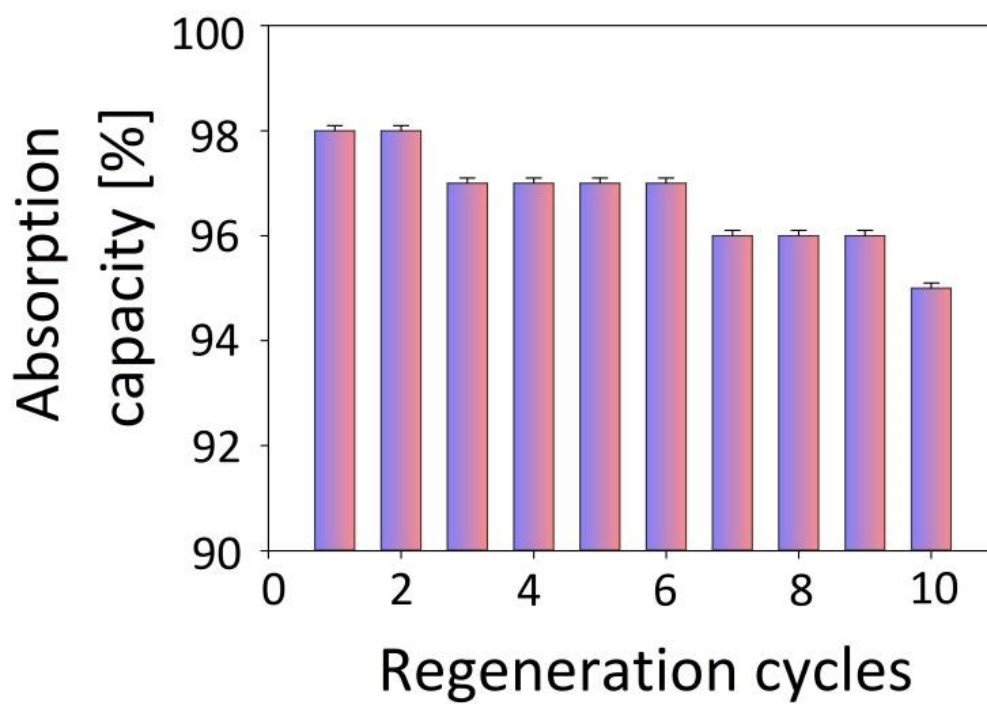
Figure S54 Absorption (10 °C) and desorption (120 °C) cycles of BTEX (initial concentration 2000 mg/m^3) in Eu:OA (1:1).
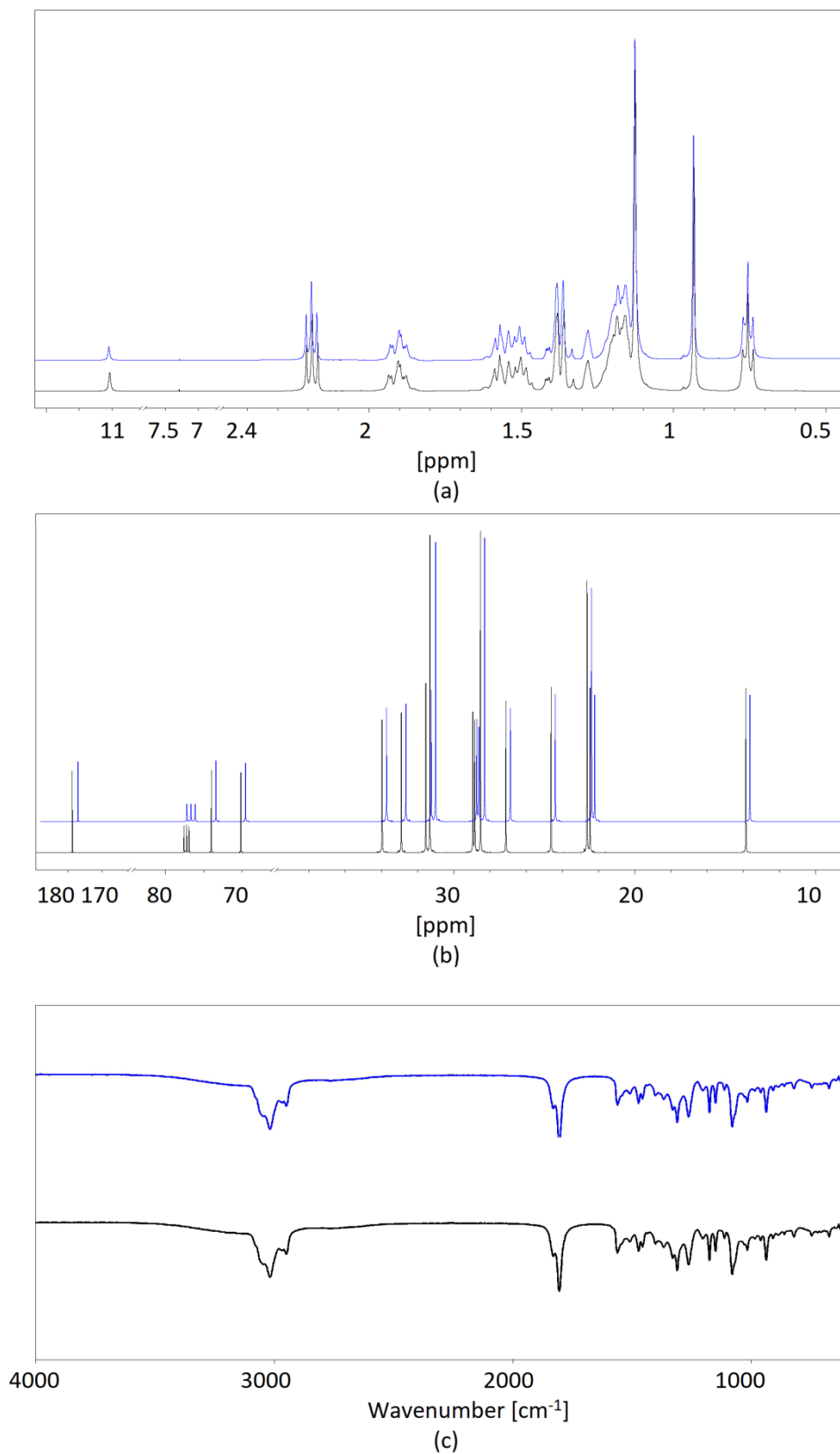
Figure S55 The fresh (black line) and regenerated (blue line) spectra for Eu: OA (1:1) was presented on (a) ^{1}H NMR, (b) [13]C

NMR, and (c) FT-IR spectrums

Table S1. Basic characteristics of the sensors used.

Sensor Type	Model	Target Gas
Photo Ionisation Detector	PID-A12	VOCs with ionisation potentials <10.6 eV
Nondispersive Infrared Sensor	NDIR CO2 2112BC4-V	Carbon dioxide
Nondispersive Infrared Sensor	NDIR CH4 2112BM4-V	Methane
Temperature and Humidity Sensor	SHT25	-

Table S2 Chemical shift values from the ^{1}H NMR and ^{13}C NMR spectra for Eu:OA (1:1).

^{1}H NMR							
HBA		DES		HBD		DES	
atom	δ (ppm)	atom	δ (ppm)	atom	δ (ppm)	atom	δ (ppm)
H1	2.02	H1	2.19	H1	11.60	H1	11.03
H2	1.66	H2	1.57	H2	2.34	H2	1.90
H3	1.51	H3	1.50	H3	1.63	H3	1.17
H4	1.41	H4	1.37	H4	1.29	H4	1.13
H5	1.24	H5	1.28	H5	0.88	H5	0.76
H6	1.05	H6	0.93				
^{13}C NMR							
C1	73.62	C1	73.98	C1	180.81	C1	178.70
C2	69.77	C2	70.13	C2	34.26	C2	33.94
C3	33.00	C3	32.88	C3	31.76	C3	31.53
C4	31.57	C4	31.30	C4	29.15	C4	28.92
C5	28.92	C5	28.51	C5	29.04	C5	28.82
C6	27.61	C6	27.10	C6	24.80	C6	24.60
C7	22.90	C7	22.62	C7	22.71	C7	22.45
				C8	14.09	C8	13.85

Table S3 Composition of prepared gas mixtures.

Chemical compound	Concentration
CH_4	0, 30, 40, 45, 50, 60, 70 % *v/v*
CO_2	0, 20, 25, 30,40, 45 % *v/v*

Table S4 Chemical shift values from ^{1}H NMR and ^{13}C NMR spectra from individual DES and genosorb components before and after the BTEX absorption process.

^{1}H NMR							
HBA				HBD			
DES		DES + BTEX		DES		DES + BTEX	
atom	δ (ppm)	atom	δ (ppm)	atom	δ (ppm)	atom	δ (ppm)
H1	2.19	H1	2.49	H1	11.03	H1	11.51
H2	1.57	H2	1.88	H2	1.90	H2	2.21
H3	1.50	H3	1.81	H3	1.17	H3	1.49
H4	1.37	H4	1.66	H4	1.13	H4	1.46
H5	1.28	H5	1.57	H5	0.76	H5	1.10
H6	0.93	H6	1.27				
^{13}C NMR							
C1	73.98	C1	74.20	C1	178.70	C1	179.60
C2	70.13	C2	70.30	C2	33.94	C2	34.29
C3	32.88	C3	33.22	C3	31.53	C3	31.88
C4	31.30	C4	31.65	C4	28.92	C4	29.24
C5	28.51	C5	28.92	C5	28.82	C5	29.14
C6	27.10	C6	27.56	C6	24.60	C6	24.93
C7	22.62	C7	23.00	C7	22.45	C7	22.83
				C8	13.85	C8	14.24
Genosorb							
^{1}H NMR				^{13}C NMR			

pure		+ BTEX		pure		+ BTEX	
atom	δ (ppm)	atom	δ (ppm)	atom	δ (ppm)	atom	δ (ppm)
H1	3,41	H1	3,77	C1	70,79	C1	71,22
H2	3,39	H2	3,75	C2	70,41	C2	70,78
H3	3,38	H3	3,74	C3	70,39	C3	70,77
H4	3,34	H4	3,69	C4	69,90	C4	70,26
H5	3,33	H5	3,68	C5	31,54	C5	31,95
H6	3,21	H6	3,57	C6	19,05	C6	19,47
H7	1,32	H7	1,70	C7	13,63	C7	14,05
H8	1,14	H8	1,51				
H9	0,68	H9	1,06				

Table S5. Equation of prepared models and their coefficients of determination

Compound		INLET STREAM		OUTLET STREAM	
BTEX	10°C	$3.5370 \cdot 10^5 * S_1 + 1.9213 \cdot 10^4$	$R^2 = 0.9878$	$9.6980 \cdot 10^4 \cdot S_1 - 3.7941 \cdot 10^3$	$R^2 = 0.9948$
	25°C	$3.0930 \cdot 10^5 \cdot S_1 + 1.3290 \cdot 10^4$	$R^2 = 0.9629$	$1,1051 \cdot 10^5 \cdot S_1 - 9.7848 \cdot 10^4$	$R^2 = 0.9882$
CO$_2$		$68.0586 \cdot S_2 - 2.7196 \cdot S_3 - 25.2984$		$R^2 = 0.9929$	
CH$_4$		$-7.0974 \cdot S_2 + 65.1165 \cdot S_3 - 21.4818$		$R^2 = 0.9976$	

S_1 – signal from PID sensor, S_2 – signal from CO$_2$ sensor, S_3 – signal from CH$_4$ sensor,

Table S6. RMSE determined for absorptivity parameter

Compound	RMSE in 10°C	RMSE in 25°C
Methane	0.024	0.028
Carbon dioxide	0.031	0.039
BTEX	0.017	0.067

Gdańsk, dnia 19.05.2023

dr inż. Patrycja Makoś-Chełstowska
....
(stopień/tytuł, imię i nazwisko)

Politechnika Gdańska
....
(Afiliacja)

OŚWIADCZENIE WSPÓŁAUTORA

Jako współautor pracy:. **"Green monoterpenes based deep eutectic solvents for effective BTEX absorption from biogas"** oświadczam, że mój własny wkład polegał na konceptualizacji, metodologii, prowadzeniu badań, wizualizacji, nadzorowaniu badań, przygotowaniu oryginalnego manuskryptu, przygotowaniu recenzji i redakcji ostatecznej wersji manuskryptu oraz finansowaniu.

Jednocześnie wyrażam zgodę na przedłożenie ww. pracy przez mgr inż. Edytę Słupek jako część rozprawy doktorskiej w formie spójnego tematycznie zbioru artykułów opublikowanych w czasopismach naukowych.

Oświadczam, że samodzielna i możliwa do wyodrębnienia część ww. pracy wykazuje indywidualny wkład mgr inż. Edyty Słupek polegający na: konceptualizacji, prowadzeniu badań, wizualizacji oraz przygotowaniu oryginalnego manuskryptu.

P. Makoś-Chełstowska
....
(podpis współautora)

Gdańsk, dnia 19.05.2023

mgr inż. Aleksandra Kramarz
....
(stopień/tytuł, imię i nazwisko)

Politechnika Gdańska
....
(Afiliacja)

OŚWIADCZENIE WSPÓŁAUTORA

Jako współautor pracy:. **"Green monoterpenes based deep eutectic solvents for effective BTEX absorption from biogas"** oświadczam, że mój własny wkład polegał na prowadzeniu badań oraz przygotowaniu oryginalnego manuskryptu.

Jednocześnie wyrażam zgodę na przedłożenie ww. pracy przez mgr inż. Edytę Słupek jako część rozprawy doktorskiej w formie spójnego tematycznie zbioru artykułów opublikowanych w czasopismach naukowych.

Oświadczam, że samodzielna i możliwa do wyodrębnienia część ww. pracy wykazuje indywidualny wkład mgr inż. Edyty Słupek polegający na: konceptualizacji, prowadzeniu badań, wizualizacji oraz przygotowaniu oryginalnego manuskryptu.

Kramarz Aleksandra
....
(podpis współautora)

Gdańsk, dnia 19.05.2023

mgr inż. Dominik Dobrzyniewski

(stopień/tytuł, imię i nazwisko)

Politechnika Gdańska

(Afiliacja)

OŚWIADCZENIE WSPÓŁAUTORA

Jako współautor pracy:. **"Green monoterpenes based deep eutectic solvents for effective BTEX absorption from biogas"** oświadczam, że mój własny wkład polegał na prowadzeniu badań oraz przygotowaniu oryginalnego manuskryptu.

Jednocześnie wyrażam zgodę na przedłożenie ww. pracy przez mgr inż. Edytę Słupek jako część rozprawy doktorskiej w formie spójnego tematycznie zbioru artykułów opublikowanych w czasopismach naukowych.

Oświadczam, że samodzielna i możliwa do wyodrębnienia część ww. pracy wykazuje indywidualny wkład mgr inż. Edyty Słupek polegający na: konceptualizacji, prowadzeniu badań, wizualizacji oraz przygotowaniu oryginalnego manuskryptu.

(podpis współautora)

Gdańsk, dnia 19.05.2023

dr inż. Bartosz Szulczyński

(stopień/tytuł, imię i nazwisko)

Politechnika Gdańska

(Afiliacja)

OŚWIADCZENIE WSPÓŁAUTORA

Jako współautor pracy:. **"Green monoterpenes based deep eutectic solvents for effective BTEX absorption from biogas"** oświadczam, że mój własny wkład polegał na prowadzeniu badań, nazdorowaniu prac badawczych oraz przygotowaniu oryginalnego manuskryptu.

Jednocześnie wyrażam zgodę na przedłożenie ww. pracy przez mgr inż. Edytę Słupek jako część rozprawy doktorskiej w formie spójnego tematycznie zbioru artykułów opublikowanych w czasopismach naukowych.

Oświadczam, że samodzielna i możliwa do wyodrębnienia część ww. pracy wykazuje indywidualny wkład mgr inż. Edyty Słupek polegający na: konceptualizacji, prowadzeniu badań, wizualizacji oraz przygotowaniu oryginalnego manuskryptu.

(podpis współautora)

dr inż. hab. Jacek Gębicki
....
(stopień/tytuł, imię i nazwisko)

Politechnika Gdańska
....
(Afiliacja)

OŚWIADCZENIE WSPÓŁAUTORA

Jako współautor pracy:. "**Green monoterpenes based deep eutectic solvents for effective BTEX absorption from biogas**" oświadczam, że mój własny wkład polegał na nadzorowaniu wstępnego planu badań oraz realizacji badań oraz przygotowaniu recenzji oraz redakcji ostatecznej wersji manuskryptu.

Jednocześnie wyrażam zgodę na przedłożenie ww. pracy przez mgr inż. Edytę Słupek jako część rozprawy doktorskiej w formie spójnego tematycznie zbioru artykułów opublikowanych w czasopismach naukowych.

Oświadczam, że samodzielna i możliwa do wyodrębnienia część ww. pracy wykazuje indywidualny wkład mgr inż. Edyty Słupek polegający na: konceptualizacji, prowadzeniu badań, wizualizacji oraz przygotowaniu oryginalnego manuskryptu.

....
(podpis współautora)

Autorzy:

E. Słupek, P. Makoś-Chełstowska, D. Dobrzyniewski, B. Szulczyński,
J. Gębicki

Tytuł publikacji:

Process Control of Biogas Purification Using Electronic Nose

Czasopismo:

CHEMICAL ENGINEERING TRANSACTIONS

DOI:

10.3303/cet2082072

Process Control of Biogas Purification Using Electronic Nose

Edyta Słupek, Patrycja Makoś, Dominik Dobrzyniewski, Bartosz Szulczyński, Jacek Gębicki*

Department of Process Engineering and Chemical Technology, Faculty of Chemistry, Gdańsk University of Technology, 11/12 Gabriela Narutowicza Street, 80-233 Gdańsk, Poland
jacek.gebicki@pg.edu.pl

Nowadays, biogas produced from landfills and wastewater treatment plants or lignocellulosic biomass is important sustainable and affordable source of energy. Impurities from biogas stream can cause a serious odor problem, especially for residents of areas immediately adjacent to production plants. Therefore, biogas pre-treatment is necessary to protect engines that convert biogas into energy and in order to increase the specific heat. Currently, there are many well-known methods of purifying biogas streams i.e. physical and chemical absorption, adsorption, membrane separation, cryogenic separation, pressure swing adsorption, advanced oxidation processes and biological separation. Among these technologies, methods based on the use of physical absorption show a high efficiency of the impurities removal from the gas phase using appropriately selected absorbents. In the presented study the purification of model biogas mixtures contaminated with cyclohexane, toluene, propionaldehyde, 1-butanol and dimethyl disuflide. Three absorbents were used in the research: hexadecane and two deep eutectic solvents: choline chloride with urea in 1:2 molar ratio and camphor with guaiacol in 1:1 molar ratio. For process efficiency monitoring the electronic nose was used. The obtained results were compared with gas chromatography analysis.

1. Introduction

Currently, biogas is considered to be modern form of bioenergy, which an alternative to conventional energy carriers, i.e.: coal, crude oil or natural gas. Waste products from various industries and agriculture (agri-food and animal waste) are increasingly used for biogas production. This is consistent with the theory of sustainable development and "green" technologies. However, biogas produced from waste materials contains (apart from the basic ingredients i.e. CH_4 and CO_2), numerous compounds that can be classified as problematic impurities, i.e.: ammonia, hydrogen sulfide, organosulfur compounds, siloxanes, aromatic and aliphatic hydrocarbons, halogenated and other volatile organic compounds (VOCs) (Andres et al., 2019). These impurities can cause a serious odor problem, especially for residents of areas immediately adjacent to production plants as well as can have environmental impacts i.e. stratospheric ozone depletion, the greenhouse effect, and effect damage to power equipment. Therefore, biogas pre-treatment is necessary to protect engines that convert biogas into energy and in order to increase the specific heat. There are many technologies to remove impurities from biogas that differ in functioning. Biogas purification methods include physical and chemical absorption, adsorption, pressure swing adsorption, membrane separation, cryogenic separation, and biological separation (Sun et al., 2019; Allegue and Hinge, 2014). The absorption process (also known as scrubbing) consists of transferring contaminants from a gas phase to a liquid phase (absorbent). This technique can select the absorbent so that it meets the designated criteria i.e. high absorption capacity of impurity, high-boiling and low vapor pressure, low viscosity and a high diffusion coefficient, safety and no toxicity, and a low cost. In addition, the development of sustainable absorbents represents one of the main challenges of "green" chemistry (Abbott et al., 2003).

Until newly, the research has been focused on Ionic Liquids (ILs) as an absorption material due to their unique properties. Recently, Deep Eutectic Solvents (DESs) have been introduced as a green alternative to ILs, due to their environmental-friendly composition, simple synthesis, low cost, and biodegradability. The literature has reported stable DESs based on natural compounds, particularly primary metabolites, such as organic acids,

polyphenols, amino acids, terpenes, and sugars (Makoś et al, 2018). Liquid DESs are obtained by the complexation of a hydrogen bond acceptor (HBA) with a hydrogen bond donor (HBD). The hydrogen bonding and electrostatic interactions are responsible for the decrease in the melting point of the mixture relative to the melting points of the raw materials. The physicochemical properties of the DESs (i.e.: viscosity, density, melting points or thermal stability) depend on the chemical nature of components and on their intermolecular interactions (Xin et al., 2017). Moreover, by appropriate selection of the components for the synthesis of DES it is possible to create a "perfect" absorbent which will allow selective removal impurities from a complex matrix i.e. biogas. Till now, DES have been successfully used to remove CO_2, H_2O, H_2S, NH_3 from biogas (Aissaoui et al., 2016). However, only a small number of works describe the use of DESs to removal of VOCs from biogas streams (Słupek et al., 2020).

In order to control the biogas purification process, mainly gas chromatography technique (GC) with selective and universal detectors is used. However, the use of GC in "off-line" or "in-line" mode results in a long delay in the results obtained, which prevents immediate correction of the fermentation broth composition, which does not allow improvement the efficiency of biogas production. Therefore, the "on-line" control system is necessary. This possibility is provided by the use of electronic noses.

Electronic noses, which are analogues of the sense of smell, allow them to be used in many fields of science and industry, such as: medical diagnostics, environmental protection, food and chemical industry or criminology. Electronic noses allow complete analysis of the gas mixture composition, without the need to separate and identify its individual components. Compared to other techniques used to analyze gas mixtures such as gas chromatography, electronic noses have additional advantages: shorter analysis time and lower price of the device. They enable independent operation in the on-line mode (Szulczyński et al., 2018).

The paper presents application of simple electronic nose for the control of odorous volatile organic compounds i.e. cyclohexane, 1-butanol, toluene, dimethyl disulphide and propionaldehyde removal from model biogas stream composed of methane and carbon dioxide. For biogas purification, hexadecane, ionic and non-ionic deep eutectic solvents composed of natural non-toxic components i.e. camphor, guaiacol, urea, choline chloride were used as new absorbents.

2. Experimental

2.1 Synthesis od DESs

DESs were synthesized by mixing two components choline chloride (ChCl) with urea (U) in 1:2 molar ratio and Camphor (C) with Guaiacol (Gu) in 1:1 molar ratio, at 70°C for 30 min using magnetic stirrer until homogeneous liquid were received. In the studies, reagents i.e. choline chloride (ChCl) (purity ≥ 99%), ±camphor (C) (purity ≥ 95%), urea (U) (purity ≥ 98%), guaiacol (purity ≥ 98%) (Sigma-Aldrich, USA) were used. The liquid DESs forms were obtained due to the formation of hydrogen bonds between -NH groups in U and chlorine anion in ChCl (Figure 1A) and between the -OH group in guaiacol and =O group in camphor (Figure 1B).
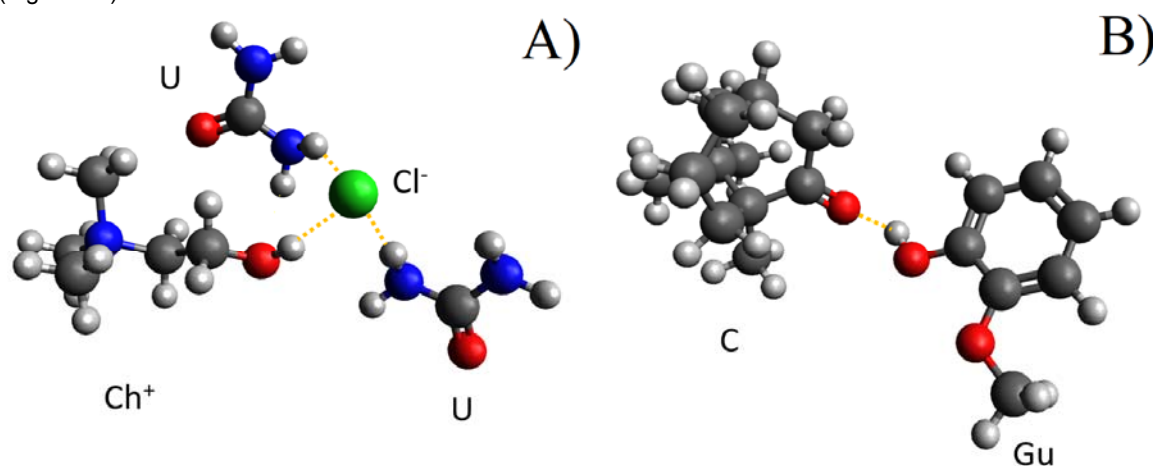
Figure 1: Molecular structures of DESs A) ChCl:U (1:2), and B) C:Gu (1:1)

2.2 Electronic nose development

In the presented study two models of chemical sensors were chosen for electronic nose application. They are commercially available metal oxide semiconductor sensors (MOS) manufactured by Figaro: TGS2600 and TGS2611. The selection of presented sensors models was caused by their high sensitivity values for volatile organic compounds, low cost, long life time and ease in signal processing.

The presented studies used qualitative analysis methods to assess the effectiveness of biogas deodorization. Points corresponding to relevant biogas samples projection onto a two-dimensional plane created by the values of the sensors used. The tests were carried out for pure biogas (methane and carbon dioxide mixture), as well as before and after the absorption process. This approach allows you to quickly analyze the performance of the biogas purification process.

2.3 Gas chromatography analysis

In order to be able to perform the analysis reliably, it was necessary to determine the exact concentrations of odorous substances in the biogas stream. For this purpose, gas chromatography combined with flame ionization detector (GC-FID) was used. In presented research Varian CP-3800 gas chromatograph was used equipped with DB-WAX column 30 m x 0.53 mm x 1 µm. The method parameters are presented in Table 1.

Table 1: Gas chromatography method parameters.

Parameter	Value
Carrier gas	Nitrogen
Column flow	$1.5 \text{ cm}^3 \text{ min}^{-1}$
Split ratio	1
Oven temperature	100°C (isothermal)
Sample volume	0.5 cm^3

The calibration for concentration determination of every odorous volatile organic compound were performed. An example chromatogram for a sample of contaminated biogas is shown in the Figure 2.
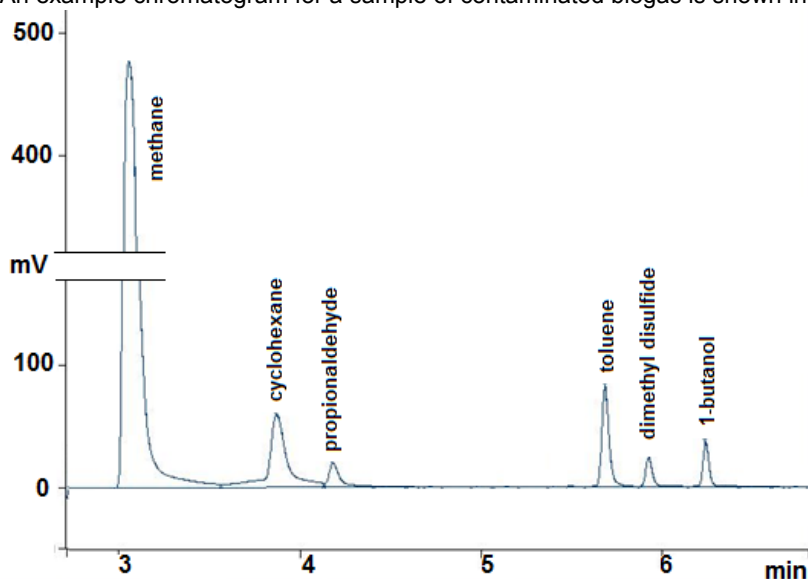
Figure 2: An example of chromatogram of impure biogas sample.

2.4 Experimental setup

The tests were carried out for three absorbents: hexadecane and two deep eutectic solvents: C:Gu (1:1), ChCl:U (1:2). The model impure biogas were prepared in Tedlar bags. the composition of the model gas was as follows: 75% methane and 25% carbon dioxide. The contaminants concentrations were equal to 16 ppm. The composition of the tested mixtures is presented in Table 2. The experimental setup is presented in Figure 3.
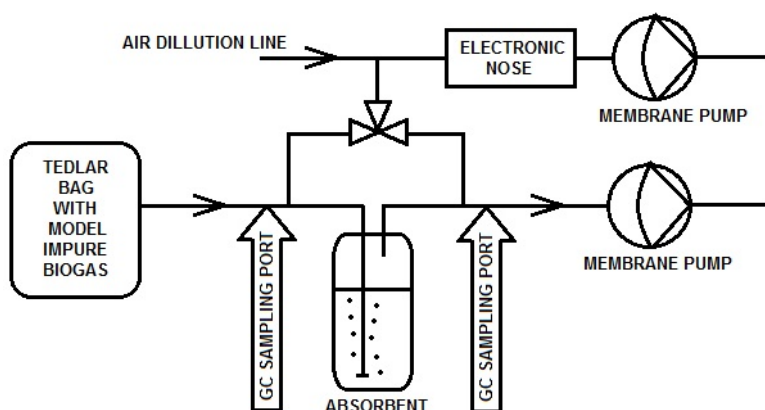
Figure 3: The schematic of the experimental setup.

The contaminated biogas flows through a vial filled with absorption liquid. At the inlet and outlet of the vial the gas samples were collected and analyzed using electronic nose and gas chromatography throughout the whole process. The recorded sensor signals were saved on the computer using the Simex SIAi-8 analog-to-digital converter. Analyzed sample was sucked by the pump and flowed through the e-nose system to the measurement chamber at a constant flow rate of 300 cm^3 min^{-1}. Due to high methane concentrations, the sample is diluted with air before entering the measuring chamber. The oxygen is necessary for the correct operation of sensors installed in the chamber. The electronic nose operated in stop-flow mode: the sample flow time through the chamber was 60 seconds, while the stop time was 30 seconds.

The sensors signal values recorded for a sample after absorption were transferred to the two-dimensional space. The purification efficiency (PE) were calculated using the formula:

$$PE_{e-nose} = \frac{a}{b} \cdot 100\% \tag{1}$$

Where: a – geometrical distance between point representing process sample and point representing impure biogas sample, b - geometrical distance between representing pure and impure biogas sample (Figure 4).
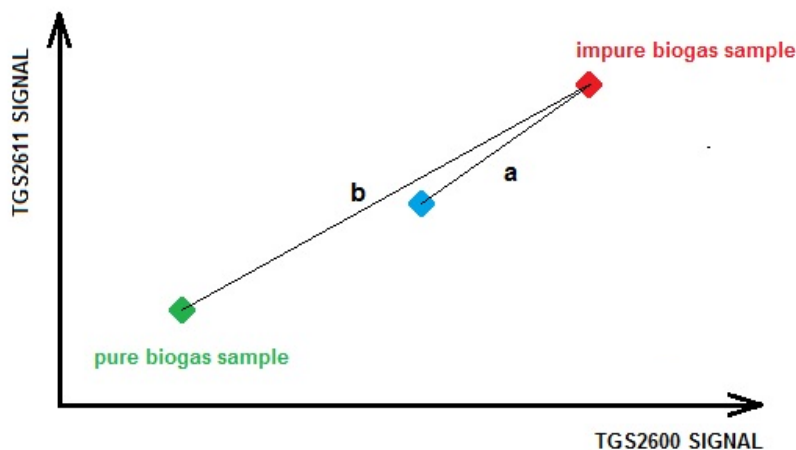
Figure 4: Purification efficiency determination using electronic nose (geometrical representation).

Every process sample were analyzed using gas chromatography. In this case, The purification efficiency were calculated using the formula:

$$PE_{GC} = \left(1 - \frac{\sum A_i}{\sum A_i^0}\right) \cdot 100\% \tag{2}$$

where: $\sum A_i$ – the sum of peaks area determined for all compounds in the process sample, $\sum A_i^0$ - the sum of peaks area determined for all compounds in the impure biogas sample.

3. Results and discussion

Model impure biogas mixtures composition and purification efficiency of its absorption process (using electronic nose and gas chromatography) in three absorbents is presented in the Table 2. Graphical representation of purification efficiency determined using electronic nose for three absorbents is presented in Figure 5.
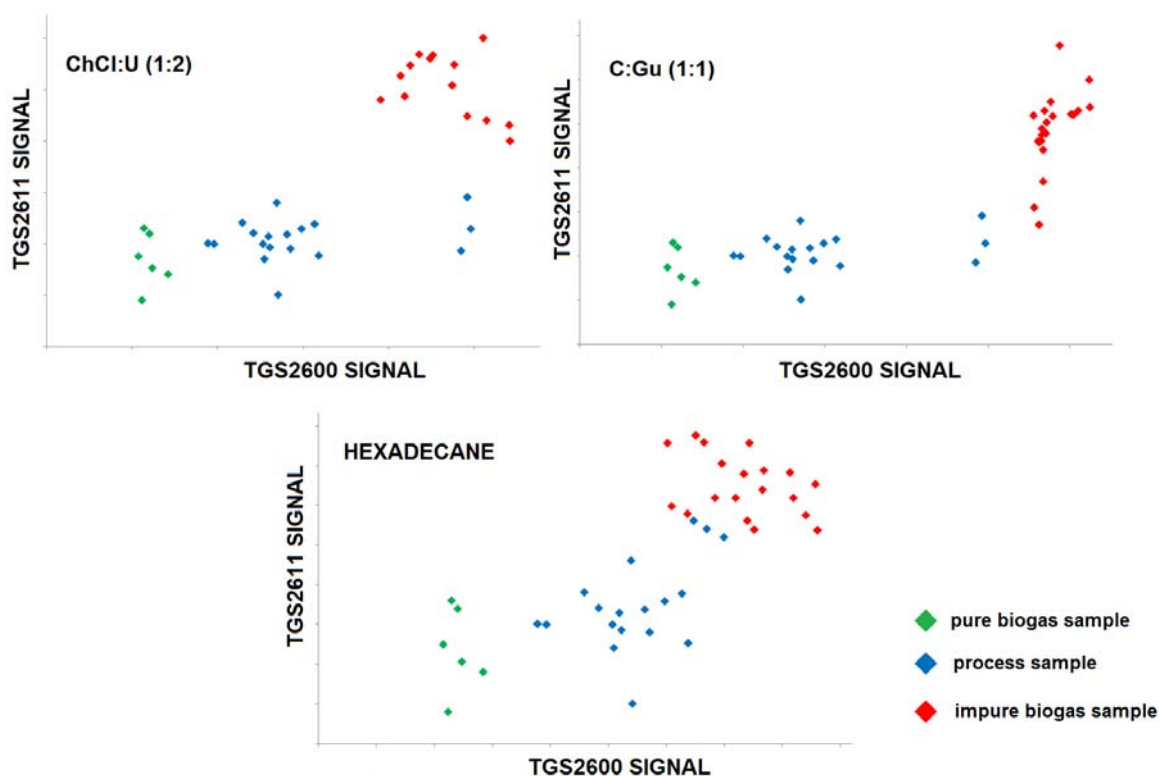
Figure 5: Results of purification efficiency determination using electronic nose (graphical representation).

Table 2: Tested mixtures composition and their purification efficiency in absorption process.

| Mixture number | Concentration in the mixture [ppm] | | | | | hexadecane | | C:Gu (1:1) | | ChCl:U (1:2) | |
	cyclohexane	DMDS	toluene	1-butanol	propionaldehyde	PE_{enose}	PE_{GC}	PE_{enose}	PE_{GC}	PE_{enose}	PE_{GC}
1	16	0	0	0	0	43.3	42.4	66.9	67.6	58.0	55.1
2	16	0	0	0	0	40.8	44.0	64.7	58.9	55.3	53.6
3	16	0	0	0	0	27.4	29.6	56.6	48.7	44.9	40.4
4	0	16	0	0	0	25.1	49.1	43.4	65.4	26.3	58.3
5	0	16	0	0	0	27.9	47.9	39.2	69.9	30.9	60.3
6	0	16	0	0	0	25.9	44.5	37.5	57.3	28.8	51.7
7	0	0	16	0	0	71.7	65.2	83.3	72.5	78.8	74.1
8	0	0	16	0	0	74.6	67.8	85.0	89.3	81.0	72.9
9	0	0	16	0	0	60.0	61.8	76.2	75.5	69.9	68.5
10	0	0	0	16	0	39.0	33.9	63.8	61.9	54.1	52.4
11	0	0	0	16	0	35.0	33.3	61.0	69.6	50.6	56.7
12	0	0	0	16	0	30.2	29.3	57.8	51.4	46.5	41.8
13	0	0	0	0	16	50.6	51.6	70.8	70.1	63.0	66.8
14	0	0	0	0	16	50.0	44.5	70.6	77.6	62.6	55.7
15	0	0	0	0	16	48.6	52.0	69.6	68.2	61.4	52.2
16	16	16	16	16	16	20.5	20.1	29.1	31.4	5.3	4.9
17	16	16	16	16	16	19.5	20.1	25.8	26.1	8.8	8.1
18	16	16	16	16	16	18.3	20.4	21.9	24.2	7.9	8.8

Analyzing the obtained results the value of the purification efficiency determined by means of electronic nose and gas chromatography should note that the results obtained from the electronic nose do not differ significantly from the values determined by the reference method (gas chromatography). Only for dimethyl disulfide, the electronic nose significantly deviates from the reference values. This is due to the very low sensitivity values for dimethyl disulfide of both sensors used for this substance. For this reason, the disulfide signals are much lower and the PE estimation error is higher. Presented results show that deep eutectic solvent - Camphor (C) with Guaiacol (Gu) in 1:1 molar ratio has the highest values of purification efficiency for purification model biogas of single volatile organic compounds and their mixture.

4. Conclusions

The research presents application of simple electronic nose for the process performance control of odorous volatile organic compounds i.e. cyclohexane, 1-butanol, toluene, dimethyl disulfide and propionaldehyde removal from model biogas stream composed of methane and carbon dioxide. The results obtained using an electronic nose are slightly different from the results obtained using gas chromatography. This shows that electronic noses can be successfully use to monitor the biogas purification process by absorption. They are significantly cheaper than chromatographs, they enable much shorter time of single analysis and easy possibility of automation. As part of the research, the usefulness of deep eutectic solvents (DES) as a green alternative to ionic liquids for biogas purification, due to their environmental-friendly composition, simple synthesis, low cost, and biodegradability has also been demonstrated. The study shows that the deep eutectic solvent consisting of Camphor (C) with Guaiacol (Gu) in 1:1 molar ratio proved to be the best choice for biogas purification from cyclohexane, dimethyl disulfide, 1-butanol, propionaldehyde and toluene.

Acknowledgments

References

Abbott A.P., Capper G., Davies D.L., Rasheed R.K., Tambyrajah V., 2003, Novel Solvent Properties of Choline Chloride /Urea Mixtures, Chemical Communications, 0, 70–71.

Allegue L.B., Hinge J., 2014, Biogas upgrading Evaluation of methods for H 2 S removal, Danish Technological Institute, 31.

Andrés C., Guardia A., Couvert A., Wolbert D., Le S., Soutrel I., Nunes G., 2019, Odor concentration (OC) prediction based on odor activity values (OAVs) during composting of solid wastes and digestates, Atmospheric Environment, 201, 1–12.

Aissaoui T., AlNashef I.M., Benguerba Y., 2016, Dehydration of natural gas using choline chloride based deep eutectic solvents: COSMO-RS prediction, Journal of Natural Gas Science and Engineering, 30, 571–577.

Makoś P., Przyjazny A., Boczkaj G., 2018, Hydrophobic deep eutectic solvents as "green" extraction media for polycyclic aromatic hydrocarbons in aqueous samples, Journal of Chromatography A, 1570.

Słupek E., Makoś P., Gębicki J., 2020, Deodorization of model biogas by means of novel non- ionic deep eutectic solvent. Archives of Environmental Protection, 46, 41–46.

Sun Q., Li H., Yan J., Liu L., Yu Z., Yu X., 2015, Selection of appropriate biogas upgrading technology-a review of biogas cleaning, upgrading and utilisation, Renewable and Sustainable Energy Reviews, 51, 521–532.

Szulczyński B., Namieśnik J., Gębicki J., 2018, Analysis of Odour Interactions in Model Gas Mixtures using Electronic Nose and Fuzzy Logic, Chemical Engineering Transactions, 68, 259-264.

Xin R., Qi S., Zeng C., Khan F.I., Yang B., Wang Y., 2017, A functional natural deep eutectic solvent based on trehalose: Structural and physicochemical properties, Food Chemistry, 217, 560–567.

Gdańsk, dnia 19.05.2023

dr inż. Patrycja Makoś-Chełstowska

....
(stopień/tytuł, imię i nazwisko)

Politechnika Gdańska

....
(Afiliacja)

OŚWIADCZENIE WSPÓŁAUTORA

Jako współautor pracy:. " **Process Control of Biogas Purification Using Electronic Nose**" oświadczam, że mój własny wkład polegał na wizualizacji oraz przygotowaniu oryginalnego manuskryptu.

Jednocześnie wyrażam zgodę na przedłożenie ww. pracy przez mgr inż. Edytę Słupek jako część rozprawy doktorskiej w formie spójnego tematycznie zbioru artykułów opublikowanych w czasopismach naukowych.

Oświadczam, że samodzielna i możliwa do wyodrębnienia część ww. pracy wykazuje indywidualny wkład mgr inż. Edyty Słupek polegający na: konceptualizacji, metodologii, gromadzeniu i przechowywaniu danych, wizualizacji oraz przygotowaniu oryginalnego manuskryptu.

(podpis współautora)

Gdańsk, dnia 19.05.2023

mgr inż. Dominik Dobrzyniewski

....
(stopień/tytuł, imię i nazwisko)

Politechnika Gdańska

....
(Afiliacja)

OŚWIADCZENIE WSPÓŁAUTORA

Jako współautor pracy:. " **Process Control of Biogas Purification Using Electronic Nose**" oświadczam, że mój własny wkład polegał na konceptualizacji, prowadzeniu badań, gromadzeniu i przechowywaniu danych oraz przygotowaniu oryginalnego manuskryptu.

Jednocześnie wyrażam zgodę na przedłożenie ww. pracy przez mgr inż. Edytę Słupek jako część rozprawy doktorskiej w formie spójnego tematycznie zbioru artykułów opublikowanych w czasopismach naukowych.

Oświadczam, że samodzielna i możliwa do wyodrębnienia część ww. pracy wykazuje indywidualny wkład mgr inż. Edyty Słupek polegający na: konceptualizacji, metodologii, gromadzeniu i przechowywaniu danych, wizualizacji oraz przygotowaniu oryginalnego manuskryptu.

(podpis współautora)

Gdańsk, dnia 19.05.2023

dr inż. Bartosz Szulczyński
....
(stopień/tytuł, imię i nazwisko)

Politechnika Gdańska
....
(Afiliacja)

OŚWIADCZENIE WSPÓŁAUTORA

Jako współautor pracy:. **" Process Control of Biogas Purification Using Electronic Nose"** oświadczam, że mój własny wkład polegał na przygotowaniu recenzji i redakcji ostatecznej wersji manuskryptu oraz finansowaniu.

Jednocześnie wyrażam zgodę na przedłożenie ww. pracy przez mgr inż. Edytę Słupek jako część rozprawy doktorskiej w formie spójnego tematycznie zbioru artykułów opublikowanych w czasopismach naukowych.

Oświadczam, że samodzielna i możliwa do wyodrębnienia część ww. pracy wykazuje indywidualny wkład mgr inż. Edyty Słupek polegający na: konceptualizacji, metodologii, gromadzeniu i przechowywaniu danych, wizualizacji oraz przygotowaniu oryginalnego manuskryptu.

....
(podpis współautora)

Gdańsk, dnia 19.05.2023

dr inż. hab. Jacek Gębicki
....
(stopień/tytuł, imię i nazwisko)

Politechnika Gdańska
....
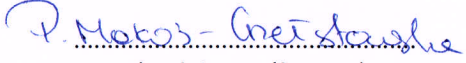(Afiliacja)

OŚWIADCZENIE WSPÓŁAUTORA

Jako współautor pracy:. **" Process Control of Biogas Purification Using Electronic Nose"** oświadczam, że mój własny wkład polegał na nadzorowaniu wstępnego planu badań oraz przygotowaniu recenzji i redakcji ostatecznej wersji manuskryptu.

Jednocześnie wyrażam zgodę na przedłożenie ww. pracy przez mgr inż. Edytę Słupek jako część rozprawy doktorskiej w formie spójnego tematycznie zbioru artykułów opublikowanych w czasopismach naukowych.

Oświadczam, że samodzielna i możliwa do wyodrębnienia część ww. pracy wykazuje indywidualny wkład mgr inż. Edyty Słupek polegający na: konceptualizacji, metodologii, gromadzeniu i przechowywaniu danych, wizualizacji oraz przygotowaniu oryginalnego manuskryptu.

....
(podpis współautora)

Autorzy:

E. Słupek, P. Makoś, J. Gębicki

Tytuł publikacji:

Theoretical and Economic Evaluation of Low-Cost Deep Eutectic
Solvents for Effective Biogas Upgrading to Bio-Methane

Czasopismo:

ENERGIES

DOI:

10.3390/en13133379

Theoretical and Economic Evaluation of Low-Cost Deep Eutectic Solvents for Effective Biogas Upgrading to Bio-Methane

Edyta Słupek[ID]**, Patrycja Makoś** *[ID] **and Jacek Gębicki**

Department of Process Engineering and Chemical Technology, Faculty of Chemistry, Gdansk University of Technology, G. Narutowicza St. 11/12, 80-233 Gdansk, Poland; edyta.slupek@pg.edu.pl (E.S.); jacek.gebicki@pg.edu.pl (J.G.)
* Correspondence: patrycja.makos@pg.edu.pl; Tel.: +48-508997100

Abstract: This paper presents the theoretical screening of 23 low-cost deep eutectic solvents (DESs) as absorbents for effective removal of the main impurities from biogas streams using a conductor-like screening model for real solvents (COSMO-RS). Based on thermodynamic parameters, i.e., the activity coefficient, excess enthalpy, and Henry's constant, two DESs composed of choline chloride: urea in a 1:2 molar ratio (ChCl:U 1:2), and choline chloride: oxalic acid in a 1:2 molar ratio (ChCl:OA 1:2) were selected as the most effective absorbents. The σ-profile and σ-potential were used in order to explain the mechanism of the absorptive removal of CO_2, H_2S, and siloxanes from a biogas stream. In addition, an economic analysis was prepared to demonstrate the competitiveness of new DESs in the sorbents market. The unit cost of 1 m^3 of pure bio-methane was estimated to be in the range of 0.35–0.37 EUR, which is comparable to currently used technologies.

1. Introduction

Due to European Union (EU) energy policies to promote the utilization of renewable resources, there has been a significant increase in biogas plants and the level of biogas production [1,2]. The number of biogas plant installations and the amount of produced bio-methane in recent years is presented in detail in Figure 1. Biogas can be produced by anaerobic digestion from different waste materials (i.e., manure and food residue, wastewater sludge, or industrial by-products) or landfill gas. Biogas mainly consists of methane (50–70%) and contaminants including carbon dioxide, water, nitrogen, oxygen, hydrogen sulfide, ammonia, and numerous organic compounds (i.e., siloxanes) [3–5]. The presence of these contaminants prevents the use of biogas as an alternative transport fuel or natural gas substitute. Among the biogas impurities, carbon dioxide, hydrogen sulfide and siloxanes are the most problematic [6,7].

Carbon dioxide is present in high concentrations in biogas and it acts as a ballast; this significantly reduces the quality of biogas because it reduces the caloric power of biogas in proportion to its concentration. Biogas should contain more than 90% pure methane, depending on its further application. During the biogas combustion process, hydrogen sulfide reacts with water, forming sulfuric acid, which corrodes the surface in the combustion chamber [8], while the siloxanes are converted into silicon dioxide (SiO_2), which can be deposited into the cylinder, impeller, valves, piston rings, liners, spark plugs, and turbochargers. Accumulation of hard deposits of SiO_2 reduces the life span of the turbines and engine efficiency, which results in detonation in the combustion chambers and an increase in the exhaust gas emissions due to unburned fuel. This also results in higher plant maintenance costs. In addition, the presence of certain groups of trace compounds in biogas can cause

the emission of toxic by-products into the atmosphere. The occurrence of these contaminants is a major barrier to the use of biogas as a renewable energy source.
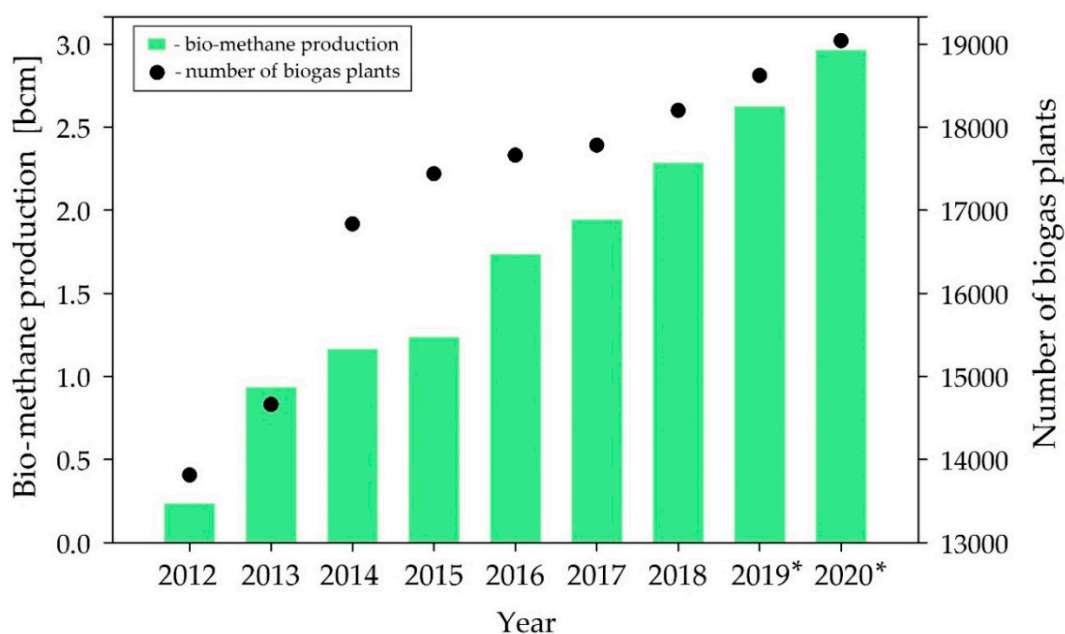
Figure 1. Number of biogas plants and bio-methane production from 2012 to 2020 in the European Union (bcm—billion cubic meters; 2019* and 2020* are estimated values).

Currently, there are several technologies for removing CO_2, H_2S, and siloxanes from biogas including adsorption, refrigeration with condensation, membrane technologies, biological methods, and absorption [9–13]. Among these technologies, physical absorption is one of the most popular. This process consists of transferring contaminants from a gas phase to an absorbent. Different types of absorbents such as water, organic compounds, and oils are used [14–16]. However, there are a few disadvantages associated with conventional organic absorbents, which can lead to equipment corrosion and harmful effects on the environment. Therefore, in the past decade, ionic liquids (ILs) have been proposed as a potential alternative for conventional absorbents for CO_2 [17–20] and H_2S [17,21–23] removal from different type of gas streams. Despite the attractive physicochemical properties of ILs (i.e., good thermal stability, non-volatile properties, and high absorption capacity [24,25]), they not found practical industrial application due to their high viscosity, potential toxicity, high cost and complicated synthesis processes [26]. Due to the limitations of both conventional solvents and ILs, alternative solutions are still in demand. Nowadays, one of the most promising group of green absorbents is deep eutectic solvents (DESs). DESs are synthesized by the direct mixing of two ingredients—hydrogen bond acceptor (HBA) with a hydrogen bond donor (HBD). DES mixtures are characterized by a lower melting point compared to the individual components [27]. In addition, DESs are characterized by specific physicochemical properties such as their non-volatility, non-flammability, high absorption capacity, non-toxic character, and high thermal stability [28,29]. A comparison of the properties of DES with other absorbents is presented in Table 1.

Table 1. Comparison of physicochemical properties of absorbents [28–37].

Properties	Water	Organic Amine	ILs	DESs
The synthesis	No	No	Multi-step synthesis	Easy
Applicability	Single function	Single function	Multifunction	Multifunction
Tunability	No	No	High	High
Thermal stability	Low	Low	Tunable, but generally high	Tunable, but generally high
Boiling Points	100 °C	111–350 °C	>250 °C	Higher than other solvents (214–1774 °C)
Environmentally friendly	Yes	No	Not all	Yes
Toxicity	No	Yes	Often increase toxicity for aquatic systems	Acceptable toxicity profiles
Corrosive nature	High	High	Low	Low
Biodegradability	Readily	Readily	Difficult	Readily
Density	Low	Medium	Tunable, but generally higher than other solvents	Tunable, but generally lower than ILs
Viscosity	Low	Medium	Tunable, but generally higher than other solvents	Tunable, but generally lower than ILs
Surface tension	High	Low	Generally lower than water and higher than organic amine	Low
Vapor pressure	High	High	Low	Low
Flammability	No	Yes	No	No
Nature	Neutral	Basic	Basic/neutral/acid	Basic/neutral/acid
Type of absorption	Physical	Chemical/Physical	Physical	Physical
Absorption capacity	Medium	Medium	High	High
Biodegradable	Yes	No	Poor	Yes
Cost	Low	Moderate	High	Low

Because of their unique properties, DESs are now successfully used as extractants [38–41] and absorption solvents [42–46] for the purification of gas and liquid streams [46–49]. Of the available DESs, solvents composed of quaternary ammonium salts are considered to be the most promising absorbents. DESs can also be synthesized from natural compounds, which makes them so-called "green solvents" due to the lack of or very low toxicity and their biodegradability [50]. Due to the high thermal stability of DESs, they can be regenerated repeatedly without loss of absorption capacity and the regeneration step requires less energy compared to other popular absorbents. Hence, the use of DESs as absorption solvents in the biogas upgrading process are considered as environmentally friendly technologies for the production of green bio-energy.

The application of upgraded biogas for the production of energy is considered as one of the most efficient methods for reducing greenhouse gas emissions to the atmosphere. For this reason, 23 deep eutectic solvents composed of quaternary ammonium salts and low-cost organic components were examined as potential absorbents for the removal of siloxanes, CO_2, and H_2S from a model biogas stream. A conductor-like screening model for real solvents (COSMO-RS) was used for the pre-selection of DESs. The selection of DESs with the highest dissolution potential for all impurities was made on the basis of the activity coefficient, excess enthalpy, and Henry's constant values. The absorption mechanism for the removal of the main impurities (CO_2, H_2S, siloxanes) was explained based on σ-profiles and σ-potential analysis. In addition, an economic analysis of the biogas upgrading processes

was prepared. To the best of our knowledge, this is the first economic analysis report dedicated to biogas upgrading processes that use DESs.

2. Materials and Methods

2.1. Procedures

2.1.1. Computational Studies

In this investigation, COSMO-RS calculations were carried out using ADF COSMO-RS software (SCM, Netherlands). The geometry optimization of all DESs were performed using the continuum solvation COSMO model at the BVP86/TZVP level of theory. This level of theory was selected due to proven high efficiency and low computational costs [51]. The list of 23 DESs is presented in Table 2. The main thermodynamic parameters, i.e., the activity coefficient, excess enthalpy, and Henry's constant were calculated based on previous studies [52,53]. The parameters were determined for model biogas composed of 64.9% of CH_4, 31% of CO_2, 3% of H_2O and 1.04 of H_2S, and 0.02% of hexamethyldisiloxane (L2), octamethyltrisiloxane (L3), and octamethylcyclotetrasiloxaan (D4), which represents the typical composition of biogas from wastewater treatment plants and landfills [8,54].

Table 2. List of deep eutectic solvents (DESs) used for the conductor-like screening model for real solvents (COSMO-RS) calculation.

No.	HBA	HBD	HBA:HBD Molar Ratio	Abbreviation
1	Choline chloride	ethylene glycol	1:3	ChCl:EG (1:3)
2	Choline chloride	glycerol	1:3	ChCl:Gly (1:3)
3	Choline chloride	levulinic acid	1:3	ChCl:Lev (1:3)
4	Choline chloride	lactic acid	1:2	ChCl:LA (1:2)
5	Choline chloride	butyric acid	1:2	ChCl:Bu (1:2)
6	Choline chloride	phenol	1:2	ChCl:Ph (1:2)
7	Choline chloride	urea	1:2	ChCl:U (1:2)
8	Choline chloride	diethylene glycol	1:2	ChCl:DEG (1:2)
9	Choline chloride	oxalic acid	1:2	ChCl:OA (1:2)
10	Choline chloride	methacrylic acid	1:2	ChCl:MthA (1:2)
11	Choline chloride	propylene glycol	1:2	ChCl:PG (1:2)
12	Tetrabutylammonium chloride	ethylene glycol	1:3	TBACl:EG (1:3)
13	Tetrabutylammonium chloride	glycerol	1:3	TBACl:Gly (1:3)
14	Tetrabutylammonium chloride	levulinic acid	1:3	TBACl:Lev (1:3)
15	Tetrabutylammonium chloride	lactic acid	1:2	TBACl:LA (1:2)
16	Tetrabutylammonium chloride	butyric acid	1:2	TBACl:Bu (1:2)
17	Tetrabutylammonium chloride	phenol	1:2	TBACl:Ph (1:2)
18	Tetrapropylammonium bromide	ethylene glycol	1:3	TEABr:EG (1:3)
19	Tetrapropylammonium bromide	glycerol	1:3	TEABr:Gly (1:3)
20	Tetrapropylammonium bromide	levulinic acid	1:3	TEABr:Lev (1:3)
21	Tetrapropylammonium bromide	lactic acid	1:2	TEABr:LA (1:2)
22	Tetrapropylammonium bromide	butyric acid	1:2	TEABr:Bu (1:2)
23	Tetrapropylammonium bromide	phenol	1:2	TBABr:Ph (1:2)

Henry's constant (K_H) was applied to systems in thermodynamic equilibrium. The K_H links the solubility of solute impurities (i) to its partial pressure above the mixture (p_i^{vap}). K_H was calculated using Equation (1).

$$K_H = \frac{1}{\gamma_i p_i^{vap}} \tag{1}$$

where γ_i is the infinite dilute activity coefficient of impurities (i), and p_i^{vap} is the vapor pressure of impurities (i).

The activity coefficient was calculated using Equation (2) and Equation (3).

$$\ln(\gamma_i) = \frac{\mu_i^{solv} - \mu_i^{pure}}{RT} \tag{2}$$

where μ_i^p is the chemical potential of pure impurities (*i*), μ_i^j is the chemical potential of impurities in the liquid phase, *T* is the temperature (K), and the universal gas constant *R* = 8.314 J/mol.

The excess enthalpy of mixtures H^E (kJ/mol) was calculated based on Gibbs-Helmholtz using Equation (3).

$$H^E = -T^2 \frac{\partial\left(\frac{G^E}{T}\right)}{\partial T} \tag{3}$$

where *T* is the temperature (K), and G^E is the excess Gibbs free energy (kJ/mol).

2.1.2. Biogas Upgrading Technology Description

The scheme for the biogas upgrading technology described in this paper is presented in Figure 2. The physicochemical properties of DESs are similar to the most commonly used absorbents (i.e., amine or water), therefore, DESs can be applied in existing and currently used absorption installations. In order to better compare the benefits of DESs application in the absorption process, the size of the installations (absorption and desorption column, compressor, pump, blower, dryer, and heat exchangers) and the process streams (inlet biogas stream 813 m^3/h and inlet air stream 403 m^3/h) was adopted from previous studies [55,56].
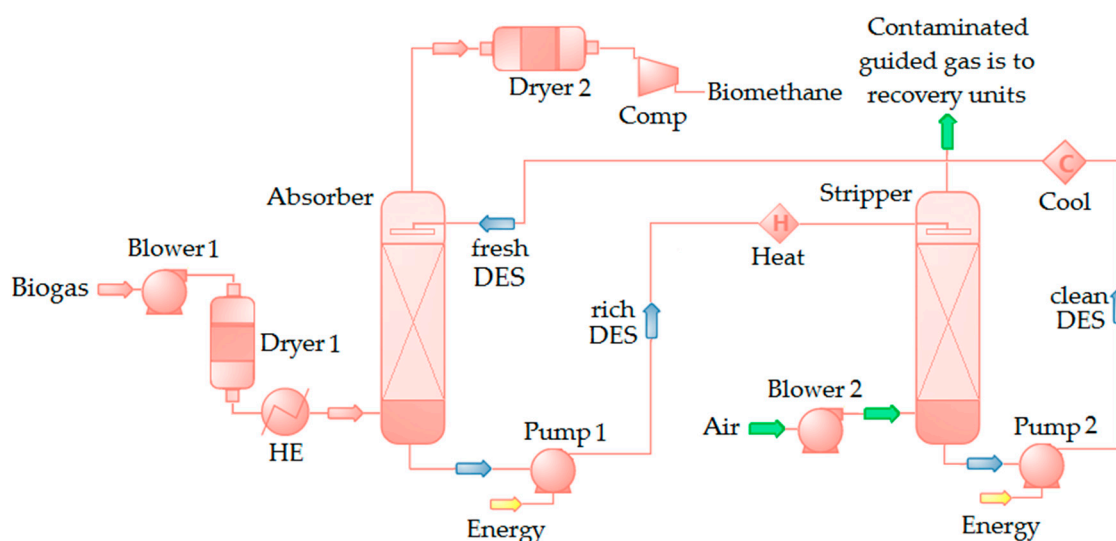
Figure 2. Scheme for the biogas upgrading technology [55,56].

In the first stage, biogas stream is introduced into Dryer 1. Then, the biogas is passed directly to the heat exchanger, after which biogas is directed into the bottom part of the absorber (813 m^3/h), which operates at a temperature of 20 °C, and pressure of 100 kPa. The biogas stream is introduced at the bottom of the absorber. The DES is introduced at the top of the column. The biogas and DES move through a counter-flow scrubbing column. In the column, the biogas comes into contact with a DES to dissolve the main impurities (L2, L3, D4, CO_2, and H_2S). This is a process of mass transfer of pollutants from the biogas phase to the liquid DES phase. The upgraded bio-methane is downloaded from the top of the absorber, drained again (Dryer 2), and compressed. The obtained renewable bio-methane can be directly injected into the distribution gas grid at 700 kPa. The biogas purification system also contains the stripper column, which is operated under a temperature of 115–125 °C and pressure of 140–170 kPa. Saturated DES from the absorption column is directed into the stripper column where

DES is purged with an inlet air stream (403 m^3/h). Most of the impurities (L2, L3, D4, CO_2, and H_2S) are liberated into a concentrated air stream that exits at the top of the stripper column. The impurities stream is directed to the H_2S, CO_2, L2, L3, and D4 recovery system. The regenerated DES is cooled and returned to the absorber column.

2.1.3. Cost and Economic Analysis

The cost simulations included an estimation of the total annual cost (*TAC*) of the biogas upgrading process. *TAC* included the annual capital investment cost (*ACIC*), and the annual operation and maintenance cost (OC and MC).

The *ACIC* was estimated based on the method of Scholz et al. [57] according to Equation (4).

$$ACIC = TCIC\frac{i(1+i)^n}{(1+i)^n - 1} \tag{4}$$

where *ACIC* is the annual capital investment cost, *TCIC* is the total capital investment cost, *i* is the interest rate (9%), and *n* is the depreciation period (15 years).

The *TCIC* was mainly estimated as the percentage value of the equipment cost (*EC*) [55]. The *EC* was estimated by Guthrie's method [58], according to Equation (5).

$$EC = PEC\left(f_{mp} + f_m - 1\right) \tag{5}$$

where *EC* is the equipment cost, *PEC is* the bare purchased equipment cost, f_{mp} the material and pressure correction factor, and f_m is the module factor, which depends on the size equipment. The values of f_{mp} and f_m were adopted according to the procedure proposed by Scholz et al. [57]. The *EC* of the absorption column, stripper column, blowers, pumps, compressors, and heat exchangers was adopted from other studies [56]. The list of basic parameters for maintenance and operation cost, which consist of operating supply cost, research, and development (R&D) costs, personnel labor cost, utility costs (i.e., electricity cost for heating and cooling, absorbent exchange cost) is presented in Table 3.

Table 3. Parameters for operation costs.

Parameter	Units	Costs	Ref.
Electricity	EUR/kWh	0.1	[59]
Heat	EUR/kWh	0.046	[57]
Personnel	EUR/h	38.88	[56]
Choline chloride	EUR/t	4550	[60]
Urea	EUR/t	218.4	[61]
Oxalic acid	EUR/t	455	[62]

The last step of the cost analysis was the estimation of the risk and economic benefits of the project. The financial assessment of the investment was carried out on the basis of the expected energy production, and total costs of the plant. The unit cost (*UC*) of 1 m^3 biogas purification was calculated according to Equation (6) [63].

$$UC = \left(\frac{\left(\frac{TCIC}{n}\right) + ((TCIC * i) + TAC)}{APB}\right) \tag{6}$$

where *UC* is the unit cost of 1 m^3 bio-methane, *i* is the interest rate (9%), *n* is the depreciation period (15 years), *APB* is the annual production of bio-methane [m^3], and *TAC* is the total annual cost.

The annual amount of cubic meters of upgraded biogas stream was determined according to Equation (7).

$$APB = BF{\cdot}\% \, CH_4 {\cdot} ML \tag{7}$$

where *BF* is the biogas flow, % *CH₄* is the percentage of methane in biogas, and *ML* is the methane loss.

3. Results and Discussion

3.1. COSMO-RS Prediction—Pre-Selection of DESs

The preselection of DESs that are characterized by high solubility of siloxanes, H_2S, CO_2, H_2O, and CH_4 was made based on the Henry's constants, activity coefficients, and excess enthalpy of mixtures that were predicted according to the COSMO-RS method. Water was omitted in the calculations because it was assumed to be removed before the biogas enters the absorption column. All parameters were determined at 20 °C and 100 kPa. The calculation results are presented in Table 4.

The activity coefficient is a thermodynamic parameter that is associated with the affinity of siloxanes, H_2S, CO_2, and CH_4 to DESs. This parameter indicates the differences in strength among DESs and impurities, which are a result of the dominant interactions. Usually, the activity coefficient values are given as $\ln(1/\gamma)$, hence these are rather negative (Table 4) [64]. The higher negative values of logarithmic activity coefficients indicate greater solubility of siloxanes, H_2S, and CO_2 in DESs. The second main thermodynamic parameter is the excess enthalpy of mixtures (H^E). H^E is a sensitive measure of the intermolecular interactions between DESs and impurities. The results of H^E calculated for all DES-impurities models are presented in Table 4. The DES, which is characterized by a higher dissolution capacity of CO_2, H_2S, and siloxanes has lower values of H^E (higher negative). The third parameter is the Henry's Law constant (K_H). The K_H describes the ratio at the equilibrium of the concentration of impurities in the gas phase to the concentration of impurities in the DES phase, and it combines vapor pressure and solubility, which can be used to estimate the likelihood that a substance will be exchanged between the gas phase and a DES. Lower K_H indicates a higher concentration of impurities in the DES phase than in the gas phase.

ChCl:U (1:2) and ChCl:OA (1:2) showed lower values for all thermodynamic parameters, relative to all impurities. Slightly higher values were obtained for the rest of the DESs composed of choline chloride such as HBA. This indicates that this type of HBA in DES structures has a major influence on absorption efficiency. This is in line with the conclusions obtained in previous studies [46]. This can be caused by several factors, including HBA alkyl chain length, different charge density on the ammonium, as well as asymmetry in ChCl ammonium with a hydroxyl group in the longest branch, and theoretically, a type of counter-ion (Cl^- or Br^-). However, the obtained results indicate that this type of counter-ion in HBA only has a slight effect on the ability of DESs to dissolve all impurities. The use of DESs containing ChCl as HBA in the absorption process is preferred because they are characterized by less viscosity compared to DESs composed of quaternary ammonium salts with long alkyl chain length [65].

Principal components analysis (PCA) was used to obtain a better interpretation of all results (the activity coefficient, excess enthalpy, and Henry's constant). The PCA plot is presented in Figure 3. The numbers on the diagram correspond to the DESs numbers in Table 4. The results indicate that DESs can be divided into three groups. The first group is marked with a yellow circle and contains two DESs (ChCl:U 1:2 and ChCl:OA 1:2) that have the greatest dissolution potential for all impurities. The second group, marked with a green circle, includes DESs that have the potential to effectively absorb siloxanes, but they have low CO_2 and H_2S dissolution potential. These DESs may have potential use for selective siloxane removal, but their solubility is insufficient in applications that require the comprehensive removal of impurities from biogas. The last group includes DESs that have the lowest absorption potential for all of the tested compounds.

Table 4. The logarithmic activity coefficient of siloxanes H$_2$S, and CO$_2$ model at infinite dilution, excess enthalpy of mixtures and Henry's constant of siloxanes calculated by COSMO-RS at 20 °C and 101325 Pa.

| No.	DES	Activity Coefficient					H^E [kJ/mol]					K_H [mol/L atm]				
		L2	L3	D4	H$_2$S	CO$_2$	L2	L3	D4	H$_2$S	CO$_2$	L2	L3 [*10^3]	D4 [*10^5]	H$_2$S	CO$_2$
1	ChCl:EG (1:3)	−5.28	−6.81	−6.57	−0.30	−1.09	−5.58	−5.57	−5.57	−5.62	−5.61	50.8	1.25	3.12	1.79	0.089
2	ChCl:Gly (1:3)	−4.86	−6.30	−6.03	−0.08	−0.83	−5.63	−5.62	−5.62	−5.68	−5.66	76.2	2.22	5.67	1.80	0.093
3	ChCl:Lev (1:3)	−3.68	−4.77	−4.42	0.16	−0.54	−5.68	−5.68	−5.68	−5.73	−5.71	151.3	5.67	15.49	1.90	0.104
4	ChCl:LA (1:2)	−5.49	−7.12	−6.81	−0.39	−1.14	−7.45	−7.44	−7.44	−7.48	−7.46	33.0	0.74	1.95	1.36	0.070
5	ChCl:Bu (1:2)	−3.13	−4.04	−3.66	0.01	−0.54	−7.52	−7.51	−7.52	−7.53	−7.52	383.8	18.57	52.76	1.89	0.119
6	ChCl:Ph (1:2)	−3.24	−4.19	−3.49	−0.14	−0.63	−7.77	−7.77	−7.82	−7.33	−7.76	366.3	17.29	69.11	1.59	0.107
7	ChCl:U (1:2)	−8.11	−10.52	−10.22	−1.15	−2.05	−7.29	−7.28	−7.30	−7.32	−7.31	1.9	0.02	0.05	0.83	0.037
8	ChCl:DEG (1:2)	−4.30	−5.57	−5.32	−0.11	−0.75	−7.65	−7.64	−7.63	−7.69	−7.67	97.5	3.17	7.94	1.49	0.086
9	ChCl:OA (1:2)	−8.11	−10.55	−9.43	−1.01	−1.88	−8.09	−8.08	−8.18	−8.12	−8.10	3.8	0.04	0.24	0.82	0.038
10	ChCl:MthA (1:2)	−3.45	−4.45	−3.98	−0.07	−0.62	−7.50	−7.50	−7.51	−7.52	−7.50	332.3	15.20	45.62	1.82	0.114
11	ChCl:PG (1:2)	−3.96	−5.10	−4.80	−0.01	−0.66	−7.77	−7.77	−7.76	−7.81	−7.79	203.7	7.94	20.31	2.06	0.118
12	TBACl:EG (1:3)	−3.39	−4.36	−4.12	0.18	−0.43	−4.13	−4.13	−4.13	−5.62	−5.61	367.9	18.13	45.69	2.04	0.120
13	TBACl:Lev (1:3)	−2.30	−2.97	−2.64	0.47	−0.09	−4.13	−4.13	−4.13	−5.73	−5.71	640.4	39.82	107.48	2.02	0.127
14	TBACl:LA (1:2)	−2.97	−3.83	−3.53	0.43	−0.11	−5.35	−5.35	−5.35	−5.38	−5.35	601.2	36.54	98.86	1.96	0.125
15	TBACl:Bu (1:2)	−1.42	−1.81	−1.49	0.38	−0.08	−5.49	−5.49	−5.50	−5.50	5.48	1413.2	109.25	293.16	2.10	0.146
16	TBACl:Ph (1:2)	−1.32	−1.69	−1.17	0.15	−0.18	−5.87	−5.88	−5.91	−5.84	−5.82	1579.3	125.21	423.11	1.63	0.128
17	TBABr:EG (1:3)	−3.46	−4.45	−4.18	0.12	−0.44	−3.85	−3.85	−3.85	−5.32	−5.30	334.4	16.01	41.41	1.90	0.118
18	TBABr:Gly (1:3)	−3.28	−4.25	−3.95	0.21	−0.34	−3.67	−3.66	−3.66	−5.37	−5.36	321.7	15.68	41.48	1.77	0.112
19	TBABr:Lev (1:3)	−2.35	−3.04	−2.70	0.41	−0.10	−3.85	−3.85	−3.85	−5.43	−5.42	593.7	36.09	98.92	1.89	0.125
20	TBABr:LA (1:2)	−3.03	−3.92	−3.59	0.03	−0.50	−4.97	−4.53	−4.98	−5.00	−4.98	261.8	11.87	32.05	1.56	0.101
21	TBABr:Bu (1:2)	−1.44	−1.84	−1.48	0.32	−0.08	−5.10	−5.10	−4.75	−5.11	−5.09	1386.6	106.58	295.07	1.97	0.145
22	TBABr:Ph (1:2)	−1.32	−1.70	−1.10	0.13	−0.18	−5.43	−5.44	−5.48	−5.39	−5.38	1567.8	124.03	449.89	1.60	0.129
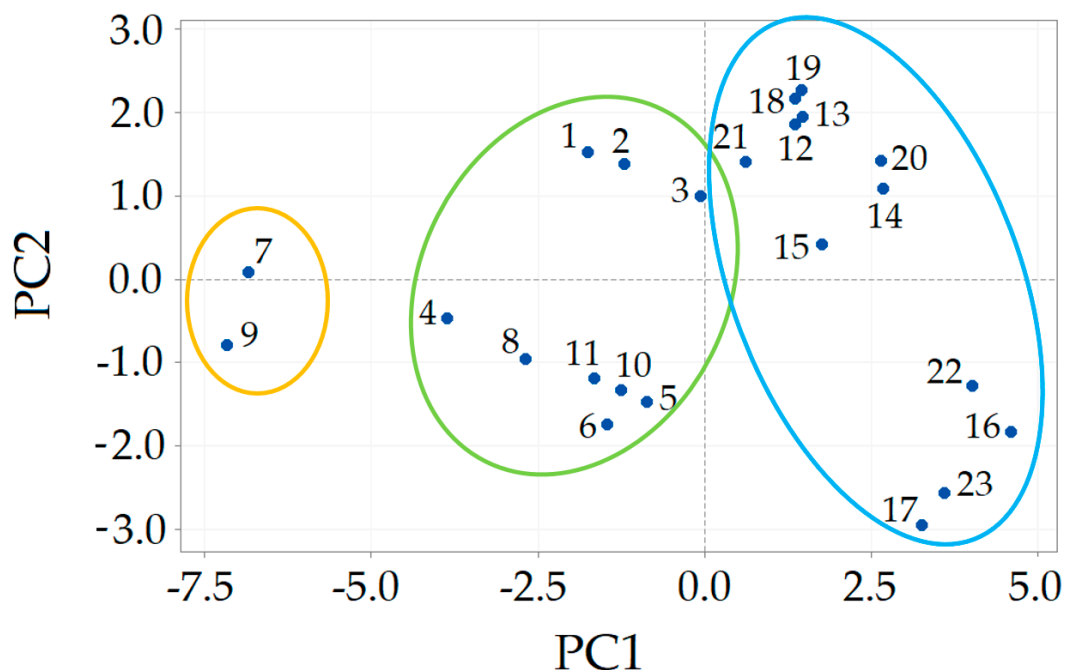
Figure 3. Principal components analysis (PCA) plot of all thermodynamic data including the activity coefficient, excess enthalpy and Henry's constant.

Based on the obtained thermodynamic results, only the DESs that showed the greatest dissolution potential for all impurities were adopted for further consideration (ChCl:U 1:2 and ChCl:OA 1:2). In practice, most of the obtained results using COSMO-RS are slightly overestimated, and this fact was more pronounced for temperatures far from room temperature. Due to the fact that all calculations were made for 20 °C, it can be concluded that the obtained results are very reliable, because the COSMO-RS model ensures acceptable accuracy (about 5%) with regard to experimental results [66,67].

3.2. Molecular Interactions

After geometric optimization, the absorption efficiency of DESs can be interpreted by molecular interactions. The geometric optimized structures of DESs are presented in Figure 4. Based on molecule-specific characteristics, the charge-related σ-profiles and σ-potential were successfully used to interpret the complex molecular interactions, according to previous studies [68–70].
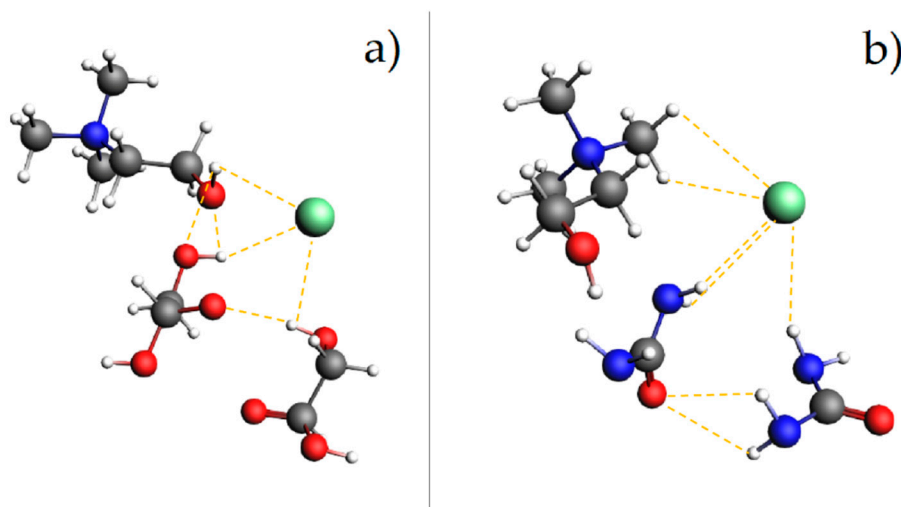

Figure 4. Optimized structures of (**a**) ChCl:OA (1:2), (**b**) ChCl:UA (1:2).

3.2.1. σ-Profiles

The σ-profile is the most important molecule-specific property because it indicates the probability distribution of the surface area of molecules that have charge density. The σ-profiles of all contaminants and DESs are presented in Figure 5. In the diagram, the range of surface area over charge density is between −0.025 and 0.025 eÅ^{-2}. This range can be divided into three segments, i.e., the non-polar region (−0.0084 eÅ^{-2} < σ < 0.0084 eÅ^{-2}), the hydrogen bond acceptor (HBA) region (−0.025 eÅ^{-2} < σ < 0.0084 eÅ^{-2}), and the hydrogen bond donor region (HBD) (0.0084 eÅ^{-2} < σ < 0.025 eÅ^{-2}). The HBA and HBD regions indicate the potential of the studied molecules to form strong hydrogen bonds. The results indicate that the σ-profile of ChCl:U (1:2) and ChCl:OA (1:2) almost overlap each other. This means that both DESs have similar properties with regard to molecular interaction. In both DESs, much larger peaks can be observed around negative values, compared to peaks around positive values, which shows more presence of HBA than HBD. The peaks of all siloxanes assume a similar shape and most of the areas are located in the non-polar area (−0.0084 eÅ^{-2} < σ < 0.0084 eÅ^{-2}), and there are small fragments of siloxane peaks in the HBD region. The opposite results can be observed for carbon dioxide, which may be a hydrogen bond acceptor to a small extent. Similar small areas of hydrogen sulfide peaks are found in the HBA and HBD parts. The σ-profile results show that the siloxanes have more negative activity coefficient values compared to CO_2 and H_2S.
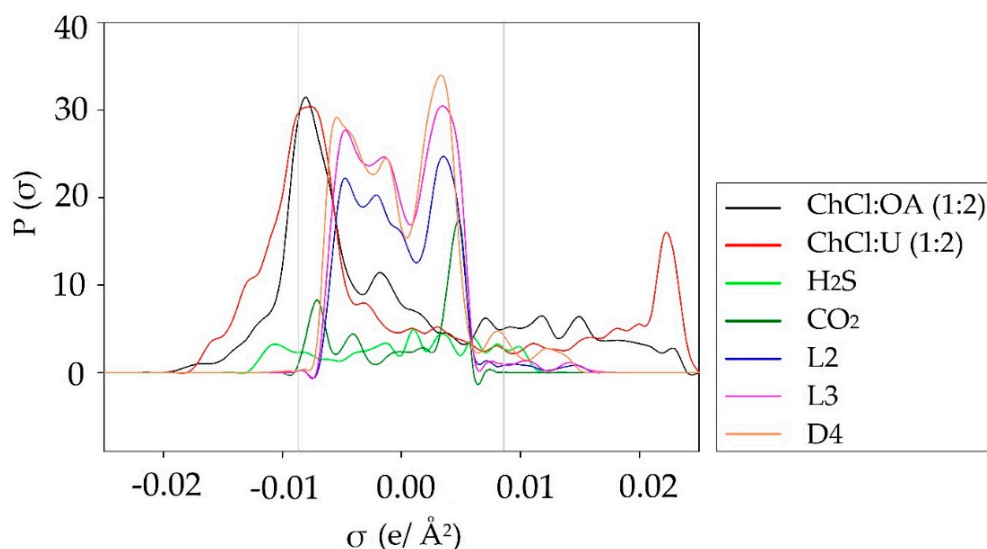
Figure 5. σ-profiles of ChCl:OA (1:2), ChCl:U (1:2), H_2S, CO_2, and siloxanes (L2, L3, D4).

3.2.2. σ-Potential

The σ-potential describes the affinity of the DESs to biogas impurities (CO_2, H_2S, L2, L3, D4) (Figure 6). The σ-potential diagram can also be divided into the same three fragments as in the σ-profile. The higher negative value of μ(σ) [kcal/molÅ] indicates stronger interaction between compounds. On the other hand, the higher positive values of μ(σ) suggest stronger repulsive interactions.
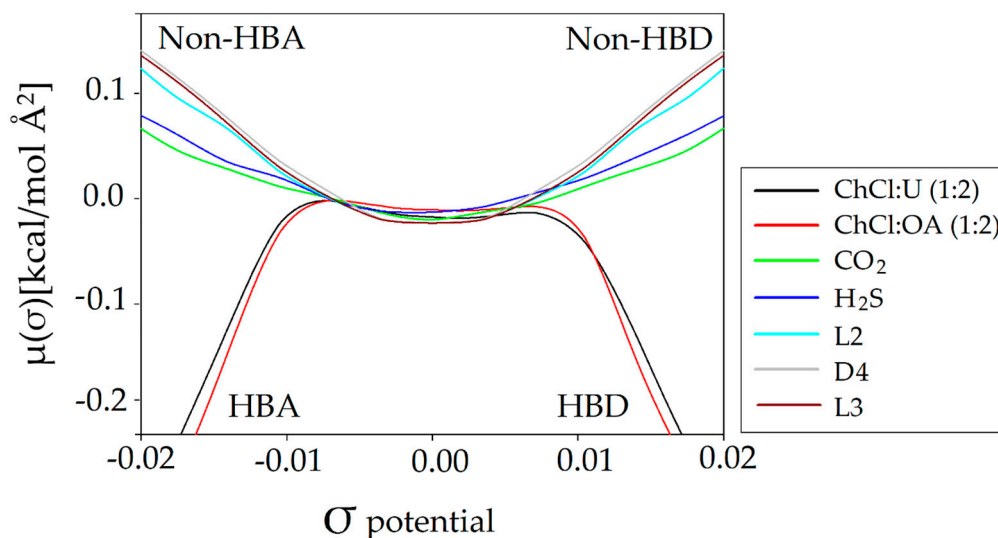
Figure 6. σ-potential of ChCl:U (1:2), ChCl:OA (1:2), CO_2, H_2S, L2, L3, and D4.

The graphic results show that all contaminants of the model biogas have parabolic curves of σ-potential. The negative values of μ(σ) in the non-polar segment indicate the non-polar nature of CO_2, H_2S, and siloxanes. The σ-potential of ChCl:U (1:2) and ChCl:OA (1:2) show negative values in the HBD, HBA, and non-polar region. This indicates that both DESs will tend to interact with hydrogen bond acceptor and donor surfaces and nonpolar molecules. The positive values of σ-potential in the HBA and HBD region of all impurities suggest that electrostatic interactions are probably the main driving force of the absorption process. In addition, the high negative value in the non-polar region of the DESs suggests a strong affinity to all biogas impurities. In addition, the similar σ-potential shape of both DESs suggests similar dissolution capabilities for all of the impurities.

3.3. Economic Evaluation

The main factor that determines the success of an investment is the economic cost [71]. The capital and running costs of biogas upgrading technology depend primarily on the size of the installation, type of technology, type of installed devices (their number and power), degree of technological advancement (degree of modernity and automation), system configuration, etc. Therefore, these costs are a function of many factors. The described technology for biogas upgrading assumes that the resulting bio-methane product will meet the quality standards of natural gas [72]. This enables the bio-methane to be introduced into natural gas installations. This is very important from an economic point of view because bio-methane does not require a specially dedicated infrastructure, which increases investment costs.

In order to better compare the cost of applying DESs, the size of installations and process streams were adopted from previous studies [55,56]. Based on an assumed biogas flow rate (813 m^3/h), estimated annual DESs consumption, and assumed biogas composition (CH_4 (64.9%; 31.0% CO_2; 3.0% H_2O; 1.04% H_2S, and 0,02% of L2, L3, and D4 [8,54]) the amount of raw biogas (7.13 Mm^3) supplied for installation per year was calculated. In addition, methane losses of 5% during the biogas upgrading process were assumed based on COSMO-RS theoretical calculations. The annual bio-methane production was calculated as 4.27 Mm^3 per year. Based on the solubility of individual biogas components in DESs, the saturation time of absorbents was calculated using the COSMO-RS model (Table 5). In order to obtain reliable information about the cost of 1 m^3 of pure bio-methane, the complete cost analysis including the total investment, operating, and maintenance costs was calculated.

Table 5. List of individual impurities and their solubility in DESs.

Type of Impurities	Impurities Concentration	Flow of Individual Impurities	Molar Mass of Impurities	ChCl:U (1:2)		ChCl:OA (1:2)	
				Solubility	Saturation Time	Solubility	Saturation Time
	[%]	[m^3/h]	[g/mol]	[mol/L DES]	[h]	[mol/L DES]	[h]
CO_2	31.0	252.03	44.01	11.53	12.89	11.49	12.84
L2	0.02	0.16	162.38	1.42	21.89	0.24	3.73
L3	0.02	0.16	236.53	0.99	20.76	0.10	2.01
D4	0.02	0.16	296.62	1.09	24.51	0.14	3.12
H_2S	1.04	8.46	34.10	32.93	1150.32	146.63	122.15

3.3.1. Investment Cost

The literature review indicated that the process scale of the biogas upgrading technology is the most important factor in the total capital investment cost (*TCIC*) calculations [73,74].

In this study, an absorption capacity of 427 m^3/h was obtained for the assumed flow rate of raw biogas, absorption and desorption column dimensions, and 8600 operating hours per year (Table 6). The assumed process parameters enabled the estimation of the individual equipment cost (*EC*) according to Equation (6). The *EC* costs (Table 6) include *EC* for the upgrading biogas section but do not include the biogas production sections. The values presented in Table 6 are average amounts from previous works [55,56]. Nevertheless, to minimize the risk of overly optimistic calculations, fluctuations in the market price of individual materials, i.e., steel and electronic components in the years from 2015–2020 were included [75].

Table 6. Estimated costs of equipment of biogas upgrading technology.

Equipment	Description	Equipment Cost (*EC*) ± SD [EUR]
Blower	Introduces biogas into the absorber	42,000 ± 3360
Absorber column	Column diameter: 1 m Column height: 15 m	50,000 ± 4000
Stripper column	Column diameter: 1 m Column height: 15 m	50,000 ± 4000
Centrifugal Pump	Pump Power	46,000 ± 3680
Heat Exchanger	Heat Exchanger	38,000 ± 3040
Centrifugal Compressor	Compressor Power	36,000 ± 2880
Dryer	Biogas water collection and disposal	25,000 ± 2000
Unlisted Equipment		300,000 ± 24,000
Total equipment cost (TEC)		587,000 ± 46,960

SD—standard deviation.

A total *EC* cost estimate was necessary to calculate the total capital investment cost (*TCIC*). *TCIC* was estimated mainly on the basis of the value of equipment cost (*EC*) [55]. In addition, statistical data for absorption technologies and laboratory processes scaling data were used for the estimation of the *TCIC* [55]. The general *TCIC* analysis for ChCl:U (1:2) and ChCl:OA (1:2) is presented in Table 7. The calculated *TCIC* for absorption using DESs was in the range of 3,152,088–3,164,929 EUR. The obtained *TCIC* is comparable to the *TCIC* of amine scrubber (3,166,000 EUR), pressure swing adsorption (3,140,000 EUR), and membrane separation (3,033,000 EUR) calculated for installations with a capacity of 500 m^3/h bio-methane. A much lower *TCIC* was obtained for the water scrubber (2,794,000 EUR) [76].

Table 7. The general estimate the total capital investment cost (*TCIC*) for DES.

Parameter	Cost ± SD [EUR] for ChCl:U (1:2)	Cost ± SD [EUR] for ChCl:OA (1:2)
Direct Cost (DC)		
Total equipment cost (TEC)	587,000 ± 46,960	587,000 ± 46,960
Installation instrumentation and control	610,480 ± 48,838	610,480 ± 48,838
Electrical and heat power	64,570 ± 5166	69,950± 5596
Building and building services and equipment installation	381,550 ± 30,524	381,550 ± 30,524
Yard improvement	58,700 ± 4696	58,700 ± 4696
External services	410,900 ± 32,872	410,900 ± 32,872
Total direct cost (TCD)	2,113,200 ± 169,056	2,118,580 ± 169,486
Indirect Cost (IC)		
Engineering and construction site	434,380 ± 34,750	434,380 ± 34,750
Law cost	23,480 ± 1878	23,480 ± 1878
Contractor's fee	129,140 ± 10,331	129,140 ± 10,331
Incidents	258,280 ± 20,662	258,280 ± 20,662
Total indirect cost (TCI)	845,280 ± 67,622	845,280 ± 67,622
Other Cost (OC)		
Floating capital	126,792 ± 10,143	126,792 ± 10,143
DES batch	66,816 ± 5345	74,277 ± 5942
Total other cost (TOC)	193,608 ± 15,489	201,069 ± 16,086
Total capital investment cost (TCIC)	3,152,088 ± 252,167	3,164,929 ± 253,194

SD—standard deviation.

3.3.2. Operation and Maintenance Cost

The annual fixed operating costs (FC) included the operation and maintenance cost (OC and MC) of biogas upgrading plants. The OC and MC included the costs of maintenance, operating, labor, and taxation, which are presented in Table 8. The cost of DESs was calculated for the scrubber volume (2.35 m^3), which was doubled in order to maintain the continuity of the process.

Table 8. General estimate of the operation cost (OC) and maintenance cost (MC) for DES.

Parameter	Cost ± SD [EUR] of ChCl:U (1:2)	Cost ± SD [EUR] of ChCl:OA (1:2)
Fixed Cost (FC)		
Regional taxes and insurance	46,066 ± 3685	46,066 ± 3685
Total fixed cost (TFC)	46,066 ± 3685	46,066 ± 3685
Direct Production Cost (DPC)		
Maintenance (M)	69,099 ± 5528	69,099 ± 5528
Salary for the operator (1500 man-hour/year) (SO) (10 Personnel)	58,320 ± 4666	58,320 ± 4666
Supervision (S)	8748 ± 700	8748 ± 700
Operating materials	10,365 ± 830	10,365 ± 830
Changes in electricity cost in the laboratory	20,425 ± 1634	20,425 ± 1634
Total direct production cost (TDPC)	166,957 ± 13,357	166,957 ± 13,357
General Expenses (GE)		
Administrative cost	1313 ± 105	1313 ± 105
Distribution, marketing and R&D cost	39,710 ± 3177	39,710 ± 3177
Total general Expenses (TGE)	41,023 ± 3282	41,023 ± 3282
DES Cost (DESC)		
DES replacement cost	334,080 ± 26,726	445,662 ± 35,653
Depreciation expense	3339 ± 267	339 ± 267
Total DES Cost (TDESC)	337,419 ± 26,994	449,001 ± 35,920
Total operation and maintenance cost (TOC and MC)	591,465 ± 47,317	703,047 ± 56,244

SD—standard deviation.

Due to the different absorption capacity of DES and regeneration cycles, the energy consumption in the absorption processes was different. Based on previous studies, it was assumed that ChCl:U (1:2) and ChCl:OA (1:2) can be regenerated 73 and 60 times, respectively, without loss of absorption capacity. From an economic and industrial point of view, recycling and reuse of DES after the absorption process is highly desirable because it reduces annual operating costs and the amount of waste. Numerous regeneration cycles can be achieved due to highly reversible absorption, which mainly depends on the structure and thermal stability of DESs. HBDs play the main role in the thermal stability of DESs, which depends mainly on the weak intermolecular interaction. The decomposition temperature of urea in ChCl:U is about 172.40 °C [77], while the decomposition temperature of oxalic acid in ChCl:OA is about 134.84 °C [78]. Both temperatures are higher than the temperature required for regeneration, which is enough to ensure long absorption–desorption cycles. However, the ChCl:OA structure and its lower decomposition temperature result in a slightly lower number of regeneration cycles. After a number of regeneration cycles, DESs must be replaced to further ensure the high quality of bio-methane. The other costs of OC and MC was estimated based on the literature [74,79] and using percentage factors of *TCIC*. The costs in Table 8 (FC, DPC, GE) are averaged values for selected European Union countries, i.e., Sweden, Germany, France, Norway, and Poland for which standard deviations have been determined. The one-time cost of replacing the absorbent is 66,816 EUR and 74,277 EUR for ChCl: U and ChCl: OA, respectively. Due to the 5-fold (ChCl: U) and 6-fold (ChCl: OA) exchange of absorbents to ensure the high quality of bio-methane, the total cost of replacement is 334,080 and 445,662 EUR for ChCl:U and ChCl:OA, respectively.

The total OC and MC cost for ChCl:OA (703,047 EUR) is comparable with amine scrubber (688,000 EUR) and membrane separation (662,000 EUR), while the total OC and MC cost for ChCl:U (591,465 EUR) is more comparable with water scrubber (513,000 EUR) and pressure swing adsorption (557,000 EUR) [76].

3.3.3. Economic Comparison of the Overall Biogas Upgrading Process

It is difficult to clearly estimate the costs of individual technologies due to the differences in the cost of components, materials and utilities, and local conditions. Therefore, is important to consider the total annual cost (*TAC*) of the biogas upgrading process, which was 982,510 ± 78,601 EUR (ChCl:U) and 1,095,685 ± 87,654 EUR (ChCl:OA) in the economic analysis. The *TAC* cost for ChCl:U was very similar to the *TAC* for pressure swing adsorption (970,000 EUR), while the *TAC* obtained for ChCl:OA was very similar to the *TAC* for amine scrubber (1,104,000 EUR) and membrane separation (1,061,000 EUR). The lowest *TAC* is for the water scrubber (880,000 EUR). Based on the above calculations, the unit cost of 1 m^3 of pure bio-methane was determined by means of Equation (4). The obtained unit cost of 1 m^3 of bio-methane was 0.35 ± 0.03 EUR/m^3 and 0.37 ± 0.03 EUR/m^3 for the physical absorption process using ChCl:U (1:2) and ChCl:OA (1:2), respectively. The unit cost for various biogas treatment technologies can be ordered as follows: amine scrubber > membrane separation > ChCl:OA (1:2) > ChCl:U (1:2) > PSA > water scrubbing [76] (Table 9). The values include the average standard deviation (8%), which was adopted based on the above calculations. Table 9 contains only the total *TAC* and UC values without standard deviations due to the lack of data from other studies. The main advantage of the innovative method based on DES is the cost of biogas upgrading compared to the most commonly used absorbents.

Table 9. Comparison of economic analysis.

Purification Methods	Total Annual Cost (*TAC*)	Unit Cost of Bio-Methane (UC)	Ref.
Amine scrubber	1,104,000 EUR	0.39 EUR/m^3	[56]
Membrane separation	1,061,000 EUR	0.38 EUR/m^3	[56]
ChCl:OA scrubber	1,095,685 EUR	0.37 EUR/m^3	This study
ChCl:U scrubber	982,510 EUR	0.35 EUR/m^3	This study
PSA	970,000 EUR	0.35 EUR/m^3	[56]
Water scrubbing	880,000 EUR	0.33 EUR/m^3	[56]

The application of traditional absorbents (water, amine), requires further biogas refinement operations, which involves additional costs, while the use of DES ensures that high-quality bio-methane is obtained in a one-step process. The obtained results indicate that biogas upgrading technology by means of DESs is a competitive technology for all currently used methods in the industry.

4. Conclusions

The study presents low-cost deep eutectic solvents (DES) as potential new sorption materials that enable one-step, effective biogas upgrading. This is a significant advantage compared to the currently used sorbents that are dedicated to removing only selected groups of impurities, which does not guarantee that the biogas will be of sufficient quality. The use of developed sorbents under absorption conditions results in biogas with high-methane gas parameters that meet the parameters for gas injected into the transmission network and transport fuel. In addition, the use of new sorbents based on DESs are highly advantageous from an economic and ecological point of view because the sorbents are synthesized from inexpensive, easily available materials that can be regenerated many times without loss of absorption capacity.

In this study, 23 low-cost DESs composed of quaternary ammonium salts and organic components were investigated. Based on the basic thermodynamic properties, i.e., the activity coefficient, excess enthalpy, and Henry's constant, two DESs (ChCl:U (1:2) and ChCl:OA (1:2)) were selected because they showed the highest dissolution potential of the siloxanes, CO_2, and H_2S. The high affinity of both DESs to all of the main biogas contaminations was confirmed by means of σ-profiles and σ-potential analysis. It was shown that the electrostatic interactions between biogas impurities and DESs are the main driving force of the absorption process. For the best DESs, economic analysis simulation was conducted in order to evaluate and compare ChCl:U (1:2) and ChCl:OA (1:2) to each other and to currently available industrial absorbents. The unit cost of DESs depend mainly on the DES structure, which is responsible for its absorption capacity, and regeneration cycles. The unit cost of obtaining 1 m^3 of high-quality bio-methane using DESs absorption is comparable to the costs of currently used technologies. However, the proposed biogas upgrading technology offers the possibility of removing CO_2, H_2S, and siloxanes in one step. This is a significant advantage compared to other commonly used technologies that only remove individual impurities. The obtained results show the great potential of DESs to improve biogas to high-quality bio-methane with properties comparable to natural gas. Such bio-methane could be injected into the natural gas network or used as an alternative to compressed natural gas fuel. However, further experimental research is needed to confirm the obtained results.

References

1. European Biogas Association (EBA). *European Biogas Association Annual Report 2019*; EBA: Brussels, Belgium, 2019.
2. European Biogas Association (EBA). *Statistical Report 2018: Annual Report*; EBA: Brussels, Belgium, 2018; Volume 68.
3. Persson, M.; Jonsson, O.; Wellinger, A. Biogas Upgrading To Vehicle Fuel Standards and Grid Injection. *IEA Bioenergy Task* **2007**, *37*, 1–34.
4. Andrés, C.; De Guardia, A.; Couvert, A.; Wolbert, D.; Le, S.; Soutrel, I.; Nunes, G. Odor concentration (OC) prediction based on odor activity values (OAVs) during composting of solid wastes and digestates. *Atmos. Environ.* **2019**, *201*, 1–12.
5. Papurello, D.; Soukoulis, C.; Schuhfried, E.; Cappellin, L.; Gasperi, F.; Silvestri, S.; Santarelli, M.; Biasioli, F. Monitoring of volatile compound emissions during dry anaerobic digestion of the Organic Fraction of Municipal Solid Waste by Proton Transfer Reaction Time-of-Flight Mass Spectrometry. *Bioresour. Technol.* **2012**, *126*, 254–265. [CrossRef] [PubMed]
6. Wasajja, H.; Lindeboom, R.E.F.; van Lier, J.B.; Aravind, P.V. Techno-economic review of biogas cleaning technologies for small scale off-grid solid oxide fuel cell applications. *Fuel Process. Technol.* **2020**, *197*, 106215. [CrossRef]
7. Paolini, V.; Petracchini, F.; Segreto, M.; Tomassetti, L.; Naja, N.; Cecinato, A. Environmental impact of biogas: A short review of current knowledge. *J. Environ. Sci. Health Part A Toxic Hazard. Subst. Environ. Eng.* **2018**, *53*, 899–906. [CrossRef] [PubMed]
8. Rasi, S.; Veijanen, A.; Rintala, J. Trace compounds of biogas from different biogas production plants. *Energy* **2007**, *32*, 1375–1380. [CrossRef]
9. Santos-Clotas, E.; Cabrera-Codony, A.; Martín, M.J. Coupling adsorption with biotechnologies for siloxane abatement from biogas. *Renew. Energy* **2020**, *153*, 314–323. [CrossRef]
10. Santos-Clotas, E.; Cabrera-Codony, A.; Boada, E.; Gich, F.; Muñoz, R.; Martín, M.J. Efficient removal of siloxanes and volatile organic compounds from sewage biogas by an anoxic biotrickling filter supplemented with activated carbon. *Bioresour. Technol.* **2019**, *294*, 122136. [CrossRef]
11. Liu, Y.H.; Meng, Z.Y.; Wang, J.Y.; Dong, Y.F.; Ma, Z.C. Removal of siloxanes from biogas using acetylated silica gel as adsorbent. *Pet. Sci.* **2019**, *16*, 920–928. [CrossRef]
12. Ruiling, G.; Shikun, C.; Zifu, L. Research progress of siloxane removal from biogas. *Int. J. Agric. Biol. Eng.* **2017**, *10*, 30–39.
13. Shen, M.; Zhang, Y.; Hu, D.; Fan, J.; Zeng, G. A review on removal of siloxanes from biogas: With a special focus on volatile methylsiloxanes. *Environ. Sci. Pollut. Res.* **2018**, *25*, 30847–30862. [CrossRef] [PubMed]
14. Xiao, Y.; Yuan, H.; Pang, Y.; Chen, S.; Zhu, B.; Zou, D.; Ma, J.; Yu, L.; Li, X. CO2 Removal from Biogas by Water Washing System. *Chin. J. Chem. Eng.* **2014**, *22*, 950–953. [CrossRef]
15. Mandal, B.P.; Biswas, A.K.; Bandyopadhyay, S.S. Selective absorption of H2S from gas streams containing H2S and CO2 into aqueous solutions of N-methyldiethanolamine and 2-amino-2-methyl-1-propanol. *Sep. Purif. Technol.* **2004**, *35*, 191–202. [CrossRef]
16. Jassim, M.S.; Rochelle, G.; Eimer, D.; Ramshaw, C. Carbon Dioxide Absorption and Desorption in Aqueous Monoethanolamine Solutions in a Rotating Packed Bed. *Ind. Eng. Chem. Res.* **2007**, *46*, 2823–2833. [CrossRef]
17. Xu, H.J.; Zhang, C.F.; Zheng, Z.S. Solubility of hydrogen sulfide and carbon dioxide in a solution of methyldiethanolamine mixed with ethylene glycol. *Ind. Eng. Chem. Res.* **2002**, *41*, 6175–6180. [CrossRef]
18. Privalova, E.; Nurmi, M.; Marañón, M.S.; Murzina, E.V.; Mäki-arvela, P.; Eränen, K.; Murzin, D.Y.; Mikkola, J. CO$_2$ removal with 'switchable' versus 'classical' ionic liquids. *Sep. Purif. Technol.* **2012**, *97*, 42–50. [CrossRef]
19. Gao, J.; Cao, L.; Dong, H.; Zhang, X.; Zhang, S. Ionic liquids tailored amine aqueous solution for pre-combustion CO$_2$ capture: Role of imidazolium-based ionic liquids. *Appl. Energy* **2015**, *154*, 771–780. [CrossRef]
20. Shiflett, M.B.; Yokozeki, A. Solubilities and Diffusivities of Carbon Dioxide in Ionic Liquids: [bmim] [PF 6] and [bmim] [BF 4]. *Ind. Eng. Chem. Res.* **2005**, 4453–4464. [CrossRef]
21. Jou, F.Y.; Mather, A.E. Solubility of hydrogen sulfide in [bmim][PF 6]. *Int. J. Thermophys.* **2007**, *28*, 490–495. [CrossRef]

22. Pomelli, C.S.; Chiappe, C.; Vidis, A.; Laurenczy, G.; Dyson, P.J. Influence of the interaction between hydrogen sulfide and ionic liquids on solubility: Experimental and theoretical investigation. *J. Phys. Chem. B* **2007**, *111*, 13014–13019. [CrossRef]

23. Rahmati-Rostami, M.; Ghotbi, C.; Hosseini-Jenab, M.; Ahmadi, A.N.; Jalili, A.H. Solubility of H2S in ionic liquids [hmim][PF6], [hmim][BF4], and [hmim][Tf2N]. *J. Chem. Thermodyn.* **2009**, *41*, 1052–1055. [CrossRef]

24. Zhang, X.; Zhang, X.; Dong, H.; Zhao, Z.; Zhang, S.; Huang, Y. Carbon capture with ionic liquids: Overview and progress. *Energy Environ. Sci.* **2012**, *5*, 6668–6681. [CrossRef]

25. Xie, Y.; Zhang, Y.; Lu, X.; Ji, X. Energy consumption analysis for CO2 separation using imidazolium-based ionic liquids. *Appl. Energy* **2014**, *136*, 325–335. [CrossRef]

26. Thuy Pham, T.P.; Cho, C.W.; Yun, Y.S. Environmental fate and toxicity of ionic liquids: A review. *Water Res.* **2010**, *44*, 352–372. [CrossRef]

27. Abbott, A.P.; Capper, G.; Davies, D.L.; Rasheed, R.K.; Tambyrajah, V. Novel Solvent Properties of Choline Chloride/Urea Mixtures. *Chem. Commun.* **2003**, *0*, 70–71. [CrossRef]

28. Azizi, N.; Dezfooli, S.; Khajeh, M.; Hashemi, M.M. Efficient deep eutectic solvents catalyzed synthesis of pyran and benzopyran derivatives. *J. Mol. Liq.* **2013**, *186*, 76–80. [CrossRef]

29. Abbott, A.P.; Barron, J.C.; Ryder, K.S.; Wilson, D. Eutectic-Based Ionic Liquids with Metal-Containing Anions and Cations. *Chem. Eur. J.* **2007**, *13*, 6495–6501. [CrossRef]

30. Mainar, A.R.; Iruin, E.; Colmenares, L.C.; Kvasha, A.; de Meatza, I.; Bengoechea, M.; Leonet, O.; Boyano, I.; Zhang, Z.; Blazquez, J.A. An overview of progress in electrolytes for secondary zinc-air batteries and other storage systems based on zinc. *J. Energy Storage* **2018**, *15*, 304–328. [CrossRef]

31. Werner, S.; Haumann, M.; Wasserscheid, P. Ionic Liquids in Chemical Engineering. *Annu. Rev. Chem. Biomol. Eng.* **2010**, *1*, 203–230. [CrossRef]

32. Sowmiah, S.; Srinivasadesikan, V.; Tseng, M.C.; Chu, Y.H. On the Chemical Stabilities of Ionic Liquids. *Molecules* **2009**, *14*, 3780–3813. [CrossRef]

33. Dai, Y.; Van Spronsen, J.; Witkamp, G.J.; Verpoorte, R.; Choi, Y.H. Ionic liquids and deep eutectic solvents in natural products research: Mixtures of solids as extraction solvents. *J. Nat. Prod.* **2013**, *76*, 2162–2173. [CrossRef] [PubMed]

34. Turosung, S.N.; Ghosh, B. Application of Ionic Liquids in the Upstream oil Industry-A Review. *Int. J. Petrochem. Res.* **2017**, *1*, 50–60. [CrossRef]

35. Smith, E.L.; Abbott, A.P.; Ryder, K.S. Deep Eutectic Solvents (DESs) and Their Applications. *Chem. Rev.* **2014**, *114*, 11060–11082. [CrossRef] [PubMed]

36. Vanda, H.; Dai, Y.; Wilson, E.G.; Verpoorte, R.; Choi, Y.H. Green solvents from ionic liquids and deep eutectic solvents to natural deep eutectic solvents. *Comptes Rendus Chim.* **2018**, *21*, 628–638. [CrossRef]

37. Marcus, Y. Estimation of the Critical Temperatures of Some More Deep Eutectic Solvents from Their Surface Tensions. *Adv. Mater. Sci. Eng.* **2018**, *2018*, 2–5. [CrossRef]

38. Makoś, P.; Słupek, E.; Gębicki, J. Extractive detoxification of feedstocks for the production of biofuels using new hydrophobic deep eutectic solvents – Experimental and theoretical studies. *J. Mol. Liq.* **2020**, in press.

39. Makoś, P.; Przyjazny, A.; Boczkaj, G. Hydrophobic deep eutectic solvents as "green" extraction media for polycyclic aromatic hydrocarbons in aqueous samples. *J. Chromatogr. A* **2018**, *1570*, 28–37. [CrossRef] [PubMed]

40. Makoś, P.; Boczkaj, G. Deep eutectic solvents based highly efficient extractive desulfurization of fuels—Eco-friendly approach. *J. Mol. Liq.* **2019**, 111916. [CrossRef]

41. Makoś, P.; Fernandes, A.; Przyjazny, A.; Boczkaj, G. Sample preparation procedure using extraction and derivatization of carboxylic acids from aqueous samples by means of deep eutectic solvents for gas chromatographic-mass spectrometric analysis. *J. Chromatogr. A* **2018**, *1555*, 10–19. [CrossRef] [PubMed]

42. Zhong, F.-Y.; Huang, K.; Peng, H.-L. Solubilities of ammonia in choline chloride plus urea at (298.2–353.2) K and (0–300) kPa. *J. Chem. Thermodyn.* **2019**, *129*, 5–11. [CrossRef]

43. Zhang, K.; Hou, Y.; Wang, Y.; Wang, K.; Ren, S.; Wu, W. Efficient and Reversible Absorption of CO2 by Functional Deep Eutectic Solvents. *Energy Fuels* **2018**, *32*, 7727–7733. [CrossRef]

44. Moura, L.; Moufawad, T.; Ferreira, M.; Bricout, H.; Tilloy, S.; Monflier, E.; Costa Gomes, M.F.; Landy, D.; Fourmentin, S. Deep eutectic solvents as green absorbents of volatile organic pollutants. *Environ. Chem. Lett.* **2017**, *15*, 747–753. [CrossRef]

45. Słupek, E.; Makoś, P.; Gębicki, J. Deodorization of model biogas by means of novel non-ionic deep eutectic solvent. *Arch. Environ. Prot.* **2020**, *46*, 41–46.

46. Słupek, E.; Makoś, P. Absorptive Desulfurization of Model Biogas Stream Using Choline Chloride-Based Deep Eutectic Solvents. *Sustainability* **2020**, *12*, 1619. [CrossRef]

47. Zhang, Y.; Ji, X.; Xie, Y.; Lu, X. Thermodynamic analysis of CO2 separation from biogas with conventional ionic liquids. *Appl. Energy* **2018**, *217*, 75–87. [CrossRef]

48. Ali, E.; Hadj-Kali, M.K.; Mulyono, S.; Alnashef, I. Analysis of operating conditions for CO2 capturing process using deep eutectic solvents. *Int. J. Greenh. Gas Control* **2016**, *47*, 342–350. [CrossRef]

49. Makoś, P.; Słupek, E.; Małachowska, A. Silica Gel Impregnated by Deep Eutectic Solvents for Adsorptive Removal of BTEX from Gas Streams. *Materials* **2020**, *13*, 1894. [CrossRef]

50. Häckl, K.; Kunz, W. Some aspects of green solvents. *Comptes Rendus Chim.* **2018**, *21*, 572–580. [CrossRef]

51. Del Olmo, L.; Lõpez, R.; García De La Vega, J.M. Effect of the molecular structure in the prediction of thermodynamic properties for 1-butyl-3-methylimidazolium chloride ionic liquid. *Int. J. Quantum Chem.* **2013**, *113*, 852–858. [CrossRef]

52. Pye, C.C.; Ziegler, T. An implementation of the conductor-like screening model of solvation within the Amsterdam density functional package. *Theor. Chem. Acc.* **1999**, *101*, 396–408. [CrossRef]

53. AMS 2019.3 COSMO-RS, SCM, Theoretical Chemistry. Vrije Universiteit: Amsterdam, The Netherlands; Available online: http://www.scm.com (accessed on 4 May 2020).

54. Rasi, S.; Läntelä, J.; Rintala, J. Upgrading landfill gas using a high pressure water absorption process. *Fuel* **2014**, *115*, 539–543. [CrossRef]

55. Ma, C.; Liu, C.; Lu, X.; Ji, X. Techno-economic analysis and performance comparison of aqueous deep eutectic solvent and other physical absorbents for biogas upgrading. *Appl. Energy* **2018**, *225*, 437–447. [CrossRef]

56. Xie, Y.; Björkmalm, J.; Ma, C.; Willquist, K.; Yngvesson, J.; Wallberg, O.; Ji, X. Techno-economic evaluation of biogas upgrading using ionic liquids in comparison with industrially used technology in Scandinavian anaerobic digestion plants. *Appl. Energy* **2018**, *227*, 742–750. [CrossRef]

57. Scholz, M.; Frank, B.; Stockmeier, F.; Falß, S.; Wessling, M. Techno-economic analysis of hybrid processes for biogas upgrading. *Ind. Eng. Chem. Res.* **2013**, *52*, 16929–16938. [CrossRef]

58. Guthrie, H.M. Capital cost estimation for the chemical and process industries. *Chem. Eng.* **1969**, *32*, 114–142.

59. Euro Statistic Explained Electricity Prices First Semester of 2017_2019 (EUR Per kWh). Available online: https://ec.europa.eu/eurostat/statistics-explained/index.php?title=File:Electricity_prices,_first_semester_of_2017-2019_(EUR_per_kWh).png (accessed on 4 May 2020).

60. Alibaba.com Choline Chloride. Available online: https://www.alibaba.com/product-detail/choline-chloride-CAS-67-48-1_62448780792.html?spm=a2700.7724857.normalList (accessed on 4 May 2020).

61. Alibaba.com Urea. Available online: https://www.alibaba.com/product-detail/price-per-ton-urea-2019-high_60456580510.html?spm=a2700.7724857.normalList.188.c2e9746du64Jbd (accessed on 4 May 2020).

62. Alibaba.com Oxalic Acid. Available online: https://www.alibaba.com/product-detail/99-6-min-Oxalic-Acid-h2c2o4_60767148271.html?spm=a2700.7724857.normalList.11.27d05ea2G45DWC&s=p&bypass=true (accessed on 4 May 2020).

63. De Hullu, J.; Massen, J.L.W.; van Meel, P.A.; Shazad, S.; Vaessen, J.M.P. *Comparing Different Biogas Upgrading Techniques-Report*; Eindhoven University of Technology: Eindhoven, The Netherlands, 2008.

64. Chu, Y.; He, X. MoDoop: An Automated Computational Approach for COSMO-RS Prediction of Biopolymer Solubilities in Ionic Liquids. *ACS Omega* **2019**, *4*, 2337–2343. [CrossRef]

65. Makoś, P.; Słupek, E.; Gębicki, J. Hydrophobic deep eutectic solvents in microextraction techniques–A review. *Microchem. J.* **2020**, *152*. [CrossRef]

66. Han, J.; Dai, C.; Yu, G.; Lei, Z. Parameterization of COSMO-RS model for ionic liquids. *Green Energy Environ.* **2018**, *3*, 247–265. [CrossRef]

67. Mu, T.; Rarey, J.; Gmehling, J. Performance of COSMO-RS with sigma profiles from different model chemistries. *Ind. Eng. Chem. Res.* **2007**, *46*, 6612–6629. [CrossRef]

68. Mullins, E.; Oldland, R.; Liu, Y.A.; Wang, S.; Sandler, S.I.; Chen, C.C.; Zwolak, M.; Seavey, K.C. Sigma-profile database for using COSMO-based thermodynamic methods. *Ind. Eng. Chem. Res.* **2006**, *45*, 4389–4415. [CrossRef]

69. Salleh, Z.; Wazeer, I.; Mulyono, S.; El-blidi, L.; Hashim, M.A.; Hadj-Kali, M.K. Efficient removal of benzene from cyclohexane-benzene mixtures using deep eutectic solvents—COSMO-RS screening and experimental validation. *J. Chem. Thermodyn.* **2017**, *104*, 33–44. [CrossRef]

70. Liu, Y.-R.; Thomsen, K.; Nie, Y.; Zhang, S.-J.; Meyer, A.S. Predictive screening of ionic liquids for dissolving cellulose and experimental verification. *Green Chem.* **2016**, *18*, 6246–6254. [CrossRef]

71. Hosseinipour, S.A.; Mehrpooya, M. Comparison of the biogas upgrading methods as a transportation fuel. *Renew. Energy* **2019**, *130*, 641–655. [CrossRef]

72. Ryckebosch, E.; Drouillon, M.; Vervaeren, H. Techniques for transformation of biogas to biomethane. *Biomass Bioenergy* **2011**, *35*, 1633–1645. [CrossRef]

73. Petersson, A.; Holm-nielsen, J.B.; Baxter, D. Biogas upgrading technologies—Developments and innovations. *IEA Bioenergy Task* **2009**, *37*.

74. Warren, W.K.E.H. A Techno-economic Comparison of Biogas Upgrading Technologies in Europe. Master's Thesis, Jyväskylän yliopisto—University of Jyväskylä, Jyväskylä, Finland, 2012; p. 44.

75. Trading Economics. Available online: https://tradingeconomics.com/commodity/steel?fbclid=IwAR12n6kfQegnqpqrIPqJZ47gjDUh2Q7OIt9BChQosYiJnZSHskCDwczPqJ8 (accessed on 21 May 2020).

76. Stürmer, B.; Kirchmeyr, F.; Kovacs, K.; Hofmann, F.; Collins, D.; Ingremeau, C.; Stambasky, J. *Technical-Economic Analysis for Determining the Feasibility Threshold for Tradable Biomethane Certificates-Report*; European Renewable Gas Registry: Brussels, Belgium, 2016; pp. 1–24.

77. Chen, W.; Xue, Z.; Wang, J.; Jiang, J.; Zhao, X.; Mu, T. Investigation on the thermal stability of deep eutectic solvents. *Wuli Huaxue Xuebao/Acta Phys. Chim. Sin.* **2018**, *34*, 904–911. [CrossRef]

78. Haz, A.; Strizincova, P.; Majova, V.; Skulcova, A.; Jablonsky, M. Thermal stability of selected deep eutectic solvents. *Int. J. Recent Sci. Res.* **2016**, *7*, 14441–14444.

79. Brown, R.C.; Brown, T.R. Biorenewable Resources: Engineering New Products from Agriculture: Second Edition. *Biorenew. Resour. Eng. New Prod. Agric. Second Ed.* **2014**, *9781118524*, 1–375.

Gdańsk, dnia 19.05.2023

dr inż. Patrycja Makoś-Chełstowska
....
(stopień/tytuł, imię i nazwisko)

Politechnika Gdańska
....
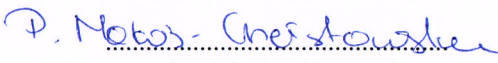(Afiliacja)

OŚWIADCZENIE WSPÓŁAUTORA

Jako współautor pracy:. **" Theoretical and Economic Evaluation of Low-Cost Deep Eutectic Solvents for Effective Biogas Upgrading to Bio-Methane"** oświadczam, że mój własny wkład polegał na konceptualizacji, metodologii, gromadzeniu i przechowywaniu danych, wizualizacji, przygotowaniu oryginalnego manuskryptu, przygotowaniu recenzji i redakcji ostatecznej wersji manuskryptu.

Jednocześnie wyrażam zgodę na przedłożenie ww. pracy przez mgr inż. Edytę Słupek jako część rozprawy doktorskiej w formie spójnego tematycznie zbioru artykułów opublikowanych w czasopismach naukowych.

Oświadczam, że samodzielna i możliwa do wyodrębnienia część ww. pracy wykazuje indywidualny wkład mgr inż. Edyty Słupek polegający na: konceptualizacji, metodologii, gromadzeniu i przechowywaniu danych, wizualizacji, przygotowaniu oryginalnego manuskryptu.

....
(podpis współautora)

Gdańsk, dnia 19.05.2023

dr inż. hab. Jacek Gębicki
....
(stopień/tytuł, imię i nazwisko)

Politechnika Gdańska
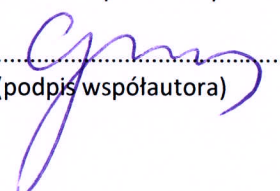...
(Afiliacja)

OŚWIADCZENIE WSPÓŁAUTORA

Jako współautor pracy:. **" Theoretical and Economic Evaluation of Low-Cost Deep Eutectic Solvents for Effective Biogas Upgrading to Bio-Methane"** oświadczam, że mój własny wkład polegał nanazdorowaniu wstępnego planu badań oraz realizacji, przygotowaniu oryginalnego manuskryptu.

Jednocześnie wyrażam zgodę na przedłożenie ww. pracy przez mgr inż. Edytę Słupek jako część rozprawy doktorskiej w formie spójnego tematycznie zbioru artykułów opublikowanych w czasopismach naukowych.

Oświadczam, że samodzielna i możliwa do wyodrębnienia część ww. pracy wykazuje indywidualny wkład mgr inż. Edyty Słupek polegający na: konceptualizacji, metodologii, gromadzeniu i przechowywaniu danych, wizualizacji, przygotowaniu oryginalnego manuskryptu.

....
(podpis współautora)